VIBRATIONS
IN PHYSICAL SYSTEMS

Volume XXIV

Editors

Czesław CEMPEL, Marian W. DOBRY

Poznan 2010

POZNAN UNIVERSITY OF TECHNOLOGY
MECHANICAL ENGINEERING AND MANAGEMENT FACULTY
INSTITUTE OF APPLIED MECHANICS
POLISH SOCIETY OF THEORETICAL AND APPLIED MECHANICS

XXIV Symposium

VIBRATIONS
IN PHYSICAL SYSTEMS

2010

XXIV SYMPOSIUM

VIBRATIONS IN PHYSICAL SYSTEMS

Będlewo (near Poznań), May 11-15, 2010

Present edition of Symposium Vibrations in Physical Systems is under auspices of

President of Poznan University of Technology
Adam HAMROL

Dean of Mechanical Engineering and Management Faculty
Jan ŻUREK

SCIENTIFIC COMMITTEE
Czesław CEMPEL – president, Andrzej TYLIKOWSKI – vice president,
Vladimir I. ALSHITC, Jan AWREJCEWICZ, Roman BOGACZ, Tadeusz BURCZYŃSKI,
Marian W. DOBRY, Zbigniew ENGEL, Antoni GAJEWSKI, Stefan JONIAK, Jan KOŁODZIEJ,
Tomasz ŁODYGOWSKI, Krzysztof MAGNUCKI, Krzysztof MARCHELEK,
Bogdan MARUSZEWSKI, Stanisław MATYSIAK, Gerard A. MAUGIN, Wolfgang MUSCHIK,
Jan HOLNICKI-SZULC, Józef NIZIOŁ, Andrzej RADOWICZ, Bogdan SKALMIERSKI,
Asja SOKOLOVA, Tomasz SZOLC, Franciszek TOMASZEWSKI, Alexandr YAVLENSKY,
Józef WOJNAROWSKI, Czesław WOŹNIAK, Andrzej P. ZIELIŃSKI

ORGANIZING COMMITTEE
Tomasz STRĘK – chairman, Małgorzata JANKOWSKA – secretary, Tadeusz WEGNER,
Marian W. DOBRY, Bogdan MARUSZEWSKI, Małgorzata WOJSZNIS, Paulina FOPP,
Tomasz MACHNICKI, Jacek BUŚKIEWICZ, Henryk KAMIŃSKI, Roman STAROSTA,
Maciej TABASZEWSKI, Zdzisław GOLEC, Paweł JASION, Jerzy LEWIŃSKI

FINANCIAL SUPPORT
Ministry of Science and Higher Education
Mechanical Engineering and Management Faculty

SPONSORS
EC Test Systems Sp. z o.o.
Brüel & Kjar Polska Sp. z o.o.
Gambit – Centrum Oprogramowania i Szkoleń

Introduction to the Volume XXIV
of Collected Papers on Vibrations in Physical Systems

Vibrations, oscillations and waves as physical phenomena are omni-present. They are the sign of life, the sign of the operation of machines and devices and they accompany any production processes. Their effects may be harmful, useful and they may also be a source of information on the technical condition of the supervised machines and devices. Volume XXIV of Vibrations in Physical Systems published every second year deals with these widespread phenomena. It comprises the papers presented by specialists from our country but also from abroad at many sessions of the XXIV Symposium of Vibrations in Physical Systems organized also every second year. The Symposium has been organized since 1960 in Poznan by a branch of the Polish Society of Theoretical and Applied Mechanics and the Institute of Applied Mechanics at Poznan University of Technology.

Topics of the publications relate to a wide range of issues connected with modelling and identification of mechanical systems, their stability and dynamics of mechanical systems as well as physical phenomena such as propagation of acoustic waves, vibrations in solid bodies, vibrations of liquids and mechanical structures.

The monograph comprises also numerously presented publications relating to the issues of dynamics in biological as well as biological and mechanical systems. They mainly concern mechanical properties of a human body and its organs (auditory bones) or parts. Other publications describe the dynamic interaction of power between human and machine (Human – Hand-held Powered Tool) or distribution of power and the energy flow in Human-Machine Systems.

Many of the publications present the results of research carried out through simulation with the application of modern digital technologies worked out for the needs of solving linear and non-linear issues of the dynamics of solid bodies or physical phenomena such as propagation of acoustic waves or complicated structures. The publications comprise the results that are analysed from the point of view of the applied methodology or accuracy of the obtained figures.

There are also quite a few publications devoted to methods of passive, active and semi-active minimizing of vibrations and noise and to modelling of vibrations damping with viscotic damper. The publications concerning dynamic issues also analysed the stability of the tested mechanical systems.

Other significant publications concern the monitoring of technical facilities with the use of the propagation of elastic waves that allow us to detect cracks in the composite structure under the test and to specify their location. They also describe methods of modelling the propagation of waves.

All the papers comprised in this volume have been reviewed by members of the Scientific Committee, and in some cases by specialists outside the Committee, should the issues concern problems outside the scope of knowledge of the Committee members. I would like to thank all those persons who help us review the papers and the published monograph and improve their quality.

Co-editor
Marian W. DOBRY

CONTENTS

INVITED PAPERS

PAPERS

ABSTRACT ONLY

Structural Health Monitoring by means of elastic wave propagation

Wiesław OSTACHOWICZ[1,2]

[1]*Gdynia Maritime University, Faculty of Navigation, Jana Pawla II 3, 81-345 Gdynia, Poland*
wieslaw@imp.gda.pl

Paweł KUDELA
[2]*Polish Academy of Sciences, Institute of Fluid-Flow Machinery*
Fiszera 14 St, 80-952 Gdansk, Poland
pk@imp.gda.pl

Abstract

The main issues regarding damage detection in elements of structures are discussed. The detection is conducted by the use of methods based on the phenomenon of elastic wave propagation. The emphasis is placed on modelling the phenomenon of elastic wave propagation in composite elements of structures, along with issues of wave interactions with damage and problems of damage location.

Keywords: elastic waves, damage detection, Structural Health Monitoring

1. Introduction

The scope of *Structural Health Monitoring* (SHM) includes constant monitoring of the structure's material condition (in real-time), for the elements of the structure as well as for the whole structure during its useful lifetime. The condition of the structure's material is to remain within the limits specified by the standards of the design process. Those standards, regarding the material, ought to take into consideration changes caused by exploitation wear during the operation process, changes caused by environmental factors, in which the structure is being used, and coincidental situations influencing the condition of the material. Owing to the fact that the monitoring process is being conducted continuously during operation, there will be a record of the complete history of utilization. Such information may be used for future condition prognosis as well as prediction of faults and the structure's safe utilization time.

Systems executing SHM processes ought to be structure integrated; this allows making modification of the structure in such a way that the probability of a failure is minor. It also enables minimization of the failure risk through management of the structure's utilization and treating it as part of a bigger system. The first layer of a SHM system is the monitoring layer specified by the type of physical phenomenon that is being monitored by the sensors. It is dependent on the damage type to be detected and the type of physical phenomenon that is being used by the sensors in order to generate the signal, mostly electrical, containing features and processable information regarding damage. Several connected sensors work together in a system measuring environmental factors influencing the condition and process of the exploitation of the structure. Data gathered from all the sensors along with historical data from previous structures allow diagnostic synthesis of information (signal fusion) regarding the condition of the structure. Once the above-mentioned information is linked with all the data from the

general system of knowledge about the phenomenon of damage and structural wear, it is possible to gain prognosis of condition and data defining the scope of any necessary repair. It is more common, that for such purposes simulation systems are used. Those systems enable extremely quick generation of the results, similar to those obtained from the chain of sensors based on familiar damage models (virtual exploitation of the structure).

The motivation for applying such systems is:

- ability to avoid failures with catastrophic consequences,
- ability to optimize the utilization process (minimization of emergency stoppage time),
- gaining essential information for designers regarding structural modification,
- ability to minimize maintenance costs and to raise the efficiency of a device thanks to the use of a methodology of repair according to condition, as well as avoiding disassembly, and replacement of non-damaged and non-used elements,
- ability to avoid operator's mistakes regarding evaluation of the condition of the structure.

Many methods used in practice to build SHM systems are being adopted from widely-known and applied disciplines e.g. NDT. Classical NDT methods can be executed continuously, such as: measurement of acoustic emission, Lamb waves, temperature, or mechanical impedance or direct monitoring of the displacement field with the use of visual methods, can be examples of applying NDT techniques in SHM systems.

A popular method, that can be applied passively as well as actively is the method based on examination of thermo-flexibility phenomena accompanying damage, especially its formation and propagation. Currently, interest in this method is increasing due to the opportunity of non-contact measurements of thermal phenomena within structures and intensive development in temperature measurement. Another method is the method of surface Lamb wave excitation within the structure. This method uses a grid of sensors/actuators. Registration and processing of transmitted waves as well as reflected waves is conducted. Evaluation of the condition of the structure takes place on the basis of wave profile deformations due to damage in the interrogated area of the structure.

2. Lamb waves

Elastic waves that propagate in solid media bounded by two free and parallel surfaces are known in the literature as Lamb waves or guided waves. Lamb waves are named after Horace Lamb in honour of his fundamental contribution in this area of research. He developed a mathematical theory that describes this kind of elastic waves, but what is very interesting he never managed to generate this type of waves in a real structure. Lamb waves propagate both as symmetric (S0, S1, S2, ...) and anti–symmetric (A0, A1, A2, ...) modes and the number of these modes depends on the product of the excitation frequency and the element thickness. Up to almost 2 MHzmm only two fundamental

Lamb wave modes S0 and A0 can propagate and be observed in a plate made out of aluminium alloy (Fig. 1–2). It has been found that just fundamental Lamb wave modes are most useful for damage detection purposes.
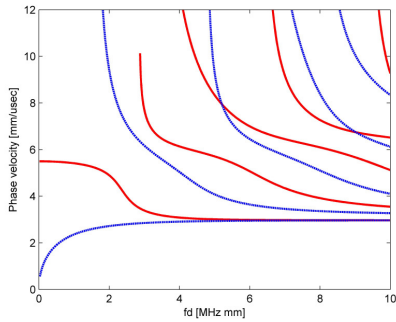
Figure 1. Phase velocities of symmetric (red) and antisymmetric (blue) modes of Lamb waves
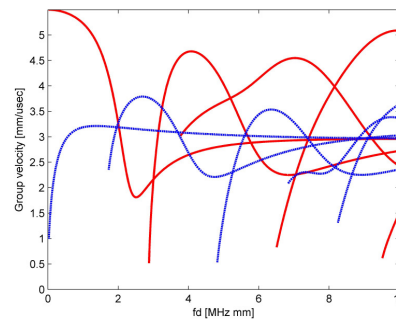
Figure 2. Group velocities of symmetric (red) and antisymmetric (blue) modes of Lamb waves

It should be noted that in composite plates dispersive relations are little more complex than in isotropic materials and solution must satisfy Christofel's equation for each layer, the continuity condition at the interfaces and the traction-free boundary conditions at the plate surfaces [1]. Alternatively, some approximate solution can be applied i.e. based on Mindlin's plate theory and material homogenisation [2]. Such approach clearly shows that group velocity of the transverse wave (which approximate A0 Lamb wave mode) is not constant, but is a function of a relative volume fraction of fibres and direction of propagation (Fig. 3).

Figure 4 show that structural discontinuity in the form of crack cause additional wave reflection. Hence, it is evident that changes in propagating waves carry information about the damage.

Figure 3. Geometry of half-pipe with crack
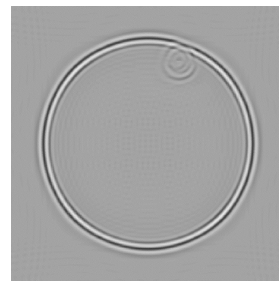
Figure 4. Interaction of elastic wave with the crack of the length 1 cm in a thin plate

3. Wave propagation modelling

Complexity of real structures cause that modelling of waves guided by boundaries of structural elements is challenging task. FFT-based Spectral Element Method proposed by Doyle [3] is efficient but it is not applicable for 3D geometry. Some of researchers try to use methods based on the Finite Element approach or the Finite Difference approach such as LISA [4]. These methods are more suitable for modelling of complex geometries. Unfortunately, both methods are inefficient and lead to errors corresponding to numerical dispersion. Only few commercial packages enable modelling of generation of elastic waves by piezoelectric transducer but they also are based on the FEM. In order to overcome disadvantages mentioned above, research group at IFFM have already implemented more accurate and efficient spectral element method [2, 4]. Recently developed spectral elements also take into account electromechanical coupling [6] (see pzt element in Fig. 7).

Exemplary numerical calculations have been carried out for a half-pipe structural element made out of aluminium alloy (Young's modulus 71 GPa, Poisson ratio 0.33, mass density 2700 kg/m^3). The radius of the element was R=0.2 m, length L=0.5 m and thickness 2 mm (figure 1). 34 piezoelectric transducers were used in which 17 for wave actuation. The placement of piezoelectric transducers along with the mesh of spectral elements is presented in Fig. 6. Each piezoelectric transducer is modelled by four spectral elements with 108 nodes each (3 nodes through the thickness). The detail of the mesh near the transducer is presented in Fig. 7. The thickness of transducers is 1 mm and it is assumed that it is made of PZT material type 4. The excitation was applied simultaneously to 17 actuators on the one side of half-pipe in the form of sine pulse of frequency 100 kHz modulated by Hanning window (3 cycles). Damage in the form of crack was modelled by splitting appropriate nodes in neighbouring elements. The crack is located at distance d=0.153 m from the end of the half-pipe (Fig. 5). Simulations have been carried out for the crack about 24.8 mm long.
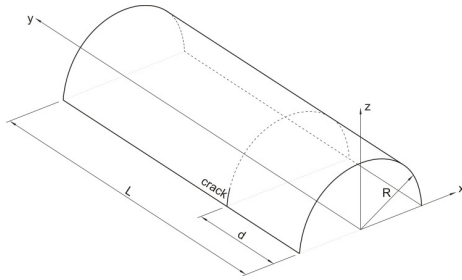
Figure 5. Geometry of half-pipe with crack
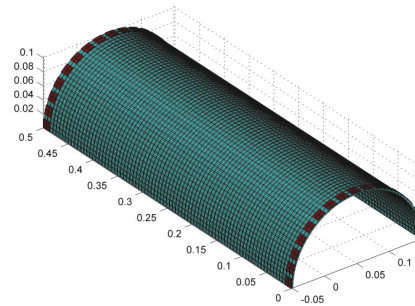
Figure 6. Mesh of spectral elements with piezoelectric transducers
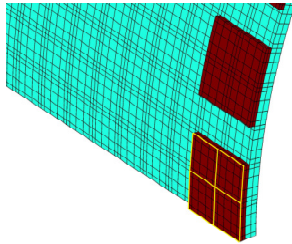
Figure 7. Detail of the mesh showing piezoelectric transducer composed of 4 spectral elements
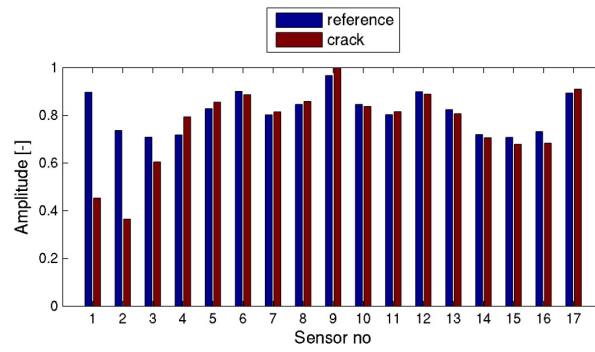
Figure 8. Energy comparison calculated for signals registered by sensors
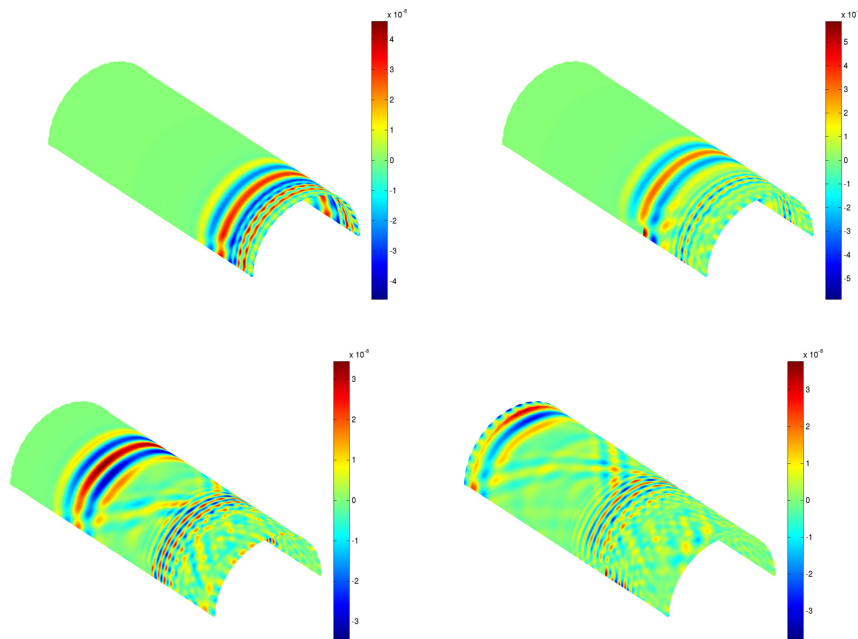
Figure 9. Displacements in *y* direction illustrate propagating waves at selected time instances

Results of numerical simulations are presented in Fig. 9. It is easy to notice that the front of symmetric mode is created and next slower antisymmetric mode propagate. Reflections between piezoelectric transducers as well as reflections from the crack are clearly visible. Reflections from the crack cause that energy transmitted to sensors drops significantly in comparison to signals for undamaged half-pipe (Fig. 8). This energy drops correlate with the position and the length of the crack. Such a simple feature can be used for damage detection purposes.

4. Damage imaging techniques

Damage localisation can be achieved by various inverse techniques performed on wave propagation signals registered by piezoelectric transducers. However, inverse techniques are computationally intensive and operate on huge amounts of data. A good alternative can be a direct method that utilises some knowledge about the wave velocity and the placement of transducers. In this case it is possible to transform the signals in such a way that damage influence maps are created [7].

The performance of the damage influence maps strongly depends on the placement of transducers and wave excitation-reception strategy [8, 9, 10].

The proposed in [7–9] methods are nothing more than signal tomography performed on the basis of some simple geometric relations. Such tomography is conducted on differential signals, i.e. based on differences between healthy state (reference signals) and damage state. The idea is to map differential signals from point locations (actuator-sensor locations) onto the surface of the analysed structure (e.g. square plate). Such mapping has been conducted for various configurations of piezoelectric transducers in order to obtain best damage localisation results. It has been found that configurations might be better suited for isotropic materials and for local inspection (focused arrays) and some are better suited for composite laminates (distributed arrays).

The basic problem with imaging techniques comes from the boundary and structural feature reflections. Imaging technique itself looks for propagating wave packet reflected from damage in order to associate reflected energy with location of the damage. This association is performed based on the knowledge of the velocity of propagating wave and the time delay of wave packet. Unfortunately, some of the energy of the wave packet is reflected back to the sensor but the rest of energy is further transmitted. Because less energy behind the damage is transmitted than in the surrounding area, reflection from boundary is also weaker. This, in turn, lead to damage influence map differences in locations not associated with damage. From practical point of view the inspection area is limited to the area enclosed in the distance from the sensor array to the nearest structural edge. It is evident that for clock-like sensor array shown in Fig. 10 (right) the algorithm is not able to find damage near plate corners (areas marked as 'dead zones') [7].

In order to overcome mentioned above difficulties triangular sensor networks were considered [8] with mapping performed separately in isolated triangular subspaces (Fig. 10 (left)). In this case the crack can be found by the algorithm regardless the boundary reflection contribution. Nevertheless, a new problem arise, namely damage indication is

ambiguous, due to symmetry between triangles. For this reason algorithm was refined in [9] for clear damage indication by multi triangular grid utilisation.
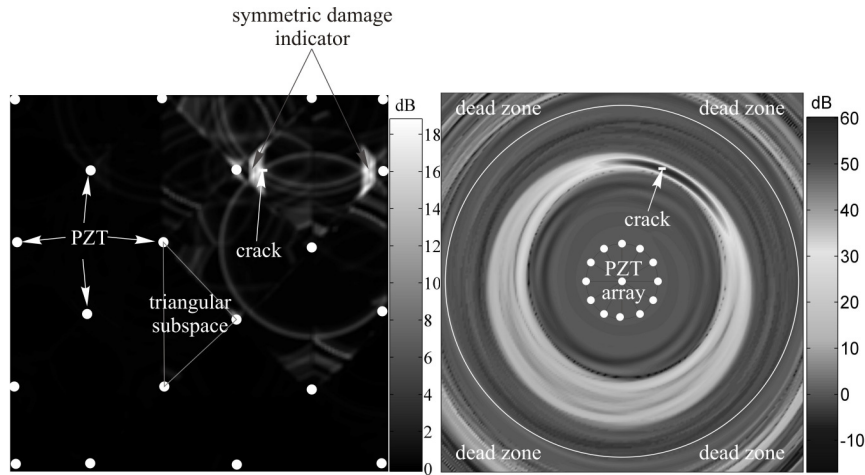
Figure 10. Damage influence maps for distributed sensor network (left) and clock–like sensor array (right).

Experimental work [11] conducted on aluminium and carbon/epoxy plates in laboratory conditions confirms that developed damage localisation algorithms are valid and can be used for detection of about 1 cm long through-thickness crack. The crack location is easily interpreted thorough damage influence maps. On the other hand delamination also can be detected with described methods but localisation of delamination is possible only to some extent.

4. Conclusions

Developed models based on the Spectral Element Method are very helpful in designing effective Structural Health Monitoring systems. Exemplary simulations show capability of modelling and testing damage detection algorithms.

It has been shown that in spite of the fact that elastic wave propagation is very complex phenomenon it can be successfully utilised for damage detection and localisation in structures.

Experimental works indicates that guided wave-based methods are reliable for inspection of simple structures like pipes, rods or even flat plates. However, for more complex shell-like structures with stiffeners, bolts or rivets developed algorithms are not yet ready to be used in real world structures.

Further work will focus on estimation of the damage size and prediction of remaining service life.

Acknowledgments

References

1. J. Rose, *Ultrasonic Waves in Solid Media*, Cambridge University Press, 1999.
2. P. Kudela, A. Zak, M. Krawczuk, W. Ostachowicz, *Modelling of wave propagation in composite plates using the time domain spectral element metod*, J. Sound Vib., **302** (2007) 728–745.
3. J.F. Doyle, *Wave Propagation in Structures*, Springer-Verlag, 1997.
4. P.P. Delsanto, R.S. Schechter, R.B. Mignogna, 1997. *Connection machine simulation of ultrasonic wave propagation in materials III: The three dimensional case*, Wave Motion, **26** (1997) 329–339.
5. W. Ostachowicz, P. Kudela, *Spectral Element Method for wave propagation modeling in 2D and 3D solids*, Proc. of the 7th Int. Conf. on SHM, **2** (2009) 2213-2221, Stanford, USA.
6. P. Kudela, W. Ostachowicz W., *3D time-domain spectral elements for stress waves modelling*," 7th Int. Conf. MPSVA, Cambridge, UK, J. Physics: Conf. Series, **181** (2009), paper no 012091
7. P. Kudela, W. Ostachowicz, A. Zak, *Damage detection in composite plates with embedded PZT transducers*, Mech. Syst. Signal Pr. **22** (2008) 1327-1335.
8. P. Kudela, W. Ostachowicz, *Lamb wave–based damage detection in composite structures: potentials and limitations*. Proc. 4th European Workshop Structural Health Monitoring, Cracow, Poland, 2008 482–490.
9. P. Kudela, W. Ostachowicz, A. Zak, *Sensor triangulation for damage localisation in composite plates*. Key Engineering Materials, **413–414** (2009) 55–62.
10. F. Schubert: *A Conceptual Study on Guided Wave Based Imaging Techniques for SHM with Distributed Transducer Array*, Proc. Structural Health Monitoring (2008) 748–757.
11. W. Ostachowicz, P. Kudela, P. Malinowski, T. Wandowski, *Damage localisation in plate-like structures based on PZT sensors*, Mech. Syst. Signal Pr. **23** (2009) 1805–1829.

Monitorowanie stanu technicznego konstrukcji przy wykorzystaniu propagacji fal sprężystych

Przedyskutowano główne problem dotyczące detekcji uszkodzeń w elementach konstrukcji. Detekcja przeprowadzana jest poprzez metody bazujące na zjawisku propagacji fal sprężystych. Położono nacisk na modelowaniu zjawiska propagacji fal sprężystych w kompozytowych elementach konstrukcji jak również na zagadnieniu interakcji fali z uszkodzeniami i zagadnieniach lokalizacji uszkodzeń.

Professor Jarosław Stefaniak 1929 – 2008

Bogdan MARUSZEWSKI
Institute of Applied Mechanics, Poznan University of Technology
3 Piotrowo Street, 60-965 Poznan, Poland
bogdan.maruszewski@put.poznan.pl

Full professor doctor habilitatus Jarosław Stefaniak was born on 17 May, 1929 in Poznań. His father was a municipal clerk, his mother unemployed. During the Second World War he worked first as a helpmate and then as a workman in Poznań Power Plant on Garbary Street. He attended a non-existing now the Berger State Lower and Upper Secondary School (a former school building on Strzelecka Street now occupied by Poznań University of Technology). In 1948 he passed examination for the secondary school certificate. Just then he began studying mathematics and physics at the Faculty of Mathematics and Science at Poznań University, later renamed as the Faculty of Mathematics, Physics and Chemistry at the Adam Mickiewicz University in Poznań. He received the diploma of Master of Science in philosophy in the field of mathematics in 1952. Yet, as a student in 1951 he took up a job as an assistant at the Chair of Mathematics at the Higher School of Engineering in Poznań and since then his professional life was connected solely with this school. In 1956 after the Higher School of Engineering received the status of Poznań University of Technology, he took a post at the Chair of Technical Mechanics whose head in those days was prof. Edmund Karaśkiewicz. Then he became deeply involved in the theory of elasticity, especially thermoelasticity. His first papers concerned thermal stresses in elastic halfspace.

The second half of the sixties was abounding with many events that contributed greatly to his career. As early as in February 1965 he defended his doctor's thesis on: Propagation of Waves in a Viscoelastic Medium with Respect to Thermomechanical Coupling, at the Faculty of Mechanical Engineering, PUT, thus obtaining the Doctor of Science degree in technical sciences in the field of mechanics. The supervisor was prof. Witold Nowacki, an outstanding scientist, the author of many fundamental papers and monographs in the field of structural mechanics, theory of elasticity and theory of fields coupled in deformable media, the IVth division chairman and president of Polish Academy of Sciences. In his next papers from the same period he analyzed the phenomena of wave propagation in viscoelastic unbounded media as well as surface waves with respect to thermomechanical coupling. Obtaining the D.Sc. degree was a significant incentive for his further scientific development and for more intensive research on thermoelasticity of the Cosserat media. In his papers before habilitation thesis Jarosław Stefaniak emphasized the possibility of presenting the loads concentrated by means of singular distribution and showed the method for solving the equations that describe the above problems. At that time special attention should be paid to generalization of the Galerkin function for nonsymmetric thermoelasticity.

From November 1967 to May 1968 J.Stefaniak ,D.Sc. served a 6 – month visiting professor fellowship at the Institute of Mathematics at Romanian Academy of Sciences in Bukarest. As a result of the studies on nonsymmetric thermoelasticity and on application of generalized functions in continuum mechanics he elaborated habilitation thesis entitled: Concentrated Loads in Nonsymmetric Thermoelasticity. On this basis in May 1969 he obtained the degree of doctor habilitatus in technical sciences in the field of thermoelasticity by the resolution of the Board of Mechanical Technological Faculty at PUT.

Following it on 1 March, 1970 the Minister of Education and Schools of Academic Rank appointed dr hab. Jarosław Stefaniak to the post of Reader at the Chair of Technical Mechanics. Research that Reader J.Stefaniak continued after being conferred the title of dr hab. concerned the problems of refraction and reflection of waves in thermoelastic media of the Cosserat type. He also showed that in micropolar media during reflection and refraction new kinds of waves are generated that are unknown in classic elastic media.

Due to his scientific achievements he was appointed to the post of deputy dean of the Mechanical Technological Faculty in 1969. He held this position till 1971.

At the end of September 1970 important organizational changes took place at PUT. The structure of institutes developed. The head of the Technical Mechanics Chair – prof. Edmund Karaśkiewicz retired. This Chair together with other units of Mechanical Technological Faculty, i.e. Division of Strength of Materials , Division of Theory of Mechanisms (so far included in the Chair of Machine Parts and Theory of Mechanisms), the Chair of Mechanics (included in the Faculty of Working Machines and Vehicles) formed the Institute of Technical Mechanics. Its first head was prof. Włodzimierz Derski, his only deputy – Reader J.Stefaniak who held this post till 1972. After prof.W.Derski took a post at the Institute of Fundamental Technological Research (Polish Academy of Sciences), Reader J.Stefaniak took over as head at the Institute of Technical Mechanics (for the first time) from 1973 to 1981. From 1981 to 1998 he was the head of the Division of Technical Mechanics at the Institute of Technical Mechanics (from 1984 at the Institute of Applied Mechanics). Then he developed his interests in magneto-thermoelasticity and diffusion in solids. With the use of distributive description of disturbance sources he investigated the conditions of mechanical wave generation by plane and linear sources in a magnetoelastic medium.

The intense development of research by Reader J.Stefaniak resulted in the title of associate professor conferred on him in 1976, at the age of 47, which was at that time very uncommon. Further research on magnetoelastic media led to the formulation of linear equations for different cases of interactions among electromagnetic, thermal, elastic fields and mass diffusion. Most of the results in this domain were published in his monograph: Influence of Electromagnetic Field on Thermodifussion in an Isotropic Medium, edited by Polish Scientific Publishers in 1982. At that time prof. J. Stefaniak began to develop another line of his research dealing with a method of controlling fictitious heat sources and its application in solving boundary problems of heat conduction. In 1989 he was conferred the title of full professor. A few months later a

new regulation about degrees and scientific titles became effective replacing the title of associate professor and full professor with one title – professor.

Prof. J. Stefaniak carried out research both on his own and in cooperation with scientific workers from the Division of Technical Mechanics run by him. He and the team often took part in big research programs financed by central authorities: interdepartmental programs and so called Central Programs for Basic Research or Central Programs for Development Research co-ordinated by main national scientific units (Institute of Fundamental Technological Research-Polish Academy of Sciences, Military University of Technology, etc.). He was a member of Co-ordinating Teams of two of them.

After the Committee of Research was set up, prof. J. Stefaniak conducted research projects financed by the state budget.

He published the results of his research not only in the form of monographs but also in well-known scientific journals in Poland and abroad. He is the author and co-author of over 100 papers of fundamental and practical character. He presented his current results at many national and international scientific conferences.

As a scientific worker of a higher technical school he was also involved in a lot of research for industry. He mainly focused on the problems of noise level and vibrations caused by different technological processes in industrial plants.

Prof. J. Stefaniak's high position made him an educator and tutor of many younger scientific workers thus initiating Poznań school of continuum mechanics that aimed at investigating interactions of different physical fields in continuum media.

So we can consider him to be the main follower of Poznań school of mechanics established at PUT by prof. Edmund Karaśkiewicz. J. Stefaniak promoted 12 doctors; 4 of them obtained later the degree of doctor habilitatus, 2 – were conferred the title of professor.

He reviewed a lot of scientific articles, a considerable number of doctoral and habilitation thesis and gave many opinions for conferring the title of professor.

From 1974 he was a co-ordinator of an international symposium – Vibrations in Physical Systems – organized every 2 years.

In 1984, together with prof. Dominik Rogula from the Institute of Fundamental Technological Research – Polish Academy of Sciences, he organized in Poznań international EUROMECH Colloquium 189: Elasticity Coupled with Thermal and Electromagnetic Effects.

During his work at PUT prof. J. Stefaniak was actively engaged in the teaching process. He gave lectures on the mechanics of a rigid body, continuum mechanics and some mathematical problems to students at all kinds of studies: full-time Master of Science and Engineer studies, evening and extramural ones. He contributed to a lot of doctoral studies at the University as a co-ordinator and a lecturer. He also co-originated the field – fundamental technological research and also modern specialization in the field of mechanical engineering – computational mechanics of constructions. He is the author of a handbook – Mechanics for Chemists.

He also used his teaching skills lecturing on mechanics and applied mathematics among other things at the Academy of Agriculture in Poznań, Military University of Automotive Vehicles in Piła and at courses organized by many scientific societies.

Prof. J. Stefaniak always attached much importance to the organization of a didactic process. Besides performing the duties of the head of the division, vice-dean, deputy head of the institute and (from 1984 -1990 for the second time) the head of the institute, he held an office of a prorector of PUT (1981 – 1984), and in 1990 – during the intense period of political changes, academic staff trusted him with the function of president of the Civic Forum at PUT – the first non-union democratic organization at the university. From 1990 to 1993 he was Rector of Poznań University of Technology.

Prof. J. Stefaniak was a member of many organizations and scientific societies both national and international, often holding high positions. He was an appointed member of Committee for Mechanics – Polish Academy of Sciences for many years, and during the last two terms of office he was one of the presiding officers. From 1975 – 1977 he was a member of the Committee for Acoustics – Polish Academy of Sciences. Moreover, he was a member of International Informatization Academy, Accademia Peloritana dei Pericolanti, American Mathematical Society, Gesellschaft für Angewandte Mathematik und Mechanik, the Committee for Mechanical and Building Sciences – Polish Academy of Sciences (Poznań branch), Poznań Society of the Friends of Sciences, Polish Society of Theoretical and Applied Mechanics, Polish Society of Acoustics as well as the Rotary Club in Poznań, which shows still another field of prof. J. Stefaniak's activity. He was an active welfare worker and a member of scientific councils of research institutions related to universities.

Prof. J. Stefaniak also maintained numerous relations with other countries, apart from his notable activity in Poland. He received fellowships from well-known universities abroad (Université de Liège, Universität Stuttgart, Technische Hochschule etc.) where he cooperated with the authorities in the field of mechanics. He was a holder of DAAD scholarship – a West German institution supporting science. He maintained many individual relations with Italy, Sweden, Ukraine, the Czech Republic, Germany, Japan, Cuba, Great Britain, France, Belgium, the Netherlands, Egypt, Lithuania.

Prof. J. Stefaniak was also a supervisor of honoris causa doctor titles of: prof. Witold Nowacki (1979) a former President of Polish Academy of Sciences and prof. Heinrich Seidl – in those days Rector of Hanover University (1995), conferred by the resolution of senate of PUT. Moreover, he was asked to review honorary doctorates of professors: Wacław Olszak (Kraków University of Technology), Witold Nowacki (Warsaw University), Michał Życzkowski (Kraków University of Technology) and Zenon Mróz (Kraków University of Technology).

Prof. J. Stefaniak was distinguished many times for his outstanding scientific achievements and didactic activity. He was knight of the Knight's Cross of Polonia Restituta Order (1977), he was awarded the Gold Cross of Merit (1972), the Medal of National Education Committee (1996), the Brown Medal for Contribution to the Development of Poznań Province (1972) and the Gold Badge of Honor for Contribution to the Development of Piła Province (1978).

He was also a winner of numerous prizes of Minister of Science, Schools of Academic Rank and Technology: a third-degree award for postdoctoral dissertation in 1970, an individual third - degree award in 1975, an individual second-degree award in 1982 and a collective second - degree award in 1983.

It is necessary to mention his unceasing activity after he retired in 1999. He gave lectures and tested students on their knowledge till the last moments. He gave his last lecture on 30 August, 2008 and was scheduled to give more. He took part actively in international scientific conferences: Trends in Continuum Physics TRECOP'04 organized by the Institute of Applied Mechanics, where he delivered a speech on his method of fictitious sources in solving problems of thermoelasticity, and Vibrations in Physical Systems – as a member of Organizing Committee. Having been the head of the Division of Technical Mechanics for many years, he did not miss scientific seminars at the Division on Monday mornings. He still reviewed applications for conferring the title of professor, doctoral and habilitation theses and dissertations, he published scientific articles and in 2008 – a handbook - Mathematical Physics. Selected problems (co-authorship). He left an unfinished handbook on mechanics.

Prof. J. Stefaniak was deeply engaged in educating and bringing up a few generations of scientists and engineers. He was a great friend of the young. He always gave advice or a hand. Not only did academic life of the institute and faculty where he worked centre around him but also many other research teams at the university and other institutions. He had a lot of friends in the scientific circle of Poznań, Poland and abroad. He was a very sociable person. If he could not persuade somebody into certain objective reasons, he used to say in the midst of his friends: look, this way of reasoning is the best which he understands and suits him most.

He liked poetry very much and was a lover of hiking.

We bid him farewell but he will remain in our thoughts and hearts.

Vibrations analysis of ossicles mechanism

Marek IWANIEC

AGH University of Science and Technology, Mickiewicz 30 av, 30-059 Cracow
llech@agh.edu.pl

Dorota MARSZALIK

AGH University of Science and Technology, Mickiewicz 30 av, 30-059 Cracow
dorota.marszalik@gmail.com

Abstract

The paper presents kinematic analysis of ossicles mechanism, which is part of the middle ear. Movement, velocity and acceleration trajectories of important points of the mechanism were determined. Influence of the length of the ossicles on the functioning of the mechanism was tested through calculating the relationship of oscillation amplitude of stapes and oscillation amplitude of incus.

Keywords: vibrations, velocity, acceleration, amplitude, malleus, incus, stapes.

1. Introduction

The middle ear consists of an eardrum, auditory ossicles (malleus, incus and stapes) and Eustachian tube. The ear bones fulfill the role of a transmission that transmits the sound from outer to inner ear through the means of converting the vibrations of the tympanic membrane, which is connected to the malleus, to vibrations of stapes footplate [1].

Sound propagates across the ear canal and stimulates vibrations of the eardrum. These vibrations bring about rotation of system of malleus – incus around the axis that crosses the centre of mass of the bones [2]. Mutual position of ossicles has significant influence on how vibrations are transmitted from outer ear to inner ear. The ossicles form a chain that functions as a lever. Vibrations of tympanic membrane cause declination of manubrium, which result in shift of incus and stapes. Oscillations of stapes affect the motion of fluid, which fills the inner ear, and excitement of hearing receptors [3 - 4].

2. Ossicles mechanism

Substitution model of middle ear was created based on the relationship of size of ossicles [1,5 - 6]. This is three elements planar mechanism. The elements of mechanism are malleus, incus and stapes.

The numbers 1 – 6 in schematic of ossicles mechanism (Fig. 1) represent important points of mechanism: number 1 – represents point of connection between eardrum and bone of ear canal, 2 – umbro (a slight rounded elevation where the malleus attaches to the eardrum), 3 – incudo-malleolar joint, 4 – incudostapedial joint, 5 – point, that marks the axis of circulation of stapes, 6 – upper edge of stapes footplate [7].
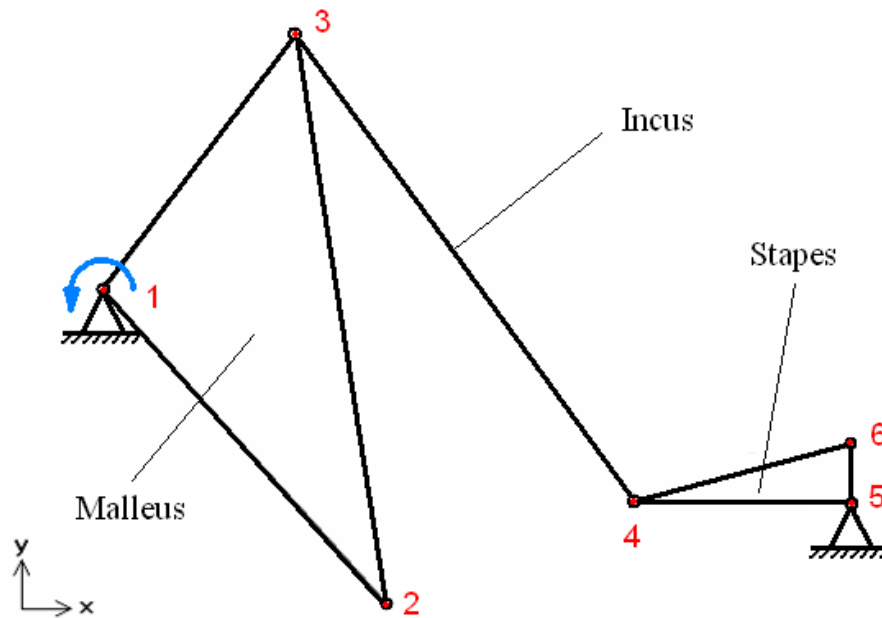
Figure 1. Schematic of ossicles mechanism

    The mechanism is propelled by rotation of the element that represents malleus connected with tympanic membrane, around point 1.

    The origin of coordinate system was set in point 1.

3. Results

Analysis of mechanism's vibration enabled determination of trajectories, velocities and accelerations of important points of mechanism. Kinematic parameters of points 1 and 5 weren't taken into consideration, because these points are stationary.

    Vibrations of eardrum are very small, therefore maximum rotation angle of propelling element was assumed 5 deg. That is way trajectories of points 2 and 3 that belong to propelling element may be approximated as straight lines. Trajectories of points 4 and 6 are nonlinear.

    Graphs of horizontal and vertical components of velocities and accelerations of points 2, 3, 4 and 6 in time function for one oscillation period were presented in figure 3. Time t=0 was assumed to relate to the point of the maximal swing of manubrium towards the ear canal and whereas time t= 0,5 T to (half of the oscillation period) relates to the maximal swing towards eardrum. The Graphs were normalized to the maximal value of velocity or acceleration respectively.

    The graphs of horizontal and vertical components of velocities in time function are symmetrical around the equilibrium point, that is point 0,5T, 0. Points 2, 4 and 6 move in

conformity with the sense of horizontal axis during oscillation of eardrum and manubrium in direction of ear canal, therefore horizontal components of velocity are positive. Sense of horizontal component of velocity of point 3 is opposite to sense of the x axis. Senses of vertical components of velocity of points 2, 3 and 4 are as per sense of y axis, however sense of Vy(6) is opposite to sense of y axis. All velocity components change sign at the point of greatest swing from the equilibrium. The largest value of horizontal component of acceleration is observed at umbro and the smallest at incudostapedial joint. The greatest value of vertical acceleration is observed at point 4 and the smallest at point 6.
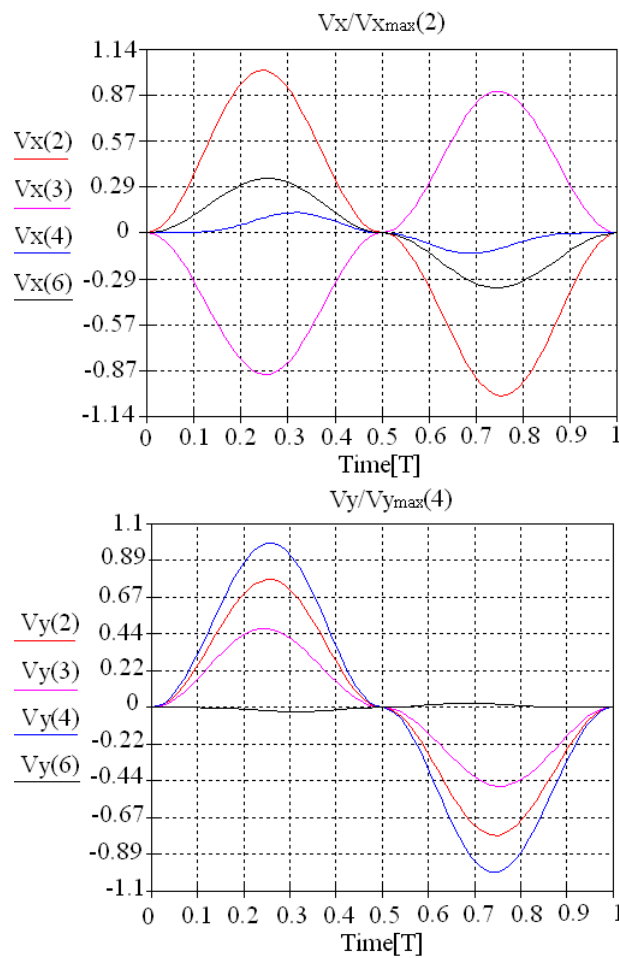
Figure 2. Graphs of horizontal and vertical components of velocities in time function.
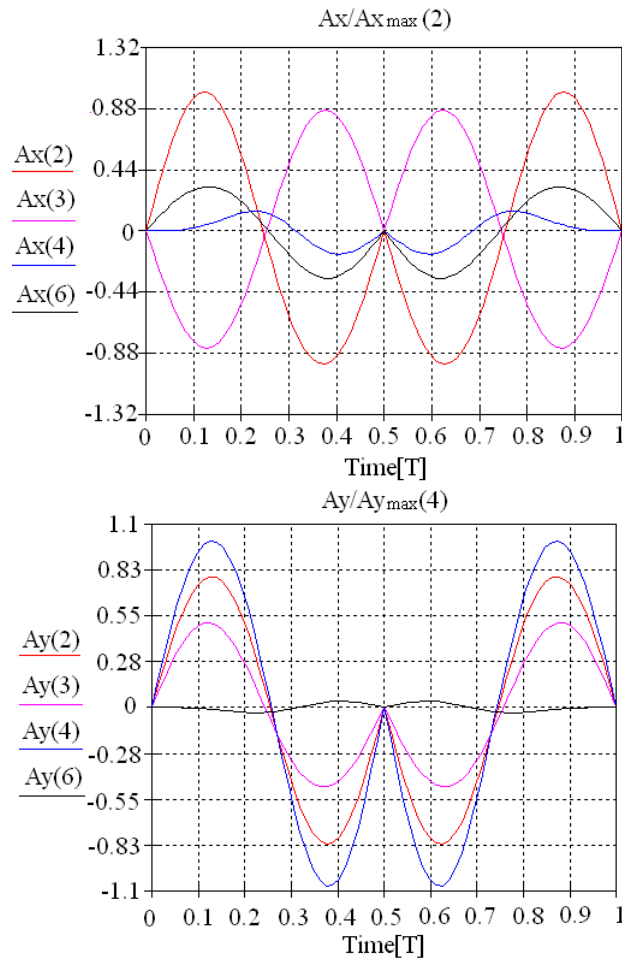
Figure 3. Graphs of horizontal and vertical components of accelerations in time function.

Graphs of horizontal and vertical components of accelerations of analysed points in time function are symmetrical around an axis that represents middle of oscillation period. In the time points that correspond to maximum values of velocity components matching acceleration components change sign.

4. Influence of ossicles size on functioning of the mechanism

Lenghts of ossicle were reduced by 2,5; 5; 7,5; and 10%, but other mechanism parameters were not modifited. Vibrations of mechanism were analysed and dependence of relationship betwen vibration amplitude of upper edge of stapes footplate (point 6)

and vibration amplitude of umbro (point2) – Axs/Axm - on lenght of malleus, incus and stapes was calculated. It was assumed that changing of the lenghts of ossicles does not affect position and motion of tympanic membrane and malleus, but only the position and motion of incus and stapes.
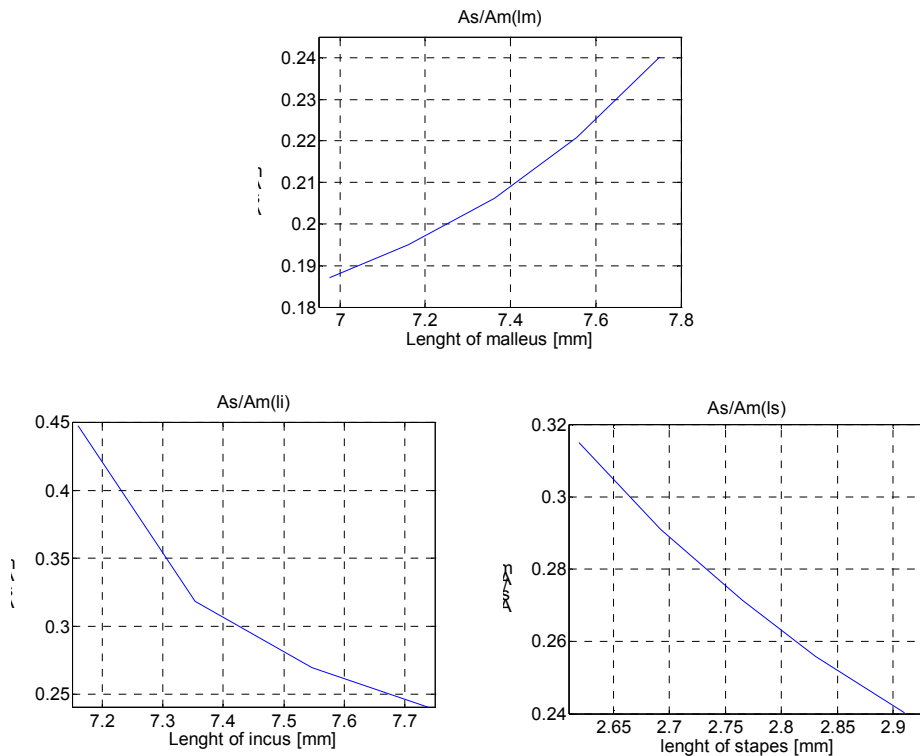
Figure 4. Graphs of dependance relationship betwen vibration amplitude of upper edge of stapes footplate and vibration amplitude of umbro – Axs/Axm - on lenght of malleus, incus and stapes

Reduced lenght of malleus entails reduced vibration amplitude of stapes footplate, while reducing dimensions of incus and stapes causes opposite effect: increase of displacement of stapes footplate.

Horizontal displacement of stapes footplate, under geometrical parameters assumed in this work, amounts to about 19 – 45% of umbro displacement.

Under basic dimensions of the mechanism, the As/Am relationship equals 0,24, which means that the vibrations of eardrum and malleus translate to fourfold less vibration of stapes footplate. As/Am increases to 0,32, when lenght of stapes is reduced

by 10% and to 0,45, when lenght of incus is reduced by 7,5%. Reducing dimensions of malleus by 10% results in decrease of As/Am to 0,19.

4. Conclusions

Performed vibrations analysis enables better understanding of properties of ossicles mechanism. It is very important in case of designing middle ear implants, as implant's proprerities should be as simmilar as possible to those of the part of body it is replacing.

The knowledge of impact of the ossicles length on vibration transmission from eardrum and malleus to stapes footplace and vistibule membrane allows for better foresight of the results of middle ear surgical interventions. It also gives important advice on sound transmission through middle ear if lengh of one of ossicles is changed

References

1. A. Bochenek, M. Reicherp, *Anatomia człowieka*, tom 5, Państwowy Zakład Wydawnictw Lekarskich, Warszawa 1989

2. S. Bobrzyk, J. Janiszewski, J. Awrejcewicz, *Dynamika kosteczek słuchowych w uchu środkowym,* II Ogólnopolska konferencja Układy dynamiki w aspekcie zachowań.

3. A. Michajlik, W. Ramotowski, *Anatomia i fizjologia człowieka*, Państwowy Zakład Wydawnictw Lekarskich, Warszawa 1980.

4. J. Buytaert, J. Aernouts, J. Dirckx, *Indentation measurements on the eardrum with automated projection moire´ profilometry*, Optics and Lasers in Engineering **47** (2009) 301-309

5. F. Zhao, T. Koike, J. Wang, H. Sienz, R. Meredith, *Finite element analysis of the middle ear transfer functions and related pathologies,* Medical Engineering & Physics, **31**(2009) 907-916

6. M. Masali, M. Cremasco, *Hoc alterum auditus organi ossiculum est: Ear Ossicles in Physical Anthropology*, Human Evolution (2006) 21 1-17

7. Q. Sun, R. Gan, K.-H. Chang, K. Dormer, *Computer-integrated finite element modeling of human middle ear*, Biomechan Model Mechanobiol 1 (2002) 109-122 Springer-Verlag 2002

Analiza drgań mechanizmu kosteczek słuchowych

Artykuł ten jest poświęcony analizie kinematycznej drgań układu kosteczek słuchowych wchodzących w skład ucha środkowego. Wyznaczono tory ruchu, prędkości oraz przyspieszenia istotnych punktów mechanizmu podczas drgań. Zbadano wpływ zmiany długości kosteczek słuchowych na działanie mechanizmu, poprzez wyznaczenie stosunku amplitudy drgań strzemiączka do amplitudy drgań kowadełka

Shaping of a Head of Cylindrical Pressure Vessel

Jerzy LEWIŃSKI

Institute of Applied Mechanics, Poznan University of Technology
3 Piotrowo Street, 60-965 Poznan, Poland
jerzy.lewinski@put.poznan.pl

Abstract

The paper is devoted to a dished head of a pressure vessel subject to internal uniform pressure. A short survey of optimal design of a pressure vessel and its head is presented. The problem of shaping of middle surface of a dished head with the use of trigonometric series is depicted. As a criterion of the shaping process the continuity of curvatures of the surfaces in the joint of the circular cylindrical shell and the dished head is assumed. Results of the numerical calculation for optimal shapes of head are presented in figures.

Keywords: thin-walled pressure vessel, dished head, minimal stress concentration

1. Introduction

Standard torispherical, ellipsoidal or hemispherical head of a pressure vessel significantly disturbs the membrane stress pattern arising in its cylindrical part. The value of the meridional principal curvature of the middle head surface is non-zero while in the cylindrical it takes zero level. In result the curvature becomes discontinuous. The problem of dished heads of the vessels has been undertaken by many investigators. Middleton [9] presented an optimal design problem of torispherical pressure vessel head. Mansfield [8] proposed the meridian shape in the form of an integral equation determining the optimal surface of revolution. Yushan et al [11,12] calculated stresses of ellipsoidal heads and noticed the stress concentration occurring there. Magnucki and Lewinski [4] described the stress state arising in a untypical torispherical head composed of circular and polynomial parts. Magnucki et al. [5] solved the problem of stress minimization of a vessel with ellipsoidal head. Magnucki and Lewinski [6] presented optimal design of an ellipsoidal head with consideration of various thickness values of the shell. Malinowski and Magnucki [7] minimized the stress concentration in sandwich ribbed flat baffle plates of a cylindrical tank. Krivoshapko [2] presented a review of strength and buckling problems of generalized and ellipsoidal shells of pressure vessels. Liu et al [3] proposed a theoretical method using finite element analysis to calculate the plastic collapse loads of pressure vessels under internal pressure and compared the analytical methods according to three criteria stated in the ASME Boiler Pressure Vessel Code. Błachut and Magnucki [1] delivered a review of strength, static stability, and structural optimization of horizontal pressure vessels. Wittembeck and Magnucki [10] shaped the dished head meridian in the form of clothoidal and circular parts. Ventsel and Krauthammer [13] delivered a monograph presenting the strength and stability problems of plates and shells with the edge effect of cylindrical shells.

The present paper is a continuation of the strength and optimization problems and deals with shaping the middle surface of dished heads with the use of trigonometric functions.

2. Mathematical description of the middle surface of the dished head

The shape of a head closing a cylindrical pressure vessel significantly affects the pattern of stress arising along its generatrix. The shape of the vessel generatrix is shown in Fig. 1.
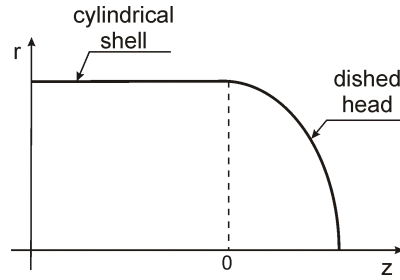
Figure 1. Example shape of the vessel generatrix

Since the stress depends, among others, on the generatrix curvature, its radius of curvature should be continuous. In order to ensure it the head profile should begin from infinite radius too. Such a shape of the head may be described by the following function:

$$r(z) = a\,\tilde{r}(\zeta), \tag{1}$$

where:

$\tilde{r}(\zeta) = \alpha_1 \cos(\pi\zeta) + \alpha_2 \cos(2\pi\zeta) + \alpha_3 \cos(3\pi\zeta) + \alpha_4 \cos(4\pi\zeta)$ $\quad$ – dimensionless radius,

$\zeta = \dfrac{z}{b_0}$ – dimensionless coordinate, b_0 – the size – a linear quantity.

Continuity conditions of the dimensionless radius for the joint of cylindrical shell and the dished head have the following form:

$$\tilde{r}(0) = 1, \qquad \text{giving} \qquad \alpha_1 + \alpha_2 + \alpha_3 + \alpha_4 = 1. \tag{2}$$

Other conditions that should be met by the function (1) in order to ensure stepless variation of the radius are as follows:

$$\left.\frac{d\tilde{r}}{d\zeta}\right|_{\zeta=0} \equiv 0 \;\text{ fulfilled by identity}\,, \qquad\qquad \left.\frac{d^2 r}{d\zeta^2}\right|_{\zeta=0} = 0 \tag{3}$$

$$\text{giving} \qquad \alpha_1 + 4\alpha_2 + 9\alpha_3 + 16\alpha_4 = 0 \tag{4}$$

The first of the above equations is satisfied by identity, while the other provides another condition for α_1, α_2, α_3, and α_4. This allows to express the coefficients α_3 and α_4 in terms of α_1 and α_2:

$$\alpha_3 = \frac{1}{7}(16 - 15\alpha_1 - 12\alpha_2), \qquad \alpha_4 = \frac{1}{7}(8\alpha_1 + 5\alpha_2 - 9) \tag{5}$$

Thus, the function (1) may smoothly match the cylindrical part of the vessel shape but in order to provide satisfactory shape of the head it must be completed by a circular part. Since the connection between cosinusoidal and circular parts of the generatrix should be smooth too the circle should begin in the point for which the centre of curvature of the cosinusoidal curve (1) reaches the axis of vessel symmetry.

The longitudinal-meridional curvature radius

$$R_m = \frac{\left(1+\left(\dfrac{dr}{dz}\right)^2\right)^{3/2}}{\left|\dfrac{d^2r}{dz^2}\right|} = a\frac{\left[1+\left(\dfrac{\pi}{\beta_0}\right)^2 \cdot f_1^2(\zeta)\right]^{3/2}}{\left(\dfrac{\pi}{\beta_0}\right)^2 \cdot f_2(\zeta)},$$

(6)

and the circumferential-parallel curvature radius

$$R_e = \frac{r(z)}{\cos\theta} = a\sqrt{1+\left(\frac{\pi}{\beta_0}\right)^2 \cdot f_1^2(\zeta)},$$

(7)

where:

$$f_1(\zeta) = \alpha_1 \sin(\pi\zeta) + 2\alpha_2 \sin(2\pi\zeta) + 3\alpha_3 \sin(3\pi\zeta) + 4\alpha_4 \sin(4\pi\zeta),$$
$$f_2(\zeta) = \alpha_1 \cos(\pi\zeta) + 4\alpha_2 \cos(2\pi\zeta) + 9\alpha_3 \cos(3\pi\zeta) + 16\alpha_4 \cos(4\pi\zeta),$$
$$\beta_0 = \frac{b_0}{a}.$$

The following expressions determine coordinates of the centre of the generatrix curvature:

$$z_c = z - \frac{1+\left(\dfrac{dr}{dz}\right)^2}{\dfrac{d^2r}{dz^2}} \cdot \frac{dr}{dz}, \quad r_c = r(z) + \frac{1+\left(\dfrac{dr}{dz}\right)^2}{\dfrac{d^2r}{dz^2}}.$$

(8)

Taking into account the relationship (5) the cosinusoidal curve (1) is determined by three parameters: α_1, α_2, and b_0. Therefore, once their values are assumed one is able to find such a point M at the cosinusoidal part of the curve from which the circular shape should begin.

In consequence, selection of the sets of three parameters α_1, α_2, and b_0 enables finding a family of the head shapes of various values of the relative depth β given by the formula

$$\beta = \frac{b}{a} = \beta_0 \zeta_M + \tilde{R}_m(1+\cos\theta_M),$$

(9)

where:　$\zeta_M = \dfrac{z_c}{b_0},$　　　　$\tilde{R}_m = \dfrac{R_m}{a}.$

3. Equivalent stress of circular cylindrical vessel

The longitudinal and circumferential stresses of the head are as follows:

$$\sigma_m = \frac{1}{2} R_m \cdot \frac{p_0}{t}, \quad \sigma_e = \frac{1}{2} R_e \left(2 - \frac{R_e}{R_m} \right) \cdot \frac{p_0}{t}, \tag{10}$$

where:

p_0 – uniformly distributed pressure, t – thickness of the head

The equivalent stress (i.e. Huber-Mises stress) may be expressed as

$$\sigma_{eq} = \frac{1}{2} R_e \sqrt{3 - 3\frac{R_e}{R_m} + \left(\frac{R_e}{R_m} \right)^2} \, \frac{p_0}{t}, \qquad \text{or } \sigma_{eq} = \widetilde{\sigma}_{eq} a \frac{p_0}{t}, \tag{11}$$

where the dimensionless equivalent stress amounts to

$$\widetilde{\sigma}_{eq} = \frac{1}{2} \widetilde{R}_e \sqrt{3 - 3\frac{R_e}{R_m} + \left(\frac{R_e}{R_m} \right)^2} \quad \text{and} \qquad \widetilde{R}_e = \frac{R_e}{a}. \tag{12}$$

An exemplary variant of the head obtained for α_1=0.8, α_2=0.52, α_3=-0.32, α_4=0 is shown in Fig. 2.
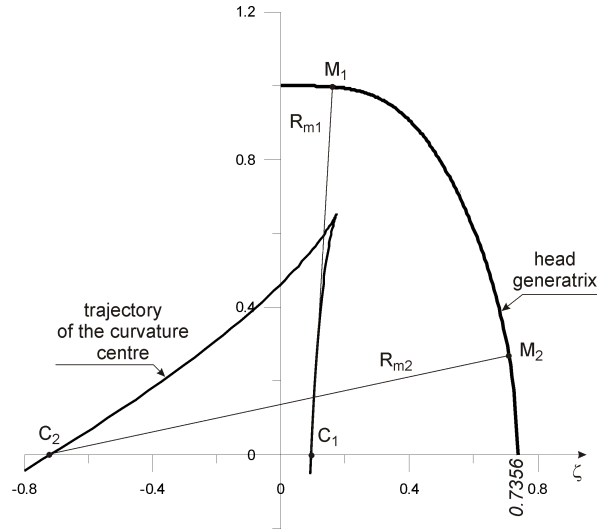
Figure 2. Example of the head solution for α_1=0.8, α_2=0.52, α_3=-0.32, α_4=0 and β_0=2

The centre of curvature runs along its trajectory and intersects twice the *x*-axis. The solution obtained with the use of the points M_2 and C_2 gives the head generatrix shown in the illustration, with the relative depth β=0.7356. Unfortunately, the pattern of the dimensionless equivalent stress of the cosinusoidal part of the head is rather unfavourable, as the stress exceeds the level of $\widetilde{\sigma}_{eq}^0 = \sqrt{3}/2$ occurring in the cylindrical part of the vessel.

Therefore, final solution of the problem should consist in finding a set of α_1, α_2 and b_0 parameters so adjusted as to obtain possibly small β value with the equivalent stress level kept below the value of $\widetilde{\sigma}_{eq}^0 = \sqrt{3}/2$. Numerical analysis carried out with the Monte Carlo method has shown that such a solution exists for α_1=1.417, α_2=-0.499 and β_0=1.34.

The MES calculation carried out with the help of the ABAQUS system confirmed the equivalent stress pattern obtained for the central line. The computation was performed for an example vessel of the radius equal to 1m and shell thickness 10mm. It became evident that in this case the stress arising at the inner part of the head shell exceeds its level occurring in the cylindrical part.

Therefore, another attempt has been undertaken with a view to find a variant so adjusted as to keep the maximum stress at the level below the one occurring in the cylindrical part. This was possible by enlarging the relative depth of the head. Finally the relative depth equal to β=0.807 gave satisfactory result depicted in Fig. 3
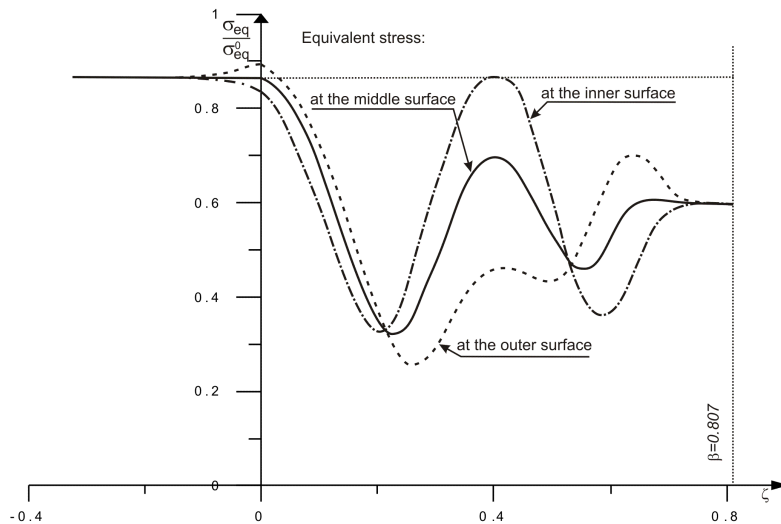
Figure 3. Equivalent stresses in the middle, inner and outer surfaces of the head for the variant with enlarged relative depth of the head

4. Conclusions

Numerical study of the stress state of a cylindrical pressure vessel with convex cosinusoidal-spherical heads enables drawing the following conclusions:

- Fulfillment of the condition of continuous curvature in the joint between the head and the cylindrical shell is not sufficient to avoid stress concentration in this place.
- Further increase in the head depth reduces the value of the concentrated stress.
- In result of shaping the head according to the boundary effect theory the relative depth β=0.7417 has been obtained for which the stress concentration should

disappear. Nevertheless, numerical test with the help of FEM has shown the opposite.

- Increase in the relative depth up to β=0.807 eliminates the stress concentration.

It should be noticed that the relative depth of standard elliptical heads amounts to the value of β=0.5 at which a remarkable stress concentration occurs.

References

1. J. Błachut, K. Magnucki, *Strength, stability, and optimization of pressure vessels: Review of selected problems*, Applied Mechanics Reviews, **61**(6)(2008) 1-33

2. S.N. Krivoshapko, *Research on general and axisymmetric ellipsoidal shells used as domes, pressure vessels, and tanks*, Applied Mechanics Review*s*, **60**(6)(2007) 336-355.

3. P-f. Liu, J-y. Zheng, L. Ma, C-j. Miao, L-l. Wu, *Calculations of plastic collapse load of pressure vessel using FEA*, Journal of Zhejiang University Science A **9**(7)(2008) 900-906.

4. K. Magnucki, J. Lewiński, *Fully stressed head of a pressure vessel*, Thin-Walled Structures*,* **38**(2000) 167-178.

5. K. Magnucki, W. Szyc, J. Lewiński, *Minimization of stress concentration factor In cylindrical pressure vessels with ellipsoidal heads*, Intl J Press Vessel Piping, **79**(2002) 841-846.

6. K. Magnucki, J. Lewiński, *Optimal design of an ellipsoidal head of a pressure cylindrical vessel*, Proc Appl Math Mech, **3**(2003) 517-518.

7. M. Malinowski, K. Magnucki, *Optimal design of sandwich ribbed flat baffle plates of a circular cylindrical tank*, Intl J Press Vessel Piping, **82**(2005) 227-233.

8. E.H. Mansfield, *An optimum surface of revolution for pressurized shells*, Intl Journal of Mechanical Science, **23**(1981) 57-62.

9. J. Middleton, *Optimal design of torispherical pressure vessel end closures*, Engineering Optimization, **4**(1979) 129-138.

10. L. Wittenbeck, K. Magnucki, Strength shaping of dished heads of pressure cylindrical vessels,: *Proceedings of the Ninth Intl Conference on Computational Structures Technology*, B.H.V. Topping and M. Papadrakakis (Editors), Civil-Comp Press, Stirlingshire, Scotland, (2008) (Paper 138, CD).

11. Z. Yushan, Z.R. Wang,, *Stress analysis of two-arc approximate ellipsoidal pressure vessel heads and parameter optimization*, Intl J Press Vessel Piping, **67**(1996a) 199-202.

12. Z. Yushan, Z.R. Wang, C. Wei, *Stress analysis of approximately ellipsoidal cold-spun tri-arc tank head and parameter optimization*, Intl J Press Vessel Piping, **68**(1996b) 237-242.

13. E. Ventsel, T. Krauthammer, *Thin plates and shells. Theory, analysis and applications*, Marcel Dekker, Inc, New York, Basel, 2001

Roots of characteristic equation versus eigenfrequencies

Krzysztof ARCZEWSKI
Institute of Aeronautics and Applied Mechanics
Warsaw University of Technology, Nowowiejska 24, 00-665 Warszaw, Poland
krisarcz@meil.pw.edu.pl

Józef PIETRUCHA
Institute of Aeronautics and Applied Mechanics
Warsaw University of Technology, Nowowiejska 24, 00-665 Warszaw, Poland
japietru@meil.pw.edu.pl

Abstract

The paper is of a purely didactic nature. We are going to focus on a distinction between two notions; i.e., the root of characteristic equation and vibration eigenfrequency of a system. The issue is well known, however, hardly any comments and satisfactory explanations can be found in handbooks on vibration theory, which may confuse the reader, particularly a student.

Keywords: Vibration thory, eigenfrequencies

1. Model of the lateral beam vibration and the characteristic equation for specific boundary conditions

Consider the simplest lateral vibration model i.e. the Euler-Bernoulli beam. Let the length of the beam be *l*. On the assumption that the mass density μ and bending stiffness *EI* are constant along the beam length, the equation of its free lateral vibration becomes

$$\frac{\partial^2 y}{\partial t^2} = -c^2 \frac{\partial^4 y}{\partial x^4} \tag{1}$$

where *c* is a constant defined as

$$c = \sqrt{EI/\mu} \tag{2}$$

A solution of equation (1) can be obtained by using the variable separation technique. At the initial stage we assume a solution in the form

$$y(x,t) = \phi(x)q(t) \tag{3}$$

where $\phi(x)$ is a space-dependent function, and $q(t)$ is a function that depends only on time. Equation (1) leads to

$$\phi^{IV} - \eta^4 \phi = 0 \tag{4}$$

$$\ddot{q} + \omega^2 q = 0 \tag{5}$$

where

$$\eta = \sqrt{\omega/c} \ . \tag{6}$$

A solution of (4) is given by

$$\phi(x) = A_1 \sinh \eta x + A_2 \cosh \eta x + A_3 \sin \eta x + A_4 \cos \eta x \qquad (7)$$

while the solution of Eq. (5) takes the form

$$q(t) = B_1 \sin \omega t + B_2 \cos \omega t \qquad (8)$$

The arbitrary constants A_1, A_2, A_3, and A_4 can be determined using boundary conditions while the constants B_1 and B_2 by means of the initial conditions. It means that the function $\phi(x)$ called mode shape depends on specific boundary conditions.

For the given boundary conditions a further procedure comprises the following steps:

a) derivation of the characteristic equation;

b) determination of the roots of this equation; i.e., numbers η_j, and in accordance with

(6) - eigenfrequencies ω_j;

c) determination of the eigenmodes corresponding to the eigenfrequencies ω_j.

The above procedure will be referred to as the standard one.

In order to formulate the essence of the matter let us consider a beam with fixed ends (Fig.1) and then a beam with free ends (Fig.2).
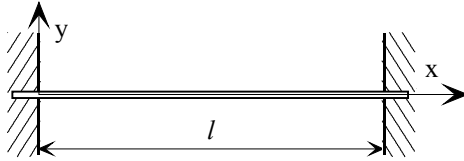
Figure 1. Beam with fixed ends   Figure 2. Beam with free ends
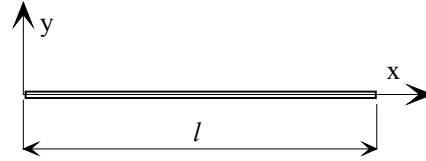
For a beam with fixed ends the boundary conditions read

$$y(0,t) = 0, \qquad\qquad y'(0,t) = 0 \qquad (9a)$$
$$y(l,t) = 0, \qquad\qquad y'(l,t) = 0 \qquad (9b)$$

while for a beam with free ends

$$y''(0,t) = 0 \qquad\qquad y'''(0,t) = 0 \qquad (10a)$$
$$y''(l,t) = 0 \qquad\qquad y'''(l,t) = 0 \qquad (10b)$$

Despite the fact that boundary conditions differ, the standard procedure leads in both cases to the identical characteristic equation, i.e.

$$\cos \eta l \cosh \eta l = 1 \qquad (11)$$

The first four roots of (11) are

$$\eta_0 l = 0, \qquad \eta_1 l = 4{,}73, \qquad \eta_2 l = 7{,}85, \qquad \eta_3 l = 10{,}99 \qquad (12)$$

The natural frequencies of the beam with free ends correspond to successive roots (12) while the same frequencies for the beam with fixed ends correspond also to successive roots except for the zero root. Here we face the question: why for a beam with fixed ends in contrast to that of free ends, the eigenfrequency $\omega = 0$ does not appear?

2. Explanation of the inconsistency

The aforementioned apparent inconsistency may be explained basing on the definition of eigenvalue, i.e., a number λ is called an eigenvalue of a matrix A if there exists a vector $\boldsymbol{x} \neq \boldsymbol{0}$ such that

$$\boldsymbol{Ax} = \lambda \boldsymbol{x} \tag{13}$$

The vector $\boldsymbol{x}$ is then called an eigenvector of the matrix A belonging to λ.

Now taking into account the above definition one should check the value $\omega = 0$ for the existence of a nontrivial eigenvector belonging to it. Note that for $\omega = 0$, equation (5) degenerates to the form:

$$d^4 \phi / dx^4 = 0 \tag{14}$$

to which a general solution is given by

$$\phi(x) = C_3 x^3 + C_2 x^2 + C_1 x + C_0 \tag{15}$$

Introducing boundary condition (9) (i.e. for a beam with fixed ends) into (15) yields

$$\phi(0) = C_0 = 0$$
$$\phi'(0) = C_1 = 0$$
$$\phi(l) = C_3 l^3 + C_2 l^2 + C_1 l + C_0 = 0 \tag{16}$$
$$\phi'(l) = 3C_3 l^2 + 2C_2 l + C_1 = 0$$

which implies $C_0 = C_1 = C_2 = C_3 = 0$. Thus the associated mode shape is $\phi(x) \equiv 0$ which means that there is no motion associated with $\omega = 0$. It is the reason why this frequency can not be considered as the eigenfrequency of the beam with fixed ends. The first three mode shapes of this beam are shown in Fig.3.
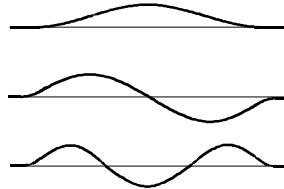
Figure 3. First three mode shapes of a beam with fixed ends.

The natural frequencies corresponding to these modes are:

$$\omega_1 = 22{,}4\sqrt{EJ/ml^3}, \quad \omega_2 = 61{,}6\sqrt{EJ/ml^3}, \quad \omega_3 = 120{,}9\sqrt{EJ/ml^3} \tag{17}$$

Let us now consider the existence of nontrivial mode shape belonging to the zero frequency for the beam with free ends. We will search for a function of a form (15) which satisfies boundary condition (10). Introducing conditions (10a) gives

$$\phi''(0) = 2C_2 = 0 \qquad \phi'''(0) = 6C_3 = 0 \tag{18a}$$

which implies $C_2 = C_3 = 0$. Remaining conditions (10b) take the form

$$\phi''(l) = 6C_3 l + 2C_2 = 0 \qquad \phi'''(l) = 6C_3 = 0 \tag{18b}$$

and these do not impose any limits on constants the C_0 and C_1. Thus the constants C_0 and C_1 may be arbitrary wherefrom the corresponding mode shape follows

$$\phi(x) = C_1 x + C_0 \qquad (19)$$

One can observe that the mode-shape given by formula (19) is a combination of translation (constant C_0) and rotation of the beam. There is no deformation of the beam associated with this mode and it is the reason why it is called a rigid-body mode shape of the beam.

The remaining deformable mode shapes of the beam corresponding to non-zero eigenfrequencies are determined on basing on solution (7), and these are shown in Fig.4.
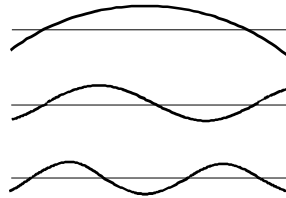
Figure 4. First three deformable mode shapes of a beam with free ends.

3. Conclusions

Like the mathematical definition of eigenvalues, the definition of eigenfrequency should be associated with a nontrivial mode shape. It is the reason why even for two vibrating systems of the same characteristic equation the sets of eigenfrequencies may be different.

Pierwiastki równania charakterystycznego a częstości drgań własnych

Referat ma charakter czysto dydaktyczny. Chcemy w nim zwrócić uwagę na konieczność rozróżniania pojęć pierwiastek równania charakterystycznego i częstość drgań własnych układu. Sprawa aczkolwiek jest znana, ale niezwykle rzadko podejmowana i wyjaśniana w podręcznikach teorii drgań, co może być przyczyną konfuzji czytelnika, zwłaszcza studenta.

Vibrations of a Mechanical System with Friction Clutch

Jan AWREJCEWICZ

Department of Automation and Biomechanics, Faculty of Mechanical Engineering of the Technical University of Łódź, 1/15 Stefanowski St., 90-924 Łódź, Poland
awrejcew@p.lodz.pl

Dariusz GRZELCZYK

Department of Automation and Biomechanics, Faculty of Mechanical Engineering of the Technical University of Łódź, 1/15 Stefanowski St., 90-924 Łódź, Poland
dariusz.grzelczyk@p.lodz.pl

Abstract

This work presents results of the numerical investigations devoted to clutch system dynamics. The general non-linear wear model has been presented and used during simulations. The influence of the considered wear model on the contact pressure distribution of the clutch discs has been investigated. Dynamics of the system is monitored via standard trajectories of motion in the system's phase space and behaviour of the system around resonance angular velocity is studied. Presented results show interesting phenomena of the investigated system and a key role of the influence of the wear process on its dynamics.

Keywords: Clutch, friction, wear

1. Introduction

Dynamic phenomena in the neighbourhood of the resonance angular velocity have the significant influence on the endurance of elements of the system and its dynamics. The mentioned phenomena can be caused by various factors like friction, wear, heat generation or/and impacts. In this work chosen issues of vibrations of a mechanical system with friction clutch are discussed and investigated. The attention is focussed on the investigation of influence of wear of clutch shields on its dynamics in the neighbourhood and far from the resonance regions.

In many monographs [1], [2], [3], [4], [5] friction and wear essential testing methods and problems of the theory of wear in such systems are described. Empirical models, which let for better understanding occurring processes are studied. However, a general relation between friction and wear has not been formulated so far.

In this work we consider general non-linear differential model of wear w in the form

$$\dot{w} = K^{(w)} P^{\alpha} \left| V_r \right|^{\beta}, \tag{1}$$

where $K^{(w)}$ is a coefficient of material wear, V_r is relative sliding velocity of surfaces touching each other, P is a contact pressure, and α, β are rates dependent on the model of wear, the step of lubricating and spreading on the contacting surfaces. For $\alpha = \beta = 1$ we obtain a particular linear Archard's wear model (see [1]).

2. Model of a System with Friction Clutch

Our investigations are concern of mechanical system with flexible-friction clutch, shown in Figure 1.
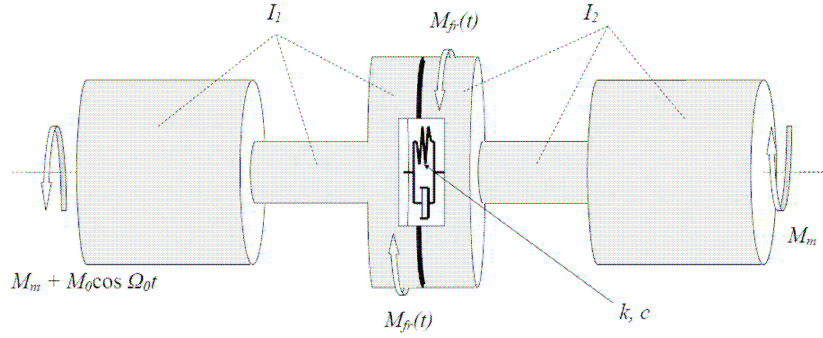
Figure 1. The model of the considered mechanical system

For a study we consider two-masses model of the system. The body 1 have the reduced moment of interia I_1, whereas the body 2 have the reduced moment of interia I_2. Vibrations in the system are caused by harmonic excitation from the side of the motor. The moment of motor is characterized by an average constant value M_m and a harmonic excitation part $M(t) = M_0 \cos \Omega_0 t$. The clutch is characterized by springiness (susceptibility) k and damping c in angular direction, and friction torque $M_{fr}(t)$ moved by the clutch. The system governing equations have the form

$$I_1 \ddot{\psi}_1 + c(\dot{\psi}_1 - \dot{\psi}_2) + k(\psi_1 - \psi_2) = M_m + M_0 \cos \Omega_0 t - M_{fr}(t)$$
$$I_2 \ddot{\psi}_2 + c(\dot{\psi}_2 - \dot{\psi}_1) + k(\psi_2 - \psi_1) = -M_m + M_{fr}(t)$$

(2)

where ψ_1 and ψ_2 are angles of driving shaft and driven shaft of the clutch, respectively. Taking $\psi = \psi_1 - \psi_2$ as the relative angular displacement of clutch shields and the reduced moment of interia $I_r = I_1 I_2 / (I_1 + I_2)$, we obtain

$$\ddot{\psi} + \frac{c}{I_r} \dot{\psi} + \frac{k}{I_r} \psi = \frac{M_m}{I_r} + \frac{M_0}{I_1} \cos \Omega_0 t - \frac{M_{fr}(t)}{I_r} .$$

(3)

Friction torque moved by the clutch $M_{fr}(t)$ is

$$M_{fr}(t) = 2\pi \int_{R_1}^{R_2} \mu R^2 P(R,t) dR ,$$

(4)

where μ is a coefficient of friction, R_1 and R_2 are internal and outside radii of contact surfaces, respectively, and $P(R,t)$ is contact pressure between shields pressed by force $Q(t)$.

Let us enrol equations on wear for the left shield and the right shield $\dot{U}_1^{(w)}(R,t) = K_1^{(w)}|V_r(R,t)|^\beta P^\alpha(R,t)$, $\dot{U}_2^{(w)}(R,t) = K_2^{(w)}|V_r(R,t)|^\beta P^\alpha(R,t)$, and axial displacements $U^{(1)}(R,t) = k_1 P(R,t)$, $U^{(2)}(R,t) = k_2 P(R,t)$ with coefficients of stiffness of shields k_1 and k_2, respectively. In what follows we obtain conditions of the contact of shields of the clutch in the form

$$U^{(1)}(R,t) + U^{(2)}(R,t) + U_1^{(w)}(R,t) + U_2^{(w)}(R,t) = \mathrm{E}(t), \tag{5}$$

where $\mathrm{E}(t)$ is a function describing distance between shields. After differentiating of equation (5) with respect to the time, taking $k_{12} = k_1 + k_2$, $K^{(w)} = K_1^{(w)} + K_2^{(w)}$, $V_r(R,t) = \Omega_r(t)R$, $\Omega_r = \dot{\psi}$, next multiplying by RdR, integrating over interval $R \in [R_1, R_2]$, and taking into account differentiation regarding time of the equation

$$Q(t) = 2\pi \int_{R_1}^{R_2} RP(R,t)dR, \tag{6}$$

we finally obtain

$$k_{12}\frac{\partial P(R,t)}{\partial t} + K^{(w)}R^\beta |\Omega_r(t)|^\beta P^\alpha(R,t) =$$
$$= \frac{2K^{(w)}}{R_2^2 - R_1^2}|\Omega_r(t)|^\beta \int_{R_1}^{R_2} R^{1+\beta} P^\alpha(R,t)dR + \frac{k_{12}}{\pi(R_2^2 - R_1^2)}\frac{dQ(t)}{dt}. \tag{7}$$

3. Non-Dimensional Form

Let us introduce the following similarity coefficients: t_*, P_*; non-dimensional time: $\tau = t/t_*$; non-dimensional radius: $r = (R - R_1)/(R_2 - R_1)$; non-dimensional geometrical parameter: $\rho = R_1/(R_2 - R_1)$; other non-dimensional parameters: $\omega_0 = \Omega_0 t_*$, $l_1 = K^{(w)}R_2^\beta t_*^{1-\beta} P_*^{\alpha-1}/(k_{12}(1+\rho)^\beta)$, $d = ct_*/I_r$, $\omega_k^2 = kt_*^2/I_r$, $F_m = M_m t_*^2/I_r$, $F_0 = M_0 t_*^2/I_1$, $k_{fr} = 2\pi t_*^2 P_* \mu R_2^3/(I_r(1+\rho)^3)$, and then following non-dimensional functions: $p(r,\tau) = P((R_2 - R_1)(r+\rho), t_*\tau)/P_*$, $F_{fr}(\tau) = M_{fr}(t_*\tau)t_*^2/I_r$, $\varphi = \psi$, $\omega = \dot{\psi}t_*$, $\omega_r = \dot{\psi}_r t_*$. Let us take $Q(t) = Q = const$, $t_* = \sqrt{I_r/k}$ and $P_* = (1+\rho)^2 Q/(\pi R_2^2(1+2\rho))$. Then, replacing integrals appearing in equations (4) and (7), after enrolling them in a non-dimensional form using method of trapezia by dividing the length of non-dimensional radius on m even segments, and taking $\Delta_r = 1/m$, $r_i = \Delta_r i$, $r_j = \Delta_r j$, $p(r_i, \tau) = p_i(\tau)$, $p(r_j, \tau) = p_j(\tau)$ (rates of the method of trapezia

are: $a_0 = a_m = 1/2$, $a_j = 1$, $j = 1,2,...m-1$), we obtain the following system of $m+3$ first order ODEs

$$\begin{cases} \dot{\omega} = -\varphi - d\omega + F_m + F_0 \cos\omega_0\tau - k_{fr}\Delta_r \sum_{j=0}^{m} a_j(r_j + \rho)^2 p_j^{\alpha}(\tau), \\ \dot{\varphi} = \omega, \\ \dot{p}_i(\tau) = -l_1|\omega_r(\tau)|^{\beta}(r_i + \rho)^{\beta} p_i^{\alpha}(\tau) + \frac{2l_1}{(1+2\rho)}|\omega_r(\tau)|^{\beta}\Delta_r \sum_{j=0}^{m} a_j(r_j + \rho)^{1+\beta} p_j^{\alpha}(\tau). \end{cases} \qquad (8)$$

4. Numerical Computations

Numerical calculations are carried out using the fourth order Runge-Kutta method with constant time step. We assumed the following initial non-dimensional parameters: $\omega_0 = 0.2$, $d = 0.0001$, $F_m = 1$, $F_0 = 0.5$, $\rho = 0.2$, $l_1 = 0.5$, $\alpha = 1$, $\beta = 1$, $m = 100$ and $F_{fr}(0) = 0.2$ for initial moment. Let us study first contact pressure distribution (Figure 2 on the left) as the function of the non-dimensional radius r of shields for different values of β parameter.
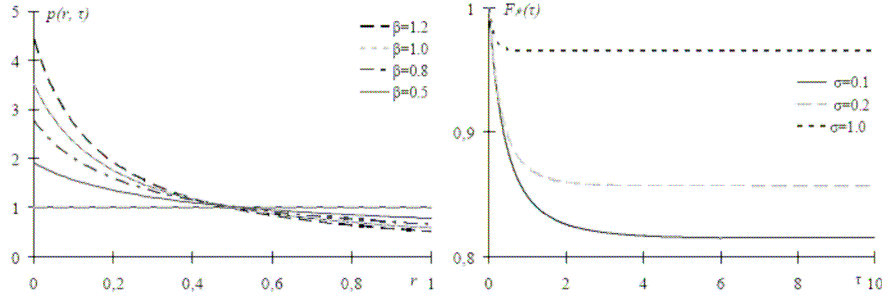
Figure 2. Contact pressures in equilibrium and changes of the friction torque moved by the clutch

Before beginning of the process of wearing of shields, the contact pressure distribution $p(r,0)$ is identical on the entire contact surface. However, contact pressure distributions $p(r,\infty)$ are different for various values of the β parameter. Figure 2 (on the right) shows changes of the friction torque moved by the clutch for various values of the geometrical ρ parameter. As can be seen, amendments of the contact pressure distribution during the wear causing reduction of the friction torque moved by the clutch. In Figure 3 we take into consideration process of wearing during vibrations of shields of clutch with a great coefficient of wear in order to observe changes in dynamics of the system. This dynamics is monitored via trajectories of motion in the system's phase for

different (rather small) values of the angle velocities of excitation, possible to appear, for example in the set-up time of the system for the slowly acting harmonic excitation.
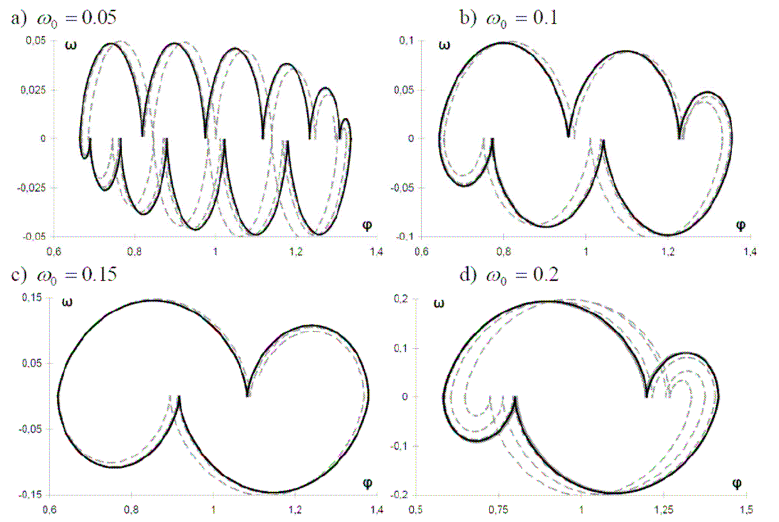
Figure 3. Phase trajectories of the system for various angular velocities including wear

As can be seen above, vibrations of the system depend both on angular velocity of harmonic excitation and friction torque moved by the clutch.

Figure 4 shows angular characteristics for various values of $F_{fr} = F_{fr}(0) = const$, (without wear process - $l_1 = 0$).
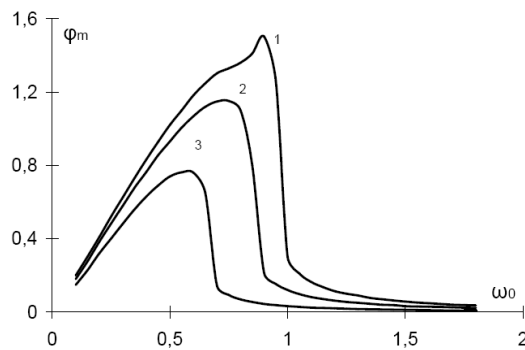
Figure 4. Angular characteristics of the system for various values of F_{fr};

curve 1 - $F_{fr} = 0.4$, curve 2 - $F_{fr} = 0.42$, curve 3 - $F_{fr} = 0.45$

Observe that the described resonance curves begin from the zero-dimensional vibration amplitude φ_m a little below value equal to zero for $\omega_0 = 0.1$, and are aspiring

asymptotically in the scope apart from resonance up to the nought. They have tendency of the gentler course in the scope apart from resonance. For smaller values of the F_{fr} resonance amplitudes have greater values. Besides, it should be noticed the phenomenon of moving of resonance on the left for more and more great values of the F_{fr}.

5. Conclusions

The considered in this work issues allow to model and analyse wear processes on the contact surface of a mechanical friction clutch and the system dynamics. Unlike many previous works, here friction clutch is treated as a friction connection of elastic (not rigid) bodies and general non-linear differential wear model is applied. Besides, mathematical model describing wear processes and equation of motion of the system are used and applied together during computer simulations. The presented in this work numerical analysis shows influence of wear processes in friction clutch on the system dynamics.

Acknowledgments

References

1. J.F. Archard, *Contact and rubbing of flat surface,* J. Applied Physics, **24**(8) (1953) 981-988.
2. Z. Lawrowski, *Tribology, friction, wear and lubrication*, PWN, Warsaw 1993 (in Polish).
3. Yu. Pyryev, *Dynamics of contact systems with including heat generation, friction and wear*, Postdoctoral thesis, Scientific Booklets no. 936, Technical University of Lodz, Lodz, Poland 2004 (in Polish).
4. J. Sadowski, *Thermodynamic interpretation of friction and wear*, Technical University of Radom, Radom, Poland 1999 (in Polish).
5. P. Solski, S. Ziemba, *Issues of wear of elements of machines caused by the friction*, PWN, Warsaw 1969 (in Polish).

Drgania Układu Mechanicznego ze Sprzęgłem Ciernym

Praca przedstawia wyniki badań numerycznych poświęconych dynamice układu mechanicznego ze sprzęgłem ciernym. Podczas symulacji przedstawiono i wykorzystano nieliniowy model zużycia. Zbadano wpływ rozważanego modelu zużycia na rozkład nacisków na tarczach sprzęgłowych. Dynamikę układu monitorowano przy użyciu trajektorii ruchu w przestrzeni fazowej oraz zachowania układu wokół rezonansowej częstości kątowej. Przedstawione wyniki pokazują interesujące i zbliżone do rzeczywistych zachowania się rozważanego układu oraz wpływ procesu zużycia na jego dynamikę.

A Stand for Forearm Flexor Muscles Examination

Jan AWREJCEWICZ

Technical University of Łódź, Faculty of Mechanics
Department of Automation and Biomechanics, Stefanowski Str. 1/15, 90-924 Łódź
awrejcew@p.lodz.pl

Jerzy MROZOWSKI

Technical University of Łódź, Faculty of Mechanics
Department of Automation and Biomechanics, Stefanowski Str. 1/15, 90-924 Łódź

Krzysztof NASIŁOWSKI

Technical University of Łódź, Faculty of Mechanics
Department of Automation and Biomechanics, Stefanowski Str. 1/15, 90-924 Łódź

Bartłomiej ZAGRODNY

Technical University of Łódź, Faculty of Mechanics
Department of Automation and Biomechanics, Stefanowski Str. 1/15, 90-924 Łódź

Abstract

In this paper a stand for forearm flexor muscles examination is presented. This stand is equipped in special cam which theoretically should extort a constant force in *biceps brachii* during arm flexion. It should allow examining maximal force of main muscle and muscles cooperation measurements. Herein an arm geometry and cam calculations is also presented.

Keywords: Muscle examination, upper limb.

1. Introduction

Muscles are biomechanical engines for animals and human beings; without them the movement or even some vital functions in biological organisms would not be possible. From biomechanical point of view, striated muscle, which are part of musculoskeletal system, are the most important part of muscle system.

Experimental examinations of muscles like measuring of damping factor, stiffness factor, length, force, cross-section, marking out static and dynamic characteristics of a muscle and so on are very important in construction mathematical models of muscles [1]. For instance a rheological model needs information on soft tissues properties. In order to build a geometrical model of muscles it is necessary to measure shape changing during contraction. The more parameters of muscles are precisely measured the better mathematical and bio-consent muscle model of actuators for artificial limbs can be built. The moments measuring, generated by muscle under conditions of maximum voluntary contraction is the most popular method for muscle strength evaluating [2].

In arm flexion the following muscles take a part (Figure 1): *biceps brachii* (1), *brachioradialis* (2), *extensor carpi radialis longus* (3), *brachialis* (4), *pronator teres, flexor carpi radialis, palmonaris longus, flexor digitorum superficiali*s.

It should be emphasized that biceps brachii and *brachialis* muscles are the most important actuators during forearm flexion [3].
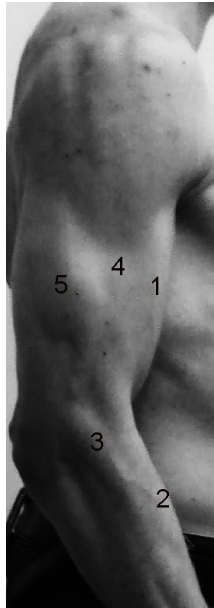
Figure 1. Main muscles of upper limb (1 – *biceps brachii*; 2 – *brachioradialis*;
3 – *extensor carpi radialis longus*; 4 – *brachialis; 5- triceps brachii*).

In the following graph it can be observed that in the human body maximum force generation occurs, when muscles are slightly stretched (see Figure 2), where L_0 is a resting length.
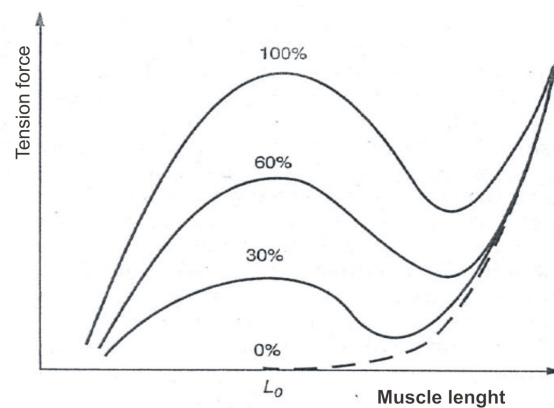
Figure 2. Force – length relationship for different levels of muscle stimulation (from [4])

A mechanism, which is presented below, is designed to extort constant force during the whole contraction of *biceps brachii* by a specially designed cam (3 in Figure 3).
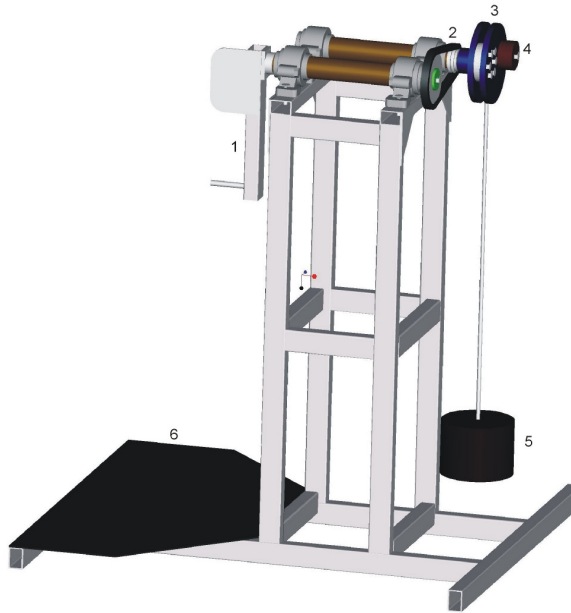
Figure 3. The stand for forearm flexor muscles examination (1 – arm holder,
2 – transmission, 3 – cam assembly, 4 – counterbalance,
5 – load, 6 – stands foundations.)

This construction allows measuring of a maximum force load for *biceps brachii* and makes possible an evaluation of work and cooperation of other muscles in an elbow joint during forearm flexion in supinated position. The use of transmission (2) was necessary because the lever angle of rotation is $180°$ in contrary to $360°$ of can rotation.

2. Arm Geometry and Cam Calculations

The arm model, shown inFigure 4, is taken under consideration, where: r_1 stands for arm length, r_2 – forearm length, r_m – distance from elbow to muscle attachment, l – muscle length, α – forearm flexion angle, β – angle between F and F_c forces, γ – angle between muscle and elbow – upper surface of *tuberositas radii* axis, F – force generated by *biceps brachii*, F_c – stands for rotational component of force F, d – high of muscle attachment (measured between an elbow – wrist axis and upper surface of *tuberositas radii*).
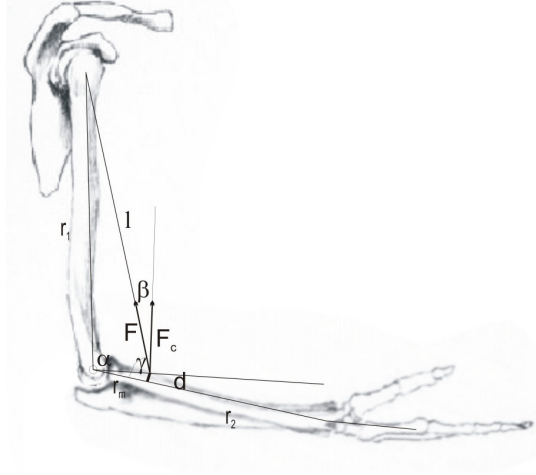
Figure 4. Arm geometry

In calculations, the following relations are used: $r_2 = 0.93\ r_1$, $r_m = 0.23\ r_2$, $d = 0.3\ r_m$. The relations between r_2, r_m and d were designated experimentally in vivo and verified to data in [4], [5] and [6]. This model gives comparable results to human arm (see [7]). Let assume that a muscle generate constant force F during contraction. Then we have.

$$F_c = F \cos\left(\frac{\pi}{2} - \beta\right) = F \sin\gamma \tag{1}$$

From the law of sines we get

$$\frac{l}{\sin\alpha} = \frac{r_1}{\sin\gamma}, \tag{2}$$

which implies

$$\gamma = \arcsin\frac{r_1 \sin\alpha}{l}. \tag{3}$$

From the law of cosines we get

$$l = \sqrt{r_1^2 + r_m^2 - 2r_1 r_m \cos\alpha}, \tag{4}$$

It follows from (1), (3) and (4), that

$$F_c = F \frac{r_1 \sin\alpha}{\sqrt{r_1^2 + r_m^2 - 2r_1 r_m \cos\alpha}}. \tag{5}$$

The following function

$$A(\alpha) = \frac{r_1 \sin\alpha}{\sqrt{r_1^2 + r_m^2 - 2r_1 r_m \cos\alpha}} \tag{6}$$

governess changing of arm load during movement from position $0°$ to $180°$.
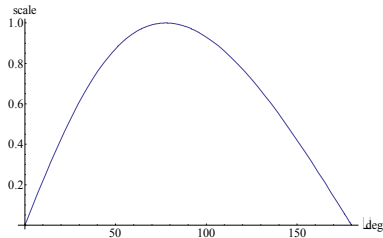
Figure 5. Plot of *A(α)* in the Cartesian coordinate system.

Changing the Cartesian coordinate system into the polar one, we receive the following function

$$r(\alpha) = \sqrt{\alpha^2 + A^2(\alpha)} \ , \ \alpha \in (0, \pi). \tag{7}$$

This allows to construct the polar plot reported in Figure 6.
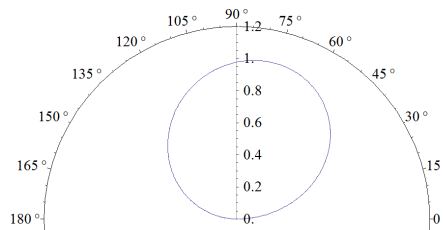
Figure 6. Plot of $A(\alpha)$ in the polar coordinate system.

Let us point out that the shape of the curve in gray was used to design the shape of the cam for the stand. Because of the positive value of the high of muscle attachment (see the parameter d in Figure. 4), it is necessary to take into account the constant difference between theoretical arm (made from straight beams) and human arm (where bones do not have regular shapes) for the cam installation, i.e. the cam must be rotated about 15°. It is also possible to modify the stand for generating maximal force in *biceps brachii* during whole arm contraction as it is shown in Figure 2 (see also [7]). The new cam will have the shape reported in Figure 7.
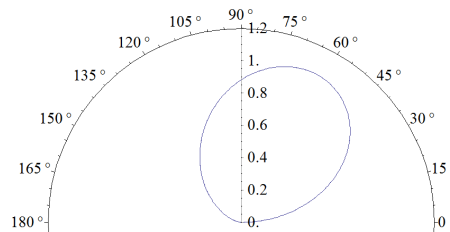
Figure 7. Plot of the new calculated cam for generating maximal force in *biceps brachii* during contraction.

3. Conclusions

Most of the researches are concerned to isometric or isotonic muscle characteristics, see for example [2] and [7]. Our presented construction is designed to measurement of isotonic arm flexor muscles. However, by changing load, it is easy to change force acting on a muscle and to examine arm behaviour. It is also possible to modify the stand in order to generate a constant force momentum by replacing the cam by a centrally mounted disc or generating maximal force in *biceps brachii* during whole arm contraction by using appropriate cam shape. For other joints examination (for example an ankle) it is possible to recalculate new cam geometry.

Acknowledgments

References

1. B. M. Nigg, W. Herzog, *Biomechanics of the Musculo – Skeletal System,* John Wiley & Sons, Chicester 1994.
2. K. Kulig, J. G. Andrews, J. G. Hay, *Human Strenght Curves*, Exercise and Sport Sciences Review, **12** (1) (1984) 417-466.
3. W. M. Murray, L. D. Scott, T. S. Buchanan, *Variation of Muscle Moment Arms With Elbow and Forearm Position,* Journal of Biomechanics, **28** I (5) (1995) 513-525.
4. J. W. Błaszczyk, *Clinical Biomechanice*, Medical Publishing House PZWL, Warsaw 2004 (In Polish).
5. A. Agur, A. Dalley, *Grant's Atlas of Anatomy, 12th Edition,* Lippincott Williams & Wilkins 2009.
6. R. L. Huston, *Principles of Biomechanics,* CRC Press, New York 2009.
7. P. Pigeon, Y. L'Hocine, A. G. Feldman, *Moment Arms and Lengths of Human Upper Limb Muscles as Function of Joint Angles,* Journal of Biomechanics, **29** (10) (1996) 1365-1370.

Stanowisko do badania zginaczy przedramienia

Mięśnie są biomechanicznymi silnikami dla zwierząt i ludzi. Mają one ogromny wpływ na ruch, a nawet pewne istotne funkcje życiowe. Z biomechanicznego punktu widzenia najważniejszą częścią układu mięśniowego są mięśnie poprzecznie prążkowane.

W artykule zaprezentowano stanowisko do badania zginaczy przedramienia. Jest ono wyposażone w specjalnie zaprojektowaną krzywkę, której zadaniem jest wymuszenie stałej siły napięcia bicepsa podczas zginania ręki. Ma to na celu umożliwienie wyznaczenia maksymalnej siły, którą może wygenerować ten mięsień oraz zbadanie współpracy mięśni przedramienia. W artykule zamieszczono również przyjętą geometrię ręki oraz obliczenia dotyczące konstrukcji krzywki.

Multi-objective optimization of the acoustic impedance distribution for room steady state sound field condition

Andrzej BŁAŻEJEWSKI
Institute of Mechatronics, Nanotechnology and Vacuum Technique
Division of Applied Mechanics and Mechatronics
75-620 Koszalin, ul. Racławicka 15-17
andrzej.blazejewski@tu.koszalin.pl

Tomasz KRZYŻYŃSKI
Institute of Mechatronics, Nanotechnology and Vacuum Technique
Division of Applied Mechanics and Mechatronics
75-620 Koszalin, ul. Racławicka 15-17
tkrzyz@tu.koszalin.pl

Abstract

In the paper problem of a room with a harmonic sound source inside and resulting acoustic field in a steady state is investigated. A question of a proper and optimum distribution of an acoustic absorption material on the room's boundaries, to obtain desirable acoustic pressure level is considered. Below the Schroeder frequency, acoustic modes are perfectly separated. Under such conditions, room's pressure distribution can be described using modal analysis assumptions. Thus, the acoustic pressure represents a sum over a set of room's eigenfunctions and time components, i.e. the modal amplitudes. Additional assumption of enough high boundaries' impedance is made, and finally the modal coupling can be neglected. By means of the analysis of the modal amplitude function, as the most important component of acoustic pressure, multi-objective function for arbitrary shaped room, with 15 different boundaries is created. Impedance values on each boundary are chosen as design variables. Research of the minimum objective function (non-dominated solutions), using genetic algorithm, is conducted. As the result, the Pareto optimal solution i.e. set of material with the specific impedance, properly distributed on boundaries has been found.

Keywords: modal amplitudes, multi-objective function, optimization, genetic algorithm

1. Introduction

The problem, how to distribute the material with specific absorption on walls, floor and other surface in the room, in order to obtain desirable acoustic field properties is commonly known. After the source of sound starts to emit a signal, losses of acoustic energy caused by absorption on room's boundaries at the same time are equalized by energy from the source, and in an enclosure acoustical steady-state is reached. In order to describe acoustic field distribution inside a room, one can use modal analysis formulation under several restrictions [1,2,3]. Using modal analysis assumptions, acoustic field distribution in a room interior can be described with its normal modes (eigenfunctions) Ψ_n and corresponding eigenfrequencies ω_n. The eigenfunctions for sufficiently enough high sound absorption related to room's boundaries impedance, approximately equals eigenfunction for the same room with Neuman boundary condition. Simultaneously orthogonal, normalized set of functions Ψ_n is required [1,2,3].

According to the above assumptions, if an acoustic field distribution in a room with harmonic source $qe^{j\omega t}$ inside describes a linear, inhomogeneous wave equation (q is a function describing source distribution in a room and its volume as well, ω is a source frequency), then the solution can be represented by a sum over a set of eigenfunctions [1]:

$$p(x,y,z,t) = \sqrt{V} \sum_{n=0}^{\infty} P_n(t)\Psi_n(x,y,z) \tag{1}$$

In equation (1), V is a volume of a room and $P_n(t)$ is the time components i.e. the modal amplitude calculated for n-th room's mode. For a steady-state and harmonic source, modal amplitudes take the form $P_n(t) = A_n\, e^{j\omega t}$, were:

$$A_n = \frac{Q_n}{\omega_n^2 - \omega^2 + 2j\omega r_n} \tag{2}$$

In equation (2), r_n is a room's damping coefficient and Q_n is an acoustic source factor [1], which are given for n-th mode by the following relation:

$$r_n = 0.5 \cdot \rho_0 \cdot c^2 \int_S \frac{\Psi_n^{\,2}}{Z_S}ds, \quad Q_n = \frac{c^2}{\sqrt{V}}\int_V q \cdot \Psi_n dV \tag{3}$$

where S describes the surface of room boundaries with the individual impedance Z_S.

2. Multi-objective function

Under assumption mentioned above, one can state that acoustic pressure (1) in each enclosure, are directly depended on modal amplitudes (2). The eigenfunctions Ψ_n and the eigenfrequencies ω_n are constant and characteristic for a particular room. Therefore the influence on the interior acoustic field can be done by modal amplitudes modification. Additionally, when a constant position of the sound source is considered, the factor Q_n in (2) is constant as well. Eventually, coefficients r_n play the main role in room's acoustic filed creation, through boundaries impedance value Z_S and its distribution. The commonly desirable situation is minimum of the acoustic pressure in enclosure under different impedance conditions. It is obvious that this can be achieved applying maximum value of impedance Z_S on all boundaries (3), from the assumed range. On the other hand, in practice higher impedance on a surface increases costs. Simultaneously, for some configurations of an impedance, absolute values of modal amplitudes are reduced, but the total sum (1) could give higher values. It results from signs of amplitudes and eigenfunctions. Thus, there are two opposite criteria, and a double criteria objective function is considered with an intention of searching optimal values of walls' impedances, which give maximal reduction of an acoustic pressure inside enclosure. The first criterion *K1* (the acoustic criterion) is: spatial root mean square value derived from (1) has to be minimal.

$$K1 = p^n{}_{rms} \rightarrow \min \tag{4}$$

where n is a number of modes taken into consideration. The second criterion *K2* (the cost criterion) is: values of impedances of particular walls have to be close to the

highest impedances from the examined range. Additionally, each separate surface, where the impedance could vary, is related to its weight w_i. Values of the weights reflect the relative importance of the surface in the enclosure. Finally, the cost criterion takes the following form:

$$K2 = \sum_{i=1}^{m} w_i (Z_{max} - Z_i) \rightarrow \min \qquad (5)$$

where m is a number of surfaces taken into consideration.

3. Sample object

As an example of optimized object, the room shown in figure 1 is taken into consideration. The volume of the enclosure is 45,27 m^3, and total surface area S with varying impedance is 84,96 m^2. 15 different surfaces are considered (walls, the floor, the ceiling, doors).
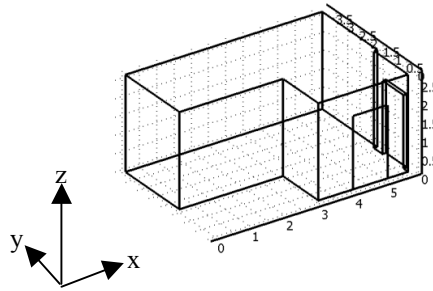
Figure 1. Shape and dimensions of the examined object

The double-objective function has been created using the relations (4) and (5). The first 500 modes are involved which is related to the eignfrequency 480,4Hz as a limit. Therefore in the case of the criterion *K1* (4), we have n=500. Modal amplitudes have been found according to (2) and factors Q_n, ω_n, r_n have been obtained numerically, using FEM method. In the case of the criterion *K2* (5) the impedance of 15 surfaces (m=15) varies from $Z_{min}=10^4$ to $Z_{max}=10^6$ Pa·s/m. The weights w_i are defined to emphasise the surfaces of small area and its sum equals unity ($\Sigma w_i =1$).

4. Genetic algorithm method

In order to examine the objective function taking into account two criteria, the genetic algorithm method [4,5] has been used. This approach has been applied due to the following reasons. The genetic algorithm does not require gradient information which could be difficult to get in a case of a large number of design variables (15 values of surfaces' impedance). The nature of the objective function is not known, the genetic algorithm converges to the global solution rather than to a local one. Additionally,

Pareto-optimal solutions are available directly. The initial population which is generated using the uniform distribution guarantees covering the whole feasible design space with equal probability.

5. Results

Results were obtained for four different sound source configurations (the position and frequency) and the phase shifted flow out from the source 0.005 m^3/s. Genetic algorithm options were: the population size-500, the number of iterations-100 and design variables tolerances 10^2 Pa·s/m. In figure 2 the Pareto optimal solutions normalized by maximal values of each criterion are shown. The quantity Cost^{max} is the value of the cost criterion (K2) in case of Z_{min} for all room's surfaces. The quantity p^{max} is the value of the acoustic criterion (K1) for Z_{max} on all surfaces.
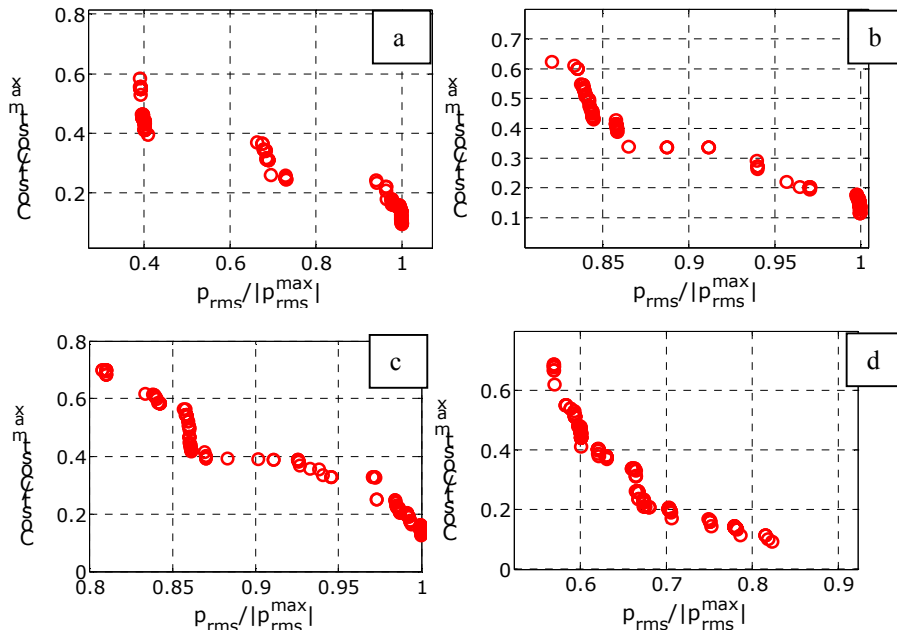
Figure 2. Normalized Pareto optimal solutions for different positions (x,y,z) and frequency (f) of the sound source: a) x=4.76m, y=2.37m, z=1.26m, f=90Hz; b) x=1.07m, y=2.50m, z=1.42m, f=90Hz; c)x=4.76m, y=2.37m, z=1.26m, f=81.5Hz; d) x=1.07m, y=2.50m, z=1.42m, f=250Hz.

Points on the Pareto curve in figure 2 are related to specific set of design variables (surface's impedances). In figure 3 the particular solutions, selected from the Pareto optimal solutions, by means of its distance evaluation from utopia point (i.e. solutions with minimal distance)[5] are shown. In figure 3, room's surfaces are put in increasing area order. The surfaces numbered from 13 to 15 are the largest, their relative areas

reaches 58% of total surfaces areas. According to the cost criteria K2, their impedances should take values in a high range of the impedance.
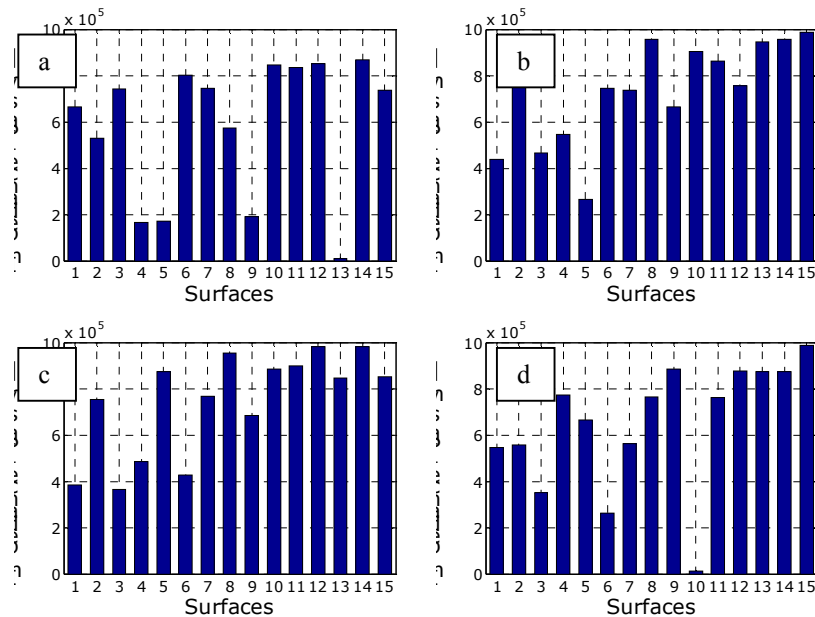
Figure 3. Solutions with minimal distance from utopia point for different positions (x,y,z) and frequency (f) of the sound source: a) x=4.76m, y=2.37m, z=1.26m, f=90Hz; b) x=1.07m, y=2.50m, z=1.42m, f=90Hz; c)x=4.76m, y=2.37m, z=1.26m, f=81.5Hz; d) x=1.07m, y=2.50m, z=1.42m, f=250Hz.

6. Conclusions

The optimization process was conducted for specific room and source configurations, but the procedure presented in the paper can be used for other applications in room acoustics, especially in cases where many factors like source prosperities, position, impedance distribution etc., can influence on the acoustic field. Particularly, using modal analysis, one can define desired optimization condition, avoiding the FEM or BEM method to calculate acoustic variables. As the result, the set of optimal solutions is available (Fig. 2) and one can decide which solution is suitable one (Fig. 3). In the case of example considered above, only the real impedances of surfaces were examined but other values are possible to obtain. Likewise, room boundaries can be divided into smaller areas but this increases the number of design variables and the cost of computing as well. Extremely, each point of boundaries can receive its specific impedance and as the optimization result, a room with varying prosperities of surfaces can be considered. Additionally, the obtained results show that the optimization strongly depends on the position and frequency of the sound source. As follows from figure 2a

and 2c, for the same position but different source frequency, even close each other, the acoustic pressure p_{rms} reduction decreases. In the case of 90Hz in the same range of expenditure, one can achieve more effects (the p_{rms} reduction) than for frequency 81,5Hz. Similar dependence appears from figure 2b and 2d. On the other hand, the same sound source placed in another position in the enclosure may change room's response likewise possibility of pressure reduction by boundaries' impedance.

Acknowledgments

References

1. M. Meissner, *Influence of wall absorption on low-frequency dependence of reverberation time in room of irregular shape*, Applied Acoustics **69** (2008) 583-590.
2. P.L. Franzoni, D.B. Bliss, *A discursion of modal uncoupling and an approximate closed-form solution for weakly coupled systems with application to acoustic*, Journal of The Acoustical Society of America **103** (1998) 1923.
3. E.H. Dowell, *Reverberation time, absorption, and impedance*, Journal of The Acoustical Society of America **64** (1978) 181.
4. A. Popov, Genetic algorithms for optimization, Programs for Matlab, Version 1.0, Hamburg 2005.
5. R.T. Marler, J.S.Arora, *Survey of multi-objective optimization methods for engineering*, Springer-Verlag, Struct Multidisc Optim **26** (2004) 369-395.

Wielokryterialna optymalizacja rozkładu materiału o określonej impedancji w pomieszczeniu, w ustalonym stanie pola akustycznego

Praca dotyczy zagadnienia pomieszczenia zamkniętego, w którym umieszczone zostało harmoniczne źródło dźwięku. Zaprezentowano problem optymalizacji rozmieszczenia na brzegach pomieszczenia materiału absorbującego akustycznie, o odpowiedniej impedancji. Poniżej częstotliwości granicznej Schroedera, mody akustyczne pomieszczenia zamkniętego są dobrze odseparowane. W tym zakresie częstotliwości, do opisu rozkładu ciśnienia akustycznego w pomieszczeniu można zastosować analizę modalną. Ciśnienie akustyczne w każdym punkcie może być przedstawione w postaci sumy funkcji własnych oraz składowych czasowych tj. amplitud modalnych. Dodatkowo założenie, wystarczająco dużej impedancji na brzegach pozwala pominąć sprzężenie między modami. Wykorzystując amplitudy modalne, jako najbardziej istotne czynniki ciśnienia akustycznego, stworzono wielokryterialną funkcję celu dla przykładowego pomieszczenia o nieregularnym kształcie i 15 powierzchniach brzegowych. Wartości impedancji na poszczególnych brzegach pomieszczenia stanowiły układ zmiennych decyzyjnych. Do poszukiwania minimum funkcji celu (rozwiązania niezdominowane) wykorzystano algorytm genetyczny. W rezultacie otrzymano zestaw rozwiązań Pareto optymalnych tj. układ materiału o specyficznej impedancji akustycznej, rozmieszczony odpowiednio na brzegach pomieszczenia.

Theoretical bases of vibration diagnostics of anchor against landslide constructions

Nadiia BOURAOU
National Technical University of Ukraine "Kiev Polytechnic Institute"
37 Peremogy Pr., Kyiv, Ukraine, 03056
burau@pson.ntu-kpi.kiev.ua

Iuliia KLOFA
National Technical University of Ukraine "Kiev Polytechnic Institute"
37 Peremogy Pr., Kyiv, Ukraine, 03056

Yuri ZSUKOVSKIJ
National Technical University of Ukraine "Kiev Polytechnic Institute"
37 Peremogy Pr., Kyiv, Ukraine, 03056

Eduard KULISH
Science-Technical Centre "Ingzaschita"
81 Kirova Str., Yalta, Ukraine,98637

Abstract

The given work is devoted to development of theoretical bases of a new vibrating diagnostics method and evaluation a current condition of the anchor. The research of the pulse response of the anchor against landslide construction is a basis of vibrating diagnostics of a tension condition an anchor, detection of feature of abatement of a tightness, and definition of character of its dependence on a changing stretching force. The elastic body with the distributed parameters (a string) is used as the diagnostic model of the tense and fixed core of an anchor. Dependences of own frequencies changing of the pulse response of an anchor on a tightness changing at deformations and displacement of a place of fastening of an anchor are defined. The discrete model of an anchor against landslide construction is developed and researched for definition of dependences between parameters of an anchor condition and vibrating characteristics of a retaining wall, which is accessible to carrying out of measurements.

Keywords: sliding processes, anchor against landslide constructions, tension of anchors, vibrating diagnostics.

1. Introduction

The anchor against landslide constructions are used for the protection of territories and the located on them buildings from distribution and catastrophic consequences of the sliding processes. They are installed in potentially dangerous places with retaining walls. Practically, their original tension is a major factor, determining density of roof-bolt setting. The anchor tension is necessary constant over a long period of anchor construction operation. However, the tension of anchors can change in due course under influence of sliding processes. In some cases it can lead to that the anchor will be pulled out from a bedrock surface and will not carry out maintaining function without any visible external attributes of change of its technical functional condition. Therefore, it is necessary to spend periodically the control of a tension of anchors, that is the important

information for an evaluation of a current condition of sliding processes and forecasting of their further development.

The anchor against landslide construction is offered by complex system enclosed a retaining wall (1), a tightener (2), a rod (3) and a locking device (4) as shown on Figure 1. A locking device serves for anchor fixation into rock, a tightener is used for stress making in an anchor rod for a decrease or elimination of a deformation and displacement of linked rocks. Practically, the steel wire rope or iron reinforcement constructions are used as a rod. Carried out theoretical researches of anchor constructions in the core touch problems of their strength and reliability for different operation phases [1]. These results allow to make demands to geometrical sizes and performances of used materials of elements of an anchor constructions, but are not sufficient for monitoring possible strains and offsets of rocks in a place of anchor fixation under natural excitation of land (for example, landslide).
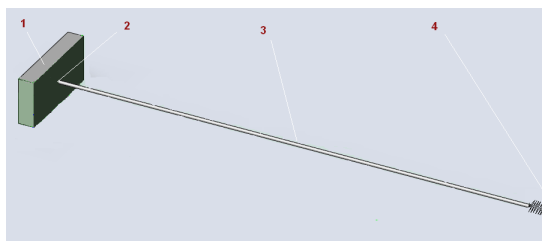
Figure 1. Configuration of an anchor against landslide construction: 1 - a retaining wall; 2 – a tightener; 3 - a rod and 4 - a locking device

The given work is devoted to development of theoretical bases of a new vibrating diagnostics method and evaluation a current condition of the anchor. The research of the pulse response of the anchor against landslide construction is a basis of vibration diagnostics of a tension condition an anchor [2], detection of feature of abatement of a tightness, and definition of character of its dependence on a changing stretching force.

2. Frequencies analysis

We use the elastic body with the distributed parameters (a string) for mathematical description of the tense and fixed rod of an anchor [3]. As a first approximation we'll not take into account a limitation of a string flexing by walls of an open test pit. String flexing (a deviation of a string in a cross plain) characterizes cross vibrations of a model. As is known, cross vibrations of a string under a influence of axial stretching force P are presented by expression

$$y = \sin\frac{n\pi}{l}x(A_n\cos\frac{an\pi}{l}t + B_n\sin\frac{an\pi}{l}t),\qquad(1)$$

where $a = \sqrt{Pgl/Q}$; g is gravitational acceleration; Q is string weight; l is string length; A_n, B_n are coefficients, which rate the amplitudes of a string oscillations on the main ($n=1$) and higher ($n=2;3;...$) oscillations shapes; x, y are axial and cross displacements.

The frequencies f_{no} of oscillations (1) are defined as:

$$f_{no} = \frac{an}{2l} = \frac{n}{2}\sqrt{\frac{Pg}{lQ}} \ . \tag{2}$$

Let an axial stretching force P is changed at a strain and offset of a place of anchor fixation:

$$P_1 = P \pm \Delta P ,$$

where ΔP is changing value of stretching force; the sign "+" corresponds to increasing of stress in an anchor rod under landslide activity and the sign "-" corresponds to a case, when rod is pulled from rocks.

Let's consider coefficient of the relative tension changing $z = \Delta P / P$, therefore force $P_1 = P(1 \pm z)$. The frequencies f_{n1} in this case are:

$$f_{n1} = \frac{n}{2}\sqrt{\frac{P_1 g}{lQ}} = f_{no}\sqrt{1 \pm z} \ . \tag{3}$$

The factor R of nature frequencies changing at the tension changing can be defined from (3) as:

$$R = \frac{f_{n1}}{f_{no}} = \sqrt{1 \pm z} \ . \tag{4}$$

Table 1 presents dependencies of frequencies changing factor on coefficient of the relative tension changing at the increasing and decreasing of axial stretching force.

Table 1. Dependencies of factor R on coefficient z of the relative tension changing.

z	0,01	0,05	0,1	0,15	0,2	0,3
$R_{(+)}$	1,005	1,025	1,049	1,072	1,095	1,140
$R_{(-)}$	0,995	0,975	0,949	0,922	0,894	0,837

Apparently from the received results, small changing of force P ($z \leq 0{,}1$) brings to changing of frequencies under all shapes of oscillations no more than 5 % both at increasing and at a decreasing of a tightness. The changing of axial stretching force in the range of $0 < z \leq 0{,}3$ brings to changing of frequencies under all shapes of oscillations about 14-16%. Thus, changing of anchor rod frequencies can be used as diagnostic feature of tension of anchors.

3. Researches of anchor discrete model

As it was noted above, rod of an anchor is unapproachable to monitoring its tightness or own frequencies. Anchor against landslide constructions are mounted in such a way that retaining wall only is accessible to carrying out of measurements (see Fig. 2).

Therefore, it is necessary to determine influence of tension changing on performances of stress, displacements and strains of a retaining wall.

We use Finite Element (FE) Analysis for the design discrete model of an anchor against landslide construction which can be representative of an actual object. For this

aim we consider anchor rod made from carbon steel rope with the following properties: Density 7850 kg/m^3; Modulus of Elasticity $2,05 \cdot 10^{11}$ N/m^2; Poison's ratio 0,29; Shear Modulus $8 \cdot 10^{10}$ N/m^2. Retaining wall is represented by concrete slab with the following properties: Density 2000 kg/m^3; Modulus of Elasticity $2,75 \cdot 10^{10}$ N/m^2; Poison's ratio 0,2. The developed discrete model consists of 8444 FE and 14572 nodes.

Figure 2. Photograph of anchor against landslide construction, installed in Crimea

The second goal was to understand the behavior of the vibrating characteristics of a retaining wall as a function of parameters of an anchor condition. For this study, rod rigidity value is changed (rigidity is decreased), relative rigidity changing ΔC is assigned of 0,15, that corresponds to R=0,97; 0,25 (R =0,87) and 0,5 (R=0,7). Figure 3 shows the example of modeling and estimation of wall displacement at the initial value of rigidity (ΔC =0).
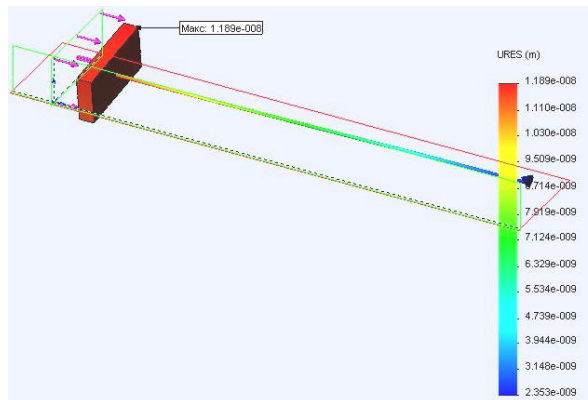
Figure 3. Example of modeling and estimation of wall displacement

   As it is possible to see from the presented figure, the maximum displacement occurs on the slab and anchor rod has minimum displacement in the area of anchor fixation. Values of maximum and minimum displacement are change at a rod rigidity changing the means specified above. These values increase at the decreasing of rod rigidity. Changing of minimum displacement can be interpreted as displacement of rocks and development of activity of landslide at the modeling and study diagnostic model of anchor against landslide construction. Relative rigidity changing of a rod and corresponding changing of frequencies are considered as parameters, which characterized functional condition of an anchor and its possibility to carry out maintaining function. Changing of maximum displacement is used in this study as a feature of changing of the anchor tightness or own frequencies. The relation between maximum and minimum values of displacement also depends on change of rod rigidity. The maximum value is different from minimum five times at the $\Delta C = 0$, and these values do not different among themselves at the $\Delta C = 0,5$, practically. In the latter case it means that the anchor against landslide construction practically does not carry out maintaining function.

   Table 2 presents dependencies of relative values of maximum and minimum displacement (ΔD_{max} and ΔD_{min}, accordingly) on relative rigidity changing ΔC. The relative values are estimated by using the following expressions:

$$\Delta D_{max} = \frac{D_{max}(\Delta C)}{D_{max}(0)} \quad \text{and} \quad \Delta D_{min} = \frac{D_{min}(\Delta C)}{D_{min}(0)}, \tag{5}$$

where $D_{max}(\Delta C)$ and $D_{min}(\Delta C)$ are displacements at the rod rigidity changing ($\Delta C \neq 0$); $D_{max}(0)$ and $D_{min}(0)$ are displacements at the initial value of rod rigidity ($\Delta C = 0$).

Table 2. Dependencies of ΔD_{max} and ΔD_{min} on relative rigidity changing of a rod

ΔC	0	0,15	0,25	0, 5
ΔD_{max}	1	1,04	2,61	28,82
ΔD_{min}	1	1,79	9,15	143,41

   The presented results show that evaluated values of minimum displacements increase too much at the decreasing of a rod rigidity. But we have not any possibility to measure these displacements. Value of maximum displacement increases slightly at the $\Delta C \leq 0,15$ (it corresponds to $R \leq 0,97$ and $z \leq 0,05$). Further decreasing of a rod rigidity causes a large increasing of values of maximum displacements. Since the mentioned displacements occurs on the slab, we can to measure these characteristics by using mounted on the retaining wall sensor.

4. Conclusions

The theoretical basis of development vibration diagnosis method is presented for monitoring and evaluation a current condition of the anchor against landslide constructions.

The elastic body with the distributed parameters (a string) is used as the diagnostic model of the tense and fixed core of an anchor, that allows to define and analyse dependencies of frequencies changing factor on coefficient of the relative tension changing at the increasing and decreasing of axial stretching force.

The discrete model of an anchor against landslide construction is developed and researched, that allows to understand the behavior of the vibrating characteristics of a retaining wall as a function of parameters of an anchor condition. The received results of anchor modeling and analysis show that decreasing of a rod rigidity causes increasing of displacements occurs on the slab and in the area of anchor fixation. Dependencies of relative values of displacements are researched on relative rigidity changing.

The received results are new and will be used for the further investigations and development of a new vibration method for monitoring and evaluation a current condition of the anchor against landslide constructions.

References

1. N. Moshkin *Perfecting of mane knots of a sling anchorage*, In Proceedings of the 12th Conference on Problems of a Mechanics and Machine Industry (2002) 213-216.
2. N. Bouraou, I. Avrutova, Yu. Zsukovskij, *Methodology of vibration diagnostics of an anchor against landslide construction for definition of a change of its tightness*, Building constructions, **67** (2007) 137-142
3. G. Pisarenko *Strength of materials*, Vischa shkola, Kiev 1979.

Vibroacoustical diagnosis of the crack-like damages of aircraft engine blades at the steady-state and non-steady-state modes

Nadiia BOURAOU

National Technical University of Ukraine "Kiev Polytechnic Institute"
37 Peremogy Pr., Kyiv, Ukraine, 03056
burau@pson.ntu-kpi.kiev.ua

Iurii SOPILKA

National Technical University of Ukraine "Kiev Polytechnic Institute"
37 Peremogy Pr., Kyiv, Ukraine, 03056
sopilk@ukr.net

Abstract

The work is devoted to condition monitoring and vibroacoustical diagnosis of the crack-like damages of the gas-turbine engines (GTE) blades at the steady-state and non-steady-state modes of GTE. The developed diagnostic model of GTE is presented and the influence of damage on the measured vibro- and acoustical signals at the steady-state and non-steady-state modes of GTE is determined. The application of the following signal processing methods: Polyspectral (Higher-Order Spectral) analysis, Wavelet-transformation and dimensionless characteristics of the vibroacoustical signals is proved. The efficiency of signal processing methods is demonstrated by the results of numerical simulations of the turbine stage at the steady-state and non-steady-state modes of vibration excitation. The fault features are detected and investigated.

Keywords: gas-turbine engine, crack-like damage, vibroacoustical diagnosis, signal processing

1. Introduction

Statistics about aircraft gas-turbine engine (GTE) failures demonstrate that the most part of these failures, led to premature taking away the engine, are provoked by the damages of the compressor components (from 20% to 76%) and the turbine ones (from 15% to 65%). The mentioned engine failures are caused by typical totality of damages as: nicks, dents, bending of compressor blades; cracks and compressor blades break; nicks and burning turbine blades. After scheduled inspections and repair, more then a half of blades are culled because of erosion, nicks, initial cracks and burning. According to analysis, the some of these damages (named crack-like damages) could be found out at initial stage of its evolution without engine disassembling if the continuous monitoring of the engine components condition was conducted.

The problem of detection of the crack-like damages of blades at the steady-state and non-steady-state modes of GTE may be solved by using the vibration and vibroacoustical diagnostic methods [1]. Creation of the monitoring system is based on application and further development of low-frequency (0-25 kHz) vibroacoustical diagnostic methods which use vibrating and acoustical noise as diagnostic information. This noise is radiated by the turbine and compressor stages at the GTE operating.

Generally monitoring is a continuous process of information gaining about the object vibrating condition, its transformation, signal processing and making decision about

object technical condition. The stages of the mentioned informative process depend on the engine operative modes. These modes define specific character of vibrating and acoustical excitation of the compressor and turbine blades, and consequently, they define the methods and algorithms of signal processing, which will allow to detect initial faults.

Initiation and increase of a crack-like damages in the blade lead the instantaneous change of its stiffness. Usually the change of stiffness is modeled by the piecewise-linear characteristic of the restoring force [1,2]. At low a level of a useful signal in vibrating and acoustic noise which is radiated by the engine at its operating, use of traditional spectral analysis is inefficient for incipient cracks detection. In this paper we propose to use the Bispectrum analysis (BS), Wavelet Decomposition (WD) and Dimensionless Peak Characteristics (DPC) of the vibroacoustical signals for the signal processing and fault features extraction.

2. Diagnostic model of GTE and measuring signal conditioning

The GTE is the compound system which consisting of many subsystems, assemblages and devices. Deriving of full mathematical exposition of GTE behavior is hampered, therefore for the purpose of diagnostic, as a rule, the simplified models of GTE are used (for example, at the engine separation on subsystems and devices with hierarchical structure of connections). According to mentioned diagnostic model of GTE has been developed. The main prominent features of diagnostic model are:

1. Model includes set of n stages (subsystems "disk-blades") which are rotation by a rotor of the engine.

2. The basic and most important source of vibration at the engine operation is the rotor, therefore rotor vibration $P(t)$ is considered as the basic entrance vibrating excitation on subsystems "disk- blades ".

3. Rotor vibration model at the steady-state mode (named m1) of GTE has been accepted in the form:

$$P(t) = \sum_{i=1}^{l} P_i(t)\sin[i\omega_p t + \varphi_i(t)] + \xi(t), \tag{1}$$

where $P_i(t)$ is the amplitude of a harmonic whith number i; ω_p is the main rotation frequency; $\xi(t)$ is the broadband normal noise.

4. Rotor vibration model at the non-steady-state modes (named m2 and m3) of GTE has been accepted in the form:

$$P(t) = \sum_{i=1}^{3} P_i(t)\sin[\omega_{p0} \pm 0,5i\beta t^2 + \varphi_i(t)] + \xi(t), \tag{2}$$

where ω_{p0} is the initial value of rotation frequency; β is speed of frequency variation of the first rotor harmonic; the sign "+" corresponds to a mode m2 with the fast increase of the rotor rotation frequency and the sign "-" corresponds to a mode m3 with the decrease of the rotor rotation frequency.

5. In relation to described above rotor excitation set of n stages is represented in the form of parallel connection of n subsystems "disk- blades". Generally reaction of system on rotor vibration represents the following n-dimensional vector of reactions:

$$R_p(t) = [R_{p1}(t),...,R_{pn}(t)] \, ,$$

where $R_{Pj}(t)$ is the reaction of subsystem with number j on excitation $P(t)$, and which are represented by the following expression in case of elastic and dynamic independence of oscillations of blades and the disk:

$$R_{Pj}(t) = \sum_{q=1}^{z_j} r_{Pjq}(t) + r_{Pjd}(t). \tag{3}$$

In the expression (3) following designations are used: $r_{Pjq}(t)$ is reaction of blade with number q; $r_{Pjd}(t)$ is reaction of disk; z_j is blades quantity at the selected stages.

6. Unfailing blades are described by the model of an linear oscillating system with natural frequency ω_* ($f_* = 600$ Hz). The impulse response of it is:

$$g_*(t) = \frac{1}{\omega_*} \sin \omega_* t \, . \tag{4}$$

The model of a blade with a crack-like damage is presented by the model of an oscillating system with piecewise-linear (asymmetrical) characteristic of the elastic force. The impulse response of this system is expansion in Fourier series at harmonics of the cracked blade model base frequency ω_0 [1]:

$$g(t) = \frac{a_0}{2} + \sum_{k=1}^{K} a_k \cos k\omega_0 t \, , \tag{5}$$

where $a_0 = \dfrac{4(1-\varsigma)}{\pi\omega_*\varsigma}$; $a_k = \dfrac{4(1+\varsigma)^3(1-\varsigma)^2}{\pi\omega_*\varsigma[(\varsigma+1)^2 - 4k^2][(\varsigma+1)^2 - 4\varsigma^2 k^2]} \cos\dfrac{\pi k}{\varsigma+1}$; $\omega_0 = \dfrac{2\omega_*\varsigma}{1+\varsigma}$;

$\varsigma = \sqrt{1-\vartheta}$; ϑ - crack parameter, relative rigidity changing at the crack presence.

The reaction of one blade on excitation $P(t)$ in the form (1) or form (2) can be defined by Duhamel integral:

$$r_{Pjq}(t) = \int_{-\infty}^{t_k} P(\tau) g_{jq}(t,\tau) d\tau \, , \tag{6}$$

where $g_{jq}(t,\tau)$ is the blade impulse response (4) or (5).

7. Each stage oscillates vibration of an aerodynamic origin $Q_j(t)$ on rotor frequency and in z_j times more. Mathematical expression of vibration similarly to (1). Other aerodynamic vibration $S_j(t)$ is excited by processes in an air-gas tract of a GTE and described as additional random entrance effects on each blade $s_{jq}(t)$. In case of not

correlated $P(t)$ and $s_{jq}(t)$ reaction of a blade on $s_{jq}(t)$ is represented additive component $r_{Sjq}(t)$ in vector of reactions by using integral (6). Let's consider also acoustical noise $B_j(t)$ directly radiated by a compressor and turbine, which model is similar (1), noise with continuous spectrum $D_j(t)$ on an exit of each stage, which is caused by turbulent phenomena and an eddy generation, and also broadband vibration of low intensity $N(t)$ from non-power elements of GTE.

Stated above has allowed to generate model of measured vibroacoustical signal $X(t)$ in the following form:

$$X(t) = \sum_{j=1}^{n} \{ \sum_{q=1}^{z_j} [r_{Pjq}(t) + r_{Sjq}(t)] + \sum_{i=1}^{n_1} Q_{ji} \sin(i\omega_p t + i z_j \omega_p t + \varphi_{j0i}) +$$
$$+ \sum_{i=1}^{n_2} B_{ji} \sin(i z_j \omega_p t + \varphi_{j0i}) + D_j(t) \} + N(t)$$

(7)

Depending on impulse response (4) or (5) model (7) reflects a state of the GTE at the absence or presence of blade crack-like damages, and it allows to research influence of a fault on behaviors of signal $X(t)$.

3. Signal processing and fault features analysis

The received model (7) is used for simulation and analysis of vibroacoustical processes which occur at the steady-state (m1) and non-steady-state (m2, m3) modes of GTE at absence and presence of small cracks in one blade of the turbine stage (the relative rigidity changing at the crack presence is considered $\vartheta=0,01;0,03;0,05;0,07;0,09$). Parameters of vibration excitation (2) at the non-steady-state modes are selected such that at least the third harmonics of excitation at increase or a decrease of rotational speed transited through a resonance region of blades. The Fig. 1 presents examples of drawings of the simulated signals.
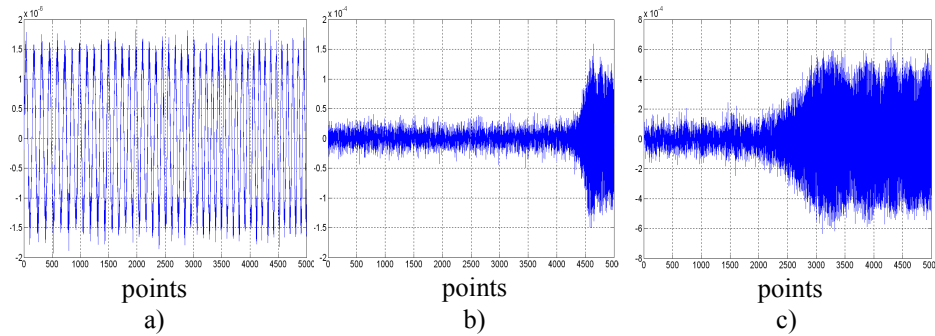
Figure 1. Examples of the simulated signals for modes m1 (a), m2 (b) and m3 (c)

Simulated signals were processed using BS, WD and DPS [2-4]. The examples of BS analysis results at the steady-state (m1) mode of GTE are shown on Fig. 2 for $\vartheta = 0$ and $\vartheta = 0,05$ at the crack presence. They are presented in a form of three-dimensional images characterizing bispectrum module dependence on frequencies f_1 and f_2.
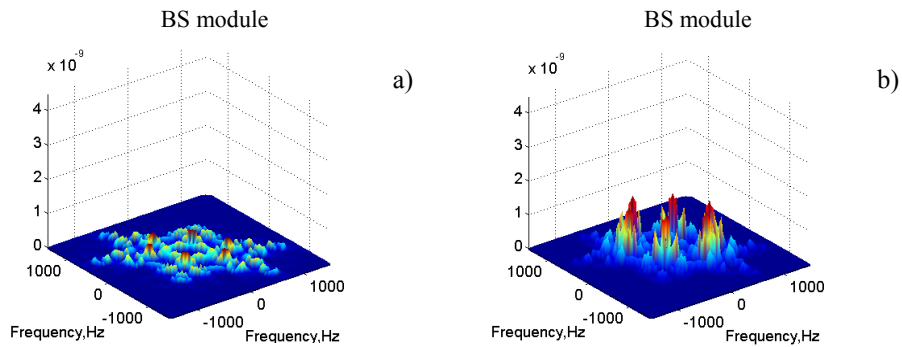
Figure 2. Examples of the BS module simulated signals for steady-state (m1) mode of GTE at the absence (a) and the presence crack (b)

As the results of diagnostic information processing demonstrate, appearance and development of a crack in the engine turbine lead to change of global and local extremum intensity of BS module estimators. We propose to use the ratio $D_{BS} = I_g / I_l$ as a fault features, where $I_{g(l)}$ is value of intensity of global (local) BS module maximum. The relationships between ϑ and D_{BS} for m1, m2 and m3 modes are illustrated in Table 1.

Table 1. Diagnostic features dependencies on a fault parameter.

ϑ	0	0,01	0,03	0,05	0,07	0,09
m1	2,10	2,23	2,55	2,82	3,02	3,30
m2	2,31	2,34	2,38	2,43	2,61	3,05
m3	1,82	1,83	1,85	1,91	1,98	2,01

The following DPC are used: J_3 - peak factor and J_4 - factor of background. The preliminary WD of signals is applied for the sensitivity increasing of DPC of the vibroacoustical signals as fault features. We used wavelets of Daubechies family db10 and 5 levels of decomposition, results are used as drawings of each level for next DPC evaluation. Fig.3 represents the values of relative speed in percents of the DPC changing (from $\vartheta = 0$ to $\vartheta = 0,05$) evaluated for initial signals and approximations (a5) and details (d1-d5) of their WD for m1 and m2 modes of GTE operation. Relative speed of the DPC changing is calculated in the following form:

$$V_r = \frac{\left|J_r - J_r^*\right|}{J_r^*} \cdot 100\% ,$$

where J_r, J_r^* are feature values at the crack presence and absence, accordingly.

| a) | b) |
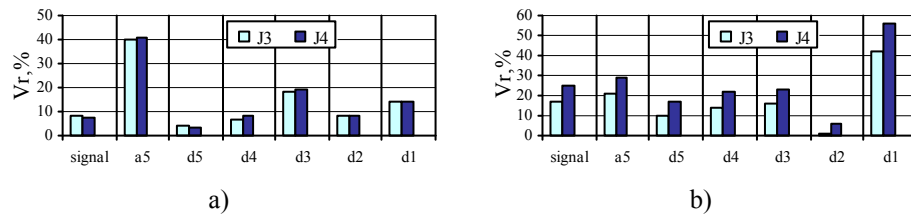
Figure 3. Relative speed of the DPC changing evaluated for signals and elements of their WD for m1(a) and m2 (b) modes of GTE

Apparently from the presented results, DPC of approximation a5 are the most sensitive fault features for a mode m1, and DPC of a detail d1 are the most sensitive fault features for a mode m2. For a mode 3 (schedules are not presented) expediently to use DPC for a detail d2, their relative speed of change makes 20%.

4. Conclusions

Developed diagnostic model of GTE allows to form the model of measured vibroacoustical signals for further simulation and analysis the influence of damages on the vibroacoustical characteristics of GTE at the steady-state and non-steady-state modes.

Application of a modern signal processing methods allows to detect fault features, which are sensitive to small crack-like damages. The received results can be used to create a vibroacoustical monitoring system for aircraft engine rotor components.

References

1. N. Bouraou, P. Marchuk, A. Tyapchenko *Condition Monitoring Diagnosis Method of Aircraft Engine Rotating Details*, In Proceedings of the 15th World Conference on Non-Destructive Testing (2000).
2. C. Cempel *Diagnostically Oriented Measures of Viroacoustical Process*, J. of Sound and Vibration, **73** (4) (1980) 547-561.
3. N. Bouraou, Yu. Sopilka, A. Protasov *The features Detection of the small rigidity faults of rotary machine elemen*, In Review of Progress in QNDE: Abstracts book (2003).
4. N. Bouraou, Yu. Sopilka, A. Protasov, O. Zazhitskiy *Decision Making of Aircraft Engine Blades on Bispectral Analysis of the Vibroacoustical Signal*, In Review of Progress in QNDE: Conference Proceedings, **24A** (2005) 760-766.

The use of genetic algorithm for identification of vibration model on the example of Bernoulli-Euler beam

Dawid CEKUS

Technical University of Częstochowa, Institute of Mechanics and Machine Design
Foundations, ul. Dąbrowskiego 73, 42-200 Częstochowa
cekus@imipkm.pcz.pl

Paweł WARYŚ

Technical University of Częstochowa, Institute of Mechanics and Machine Design
Foundations, ul. Dąbrowskiego 73, 42-200 Częstochowa
warys@imipkm.pcz.pl

Abstract

In the paper, in the discrete-continuous model, the spring constants replacing the rotational and translational restrained end of the Bernoulli-Euler beam have been identified on the basis experimental investigations and formulation of optimization problem. The mathematical model of free vibration problem of analyzed system has been formulated and solved according to the Lagrange multiplier formalism. Frequencies and mode shapes of free vibration, which have been obtained from the experimental investigations, have been used to formulate optimization problem. Optimization has been based on the genetic algorithm. The presented proceeding's stages allow identification any parameters of discrete-continuous systems.

Keywords: genetic algorithm, experimental modal analysis, free vibration, the Bernoulli-Euler beam

1. Introduction

The genetic algorithms were first developed by John Holland [1] in the early 1970s. At present the genetic algorithms [2, 3 and 4] are widely applied in a lot of field of knowledge. Their effective mechanism of searching the large space solution is the most important advantage. It allows using the genetic algorithms in optimization problems [5, 6].

In this paper the applying of the genetic algorithm, experimental modal analysis and the Lagrange multiplier formalism [7, 8] to identify the chosen parameters of discrete-continuous systems are presented. Identification of parameters has been carried out on the example of the Bernoulli-Euler beam, which has been elastically restrained at the end. This way restrained of the beam has been showed in the articles [9, 10]. Additionally in the paper [9] the concentrated mass at an arbitrary position along the beam length has been added, while in the paper [10] the translational spring at the intermediate point has been restrained.

2. Formulation of the problem

The vibration model of the uniform Bernoulli-Euler beam with discrete elements (substituting the elastically restrained end) is presented in the figure 1. The translational

restraint is characterized by spring constant K and the rotational restraint by the spring constant C.

a)   b)
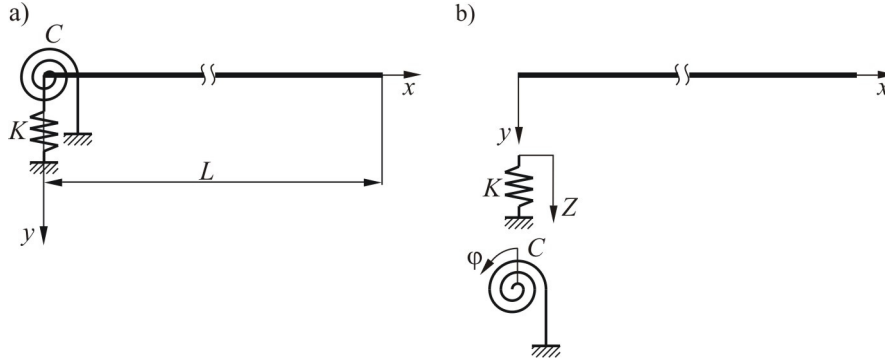
Figure 1. Scheme of the beam elastically restrained at the end: a) the whole system,
b) the separated element system

Acting on the Lagrange multiplier formalism [7, 8] the free vibration problem of analyzed system has been formulated and the solution has been reduced to matrix system of equations in the following form:

$$\begin{bmatrix} C_{1,1} + \varepsilon_1 & C_{1,2} \\ C_{2,1} & C_{2,2} + \varepsilon_2 \end{bmatrix} \begin{bmatrix} \Lambda_1 \\ \Lambda_2 \end{bmatrix} = 0 \qquad (1)$$

where Λ_1 and Λ_2 are the amplitudes of Lagrange multipliers. Coefficients $C_{k,r}$, which characterize beam to boundary conditions respectively, are described by relationship:

$$C_{k,r} = \sum_{i=0}^{N} \frac{b_{i,k} b_{i,r}}{K_i - \omega^2 M_i}, \quad i = 0,1,2,...,N, \ k = 1,2, \ r = 1,2 \qquad (2)$$

and coefficients:

$$\varepsilon_1 = \frac{1}{K}, \ \varepsilon_2 = \frac{1}{C} \qquad (3a, b)$$

characterize the type of discrete elements joining to the beam.

In the formula (2) the following relationships (according to work [8]) have been accepted:

$$K_i = \frac{EI}{L^3} k_i, \quad M_i = \rho A L m_i, \quad i = 0,1,2,...,N \qquad (4a, b)$$

where the symbols denote: ρ – density, E – the longitudinal modulus of elasticity, A – cross-sectional area, I – moment of inertia and L – length of beam, while:

$$b_{i,(k,r=1)} = Y_i(0), \ b_{i,(k,r=2)} = Y_i'(0) \qquad (5a, b)$$

represent the mode shapes of the free-free beam calculated without any influence of the other elements. Coefficients k_i and m_i occurring in formula (4a, b) can derive on the basis of dependences appearing among other things in work [8].

The equation set (1) yields the eigenvalue equation:

$$\det\begin{bmatrix} C_{1,1} + \varepsilon_1 & C_{1,2} \\ C_{2,1} & C_{2,2} + \varepsilon_2 \end{bmatrix} = 0 \qquad (6)$$

which enables one to calculate the free vibration frequency values ω_k of the system. When the values of free vibration frequency are known and on the basis of equation (1) the amplitudes of Lagrange multipliers are determined, then the mode shapes can be described with the use of following expression:

$$Y_k(x) = \sum_{i=0}^{N} \frac{\sum_{r=1}^{2} \Lambda_r(\omega_k) b_{ir}}{K_i - \omega_k^2 M_i} Y_i(x) \qquad (7)$$

3. Experimental investigations

The measurement system which has been used to the experimental investigations is presented in the figure 2. This system consists of the fixed beam (1), PC computer (2) with appropriate software, four-channel vibration analyzer (3), amplifier (4), exciter body with exciter head (5), force detector (6), one-axial piezoelectric accelerometer (7).
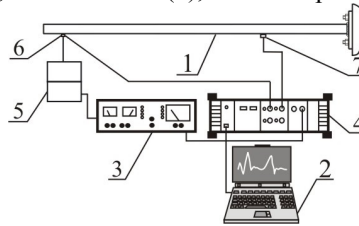
Figure 2. Scheme of the measuring set

The modal model (set of natural frequencies, coefficients of damping and modes of vibrations) of the system has been obtained as a result of the experimental investigations.

In the figure 3 first three received natural frequencies and corresponding modes of vibrations are showed.

$\omega_1 = 36.6$ Hz

$\omega_2 = 234$ Hz

$\omega_3 = 644$ Hz
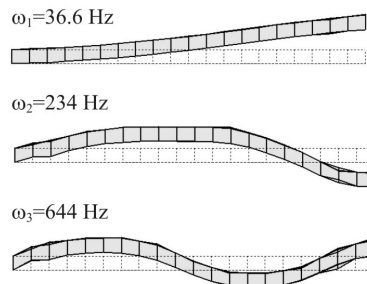
Figure 3. The experimental free vibration frequencies and the modes of the beam

4. Genetic algorithm

The looked values of spring constants substituting the elastically restrained end of beam can be determined on the basis of the derived relationships and obtained experimental free vibration frequencies. In order to formulate optimization problem the genetic algorithm has been used.

The genetic algorithm bases on the principles of genetics and natural selection and it works as follows (fig. 4): first, population of chromosomes that are solution candidates to a problem is randomly generated; then the fitness function of each chromosomes in the population is calculated; next Selection, Crossover and Mutation are repeated until a steady number of offspring will be created or the value of solution will be satisfactory.
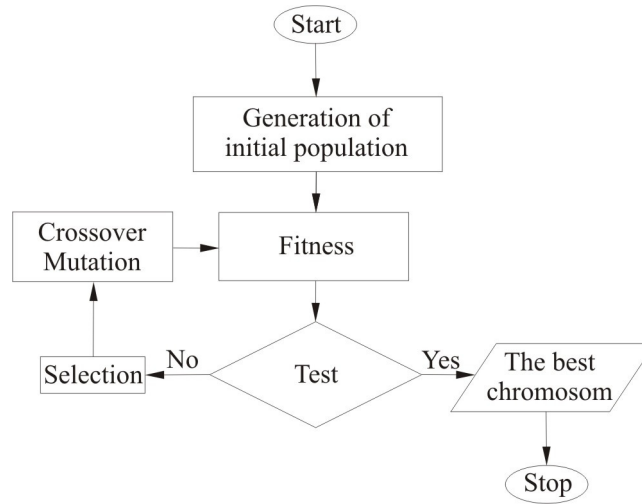
Figure 4. Simple genetic algorithm

The selection operator selects chromosomes in the population for reproduction. The fitter the chromosome, the more times it is likely to be selected to reproduce. Crossover and mutation are the reproduction operators, the former forms a new chromosome by combining parts of each of the two parental chromosomes and the latter forms a new chromosome by making alterations to the values of genes in a copy of a single parent chromosome.

In the examined case, objective function (fitness function) has been written by the formula:

$$f(K,C) = \frac{\sum\limits_{i=1}^{n} \left| \dfrac{\omega_t^{(n)} - \omega_e^{(n)}}{\omega_t^{(n)}} \right| \cdot 100\%}{n}, \ \ for \ n = 3, \tag{8}$$

which means that relative average error between theoretical and experimental frequencies is optimized.

5. Sample results

Based on the presented mathematical model, the experimental investigations and the genetic algorithm the numerical program has been worked out. This program enables to identify the spring constants K and C representing the elastically restrained end of beam.

The exemplary numerical calculations have been completed for the following data:
- the beam parameters: the length – 1 m, the dimensions of the cross section of the box shaped member: the external height and width – 0.04 m, the internal height and width – 0.036 m; the beam's material: the density – 7850 kg/m^3, the Young's modulus – $2.1 \cdot 10^{11}$ N/m^2,
- the genetic algorithm parameters: the crossover probability – 0.5, the mutational probability – 0.1, and selection has been carried out according to rank selection,
- the values of spring constants (K, C) were looked for in the range [100, $1 \cdot 10^{10}$] N/m.

On the basis of numerical calculations the spring constants modeling the elastically restrained end of beam have been amounted: $C=9.23795 \cdot 10^4$ N/m, $K=1.51182 \cdot 10^7$ N/m and the relative average error (8) between theoretical and experimental frequencies has been equal 0.23%.

In figure 5 the theoretical natural frequencies and corresponding modes of analyzed system are presented with the consideration of the determined spring constants K and C.
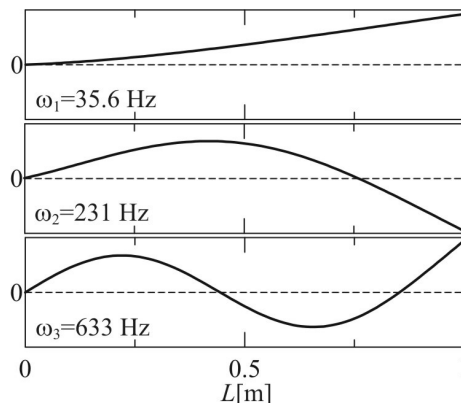
Figure 5. The theoretical free vibration frequencies and the modes of the analyzed beam

6. Summary

In this paper the use of genetic algorithm for identification of constants of discrete elements which are joined to continuous element has been presented. Identification has been carried out on the example of the Bernoulli-Euler beam which has been elastically restrained by translational and rotational springs at the end. To the formulation and solution of the problem has been used the Lagrange multiplier formalism and the experimental modal analysis, too. The mathematical formulation is completed by the exemplary numerical results.

Acknowledgments

References

1. J.H. Holland, *Adaptation in Natural and Artificial Systems*, University of Michigan Press, Ann Arbor, MI, 1975.
2. D.E. Goldberg, *Genetic Algorithms in Search, Optimization, and Machine Learning*, Addison-Wesley, Reading, MA, 1989.
3. Z. Michalewicz, *Genetic Algorithms + Data Structures = Evolution Programs*, Springer-Verlag Berlin Heidelberg New York, USA, 1996.
4. M. Mitchel, *An Introduction to Genetic Algorithms*, A Bradford Book The MIT Press, Cambridge, Massachusetts London, England, 1999.
5. P. Wang Bo, L. Chen Jahau, *Application of genetic algorithm for the support location optimization of beams*, Computer & Structures, **58** (4) (1996) 797-800.
6. R.J. Jiang, F.T.K. Au, Y.K. Cheung, *Identification of masses moving on multi-span beams based on a genetic algorithm*, Computer & Structures, **81** (2003) 2137-2148.
7. B. Posiadała, *Use of Lagrange multiplier formalism to analyze free vibration of combined dynamical systems*, Journal of Sound and Vibration, **176**(4) (1994) 563-572.
8. B. Posiadała, Modelling and analysis of continuous-discrete mechanical systems. Application of the Lagrange multiplier formalism, Wydawnictwo Politechniki Częstochowskiej, Częstochowa, 2007 (in Polish).
9. M.A. De Rosa, S. Ascoli, S. Nicastro, *Exact dynamic analysis of beam-mass system*, Journal of Sound and Vibration, **196**(4) (1996) 529-533.
10. C.M. Albarracin, L. Zannier, R.O. Grossi, *Some observations in the dynamics of beams with intermediate supports*, Journal of Sound and Vibration, **271** (2004) 475-480.

Zastosowanie algorytmu genetycznego do identyfikacji modelu drgań na przykładzie belki Bernoulliego-Eulera

W pracy na podstawie przeprowadzonych badań eksperymentalnych oraz sformułowania zadania optymalizacyjnego zidentyfikowano stałe sprężystości sprężyn rotacyjnej i translacyjnej zastępujących w modelu dyskretno-ciągłym zamocowanie jednostronne belki Bernoulliego-Eulera. Model matematyczny zagadnienia drgań swobodnych analizowanego układu został sformułowany i rozwiązany zgodnie z formalizmem mnożników Lagrange'a. Jako rezultat przeprowadzonych badań eksperymentalnych otrzymano częstości i postacie drgań własnych, które wykorzystano do sformułowania zagadnienia optymalizacyjnego. Algorytm optymalizacyjny bazował na algorytmie genetycznym. Przedstawione etapy postępowania pozwalają na identyfikację dowolnych parametrów układów dyskretno-ciągłych.

Operational excitations in experimental research into dynamics of Light Rail Vehicles

Bartosz CZECHYRA

Poznan University of Technology, ul. Piotrowo 3, 60-965 Poznań, Poland
bartosz.czechyra@put.poznan.pl

Abstract

Modern railways, as light and classic vehicles, are designed with a new construction concept/trend. Expression of this thesis is the increase of safety standards and loads/performance of vehicle elements with simultaneous reduction of the vehicle mass. The newest constructions of trains and trams have applied many parts which are made of light metal alloys, aluminium and plastic profiles, ceramic, fibber and glass. Consequently those materials have major influence on a vehicle dynamics.

This article presents a first approach of a structural dynamics of a tram body during a ride test. Author analyzed the vibration signals recorded on two different trams drive units and tram body. The vibrations are analyzed in ride safety category and human vibration exposure of operator/passenger aspect. Author presents rationales to use of ride-source vibrations as a potential excitation in OMA test technique. Paper includes a methodology of the experiment and first results from performed investigation.

Keywords: operational excitation , tram dynamics, modal test

1. Introduction

Popularity of railway transport and its revival (particularly in fast railway as well as in trams) stem from advantages of this form of relocating. It has, including but not limited to, the following advantages:
- ride safety,
- continually rising ride speed,
- possibility to travel in „City-to-City" system,
- little sensitivity to weather conditions,
- separated communication routes – minimal traffic congestion.

The last two advantages are especially important in case of trams and specific conditions of their exploitation. In recent years those vehicles have experienced a revival connected with dynamic development of cities and rising problems in individual car communication. Possibility to operate big traffic steams and little urban requirements result in dynamical development of tram market in Europe and in the world.

Classic and light rail vehicles undergo strict tests connected with investigation of construction dynamics. These tests comprise two domains:
- ride safety,
- ride comfort of passengers.

In the first case, the most commonly used criterion of assessing ride safety of a railway vehicle is Nadal's criterion, which is the ratio between transverse dynamic force and vertical dynamic force Y/Q according to UIC 518 chart [1]. Another values connected with vehicle ride on the rails are also acceptable, e.g. the sum of leading

forces affecting the rails, vertical pressure of wheels on the rails, transverse and vertical acceleration measured in selected points in the vehicle or stiffness of susceptible parts of vehicle suspension [1,2].

In case of the ride comfort investigation, parameters of ride characteristics of the vehicle or adequate dosimeter parameters according to European Union Directive 2002/44/EC may be used. Broad numeric investigations connected with dynamics of vehicle move in the rails are also carried out. The aim of these investigations is to support, describe and explain through simulation the processes connected with wheel interaction on the rail in the vibro-acoustic aspect.

In the all mentioned situations the dynamic susceptibility of the suspension as an element that has influence on safety and comfort of rail vehicle ride, is omitted.

2. Structural dynamics of a tram

In dynamic investigation of rail vehicles, because of security against derailment, particular attention is paid to cooperation between the wheel and the rail. The further step of the designer is developing a suspension system meeting the following postulates:
- safe vehicle drive in the railway track,
- fulfilling requirements of vehicle gauge,
- transfer of driving and braking forces from the body to the bogie and from the bogie to the body,
- possibly effective insulation (expansion) of vibrations transferred from the tram drive unit to the car body and further to passenger and driver seats,
- fulfilling requirements of ride comfort with assumption that the vehicle body is a stiff solid.

A bogie is a widely used solution, which constitutes a good basis for a compromise between safety and ride comfort. In case of trams, the bogie is a complicated riding structure, which enables building up two or three grades of de-springing. For the necessity of model testing of bogies,

7-mass-model with nonlinear damping is commonly accepted. Unfortunately, in detailed investigation of tram ride dynamics, such models are not precise enough [3]. That is why e.g. 19-mass-models are built, which is presented schematically in Fig.1.
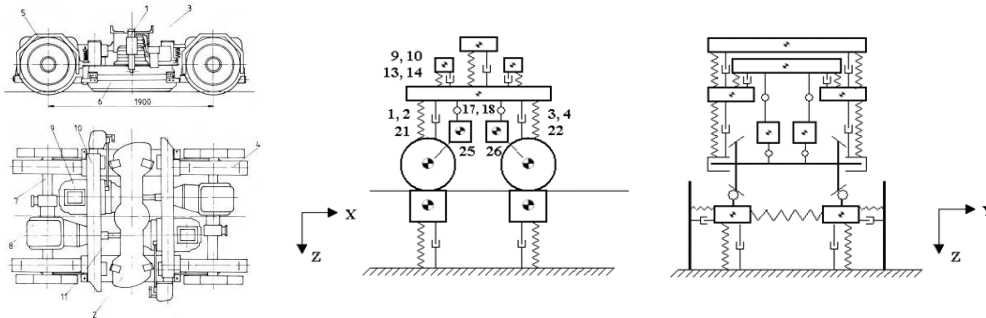
Figure 1. Scheme of tram bogie 105Na and its model [3]

With bogie models defined in the mentioned way, there is possibility to carry out broad numeric and experimental investigations to optimize construction parameters with accepted assessing criteria.

In actual constructions of the tram drive unit, full mechano-acoustic separation of the under-carriage from the tram body is not possible. A part of energy will be transferred to the vehicle body, which will excite vibrations of the vehicle construction.
It is commonly accepted that the car body constitutes a solid which joins the vehicle bogies. It has been suggested to verify this thesis. It is especially important that very often light construction materials are used for suspension elements (light metal alloy, composites). Enlarging glass surfaces and door-ways is also significant as it influences construction susceptibility to elastic deformations. Modernization of older types of trams is observed. The purpose of it is to increase their functionality without particular consideration of consequences of performed works

Transfer of excitations from the tram drive unit to the tram body results in vibro-acoustic effects affecting passengers and the tram driver. Taking into consideration structural dynamics of the tram body itself it may turn out that the mechano-acoustic susceptibility as well as global and local resonances of the tram body may significantly affect safety and ride comfort. This hypothesis be-came the basis of tram investigations in standard exploitation conditions. Cracks in top beam of the tram car resulting from dynamic interaction between vehicle and rails, serve as another argument.

3. Investigation methodology

The purpose of this experiment was to define prospects of using exploitation excitation for modal investigation of a tram car. As this investigation has a diagnosing character in the first step only a vertical excitation was taken into consideration.

The excitation from the tram drive unit is a natural excitation for a certain vehicle and exploitation conditions. As measurement of dynamic forces affecting the car body is not possible, it was decided to use techniques of OMA. The priority of the investigation is to determine frequencies characteristic for a tram in excitation frequency from the tram drive unit because global and local construction resonances may occur.

The scope of frequencies, which should be taken for the analysis, results from taking into ac-count frequencies characteristic for safety (kinematics and dynamics of a vehicle in the railway track) and ride comfort. In safety aspect a few characteristic frequencies may be defined [3,4]:

- approx. 2-20 Hz connected with basic hunting oscillation of wheel sets,
- approx. 4-10 Hz harmonics vibrations of individual bogie elements,
- approx. 20-60 Hz vibrations caused by cooperation between a wheel and a rail for wheels with elastomeric inserts.

However, in ride comfort aspect and endangering a tram driver with excessive vibrations, the scope of frequencies and their weight contribution in particular kinds of influence on human body are defined by EU Directive2002/44/EC and commonly acknowledged human vibration model [5].

Carried analyses show that it is purposeful to carry out investigations in frequency scope from min. 2 to approx. 200 Hz. Such defined band of frequencies covers with its scope, all effects that are the subject of investigation.

4. Experiment results

The investigation was carried out with two types of jointed trams (from the left side: A and B) with significant contribution of the low floor (Fig. 2).

Figure 2. Objects of comparative investigation; from the left side: type A and type B

Test rides were carried out on a classic ballast track, on the same parts of the straight track with speed limit to 40 km/h. The signal of vibration acceleration was registered on the floor inside the tram car directly over the pivot. In the investigation, vibration transducers of Brüel & Kjær type 4504A were used. Portable data acquisition unit type B&K 3560C with 17 input channels constitutes the central unit of the measurement set [6]. Because of the character of the recorded signal and assumed estimation accuracy, the signal of vibration acceleration was recorded in band 3.2 kHz.

The results of preliminary analysis are displayed in Fig. 3 and 4, where the signal time flow and its spectrum are presented. The analysis was carried out in band 2-200Hz with resolution of 0.5Hz and accuracy of amplitude estimation of 0.5dB [7].
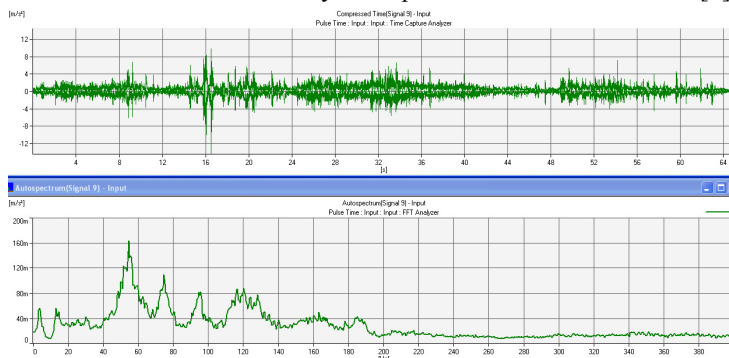
Figure 3. Signal registered in a tram type A
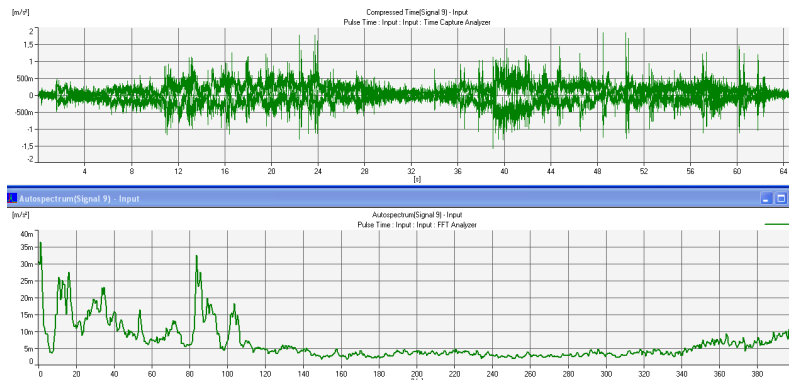
Figure 4. Signal registered in a tram type B

As it can be concluded from the presented diagrams, obtained frequency characteristics of registered signals in particular types of trams are different. For a tram type A, characteristic frequencies are explicitly exposed in amplitude spectrum (Fig.3.) of 54,5Hz, 74.5Hz and 95.5Hz. At the same time attention is drawn to amplitude rising of the signal in band from 110 to 130Hz. For a tram type B characteristic and dominant spectra are 2.5Hz and 84Hz.

Analyzing the distribution of vibration energy of registered signals, it was observed that for a tram type B vibration energy is comprised in band 2.5 to 110Hz, whereas for a tram type A, vibro-acoustic activity is shifted to higher frequencies 14-190Hz. This may stem from the fact that a tram type B has a more elastic structure and more modern set of the suspension over four times lowering the level of registered vibrations in comparison to type A (respectively for type B and A: 178mm/s^2 and 813mm/s^2 on the investigated part of the railway track).

5. Conclusion

Presented investigation results have cognitive character and refer to prospects of using the test ride in investigations of structural dynamics of a tram car.

This article presents the genesis of the subject and analyses referring to methodology assumptions of the experiment. The effects connected with tram move and influencing vibration generation were systematized. The author suggested accepting a scope of frequencies for the analysis in safety aspect and ride comfort aspect. Preliminary investigation results of two types of joint trams confirmed that the assumed analysis band was correct. At the same time possible origin of changes in amplitude structure of spectra of recorded signals was indicated.

The further step in the investigation of prospects of using the ride test for structure modal analysis will be an analysis in three directions.

References

1. UIC Chart 518 Testing and approval of railway vehicles from the point of view of their dynamic behavior – Safety – Track fatigue – Ride quality. 2003
2. A. Chudzikiewicz, *Elementy diagnostyki pojazdów szynowych*. Biblioteka Problemów Eksploatacji, Warszawa – Radom 2002.
3. B. Firlik, Light *Rail Vehicle Running Safety Analysis on a Worn Track Profile*, I[st] International Interdisciplinary Technical Conference of Young Scientists InterTech'2008, 17-18.04.2008 Poznan.
4. B. Czechyra, B. Firlik, F. Tomaszewski, *Technical state monitoring method of light rail track wear*, Proceedings of the Fourth European Workshop on Structural Health Monitoring 2008, Edited by: UHL, OSTROWSKI, HOLNICKI-SZULC; DEStrech Publications, Inc., 439 North Duke Street Lancaster, Pennsylvania 17602 USA; page 167-174; ISBN 978-1-932078-94-7
5. E. Aflalo, *Human Vibration European directive 2002/44/EC and a new human vibration analysis tool for field measurements of vibration doses*. Brüel & Kjær University Seminar, Naerum Denmark 2007
6. www.bksv.com
7. R.B. Randall, Frequency Analysis. Brüel & Kjær, Denmark 1987

Wymuszenie eksploatacyjne w eksperymentalnych badaniach dynamiki lekkich pojazdów szynowych

Nowoczesne pojazdy szynowe, tak lekkie jak i klasyczne, podlegają najnowszym tendencjom panującym w projektowaniu i konstruowaniu pojazdów. Wyrazem tego jest maksymalizowanie współczynnika wysilenia konstrukcji, co przekłada się na obniżanie masy własnej pojazdu. Coraz częściej do budowy pojazdów wykorzystuje się materiały ze stopów metali lekkich, szkła oraz kompozytów. Rodzaj użytych materiałów ma jednak bezpośredni wpływ na własności dynamiczne konstrukcji pojazdów.

W artykule przedstawiono koncepcję wykorzystania wymuszenia eksploatacyjnego tramwaju w badaniach dynamiki strukturalnej jego pudła. Przeanalizowano możliwości i ograniczenia w metodologii estymacji własności modalnych pojazdu z wykorzystaniem techniki Operacyjnej Analizy Modalnej w zastosowaniu do pudła tramwaju.

Numerical methods for vibration analysis of Timoshenko beam subjected to inertial moving load

Bartłomiej DYNIEWICZ

Institute of Fundamental Technological Research, Polish Academy of Sciences,
Pawińskiego 5b, 02-106 Warsaw, Poland
bdynie@ippt.gov.pl

Czesław I. BAJER

Institute of Fundamental Technological Research, Polish Academy of Sciences,
Pawińskiego 5b, 02-106 Warsaw, Poland
cbajer@ippt.gov.pl

Abstract

The paper deals with the problem of modeling of the moving mass particle in numerical computation by using the finite element method in one dimensional wave problems in which both the displacement and angle of the pure bending are described by linear shape functions. The analysis is based on the Timoshenko beam theory. We consider the simply supported beam, in a range of small deflections with zero initial conditions.

Keywords: numerical method, moving mass, moving inertial load, vibrations

1. Introduction

Rail and road transport development needs a closer understanding of phenomena accompanying travelling load. Most applications can be found in the interaction between railway wheels and rail or track, the effect of a moving vehicle on a bridge, interaction between rail power collector and traction power network, as well as magnetic rail, aerospace technology, automotive industry, and robotics. Despite of the wide interest in moving loads for more than a century, still many issues remain unresolved. In the case of non-inertial loads, for example the gravitational force or forces described by harmonic functions, complete analytical solutions in the series are known [1, 2]. Solutions differ in the case of inertial loads. A moving inertial load problem can not be solved fully analyticaly, except special cases such as the massless string [3]. There are semi-analytical solutions [4, 5, 6] which take into account the influence of a mass particle moving along the structure.
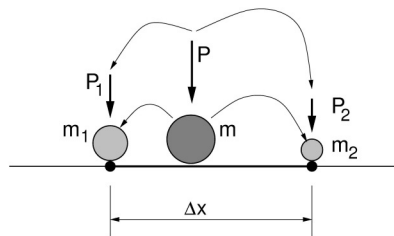
Figure 1. Ad hoc mass lumping in nodes

Modelling of the moving forces does not take into account the inertia of a moving point and is relatively simple. In practice it reduces to the modification of the right-hand-side vector at each time step. Inclusion of the inertia of a moving load requires the modification of the inertia, damping and stiffness matrices at every time step. A simple modification of the diagonal of the inertia matrix (Fig.1) is incorrect and results in divergence of the solution. Errors, due to incorrect modeling, increase with increasing speed of a moving inertial load. According to the Renaudot formula [7] the acceleration of the material point moving with a constant speed *v*, is composed of three elements:

$$\frac{\mathrm{d}^2 w(vt, t)}{\mathrm{d}t^2} = \left. \frac{\partial^2 w(x, t)}{\partial t^2} \right|_{x=vt} + 2v \left. \frac{\partial^2 w(x, t)}{\partial x \mathrm{d}t} \right|_{x=vt} + v^2 \left. \frac{\partial^2 w(x, t)}{\partial x^2} \right|_{x=vt} . \quad (1)$$

We can show the components corresponding to transverse acceleration, Coriolis acceleration and centrifugal acceleration.

There are numerous publications on numerical modelling of inertial moving load using the finite element method [8, 9, 10]. In most of them displacements and rotations are approximated as cubic functions. They can be applied to all the terms of the equation (1). In the case of wave problems in a string or the Timoshenko beam we have to use linear shape functions to describe independently displacements and rotations in pure bending. It entails mathematical consequences. We can not compute the second derivative of the displacement *x*. In such a case we should have to neglect the effect of centrifugal acceleration of the moving material point in the formula (1). It leads to incorrect solution.

Below we present recent results which enables us to solve the problem of a moving mass travelling on the Timoshenko beam with an arbitrary velocity. Numerical examples prove the efficiency of the proposed method.

2. Timoshenko beam theory

Let us consider the Timoshenko beam with the length *l*, mass density ρ, cross-sectional area *A* and moment of inertia *I*, subjected to the mass particle *m* accompanied by the force *P*, moving with the constant speed *v*. Denoting the transverse displacement by *w(x,t)* and the pure bending angles by *ψ(x,t)*, the kinetic energy of the Timoshenko beam and moving material point with mass *m* is expressed by the equation

$$T = \frac{1}{2}\rho A \int_0^l \left[\frac{\partial w(x,t)}{\partial t} \right]^2 \mathrm{d}x + \frac{1}{2}\rho I \int_0^l \left[\frac{\partial \psi(x,t)}{\partial t} \right]^2 \mathrm{d}x + \frac{1}{2}mv^2 + \frac{1}{2} m \left[\frac{\mathrm{d}w(vt,t)}{\mathrm{d}t} \right]^2 .$$

$$(2)$$

The potential energy of the Timoshenko beam and a moving gravitational force is described as follows

$$U = \frac{1}{2}EI \int_0^l \left[\frac{\partial \psi(x,t)}{\partial x} \right]^2 \mathrm{d}x + \frac{1}{2} \frac{GA}{k} \int_0^l \left[\frac{\partial w(x,t)}{\partial x} - \psi(x,t) \right]^2 \mathrm{d}x - Pw(vt,t) .$$

$$(3)$$

E is the elastic modulus, G is the shear modulus and k is the cross-section shape ratio. Based on the second kind Lagrange equation, we determine two coupled equations describing the motion of the Timoshenko beam subjected to a moving load

$$\begin{cases} \rho A \frac{\partial^2 w(x,t)}{\partial t^2} - \frac{GA}{k}\left(\frac{\partial^2 w(x,t)}{\partial x^2} - \frac{\partial \psi(x,t)}{\partial x}\right) = \delta(x - vt)P - \delta(x - vt)m\frac{\mathrm{d}^2 w(vt,t)}{\mathrm{d}t^2}, \\ \rho I \frac{\partial^2 \psi(x,t)}{\partial t^2} - EI\frac{\partial^2 \psi(x,t)}{\partial x^2} - \frac{GA}{k}\left(\frac{\partial w(x,t)}{\partial x} - \psi(x,t)\right) = 0 \ . \end{cases}$$

(4)

The equations (4) can be transformed into one equation of motion. It depends only on displacements or rotations. Let us consider displacements first

$$\frac{\partial^4 w(x,t)}{\partial t^4} - \left(c_1^2 + c_2^2\right)\frac{\partial^4 w(x,t)}{\partial x^2 \partial t^2} + \frac{A}{I}c_1^2\frac{\partial^2 w(x,t)}{\partial t^2} + c_1^2 c_2^2\frac{\partial^4 w(x,t)}{\partial x^4} =$$
$$= c_1^2 c_2^2 q(x,t) - \frac{c_2^2}{\rho A}\frac{\partial^2 q(x,t)}{\partial x^2} + \frac{1}{\rho A}\frac{\partial^2 q(x,t)}{\partial t^2} \ ,$$

(5)

where the external load is given by the formula

$$q(x,t) = \delta(x - vt)P - \delta(x - vt)m\frac{\mathrm{d}^2 w(vt,t)}{\mathrm{d}t^2} \ . \tag{6}$$

$c_1 = \sqrt{G/(k\rho)}$ is the shear wave speed and $c_1 = \sqrt{E/\rho}$ is the bending wave speed. We assume a simply supported beam

$$w(0,t) = 0, \quad w(l,t) = 0, \quad \left.\frac{\partial^2 w(x,t)}{\partial x^2}\right|_{x=0} = 0, \quad \left.\frac{\partial^2 w(x,t)}{\partial x^2}\right|_{x=l} = 0, \tag{7}$$

with zero initial conditions

$$w(x,0) = 0, \quad \left.\frac{\partial w(x,t)}{\partial t}\right|_{t=0} = 0 \ . \tag{8}$$

Equation (5) is a partial differential equation of the fourth order with respect to time. Its solution requires additional initial conditions

$$\left.\frac{\partial^2 w(x,t)}{\partial t^2}\right|_{t=0} = \frac{1}{\rho A}q(x,0), \quad \left.\frac{\partial^3 w(x,t)}{\partial t^3}\right|_{t=0} = \frac{1}{\rho A}\left.\frac{\partial q(x,t)}{\partial t}\right|_{t=0} \ . \tag{9}$$

3. Semi-analytical solution

We can develop displacements of the beam into the sine Fourier series in a finite interval, which fulfil boundary conditions (7)

$$w(x,t) = \sum_{i=1}^{n} Q_i(t)\sin\frac{i\pi x}{l} \ . \tag{10}$$

By substituting the series (10) to the equation (5) we obtain a set of ordinary differential equations of the form

$$\mathbf{\Gamma} \begin{bmatrix} \dddot{Q}_1(t) \\ \dddot{Q}_2(t) \\ \vdots \\ \dddot{Q}_n(t) \end{bmatrix} + \mathbf{U} \begin{bmatrix} \dddot{Q}_1(t) \\ \dddot{Q}_2(t) \\ \vdots \\ \dddot{Q}_n(t) \end{bmatrix} + \mathbf{M} \begin{bmatrix} \ddot{Q}_1(t) \\ \ddot{Q}_2(t) \\ \vdots \\ \ddot{Q}_n(t) \end{bmatrix} + \mathbf{C} \begin{bmatrix} \dot{Q}_1(t) \\ \dot{Q}_2(t) \\ \vdots \\ \dot{Q}_n(t) \end{bmatrix} + \mathbf{K} \begin{bmatrix} Q_1(t) \\ Q_2(t) \\ \vdots \\ Q_n(t) \end{bmatrix} = \mathbf{P} . \quad (11)$$

This method lead us to the system of differential equation of variable coefficients (11) solved by the Runge-Kutta 4 order method. We compute numerically the vector $\mathbf{Q}$ and then insert it to the resulting series (10).

4. Numerical solution by the finite element method

Let us consider the finite element of the length b of the Timoshenko beam. The element carries the inertial particle of the mass m, travelling with a constant velocity v. The equation of the virtual work which describes the influence of the inertial particle can be written in the following form

$$\int_0^b w^*(x)\delta(x - x_0 - vt)\, m\, \frac{\mathrm{d}^2 w(vt, t)}{\mathrm{d}t^2} \mathrm{d}x = 0 . \quad (12)$$

We impose the linear shape function describing the transversal displacement in finite element nodes

$$w(x, t) = \left(1 - \frac{x}{b}\right) w_1(t) + \frac{x}{b} w_2(t) . \quad (13)$$

Equation (1) describes the acceleration of a moving material point. It can be expressed in the form

$$\frac{\mathrm{d}^2 w(vt, t)}{\mathrm{d}t^2} = \left.\frac{\partial^2 w(x, t)}{\partial t^2}\right|_{x=vt} + v \left.\frac{\partial^2 w(x, t)}{\partial x \partial t}\right|_{x=vt} + v \frac{\mathrm{d}}{\mathrm{d}t}\left[\left.\frac{\partial w(x, t)}{\partial x}\right|_{x=vt}\right] . \quad (14)$$

The third term of (14) is developed into the Taylor series in terms of the time increment $\Delta t = h$

$$\left[\left.\frac{\partial w(x, t)}{\partial x}\right|_{x=vt}\right]^{t+h} = \left[\left.\frac{\partial w(x, t)}{\partial x}\right|_{x=vt}\right]^t + \left\{\frac{\mathrm{d}}{\mathrm{d}t}\left[\left.\frac{\partial w(x, t)}{\partial x}\right|_{x=vt}\right]\right\}^t (1 - \alpha)\, h +$$

$$+ \left\{\frac{\mathrm{d}}{\mathrm{d}t}\left[\left.\frac{\partial w(x, t)}{\partial x}\right|_{x=vt}\right]\right\}^{t+h} \alpha h. \quad (15)$$

Upper indices indicate time in which respective terms are defined. We assume the backward difference formula $(\alpha = 1)$. In this case we have

$$\left\{\frac{\mathrm{d}}{\mathrm{d}t}\left[\left.\frac{\partial u(x, t)}{\partial x}\right|_{x=vt}\right]\right\}^{t+h} = \frac{1}{h}\left[\left.\frac{\partial u(x, t)}{\partial x}\right|_{x=vt}\right]^{t+h} - \frac{1}{h}\left[\left.\frac{\partial u(x, t)}{\partial x}\right|_{x=vt}\right]^t . \quad (16)$$

The energy (12), with respect to (14) and (16) allows us to write the results in the matrix equation, after classical minimisation

$$\mathbf{M}_m \ddot{\mathbf{w}}^{i+1} + \mathbf{C}_m \dot{\mathbf{w}}^{i+1} + \mathbf{K}_m \mathbf{w}^{i+1} = \mathbf{e}_m^i \ . \tag{17}$$

where

$$\mathbf{M}_m = m \begin{bmatrix} (1-\kappa)^2 & \kappa(1-\kappa) \\ \kappa(1-\kappa) & \kappa^2 \end{bmatrix} \ , \quad \mathbf{C}_m = \frac{mv}{b} \begin{bmatrix} -(1-\kappa) & 1-\kappa \\ -\kappa & \kappa \end{bmatrix} \ ,$$

$$\mathbf{K}_m = \frac{mv}{bh} \begin{bmatrix} -(1-\kappa) & 1-\kappa \\ -\kappa & \kappa \end{bmatrix} \quad \mathbf{e}_m = \frac{mv}{bh} \begin{bmatrix} (1-\kappa)(u_2 - u_1) \\ \kappa(u_2 - u_1) \end{bmatrix} \ , \tag{18}$$

with the coefficient $\kappa = (x_0 + vh)/b$, $0 < \kappa \le 1$. It determines the force equilibrium of the mass travelling over the finite element of a Timoshenko beam. Matrix factors $\mathbf{M}_m$, $\mathbf{C}_m$ and $\mathbf{K}_m$ can be called mass, damping, and stiffness matrices, since they have similar forms to matrices derived for pure finite element of the Timoshenko beam. The last term $\mathbf{e}_m$ describes nodal forces at the beginning of the time interval [0; h]. We must emphasise here that matrices (18) and the vector $\mathbf{e}$ contribute only the moving inertial particle effect. Pure classical matrices of the finite element of a string must be added to the global system of equations.

5. Examples

We choose the steel beam of the rectangular cross-section A=0.015 m^2 and the length l=2 m. We assume other data: ρ=7860 kg/m^3, I=0.0000281 m^4, m=200 kg, P=mg, g=9.81 m/s^2, E=2.1·10^5 MPa, G=8.1·10^4 MPa, k=1.2. Fig.2 shows a comparison of the results obtained by semi-analytical method presented earlier, and the finite element method using matrices describing the moving material point of mass m. The obtained results confirm the correct way of modelling a moving mass particle.
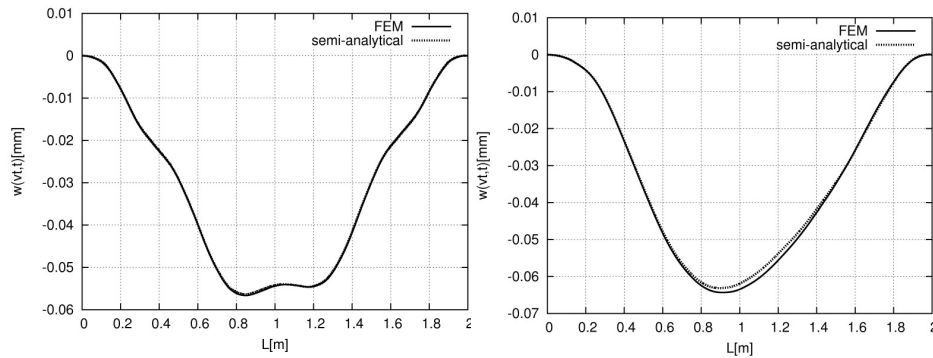
Figure 2. Trajectories of a mass particle travelling along the Timoshenko beam
at the speed $v = 30 \, m/s$ (left picture) and $v = 60 \, m/s$ (right picture)

6. Conclusions

The paper deals with the problem of vibrations of the Timoshenko beam subjected to a moving inertial particle. The presented approach allows accurate modeling of a mass particle travelling with a constant velocity in numerical computation by using finite element method. These matrices can be applied to every wave problem, where the displacement and rotations of the pure bending are described by linear shape functions.

References

1. L. Frỳba. *Vibrations of solids and structures under moving loads*. Thomas Telford House, 1999.
2. W. Szcześniak. *Inertial moving loads on beams* (in Polish). Scientific Reports, Warsaw University of Technology, Civil Engineering **112**, 1990.
3. C.E. Smith. *Motion of a stretched string carrying a moving mass particle*. J. Appl. Mech., **31**(1)(1964) 29-37.
4. B. Dyniewicz and C.I. Bajer. *Paradox of the particle's trajectory moving on a string*. Arch. Appl. Mech., **79**(3)(2009) 213-223.
5. E.C. Ting, J. Genin and J.H. Ginsberg. *A general algorithm for moving mass problems*. J. Sound Vib., **33**(1)(1974) 49-58.
6. G.T. Michaltsos. *Dynamic behaviour of a single-span beam subjected to loads moving with variable speeds*. J. Sound Vibr., **258**(2)(2002) 359-372.
7. A. Renaudot. *Etude de l'influence des charges en mouvement sur la resistance, des ponts metallique a poutres droites*. Annales des Ponts et Chausses, **1**(1861) 145-204.
8. C.I. Bajer and B. Dyniewicz. *Numerical modelling of structure vibrations under inertial moving load*. Arch. Appl. Mech., **79**(6-7)(2009) 499-508.
9. F.V. Filho. *Finite element analysis of structures under moving loads*. The Shock and Vibration Digest, **10**(8)(1978) 27-35.
10. T. Borowicz. *Strength of beams under moving load* (in Polish). Archives of Civil Engineering, **24**(2)(1978) 219-235.

Metody numeryczne analizy drgań belki Timoshenki pod inercyjnym obciążeniem ruchomym

Praca omawia problem modelowania numerycznego poruszającej się cząstki masowej metodą elementów skończonych w zadaniu jednowymiarowym. Przemieszczenia i obroty opisano liniowymi funkcjami kształtu. Analizę oparto na teorii belki Timoshenki.

A discrete elastic-dissipative system as a model of a rope

Paweł FRITZKOWSKI
Institute of Applied Mechanics, Poznan University of Technology
Piotrowo 3, 60-965 Poznan, Poland
pawel.fritzkowski@gmail.com

Henryk KAMIŃSKI
Institute of Applied Mechanics, Poznan University of Technology
Piotrowo 3, 60-965 Poznan, Poland
henryk.kaminski@put.poznan.pl

Abstract

Motion of a hanging rope is considered and a discrete model of the body is discussed. The system consists of identical members which are connected by rotational joints. Various character of both the elements and joints is considered, and equations of motion are presented. Consequently, there are several options: an extensible or non-extensible model, whose joints are ideal, elastic, dissipative or elastic-dissipative. Nevertheless, a concise generalized mathematical model is presented which is suitable for all the variants.

Keywords: rope, modelling, elastic-dissipative joints

1. Introduction

Already in 19th century D. Bernoulli (1732) and Euler (1781) considered and solved the problem of small vibrations of a perfectly flexible, uniform rope which is fixed at one end [1]. However, even now it is a non-trivial task to mathematically describe motion of the rope in a general case and to perform computer simulations of such a phenomenon.

Usually research on dynamics of such bodies as ropes, chains, whips or fly lines involves continuous models [5, 6, 7]. Although the approach seems to be very natural, we consider a discrete model of the rope. The main advantage of this conception is relatively simple description of the problem by means of analytical mechanics. On the basis of the works [1, 2, 3, 4] we present equations of motion of the system and concentrate on the included features: longitudinal elasticity, transverse elasticity and damping.

2. Basic mathematical models

Let us consider planar motion of a discrete system consisting of n identical members that are connected by rotational joints. One end of the body is attached to a point P_0. Generally, we treat the point as non-stationary, so that its position is specified by the pair of time dependent functions: $x_0 = x_0(t)$, $y_0 = y_0(t)$. The motion takes place in a gravitational field, but air resistance is neglected.

The simplest model of the rope can be represented by a multiple physical pendulum [1], which is shown in Fig. 1a. It is assumed that every element is a rigid prismatic rod of length l and mass m, the joints, in turn, are ideal (frictionless). Using the

angular generalized coordinates φ_i ($i=1, 2, \ldots, n$), one can derive the following equations of motion:

$$\sum_{j=1}^{n} a_{ij} \ddot{\varphi}_j \cos(\varphi_i - \varphi_j) + \sum_{j=1}^{n} a_{ij} \dot{\varphi}_j^2 \sin(\varphi_i - \varphi_j) + \frac{b_i}{l} \left(g \sin \varphi_i + \ddot{x}_0 \cos \varphi_i - \ddot{y}_0 \sin \varphi_i \right) = 0 , \quad (1)$$

where $i=1, 2, \ldots, n$ and the coefficients a_{ij}, $b_i \in \Re$.

This system is modified in paper [2] by a simple longitudinal elasticity conception. As in Fig. 1b, each of the rods is attached to a linear spring, thus, every segment has two parts with a common longitudinal axis. The springs are assumed to be identical – their free length is denoted by l_s and stiffness by k_L. If we introduce the additional variables z_i ($i=1, 2, \ldots, n$) expressing elongations of the springs, then the mathematical model takes the form:

$$\begin{cases} \displaystyle\sum_{j=1}^{n} A_{ij}^{\varphi} \ddot{\varphi}_j \cos(\varphi_i - \varphi_j) - \frac{1}{l} \sum_{j=1}^{n} B_{ij}^{\varphi} \ddot{z}_j \sin(\varphi_i - \varphi_j) + \sum_{j=1}^{n} A_{ij}^{\varphi} \dot{\varphi}_j^2 \sin(\varphi_i - \varphi_j) + \\[2mm] + \displaystyle\frac{2}{l} \sum_{j=1}^{n} B_{ij}^{\varphi} \dot{\varphi}_j \dot{z}_j \cos(\varphi_i - \varphi_j) + \frac{1}{l} B_{ii}^{\varphi} \left(g \sin \varphi_i + \ddot{x}_0 \cos \varphi_i - \ddot{y}_0 \sin \varphi_i \right) = 0, \\[3mm] \displaystyle\sum_{j=1}^{n} A_{ij}^{z} \ddot{\varphi}_j \sin(\varphi_i - \varphi_j) + \frac{1}{l} \sum_{j=1}^{n} B_{ij}^{z} \ddot{z}_j \cos(\varphi_i - \varphi_j) - \sum_{j=1}^{n} A_{ij}^{z} \dot{\varphi}_j^2 \cos(\varphi_i - \varphi_j) + \\[2mm] + \displaystyle\frac{2}{l} \sum_{j=1}^{n} B_{ij}^{z} \dot{\varphi}_j \dot{z}_j \sin(\varphi_i - \varphi_j) + \frac{1}{l} B_{ii}^{z} \left(-g \cos \varphi_i + \ddot{x}_0 \sin \varphi_i + \ddot{y}_0 \cos \varphi_i \right) + \frac{k_L z_i}{ml} = 0, \end{cases} \quad (2)$$

where $i=1, 2, \ldots, n$ and A_{ij}^{φ}, B_{ij}^{φ}, A_{ij}^{z}, $B_{ij}^{z} \in \Re$.
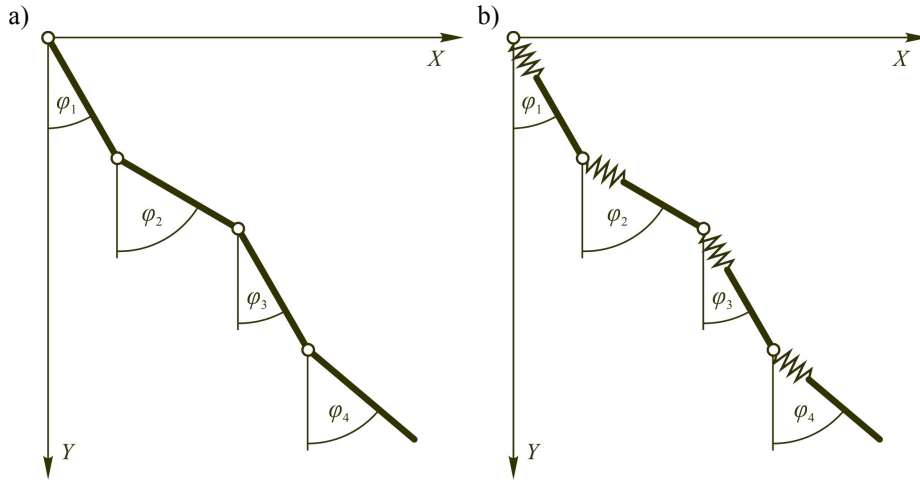
Figure 1. Basic models of a rope: a) model of an inelastic rope, b) model of an extensible rope

3. Elastic-dissipative joints

It should be noted that the ideal joints enable to bend the rope freely, which is far from its real behaviour. Hence, we try to modify the character of the joints within the discrete approach.

Let us recall the bending stiffness idea discussed in [3]. Schematically, every joint is enriched with a torsional spring whose constant is denoted by k_T (see Fig. 2). To determine a characteristics of the springs, we consider a fragment of the rope shown in Fig. 3. According to the classical formula:

$$\frac{1}{r} = \frac{M}{K} , \tag{3}$$

where M is the bending moment and K is the flexural rigidity of a beam. Moreover, the radius of a plane curve parameterized by the functions $x(s)$ and $y(s)$ may be expressed as

$$r = \frac{\left(x'^2 + y'^2\right)^{3/2}}{x'\,y'' - x''\,y'} , \tag{4}$$

where:

$$x' = \frac{dx}{ds}, \quad y' = \frac{dy}{ds}, \quad x'' = \frac{d^2 x}{ds^2}, \quad y'' = \frac{d^2 y}{ds^2} . \tag{5}$$
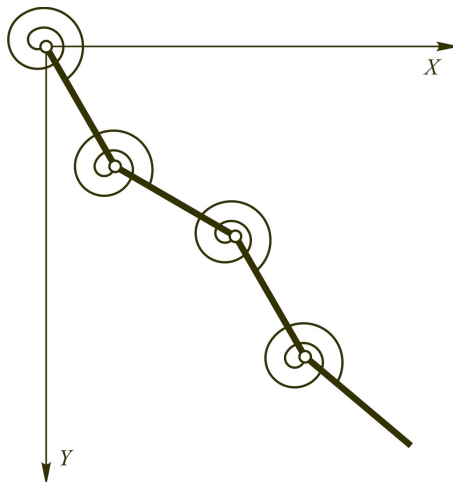
Figure 2. Model of a rope with elastic joints

If we assume that s is the curvilinear coordinate along the rope, it is easy to approximate the above derivatives by central difference schemes, which are based on the discrete representation of the rope. Consequently, one can obtain

$$r_i = -\frac{1}{2} l \cos \frac{\theta_i}{2} \operatorname{ctg} \frac{\theta_i}{2} , \tag{6}$$
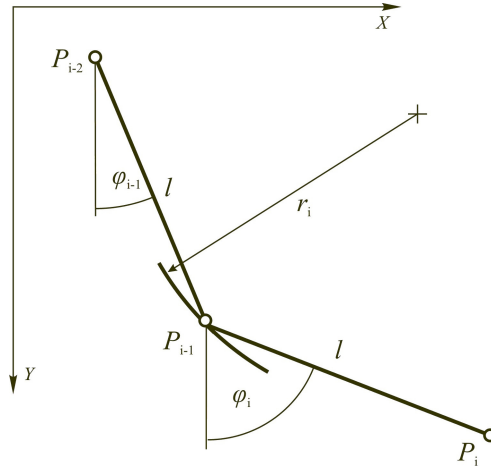
Figure 3. Fragment of a rope

where θ_i denotes the relative generalized coordinate:

$$\theta_i = \begin{cases} \varphi_i & \text{for } i = 1 \\ \varphi_i - \varphi_{i-1} & \text{for } i = 2, 3, \ldots, n \end{cases} \tag{7}$$

Finally, inserting (6) into (3) gives

$$M_i = \frac{K}{r_i} = -\frac{2k_T}{l} \frac{\text{tg}(\theta_i / 2)}{\cos(\theta_i / 2)}. \tag{8}$$

As it can be seen in Fig. 4, the nonlinear characteristics of the springs is specific – as the relative coordinate θ tends to $\pm\pi$, value of the elastic moment M increases infinitely.
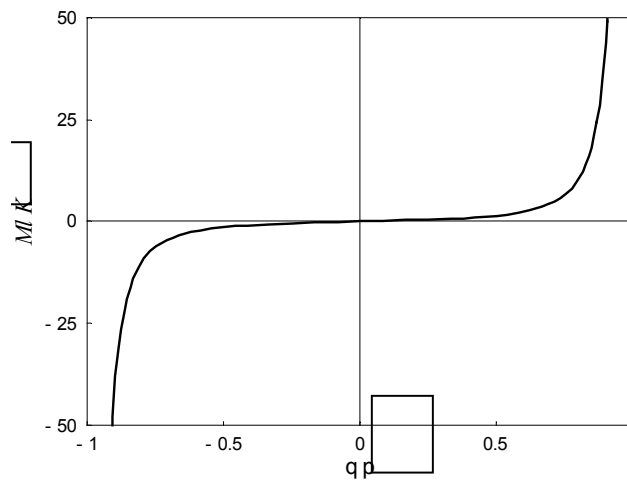
Figure 4. Characteristics of the springs

Since the formulas (6) and (8) have been derived for the model of inelastic rope (1), let us consider the other case. A length of the ith segment, consisting of a rod and spring, can be denoted by $l_i = l_0 + z_i$, where the component $l_0 = l + l_s$ is constant. Assuming that $z_i/l_0 \ll 1$ for $i = 1, 2, \ldots, n$, each of the products $z_i z_j$ for $i, j = 1, 2, \ldots, n$ can be treated as negligible. Then (6) and (8) take the forms:

$$r_i = -\frac{1}{2}\sqrt{l_0(\Delta l_i + l_0)} \cos\frac{\theta_i}{2} \operatorname{ctg}\frac{\theta_i}{2}, \tag{9}$$

$$M_i = -\frac{2k_T}{\sqrt{l_0(\Delta l_i + l_0)}} \frac{\operatorname{tg}(\theta_i/2)}{\cos(\theta_i/2)}, \tag{10}$$

where:

$$\Delta l_i = \begin{cases} z_i & \text{for } i = 1 \\ z_{i-1} + z_i & \text{for } i = 2, 3, \ldots, n \end{cases} \tag{11}$$

In case of both the systems shown in Fig. 1, the generalized elastic forces can be written as follows:

$$Q_i^T = \begin{cases} M_i - M_{i+1} & \text{for } i = 1, 2, \ldots, n-1 \\ M_i & \text{for } i = n \end{cases} \tag{12}$$

At last, let us introduce dissipation into the mathematical description. In this work we apply simply the viscous damping model [4]. Beside the torsional spring, we can place a damper in every joint. Denoting a damping coefficient by c, one can specify the Rayleigh dissipation function as

$$R = \frac{1}{2}c\sum_{i=1}^{n}\dot{\theta}_i^2. \tag{13}$$

Hence, the generalized dissipative forces have the form:

$$Q_i^D = -\frac{\partial R}{\partial \dot{\varphi}_i} = \begin{cases} c\left(\dot{\theta}_{i+1} - \dot{\theta}_i\right) & \text{for } i = 1, 2, \ldots, n\text{-}1 \\ -c\dot{\theta}_i & \text{for } i = n \end{cases} \tag{14}$$

A combination of the forces (12) and (14) produces elastic-dissipative joints.

Typically for the Lagrange equations, it is easy to introduce Q_i^T and/or Q_i^D to the model (1) and (2). Thus, the generalized forces can be put in the right-hand side of the equations related to the rotational degrees of freedom. For instance, a model of an inextensible rope with the elastic-dissipative joints has the form:

$$\sum_{j=1}^{n} a_{ij}\ddot{\varphi}_j \cos(\varphi_i - \varphi_j) + \sum_{j=1}^{n} a_{ij}\dot{\varphi}_j^2 \sin(\varphi_i - \varphi_j) + \frac{b_i}{l}\left(g\sin\varphi_i + \ddot{x}_0\cos\varphi_i - \ddot{y}_0\sin\varphi_i\right) =$$
$$= \frac{1}{ml^2}\left(Q_i^T + Q_i^D\right), \qquad i = 1, 2, \ldots, n. \tag{15}$$

4. Generalized mathematical model

In a general case, a system of the dynamics equations can be written as follows:

$$\mathbf{M}(\mathbf{q})\ddot{\mathbf{q}} = \mathbf{f}(t, \mathbf{q}, \dot{\mathbf{q}}), \tag{16}$$

where **q** denotes the generalized coordinates vector. Obviously, the following initial conditions must be satisfied:

$$\mathbf{q}(0) = \mathbf{q}_0, \quad \dot{\mathbf{q}}(0) = \mathbf{u}_0 \tag{17}$$

It should be emphasized that, in the given problem, **M** is a full, non-symmetric and time-dependent matrix, which complicates solution procedures in a numerical sense.

3. Conclusions

The presented mathematical model is suitable for all various combinations of the discussed model properties. It allows to generalize consideration on numerical integration of the dynamics equations. Moreover, many simulations based on this model provide interesting results [1, 2, 3, 4], however, their presentation is beyond the scope of this work.

The elastic-dissipative joints seem to be useful in modelling other multi-body systems which may take a form of closed-loop mechanisms and play a practical role in mechanical engineering.

References

1. P. Fritzkowski, H. Kaminski, *Dynamics of a rope as a rigid multibody system*, J. Mech. Mater. Struct., **3**(6) (2008) 1059 – 1075.
2. P. Fritzkowski, H. Kaminski, Dynamics of a rope modeled as a discrete system with extensible members, Comput. Mech., **44**(4) (2009) 473 – 480.
3. P. Fritzkowski, H. Kaminski, *Discrete model of a rope with bending stiffness,* Proceedings of the 10th Conference on Dynamical Systems - Theory and Applications, Lodz 2009, 905 – 912.
4. P. Fritzkowski, H. Kaminski, *Discrete model of a rope with viscous damping,* Proceedings of the 10th Conference on Dynamical Systems - Theory and Applications, Lodz 2009, 913 – 918.
5. A. Goriely, T. McMillen, *Shape of a cracking whip,* Phys. Rev. Lett., **88**(24) (2002) 1 – 4.
6. D. Yong, *Strings, chains and ropes,* SIAM Rev., **48**(4) (2006) 771 – 781.
7. C. Wong, K. Yasu, *Falling chains*, Phys. Rev. Lett., **74**(6) (2006) 490 – 496.

Dyskretny sprężysto-dyssypatywny układ jako model liny

W pracy rozważono ruch liny zawieszonej jednym końcem i omówiono jej dyskretny model. Układ złożony jest z jednakowych członów połączonych przegubowo. Rozważono różny charakter zarówno elementów, jak i połączeń oraz zaprezentowano równania ruchu. W konsekwencji istnieje kilka możliwości: model rozciągliwy lub nierozciągliwy, których przeguby są idealne, sprężyste, dyssypatywne lub sprężysto-dyssypatywne. Niemniej jednak pokazano zwięzły, uogólniony model matematyczny, właściwy dla każdego z wariantów.

Regular motion of a hanging rope

Paweł FRITZKOWSKI
Institute of Applied Mechanics, Poznan University of Technology
Piotrowo 3, 60-965 Poznan, Poland
pawel.fritzkowski@gmail.com

Henryk KAMIŃSKI
Institute of Applied Mechanics, Poznan University of Technology
Piotrowo 3, 60-965 Poznan, Poland
henryk.kaminski@put.poznan.pl

Abstract

Plane motion of a rope fixed at one end is considered. The body is modelled as a discrete system including transverse elasticity and dissipation. Mathematical model is presented and some numerical aspects are outlined. In simulations of dynamics vibrations of the system are excited by non-stationary constraints. It is shown that appropriate model properties and the excitation parameters can lead to quasi-periodic motion of the rope.

Keywords: rope, nonlinear dynamics, numerical simulation

1. Introduction

Usually forced vibrations are considered in the context of an external harmonic force acting on a system. However, rheonomic constraints can lead to similar effects, although the nature of such an excitation is kinematic. As with the external force, the time dependent constraints make the system non-autonomous. Moreover, due to the variable inertial terms resulting from the excitation, the motion may be treated as parametric vibrations. All in all, kinematically driven systems can be very interesting subjects of study in the area of nonlinear dynamics.

In this work forced vibrations of a hanging rope are considered. To simulate dynamics of the system, a discrete model of the rope is used. As an extension of papers [3, 4] we present equations of motion of the rope with transverse elasticity and viscous damping. In several numerical examples the discrete system with multiple degrees of freedom is analysed, whose vibrations are excited by non-stationary constraints. It is shown that selection of appropriate model properties (damping coefficient and bending stiffness) and the excitation parameters can produce quasi-periodic motion.

2. Mathematical and numerical model

Let us consider planar motion of the rope presented in Fig. 1a. One end of the body is attached to a point P_0, whose position is specified by the pair of time dependent functions:

$$x_0 = x_0(t), \quad y_0 = y_0(t). \tag{1}$$

The system consists of n simple elements – rigid prismatic rods of length l and mass m, which are connected by rotational joints. However, character of the joints is not idealized – they involve both elasticity and damping. In a schematic manner, a torsional spring and viscous damper is placed in each of the joints (see Fig. 1b). We assume that all the springs have identical stiffness k_T; similarly, one damping coefficient c is associated to all the dampers.
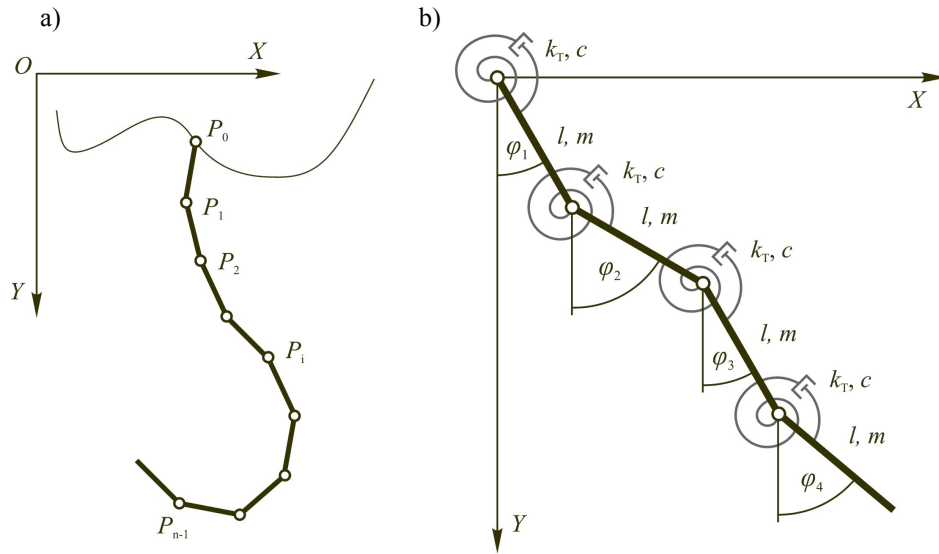
Figure 1. Discrete model of a rope: a) general conception, b) system with transverse elasticity and damping

In view of the above assumptions, the rope is modelled by a multiple physical pendulum with joints which are both flexible and dissipative. Such a discrete system can be described with use of the angular generalized coordinates φ_i (i=1, 2, …, n). Taking into account the mathematical models discussed in [3] and [4], equations of motion of the given system can be written as follows

$$\sum_{j=1}^{n} a_{ij} \ddot{\varphi}_j \cos(\varphi_i - \varphi_j) + \sum_{j=1}^{n} a_{ij} \dot{\varphi}_j^2 \sin(\varphi_i - \varphi_j) + \frac{b_i}{l}(\ddot{x}_0 \cos\varphi_i - \ddot{y}_0 \sin\varphi_i) =$$
$$= \frac{1}{ml^2}(Q_i^G + Q_i^T + Q_i^D), \qquad i = 1, 2, …, n,$$
(2)

where the coefficients

$$a_{ij} = \begin{cases} n-i+1/2 & \text{for } j < i \\ n-i+1/3 & \text{for } j = i \\ n-j+1/2 & \text{for } j > i \end{cases} \qquad b_i = n-i+1/2 \qquad (3)$$

and the generalized forces are determined below:

a) potential forces resulting from gravity

$$Q_i^G = -mgl\, b_i \sin \varphi_i \, ; \tag{4}$$

b) potential elastic forces

$$Q_i^T = \begin{cases} M_i - M_{i+1} & \text{for } i = 1, 2, \ldots, n-1 \\ M_i & \text{for } i = n \end{cases} \tag{5}$$

where the elastic moment

$$M_i = -2 \frac{k_T}{l} \frac{\tan(\theta_i / 2)}{\cos(\theta_i / 2)} \tag{6}$$

is expressed in terms of the relative generalized coordinate:

$$\theta_i = \begin{cases} \varphi_i & \text{for } i = 1 \\ \varphi_i - \varphi_{i-1} & \text{for } i = 2, 3, \ldots, n \end{cases} \tag{7}$$

c) dissipative (viscous) forces

$$Q_i^D = \begin{cases} c(\dot{\theta}_{i+1} - \dot{\theta}_i) & \text{for } i = 1, 2, \ldots, n-1 \\ -c\dot{\theta}_i & \text{for } i = n \end{cases} \tag{8}$$

The system of second order differential equations (2) may be written in the following concise form:

$$\mathbf{M}(\mathbf{q})\ddot{\mathbf{q}} = \mathbf{f}(t, \mathbf{q}, \dot{\mathbf{q}}), \tag{9}$$

where $\mathbf{q}$ denotes the generalized coordinates vector. Additionally, the initial conditions must be fulfilled:

$$\mathbf{q}(0) = \mathbf{q}_0, \quad \dot{\mathbf{q}}(0) = \mathbf{u}_0 \tag{10}$$

After reformulation, the initial value problem has a form convenient for numerical computation:

$$\hat{\mathbf{M}}(\mathbf{X})\dot{\mathbf{X}} = \hat{\mathbf{f}}(t, \mathbf{X}) \tag{11}$$

$$\mathbf{X}(0) = \mathbf{X}_0 \tag{12}$$

where:

$$\hat{\mathbf{M}} = \begin{bmatrix} \mathbf{I} & \mathbf{0} \\ \mathbf{0} & \mathbf{M} \end{bmatrix}, \quad \hat{\mathbf{f}} = \begin{bmatrix} \mathbf{u} \\ \mathbf{f} \end{bmatrix}, \quad \mathbf{X} = \begin{bmatrix} \mathbf{q} \\ \mathbf{u} \end{bmatrix}, \quad \mathbf{u} = \dot{\mathbf{q}} \tag{13}$$

and $\mathbf{I}$ denotes the identity matrix.

It should be noted that, due to the matrix $\mathbf{M}$ which couples the equations of motion, the system (11) is classified as an implicit ordinary differential equation (IODE) system. What is more, the matrix is time dependent, hence, the given problem is numerically much more demanding than the standard explicit ordinary differential equation (ODE) systems. In our simulations we use the MEBDFV solver written by Abdulla and Cash (Imperial College, London); the code is based on the modified extended backward differentiation formulae (MEBDF) of Cash (1980) [1, 2].

3. Numerical experiments

Let us turn now to some examples which show regular motion of the system. We consider a rope of a total length 1 [m] and total mass 0.5 [kg]. The supposed number of elements $n=20$ and the parameters: $k_T=10^{-3}$ [Nm^2], $c=10^{-3}$ [Nms]. Initially, the rope hangs down, so that $\mathbf{q}_0= \mathbf{0}$ and $\mathbf{u}_0= \mathbf{0}$. Vibration of the system are enforced by horizontal motion of the point P_0 according to the function:

$$x_0(t) = A\sin^2(\pi Bt),\tag{14}$$

where A and B are constants. Is it possible to find such values of A and B which ensure periodic or quasi-periodic motion of the discrete system? Is there any method to generate regular motion of such a complex system, which actually is not a mechanism?

Let us take into account a system which is simpler than the given one – a multiple physical pendulum whose motion is governed by the equations (2) as $Q_i^T=Q_i^D=0$ for $i=1, 2, \ldots, n$. If we linearize this system and solve the related eigenvalue problem, we obtain the following natural frequencies:

$$\omega_1 \approx 3.766\,[1/s], \quad \omega_2 \approx 8.667\,[1/s], \quad \ldots, \quad \omega_{20} \approx 186.127\,[1/s]\tag{15}$$

It turns out that applying the kinematic excitation (14) with small amplitude A and the value $2\pi B$ nearby ω_1 can produce regular vibrations. In the examples below we take $A=0.05$ [m] and:

a) $B = 0.56\,[1/s] \;\Rightarrow\; 2\pi B = 3.519\,[1/s]$,

b) $B = 0.57\,[1/s] \;\Rightarrow\; 2\pi B = 3.581\,[1/s]$.

Figure 2 illustrates the generalized coordinate φ_{20} as a function of time in the first case. As it can be seen, the quasi-periodic motion exhibit two non-commensurable frequencies: the higher frequency refers to the motion itself, whereas the other one is connected to the amplitude modulation. The angular velocity versus time graph indicates similar effect. Consequently, the phase trajectory densely fill the plane $(\varphi_{20}, \dot{\varphi}_{20})$ in a quite regular manner (see Fig. 3).
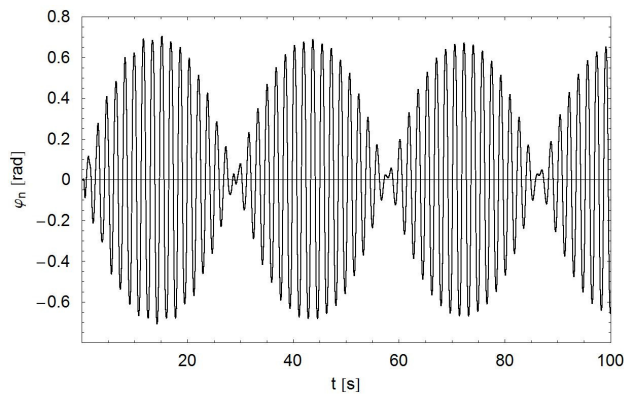
Figure 2. The last generalized coordinate for $A=0.05$ and $B=0.56$
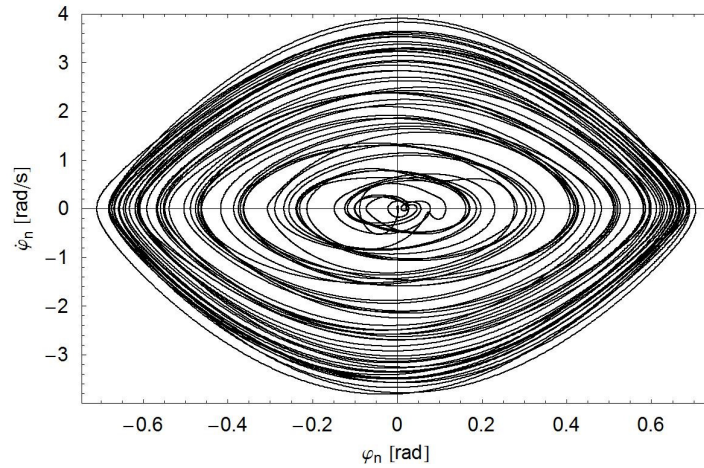
Figure 3. Phase portrait for *A*=0.05 and *B*=0.56
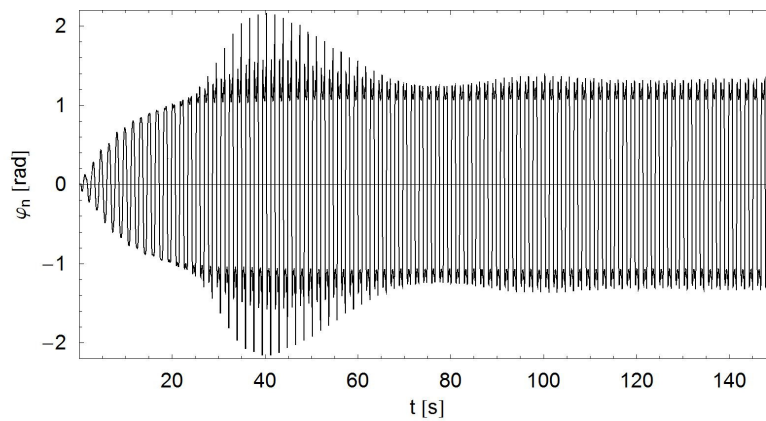
Figure 4. The last generalized coordinate for *A*=0.05 and *B*=0.57

There are many values of *B* which give similar effects but weaker amplitude modulation. An extreme case is presented in Fig. 4. After some period of transient motion, when higher harmonics appear, the vibrations become regular and their amplitude hardly changes.

3. Conclusions

On the basis of our previous papers, the discrete model of a rope with transverse elasticity and dissipation has been presented. Numerically, the problem leads to implicit ordinary differential equations.

Although the hanging rope is not a mechanism and the discrete model has multiple degrees of freedom, the performed numerical simulations show that the system can experience regular motion. Coupling the two features, bending stiffness and damping, plays a key role, since it affects the transverse vibrations of the system. Appropriate values of the parameters k_T and c in conjunction with specific rheonomic constraints can ensure rough equilibrium between the energy provided and dissipated, which produces quasi-periodic behaviour. We feel that the work may be useful for further analysis of the discrete model, other complex chain-like mechanical systems and their regular motion.

References

1. J.R. Cash, S. *Considine, An MEBDF code for stiff initial value problems,* ACM Trans. Math. Soft., **18**(2) (1992) 142-155.
2. J.R. Cash, *Modified extended backward differentiation formulae for the numerical solution of stiff initial value problems in ODEs and DAEs*, J. Comput. Appl. Math., **125** (2000) 117-130.
3. P. Fritzkowski, H. Kaminski, *Discrete model of a rope with bending stiffness,* Proceedings of the 10th Conference on Dynamical Systems – Theory and Applications, Lodz 2009, 905-912.
4. P. Fritzkowski, H. Kaminski, *Discrete model of a rope with viscous damping,* Proceedings of the 10th Conference on Dynamical Systems – Theory and Applications, Lodz 2009, 913-918.

Ruch regularny wiszącej liny

W pracy rozważa się ruch płaski liny zawieszonej jednym końcem. Ciało jest zamodelowane jako układ dyskretny, ujmujący sprężystość poprzeczną i dyssypację energii. Zaprezentowano model matematyczny i zarysowano pewne aspekty numeryczne. W symulacjach dynamiki drgania układu zostają wymuszone za pomocą więzów niestacjonarnych. Pokazano, że odpowiednie własności modelu, jak i parametry wymuszenia mogą prowadzić do prawie okresowego ruchu liny.

Parametric Oscillations of a Torsional Pendulum

Leszek GADOMSKI

The College of Finance and Management, ul. Sokolowska 172, Siedlce, 08-110 Poland
leszek.gadomski@wsfiz.siedlce.pl

Alexander PROKOPENYA

The College of Finance and Management, ul. Sokolowska 172, Siedlce,08-110 Poland
Brest State Technical University, ul. Moskowskaya 267, Brest, 224017 Belarus
prokopenya@brest.by

Abstract

We study parametric oscillations of a torsional pendulum excited by means of varying a moment of inertia of the rotating body. Motion of the system is determined by the second order differential equation with periodic coefficients. We have studied stability of this equation and proved that parametric resonance in the system can occur only if the excitation frequency Ω is sufficiently close to the value $2\omega_0/N$ (N=1,2,3,…), where ω_0 is a natural frequency of the pendulum, and the damping coefficient β_0 is sufficiently small. Moreover, for any positive β_0 parametric resonance can occur only if the excitation amplitude ε is greater than some threshold value. Using the infinite determinant method, we have found analytically the boundaries of the resonance domains in the parameter space for N=1,2,3.

Keywords: Parametric oscillations, characteristic multipliers, stability, parametric resonance.

1. Introduction

External influence on a vibrating system is often reduced to varying parameters of the system with time. In such a case vibrations of the system are called the parametric oscillations. As a physical example we consider a torsional pendulum excited by means of alternating its moment of inertia. The pendulum may be realized as a massive disk mounted on an elastic shaft and two point bodies of equal masses m being placed on its surface symmetrically with respect to the axis of the shaft. If a distance of each body from the axis of the shaft oscillates near some equilibrium value r_0 according to the law

$$r(t) = r_0(1 + \varepsilon \cos(\Omega t)) ,$$

where Ω and $|\varepsilon| < 1$ are the excitation frequency and amplitude, respectively, then moment of inertia of the pendulum alternates as

$$I(t) = I_0 + 2mr^2 = I_0 + 2mr_0^2(1 + \varepsilon \cos(\Omega t))^2 , \tag{1}$$

where I_0 is a moment of inertia of the disk. Denoting a twist angle of the disk by ϑ, we can write equation of motion of the system in the form

$$\frac{d}{dt}\left(I(t)\frac{d\vartheta}{dt}\right) = -\gamma \frac{d\vartheta}{dt} - c\vartheta , \tag{2}$$

where γ is a coefficient of viscous friction and c is a stiffness of the shaft. Taking into account expression (1) and introducing the following notations

$$p = \frac{2mr_0^2}{I_0 + 2mr_0^2} \; , \; \beta_0 = \frac{\gamma}{2(I_0 + 2mr_0^2)} \; , \; \omega_0^2 = \frac{c}{I_0 + 2mr_0^2} \; ,$$

we can rewrite equation (2) in the form

$$\frac{d^2\vartheta}{dt^2} + \frac{2(\beta_0 - \varepsilon p\Omega\sin(\Omega t)(1 + \varepsilon\cos(\Omega t)))}{1 + \varepsilon p\cos(\Omega t)(2 + \varepsilon\cos(\Omega t))}\frac{d\vartheta}{dt} + \frac{\omega_0^2}{1 + \varepsilon p\cos(\Omega t)(2 + \varepsilon\cos(\Omega t))}\vartheta = 0 \; . \quad (3)$$

In the case of $\varepsilon = 0$ equation (3) reduces to differential equation with constant coefficients determining damped oscillations of the pendulum. But for $\varepsilon > 0$ there may exist such values of the excitation frequency Ω and amplitude ε for which the solution $\vartheta(t)$ increases unboundedly with time. This phenomenon is known as a parametric resonance. From mathematical point of view parametric resonance corresponds to instability of equilibrium position of the pendulum. Therefore, seeking the conditions under which parametric resonance can occur is equivalent to studying the stability of a trivial solution of equation (3).

It should be noted that equation (3) is a differential equation with periodic coefficients and general theory of such equations has been developed quite well (see, for example, [1]). The most general method for studying behaviour of their solutions is the classic Floquet method which is based on calculation of a monodromy matrix and analysis of its eigenvalues. Just such approach was realized in paper [2], where a monodromy matrix was found in the form of power series in terms of ε accurate up to the second order. But if we are looking for such values of the system parameters for which a trivial solution of equation (3) is unstable the method of infinite determinant turns out to be more effective [3].

The main purpose of the present paper is to find the domains of instability of equation (3) in the parameter space and to calculate their boundaries assuming that excitation frequency Ω is given while the amplitude ε and the system parameters β_0 and ω_0 can be changed. As the corresponding calculations are rather bulky we use the computer algebra system Mathematica [4] for doing necessary analytical calculations.

2. Characteristic multipliers of the system

Behaviour of solutions of equation (3) is determined by its characteristic multipliers ρ which are the eigenvalues of a monodromy matrix $X(T)$ and, hence, are determined as roots of the characteristic equation

$$\det(X(T) - \rho E_2) = 0 \; , \quad (4)$$

where E_2 is the 2×2 identity matrix and $T = 2\pi / \Omega$. Here $X(t)$ is a principal fundamental matrix for the equation (3) which is defined as

$$X(t) = \begin{pmatrix} \vartheta_1(t) & \vartheta_2(t) \\ \vartheta'_1(t) & \vartheta'_2(t) \end{pmatrix},$$

where $\vartheta_1(t)$ and $\vartheta_2(t)$ are two linearly independent solutions of equation (3) satisfying the following initial conditions

$$\vartheta_1(0) = 1, \ \vartheta'_1(0) = 0, \ \vartheta_2(0) = 0, \ \vartheta'_2(0) = 1. \tag{5}$$

Calculation shows that characteristic equation (5) can be represented in the form

$$\rho^2 - 2A\rho + B = 0, \tag{6}$$

where A and B are real-valued parameters given by

$$A = \frac{1}{2}\left(\vartheta_1(T) + \vartheta'_2(T)\right), \ B = \vartheta_1(T)\vartheta'_2(T) - \vartheta'_1(T)\vartheta_2(T).$$

Obviously, equation (6) has two roots

$$\rho_{1,2} = A \pm \sqrt{A^2 - B}. \tag{7}$$

Therefore, characteristic multipliers (7) are either two complex conjugate numbers with absolute values being equal to $\sqrt{B}$ (if $B > A^2$) or two real numbers of the same sign satisfying the conditions $|\rho_1| \geq \sqrt{B}$, $0 < |\rho_2| \leq \sqrt{B}$ (when $B < A^2$). As functions $\vartheta_1(t)$, $\vartheta_2(t)$ satisfy equation (3) and initial conditions (5), one can readily show that parameter B is bounded by the inequality

$$0 < B \leq 1. \tag{8}$$

It means that in the case of $|\rho_1| < 1$ a trivial solution of equation (3) is stable and it becomes unstable when $|\rho_1| > 1$. The case $|\rho_1| = 1$ corresponds to the boundary between stable and unstable behaviour.

3. Determination of the stability boundaries

In order to simplify calculations let us rewrite equation (3) in the form

$$(1 + \varepsilon p \cos\tau(2 + \varepsilon \cos\tau))\frac{d^2\vartheta}{d\tau^2} + 2(\beta - \varepsilon p \sin\tau(1 + \varepsilon \cos\tau))\frac{d\vartheta}{d\tau} + \omega^2\vartheta = 0, \tag{9}$$

where $\beta = \beta_0/\Omega$, $\omega = \omega_0/\Omega$, $\tau = \Omega t$. The boundaries between stable and unstable behaviour of solutions of equation (3) in the parameter space are determined from the condition $\rho_1 = -1$ or $\rho_1 = 1$ what means that equation (9) must have periodic solution with a period 4π or 2π, respectively. Hence, we can attempt to determine these boundaries directly by seeking a solution of equation (9) in the form of Fourier series

$$\vartheta = a_0 + \sum_{k=1}^{\infty}\left(a_k \cos(k\tau/2) + b_k \sin(k\tau/2)\right). \tag{10}$$

Note that Fourier series (10) corresponding to 4π-periodic function $\vartheta(\tau)$ can be also used to obtain 2π-periodic solution by setting to zero odd coefficients a_{2k-1}, b_{2k-1}.

Substituting solution (10) into equation (9) and setting coefficients of $\cos(k\tau/2)$ and $\sin(k\tau/2)$ to zero, we obtain two infinite sequences of linear algebraic equations determining coefficients a_k and b_k of the Fourier series (10). The first sequence of equations determines odd coefficients a_{2k-1}, b_{2k-1} and is given by

$$\left(\omega^2 - \frac{1}{4} + \frac{p\varepsilon}{8}(2-\varepsilon)\right)a_1 + \beta b_1 - \frac{3p\varepsilon}{16}(4-\varepsilon)a_3 - \frac{5p\varepsilon^2}{16}a_5 = 0,$$

$$-\beta a_1 + \left(\omega^2 - \frac{1}{4} - \frac{p\varepsilon}{8}(2+\varepsilon)\right)b_1 - \frac{3p\varepsilon}{16}(4+\varepsilon)b_3 - \frac{5p\varepsilon^2}{16}b_5 = 0,$$

$$-\frac{3p\varepsilon}{16}(4-\varepsilon)a_1 + \left(\omega^2 - \frac{9}{8}(2+p\varepsilon^2)\right)a_3 + 3\beta b_3 - \frac{15p\varepsilon}{4}a_5 - \frac{21p\varepsilon^2}{16}a_7 = 0,$$

$$-\frac{3p\varepsilon}{16}(4+\varepsilon)b_1 - 3\beta a_3 + \left(\omega^2 - \frac{9}{8}(2+p\varepsilon^2)\right)b_3 - \frac{15p\varepsilon}{4}b_5 - \frac{21p\varepsilon^2}{16}b_7 = 0,$$

$$\vdots \tag{11}$$

$$-\frac{p\varepsilon^2}{16}(2k-1)((2k-5)a_{2k-5} + (2k+3)a_{2k+3}) + \left(\omega^2 - \frac{1}{8}(2k-1)^2(2+p\varepsilon^2)\right)a_{2k-1} +$$

$$+ (2k-1)\beta b_{2k-1} - \frac{p\varepsilon}{4}(2k-1)((2k-3)a_{2k-3} + (2k+1)a_{2k+1}) = 0,$$

$$-\frac{p\varepsilon^2}{16}(2k-1)((2k-5)b_{2k-5} + (2k+3)b_{2k+3}) + \left(\omega^2 - \frac{1}{8}(2k-1)^2(2+p\varepsilon^2)\right)b_{2k-1} -$$

$$- (2k-1)\beta a_{2k-1} - \frac{p\varepsilon}{4}(2k-1)((2k-3)b_{2k-3} + (2k+1)b_{2k+1}) = 0,\ldots$$

The second sequence of equations determines even coefficients a_{2k}, b_{2k} and has a form

$$a_0\omega^2 = 0,$$

$$\left(\omega^2 - 1 - \frac{p\varepsilon^2}{4}\right)a_2 + 2\beta b_2 - 2p\varepsilon a_4 - \frac{3p\varepsilon^2}{4}a_6 = 0,$$

$$-2\beta a_2 + \left(\omega^2 - 1 - \frac{3p\varepsilon^2}{4}\right)b_2 - 2p\varepsilon b_4 - \frac{3p\varepsilon^2}{4}b_6 = 0,$$

$$-2p\varepsilon a_2 + \left(\omega^2 - 4 - 2p\varepsilon^2\right)a_4 + 4\beta b_4 - 6p\varepsilon a_6 - 2p\varepsilon^2 a_8 = 0,$$

$$-2p\varepsilon b_2 - 4\beta a_4 + \left(\omega^2 - 4 - 2p\varepsilon^2\right)b_4 - 6p\varepsilon b_6 - 2p\varepsilon^2 b_8 = 0, \tag{12}$$

$$\vdots$$

$$-\frac{kp\varepsilon^2}{4}((k-2)a_{2k-4} + (k+2)a_{2k+4}) + \left(\omega^2 - k^2 - \frac{pk^2\varepsilon^2}{2}\right)a_{2k} +$$

$$+ 2k\beta b_{2k} - kp\varepsilon((k-1)a_{2k-2} + (k+1)a_{2k+2}) = 0,$$

$$-\frac{kp\varepsilon^2}{4}((k-2)b_{2k-4} + (k+2)b_{2k+4}) + \left(\omega^2 - k^2 - \frac{pk^2\varepsilon^2}{2}\right)b_{2k} -$$

$$- 2k\beta a_{2k} - kp\varepsilon((k-1)b_{2k-2} + (k+1)b_{2k+2}) = 0,\ldots$$

For a solution of the systems (11), (12) to exist, determinants of their matrices must vanish, thus giving equations for determination of the stability boundaries.

Note that matrices of the systems (11), (12) have infinite dimensions and, of course, we can not calculate their determinants exactly. So we have to truncate the infinite

sequences of equations (11), (12) after the *n*th term, where *n* is a suitably large number, and to calculate the corresponding finite determinant analytically.

Calculation shows that in the case of $\varepsilon = 0$ determinants of the systems (11), (12) reduce to the product of terms of the form

$$\left(\omega^2 - k^2/4\right)^2 + k^2\beta^2 ,$$

which are equal to zero only if

$$\omega = k/2 , \ \beta = 0 , \ k = 0,1,2,3,... \tag{13}$$

As determinants are analytic functions of the parameter ε we can conclude that the domains of parametric resonance in the $\omega - \beta - \varepsilon$ space may exist only in the neighbourhood of the points (13). Therefore, for sufficiently small ε we can seek the boundaries of these domains in the form

$$\omega = N/2 + \omega_1\varepsilon + \omega_2\varepsilon^2 + .. , \ \beta = \beta_1\varepsilon + \beta_2\varepsilon^2 + .. , \ N = 1,2,3,... , \tag{14}$$

where coefficients ω_k, β_k should be found from the condition that the corresponding determinants of the systems (11), (12) are equal to zero. To find these coefficients we substitute (14) into the expressions for determinants and expand them in powers series in terms of ε. Equating coefficients of ε^k ($k = 1,2,3,...$) to zero, we obtain a system of algebraic equations giving the coefficients ω_k, β_k in the neighbourhood of each point (13). In the case of $N = 1$, for example, the first two equations are given by

$$\omega_1^2 + \beta_1^2 = p^2/16 , \ 128(\omega_1\omega_2 + \beta_1\beta_2) + \omega_1(16\omega_1^2 - 112\beta_1^2 - p(16 - 43p)) = 0 . \tag{15}$$

Eliminating coefficients ω_1, ω_2, β_1, β_2 from the expressions (14), (15), we obtain an equation determining the stability boundary in the neighbourhood of the point $\omega = 1/2$

$$\left(\omega - \frac{1}{2}\right)^3 - 7\beta^2\left(\omega - \frac{1}{2}\right) + 4\left(\omega - \frac{1}{2}\right)^2 + 4\beta^2 - \frac{p\varepsilon^2}{16}(16 - 43p)\left(\omega - \frac{1}{2}\right) = \frac{p^2\varepsilon^2}{4} , \tag{16}$$

where an error term is $O(\varepsilon^4)$. The cross-sections of this surface by the planes $\beta = const$ and $\varepsilon = const$ are shown in Figure 1.

Doing similar calculations in the cases of $N = 2$ and $N = 3$ we obtain the corresponding stability boundaries in the form

$$\left(\omega - 1 - \frac{p\varepsilon^2}{12}(3 - 8p)\right)^2 + \beta^2 = \frac{p^2\varepsilon^4}{64} , \tag{17}$$

$$\left(\omega - \frac{3}{2} - \frac{3p\varepsilon^2}{64}(8 - 23p)\right)^2 + \beta^2 = \frac{9p^4(4 + p)^2\varepsilon^6}{65536} . \tag{18}$$

4. Conclusions

In the present paper we have studied parametric oscillations of the torsional pendulum with damping which are described by the second order differential equation with periodic coefficients. We have shown that parametric resonance in the system can occur

only if excitation frequency Ω is sufficiently close to the value $2\omega_0/N$ ($N=1,2,..$), damping coefficient β_0 is sufficiently small, and for any $\beta_0 > 0$ excitation amplitude ε is greater than some threshold value. Using the infinite determinant method and taking into account more equations from the sequences (11), (12), one can easily increase accuracy of calculation of the stability boundaries (16)-(18).
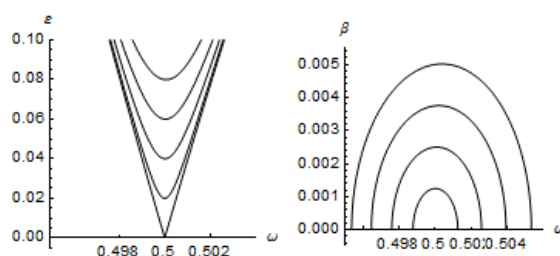
Figure 1. Cross-sections of the boundary surface by the planes $\beta = 0.0005(k-1)$ and $\varepsilon = 0.05k$ for $N=1$, $p=0.1$, $k=1,2,3,4,5$

References

1. V.A. Yakubovich, V.M. Starzhinskii, *Linear differential equations with periodic coefficients*, John Wiley, New York 1975.
2. C. Cattani, E.A. Grebenikov, A.N. Prokopenya, *On stability of the Hill's equation with damping,* Nonlinear Oscillations, **7** (2004) 169-179.
3. A.N. Prokopenya, Determination of the stability boundaries for the Hamiltonian systems with periodic coefficients, Mathematical Modelling and Analysis, **10** (2005) 191-204.
4. S. Wolfram, *The Mathematica book*, Cambridge University Press 1999.

Drgania parametryczne wahadła skrętnego

W pracy rozważane są drgania parametryczne wahadła skrętnego pobudzanego przez zmienny moment bezwładności obracającego się ciała. Ruch układu opisany jest przez równanie różniczkowe rzędu drugiego ze współczynnikami okresowymi. Zbadano stabilność tego równania i udowodniono, że rezonans parametryczny tego układu może wystąpić tylko wtedy, gdy częstotliwość pobudzania Ω jest wystarczająco bliska wartości $2\omega_0$/N (N=1,2,3,…), gdzie ω_0 jest naturalną częstością drgań wahadła a współczynnik tłumienia β_0 jest dostatecznie mały. Ponadto wykazano, dla dowolnej dodatniej wartości β_0 rezonans parametryczny może wystąpić tylko wówczas, gdy amplituda pobudzenia ε jest większa niż pewna wartość progowa. Stosując metodę nieskończonych wyznaczników znalezione zostały, w sposób analityczny, granice obszarów rezonansowych w przestrzeni parametrów dla N=1,2,3.

Compensative Control Chart of Angular Velocity Sensor on Basis of Wave Solid-State Gyroscope

Zinaida GANKEVYCH
Student, National Technical University of Ukraine "Kiev Polytechnic Institute"
37 Peremogy Pr, Kyiv, Ukraine, 03056
zina-1@bigmir.net

Sergey KUCHER
Student, National Technical University of Ukraine "Kiev Polytechnic Institute"
37 Peremogy Pr, Kyiv, Ukraine, 03056
rusty_serg@ukr.net

Pavel BONDAR
D.Sc, National Technical University of Ukraine "Kiev Polytechnic Institute"
37 Peremogy Pr, Kyiv, Ukraine, 03056
pbon43@mail.ru

Abstract

This work is devoted to results of research wave solid-state gyroscope (WSG) with a metallic cylinder resonator and piezoelectric systems of excitation and pickup information, which works in the mode of compensation angular velocity sensor. This type of device becomes more and more attractive thanks to its low cost, considerable vibrostability, shockproof and enough high precision characteristics. In the work there are results of design the power balancing channel, which provides functioning of gyroscope in the compensative mode in the environment of MatLAB-Simulink. Numerical parameters, namely basic mode frequencies of vibration, which are used in model, were got by means of finite element analysis of real resonator model in the environment of ANSYS. It is shown that application of integral-position control law gives the desired dynamic characteristics both to the action of permanent angular speed and to the change of it by harmonic law.

Keywords: resonator, standing wave, vibration loop, vibration node, Coriolis's force, power balancing channel.

1. Introduction

Wave solid-state gyroscopes (WSG) are perspective information sensors about object angular motion in many application fields – from navigation systems of middle precision class, to orientation's control system for microsatellites. This type of device becomes more and more attractive thanks to its low cost, considerable vibrostability, shockproof and enough high precision characteristics.

Principle of WSG's operation is based on inertial properties of resilient waves, which are generated in resonator with acoustical frequencies. In the resonator a standing wave is generated by the second resonance mode of vibration (basic wave), which is characterized by four loops and nodes of vibration. During the rotation of resonator at a angular velocity of Ω the Coriolis's forces are affecting and generating additional wave in the direction of resulting force action. This additional wave is oriented at an angle of

ψ to the basic wave. There can be two types of WSG's resonators – cylindrical and hemispherical forms.

WSG can work in two modes – in mode of angular velocity sensor (AVS) and in the integrating mode. The object of research of this work is WSG with cylindrical resonator in the mode of AVS. There are two methods of such WSG's construction – method of the direct measuring and compensative.

Compensative chart in comparison with the method of the direct measuring has some advantages. Using direct measuring leads to necessity of compromise between frequency band width and sensitivity. Because increase of mode distributing on frequency and increase of damping lead to lower values of a long-term response on this angular velocity. This compromise is removed by realization of compensative method, which is more precisely. Therefore exactly compensative method was chosen for research.

2. Mathematical Model

The construction of WSG with a metallic cylinder resonator is presented on figure 1. A basic element is a metallic cylinder resonator with diameter from 20 to 42 mm. The piezoelectric systems of excitation and pickup information are placed on its diaphragm.

A resonator with a diameter of 42 mm was selected for research (figure 2).

1. Foundation
2. Bush
3. Electrode
4. Resonator
5. Bearing
6. Cover
7. Stem
8. Screw
9. Spring washer
10. Washer
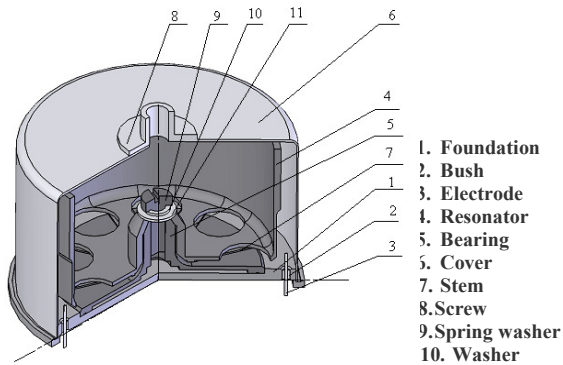
Figure 1. Chart of WSG with position excitation   Figure 2. Resonator of WSG

There are three channels in the base construction chart of compensative WSG [1] – following the resonator's eigenfrequency channel, maintenance the vibration's basic mode amplitude channel and the wave's power balancing channel. The last one retains the turning angle of standing wave on the specified value.

Then it is considered the wave's power balancing chart (figure 3). Amplitude of additional wave, generated by Coriolis's forces, is measured by piezoelectric, which is set in one of the basic wave vibration node. This signal through power balancing channel shall be applied to another node of basic wave.

In the capacity of resonator's model there were used equations in toroidal coordinates [2] at mathematical simulation. These equations are presented below:

$$\begin{cases} \ddot{x}+\left(\dfrac{1}{\tau_1}+\dfrac{1}{\tau_2}\right)\dot{x}+\left(\dfrac{1}{\tau_1}-\dfrac{1}{\tau_2}\right)\left(\dot{x}\cos 2\theta_\tau+\dot{y}\sin 2\theta_\tau\right)+\dfrac{\omega_1^2+\omega_2^2}{2}x-\dfrac{\omega_1^2-\omega_2^2}{2}\left(x\cos 2\theta_\omega+y\sin 2\theta_\omega\right)=g_x \\[3mm] \ddot{y}+\left(\dfrac{1}{\tau_1}+\dfrac{1}{\tau_2}\right)\dot{y}+\left(\dfrac{1}{\tau_1}-\dfrac{1}{\tau_2}\right)\left(-\dot{x}\sin 2\theta_\tau+\dot{y}\cos 2\theta_\tau\right)+\dfrac{\omega_1^2+\omega_2^2}{2}y-\dfrac{\omega_1^2-\omega_2^2}{2}\left(-x\sin 2\theta_\omega+y\cos 2\theta_\omega\right)= \\[3mm] \qquad\qquad\qquad\qquad\qquad\qquad\qquad\qquad\qquad\qquad\qquad\qquad\qquad\qquad = g_y-2\Omega\dot{x} \end{cases} \quad (1)$$

where x and y – movement of resonator's nodes and loops, respectively;

g_x, g_y – forces, putted by piezoelectric drive, respectively to the nodes and loops axes of sensing element, and besides $g_y=F(y)$;

τ_1 and τ_2 – time constant of main axes good quality;

ω_1 and ω_2 – eigenfrequencies of main axes;

θ_τ and θ_ω – parameters which are determined the defects of WSG's making resonator.
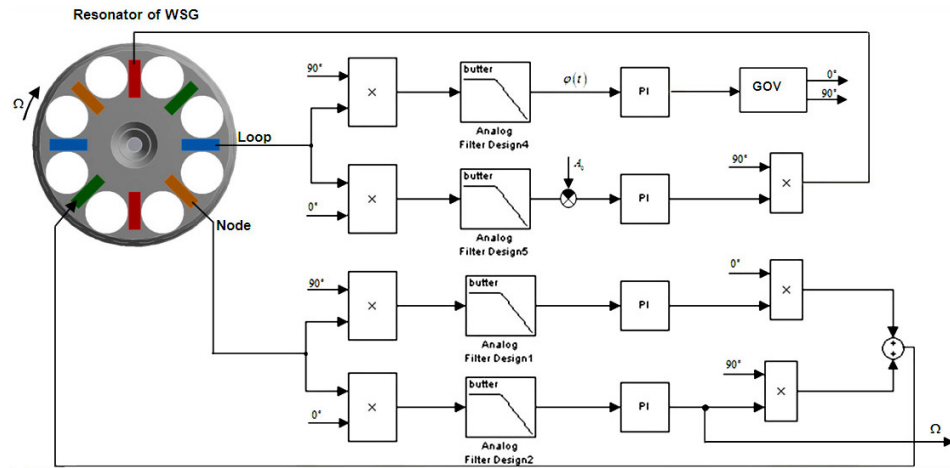
Figure 3. The wave's power balancing chart

Equations (1) describe the operation of WSG in the compensative mode. The first of them characterizes motion in the resonator's nodes, the second one characterizes motion in the loops. It is obvious from these equations, that equation of nodes carries information about angular velocity, which is affecting a gyroscope. Thus in this case signals g_x, and g_y are created by piezoelectric (7), located on the bottom of resonator (4) (see figure 1).

The eigenfrequency vibration value of investigated resonator, used in equations, was gained as a result of resonator's model research in the environment of ANSYS. Models from the environment of ANSYS are presented on figure 4. The sensing element frequency, which was found is equal to ω_1=2106,5 Hertz.
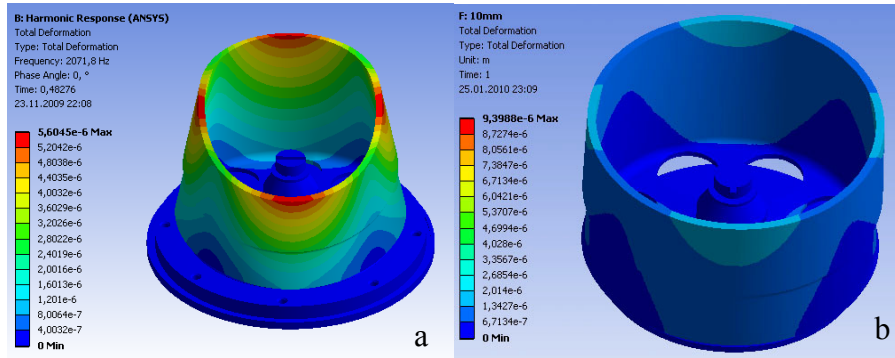
Figure 4. ANSYS models of resonator:
a – eigenfrequency of the second mode of vibration; b –deformation under
piezoelectric.

3. Simulation Data

In the environment of Matlab there was created WSG's model with taking into account invariability of resonator's parameters. It is presented on figure 5. It is necessary to notice that channel of following the resonator's eigenfrequency and channel of maintenance the vibration's basic mode amplitude are ignored, so long as ideal resonator's model was used. For forming supporting signals of phase detectors and modulators with phases shift 0° and 90° on the additional wave were used output signal x and its derivative x'.
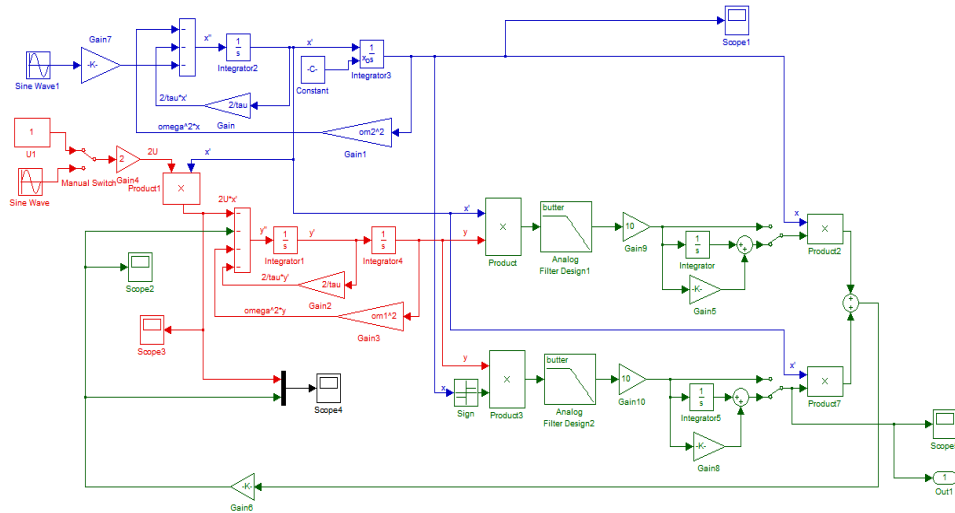
Figure 5. Simulink model

Simulation results are presented on figures 6, 7 and 8. They represent the system behavior with two types of correction in the feedback channel – proportional and integral-positional. Also there was analyzed the system behavior when angular velocity is constant and when it changes according to harmonic law.
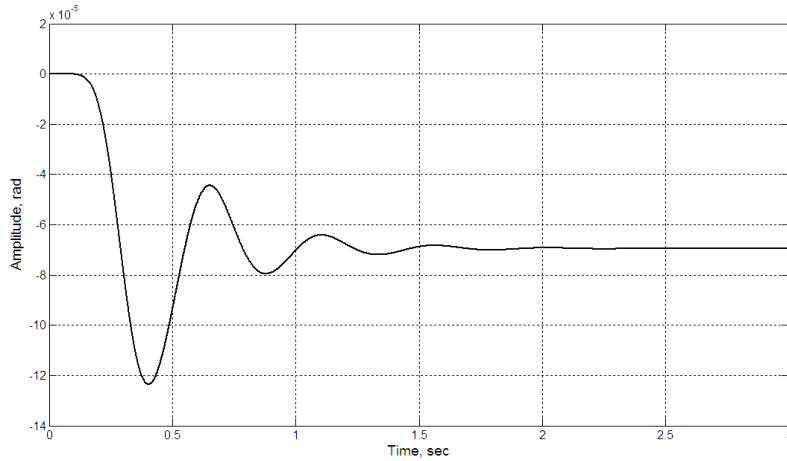
Figure 6. Diagram of WSG's output signal with proportional correction
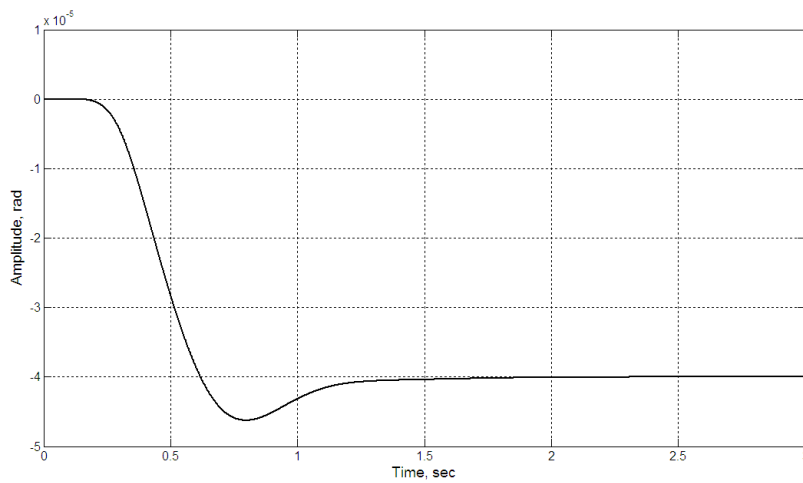
Figure 7. Diagram of WSG's output signal with integral- positional correction
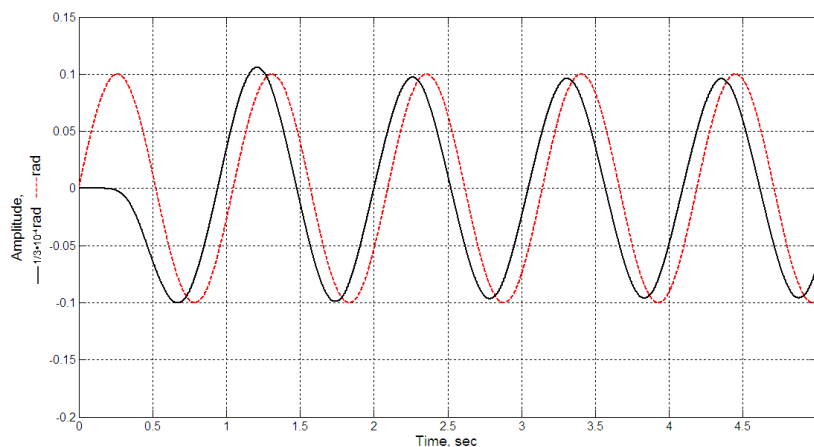
Figure 8. Diagram of WSG's output signal with integral- positional correction and change of entrance signal according to harmonic law

(———— output signal; - - - - - - measured velocity)

4. Conclusions

The power balancing system with the proportional correction does not provide the required quality of the transient. In this case overshoot reaches 74%.

For ensuring acceptable characteristics integral-positional correction should be used. Its use leads to increasing the fast-acting of the system. In this case, the overshoot is reduced approximately 4-fold to a value of 17,5%.

Question of reducing the dynamic errors requires further consideration.

References

1. D. Lynch *Coriolis Vibratory Gyros* Symposium Gyro Technology, Stuttgart, Germany 1998.
2. D. Lynch *Vibrating Gyro Analysis by the Method of Averaging* 2nd St. Petersburg International Conference on Gyroscopic Technology and Navigation, St. Petersburg, Russia, May 24-25, 1995 – p. 26-34.

Application of an oscillating flap to improve glider aerodynamical characteristics

Dominik GŁOWACKI

Warsaw University of Technology, The Institute of Aeronautics and Applied Mechanics
dglowacki@meil.pw.edu.pl

Jakub GŁOWACKI

Warsaw University of Technology, The Faculty of Power and Aeronautical Engineering
yaqb3@wp.pl

Michał KAWALEC

Warsaw University of Technology, The Faculty of Power and Aeronautical Engineering
michal.kawalec@gmail.com

Józef PIETRUCHA

Warsaw University of Technology, The Institute of Aeronautics and Applied Mechanics
japietru@meil.pw.edu.pl

Abstract

This paper summarizes the results of the first stage of the project tilted "Multifunctional two person motoglider driven by an electrical motor" conducted at The Institute of Aeronautics and Applied Mechanics at Warsaw Technical University, Warsaw, Poland.. The goal of this stage was to build a flying laboratory including a mechanism with an oscillating flap. According to on the previously published results of research done by Boldyriev the average drag of a wing with an oscillating flap is much lower than the drag of the fix wing. The results were so good that we decided to verify them by repeating some of his tests. Discussion of our experiments, test results and supporting numerical calculations are also presented in this paper.

Key words: oscillating flap, experimental model, numerical simulation.

1. Introduction

The goal that all aeronautical designers want to achieve is enhancement of the highest gilder glide ratio. Traditional approach, which includes application of different laminar shapes in the wing design requires huge money investment and the results are still deceiving. Further increase of the already high glide ratio is possible only with the use of unconventional methods. Multiple flying techniques observed in nature suggest use of a flapping wing. One implementation of this flying technique is described in a very interesting, but not commonly known work describing an oscillating flap [1] by Aleksander Iwanowicz Boldyriev (Department of Aerodynamics of Moscow Aeronautical Institute – MAI) in early thirties of the twenty century. At that time the book "Hydro- und Aerodynamik" [2], was published. In this book an interesting phenomena was investigated: The top surface of a wing was subjected to an intensive flow rate, which significantly increased the lift force and decreased the take-off distance of an aircraft. Multiple experiments with models of this type of wing were conducted in

1940 and beyond. Flying models and tests in a wind tunnel suggested a new aerodynamical phenomena: the thrust force appeared and the lift force increased when the flap which was inserted just above and ahead of the leading edge was brought to oscillations with the ±15°amplitude (Fig.1a).

A model in the 1:2 scale was built and tested by Boldyriev in a wind tunnel. Published results were surprisingly good (Fig. 1b) so good that we decided to verify them. Moreover, even thou that Boldyriev built an experimental aircraft, his work has never been commercially implemented and the records related to the plane tests have been lost. It may suggest that Boldyriev met some technical difficulties that we are not aware about.
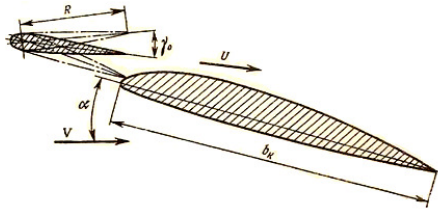
a)   **b)**
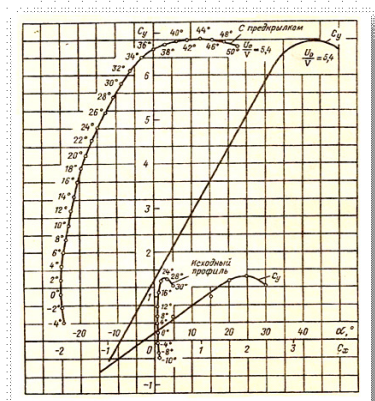
Figure 1. Experimental results achieved by Bołdyriew

2. Experimental model

To check experimental results made in MAI and to verify numerical simulation, a model of the oscillating flap was built (fig.2). Technical details of this model are presented below:
 - wing span – 530 mm
 - wing chord – 150 mm (with the 200 mm flap)
 - angle of flapping movement oscillation - ±15deg
 - frequency 40Hz (for a short period of time 60Hz)
 - wing airfoil NACA23020

Composite structure was chosen for the model. It consisted of a mobile platform with the vertically fastened object in a wing shape having a movable front flap and a driving mechanism.
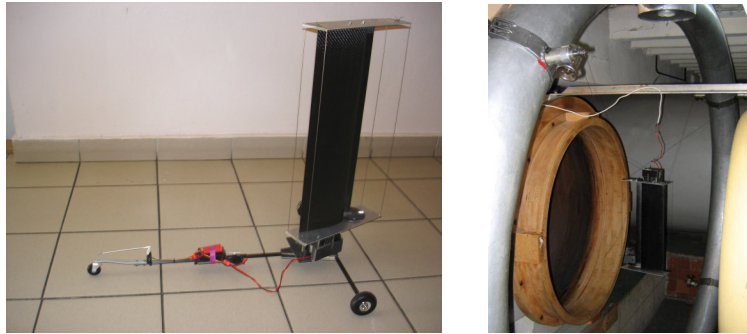
Figure 2. Experimental model of the oscillating flap: a), on mobile platform, b) in wind tunnel

All elements were made from polymer composites which were strengthen with carbon fibers. The driving mechanism consisted of an electrical motor, gear and crank mechanisms and a connection rod. This driving mechanism allowed oscillation of the flap with designed amplitude and frequency.

3. Experiments in the wind tunnel

Experimental investigation was conducted in The Institute of Aeronautics and Applied Mechanics' wind tunnel. The tested element was fixed to the wind tunnel weight using 8 ties (Fig. 3)
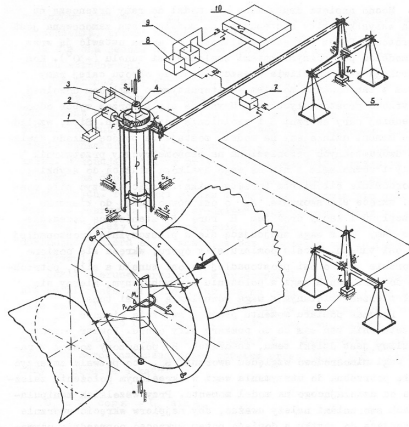
Figure 3. The wind tunnel weight

All the measurement were conducted for the angles of attack ranging from -5 to +20° with the stream velocity equal to 6m/s. Experiments were conducted using the Reynolds and Strouhal numbers defined as follow:

$$\mathrm{Re} = \frac{\rho \cdot u \cdot l}{\mu} \qquad\qquad Sr = \frac{l \cdot f}{u}$$

where:
ρ – air density = 1.225kg/m^3
u – free stream velocity = 6m/s
l – linear dimension =150mm
μ – dynamical viscosity = 17,08·10^{-6} Pa·s
f – frequency of the oscillations.

As the result of the experiment two diagrams showing dependence between the lift force and the drag force in the function of the angle of attack for different frequencies of the oscillating flap were obtained (Fig.4).
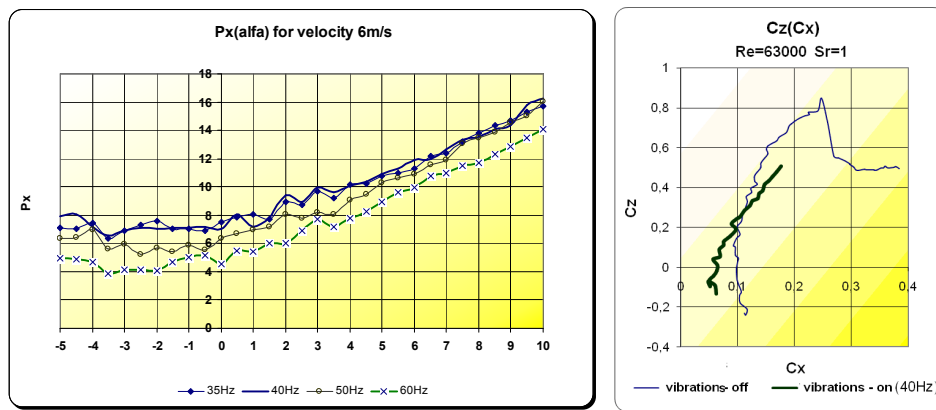
Figure 4. Aerodynamical characteristics of the oscillating flap

An increase of frequency of the flap oscillations on the wing drag is evident according to the Fig.4. It causes increase of the glade ratio. However we have never achieved a negative value of that force contrary to the results that were obtained at MAI. It may be at least two reasons for it. Firstly, we couldn't reach any higher frequency than 60Hz. A further increase of the frequency caused the resonance of the tested element with the wind tunnel weight leading to destruction of the test sample. Secondly, small dimensions of our model prevented us from obtaining higher Reynolds and Strouhal numbers.

What is also worth to mention is the dependency between the lift coefficient and the angle of attack. It can be easily observed that lift coefficient is lower when the oscillating flap is used. This observation is quite contrary to what it was obtained in MAI.

Comparing our results with the results that are presented on Fig 1, we came into conclusion that Bołdyriev results are too optimistic.

4. Comparison of the numerical and experimental simulations.

All the numerical simulations were made using commercial software FLUENT. The results showing pressure and velocity distribution near the airfoil is presented below.
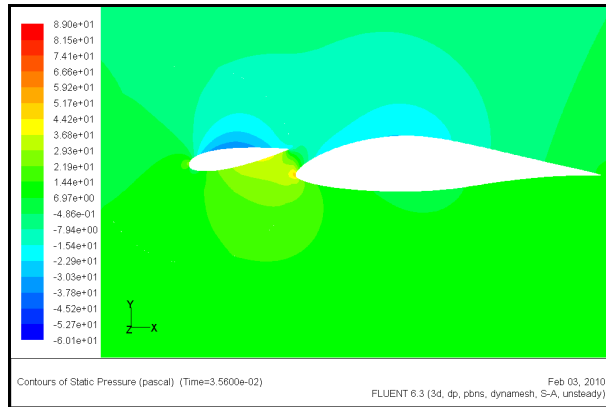
Figure 6. Pressure distribution around the airfoil with the oscillating flap
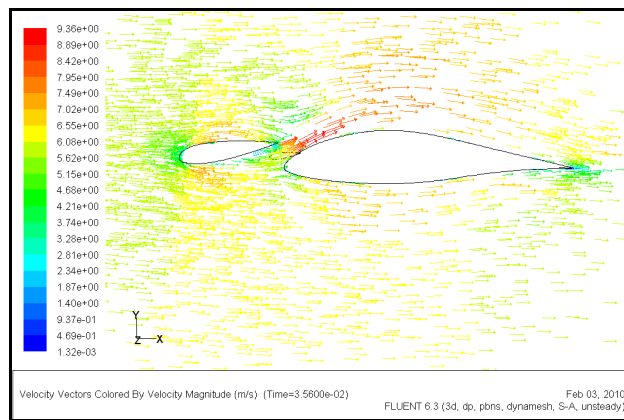
Figure 7.Velocity vectors around the airfoil with the oscillating flap

Dependency between the drag force and the lift force in a function of time are shown on Fig.8

Pz(t)

Px(t)
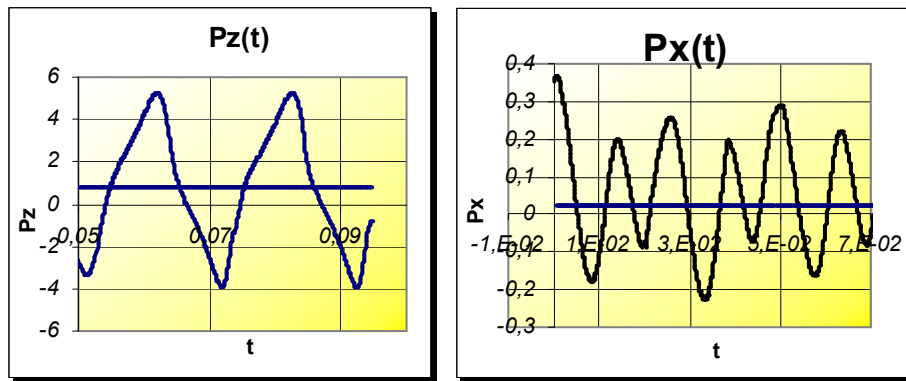
Figure 8. The drag and lift forces showing mean values in a function of time

The mean values of the drag and lift forces characteristics $C_x(\alpha)$, $C_z(\alpha)$ were obtained, and compared with the tunnel experimental results (Fig. 9).

Cz(Cx)
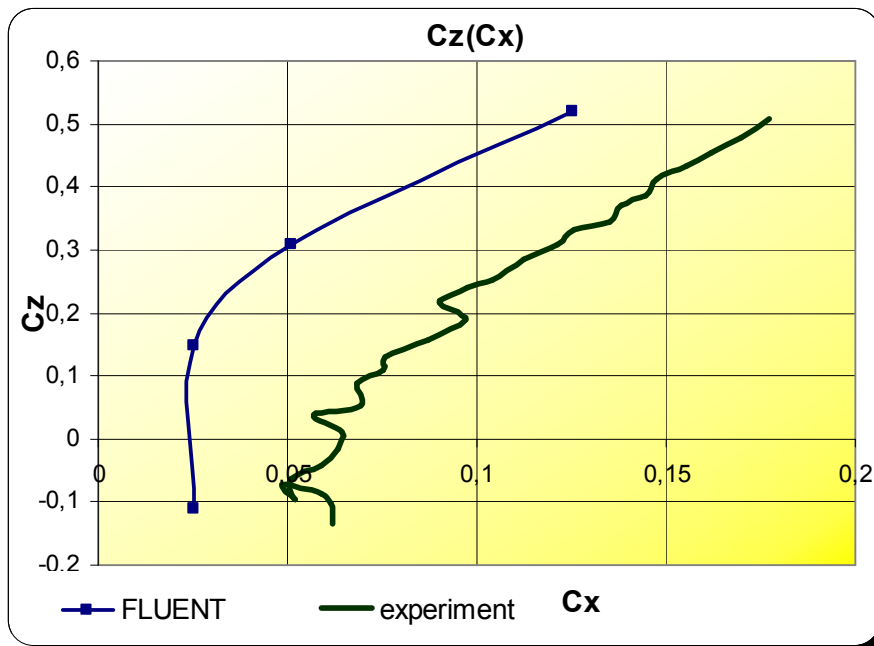
Figure 9. The lift coefficient and the drag coefficient in function of time

Numerical simulation made in FLUENT and the experimental results are comparable. It proves that the results gained with the finite volume method are correct and very close to those observed in the experiment.

Further simulations for different cases were also conducted. We decided to rerun our simulation for higher Reynolds and Strouhal numbers. To do it, we changed following inputs of the simulation:

chord = 465mm

Free stream velocity = 6m/s

Frequency of oscillation =60Hz and 120Hz

Received results are presented on Fig. 10.
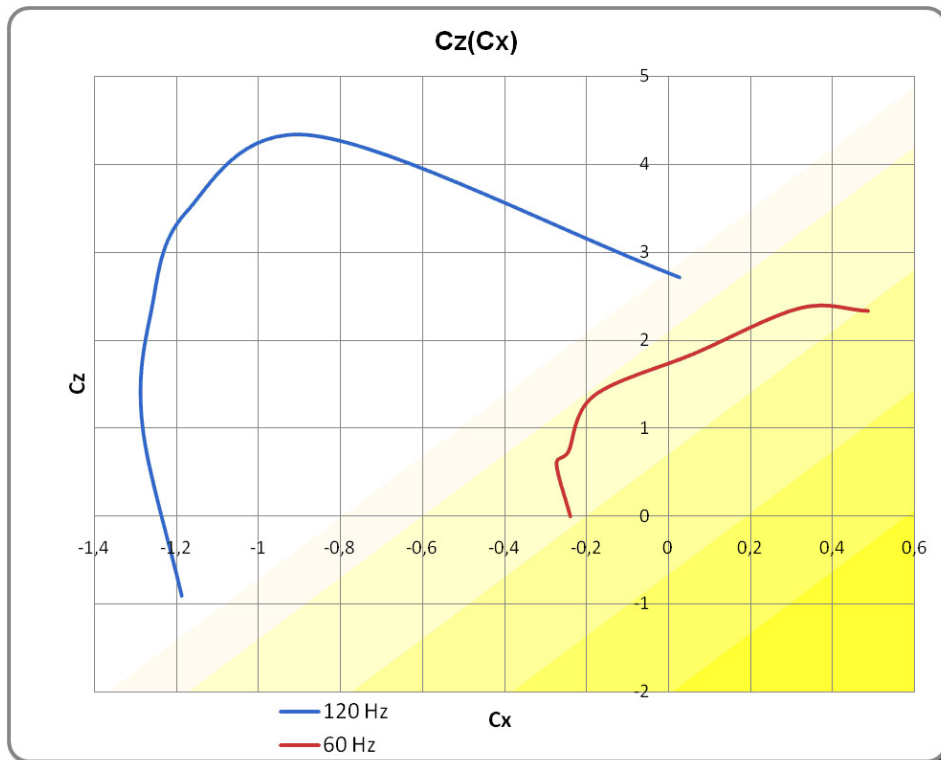
Figure 10. Dependency between the lift coefficient and the drag coefficient for different frequency of the oscillating flap

5. Conclusions

Both the wind tunnel and the numerical simulations results are very promising. They show the reduction of the drag force and increase of the lift force due to the use of the flapping wing.. However, we couldn't obtain as good results as those claimed by Boldyriev in his publications. In spite of that, the application of the oscillating flap represents a huge potential for further improvements in the construction of gliders.

It is also worth to mention that a high frequency of oscillations is essential to obtain a visible drag reduction and a substantial lift generation. This frequency may lead to an unwanted transmission of the generated vibrations into different parts of an aircraft. We think that it is at least a partial explanation to the mechanical failure of the first prototype that was built and tested in the 40's.

Acknowledgments

References

1.   Ю.В. Макаров, *Летательные аппараты МАИ,* Москва иэдательство МАИ 1994
2.   L. Prandtl, O. Tietjens, *Hydro- und Aerodynamik*, Berlin 1929-1931

Zastosowanie wibroklapy do polepszania charakterystyk aerodynamicznych szybowców

Celem pracy podjętej w ramach projektu „wielofunkcyjny dwumiejscowy motoszybowiec z napędem elektrycznym AOS-71", a której wybrane wyniki są przedmiotem zgłaszanego referatu, jest zbudowanie latającego laboratorium, które m.in. będzie zawierało urządzenie z wibroklapy.

Dotąd okazało się, że średni opór skrzydła z wibroklapą jest mniejszy od oporu skrzydła nieruchomego, co już daje , zwiększenie doskonałości. Jednym z głównych problemów, które się pojawiały był dobór najodpowiedniejszej częstości i amplitudy drgań wibroklapy. Zagadnieniu temu, jak i samej metodzie obliczeń oraz weryfikacji doświadczalnej, poświęcony będzie nin. referat.

Properties of resonance-type and dynamic vibration eliminators

Zdzisław GOLEC

Poznan University of Technology, Institute of Applied Mechanics
3 Piotrowo Street, PL 60-965 Poznan
zdzislaw.golec@put.poznan.pl

Abstract

The paper presents a rheological model of a body, which properties are described by means of a fractional derivative of its deformation. Such a model of a body was used to describe the coupling between a protected object and vibration eliminator. Then differential equations of motion were solved and effectiveness of vibration elimination was determined.

Keywords: vibration eliminators, models of rheological bodies, fractional derivatives

1. Introduction

In the task of vibration elimination the forces of reaction of an eliminator on a protected object may be described as a continuum, which properties are described as follows:

$$R(\varepsilon, \sigma, t) = 0 , \qquad (1)$$

where ε is deformation, σ is stress and t is time.

Basic rheological models of bodies can be described for different forms of Equation (1). Selected rheolgical models of bodies are shown in Table 1 [1].

Table 1. Basic rheological models of bodies

Model name	Model schema	Constitutive equation
Hook model	E	$\sigma = E\varepsilon$
Newton model	η	$\sigma = \eta\dot{\varepsilon}$
Kelvin – Voigt model	E η	$\sigma = E\varepsilon + \eta\dot{\varepsilon}$
Maxwell model	E $\quad$ η	$\dot{\varepsilon} = \dfrac{1}{E}\dot{\sigma} + \dfrac{1}{\eta}\sigma$
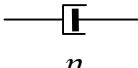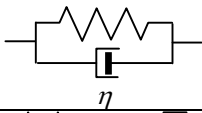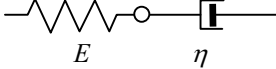
Taking a simple discrete two-degree-of-freedom model of a protected system with an eliminator (rys.1) into consideration, the force interaction S between the protected object
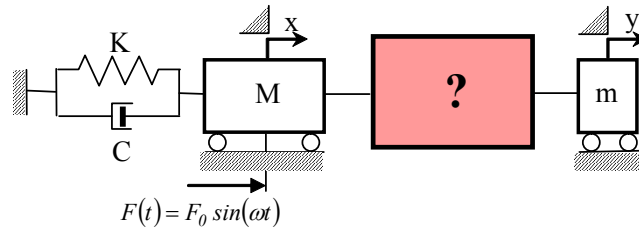
Figure 1. Physical model of a protected system with a vibration eliminator

M and the eliminator m is a function of deformation $(x - y)$ and deformation velocity $(\dot{x} - \dot{y})$ of a coupling object:

$$S = S[(x - y), (\dot{x} - \dot{y})] \tag{2}$$

Hence, for the first two models one can write that force S is proportional:
  - in the Hook model – to the zero derivative of deformation with respect to time - $S \sim (x - y)$,

  - in the Newton model – to the first derivative of deformation - $S \sim \dfrac{d}{dt}(x - y)$.

The first case concerns a dynamic eliminator, and the second case – a viscous one. Properties of both eliminator types may be compared with the assumption that the force of interaction between the eliminator and the protected system is proportional to the fractional derivative of coupling element deformation with respect to time

$$S \sim \frac{d^\alpha}{dt^\alpha}(x - y), \ 0 \le \alpha \le 1 \ [2].$$

2. Physical model of a protected system with an eliminator described using a fractional derivative

Let us consider a simple model of a system protected by a vibration eliminator. The protected system has been assumed as a linear single-degree-of-freedom system of mass M, stiffness K and damping C, which is moved by a harmonic force of constant amplitude (Fig. 2). The eliminator has also one degree of freedom, and the coupling between the two masses is described as follows:

$$S = k_\alpha D_t^\alpha(x - y), \quad 0 \le \alpha \le 1, \tag{3}$$

where the operator $D_t^\alpha(\bullet) \equiv \dfrac{d^\alpha}{dt^\alpha}(\bullet)$
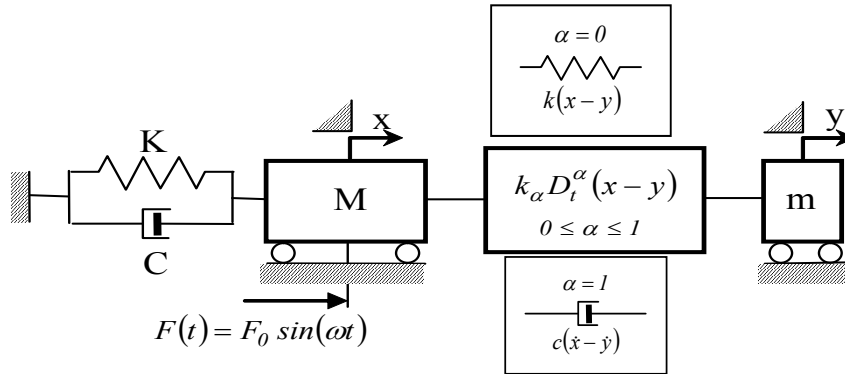
Figure 2. Diagram of a protected system with an eliminator with coupling described by means of a fractional derivative

At present it is difficult to find a physical interpretation of coefficient k_α. It describes some elastic-lossy properties of the coupling of the two subsystems. For boundary values of quantity α it has the following interpretation:

- $\alpha = 0 \rightarrow k_\alpha = k$ - stiffness coefficient,
- $\alpha = 1 \rightarrow k_\alpha = c$ - damping coefficient.

Equations of motion of the system shown in Fig. 2 for any value of α ($0 \le \alpha \le 1$) may be written as:

$$M\ddot{x} + C\dot{x} + Kx + k_\alpha D_t^\alpha (x - y) = F_0 \sin(\omega t)$$
$$m\ddot{y} - k_\alpha D_t^\alpha (x - y) = 0, \qquad 0 \le \alpha \le 1$$

(4)

where the fractional derivative of function *f(t)* is defined as follows [2]:

$$D_t^\nu [f(t)] = \frac{1}{\Gamma(1-\nu)} \frac{d}{dt} \int_0^t \frac{f(\tau)}{(t-\tau)^\nu} \, d\tau, \; 0 \le \nu \le 1$$

(5)

The exact solution can be found using Laplace integral transform. The Laplace form of solutions to Equations (5) may be written:

$$X(s) = F_0 \frac{\omega}{s^2 + \omega^2} \frac{ms^2 + k_\alpha s^\alpha}{\left(Ms^2 + Cs + k_\alpha s^\alpha + K\right)\left(ms^2 + k_\alpha s^\alpha\right) - \left(k_\alpha s^\alpha\right)^2}$$

$$Y(s) = F_0 \frac{\omega}{s^2 + \omega^2} \frac{k_\alpha s^\alpha}{\left(Ms^2 + Cs + k_\alpha s^\alpha + K\right)\left(ms^2 + k_\alpha s^\alpha\right) - \left(k_\alpha s^\alpha\right)^2}$$

(6)

$$dla \quad D_t^{n+\alpha} [x(t)]_{t=0} = 0$$

The solution to equations (5) obtained using inverse Fourier transform is rather complicated. The paper presents an approximate solution.

3. Approximate solution to the equations of motion of the system

For limiting values of k_α $(k_\alpha = 0$ i $k_\alpha = 1)$ and harmonic forcing $F(t) = F_0 \sin(\omega t)$ the stationary solution to Equations (5) are harmonic:

$$x(t) = A \sin(\omega t - \varphi_1), \quad y(t) = B \sin(\omega t - \varphi_2) \tag{7}$$

Taking the above into consideration it has been assumed, that the solution to Equations (5) for any value of coefficient k_α from interval $\langle 0,1 \rangle$ will be approximately harmonic:

$$x = A_c \cos(\omega t) + A_s \sin(\omega t), y = B_c \cos(\omega t) + B_s \sin(\omega t). \tag{8}$$

If we substitute the assumed solution (8) in Equations (5), then the unknowns (amplitude-frequency characteristics) A_c, A_s, B_c, B_s must satisfy the system of algebraic equations:

$$G \cdot A = F \tag{9}$$

where:

$$G =$$

$$\begin{Bmatrix} 1 - \delta^2 + k_{\alpha 1}\delta^\alpha \cos\left(\alpha\frac{\pi}{2}\right) & 2\xi\delta + k_{\alpha 1}\delta^\alpha \sin\left(\alpha\frac{\pi}{2}\right) & -k_{\alpha 1}\delta^\alpha \cos\left(\alpha\frac{\pi}{2}\right) & -k_{\alpha 1}\delta^\alpha \sin\left(\alpha\frac{\pi}{2}\right) \\ -2\xi\delta - k_{\alpha 1}\delta^\alpha \sin\left(\alpha\frac{\pi}{2}\right) & 1 - \delta^2 + k_{\alpha 1}\delta^\alpha \cos\left(\alpha\frac{\pi}{2}\right) & k_{\alpha 1}\delta^\alpha \sin\left(\alpha\frac{\pi}{2}\right) & -k_{\alpha 1}\delta^\alpha \cos\left(\alpha\frac{\pi}{2}\right) \\ -k_{\alpha 1}\delta^\alpha \cos\left(\alpha\frac{\pi}{2}\right) & -k_{\alpha 1}\delta^\alpha \sin\left(\alpha\frac{\pi}{2}\right) & -\mu\omega^2 + k_{\alpha 1}\delta^\alpha \cos\left(\alpha\frac{\pi}{2}\right) & k_{\alpha 1}\delta^\alpha \sin\left(\alpha\frac{\pi}{2}\right) \\ k_{\alpha 1}\delta^\alpha \sin\left(\alpha\frac{\pi}{2}\right) & -k_{\alpha 1}\delta^\alpha \cos\left(\alpha\frac{\pi}{2}\right) & k_{\alpha 1}\delta^\alpha \sin\left(\alpha\frac{\pi}{2}\right) & -\mu\omega^2 + k_{\alpha 1}\delta^\alpha \cos\left(\alpha\frac{\pi}{2}\right) \end{Bmatrix}$$

$$A = \begin{Bmatrix} A_{c1} \\ A_{s1} \\ B_{c1} \\ B_{s1} \end{Bmatrix}, \quad F = \begin{Bmatrix} 0 \\ F_{01} \\ 0 \\ 0 \end{Bmatrix} \tag{10}$$

The following dimensionless parameters were introduced in Equation (9):

$$\xi = \frac{C}{2\sqrt{KM}}, \; k_{\alpha 1} = k_\alpha \frac{\omega_0^\alpha}{K}, \; \omega_0 = \sqrt{\frac{K}{M}}, \; \delta = \frac{\omega}{\omega_0}, \; \mu = \frac{m}{M}, \; F_{01} = \frac{F_0}{Mg},$$

$$A_{c1} = \frac{A_c}{Mg/K}, \; A_{s1} = \frac{A_s}{Mg/K}, \; B_{c1} = \frac{B_c}{Mg/K}, \; B_{s1} = \frac{B_s}{Mg/K},$$

Hence, the dimensionless solution to the system of differential equations (5) assumes the form:

$$x_1 = A_1(\delta)\sin(2\pi\delta\tau + \beta), \; y_1 = B_1(\delta)\sin(2\pi\delta\tau + \gamma) \tag{11}$$

where

$$A_1(\delta) = \sqrt{A_{c1}^2(\delta) + A_{s1}^2(\delta)}, \quad B_1(\delta) = \sqrt{B_{c1}^2(\delta) + B_{s1}^2(\delta)}, \qquad \text{amplitude-frequency}$$

characteristics, $\beta(\delta) = arctg\left(\dfrac{A_{s1}(\delta)}{A_{c1}(\delta)}\right)$, $\gamma(\delta) = arctg\left(\dfrac{B_{s1}(\delta)}{B_{c1}(\delta)}\right)$ phase-frequency

characteristics, $\tau = \dfrac{t}{T_0}, T_0 = \dfrac{2\pi}{\omega_0}$ dimensionless time

Fig. 3 shows examples of computed dimensionless vibration amplitudes for a protected object with an eliminator A_1 and without an eliminator A_{01} for given parameter values.
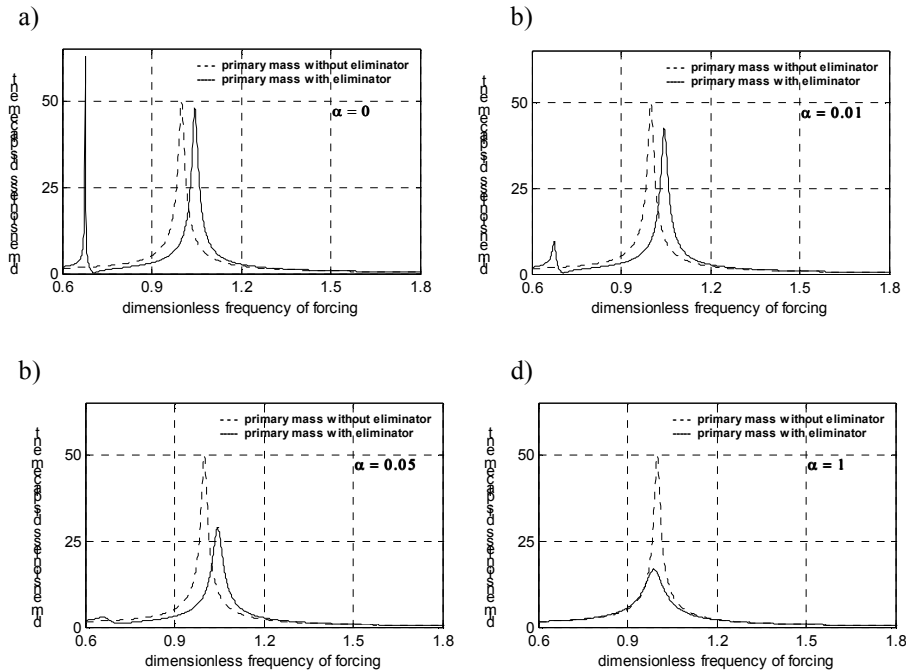
Figure 3. Dimensionless vibration amplitudes for a protected object with an eliminator A_1 – solid curve, and without an eliminator A_{01} – dotted curve as a function of dimensionless frequency of forcing for parameter values $\xi = 0.01, \mu = 0.1, k_{\alpha 1} = 0.05$ and various α values

From the presented curses of vibration amplitudes for a protected object it can be stated that the presented model of coupling between the protected system and the eliminator enables to observe the change of curve A_1 as a two-modal curve (two-degree-of freedom system with elastic coupling) into a one-modal one (two-degree-of freedom system with lossy coupling),

4. Effectiveness of vibration elimination of an eliminator

Effectiveness of vibration reduction in the task of vibration elimination has been assessed based on the function of effectiveness of vibration elimination defined here as a ratio of a vibration amplitude for the protected system without an eliminator to the one for the system with such an eliminator:

$$E(\delta) = \frac{A_{01}(\delta)}{A_1(\delta)} \tag{12}$$

If the value is greater than one, $E > 1$, then the eliminator fulfils its task and we can observe reduction of the vibration amplitude of the protected system. Comparing curves A_1 and A_{01} from Fig. 3 one can easily find out that in some ranges of forcing frequency δ vibration reduction can be observed, $A_1 < A_{01}$, (the paper does not present any results of computation of effectiveness of vibration elimination for an eliminator described using fractional derivatives).

5. Conclusions

Based on the conducted numerical research the following conclusions may be drawn:

- Description of dynamic properties of mechanical systems using fractional derivatives makes possible a generalized description of dynamics of classical vibration eliminators.

- For $0 \leq \alpha \leq 1$ we can freely take elastic-lossy properties of the coupling between a protected system and an eliminator into consideration, and therefore we can freely model the effectiveness of vibration elimination.

References

1. Z. OSiński [red.] *Tłumienie drgań mechanicznych*, PWN, Warszawa 1986.
2. Z. GOLEC, M. GOLEC, *Model of Damper of Vibration with interaction described by Means of Fractional Derivatives*, Proceedings of XIXth Symposium Vibrations in Physical Systems, Poznań – Błażejewko, May 23 – 27,2000
3. Ch. D. MORGAN, *Effect of Fractional Based Damping of Dynamic System Response*, PhD Thesis, University of Akron, 1998

Właściwości rezonansowych i dynamicznych eliminatorów drgań

W pracy przedstawiono model reologiczny ciała, którego własności opisano niecałkowitą pochodną jego deformacji. Taki model ciała wykorzystano w opisie sprzężenia obiektu chronionego z eliminatorem drgań. Rozwiązano różniczkowe równania ruchu i określono skuteczność eliminacji drgań mechanicznych.

Dice Throw Dynamics Including Bouncing

Juliusz GRABSKI
Technical University of Łódź, 90-924 Łódź, Stefanowskiego 1/15
julgrabs@p.lodz.pl

Jarosław STRZAŁKO
Technical University of Łódź, 90-924 Łódź, Stefanowskiego 1/15
jstrzalk@poczta.onet.pl

Tomasz KAPITANIAK
Technical University of Łódź, 90-924 Łódź, Stefanowskiego 1/15
tomaszka@p.lodz.pl

Abstract

In the paper some aspects of die throw dynamics are presented. Free fall of die as well as their collisions with table are analysed. Two models of collision are compared: first based on Newton's hypothesis and the second on Poisson's hypothesis. It is shown that from the point of view of dynamical systems dynamics of die is predictable.

Keywords: dice throw, collisions, predictability

1. Introduction

The dynamics of popular randomizer based on throw of a die is considered. The dynamics of this type of gambling can be described in the terms of the Newtonian mechanics so one can expect that the outcome can be predicted. However, due to high sensitivity to initial conditions, very precise devices are necessary to predict the outcome. Therefore, the result is practically pseudorandom. Evidence that the pseudorandomness in mechanical systems can be fully understood in terms of nonlinear dynamics as temporal sensitivity to the initial conditions generated by nonsmooth properties of the randomizers is given in [1].

A throw of a fair die is commonly considered as a paradigm for chance. The die is usually a cube of a homogeneous material. The symmetry suggests that such a die has the same chance of landing on each of its six faces after a vigorous roll so it is considered to be fair. Generally, a die with a shape of convex polyhedron is fair by symmetry if and only if it is symmetric with respect to all its faces [2]. The polyhedra with this property are called the isohedra. The commonly known examples of isohedra are: tetrahedron, hexahedron (cube), octahedron, dodecahedron and icosahedron which are also used as the shapes for dice. Typical isohedra are shown in Fig. 1.

Two models of collision are used in the analysis: first based on Newton's hypothesis and the second on Poisson's hypothesis. In Newton's model of an impact tangential impulses cannot influence on normal impulses whereas Poisson's hypothesis allows an energy transfer between tangential and normal directions.
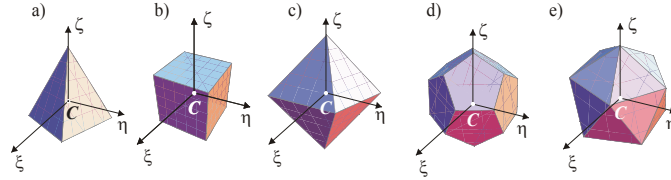
Figure 1. Isohedral dice: a) tetrahedron, b) hexahedron (cube), c) octahedron,
d) dodecahedron, e) icosahedron

2. Dynamics of coin toss and die throw

Rigid body dynamics equations can be expressed as two equations in matrix form that describe:

– motion of the body mass centre

$$\mathbf{M}\left(\mathbf{a}_B + \dot{\boldsymbol{\Omega}}\mathbf{r}_C + \boldsymbol{\Omega}\boldsymbol{\Omega}\mathbf{r}_C\right) = \mathbf{f}, \tag{1}$$

– spatial orientation of the body

$$\mathbf{J}_B\dot{\boldsymbol{\omega}} + \boldsymbol{\Omega}\mathbf{J}_B\boldsymbol{\omega} + \mathbf{M}\mathbf{R}_C\,\mathbf{a}_B = \mathbf{m}_B. \tag{2}$$

In mentioned equations $\mathbf{M}$ is the mass matrix of the coin or the die, $\mathbf{a}_B$ denotes absolute acceleration of the point B, $\mathbf{r}_C$ and $\mathbf{R}_C$ include coordinates of the vector $\mathbf{r}_C$, describing the position of centre mass (C) relative to the origin B, $\mathbf{J}_B$ is the body moment of inertia matrix (determined with respect to the body embedded frame $\xi_B\eta_B\zeta_B$ – parallel to the $\xi\eta\zeta$ and with origin B), and $\mathbf{m}_B$ is the body force moment with respect to the B, $\boldsymbol{\omega}$ and $\boldsymbol{\Omega}$ are the body angular velocity vectors in the form of column and antisymmetric matrices. In general case, for nonsymmetric or nonhomogenous coin, the matrix $\mathbf{J}_B$ is not diagonal, because the axes ξ_B, η_B, ζ_B are not principal axes (some nonzero inertia products in $\mathbf{J}_B$ appear).

The column matrices $\mathbf{a}_B$ and $\mathbf{f}$ are expressed by vector components with respect to the fixed frame (xyz). On the other hand, it is more convenient to describe rotations of the body by their components with respect to the body embedded frame ($\xi\eta\zeta$).

The equations (1) and (2) are coupled equations even though free fall of a coin or a die is considered, i.e. even if the air resistance is neglected.

3. Modelling of a collision

In the analysis of die–table collision impact hypothesis, the laws of linear momentum and angular momentum of rigid body as well as constraint equations are employed. To describe a collision of the body with a table we assume that: (i) the table is modelled as flat, horizontal, elastic body (fixed), (ii) a friction force between the table and the die is included, (iii) only one point of the die is in contact with the table during each collision.

In most of papers ([1], [3], [4]) the coin collision with the table are analysed using Newton's hypothesis. With those assumptions one gets

$$v''_{Ay} = -\chi \, v'_{Ay} \,. \tag{3}$$

where χ is the coefficient of restitution, A stands for the coin point that is in contact with the floor at the instant of impact, v'_{Ay} and v''_{Ay} are projections of the velocity of point A on the direction (y) normal to the impact surface respectively before and after the impact. Such an idealization can be used if the energy balance allows it.

Kane [5] shown, that Newton's hypothesis used in collision of bodies including friction leads – for certain values of friction coefficient μ and restitution coefficient χ – to erroneous results. The illustration of such situations is presented in Fig. 2, where the mechanical energy loss during the collision is shown. For some regions (coloured in green and yellow) the mechanical energy after the collision is bigger than before.
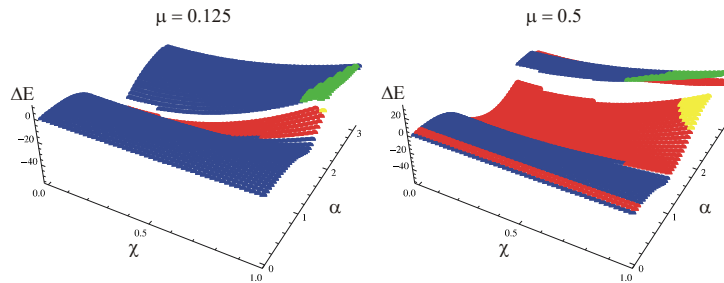
Figure 2. Energy loss and energy growth after collision (Newton's hypothesis)

Using Poisson's hypothesis [6], i.e. assuming that the normal components of impulse vectors in compression phase (**S'**) and expansion phase (**S''**) are proportional we avoid such difficulties as the energy increase after a collision.

The normal and tangent impulses for the compression phase can be expressed as:

$$S'_N = \lim_{t_C \to t_A} \int_{t_A}^{t_C} N' \, dt \,, \qquad S'_T = \lim_{t_C \to t_A} \int_{t_A}^{t_C} T' \, dt \,, \tag{4}$$

and Poisson's impact law in the normal direction for the compression phase is characterized by:

$$S'_N \geq 0 \,, \qquad v'_{Ay} \geq 0 \,. \tag{5}$$

The impact law for the phase of expansion is described by

$$S''_N = \chi \, S'_N \,, \qquad v''_{Ay} \geq 0 \,. \tag{6}$$

From Coulomb's hypothesis of friction we get

$$\left| S'_T \right| \leq \mu \, S'_N \,, \qquad \left| S''_T \right| \leq \mu \, S''_N \,. \tag{7}$$

(More details on impacts with friction analysis by Poisson's law can be found in the book of Pfeiffer and Glocker [6].)

Results shown in Fig. 3 were obtained for the same parameters as used in the cases presented in Fig. 2. It can be observed that there are no regions where the energy after the collision is bigger than before.
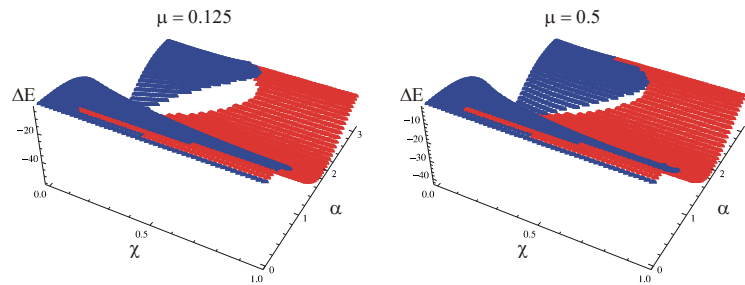
Figure 3. Energy loss after collision (Poisson's hypothesis)

3. Simulation results

In Figures 4–6 we present some exemplary results of dice throw simulation. The trajectory of dice vertices as well as the dice position and orientation during the collisions are shown. (For numerical simulations we used Mathematica package [7].)

a)   b)
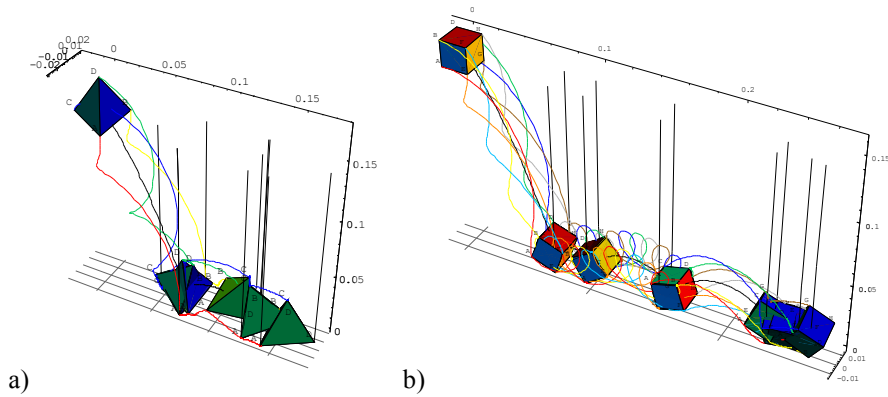
Figure 4. Die throw simulation: a) tetrahedron die, b) hexahedron (cube) die,
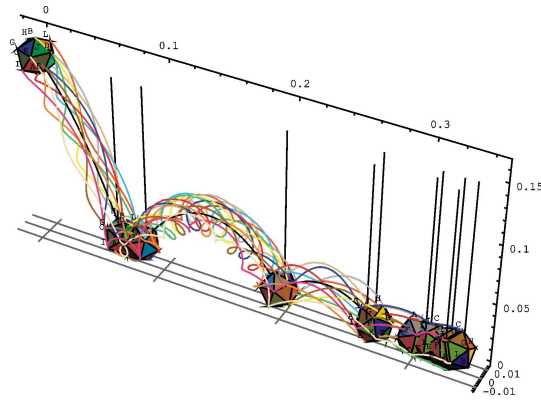
Figure 5. Die throw simulation – icosahedron die

In Figure 6 the outcome results of perfect homogenous cube die throw are compared with results obtained for imperfect (nonhomogenous) cube die. Simulations were performed for the same parameters (except of the mass centre position coordinate ζ_d) and initial conditions for $i=30$ throws of the dice. Final results of the die throw is depicted by the colour corresponding of bottom die face. Obviously the imperfection change the result of die throw. The number of analysed collisions was $n=20$ and we point out that there are not changes in outcome results after $n>12$ collisions (for the assumed coefficient of restitution and the die parameters). Bar charts illustrate probability of outcome result for each face (f) of the die.
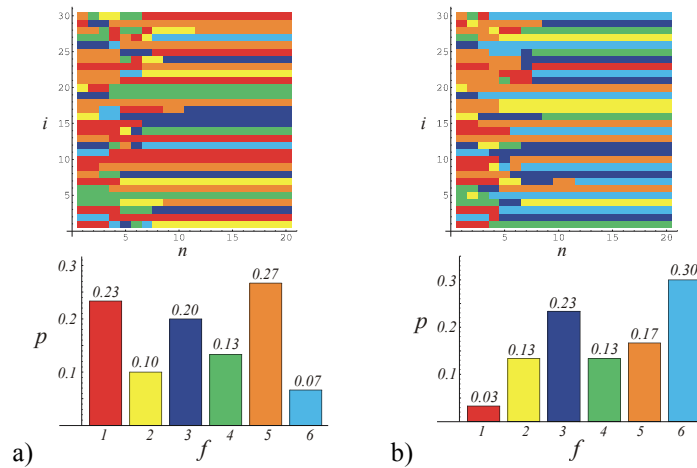
Figure 6. Die throw final results for: a) perfect cube die,
b) imperfect (unfair) cube die

4. Conclusions

To avoid the mechanical energy increase due to collisions of the die and the table Poisson's hypothesis, based on the assumption that the normal components of impulse vectors in compression phase and expansion phase are proportional, is used. Poisson's hypothesis allows an energy transfer between tangential and normal directions. It can be observed that for this model there are no regions where the energy after the collision is bigger than before.

Die throw simulation results presented in the paper show that there are no changes in the results after n collisions and that the outcome of the die throw is predictable. The final result strongly depends on the initial conditions.

References

1. J. Strzałko, J. Grabski, P. Perlikowski, A. Stefański, T. Kapitaniak, *Dynamics of Gambling: Origins of Randomness in Mechanical Systems*, Series: Lecture Notes in Physics, **792**, Springer 2009.
2. P. Diaconis, J.B. Keller, *Fair dice*. Amer. Math. Mon., **96** (1989) 337–339.
3. Strzałko J., Grabski J., Kapitaniak T., Les dés sont pipés, Pour la Science 385 (2009) 30–36.
4. R. Feldberg, M. Szymkat, C. Knudsen, E. Mosekilde, *Iterated-map approach to die tossing*, Phys. Rev. A **42**/8 (1990) 4493–4502.
5. T.R. Kane, *A Dynamic Puzzle*, Stanford Mechanics Alumni Club Newsletter, (1984) pp. 6.
6. F. Pfeiffer, Ch. Glocker, *Multibody Dynamics with Unilateral Contacts*, John Wiley & Sons, Inc. 1996.
7. S. Wolfram, *The Mathematica Book*, 5th ed. Wolfram Media, Inc. 2004.

Dynamika rzutu kostki do gry z uwzględnieniem zderzeń

Przedmiotem opisanych badań jest analiza zderzeń kostki do gry ze stołem.

Przeprowadzone obliczenia numeryczne i analiza równań wykazały, że użycie hipotezy Newtona do opisu zderzeń dla niektórych wartości współczynnika restytucji może prowadzić do błędnych rozwiązań. W takich przypadkach obserwuje się wzrost wartości energii mechanicznej ciała po uderzeniu w stosunku do jej wartości przed uderzeniem. Wykorzystanie hipotezy Poissona pozwala na uniknięcie takich niespodzianek.

Na podstawie otrzymanych wyników obliczeń numerycznych stwierdzono, że wynik rzutu jest zdeterminowany przez warunki początkowe, że kolejne zderzenia powodują zmiany wyniku rzutu kostką, ale od pewnej liczby zderzeń rezultat rzutu nie ulega zmianie.

Energy experimental method verification dynamical model of human under whole body vibration

Magdalena GRYGOROWICZ
Poznan University of Technology, Institute of Applied Mechanics
3 Piotorwo Street, 60-965 Poznan, POLAND
magdalena.grygorowicz@put.poznan.pl

Marian W. DOBRY
Poznan University of Technology, Institute of Applied Mechanics
3 Piotorwo Street, 60-965 Poznan, POLAND
marian.dobry@put.poznan.pl

Maciej TABASZEWSKI
Poznan University of Technology, Institute of Applied Mechanics
3 Piotorwo Street, 60-965 Poznan, POLAND
maciej.tabaszewski@put.poznan.pl

Abstract

The article presents energetic experimental method of verification dynamical model of human under whole body vibration. There are two phases of this method. Base of the first one is laboratory measurements of strength stimulation power and energy flow. Measurement is made in point of connection actuator and seat loaded sitting operator for slow turn of standard frequency band for whole body vibration.

The second phase its digital simulation of power distribution and energy flow in biodynamical structure of physical model human seated also at this some frequency.

Compare e.g. two energy flow curves into biodynamical structure of human body and energy dose, which passed in this time to man, allows to assess the correctness of the structure and dynamical parameters of physical models.

Keywords: Human body model, whole body vibration, energy flow, power distribution

1. Introduction

The average man seems to be safety at work place. Man might think that there are no more possibilities to improve conditions and safety of work. Nowadays very important is ergonomic of work environmental. Using its principles man can design places of work significantly less harmful effects on health workers.

Appreciated are also other areas of technical sciences, a team of specialists invite medicine doctors of work, anthropologist, constructors, mechanics, mechatronics, acoustics, etc.

Modern work stations are first tested not by humans, but using dummies and human models. These stations must compliance with requirements European directives and ISO standards. Correctness of biodynamical structure, mapping the human body and its parameters depends on the final success of teem construct equipment work stations. In

this article proposed energy method of verification physical models of human under whole body vibrations used in ergonomics.

2. Enerty experimental method of verification dynamical models of human

Energy experimental verification methods of human models based on comparison energy flow domain at a specific point of experimental stand and point reduction biomechanical model in time and frequency range. The energy modeling process has already been widely described in the literature [1-6]. It consists of three phases and the most important is the real object transformation, which is the subject of research in the field of power distribution and energy flow in test pattern. In the case of research it was biological subsystem a human-operator, taking a sitting position of their work (fig 1a). The real object transformation is to describe the phenomena of the energy in object biodynamical structure by physical and mathematical energy model. In Figure (1. b) shows the verified energy physical model of human D-G-HB 2005 seated, an effect of research. The substitute dynamic parameters as masses, elastic deformation and damping of 28 degrees of freedom model have been establish in research.
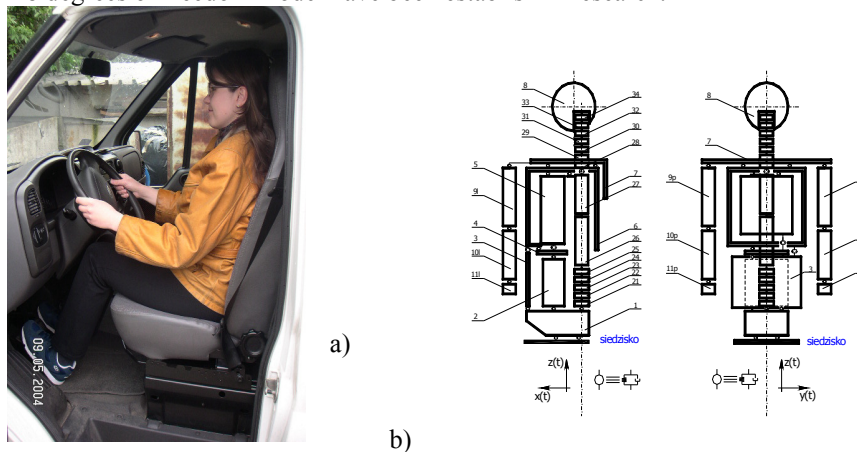
Figure 1. a) The real object – man – operator seated, b) physical model of human D-G-HB 2005 [6]

Physical model was the basis for elaborate a mathematical model using Lagrange equations II type. Solve mathematical model constituting layout 28 differential equations of motion has been done by digital simulation method using special programme MATLAB/silumink.

The energy model of investigate object is obtained by use of elementary Energy Processor MWD for each degree of freedom by extending dynamics digital simulation program. Those Processors enable pass from analysis of the amplitude acceleration, velocity and displacement to areas: power distribution and energy flow in an investigated structure. Dynamic and energy analysis synchronously during various dynamic tests. Selection of dynamic parameters elastic deformation and damping were based on the

acceleration transmitance module Seat-Head. Its known course of experimental – fig. 4.a, let determine correctness changes values in amplitude and frequency scale.

Known from literature physical model HBMN-3 [8] showed large differences in dynamic parameters, and its transfer function acceleration (fig. 4. b) significantly differ from experimental (average 25 measurements): 36% frequency characteristic domain and 1400% as regards maximum amplitude.

Experimental studies had been done in the Laboratory of Dynamic and Ergonomics Metasystem: Man – Technical Object – Environment. Figure 2 shows the test site for dynamic and ergonomic research involving people. It's the most important element was electromagnetic inductor DVC 48 from LDS. On the inductor table was piezoelectric sensor acceleration vibrations fasten as reference sensor join return stabilization amplitude acceleration the frequency band.
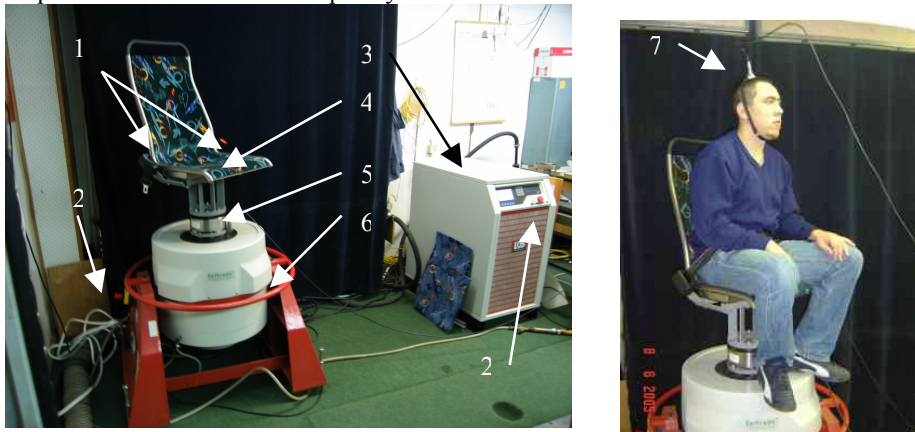
Figure. 2. View of the test stand to test the influence of whole body vibrations on a man in a sitting position; 1-a two-point security belt, 2-button Stop Energy, 3- amplifier LDS, 4-seat's Ster company, 5 – sensor force CL 16, 6 – inductor LDS, 7 – mount vibration sensor head [6].

Scheme of the measuring system, built for experimental research of identification and allocation of power distribution and energy flow in the human biodynamic structure, shown in figure. 3.

Dynamic studies had enabled construction of a new physical model of human called in short D-G-HB 2005 seated (fig 1b).

Constructed structure and its new dynamic parameters were subjected to dynamic simulation investigation. The values of the acceleration transmittance model of seat-Seat-Head assistance for D-G-HB 2005 model in a sitting position are presented below in the frequency range 4 to 80 [Hz] (fig 5).

Comparison of the percentage difference in the values of characteristic frequency and maximum values of the acceleration transmittance module of Seat-Head assistance experiment with tests on D-G-HB 2005 model rendered similar results. This mainly concerned the frequency of vibrations, where both types of transmittance reached

maximum values. The error here was only 3,64 %. The difference between the maximum values reached in both cases was also within the error range, it amounted to 12 %. It was the first successful attempt to adjust the model to the real life object.
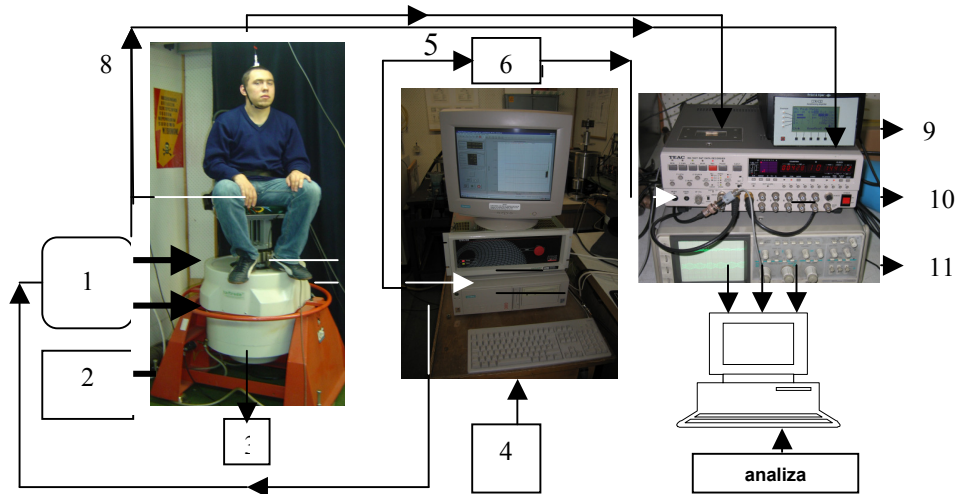
Figure 3. The scheme of measuring system built for experimental power distribution and energy flow in the biodynamic structure of human [6]: 1 – LDS amplifier power 2 – compressor, 3 – solenoid inducer, 4- digital driver system DVC 48, 5-tensometric receptor force CL 16, 6 – amplifier CAX 1304, 7- vibration sensor acceleration, 8 - 4391 B&K 4322 acceleration sensor vibrations, 9 – preamplifier *NEXUS* 2692, 10 – digital recorder TEAC RD135 , 11-*100 MHz* Digital oscilloscope 5501 U.
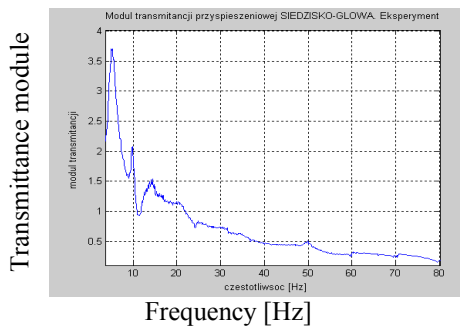
Figure 4a. Mean value of acceleration transmittance module Seat-Head assistance. Experiment [5]
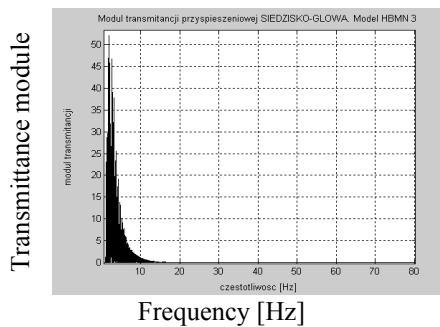
Figure 4b. Mean value of acceleration transmittance module Head-Seat assistance HBMN-3 model [5]

To definitely confirm the compliance of D-G-HB 2005 model with the real life object, flow of input energy applied to the tested object in the two cases was calculated within the tested range of frequency. Fig. 6 present the functions of the energy increase in case of the experiment and D-G-HB 2005 model respectively.
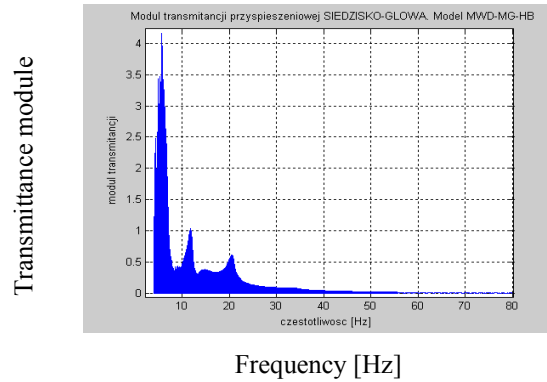
Figure. 5. The acceleration transmittance module Seat-Head performed for model D-G-HB 2005 for seated at frequencies 4 ÷ 80 [Hz] [6].
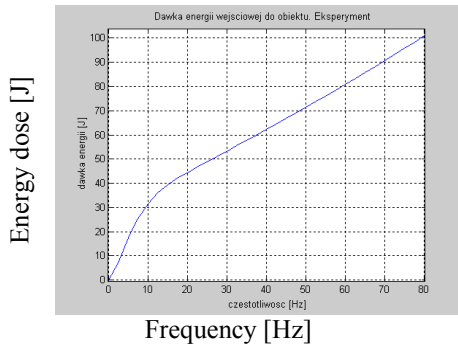
Figure. 6a. Dose of the input energy flow at the tested object: Experiment [6].
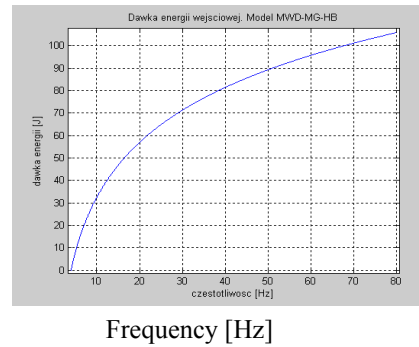
Figure. 6b. Dose of the input energy flow at the tested object: D-G-HB 2005[6].

Comparing the two functions, it may be observed that their courses are similar. Detailed analysis of both flow performance graphs of the energy flow (energy dose) has shown slight deviations with regard to the input energy dose applied to the tested object e.g. in both flow performance graphs in the frequencies of 10 and 80 [Hz]. Difference in the energy dose in the experiment and in case of D-G-HB 2005 model is ~ 3% for the frequency of 10 [Hz] and ~ 4,5 % for the frequency 80 [Hz]. The results confirmed the correctness of the new human body model D-G-HB 2005 in a sitting position as the input energy depends on the entire dynamic structure of the tested subsystem of man.

On the basis of the carried out analyses, it was assumed that the structure and dynamic parameters of the new model are correct. Therefore, we could continue the research on power distribution and energy flow in the biodynamic structure of man exposed to whole body vibrations.

3. Summary

Presented in this article energy experimental method verification of human physical models allows clearly validates the biodynamical structure of new model MWD-MG-HB 2005 man seated. This method allegations of occupational literature that science has not yet sufficiently far away to explore energy passing through the human body [7]. Except this, proposed energy propagation method allows to test power distribution and energy flow in all structural elements: masses, elastic deformation and damping. So far in studies of the effect of whole body vibrations and its assessment on human overlooked resilient and damping biodynamical structure, therefore their results may differ from reality.

References

1. Dobry M. W. (1996), „Zasada przepływu energii jako podstawa uogólnionej analizy dynamicznej systemu mechanicznego". Raport wewnętrzny nr 265 IMS PP, Poznań.
2. Dobry M.W. (1998) „Optymalizacja przepływu energii w systemie Człowiek – Narzędzie – Podłoże (CNP). Rozprawa habilitacyjna. Seria „Rozprawy" nr 330. Wyd. PP, Poznań.
3. Dobry M. W. (2000a), „Pierwsza Zasada Przepływu Energii w Systemie Mechanicznym jako podstawa teoretyczna uogólnionej – energetycznej metody analizy dynamicznej". Seminarium otwarte nr 984 Zakładu Dynamiki i Wibroakustyki Systemów PP. Semestr letni marzec 2000.
4. Dobry M. W. (2000b), „Advanced Analysis of Human – Machine System in Energy Flow Domain" 35th United Kingdom Group Meeting on Human Responses to Vibration, held at ISVR, University of Southampton, Southampton, England, 13-15 September, pp. 89-99.
5. Dobry M. W. (2004), „Energetyczna metoda diagnostyki technicznych i inteligentnych biologiczno-technicznych systemów oraz jej zastosowania". Diagnostyka Vol. 30, tom 1, 2004.
6. Grygorowicz M., „Rozdział mocy i przepływ energii w strukturze biodynamicznej człowieka poddanego wibracji ogólnej". Rozprawa doktorska, Politechnika Poznańska WBMiZ 2006.
7. Marek K. (2003), „Choroby zawodowe" Wydawnictwo Lekarskie PZWL.
8. Nader M. (2001), „Modelowanie i symulacja oddziaływania drgań pojazdów na organizm człowieka" Rozprawa habilitacyjna, Transport, z. 46, Oficyna Wydawnicza Politechniki Warszawskiej, Warszawa.

Hybrid Reduced Model of Continuous System

Rafał HEIN

Gdańsk University of Technology, Department of Mechanical Engineering
G. Narutowicza 11/12, 80-233 Gdansk

Cezary ORLIKOWSKI

Gdańsk University of Technology, Department of Mechanical Engineering
G. Narutowicza 11/12, 80-233 Gdansk

Abstract

The paper introduces an alternative method of modelling and modal reduction of continuous systems. Presented method is a hybrid one. It combines the advantages of modal decomposition method and the rigid finite element method. In the proposed method continuous structure is divided into one-dimensional continuous elements. For each 1D element modal decomposition and reduction is applied. Interactions between substructures are described by lumping techniques. Presented method enables to obtain reduced, low order modal model of considered system. The proposed approach is illustrated by selected examples.

Keywords: modelling, model reduction, modal analysis, mechanical system, dynamic systems, vibration.

1. Introduction

In the static and dynamic analysis of the elastic bodies the Finite Element Method (FEM) is widely used. The conventional discretization (Fig. 1a,c) yields to a set of ordinary differential equations. However, to obtain accurate results it is necessary to apply a great number of finite elements and to solve high order model (a big number of the second order differential equations). To avoid such problem, different methods of model order reduction can be applied. Modal decomposition and reduction is one of them [1]. However, in standard approach to obtain modal reduced order model it is necessary to derive and consider high order model by FEM.

In the paper a new, alternative method of model order reduction is described. It is a hybrid one and combines two well known approaches: modal decomposition method and the rigid finite element method.

In the proposed method the body is divided into strips (for 2D system - Fig. 1b) and prism (for 3D system - Fig. 1c). Each strip or prism represents one-dimensional distributed system and it is described by appropriate second order partial differential equation. However, these equations have also terms related to interactions between strip/prism. Hence, the given system can be described by set of a couplet second order partial differential equations. For each 1D element modal decomposition and reduction is applied whereas interactions between elements are described by lumping technique. In this case no complex FEM model is considered for modal decomposition.

Appropriate mathematical description of 2D system is presented below.
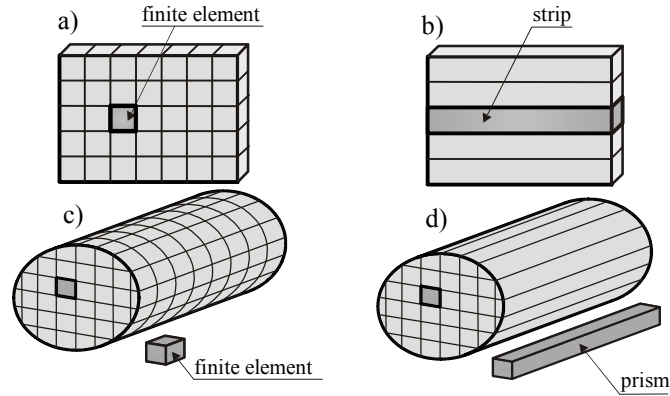
Figure 1. Spatial discretization of 2D and 3D body: a), c) conventional finite element method, b), d) proposed hybrid method

3. Hybride model of 2D body

Applying Rigid Final Element Method to 2D body divided into $n_x \times n_y$ finite elements one obtains appropriate system of ordinary differential equations ($n_x \times n_y$ second order equations) [1]. Such FEM model can be transformed to the continuum representation by letting $dx \rightarrow 0$. In that way small differences divided by dx become derivatives.
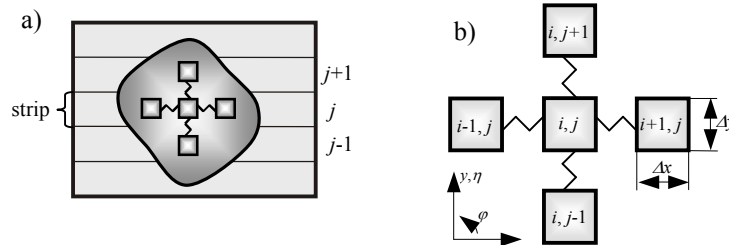
Figure 2. Discrete model of the hybrid 2D structure: a) continuous body, b) elementary

Thus, 2D body can be described by the following, n_y partial differential equations (after Laplace transform with respect to time):

$$f_{xj}\Delta y = \underline{\Delta y b \rho \xi_j s^2 - Eb\Delta y \xi_j''} + \frac{2\kappa Gb}{\Delta y}\xi_j - \frac{\kappa Gb}{\Delta y}\xi_{j+1} - \frac{\kappa Gb}{\Delta y}\xi_{j-1} + \frac{\kappa Gb}{2}\varphi_{j+1} - \frac{\kappa Gb}{2}\varphi_{j-1}, \quad (1)$$

$$f_{yj}\Delta y = \underline{\Delta y b \rho \eta_j s^2 - \kappa Gb\Delta y \eta_j''} + \frac{2Eb}{\Delta y}\eta_j - \frac{Eb}{\Delta y}\eta_{j-1} - \frac{Eb}{\Delta y}\eta_{j+1} + \kappa Gb\Delta y \varphi', \quad (2)$$

$$\tau_j \Delta y = \underline{\rho I_y \varphi_j s^2 - E I_y \varphi_j''} - \kappa G b \Delta y \eta_j' + \frac{\kappa G b}{2}(\xi_{j-1} - \xi_{j+1}) + \frac{3}{2}\kappa G b \Delta y \varphi_j +$$

$$+ \frac{\kappa G b \Delta y}{4}(\varphi_{j-1} + \varphi_{j+1}), \qquad j = 1, 2, 3, \ldots, n_y, \tag{3}$$

where: E – Young's modulus, G – shear modulus, I – area moment of inertia, A – cross section area, κ – numerical shape factor of cross section, ρ – mass per unit volume, ξ, η – transverse displacements, φ – rotation (angular displacement), f – distributed force (excitation), τ – distributed torque moment (excitation), $i=1,2,\ldots,n_x, j=1,2,\ldots,n_y$.

Solution of these equations with appropriate boundary conditions gives accurate prediction of static and dynamic response (displacement, strain, stresses etc.) for many 2D elastic body. Applying modal decomposition for underlined parts of equations (1, 2, 3) and applying FEM for remained parts one can obtain discrete model of the considered system written in the form:

$$\boldsymbol{M}_{xj}\ddot{\boldsymbol{q}}_{xj} + \boldsymbol{K}_{xj}\boldsymbol{q}_{xj} = \boldsymbol{\Phi}_{xj}^T \left[\frac{\kappa G b}{\Delta y}\boldsymbol{\Phi}_{x,j+1}\boldsymbol{q}_{x,j+1} - \frac{2\kappa G b}{\Delta y}\boldsymbol{\Phi}_{xj}\boldsymbol{q}_{xj} + \frac{\kappa G b}{\Delta y}\boldsymbol{\Phi}_{x,j-1}\boldsymbol{q}_{x,j-1} + \right.$$

$$\left. - \frac{\kappa G b}{2}\boldsymbol{\Phi}_{\varphi,j+1}\boldsymbol{q}_{\varphi,j+1} + \frac{\kappa G b}{2}\boldsymbol{\Phi}_{\varphi,j-1}\boldsymbol{q}_{x,j-1} \right]\Delta x + \boldsymbol{\Phi}_{xj}^T \boldsymbol{f}_{xj}, \tag{4}$$

$$\boldsymbol{M}_{yj}\ddot{\boldsymbol{q}}_{yj} + \boldsymbol{K}_{yj}\boldsymbol{q}_{yj} = \boldsymbol{\Phi}_{yj}^T \left[\frac{E b}{\Delta y}\boldsymbol{\Phi}_{y,j+1}\boldsymbol{q}_{y,j+1} - \frac{2E b}{\Delta y}\boldsymbol{\Phi}_{yj}\boldsymbol{q}_{yj} + \right.$$

$$\left. + \frac{E b}{\Delta y}\boldsymbol{\Phi}_{y,j-1}\boldsymbol{q}_{y,j-1} - \kappa G b \boldsymbol{\Phi}_{\varphi j}' q_{\varphi j} \right]\Delta x + \boldsymbol{\Phi}_{yj}^T \boldsymbol{f}_{yj}, \tag{5}$$

$$\boldsymbol{M}_{\varphi j}\ddot{\boldsymbol{q}}_{\varphi j} + \boldsymbol{K}_{\varphi j}\boldsymbol{q}_{\varphi j} = \boldsymbol{\Phi}_{\varphi j}^T \left[\kappa G b \Delta y \boldsymbol{\Phi}_{yj}' \boldsymbol{q}_{yj} - \frac{\kappa G b}{2}\boldsymbol{\Phi}_{x,j-1}\boldsymbol{q}_{x,j-1} + \frac{\kappa G b}{2}\boldsymbol{\Phi}_{x,j+1}\boldsymbol{q}_{x,j+1} + \right.$$

$$\left. - \frac{3}{2}\kappa G b \Delta y \boldsymbol{\Phi}_{\varphi j}\boldsymbol{q}_{\varphi j} - \frac{\kappa G b \Delta y}{4}\boldsymbol{\Phi}_{\varphi,j-1}\boldsymbol{q}_{\varphi,j-1} - \frac{\kappa G b \Delta y}{4}\boldsymbol{\Phi}_{\varphi,j+1}\boldsymbol{q}_{\varphi,j+1} \right]\Delta x + \boldsymbol{\Phi}_{\varphi j}^T \boldsymbol{f}_{\varphi j}, \tag{6}$$

where: $\boldsymbol{M}_{xj} = diag(m_{xj1} \quad \cdots \quad m_{xjn})$, $\boldsymbol{M}_{yj} = diag(m_{yj1} \quad \cdots \quad m_{yjn})$,

$\quad\quad\quad \boldsymbol{M}_{\varphi r} = diag(m_{\varphi j1} \quad \cdots \quad m_{\varphi jn})$, $\boldsymbol{K}_{xj} = diag(k_{xj1} \quad \cdots \quad k_{xjn})$,

$\quad\quad\quad \boldsymbol{K}_{yj} = diag(k_{yj1} \quad \cdots \quad k_{yjn})$, $\boldsymbol{K}_{\varphi j} = diag(k_{\varphi j1} \quad \cdots \quad k_{\varphi jn})$,

$\quad\quad\quad \boldsymbol{f}_{xj} = \Delta x \cdot \Delta y \cdot col(f_{xj1} \quad \cdots \quad f_{xjn_x})$, $\boldsymbol{f}_{yj} = \Delta x \cdot \Delta y \cdot col(f_{yj1} \quad \cdots \quad f_{yjn_x})$,

$\quad\quad\quad \boldsymbol{f}_{\varphi j} = \Delta x \cdot \Delta y \cdot col(\tau_{\varphi j1} \quad \cdots \quad \tau_{\varphi jn_x})$, $\boldsymbol{q}_{xj} = col(q_{xj1} \quad \cdots \quad q_{xjn_x})$,

$\quad\quad\quad \boldsymbol{q}_{yj} = col(q_{yj1} \quad \cdots \quad q_{yjn_x})$, $\boldsymbol{q}_{\varphi j} = col(q_{\varphi j1} \quad \cdots \quad q_{\varphi jn_x})$,

$$\boldsymbol{\Phi}_{xj} = \begin{bmatrix} Y_{xj1}(x_1) & \cdots & Y_{xjn}(x_1) \\ \vdots & & \vdots \\ Y_{xj1}(x_{n_x}) & \cdots & Y_{xjn}(x_{n_x}) \end{bmatrix}, \boldsymbol{\Phi}_{yj} = \begin{bmatrix} Y_{yj1}(x_1) & \cdots & Y_{yjn}(x_1) \\ \vdots & & \vdots \\ Y_{yj1}(x_{n_x}) & \cdots & Y_{yjn}(x_{n_x}) \end{bmatrix},$$

$$\boldsymbol{\Phi}_{\varphi j} = \begin{bmatrix} Y_{\varphi j1}(x_1) & \cdots & Y_{\varphi jn}(x_1) \\ \vdots & & \vdots \\ Y_{\varphi j1}(x_{n_x}) & \cdots & Y_{\varphi jn}(x_{n_x}) \end{bmatrix},$$

wheras: q – modal coordinates, m – modal coefficients of inertia, k – modal coefficients of stiffness, Y – eigenfunction, n – number of retained modes, n_x – number of ports for lumped interactions, $j=1,\ldots, n_y$, n_y – number of strips, f – generalized external force, $\boldsymbol{\Phi}' = d\boldsymbol{\Phi} / dx$, subscripts x, y, φ are related to translations in x, y directions and rotation respectively.

It is very easy to construct the modal models because eigenvalues and eigenfunctions related to one-dimensional second order systems are known. Fig.3 presents general concept of developed hybrid model. Proposed approach can be applied for modeling of 2D, 3D and 1D continuous systems. Of course, in the case of 1D system, there are not interactions between strips/prisms. In this case the method can be applied for modelling of discrete-distributed systems with non-self-adjoined components – see illustrative example 2 and [2, 3, 4].
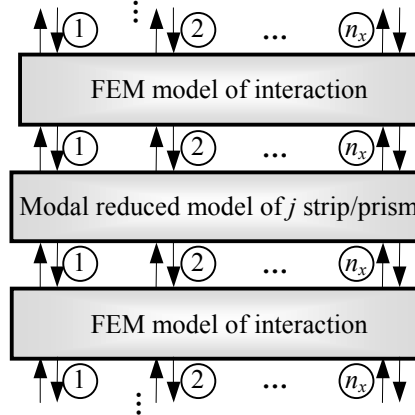
Figure 3. General block diagram of hybrid model

3.1. Illustrative Example 1

As an simple example let us consider one-strip system - the Timoshenko beam model (Fig. 4) which is described by the following equations (they can be obtain as the special case of equations (1÷3)):

$$f - \kappa A G \eta' = \underline{F = \rho A s^2 \eta - \kappa A G \eta''}, \tag{7}$$

$$\tau - \kappa A G \varphi + \kappa A G \eta' = \underline{T = \rho I s^2 \varphi - E J \varphi''}. \tag{8}$$
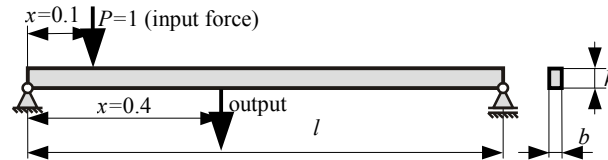
Figure 4. Simply supported beam with the following parameters: $E = 2 \cdot 10^{11}$, $G = 7.93 \cdot 10^{10}$, $\rho = 8000$, $b=0.05$, $h=0.1$, $\kappa = 1.2$, $l=1$.

The results are presented in Fig. 5. Frequency characteristics of the beam are obtained for the hybrid models with 6 retained modes and with 12 finite elements. From these one can see that in the range of frequency related to a number of retained modes frequency responses for reduced models have the same shape as for the reference continuous one.
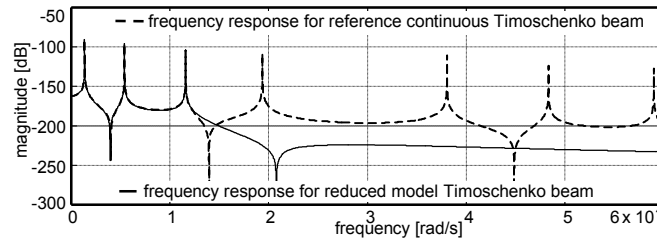
Figure 5. Verification of the reduced Timoshenko beam model

3.2. Illustrative Example 2

As the second example let us consider the rotor presented in Fig. 6a.
The difficulties in modal analysis of rotor system arise from the non-self-adjointness. To avoid that problem the following approach is proposed. Modal reduced model is built up for the system without gyroscopic effect.
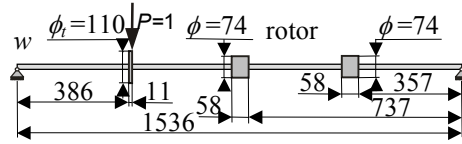
Figure 6. Rotor: $E = 1.9995 \cdot 10^{11}$ [Pa],
$\rho = 7834.6$ [kg/m^3], $G = 7.5842 \cdot 10^{10}$ [Pa],
$\kappa = 32/27$ (shape factor of cross section)
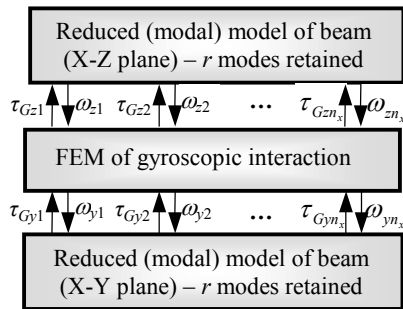
Figure 7. General block diagram of
hybrid model of rotor

Figure 8. Frequency response with gyroscopic phenomena for reduced and non-reduced model $\Omega=1000$ [rad/s] (a) and scaled up (b)

Gyroscopic moments are then modeled by application of rigid finite element method. Because of above reduced modal model must contain an appropriate number of inputs and outputs needed to connect lumped elements related to gyroscopic interactions between beams vibrating in X-Z and Y-Z planes.

Frequency characteristics of the rotor (Fig. 8) are obtained for the unit step force input signal acting at the left disk (Fig. 6) and the displacement output signal observed at the same point. From these one can see that in the range of frequency related to a number of retained modes frequency responses for reduced models have the same shape as for the reference model.

4. Conclusions

In this paper model reduction of continuous systems is presented. Two techniques: modal decomposition and finite element approach are applied simultaneously. The final reduced model consists of two parts - the reduced modal model and the finite element model. General idea of such approach has been presented in simple illustrative examples. The proposed approach enables to obtain accurate low order lumped parameter model representation of considered system. Computer simulations and numerical calculations proved that the proposed method is efficient and can be applied for others, more complex systems.

Acknowledgments

References

1. R. Hein, C. Orlikowski, *Reduced order model of 2d system*, Selected problems of modal analysis of mechanical systems, Editor T. Uhl, AGH, Kraków 2009, Poland
2. C. Orlikowski, *Modeling, analysis and synthesis of dynamic systems with bond graph application*, WPG, Gdansk 2005 [in Polish],
3. C. Orlikowski, R. Hein, *Reduced model of gyroscopic system*, Wybrane zagadnienia analizy modalnej konstrukcji mechanicznych, Editor T. Uhl, AGH, Kraków 2007, Poland
4. C. Orlikowski, R. Hein, *Hybrid model of axially moving continua*, Wybrane zagadnienia analizy modalnej konstrukcji mechanicznych, Editor T. Uhl, AGH, Kraków 2008, Poland

Hybrydowe modele zredukowane układów ciągłych

W artykule przedstawiono alternatywną metodę modelowania i modalnej redukcji układów ciągłych. Zaprezentowana metoda jest metodą hybrydową. Łączy zalety metod dekompozycji modalnej i sztywnych elementów skończonych. W proponowanej metodzie układ ciągły dzielony jest na jednowymiarowe podukłady ciągłe. Dla każdego podukładu jednowymiarowego budowany jest modalny model zredukowany. Poszczególne modele zredukowane wiąże się ze sobą poprzez oddziaływania między nimi modelowane za pomocą metody sztywnych elementów skończonych. Zaprezentowana metoda umożliwia otrzymanie zredukowanego modelu modalnego niskiego rzędu. Proponowane podejście jest zilustrowane prostymi przykładami.

Newton's Law for the Point Particle with Changing Mass in Static Moment Description

Tadeusz J. HOFFMANN
Institute of Applied Mechanics, Poznan University of Technology
3 Piotrowo Street, 60-965 Poznan
tadeusz.hoffmann@put.poznan.pl

Marta CHUDZICKA-ADAMCZAK
Polytechnic Institute, Higher Vocational State School in Piła
10 Podchorążych Street, 64-920 Piła
martachudzicka@wp.pl

Radoslaw PYTLIŃSKI
Institute of Technology, Higher Vocational State School in Kalisz
140 Częstochowska Street, 62-800 Kalisz

Abstract

The trial of the mechanic's description of material point with variable mass where the classical position vector was replaced with the static moment vector was presented. In this way, the present position and the current mass were bound into a single quantity. The description contains: the dynamic motion formulae, the momentum and the impulse of force, work, kinetic energy, the equivalence of the work and of the kinetic energy as well as the conservation law of mechanical energy. The example of the fall of the evaporating drop in the gravitational field was shown.

Keywords: system with changing mass, dynamic system, static moment

1. Introduction

Mechanics with variable mass as classically defined contains the following cases:
- changes in mass in the system,
- changes in mass distribution in the system,
- the changes of mass as well as of its distribution.

History and achievements in the examinations of systems with variable mass are described in literature [1], [2].

In the paper, the material point in which the change in mass occurs is analyzed. The vector of static moment joining the position of the point with its present mass is used instead of the position vector. Such an attitude in authors' conception constitutes a formal experiment.

2. The vector of static moment

If the material point has a mass m and the position described with the coordinates x_i in the given system of coordinates, then the vector of static moment is defined with the following formula:

$$s_i = mx_i. \tag{1}$$

The derivative of this vector is calculated:

$$ds_i = x_i dm + mdx_i. \tag{2}$$

It is easy to notice that the above derivative is a vector created from the addition of the two components:

- $x_i dm$ − with the direction of the position vector,

- mdx_i − with direction tangent to the trajectory of the point in the given point (in kinematical understanding).

3. Momentum and the dynamic equations of the motion

Based on the definition (1) the momentum of material point can be calculated in the form:

$$m\dot{x}_i = \dot{s}_i - \dot{m}x_i. \tag{3}$$

The time derivative of the momentum (3) is given with the following expression:

$$\frac{d}{dt}(m\dot{x}_i) = \ddot{s}_i - \frac{\dot{m}}{m}\dot{s}_i - \left[\frac{\ddot{m}}{m} - \left(\frac{\dot{m}}{m}\right)^2\right]s_i. \tag{4}$$

The above result allows to write the dynamic equation of motion:

$$\ddot{s}_i - \frac{\dot{m}}{m}\dot{s}_i - \left[\frac{\ddot{m}}{m} - \left(\frac{\dot{m}}{m}\right)^2\right]s_i = f_i, \tag{5}$$

where f_i is a given external force.

The equation (5) is the quadratic ordinary differential equation relative to the time with the variable coefficients. The equation (5) must be completed with the initial conditions put on the searched function and its first time derivative. It is also necessary to assume the open form of the mass evolution.

4. Kinetic energy and differentiated work

Momentum (3) can be depicted in the new form using (1):

$$m\dot{x}_i = \dot{s}_i - \frac{\dot{m}}{m}s_i, \tag{6}$$

then kinetic energy

$$T = \frac{1}{2}m\dot{x}_i\dot{x}_i \tag{7}$$

will get a form:

$$T = \frac{1}{2m}\dot{s}_i\dot{s}_i - \frac{\dot{m}}{m^2}\dot{s}_i s_i + \frac{1}{2}\frac{\dot{m}^2}{m^3}s_i s_i, \tag{8}$$

so the kinetic energy is the function of variables

$$T = T(m, \dot{m}, s_i, \dot{s}_i). \tag{9}$$

The differentiated work is described with the commonly-known expression:

$$dL = f_i dx_i. \tag{10}$$

Thanks to the equation (2) the following can be obtained:

$$dx_i = \frac{1}{m} ds_i - \frac{1}{m^2} s_i dm, \tag{11}$$

hence the differentiated work (10) gets a new form:

$$dL = \frac{1}{m} f_i ds_i - \frac{1}{m^2} f_i s_i dm. \tag{12}$$

It seems that the equivalence of work and kinetic energy should occur, however, the authors were not able to show it.

5. Free fall of the drop evaporating in the gravitational field

In case of evaporating drop, in accordance with literature [1], the open form of the evolution of mass is taken into account:

$$m(t) = m_0 e^{-\lambda t}, \tag{13}$$

where m_0 – the initial mass, λ – the constant parameter of vaporization.

In such case, the dynamic equation of motion (5) is simplified to the form:

$$\ddot{s}_i + \lambda \dot{s}_i = f_i. \tag{14}$$

It is assumed that fall is carried out along vertical axis with the direction of gravitational force. The equation of this matter of contention has a form:

$$\ddot{s} + \lambda \dot{s} = mg, \tag{15}$$

where g - gravity acceleration.

Using the homogenous initial conditions:

$$t = 0, \ \dot{s}(0) = 0, \ s(0) = 0, \tag{16}$$

the solutions is obtained:

$$s = m_0 g \left[-\frac{1}{\lambda} t e^{-\lambda t} + \frac{1}{\lambda^2} \left(1 - e^{-\lambda t} \right) \right]. \tag{17}$$

The equation (15) and the solution (17) in the formal form refer to the issues of fall in the medium constituting resistance.

6. Conclusions

The presentation of the benefit of application in the description of the static moment is difficult to point out at the current phase of the research. However, it seems that this formal experiment opens new scientific fields. In the continuous systems, mass could take tensor's properties what would broaden significantly the theoretical horizons.

Acknowledgments

References

1. G. Białkowski,, *Classical mechanics* [in Polish], PWN, Warszawa 1975.
2. E. Jarzębowska, W. Jarzębowski, *General mechanics* [in Polish], PWN, Warszawa 2000.

Prawo Newtona dla punktu materialnego o zmiennej masie w opisie momentu statycznego

Przedstawiona została próba opisu mechaniki punktu materialnego o zmiennej masie w której zastąpiono klasyczny wektor położenia wektorem momentu statycznego. W ten sposób połączono w jednej wielkości aktualne położenie z aktualną masą. W tym opisie przedstawiono : dynamiczne równania ruchu, pęd i popęd, pracę, energię kinetyczną, równoważność pracy i energii kinetycznej oraz zasadę zachowania energii mechanicznej. Przedstawiono przykład spadku kropli parującej w polu siły ciężkości.

Image Noise Reduction by Means of Regularization Methods – Part I

Joanna IWANIEC

Department of Robotics and Mechatronics, Faculty of Mechanical Engineering
and Robotics, AGH University of Science and Technolog
Mickiewicz Alley 30, 30-059 Krakow, Poland
jiwaniec@agh.edu.pl

Abstract

In practical applications of vision systems to mechanical systems vibration measurements, the problem of image reconstruction on the basis of registered noisy image is frequently encountered [6]. Such problem is an inverse, ill-posed problem, which means that even small disturbances of the registered image have significant influence on the accuracy of its reconstruction. For the purposes of image noise reduction, regularization methods were used. In the current paper (part I), noise reduction of the test image was carried out by means of the algorithm requiring decomposing matrix modelling noise into singular values, which, in case of images of significant dimensions, requires significant computational effort. Therefore, for the purposes of regularization of images of significant dimensions, in the second paper (part II) the iterative approximate method formulated by the author was used. Obtained results proved that formulated and implemented methods find application to noise reduction of images, the reconstruction of which is impossible to carry out by means of other methods because of the excessive loss of information resulting from imposed noise.

Keywords: noise reduction, image reconstruction, regularization

1. Introduction

The problem of image reconstruction on the basis of registered noisy image is an inverse ill posed-problem [1, 7] (Fig. 1), which means that even small disturbances of registered image have significant influence on the accuracy of its reconstruction. Therefore, in this paper, for the purposes of the analysed images noise reduction, regularization methods were used [1, 2, 7]. Images burdened with noise were filtered by means of the Tikhonov regularization method, Truncated SVD (TSVD), Damped SVD (DSVD) and Maximal Entropy (ME) methods [2, 4]. Algorithm of direct image regularization (Fig. 2) formulated by the author consists in:

1. Transformation of matrix describing registered noisy image $\{b_{sz}\}_{N \times N}$ into column vector $\{b_{1\,sz}\}_{N \times 1}$ by writing consecutive columns one below the other.
2. Estimation of noise matrix $[A]_{N^2 \times N^2}$ modelling disturbances appearing in the process of image registration.
3. Computing vector describing filtered image $\{x_{1reg}\}$ by regularization of problem: $[A]_{N^2 \times N^2}\{x_{1reg}\}_{N \times 1}=\{b_{1sz}\}_{N \times 1}$ by means of the selected regularization method.
4. Computing matrix describing regularized image $[X_{reg}]_{N \times N}$ by transformation of vector $\{x_{1reg}\}_{N \times 1}$.

At the present stage of development of commonly available PC computers, the proposed algorithm of noise reduction with the use of regularization methods (Fig. 2) can not be applied to filtration of images of significant dimensions. Image regularization

according to that algorithm requires decomposition of matrix modelling noise into singular values, which in case of matrices of significant dimensions, requires great computational effort. Matrix modelling noise of image of dimensions $N{\times}N$ is of dimensions $N^2{\times}N^2$.
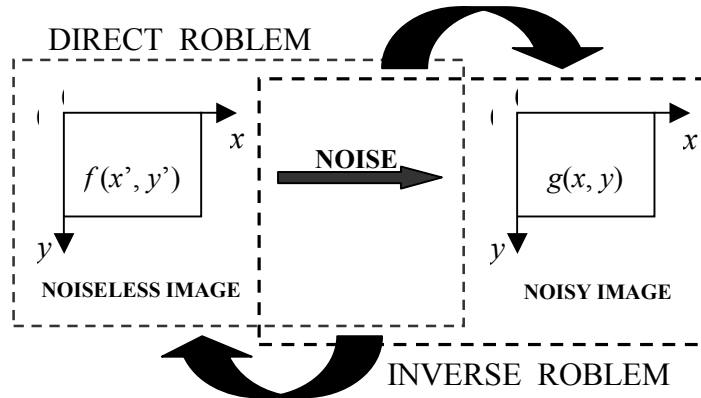
Figure 1. Image reconstruction on the basis of registered noisy image.
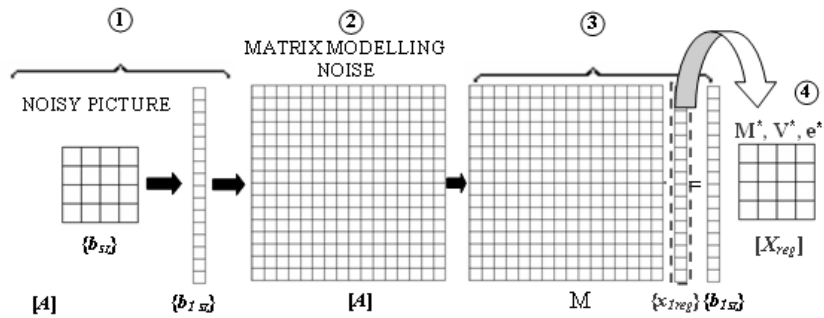
Figure 2. Algorithm of direct image regularization.

Therefore for the purposes of regularization of images of significant dimensions (e.g. 512×512 pixels) the iterative approximate method formulated by author was used (Fig. 3). The idea of the method consists in application of the selected method to regularization of the following issue:

$$\left[A_1^{(k)}\right]_{M^2 \times M^2} \left\{x_1^{(k)}\right\}_{M \times 1} = \left\{b_{1sz}^{(k)}\right\}_{M \times 1} \tag{1}$$

where $[A_1^{(k)}]$ is a matrix consisted of elements lying in the vicinity of matrix $[A]$ main diagonal, corresponding to the kth fragment of image written in the form of vector.

$k = 1, \ldots,$
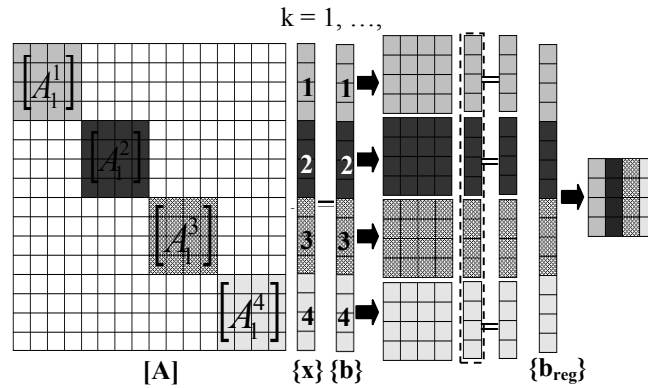
Figure 3. Proposed algorithm of regularization of images of significant dimensions.

The issue of image reconstruction on the basis of registered noisy image (Fig. 4) can be also described by means of the Fredholm integral equation of the first kind [3] in the following form:

$$\int\limits_0^1 \int\limits_0^1 \{k_1(x,s)\} \cdot \{k_2(y,t)\} \cdot \{f(x,y)\} dxdy = \{g(s,t)\} \tag{2}$$

where: $\{k_1(x, s)\}$, $\{k_2(y, t)\}$ integrands (known), defined for horizontal ($\{k_1(x, s)\}$) and vertical $\{k_2(y, t)\}$ directions, $\{g(s, t)\}$: right side of the equation (known function), $\{f(x, y)\}$: solution.
Mathematical proof of the fact that the Fredholm integral equation of the first kind is always ill-conditioned can be found in [5].
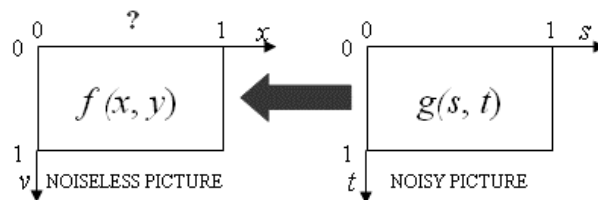
Figure 4. Description of the image noise reduction issue by means of the Fredholm differential equation of the first kind.

Such a description is valid for images burdened with noise distributed uniformly, for which disturbances in vertical and horizontal directions are independent [3]. As a result of discretization of relation (2), equation describing the problem of registered image noise reduction has the following form:

$$([K_1(x,s)] \otimes [K_2(y,t)]) \cdot \{F(x,y)\} = \{G(s,t)\} \tag{3}$$

where $\otimes$: Kronecker product, defined for matrices $[A]$ and $[B]$ as [3]:

$$[A] \otimes [B] = \begin{bmatrix} a_{11}[B] & a_{12}[B] & \dots & a_{1n}[B] \\ a_{21}[B] & a_{22}[B] & \dots & a_{2n}[B] \\ \vdots & \vdots & \ddots & \vdots \\ a_{n1}[B] & a_{n2}[B] & \dots & a_{nn}[B] \end{bmatrix} \tag{4}$$

Description of the issue of image reconstruction on the basis of registered noisy image by the use of the Fredholm integral equation of the first kind was implemented in the software package *MOORe TOOLs* (ang. ***M**odular **O**bject **O**riented **R**egularization **T**ools*) [5] dedicated for MATLAB environment.

1.1. Matrix modelling noise

Reduction of image disturbances by the use of the presented algorithms of image regularization requires identification of character of disturbances influencing image registration process. Below there are presented relations making it possible to formulate matrix [K] modelling frequently encountered disturbances of image registration process [3, 5]:

$$[K] = [K_1] \otimes [K_2] \tag{5}$$

where [K_1], [K_2]: matrices modelling noise in horizontal ([K_1]) and vertical ([K_2]) directions.

In the literature [5], under the term of *atmospheric blur,* the phenomena of blurring remote objects contours by vibrating air masses is understood. Elements of matrix [K] modelling noise of that type is described by the following relation [5]:

$$(K)_{ij} = \frac{1}{\pi\sigma} \cdot \exp\left(-\frac{(x-s)^2 + (y-t)^2}{\sigma^2} \right) \tag{6}$$

where σ: standard deviation of noise.

2. Filtration of test image burdened with noise of known statistical properties

Test image of dimensions 16×16 pixels (Fig. 5a) was burdened with the atmospheric Gaussian blur of zero mean value and $\sigma = 0{,}7$. Regularization of noisy image (Fig. 5b) was carried out by means of the software realizing the algorithm presented in the Fig. 2 with the use of functions implemented in the *Regularization Tools* package. Results of the filtration of the considered test image carried out with the use of different regularization methods are presented in the Fig. 5c, d, e, f [4].

In order to assess quality of the obtained results, the differences between the noiseless and noisy image (Fig. 6a) as well as between the noiseless image and images reconstructed by means of the considered regularization methods were computed (Fig. 6b, c, d, e). The smallest differences between the noiseless and regularized image were observed for the Tikhonov (Fig. 6b) and ME (Fig. 6e) methods, the most significant differences for the TSVD method (Fig. 6c).
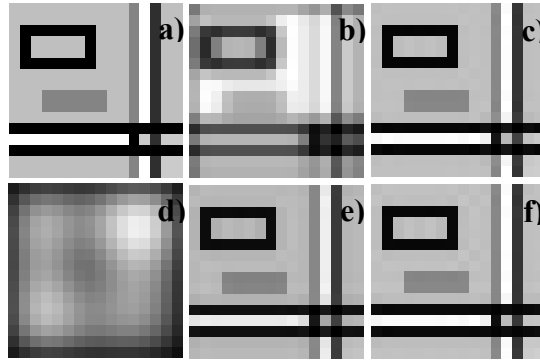
Figure 5. Image of dimensions 16×16 pixels: a) noiseless, b) burdened with Gaussian noise of zero mean value and $\sigma = 0.7$ and regularized by means of the c) Tikhonov, d) TSVD, e) DSVD and f) ME methods.
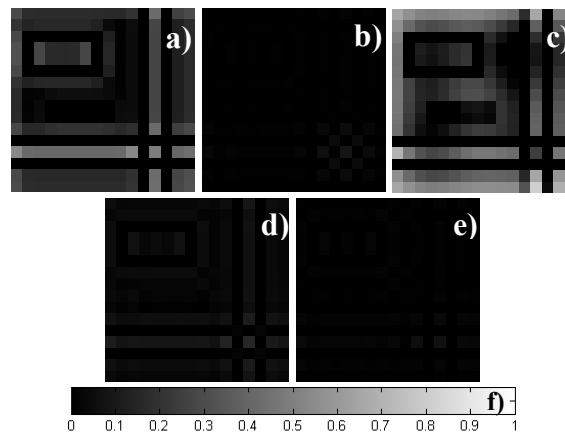
Figure 6. Differences between noiseless image and image a) burdened with Gaussian noise of $\sigma = 0.7$, and filtered by means of the b) Tikhonov method, c) TSVD, d) DSVD, e) ME methods and f) assumed intensity scale.

In the Fig. 7 there are presented histograms illustrating the number of points of different intensity values in the noiseless image (Fig. 5a), image burdened with an atmospheric Gaussian blur of considered statistical properties (Fig. 5b) and noisy image filtered with the use of the considered regularization methods (Fig. 5c, d, e, f).

Histograms obtained for images filtered by means of the Tikhonov regularization method (Fig. 7c) and maximal entropy method ME (Fig. 7f) bear most resemblance to the histogram of noiseless image (Fig. 7a) and are characterized by a slight broadening of main peaks of noiseless image into side peaks.
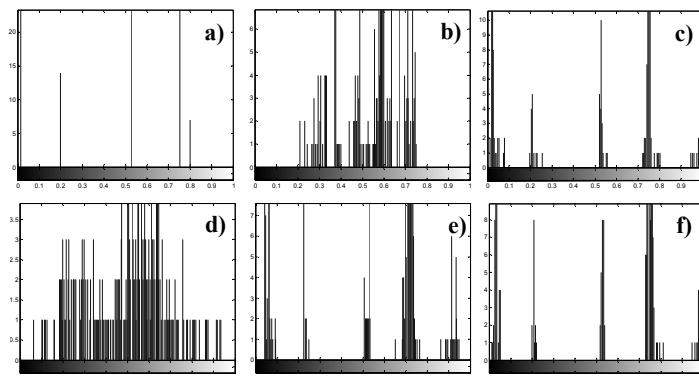
Figure 7. Histograms for a) noiseless image, b) image burdened with Gaussian noise of
$\sigma = 0{,}7$ and filtered by means of the c) Tikhonov regularization method, d) TSVD,
c) DSVD and d) ME methods.

3. Conclusions and final remarks

Obtained results proved suitability of the algorithm of direct image regularization
(Fig. 2) formulated and implemented in the Matlab environment by the author for
filtration of small noisy images [4]. Results of reconstruction of images of significant
dimensions carried out by means of the elaborated iterative approximate method are
presented in the paper under the same title (part II) that stands for the continuation of this
paper.

4. Literature

1. Hansen P.C.: *Regularization Tools – A Matlab Package for Analysis and Solution of Discrete Ill-Posed Problems*, Numerical Algorithms 6, 1994.
2. Horn K.F., Holfort I.K.: *Deblurring of Digital Colour Images*, Department of Informatics and Mathematical Modelling, Technical University of Denmark.
3. Iwaniec J.: *Wybrane zagadnienia identyfikacji układów nieliniowych w warunkach eksploatacyjnych*, ITE Radom, Kraków, 2009.
4. Jacobsen M.: *Modular Regularization Algorithms*, PhD thesis of Technical University of Denmark, 2004.
5. Engl H.W., Hanke M., Neubauer A.: *Regularization of Inverse Problems,* Mathematics and its Applications, Kluwer Academic Publishers, 1996.
6. Tadeusiewicz R., Flasiński M.: Rozpoznawanie obrazów, PWN, 1991.
7. Tikhonov A.N., Arsenin V.Y.: *Solutions of Ill-Posed Problems*, Scripta Series in Mathematics, John Wiley and Sons, New York, 1977.

Zastosowanie metod regularyzacji do redukcji zakłóceń rejestrowanych obrazów – część I

Praca dotyczy zagadnienia redukcji szumów pomiarowych obrazów z zastosowaniem metody regularyzacji Tichonowa, TSVD, DSVD oraz ME. Rekonstrukcję obrazów przeprowadzono z zastosowaniem sformułowanych i zaimplementowanych przez autorkę algorytmów. Wykazano przydatność sformułowanych metod w przypadku obrazów, których rekonstrukcja nie jest możliwa do przeprowadzenia innymi metodami ze względu na zbyt dużą utratę informacji spowodowaną nałożeniem szumów.

Image Noise Reduction by Means of Regularization Methods – Part II

Joanna IWANIEC

Department of Robotics and Mechatronics, Faculty of Mechanical Engineering and Robotics, AGH University of Science and Technology
Mickiewicz Alley 30, 30-059 Krakow, Poland
jiwaniec@agh.edu.pl

Abstract

In practical applications of vision systems to mechanical systems vibration measurements, the problem of image reconstruction on the basis of registered noisy image is frequently encountered [6]. Such problem is an inverse [1], ill-posed problem [2, 7], which means that even small disturbances of the registered image have significant influence on the accuracy of its reconstruction. The first paper, denoted as part I, concerns the issue of the test image noise reduction carried out by means of the direct image regularization method. The main step of the method algorithm consists in decomposing matrix modelling noise into singular values, which, in case of images of significant dimensions, requires significant computational effort. Therefore, for the purposes of regularization of images of significant dimensions, in the current paper (part II), the iterative approximate method formulated by the author was used. Obtained results proved that formulated and implemented methods find application to noise reduction of images, the reconstruction of which is impossible to carry out by means of other methods because of the excessive loss of information resulting from imposed noise.

Keywords: noise reduction, image reconstruction, regularization

1. Introduction

The research presented in the paper stands for the continuation of the research presented in the first paper (denoted as part I) and concerns reconstruction of the image of dimensions 512×512 pixels (Fig. 1a), depicting man eating an orange. The image was burdened with the atmospheric Gaussian blur of zero mean value, magnitude $A = 1$ and $\sigma = 2$ (Fig. 1b) and regularized [2, 4, 7] by means of the Tikhonov regularization method (Fig. 1c), Truncated SVD (TSVD, Fig. 1d), Damped SVD (DSVD, Fig. 1e) and Maximum Entropy (ME, Fig. 1f) methods. Taking into account significant dimensions of the considered image, for the purposes of noise reduction, the iterative approximated method formulated by the author was applied. Detailed description of the method algorithm is provided in the paper under the same title denoted as part I. In spite of the fact that the image filtration was carried out by means of the approximate method, the overall time of computations carried out in the MATLAB 5.3 environment (for PC computer equipped with the 2 [GHz] processor and dual 512 MB) amounted to 7 hours.

2. Results of filtration of image of dimensions 512×512 pixels burdened with noise of known statistical properties

In order to assess the quality of images reconstructed with the use of the considered regularization methods, the differences between the noiseless image and noisy deblurred images were computed (Fig. 2a, b, c, d).

Figure 1. Image a) noiseless, b) burdened with the atmospheric Gaussian blur and filtered with the use of the c) Tikhonov regularisation method, d) TSVD, e) DSVD and f) ME methods.
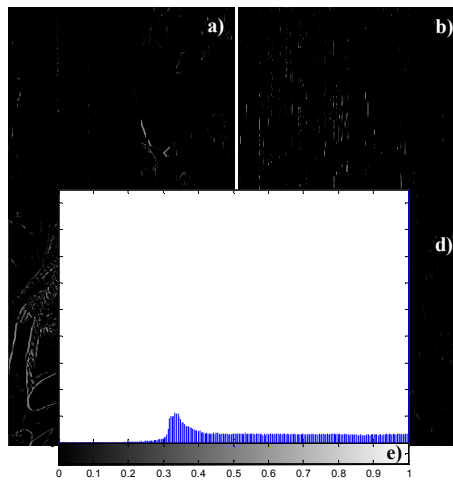
Figure 2. Differences between noiseless image and noisy images filtered with the use of the a) Tikhonov regularization method, b) TSVD, c) DSVD and d) ME methods, e) assumed intensity scale.

The smallest differences were observed for images reconstructed by means of the Tikhonov regularization and ME methods.

In the Fig. 3 there are presented histograms illustrating the number of pixels of a given intensity value for noiseless image (Fig. 3a), image burdened with the atmospheric Gaussian blur of given statistical properties (Fig. 3b) and noisy images reconstructed by means of the considered regularization methods (Fig. 3c, d, e, f).
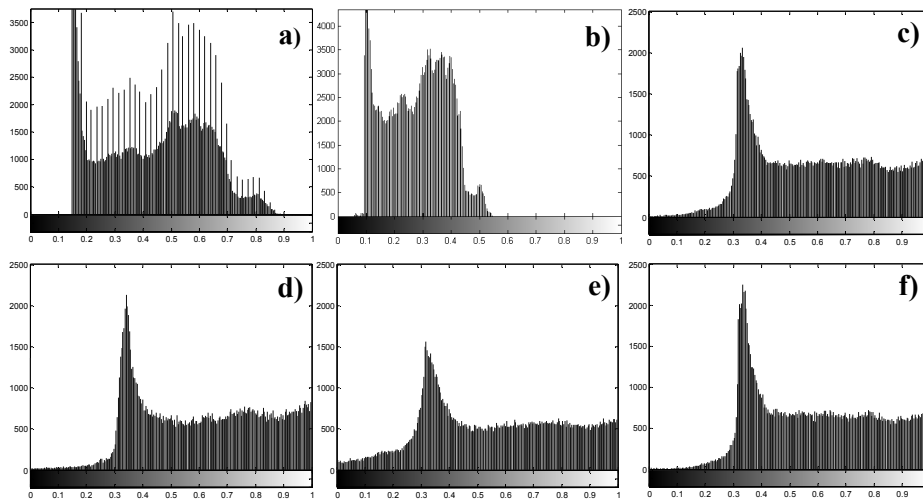
Figure 3. Histogram of images presented in the Figure 2.

The noise imposed on the considered image resulted in the information loss in the $0,55 \div 1$ range of the intensity scale. As the result of application of the elaborated approximate image regularization method most of the previously lost information was retrieved.

Cutting out of the histograms values from the $0 \div 0,3$ range of the intensity scale results from the specific properties of the applied iterative approximate method dedicated to regularization of pictures of significant dimensions, the essence of which consists in analyzing only the fragments lying in the vicinity of the image main diagonal. Therefore obtained regularized images (Fig. 1c, d, e, f) are brighter than the original noiseless image.

The further research concerned the image of man eating an orange (Fig. 4a), burdened with the atmospheric Gaussian blur of the zero mean value, magnitude $A = 3$ and $\sigma = 2$ (Fig. 4b). Introduction of noise of discussed properties resulted in the loss of image sharpness in such a degree that, on the basis of noisy image, it is difficult to figure out what was depicted in the original image. In order to reduce the introduced noise, the consecutive image fragments were regularized with use of the Tikhonov regularization method (Fig. 4c), TSVD (Fig. 4d), DSVD (Fig. 4e) and maximal entropy (Fig. 4f) methods. Histograms of images presented in the Fig. 4 are shown in the Fig. 5.

Figure 4. Image a) noiseless, b) burdened with the atmospheric Gaussian blur of zero mean value, $A = 3$ and $\sigma = 2$ and filtered with the use of the c) Tikhonov regularization d) TSVD, e) DSVD, f) ME methods.
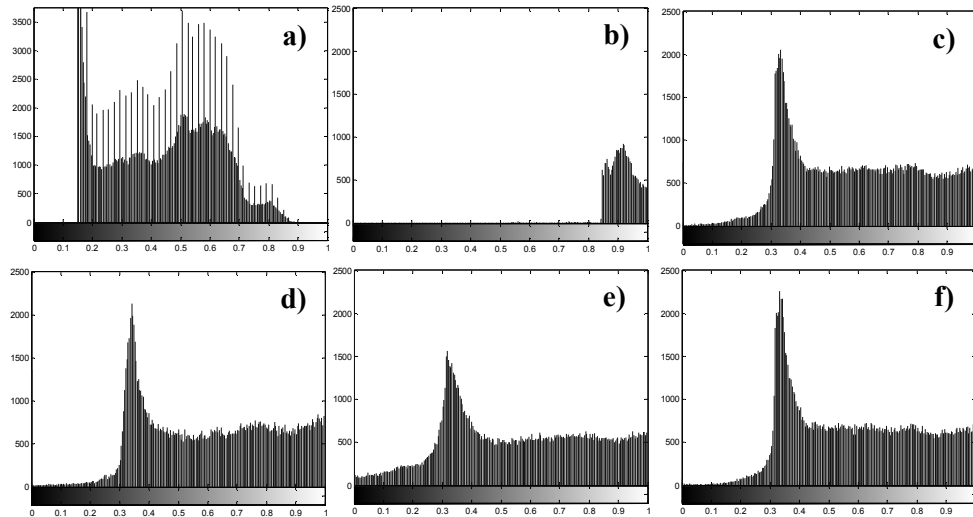
Figure 5. Histograms of images presented in the Figure 4.

Application of the elaborated iterative approximate method made it possible to retrieve information in the 0,3 ÷ 1 range of the intensity scale, lost as the result of imposing the atmospheric Gaussian blur on the original noiseless image. In the considered case the classical image filtration methods fail. Therefore, the possibility of image reconstruction compensates for inconveniences related to application of the elaborated method, such as long computational time and characteristic brightening of the filtered image with respect to the original image.

2. Conclusions and final remarks

The paper concerns noise reduction of images of significant dimensions carried out by means of the elaborated iterative approximate method based on the regularization method. The paper stands for the continuation of the paper under the same title denoted as part I, in which the issue of small images filtering with the use of direct application of the regularization methods was discussed.

On the basis of the obtained results it can be stated that elaborated image filtration algorithms based on the regularization methods, due to their specific properties such as e.g. required great computational effort and long time of computations, should not be applied in cases when application of 'conventional' image processing methods leads to obtaining results of satisfactory accuracy. Their application becomes indispensable in case of images, the reconstruction of which is impossible to carry out by means of other methods because of the excessive loss of information resulting from imposed noise.

References

1. Engl H.W., Hanke M., Neubauer A.: *Regularization of Inverse Problems,* Mathematics and its Applications, Kluwer Academic Publishers, 1996.
2. Hansen P.C.: *Regularization Tools – A Matlab Package for Analysis and Solution of Discrete Ill-Posed Problems*, Numerical Algorithms 6, 1994.
3. Horn K.F., Holfort I.K.: *Deblurring of Digital Colour Images*, Department of Informatics and Mathematical Modelling, Technical University of Denmark.
4. Iwaniec J.: *Wybrane zagadnienia identyfikacji układów nieliniowych w warunkach eksploatacyjnych*, ITE Radom, Kraków, 2009.
5. Jacobsen M.: *Modular Regularization Algorithms*, PhD thesis of Technical University of Denmark, 2004.
6. Tadeusiewicz R., Flasiński M.: Rozpoznawanie obrazów, PWN, 1991.
7. Tikhonov A.N., Arsenin V.Y.: *Solutions of Ill-Posed Problems*, Scripta Series in Mathematics, John Wiley and Sons, New York, 1977.

Zastosowanie metod regularyzacji do redukcji zakłóceń rejestrowanych obrazów – część II

Często spotykanym w praktyce problemem przetwarzania sygnałów jest rekonstrukcja obrazu na podstawie zarejestrowanego obrazu zaszumianego. Problem ten jest zagadnieniem odwrotnym źle zdefiniowanym, co oznacza, że niewielkie zakłócenia rejestrowanego obrazu mają znaczący wpływ na dokładność rekonstrukcji obrazu. W pierwszym artykule (oznaczonym jako „część I") przedstawiono rezultaty redukcji zakłóceń obrazu testowego uzyskane z zastosowaniem sformułowanego przez autorkę algorytmu opartego o metody regularyzacji Tichonowa, TSVD, DSVD oraz ME. Przeprowadzenie regularyzacji obrazu zgodnie z tym algorytmem wymaga dokonania rozkładu macierzy modelującej szum na wartości szczególne, co w przypadku macierzy o dużym rozmiarze wymaga bardzo dużych nakładów obliczeniowych. Z tego względu w niniejszym artykule (oznaczonym jako „część II"), do redukcji obrazów o znacznych rozmiarach, zastosowano sformułowaną przez autorkę iteracyjną metodę przybliżoną. Na podstawie analizy rezultatów przeprowadzonych badań nasuwa się wniosek, że metody regularyzacji nie powinny być stosowane w przypadkach gdy zastosowanie „konwencjonalnych" metod analizy prowadzi do uzyskania rezultatów o zadawalającej dokładności. Ich zastosowanie staje się konieczne w przypadku obrazów, których rekonstrukcja nie jest możliwa do przeprowadzenia innymi metodami ze względu na zbyt dużą utratę informacji spowodowaną nałożeniem szumów.

Voice control

Marek IWANIEC

AGH University of Science and Technology, Mickiewicz 30 av, 30-059 Cracow
iwaniec@agh.edu.pl

Agnieszka MIETŁA
AGH University of Science and Technology, Mickiewicz 30 av, 30-059 Cracow
mietla@agh.edu.pl

Abstract

The article describes the voice control system. It is based on comparing feature vector sequence, which represents spoken word, with patters. For this purpose Dynamic Time Warping algorithm was implemented. Features extracted from voice record are Mel cepstral coefficients. Delta and delta-delta parameters were also tested. Important part of system is algorithm detecting word boundaries. It uses fundamental frequency and energy.

Keywords: voice control, Dynamic Time Warping, speech recognition

1. Introduction

For a human the most intuitive way of communication is speech. Meanwhile, in the case of control, voice commands are seldom used. This is because the developers of such systems are facing with many problems like noise reduction or speaker independence. However, there is no shortage of ideas on the use of this type of control. The article [4] describes a robot control system with a mobile phone. Commands are described in simple grammar. In [10] such a system is used to control the wheelchair.

An important issue is the selection of appropriate signal features which reflect differences between words. In this work Mel-frequency cepstral coefficients and their derivatives are used. Detected word is divided into frames for which the coefficients are calculated. Other solutions can be found in the literature. In [4] author used vectors with 26 elements: mean power, mean zero crossing and 24 frequency features.

Separate issue is the selection of a classifier which decides, on the basis of features, what was spoken. In this work a Dynamic Time Warping algorithm was described and implemented. It calculates the similarity between the data series. These data may be either single or multidimensional. Series may be of different length and can be shifted in phase relative to each other. These are very desirable features for speech recognition because nobody can say the same word twice in the same way.

Undoubted advantage of the algorithm is its simplicity. Currently more advanced systems can be used such as neural networks or hidden Markov models.

2. Word segmentation and representation

Extremely important issue in speech recognition is detection of word beginning and end (word segmentation). In this work a solution based on signal energy and fundamental frequency has been used.

Fundamental frequency is associated with vibration of vocal folds [7]. It is characteristic of voiced sounds and it lies in the range between 80Hz and 350Hz [3]. Thus by measuring the fundamental frequency for parts of record we can conclude which contains a human voice. But the problem remains with voiceless sounds which are not detected and with some noise that may by recognized as the voice. Therefore a second parameter was introduces, the signal energy.

The figure below shows the word 'dziewięć' with a part determined by the fundamental frequency (upper chart, marked in red). At the bottom graph the signal energy is presented. Energy lower than 10% of the maximum is removed.

Combination of these two parameters allows the better word boundaries detection.
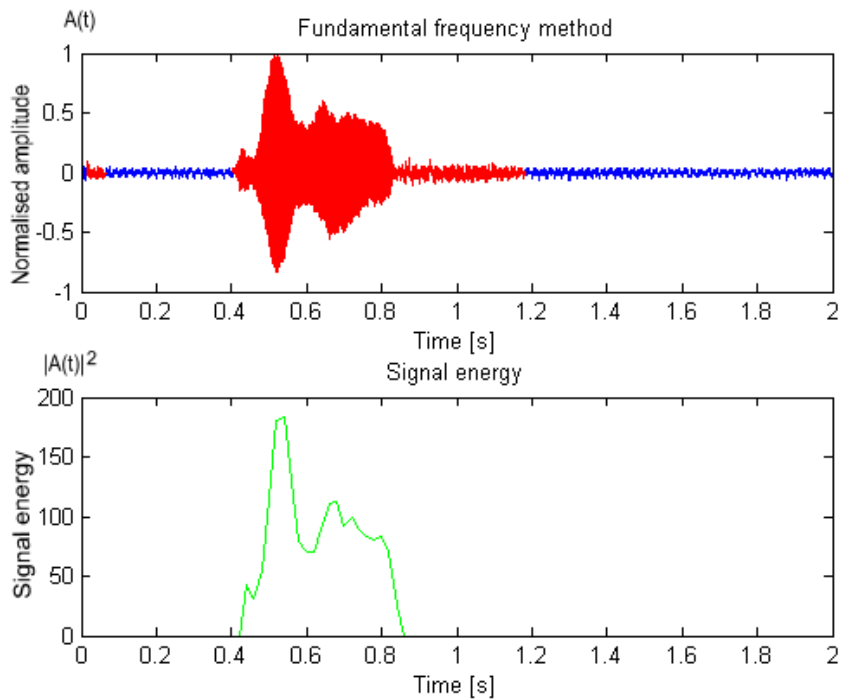
Figure 1. Word 'dziewiec' boundaries set by using the fundamental frequency and signal energy.

Mel cepstral coefficients are commonly used is speech recognition. The counting procedure is as follows [9]:

1. Signal is cut into overlapping frames (20-30 ms length) which are multiplied by the Hamming window.
2. FFT is computed for each frame.
3. Spectrum power (for each frame) is mapped to set of bands using Mel scale triangular overlapping windows.
4. Discrete cosine transform (DCT) is computed for logarithm of each band.

The first (delta parameter) and the second derivative (delta-delta parameter) in time of Mel cepstral coefficient are also used in speech recognition.

3. Dynamic Time Warping algorithm

Algorithm is used to compare the time series which may be of different lengths and shifted in phase relative to each other. Having two series:

$$A = a_1, a_2, \ldots a_n \quad n \in \aleph$$
$$B = b_1, b_2, \ldots b_m \quad m \in \aleph \tag{1}$$
$$a, b \in \Re^k \quad k \in \aleph$$

it is necessary to specify the distance function:

$$d : \Re^k \times \Re^k \to \Re \tag{2}$$

Most commonly used is the Euclidean distance.

First step of algorithm is to calculate the n-by-m matrix. The (i,j)-element of the matrix has a value equal to d(a_i,b_j). Next the warping (alignment) path is determined. It consists of matrix elements:

$$P = p_1, p_2, \ldots p_q \quad \max(m,n) \le q \le m + n + 1 \tag{3}$$

This path must meet several conditions [8]. First concerns the beginning and end of the path i.e. p_1=(1,1) and p_q=(m,n). The second ensures the continuity and monotonicity of the path. For two consecutive elements p_i=(x,y) and p_{i-1}=(x',y') the following relation is satisfied:

$$0 \le x - x' \le 1$$
$$0 \le y - y' \le 1 \tag{4}$$

There may be more than one such path. Algorithm selects the path with the least warping cost:

$$DTW(A,B) = \min \left\{ \frac{\sqrt{\sum_{i=1}^{q} p_i}}{q} \right. \tag{5}$$

The figure below show a cost matrix with a sample path satisfying the above conditions.
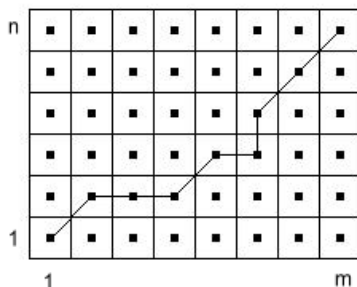
Figure 2. Cost matrix with warping path.

4. Grammar

In order to man-machine communication it is necessary to agree not only vocabulary but also grammar. For a testing purposes a simple grammar was written. Vocabulary consists of 16 polish words (in brackets are the English meanings of words): jeden (one), dwa (two), trzy (trzy), cztery (four), pięć (five), sześć (six), siedem (seven), osiem (eight), dziewięć (nine), dziesięć (ten), zero, stop, prawo (right), lewo (left), góra (up), dół (down), kropka (point). These words form the following grammar:

$$
\begin{aligned}
\langle\text{digit}\rangle \quad &= \quad \text{zero} \mid \text{jeden} \mid \text{dwa} \mid \text{trzy} \mid \text{cztery} \mid \text{pięć} \mid \\
&\qquad \text{sześć} \mid \text{siedem} \mid \text{osiem} \mid \text{dziewięć} \\
\langle\text{integer}\rangle \quad &= \quad \{\langle\text{digit}\rangle\}+ \\
\langle\text{float}\rangle \quad &= \quad \{\langle\text{digit}\rangle\}+ \text{ kropka } \{\langle\text{digit}\rangle\}* \\
\langle\text{keyword}\rangle \quad &= \quad \text{prawo} \mid \text{lewo} \mid \text{góra} \mid \text{dół} \\
\langle\text{command}\rangle \quad &= \quad \langle\text{keyword}\rangle \langle\text{digit}\rangle \\
&\qquad \mid \langle\text{keyword}\rangle \langle\text{integer}\rangle \\
&\qquad \mid \langle\text{keyword}\rangle \langle\text{float}\rangle \\
&\qquad \mid \langle\text{keyword}\rangle \text{ stop} \\
&\qquad \mid \langle\text{command}\rangle \text{ stop} \\
&\qquad \mid \text{stop}
\end{aligned}
$$

Such a grammar can be used to control a simple robot. It allows to run commands consisting of direction and distance. The word 'stop' can be used in case of operator or system confusion. It cause the entering of the command is not continued.

5. Results

All calculation were carried out in MATLAB.

Recognition effectiveness of 16 word was tested. In the first experiment feature vector consisted of 12 Mel cepstral coefficients per frame. In pattern database there was one representative for each word. Word recognition is based on vector sequence comparison with patterns using DTW. Next the shortest warping path is chosen. Mean

efficiency was 95.9%. After redoubling the amount of patterns in database 98.7% efficiency was obtained. Recognition effectiveness of individual words is presented in figure 3.
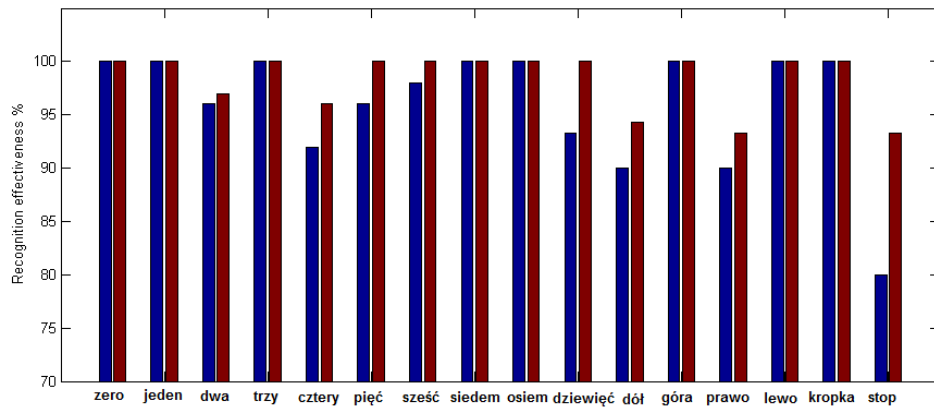
Figure 3. Recognition effectiveness for system with one pattern for each word (blue bar) and two patterns for each word (red bar).

Next the delta and delta-delta parameters were added to feature vector in order to verify whether this will improve the efficiency. Unfortunately it turned out that the efficiency decreased to 76.5% (figure 4).
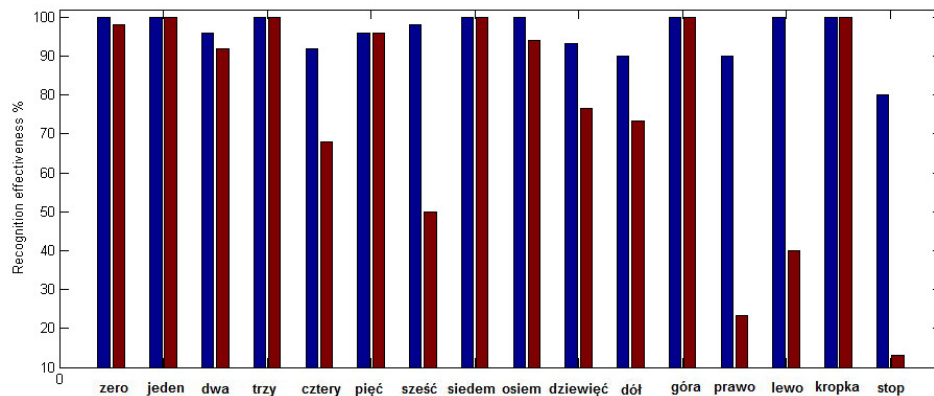
Figure 4. Recognition effectiveness for individual words. Feature vector with Mel cepstral coefficient (blue bar). Feature vector with Mel cepstral coefficient, delta and delta-delta parameters (red bar).

6. Conclusions

DTW algorithm is very simple and well known. As was shown by experiments it gives good results (98.7%) in recognizing words from a small vocabulary.

It was found that delta and delta-delta parameters deteriorated the effectiveness.

Problem may occur with bigger vocabulary as it involves comparing each word with all patterns from database. It can lead to system deceleration (what was observed when number of patterns was doubled).

References

1. P. Senin, *Dynamic Time Warping Algorithm Review*, Information and Computer Science Departament University of Hawaii, Honolulu 2008.
2. M. Petroni, A.S. Malowany, C.C. Johnston, B.J. Stevens, *A new, robust vocal fundamental frequency (F_0) determination method for the analysis of infant cries*, Seventh Annual IEEE Symposium on Computer-Based Medical Systems, 1994
3. B. Plannerer, *An introduction to speech recognition*, 2005
4. M. S. Haleem, *Voice Controlled Automation System*, Proceedings of the 12th IEEE International Multitopic Conference, 2008
5. T. Kubik, M. Sugisaka, Use of acellular phone in mobile robot voice control, SICE, 2001
6. U. H. Langanke, *Direct Voice Control – Speech Data Entry and Database Query Models*, International Symposium on Logistics and Industrial Informatics, 2007
7. A. F. Johnson, B. H. Jacobson, *Medical Speech-Language Pathology A practitioner's Guide*, Thieme, 2007
8. E. J. Keogh, M. J. Pazzani, *Scaling up Dynamic Time Warping to Massive Dataset*, Principles of data mining and knowledge discovery: Third European Conference, Prague, 1999
9. S. Molau, M. Pitz, R. Schluter, H. Ney, *Computing Mel-frequency cepstral coefficients on the Power spectrum*, Acoustics, Speech and Singla Processing Proceedings, **1** (2001) 73-76
10. R. C. Simpson, S. P. Levine, Voice Control of a Powered Wheelchair, IEEE Transactions on neural systems and rehabilitation engineering, **10** (2002) 122-125

Sterowanie głosowe

W artykule opisano system sterowania głosowego. Opiera się on na porównywaniu sekwencji wektorów cech, która reprezentuje wypowiedziane słowo, z bazą wzorców. W tym celu zaimplementowano algorytm Dynamic Time Warping. Jako cech ekstrahowanych z nagrań użyto współczynników Mel cepstrum. Przetestowano także parametry delta oraz delta-delta. W skład systemu wchodzi również algorytm wykrywający granice wypowiedzianego słowa, działający w oparciu o częstotliwość podstawową oraz energię.

Comparison of the Interval Multistep Methods of Adams Type on Some Dynamical Systems

Malgorzata A. JANKOWSKA

Poznan University of Technology, Piotrowo 3, 60-965 Poznan, Poland
malgorzata.jankowska@put.poznan.pl

Abstract

In the paper we compare the explicit and implicit interval multistep methods of Adams type on some dynamical systems. The methods considered can be used for solving the initial value problem (IVP) for ordinary differential equations (ODEs). As a results we obtain the interval solution that include the exact solution of the IVP. The interval methods are examined on efficiency and numerical precision of the results.

Keywords: initial value problem, ordinary differential equations, interval floating-point arithmetic, interval multistep methods of Adams type

1. Introduction

The development of interval methods for solving the IVP for ODEs started with methods based on Taylor series. Such methods were introduced by Moore [26]-[27], Krückberg [17], Eijgenraam [3], Lohner [18], Corliss and Rihm [2]. Explicit interval methods of Runge-Kutta type and explicit interval multistep methods of Adams-Bashforth type have been given by Kalmykov, Šokin and Juldašev [16], [28]. Another approach is represented by a method based on high-order Taylor series proposed by Berz and Makino [1], [19]. The research stared by Makino has been continued by Hoefkens [7]-[8]. An implicit interval Hermite-Obreschkoff (IHO) method for solving the IVP with predictor and corrector phases has been constructed by Jackson and Nedialkov [23]-[24].

Studies on the explicit interval one-step methods of Runge-Kutta type and the interval multistep methods of Adams type for the IVP introduced by Šokin [16], [28] have been going on in Poznan University of Technology since the 1990s. Let us mention one- and two-stage implicit interval methods of Runge-Kutta type (see Marciniak and Szyszka [5], [20], [22]) and three- and four-stage implicit interval methods of Runge-Kutta type (see Marciniak, Gajda and Szyszka [4]-[5], [20]). The explicit and implicit interval multistep methods of Adams type have been proposed by Marciniak and Jankowska (see e.g. [5], [9], [13]-[15], [20]). Finally, the explicit interval multistep methods of Nyström type and the implicit interval methods of Milne-Simpson type have been developed by Marciniak [20].

Computer implementation of the methods considered in the floating-point interval arithmetic (see [6], [10]-[12], [25]), together with the representation of initial data in the form of machine intervals, let us achieve interval solutions that contain all possible errors (i.e. the errors of inexact input data that is often obtained through the experiment, the errors caused by the representation of real numbers in computer, the rounding errors and the errors of the approximate methods).

The paper deals with a comparison of the interval multistep methods of Adams type. Their formulas are not mentioned but can be found in e.g. [9]. Essential notations and assumptions are given in Section 2. In Section 3 we solve some example dynamical systems. The results in the form of interval solutions obtained with the interval methods considered and the widths of such interval solutions are presented and compared. Comments on the efficiency of the methods and the numerical precision of the results obtained bring this paper to the end.

2. Notations and Assumptions

Let us consider the initial value problem for ordinary differential equations of the form

$$y' = f(t, y), \quad y(0) = y_0,$$
(1)

where $t \in [0, \xi]$, $\xi \in \mathbf{R}$, $y = y(t) \in \mathbf{R}^N$, $f : [0, \xi] \times \mathbf{R}^N \to \mathbf{R}^N$.

We choose a positive integer m and select the mesh points $t_0, t_1, \ldots, t_m$, where $t_n = nh$ for each $n = 0, 1, \ldots, m$ and $h = \xi / m$. Moreover, we denote by Δ_t and Δ_y the sets in which the function $f(t, y)$ of the IVP (1) is defined as follows:

$$\Delta_t = \{ t \in \mathrm{R} : 0 \leq t \leq \xi, \quad \xi \in \mathrm{R} \},$$

$$\Delta_y = \left\{ y = (y_1, y_2, \ldots, y_N)^T \in \mathrm{R}^N : \underline{b}_i \leq y_i \leq \overline{b}_i, \ \underline{b}_i, \overline{b}_i \in \mathrm{R}, \ i = 1, 2, \ldots, N \right\}.$$

Furthermore, if we denote by $y(t_i), i = 0, 1, \ldots, m$, the exact value of the function y at t_i, then $Y(t_i)$ is an interval solution such that $y(t_i) \in Y(t_i)$. Note that for any interval $A = [\underline{x}, \overline{x}]$ we define its width (diameter) in the following way $d(A) = \overline{x} - \underline{x}$.

The interval methods considered are interval multistep methods. Hence, before we start the method, we have to know k previous interval solutions obtained with some one step interval methods. The parameter k is known as the number of method steps.

We introduce some abbreviations of the names of the interval methods considered. Namely, the IMA methods for any interval multistep method of Adams type, the EIAB methods for the explicit interval methods of Adams-Bashforth type, the IIAM methods for the implicit interval methods of Adams-Moulton type, the IIAPC1 methods for the implicit interval $P(EC)^sE$ predictor-corrector methods of Adams type, and the IIAPC2 methods for the implicit interval $P(EC)^s$ predictor-corrector methods of Adams type. For the interval predictor-corrector methods of Adams type the number k of method steps in the predictor formula is denoted by k_p, and in the corrector formula by k_c.

3. Numerical experiments

3.1. The Simple Pendulum Problem

We consider the motion of a simple pendulum given by the equation of the form

$$\ddot{\varphi} + u^2 \sin \varphi = 0,$$
(2)

where $\varphi = \varphi(t)$, $u = \sqrt{g/L}$, g is the gravitational acceleration at Earth's surface and L denotes the pendulum length. Under the assumption of small angles, the above equation reduces to the equation of simple harmonic motion

$$\ddot{\varphi} + u^2\varphi = 0. \tag{3}$$

The simple harmonic solution is $\varphi(t) = \varphi_0 \cos(ut)$, where φ_0 is an initial angle.

Denoting $y_1 = \dot{\varphi}$, $y_2 = \varphi$, where $y_1 = y_1(t)$, $y_2 = y_2(t)$, we transform (2) and (3) with the initial conditions $\dot{\varphi}(0) = 0$, $\varphi(0) = \varphi_0$ into the following systems of first order differential equations

$$\dot{y}_1 = -u^2 \sin y_2, \quad \dot{y}_2 = y_1, \tag{4}$$

and

$$\dot{y}_1 = -u^2 y_2, \quad \dot{y}_2 = y_1, \tag{5}$$

with the initial conditions

$$y_1(0) = 0, \quad y_2(0) = \varphi_0. \tag{6}$$

Let us integrate (5) with (6) for $t \in [0, 7.2]$, where $\varphi_0 = \pi/60$ [rad]. Hence, $\Delta_t = [0, 7.2]$ and we take

$$Y_1(0) = [0, 0], \quad Y_2(0) = [0.05235987755982987, 0.05235987755982989].$$

Finally, we specify Δ_y depending on the stepsize h and the number k of method steps such that the computations could be finished successfully at least for the implicit interval methods of Adams type. Then, the results of computations are given as follows.

Table 1. Widths of the interval solution $Y_1(t)$ obtained from the integration of (5) with (6) by the IMA methods for $k = k_p = k_c = 1$, where h = 1E-4, 1E-5, 1E-6.

t	h	$d(Y_1(t))$			
		EIAB	IIAM	IIAPC1	IIAPC2
0.8	1E-4	6.779460E-07	3.527207E-11	3.527207E-11	3.527207E-11
	1E-5	2.135499E-09	1.745521E-14	1.745571E-14	1.745637E-14
	1E-6	2.141428E-11	5.907261E-14	5.909413E-14	5.911725E-14
4.0	1E-4	1.660386E-02	8.669055E-07	8.669056E-07	8.669057E-07
	1E-5	5.252683E-05	4.233049E-10	4.233187E-10	4.233339E-10
	1E-6	5.266869E-07	1.413396E-09	1.413917E-09	1.414477E-09
7.2	1E-4	–	1.953324E-02	1.953324E-02	1.953324E-02
	1E-5	–	9.537963E-06	9.538273E-06	9.538617E-06
	1E-6	1.186738E-02	3.184684E-05	3.185857E-05	3.187119E-05

Table 2. Widths of the interval solution $Y_1(t)$ obtained from the integration of (5) with (6) by the IMA methods for $k = k_p = k_c = 2$, where h = 1E-4, 1E-5, 1E-6.

t	h	$d(Y_1(t))$			
		EIAB	IIAM	IIAPC1	IIAPC2
0.8	1E-4	1.166908E-09	1.623019E-14	1.623432E-14	1.624167E-14
	1E-5	4.108713E-13	8.329776E-15	8.331098E-15	8.333341E-15
	1E-6	3.622299E-13	7.783052E-14	7.783177E-14	7.783194E-14
4.0	1E-4	5.909160E-01	2.044427E-09	2.044964E-09	2.045867E-09
	1E-5	2.097162E-04	1.034466E-09	1.034675E-09	1.035003E-09
	1E-6	1.848350E-04	9.688477E-09	9.688654E-09	9.688734E-09
7.2	1E-4	–	2.445918E-04	2.446560E-04	2.447641E-04
	1E-5	–	1.238637E-04	1.238887E-04	1.239281E-04
	1E-6	–	1.160164E-03	1.160185E-03	1.160195E-03

Table 3. Widths of the interval solution $Y_1(t)$ obtained from the integration of (5) with (6) by the IMA methods for $k = k_p = k_c = 3$, where h = 1E-4, 1E-5, 1E-6.

t	h	$d(Y_1(t))$			
		EIAB	IIAM	IIAPC1	IIAPC2
0.8	1E-4	2.370461E-11	2.341904E-15	2.364767E-15	2.423415E-15
	1E-5	1.483387E-12	1.307405E-14	1.307453E-14	1.307554E-14
	1E-6	1.196633E-11	1.204806E-13	1.204787E-13	1.204800E-13
4.0	1E-4	–	3.464933E-09	3.500707E-09	3.590804E-09
	1E-5	–	1.954756E-08	1.954903E-08	1.955274E-08
	1E-6	–	1.804542E-07	1.804522E-07	1.804563E-07
7.2	1E-4	–	5.069395E-03	5.121734E-03	5.253552E-03
	1E-5	–	2.867079E-02	2.867294E-02	2.867839E-02
	1E-6	–	2.647419E-01	2.647390E-01	2.647451E-01

Now, let us integrate (4) with (6) for $t \in [0,1]$, where $\varphi_0 = \pi/60$ [rad]. We get the following comparison of the widths of the interval solutions
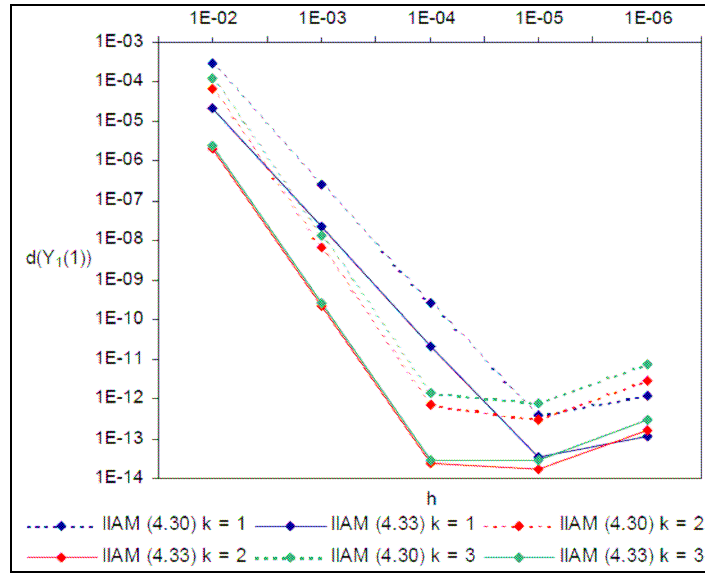
Figure 1. Widths of the interval solution $Y_1(1)$ obtained from the integration of (4) with (6) by the IIAM for $k = 1,2,3$, vs. the stepsize h.
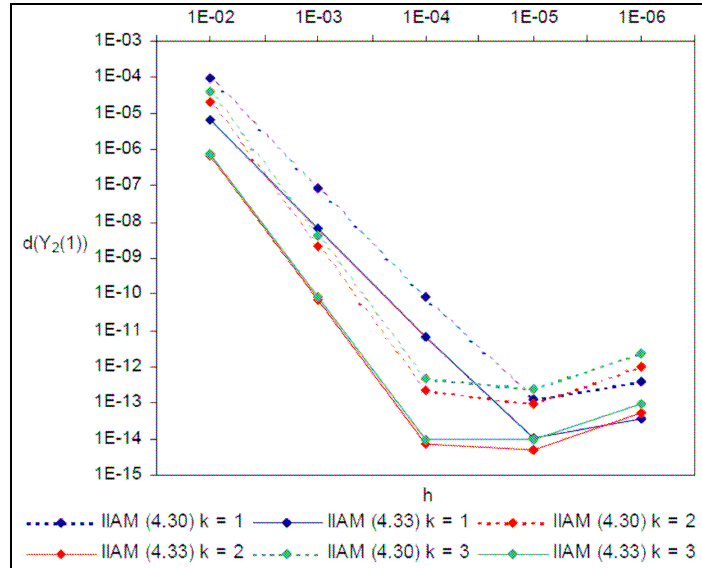
Figure 2. Widths of the interval solution $Y_2(1)$ obtained from the integration of (4) with (6) by the IIAM for $k = 1,2,3$, vs. the stepsize h.

3.2. The Two-Body Problem

Let us consider the system of two material points with the masses m_1 and m_2. We put the origin of the rectangular coordinate system at the material point with the mass m_2. Such a frame is an uninertial one and can be considered as an inertial frame if the mass m_2 is significantly larger then the mass m_1.

The equations of relative motion of material point with the mass m_1 with respect to the material point with the mass m_2 are of the form

$$\ddot{x} = -G(m_1 + m_2)\frac{x}{r^3}, \quad \ddot{y} = -G(m_1 + m_2)\frac{y}{r^3}, \quad \ddot{z} = -G(m_1 + m_2)\frac{z}{r^3}, \tag{7}$$

where $x = x(t)$, $y = y(t)$, $z = z(t)$, $r = \sqrt{x^2 + y^2 + z^2}$ and G is the gravitational constant.

We assume that the material points are located in the plane, i.e. $z = 0$. Denoting $u_1 = x$, $u_2 = y$, $u_3 = \dot{x}$, $u_4 = \dot{y}$, where $u_1 = u_1(t)$, $u_2 = u_2(t)$, $u_3 = u_3(t)$, $u_4 = u_4(t)$, $r = \sqrt{u_1^2 + u_2^2}$, we transform (7) with the initial conditions $x(0) = x_0$, $y(0) = y_0$, $\dot{x}(0) = v_{x0}$, $\dot{y}(0) = v_{y0}$, into the system of differential equations of the first order as follows

$$\dot{u}_1 = u_3, \quad \dot{u}_2 = u_4, \quad \dot{u}_3 = -G(m_1 + m_2)\frac{u_1}{r^3}, \quad \dot{u}_4 = -G(m_1 + m_2)\frac{u_2}{r^3}, \tag{8}$$

with the initial conditions

$$u_1(0) = x_0, \quad u_2(0) = y_0, \quad u_3(0) = v_{x0}, \quad u_4(0) = v_{y0}. \tag{9}$$

Now, let us take the mass of the Earth as the mass unit, the astronomical unit as the length unit, and the sideral year as the time unit. For these units we have the gravitational constant $G = 1.185684121E\text{-}4$. Now, we assume that the material points with the masses $m_1 = 1$ and $m_2 = 332958$, where m_2 is the mass of the Sun in the given mass unit, fulfil at the initial moment $t = 0$ the following conditions

$$u_1(0) = 1, \quad u_2(0) = 0, \quad u_3(0) = 0, \quad u_4(0) = \sqrt{G(m_1 + m_2)}. \tag{10}$$

The analytical solution of (8) with (10) has the form (see also [21])

$$u_1(t) = \cos(Mt), \quad u_2(t) = \sin(Mt), \quad u_3(t) = -M\sin(Mt), \quad u_4(t) = M\cos(Mt),$$

where $M = \sqrt{G(m_1 + m_2)}$.

We integrate (8) with (10) for $t \in [0,1]$. Hence, $\Delta_t = [0,1]$ and we take

$$U_1(0) = [1,1], \quad U_2(0) = [0,0], \quad U_3(0) = [0,0],$$
$$U_4(0) = [6.28318549180301535, 6.28318549180301537].$$

Then, we get the following results.

Table 4. Values of the exact solution and the interval solutions $U_i(t), i = 1,2,3,4,$ obtained from the integration of (8) with (10) by the IIAM method for $k = 2$, where $h =$ 1E-5.

t	$u_1(t)$	$U_1(t)$
0.2	3.09016959257484E-1	[3.0901695925747969E-1, 3.0901695925748894E-1]
0.4	-8.09017037782516E-1	[-8.0901703778257027E-1,-8.0901703778246288E-1]
0.6	-8.09016929263585E-1	[-8.0901692926487735E-1,-8.0901692926229403E-1]
0.8	3.09017134844796E-1	[3.0901713483060309E-1, 3.0901713485898777E-1]
1.0	9.99999999999982E-1	[9.9999999974702492E-1, 1.0000000002529414E+0]

t	$u_2(t)$	$U_2(t)$
0.2	9.51056527705508E-1	[9.5105652770550377E-1, 9.5105652770551289E-1]
0.4	5.87785192547074E-1	[5.8778519254698043E-1, 5.8778519254717017E-1]
0.6	-5.87785341910564E-1	[-5.8778534191141762E-1,-5.8778534190971036E-1]
0.8	-9.51056470653721E-1	[-9.5105647067212342E-1,-9.5105647063532045E-1]
1.0	1.84623428883101E-7	[1.8435716556183061E-7, 1.8488969007326329E-7]

t	$u_3(t)$	$U_3(t)$
0.2	-5.97566457676380E+0	[-5.9756645767638517E+0,-5.9756645767637525E+0]
0.4	-3,69316339410842E+0	[-3.6931633941091693E+0,-3.6931633941076792E+0]
0.6	3.69316433258693E+0	[3.6931643325702719E+0, 3.6931643326035890E+0]
0.8	5.97566421829684E+0	[5.9756642181779058E+0, 5.9756642184157832E+0]
1.0	-1.16002324980522E-6	[-1.1633906352060689E-6,-1.1566558509050039E-6]

t	$u_4(t)$	$U_4(t)$
0.2	1.94161087512770E+0	[1.9416108751276484E+0, 1.9416108751277690E+0]
0.4	-5.08320411441656E+0	[-5.0832041144176589E+0,-5.0832041144154596E+0]
0.6	-5.08320343257198E+0	[-5.0832034325811353E+0,-5.0832034325628382E+0]
0.8	1.94161197837535E+0	[1.9416119781338048E+0, 1.9416119786169041E+0]
1.0	6.28318549180290E+0	[6.2831854895478384E+0, 6.2831854940579771E+0]
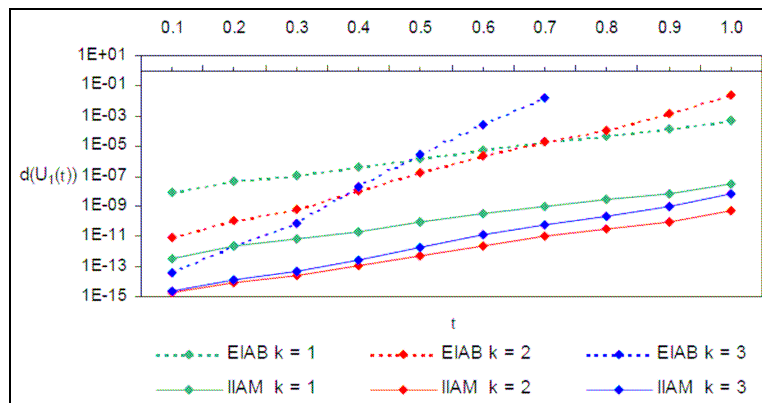
Figure 3. Widths of the interval solution $U_1(t)$ obtained from the integration of (8) with (10) by the EIAB methods for $k = 1,2,3$, and the IIAM methods for $k = 1,2,3$, where $h =$ 1E-5.
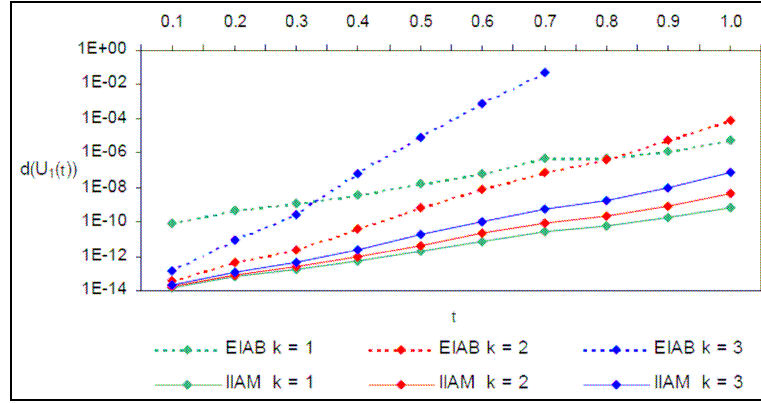
Figure 4. Widths of the interval solution $U_1(t)$ obtained from the integration of (8) with (10) by the EIAB methods for $k = 1,2,3$, and the IIAM methods for $k = 1,2,3$, where $h = 1E\text{-}6$.

3.3. Hill Equations

Finally, we consider the equations of motion of the Moon given by Hill (see e.g. [21]). We assume that the origin of the frame is placed in the center of the Earth, the plane xy is in line with the Sun's orbit plane and the frame rotates with the constant angular velocity v', where v' denotes the mean motion of the Sun. Moreover, we assume that in the considered frame of reference the axis x goes across the center of the Sun and the Sun revolves around the Earth along the circular orbit. The equations of motion of the Moon (called the Hill equations) are of the form

$$\frac{d^2x}{d\tau^2} = 2M\frac{dy}{d\tau} - \left(\frac{\kappa}{r^3} - 3M^2\right)x, \quad \frac{d^2y}{d\tau^2} = -2M\frac{dx}{d\tau} - \frac{\kappa}{r^3}y, \quad \frac{d^2z}{d\tau^2} = -\left(\frac{\kappa}{r^3} + M^2\right)z, \quad (11)$$

where $x = x(\tau)$, $y = y(\tau)$, $z = z(\tau)$, $\tau = (v - v')(t - t_0)$, $r = \sqrt{x^2 + y^2 + z^2}$. Moreover, the parameters M and κ in (11) are introduced as follows

$$M = \frac{v'}{v - v'}, \quad \kappa = G\frac{m_0 + m_1}{(v - v')^2}, \quad (12)$$

where v is the mean motion of the Moon, G is the gravitational constant, and m_0, m_1 denote the masses of the Earth and the Moon, respectively.

Taking into account a small inclination of the Moon's orbit to the ecliptic, we can also assume $z = 0$. Finally, denoting $u_1 = x$, $u_2 = y$, $u_3 = dx/d\tau$, $u_4 = dy/d\tau$, where $u_1 = u_1(\tau)$, $u_2 = u_2(\tau)$, $u_3 = u_3(\tau)$, $u_4 = u_4(\tau)$, we transform (11) with the initial conditions $x(0) = x_0$, $y(0) = y_0$, $dx/d\tau(0) = v_{x0}$, $dy/d\tau(0) = v_{y0}$ into the following system of differential equations of the first order

$$\frac{du_1}{d\tau} = u_3, \quad \frac{du_2}{d\tau} = u_4, \quad \frac{du_3}{d\tau} = 2Mu_4 - \left(\frac{\kappa}{r^3} - 3M^2\right)u_1, \quad \frac{du_4}{d\tau} = -2Mu_3 - \frac{\kappa}{r^3}u_2, \quad (13)$$

with the initial conditions

$$u_1(0) = x_0, \quad u_2(0) = y_0, \quad u_3(0) = v_{x0}, \quad u_4(0) = v_{y0}, \quad (14)$$

where $r = \sqrt{u_1^2 + u_2^2}$.

In order to test the methods considered we determine the initial conditions (14) as follows

$$u_1(0) = 1, \quad u_2(0) = 0, \quad u_3(0) = 0, \quad u_4(0) = 1, \quad (15)$$

and

$$u_1(0) = -0.9447782, \quad u_2(0) = -0.2673999,$$
$$u_3(0) = 0.3286969, \quad u_4(0) = -0.9500594. \quad (16)$$

Finally, we specify the parameters M and κ in (13) as

- $M = 0$, $\kappa = 1$, and
- $M = 0.080848933808312$, $\kappa = 1.171418459184516$, respectively.

Then, we get the following results.
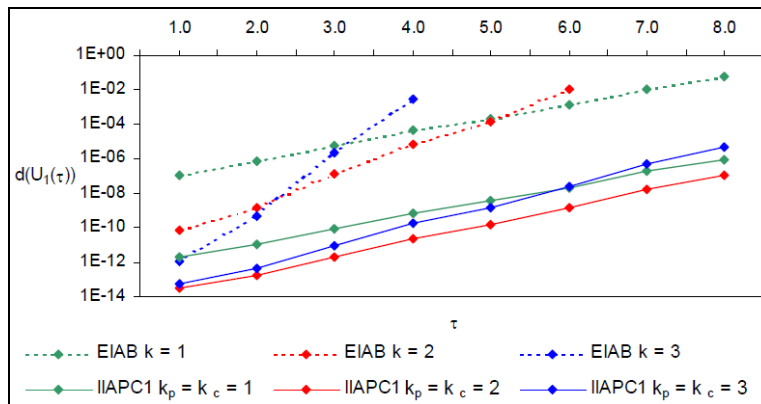
Figure 5. Widths of the interval solution $U_1(\tau)$ obtained from the integration of the Hill equations (13) with (15), with $M = 0$, $\kappa = 1$, by the EIAB methods for $k = 1,2,3$, and the IIAPC1 methods for $k = k_p = k_c = 1,2,3$, where $h = 1E\text{-}5$.
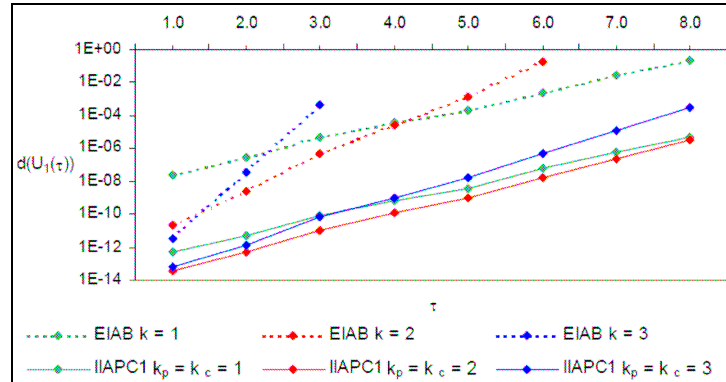
Figure 6. Widths of the interval solution $U_1(\tau)$ obtained from the integration of the Hill equations (13) with (16), with $M \approx 0.08$, $\kappa \approx 1.17$, by the EIAB methods for $k = 1,2,3$, and the IIAPC1 methods for $k = k_p = k_c = 1,2,3$, where $h = $ 1E-5.

4. Conclusions

Comparison of the numerical results obtained with the explicit and implicit interval methods of Adams type let us formulate the following conclusions:

- The implicit interval methods of Adams type yield better results, i.e. interval solutions of a smaller width, than the explicit ones applied with the same number k of method steps and the same stepsize h.

- For the explicit and implicit interval methods of Adams type the increase in the number k of method steps for the same stepsize h contributes to the decrease in the widths of the interval solutions. A similar effect can be observed if we reduce the stepsize h for the same value of parameter k. Such a behavior of these methods is true mainly for short integration intervals. Otherwise for each particular IVP the suitable interval multistep method with the appropriate number k of method steps and the stepsize h should be chosen to get the best acceptable result.

- For a given stepsize there exists an optimal number of method steps, and for a given number of method steps the optimal stepsize can be found.

- The widths of the interval solutions obtained by the implicit interval methods of Adams type and both kinds of interval predictor-corrector methods of Adams type are of the same order. We recommend applying the interval predictor-corrector methods due to a significant reduction in the number of iterations involved. The number of iterations is usually reduced by half in comparison to the interval methods of Adams-Moulton type. Hence, computation time is saved.

- The implicit interval $P(EC)^s E$ predictor-corrector methods of Adams type yield interval solutions of somewhat smaller widths then the $P(EC)^s$ ones. On the other

hand the additional computation of $F_n^{(s)} = F(T_n, Y_n)$ performed in each step of the method makes them a little bit more laborious than the $P(EC)^s$ ones.

- As numerical tests show, the interval solutions of the smallest widths are mostly produced by the interval methods of Adams type for $k > 1$. For this reason, just the interval multistep methods of Adams type rather than the interval one-step ones should be taken into account before the integration of the given IVP starts.

References

1. Berz M., Makino K., Verified integration of ODEs and flows with differential algebraic methods on Taylor models, *Reliable Computing* **4** (**4**), (1998) 361-369
2. Corliss G.F., Rihm R., Validating an a priori enclosure using high-order Taylor series, in Alefeld G., Frommer A., editors, *Scientific Computing, Computer Arithmetic and Validated Numerics*, Akademie Verlag, Berlin (1996) 228-238
3. Eijgenraam P., The Solution of Initial Value Problems Using Interval Arithmetic, *Mathematical Centre Tracts* No. **144**, Stichting Mathematisch Centrum, Amsterdam (1981)
4. Gajda K., Marciniak A., Szyszka B., Three- and Four-Stage Implicit Interval Methods of Runge-Kutta Type, *Computational Methods in Science and Technology* **6**, (2000) 41-59
5. Gajda K., Jankowska M., Marciniak A., Szyszka B., A Survey of Interval Runge-Kutta and Multistep Methods for Solving the Initial Value Problem, *Lecture Notes in Computer Science* **4967,** (2008) 1361-1371
6. Hammer R., Hocks M., Kulisch U., Ratz D., *Numerical Toolbox for Verified Computing I. Basic Numerical Problems*, Springer-Verlag, Berlin (1993)
7. Hoefkens J., *Rigorous Numerical Analysis with High-Order Taylor Models*, Ph.D. Thesis, Michigan State University, East Lansing (2001)
8. Hoefkens J., Berz M., Makino K., Controlling the Wrapping Effect in the Solution of ODEs for Asteroids, *Reliable Computing* **8**, (2003) 21-41
9. Jankowska M.A., Interval Multistep Methods of Adams type and their Implementation in the C++ Language, Ph.D. Thesis, Poznan University of Technology, Poznan (2006)
10. Jankowska M.A., Introduction to the C++ Libraries for Floating-Point Conversions and Interval Arithmetic, *Polish Journal of Environmental Studies* Vol. **18**, No. **3B**, (2009) 131-137
11. Jankowska M.A., C++ *Library for Floating-Point Conversions. User and Reference Guide*, Poznan University of Technology, last updated 2009, available in Software at http://www.mjank.user.icpnet.pl/
12. Jankowska M.A., C++ *Library for Floating-Point Interval Arithmetic. User and Reference Guide*, Poznan University of Technology, last updated 2009, available in Software at http://www.mjank.user.icpnet.pl/

13. Jankowska M.A., Marciniak, A., Implicit Interval Multistep Methods for Solving the Initial Value Problem, *Computational Methods in Science and Technology* **8** (**1**), (2002) 17-30

14. Jankowska M.A., Marciniak A., On Explicit Interval Methods of Adams-Bashforth Type, *Computational Methods in Science and Technology* **8** (**2**), (2002) 46-57

15. Jankowska M.A., Marciniak A., On Two Families of Implicit Interval Methods of Adams-Moulton Type, *Computational Methods in Science and Technology* **12** (**2**), (2006) 109-113

16. Kalmykov S.A., Šokin Ju.I., Juldašev E.Ch., *Methods of Interval Analysis* [in Russian], Nauka, Novosibirsk (1986)

17. Krückberg F., Ordinary differential equations, in Hansen E., editor, *Topics in Interval Analysis*, Clarendon Press, Oxford (1969) 91-97

18. Lohner R.J., Enclosing the solutions of ordinary initial and boundary value problems, in Kaucher E.W., Kulisch U.W., Ullrich Ch., editors, *Computer Arithmetic: Scientific Computation and Programming Languages*, Wiley-Teubner Series in Computer Science, Stuttgart (1987) 255-286

19. Makino K., *Rigorous Analysis of Nonlinear Motion in Particle Accelerators*, Ph.D. Thesis, Michigan State University, East Lansing, Michigan, USA (1998)

20. Marciniak A., *Selected Interval Methods for Solving the Initial Value Problem*, Publishing House of Poznan University of Technology, Poznan (2009)

21. Marciniak A., Numerical Solutions of the N-body Problem, Reidel, Dordrecht (1985)

22. Marciniak A., Szyszka B., One- and Two-Stage Implicit Interval Methods of Runge-Kutta Type, *Computational Methods in Science and Technology* **5**, (1999) 53-65

23. Nedialkov N.S., Jackson K.R., An interval Hermite-Obreschkoff method for computing rigorous bounds on the solution of an initial value problem for an ordinary differential equation, *Reliable Computing* **5** (**3**), (1999) 289-310

24. Nedialkov N.S., Computing Rigorous Bounds on the Solution of an Initial Value Problem for an Ordinary Differential Equation, Ph.D. Thesis, University of Toronto (1999)

25. Jaulin L., Kieffer M., Didrit O., Walter É., *Applied Interval Analysis*, Springer-Verlag, London (2001)

26. Moore R.E., *Interval Analysis*, Prentice-Hall, Englewood Cliffs, NJ (1966)

27. Moore R.E., Kearfott R.B., Cloud M.J., *Introduction to Interval Analysis*, SIAM, Philadelphia (2009)

28. Šokin Ju.I., *Interval Analysis* [in Russian], Nauka, Novosibirsk (1981)

Porównanie przedziałowych metod wielokrokowych typu Adamsa na przykładzie wybranych układów dynamicznych

W pracy porównane zostały jawne i niejawne przedziałowe metody typu Adamsa na przykładzie wybranych układów dynamicznych. Rozważane metody mogą być wykorzystane do rozwiązywania zagadnienia początkowego dla równań różniczkowych zwyczajnych. W wyniku zastosowania wspomnianych metod otrzymujemy przedział rozwiązanie, które zawiera w sobie rozwiązanie dokładne danego zagadnienia początkowego. Metody przedziałowe zostały zbadane ze względu na efektywność ich działania oraz dokładność otrzymanego rozwiązania.

Interval Multistep Predictor-Corrector Methods
of Adams Type for Solving the Initial Value Problem
for Ordinary Differential Equations

Malgorzata A. JANKOWSKA

Poznan University of Technology, Piotrowo 3, 60-965 Poznan, Poland
malgorzata.jankowska@put.poznan.pl

Abstract

In the paper we propose the interval multistep predictor-corrector methods of Adams type for solving the initial value problem (IVP) for ordinary differential equations (ODEs). These methods are based on the explicit interval methods of Adams-Bashforth type and the implicit interval methods of Adams-Moulton type. The interval methods considered belong to a class of algorithms that allow to obtain the guaranteed result, i.e. the interval solution that contain the exact solution of the problem.

Keywords: initial value problem, ordinary differential equations, floating-point interval arithmetic, interval methods, interval predictor-corrector methods of Adams type

1. Introduction

Interval methods have been first proposed for verified computing by Sunaga (see [14]) and Moore (see e.g. [12]-[13]). Growing interest in such algorithms (see e.g. [2], [11]) results from the fact that interval solutions obtained by theses methods include the exact solution of the problem. Computer implementation of the methods considered in the floating-point interval arithmetic (for some information on the C++ libraries for floating-point conversion and interval arithmetic see [4]-[6]), together with the representation of initial data in the form of machine intervals, let us achieve interval solutions that contain all possible errors (i.e. the errors of inexact input data that is often obtained through the experiment, the errors caused by the representation of real numbers in computer, the rounding errors and the errors of the approximate methods).

The development of the interval methods for solving the IVP for ODEs started with methods based on Taylor series (the detailed bibliography concerned with all verified methods devoted for the IVP is available in e.g. [3] and [10]). The interval multistep predictor-corrector methods of Adams type introduced in the paper are based on the explicit interval multistep methods of Adams-Bashforth type (see [1], [3], [8], [10]) and the implicit interval multistep methods of Adams-Moulton type (see [1], [3], [7], [9]-[10]). In the paper we give the detailed theoretical description of the interval predictor-corrector methods (the results of numerical experiments can be found in [3]).

The interval methods presented in the paper can be used for solving the IVP that occurs very frequently in physics and other sciences. For example in the area of dynamical systems the differential equation is an evolution equation that specifies how, with a given initial condition, the system will evolve in time.

2. Initial Value Problem and Interval Explicit and Implicit Multistep Methods of Adams Type

Let us consider the initial value problem for ordinary differential equations of the form

$$y' = f(t, y), \quad y(0) = y_0, \tag{1}$$

where $t \in [0, \xi]$, $\xi \in \mathbf{R}$, $y = y(t) \in \mathbf{R}^N$, $f : [0, \xi] \times \mathbf{R}^N \to \mathbf{R}^N$.

Now, let us choose a positive integer m and select the mesh points $t_0, t_1, \ldots, t_m$, where $t_n = nh$ for each $n = 0, 1, \ldots, m$ and $h = \xi / m$. Moreover, we denote by Δ_t and Δ_y the sets in which the function $f(t, y)$ of the IVP (1) is defined as follows:

$$\Delta_t = \{ t \in \mathbf{R} : 0 \leq t \leq \xi, \quad \xi \in \mathbf{R} \},$$
$$\Delta_y = \{ y = (y_1, y_2, \ldots, y_N)^T \in \mathbf{R}^N : \underline{b}_i \leq y_i \leq \overline{b}_i, \ \underline{b}_i, \overline{b}_i \in \mathbf{R}, \ i = 1, 2, \ldots, N \}.$$

Let $F(T, Y)$ be an interval extension of $f(t, y)$, and $\Psi(T, Y)$, $\overline{\Psi}(T, Y)$ be interval extensions of functions $\psi(t, y)$ and $\overline{\psi}(t, y)$ (for details see [3]) determined as follows:

$$\psi(\eta, y(\eta)) \equiv f^{(k)}(\eta, y(\eta)) \equiv y^{(k+1)}(\eta), \quad \eta \in [t_{n-k}, t_n],$$
$$\overline{\psi}(\eta, y(\eta)) \equiv f^{(k+1)}(\eta, y(\eta)) \equiv y^{(k+2)}(\eta), \quad \eta \in [t_{n-k}, t_n].$$

We also assume that

- $F(T, Y)$ is defined and continuous for all $T \subset \Delta_t$ and $Y \subset \Delta_y$,
- $F(T, Y)$ is monotonic with respect to inclusion, i.e.
$$T_1 \subset T_2 \wedge Y_1 \subset Y_2 \Rightarrow F(T_1, Y_1) \subset F(T_2, Y_2),$$
- for each $T \subset \Delta_t$ and for each $Y \subset \Delta_y$ there exists a constant $L > 0$ such that
$$d(F(T, Y)) \leq L(d(T) + d(Y)),$$
  where $d(A)$ denotes the width (diameter) of A; if $A = [\underline{x}, \overline{x}]$ then $d(A) = \overline{x} - \underline{x}$; if $A = (A_1, A_2, \ldots, A_N)^T$ then $d(A)$ is defined by $d(A) = \max_{i=1,2,\ldots,N} d(A_i)$,
- $\Psi(T, Y)$, $\overline{\Psi}(T, Y)$ are defined for all $T \subset \Delta_t$ and $Y \subset \Delta_y$,
- $\Psi(T, Y)$, $\overline{\Psi}(T, Y)$ are monotonic with respect to inclusion.

2.1. Explicit Interval Methods of Adams-Bashforth Type

Let us assume that $y(0) \in Y_0$, $Y_0 \subset \Delta_y$ and the intervals $Y_i \subset \Delta_y$, such that $y(t_i) \in Y_i$, $i = 1, 2, \ldots, k-1$, are known. An integer $k = 1, 2, \ldots$ states how many interval-solutions Y_i are required to apply the k-step multistep method and it is referred to as the number of method steps. We obtain $Y_i, i = 1, 2, \ldots, k-1$ by applying an interval one-step method (e.g. an explicit interval method of Runge-Kutta type (see e.g. [10]) or an explicit

interval method of Adams-Bashforth type with $k = 1$). Then the explicit interval method of Adams-Bashforth type (see also [3]) can be given in the form

$$
\begin{aligned}
Y_n = Y_{n-1} + h \sum_{j=0}^{k-1} \gamma_j \, \nabla^j F\left(T_{n-1}, Y_{n-1}\right) \\
+ h^{k+1} \gamma_k \, \Psi\left(T_{n-1} + \left[-(k-1)h, h\right], Y_{n-1} + \left[-(k-1)h, h\right] F\left(\Delta_t, \Delta_y\right)\right),
\end{aligned}
\tag{2}
$$

for $n = k, k+1, \ldots, m$,

where $t_i = ih \in T_i$, $i = 0,1,\ldots,m$, γ_j, $j = 0,1,\ldots,k$ and $\nabla^j F\left(T_{n-1}, Y_{n-1}\right)$ are given by

$$
\gamma_0 = 1, \quad \gamma_j = \frac{1}{j!} \int_0^1 s(s+1)\cdots(s+j-1)\,ds, \quad j = 1,2,\ldots,k,
$$

$$
\nabla^j F\left(T_{n-1}, Y_{n-1}\right) = \sum_{m=0}^{j} (-1)^m \binom{j}{m} F\left(T_{n-1-m}, Y_{n-1-m}\right).
\tag{3}
$$

The formula of the explicit interval methods of Adams-Bashforth type equivalent to (2) can be written as follows

$$
\begin{aligned}
Y_n = Y_{n-1} + h \sum_{j=1}^{k} \beta_{kj} F\left(T_{n-j}, Y_{n-j}\right) \\
+ h^{k+1} \gamma_k \, \Psi\left(T_{n-1} + \left[-(k-1)h, h\right], Y_{n-1} + \left[-(k-1)h, h\right] F\left(\Delta_t, \Delta_y\right)\right),
\end{aligned}
\tag{4}
$$

for $n = k, k+1, \ldots, m$,

where β_{kj} are defined as follows

$$
\beta_{kj} = (-1)^{j-1} \sum_{m=j-1}^{k-1} \binom{m}{j-1} \gamma_m, \quad j = 1,2,\ldots,k.
\tag{5}
$$

2.2. Implicit Interval Methods of Adams-Moulton Type

Let the assumptions about Y_i, $i = 0,1,\ldots,k-1$, be the same as in Sec. 2.1. Then the implicit interval method of Adams-Moulton type (see also [3]) can be given in the form

$$
\begin{aligned}
Y_n = Y_{n-1} + h \sum_{j=0}^{k} \bar{\gamma}_j \, \nabla^j F\left(T_n, Y_n\right) \\
+ h^{k+2} \bar{\gamma}_{k+1} \, \overline{\Psi}\left(T_n + \left[-kh, 0\right], Y_n + \left[-kh, 0\right] F\left(\Delta_t, \Delta_y\right)\right),
\end{aligned}
\tag{6}
$$

for $n = k, k+1, \ldots, m$,

where $t_i = ih \in T_i$, $i = 0,1,\ldots,m$, $\bar{\gamma}_j$, $j = 0,1,\ldots,k+1$ and $\nabla^j F\left(T_n, Y_n\right)$ are given by

$$\bar{\gamma}_0 = 1, \quad \bar{\gamma}_j = \frac{1}{j!} \int_{-1}^{0} s(s+1)\cdots(s+j-1)ds, \quad j = 1, 2, \ldots, k+1,$$

$$\nabla^j F(T_n, Y_n) = \sum_{m=0}^{j} (-1)^m \binom{j}{m} F(T_{n-m}, Y_{n-m}). \tag{7}$$

The equation (6) can be written in the equivalent form

$$Y_n = Y_{n-1} + h \sum_{j=0}^{k} \bar{\gamma}_j F(T_n, Y_n) + h \sum_{j=1}^{k} \bar{\gamma}_j \sum_{m=1}^{j} (-1)^m \binom{j}{m} F(T_{n-m}, Y_{n-m})$$

$$+ h^{k+2} \bar{\gamma}_{k+1} \overline{\Psi}(T_n + [-kh, 0], Y_n + [-kh, 0] F(\Delta_t, \Delta_y)), \tag{8}$$

for $n = k, k+1, \ldots, m$.

Another kind of the implicit interval methods of Adams-Moulton type (which are not equivalent to (6) and (8)) are of the following form

$$Y_n = Y_{n-1} + h \bar{\beta}_{k0} F(T_n, Y_n) + h \sum_{j=1}^{k} \bar{\beta}_{kj} F(T_{n-j}, Y_{n-j})$$

$$+ h^{k+2} \bar{\gamma}_{k+1} \overline{\Psi}(T_n + [-kh, 0], Y_n + [-kh, 0] F(\Delta_t, \Delta_y)), \tag{9}$$

for $n = k, k+1, \ldots, m$,

where $\bar{\beta}_{kj}$ are defined as follows

$$\bar{\beta}_{kj} = (-1)^j \sum_{m=j}^{k} \binom{m}{j} \bar{\gamma}_m, \quad j = 0, 1, \ldots, k. \tag{10}$$

Let us note that (6) (or (8)) and (9) are both nonlinear interval equations with respect to Y_n, $n = k, k+1, \ldots, m$. It implies that in each step of these methods we have to solve an interval equation of the form

$$Y = G(T, Y), \tag{11}$$

where

$$T \in I(\Delta_t) \subset IR, \quad Y = (Y_1, Y_2, \ldots, Y_N)^T \in I(\Delta_y) \subset IR^N, \quad G : I(\Delta_t) \times I(\Delta_y) \to IR^N,$$

IR denotes the set of real intervals and $I(\Delta_t)$, $I(\Delta_y)$ – the sets of intervals which are contained in Δ_t and Δ_y (or the sets of subintervals of Δ_t and Δ_y), respectively.

If we assume that G is a contraction mapping, then the fixed-point theorem implies that the iteration process

$$Y^{(l+1)} = G(T, Y^{(l)}), \quad l = 0, 1, \ldots, \tag{12}$$

is convergent to an unique element Y^*, i.e. $\lim_{l \to \infty} Y^{(l)} = Y^*$, for an arbitrary choice of $Y^{(0)} \in I(\Delta_y)$.

For the interval methods of Adams-Moulton type given by (6) (or (8)), the iteration process (12) is of the form

$$Y_n^{(l+1)} = Y_{n-1} + h\sum_{j=0}^{k} \bar{\gamma}_j \, F\left(T_n, Y_n^{(l)}\right) + h\sum_{j=1}^{k} \bar{\gamma}_j \sum_{m=1}^{j} (-1)^m \binom{j}{m} F\left(T_{n-m}, Y_{n-m}\right)$$
$$+ h^{k+2}\, \bar{\gamma}_{k+1}\, \overline{\Psi}\left(T_n + [-kh, 0], Y_n^{(l)} + [-kh, 0] F\left(\Delta_t, \Delta_y\right)\right),$$

for $n = k, k+1, \ldots, m$.

Similarly, for the methods described by (9) we have

$$Y_n^{(l+1)} = Y_{n-1} + h\bar{\beta}_{k0}\, F\left(T_n, Y_n^{(l)}\right) + h\sum_{j=1}^{k} \bar{\beta}_{kj}\, F\left(T_{n-j}, Y_{n-j}\right)$$
$$+ h^{k+2}\, \bar{\gamma}_{k+1}\, \overline{\Psi}\left(T_n + [-kh, 0], Y_n^{(l)} + [-kh, 0] F\left(\Delta_t, \Delta_y\right)\right),$$

for $n = k, k+1, \ldots, m$.

Note that for the above iteration processes we usually choose $Y_n^{(0)} = Y_{n-1}$.

3. Interval Predictor-Corrector Multistep Methods of Adams Type

The implicit interval methods of Adams-Moulton type described in Sec. 2.2 can be realized in another way. Let us assume that the iteration processes (12) is initiated by the interval solution obtained by applying the explicit interval k-step method of Adams-Bashforth type, instead of Y_{n-1}, as we proposed in Sec. 2.2. Such an initialization is characteristic of predictor-corrector methods. Hence, we define the interval predictor-corrector methods of Adams type in the following way.

Let the assumptions about Y_i, $i = 0, 1, \ldots, k-1$, be the same as in Sec. 2.1. Consider the explicit interval k-step method of Adams-Bashforth type as a predictor and the implicit interval k-step method of Adams-Moulton type as a corrector. We assume that both predictor and corrector formulas describe the interval multistep methods such that the number k of method steps is the same. Moreover, we denote by s ($s \geq 1$) the number of iterations that are performed in each step of the method.

The assumptions about k and s have been made to simplify the notation of the interval predictor-corrector methods of Adams type and can be neglected while developing the specific predictor-corrector formulas.

For the interval methods of Adams-Moulton type given by (6) (or (8)), the interval $P(EC)^s E$ predictor-corrector methods of Adams type are of the following form:

$$P: \quad Y_n^{(0)} = Y_{n-1}^{(s)} + h\sum_{j=1}^{k} \beta_{kj}\, F\left(T_{n-j}, Y_{n-j}^{(s)}\right)$$
$$+ h^{k+1}\gamma_k\, \Psi\left(T_{n-1} + [-(k-1)h, h], Y_{n-1}^{(s)} + [-(k-1)h, h] F\left(\Delta_t, \Delta_y\right)\right), \tag{13}$$

$$E: \quad F_n^{(l)} = F\left(T_n, Y_n^{(l)}\right), \tag{14}$$

$$C: \quad Y_n^{(l+1)} = Y_{n-1}^{(s)} + h \sum_{j=0}^{k} \bar{\gamma}_j F_n^{(l)}$$

$$+ h \sum_{j=1}^{k} \bar{\gamma}_j \sum_{m=1}^{j} (-1)^m \binom{j}{m} F\left(T_{n-m}, Y_{n-m}^{(s)}\right) \tag{15}$$

$$+ h^{k+2} \bar{\gamma}_{k+1} \overline{\Psi}\left(T_n + [-kh, 0], Y_n^{(l)} + [-kh, 0] F\left(\Delta_t, \Delta_y\right)\right),$$

$$\text{for } l = 0, 1, \ldots, s-1,$$

$$E: \quad \text{if } n < m, \text{ then } F_n^{(s)} = F\left(T_n, Y_n^{(s)}\right), \tag{16}$$

for $n = k, k+1, \ldots, m$.

Similarly, for the interval methods determined by (9) we have

$$P: \quad Y_n^{(0)} = Y_{n-1}^{(s)} + h \sum_{j=1}^{k} \beta_{kj} F\left(T_{n-j}, Y_{n-j}^{(s)}\right)$$

$$+ h^{k+1} \gamma_k \Psi\left(T_{n-1} + [-(k-1)h, h], Y_{n-1}^{(s)} + [-(k-1)h, h] F\left(\Delta_t, \Delta_y\right)\right), \tag{17}$$

$$E: \quad F_n^{(l)} = F\left(T_n, Y_n^{(l)}\right), \tag{18}$$

$$C: \quad Y_n^{(l+1)} = Y_{n-1}^{(s)} + h \bar{\beta}_{k0} F_n^{(l)} + h \sum_{j=1}^{k} \bar{\beta}_{kj} F\left(T_{n-j}, Y_{n-j}^{(s)}\right)$$

$$+ h^{k+2} \bar{\gamma}_{k+1} \overline{\Psi}\left(T_n + [-kh, 0], Y_n^{(l)} + [-kh, 0] F\left(\Delta_t, \Delta_y\right)\right), \tag{19}$$

$$\text{for } l = 0, 1, \ldots, s-1,$$

$$E: \quad \text{if } n < m, \text{ then } F_n^{(s)} = F\left(T_n, Y_n^{(s)}\right), \tag{20}$$

for $n = k, k+1, \ldots, m$.

For the interval methods of Adams-Moulton type given by (6) (or (8)), the interval $P(EC)^s$ predictor-corrector methods of Adams type are of the form

$$P: \quad Y_n^{(0)} = Y_{n-1}^{(s)} + h \sum_{j=1}^{k} \beta_{kj} F\left(T_{n-j}, Y_{n-j}^{(s-1)}\right)$$

$$+ h^{k+1} \gamma_k \Psi\left(T_{n-1} + [-(k-1)h, h], Y_{n-1}^{(s)} + [-(k-1)h, h] F\left(\Delta_t, \Delta_y\right)\right), \tag{21}$$

$$E: \quad F_n^{(l)} = F\left(T_n, Y_n^{(l)}\right), \tag{22}$$

$$C: \quad Y_n^{(l+1)} = Y_{n-1}^{(s)} + h \sum_{j=0}^{k} \overline{\gamma}_j F_n^{(l)}$$

$$+ h \sum_{j=1}^{k} \overline{\gamma}_j \sum_{m=1}^{j} (-1)^m \binom{j}{m} F\left(T_{n-m}, Y_{n-m}^{(s-1)}\right) \tag{23}$$

$$+ h^{k+2} \overline{\gamma}_{k+1} \overline{\Psi}\left(T_n + [-kh, 0], Y_n^{(l)} + [-kh, 0] F\left(\Delta_t, \Delta_y\right)\right),$$

$$\text{for } l = 0, 1, \dots, s-1,$$

for $n = k, k+1, \dots, m$.

Similarly, for the interval methods determined by (9) we have

$$P: \quad Y_n^{(0)} = Y_{n-1}^{(s)} + h \sum_{j=1}^{k} \beta_{kj} F\left(T_{n-j}, Y_{n-j}^{(s-1)}\right)$$

$$+ h^{k+1} \gamma_k \Psi\left(T_{n-1} + [-(k-1)h, h], Y_{n-1}^{(s)} + [-(k-1)h, h] F\left(\Delta_t, \Delta_y\right)\right), \tag{24}$$

$$E: \quad F_n^{(l)} = F\left(T_n, Y_n^{(l)}\right), \tag{25}$$

$$C: \quad Y_n^{(l+1)} = Y_{n-1}^{(s)} + h \overline{\beta}_{k0} F_n^{(l)} + h \sum_{j=1}^{k} \overline{\beta}_{kj} F\left(T_{n-j}, Y_{n-j}^{(s-1)}\right)$$

$$+ h^{k+2} \overline{\gamma}_{k+1} \overline{\Psi}\left(T_n + [-kh, 0], Y_n^{(l)} + [-kh, 0] F\left(\Delta_t, \Delta_y\right)\right), \tag{26}$$

$$\text{for } l = 0, 1, \dots, s-1,$$

for $n = k, k+1, \dots, m$.

Let us note that the symbol P denotes a prediction that determines the initial interval solution $Y_n^{(0)}$ by the explicit interval k-step method of Adams-Bashforth type. The symbol C means a correction that performs several iterations using the implicit interval k-step method of Adams-Moulton type, and E – an evaluation that computes $F_n^{(l)} = F\left(T_n, Y_n^{(l)}\right)$ for $l = 0, 1, \dots, s-1$. Furthermore, for the methods of $P(EC)^s E$ type, after computing the last iteration, the additional evaluation of $F_n^{(s)} = F\left(T_n, Y_n^{(s)}\right)$ is required and used in the next step. Hence, these methods require more work than the $P(EC)^s$ ones.

Remark 1

For the above algorithms of interval $P(EC)^s E$ and $P(EC)^s$ predictor-corrector methods of Adams type, given by (13)-(16), (17)-(20) and (21)-(23), (24)-(26) the following issues should be taken into account:

1. Since $Y_{k-1} \subset \Delta_y$, then before applying the method we only have to check that

$$Y_{k-1} + [-(k-1)h, h] F\left(\Delta_t, \Delta_y\right) \subset \Delta_y.$$

2. From the assumption made on the function F the interval solution $Y_n^{(l)}$ obtained at t_n, $n = k, k+1, \ldots, m$, is acceptable if for each $l = 0, 1, \ldots s$ we have

$$Y_n^{(l)} \subset \Delta_y.$$

3. Suppose that the interval solution $Y_n^{(l)}$ for a given l is such that the above condition is satisfied. Then, from the assumption made on the function $\overline{\Psi}$, the computation of $Y_n^{(l+1)}$ is allowed if

$$Y_n^{(l)} + \left[-kh, 0 \right] F\left(\Delta_t, \Delta_y \right) \subset \Delta_y.$$

4. Suppose that $Y_n^{(s)} \subset \Delta_y$. Then, from the assumption made on the function Ψ, the computation of $Y_{n+1}^{(0)}$ is allowed if

$$Y_n^{(s)} + \left[-k(k-1)h, h \right] F\left(\Delta_t, \Delta_y \right) \subset \Delta_y.$$

Note that in each step of the method it is necessary to check that the above conditions hold. If one of them is not satisfied then the computation should be aborted.

Remark 2

Note that from the assumptions made in Sec. 2.2. the iteration processes (13)-(16), (17)-(20) and (21)-(23), (24)-(26) are convergent to Y_n, i.e. $\lim_{s \to \infty} Y_n^{(s)} = Y_n$, where Y_n, $n = k, k+1, \ldots, m$, are obtained from (6) (or (8)) and (9), respectively. Hence, for $s \to \infty$ the predictor-corrector methods considered turn into the interval methods of Adams-Moulton type given by (6) (or (8)) and (9).

3. Conclusions

Comparison of the numerical results (see [3]) obtained with the implicit interval methods of Adams-Moulton type and the interval predictor-corrector methods of Adams type let us formulate the following remarks:

- The widths of the interval solutions obtained by the implicit interval methods of Adams type and both kinds of interval predictor-corrector methods of Adams type are of the same order.

- We recommend applying the interval predictor-corrector methods due to a significant reduction in the number of iterations involved. The number of iterations is usually reduced by half in comparison to the interval methods of Adams-Moulton type. Hence, computation time is saved.

- The implicit interval $P(EC)^s E$ predictor-corrector methods of Adams type yield interval solutions of somewhat smaller widths then the $P(EC)^s$ ones. On the other hand the additional computation of $F_n^{(s)} = F\left(T_n, Y_n \right)$ performed in each step of the method makes them a little bit more laborious than the $P(EC)^s$ ones.

References

1. Gajda K., Jankowska M., Marciniak A., Szyszka B., A Survey of Interval Runge-Kutta and Multistep Methods for Solving the Initial Value Problem, *Lecture Notes in Computer Science* **4967,** (2008) 1361-1371

2. Hammer R., Hocks M., Kulisch U., Ratz D., *Numerical Toolbox for Verified Computing I. Basic Numerical Problems*, Springer-Verlag, Berlin (1993)

3. Jankowska M.A., Interval Multistep Methods of Adams type and their Implementation in the C++ Language, Ph.D. Thesis, Poznan University of Technology, Poznan (2006)

4. Jankowska M.A., Introduction to the C++ Libraries for Floating-Point Conversions and Interval Arithmetic, *Polish Journal of Environmental Studies* Vol. **18**, No. **3B**, (2009) 131-137

5. Jankowska M.A., *C++ Library for Floating-Point Conversions. User and Reference Guide*, Poznan University of Technology, last updated 2009, available in Software at http://www.mjank.user.icpnet.pl/

6. Jankowska M.A., *C++ Library for Floating-Point Interval Arithmetic. User and Reference Guide*, Poznan University of Technology, last updated 2009, available in Software at http://www.mjank.user.icpnet.pl/

7. Jankowska M.A., Marciniak, A., Implicit Interval Multistep Methods for Solving the Initial Value Problem, *Computational Methods in Science and Technology* **8** (**1**), (2002) 17-30

8. Jankowska M.A., Marciniak A., On Explicit Interval Methods of Adams-Bashforth Type, *Computational Methods in Science and Technology* **8** (**2**), (2002) 46-57

9. Jankowska M.A., Marciniak A., On Two Families of Implicit Interval Methods of Adams-Moulton Type, *Computational Methods in Science and Technology* **12** (**2**), (2006) 109-113

10. Marciniak A., *Selected Interval Methods for Solving the Initial Value Problem*, Publishing House of Poznan University of Technology, Poznan (2009)

11. Jaulin L., Kieffer M., Didrit O., Walter É., *Applied Interval Analysis*, Springer-Verlag, London (2001)

12. Moore R.E., *Interval Analysis*, Prentice-Hall, Englewood Clis, NJ (1966)

13. Moore R.E., Kearfott R.B., Cloud M.J., *Introduction to Interval Analysis*, SIAM, Philadelphia (2009)

14. Sunaga T., Theory of interval algebra and its application to numerical analysis, *Research Association of Applied Geometry* (*RAAG*) *Memoirs*, Ggujutsu Bunken Fukuy-kai, Tokyo, Japan, Vol. **2**, (1958) 29-46 (547-564)

Przedziałowe metody wielokrokowe predyktor-korektor typu Adamsa rozwiązywania zagadnienia początkowego dla równań różniczkowych zwyczajnych

W pracy zaproponowane zostały przedziałowe metody wielokrokowe predyktor-korektor typu Adamsa rozwiązywania zagadnienia początkowego dla równań różniczkowych zwyczajnych. Metody te oparte są na jawnych przedziałowych metodach typu Adamsa-Bashfortha oraz niejawnych przedziałowych metodach typu Adamsa-Moultona. Metody przedziałowe należą do klasy algorytmów, które pozwalają otrzymać rozwiązanie danego problemu w postaci przedziału-rozwiązania, który zawiera w sobie rozwiązanie dokładne.

Velocity and acceleration distribution in the relative motion

Janusz JANKOWSKI

Poznan University of Technology, Institute of Applied Mechanics
Piotrowo 3, 60-965 Poznan
janusz.jankowski@put.poznan.pl

Abstract

The kinematical problem of a two rigid body general motion is treated. Introduced in the paper the stiffness condition method for to appoint the relative rigid body motion is based on the absolute rigid body motion formulae. It allows us to derive the velocity and acceleration distributions in the way by analogy to rigid body kinematics. Emphasis is placed on the investigation of the stiffness condition in the general motion. In one place only we have to use the ordinary formulae for the absolute, drift or Coriolis components Examples are given to illustrate the practical applications to the mechanisms.

Keywords: relativity, drift, Coriolis, stiffness

1. Introduction

The principles of conservations i the Newton dynamics suggest that the description of the physical phenomena should be of global nature [1]. But the velocity is locally defined and its relative character means that the every result is of the same importance. Hence, the physical meaning of the velocity may concern to the fraction of the body only (locality) and its derivation is acceptable with respect to other bodies only (relativity). The conception of local-relative velocity, which is with respect to chosen reference system defined, was named in mechanics absolute velocity. But the subjectivity of the choice of the reference system question the sense of existence of the conception. Only the appointment of absolute motion in the same reference system for another fraction, named observer, allows to receive the results that are comparable for the both bodies. The difference of this both absolute motions we are called the relative motion.

2. Absolute motion

Let the body model takes the region Ω in 3D Euclidean space. Element $A \in \Omega$ of the region is called the place. Similarly, the interval $(0,\infty)$ of the real numbers in 1D space is called the time, and its element $t \in (0,\infty)$ is called the instant.

The location $\mathbf{r}$ of a place $A \in \Omega$ in the space may be expressed by a position vector $\mathbf{xA}$ in the reference frame with a set of orthogonal axes $O_1 \mathbf{e}_2 \mathbf{e}_3 \mathbf{e}$ named Cartesian coordinate system:

$$\mathbf{r}(A) = \mathbf{xA}(t), \quad t \in (0,\infty) \tag{1}$$

The absolute linear velocity $\mathbf{vb}(A)$ of a place $A \in \Omega$ is the time derivative of the position vector:

$$\mathbf{vb}(A) = \frac{d}{dt}\mathbf{xA}(t), \quad t \in (0, \infty) \tag{2}$$

But the absolute linear velocity does not determined unambiguously the motion of the place $A \in \Omega$ [2]. Following Chasles theorem [3] rotation of a rigid body can be described by a temporary rotation axe where the absolute angular velocity vector $\omega\mathbf{b}(A)$ of the place $A \in \Omega$ is being. Hence, the absolute motion of the rigid body is locally determined be the two vector functions of time:

$$\mathbf{vb}(A) = \mathbf{g}(t), \quad \omega\mathbf{b}(A) = \mathbf{h}(t), \quad t \in (0, \infty) \tag{3}$$

Global properties of absolute motion gives the so called stiffness condition:

$$\mathbf{vb}(B) = \mathbf{vb}(A) + \omega\mathbf{b}(A) \times (\mathbf{r}(B) - \mathbf{r}(A)), \quad \omega\mathbf{b}(B) = \omega\mathbf{b}(A), \quad A, B \in \Omega \tag{4}$$

The formulae (3-4) describe the absolute motion of a rigid body. Note that according to the formula (4) there can be change the place $B \in \Omega$ in the region. It gives a possibility of determining the absolute motion of the rigid body treated as the set of all the places in the region. Remaining in that way results allows to define the fields of the absolute linear velocity and the absolute angular velocity vectors in the region of the considered body. The graphical representation of this fields are called the velocity time-tables in the theory of mechanisms.

The derivatives with respect to time of the velocity vectors are called the absolute linear and angular accelerations of the place $A \in \Omega$:

$$\mathbf{ab}(A) = \dot{\mathbf{g}}(t), \quad \varepsilon\mathbf{b}(A) = \dot{\mathbf{h}}(t), \quad t \in (0, \infty) \tag{5}$$

The absolute acceleration time-tables we can receive if we will differentiate the formula (4) with respect to time:

$$\mathbf{ab}(B) = \mathbf{ab}(A) + \varepsilon\mathbf{b}(A) \times (\mathbf{r}(B) - \mathbf{r}(A)) + \omega\mathbf{b}(A) \times [\omega\mathbf{b}(A) \times (\mathbf{r}(B) - \mathbf{r}(A))]$$
$$\varepsilon\mathbf{b}(B) = \varepsilon\mathbf{b}(A), \quad A, B \in \Omega \tag{6}$$

The double vector product follows from the formula (2).

3. Drift motion

The absolute motion of the observer it is adopt to call the drift motion. Let the model of the observer body occupies in the space the region Θ, which elements $C \in \Theta$ we will call the points. The location $\mathbf{q}$ of a point $C \in \Theta$ in the space may be expressed by a position vector $\mathbf{y}$ in the same reference frame with a set of orthogonal axes $O_1\mathbf{e}_2\mathbf{e}_3\mathbf{e}$:

$$\mathbf{q}(C) = \mathbf{yC}(t), \quad t \in (0, \infty) \tag{7}$$

The drift linear velocity $\mathbf{vu}(C)$ of a point $C \in \Theta$ is the time derivative of the position vector $\mathbf{yC}$. The drift motion of the observer is locally determined by the vector functions of time:

$$\mathbf{vu}(C) = \hat{\mathbf{g}}(t), \quad \omega\mathbf{u}(C) = \hat{\mathbf{h}}(t), \quad t \in (0, \infty) \tag{8}$$

Global properties of the drift motion gives kinematical stiffness condition:

$$\mathbf{vu}(D) = \mathbf{vu}(C) + \omega\mathbf{u}(C) \times (\mathbf{r}(D) - \mathbf{r}(C)), \quad \omega\mathbf{u}(D) = \omega\mathbf{u}(C), \quad C, D \in \Theta \tag{9}$$

The formulae (8-9) describe the drift motion of an observer. The derivatives with respect to time of the velocity vectors (8) are called the drift linear and angular accelerations of the point:

$$\mathbf{au}(C) = \dot{\mathbf{g}}(t), \quad \varepsilon\mathbf{u}(C) = \dot{\mathbf{h}}(t), \quad t \in (0,\infty) \tag{10}$$

Drift linear and angular accelerations we can receive if we will differentiate the formula (9) with respect to time:

$$\mathbf{au}(D) = \mathbf{au}(C) + \varepsilon\mathbf{u}(A)\times(\mathbf{r}(D)-\mathbf{r}(C)) + \omega\mathbf{u}(C)\times[\omega\mathbf{u}(C)\times(\mathbf{r}(D)-\mathbf{r}(C))]$$
$$\varepsilon\mathbf{u}(D) = \varepsilon\mathbf{u}(C), \quad C, D \in \Theta \tag{11}$$

The formula (9) can be of use as the definition of a new set of points in the space. The points of this set have some kinematical properties like the points belonging to the observer. The set we marked $\hat{\Omega}$ and called the kinematical region. Hence, the point $E \in \hat{\Omega}$ is deriving by the formula:

$$\mathbf{vu}(E) = \mathbf{vu}(C) + \omega\mathbf{u}(C)\times(\mathbf{r}(E)-\mathbf{r}(C)), \quad \omega\mathbf{u}(E) = \omega\mathbf{u}(C), \quad C \in \Theta, E \in \hat{\Omega} \tag{12}$$

Note that the point $E \in \hat{\Omega}$ is unlimited in the space. Hence we can accept that its position vector is covered with the position vector of a place in the region:

$$\mathbf{xE}(t) = \mathbf{yE}(t), \quad t \in (0,\infty) \tag{13}$$

Hence in every place of the region occupied by the considered body in the space we can define both absolute and drift velocity vectors.

The global properties of the drift motion are valid in the original version in the kinematical region. It allows to write the kinematical drift stiffness condition:

$$\mathbf{vu}(F) = \mathbf{vu}(E) + \omega\mathbf{u}(E)\times(\mathbf{r}(F)-\mathbf{r}(E)), \quad \omega\mathbf{u}(F) = \omega\mathbf{u}(E), \quad E, F \in \hat{\Omega} \tag{14}$$

Note that the formula (14) allows to replace the choice of a point $F \in \hat{\Omega}$ in the kinematical region. It gives a possibility to derive the drift motion for a whole the kinematical region as the set of all the points $F \in \hat{\Omega}$. The results that are receiving in that way allows to determine the drift linear and angular velocity time-tables in the region occupies in the space by the considered body.

The drift acceleration time-tables we can receive if we will differentiate the formula (14) with respect to time:

$$\mathbf{au}(F) = \mathbf{au}(E) + \varepsilon\mathbf{u}(E)\times(\mathbf{r}(F)-\mathbf{r}(E)) + \omega\mathbf{u}(E)\times[\omega\mathbf{u}(E)\times(\mathbf{r}(F)-\mathbf{r}(E))]$$
$$\varepsilon\mathbf{u}(F) = \varepsilon\mathbf{u}(E), \quad E, F \in \Omega \tag{15}$$

Here the drift accelerations are deriving in all the places of the region occupies in the space by the considered body on the base of points in the region of the observer.

4. Relative motion

Relative motion is comprehended in mechanics as the motion of some places occupies in the space by the considered body that is determined with respect to the points of the observer region, which is treated as the motionless reference frame. Relative linear velocity $\mathbf{vw}(A)$ and relative angular velocity $\omega\mathbf{w}(A)$ of the place $B \in \Omega$ in the region

of the body are defined as the corrections to the drift velocities that are necessary to receive some suitable absolute velocities:

$$\mathbf{vb}(A) \equiv \mathbf{vu}(A) + \mathbf{vw}(A), \quad \omega\mathbf{b}(A) \equiv \omega\mathbf{u}(A) + \omega\mathbf{w}(A), \quad A \in \Omega \tag{16}$$

It is worth to notice that the formula is valid locally in the region of the body. Hence, the definition (16) is inconsistent because of the place $B \in \Omega$ is not the point of the observer region Θ, in which the drift velocity is defined. That is why the drift motion seems impossible to derive. But the observer region Θ can be extend to the kinematical region $\hat{\Omega}$, in order to exist the inclusion: $\Omega \subset \hat{\Omega}$. Then the definition (16) contains only the vectors correctly specified. It allows for the symbolical notation:

$$\langle vb, \omega b \rangle(B) = \langle vu, \omega u \rangle(B) + \langle vw, \omega w \rangle(B), \quad A \in \Omega \tag{17}$$

Inserting the stiffness conditions (4) and (14) into formula (17) one can obtain the relative linear and angular velocity distributions:

$$\mathbf{vw}(B) = \mathbf{vw}(A) + \omega\mathbf{w}(A) \times (\mathbf{r}(B) - \mathbf{r}(A)), \quad \omega\mathbf{w}(B) = \omega\mathbf{w}(A), \quad A, B \in \Omega \tag{18}$$

For the accelerations the symbolical notation (17) should be develop:

$$\langle ab, \varepsilon b \rangle(B) = \langle au, \varepsilon u \rangle(B) + \langle aw, \varepsilon w \rangle(B) + \langle ac, \varepsilon c \rangle(B), \quad B \in \Omega \tag{19}$$

because of the Coriolis acceleration presence:

$$\mathbf{ac}(A) = 2\omega\mathbf{u}(A) \times \mathbf{vw}(A), \quad \varepsilon c(A) = \omega\mathbf{u}(A) \times \omega\mathbf{w}(A), \quad A \in \Omega \tag{20}$$

Then the relative linear acceleration $\mathbf{aw}(B)$ and relative angular acceleration $\varepsilon\mathbf{w}(A)$ of the place $B \in \Omega$ are locally defined as the corrections to the drift and Coriolis accelerations that are necessary to receive some suitable absolute accelerations:

$$\mathbf{ab}(A) \equiv \mathbf{au}(A) + \mathbf{ac}(A) + \mathbf{aw}(A), \quad \varepsilon b(A) \equiv \varepsilon u(A) + \varepsilon c(A) + \varepsilon \mathbf{w}(A), \quad A \in \Omega \tag{21}$$

The formula (21) is inserting to the absolute linear acceleration time-table

$$\begin{aligned}
\mathbf{au}(B) + \mathbf{ac}(B) + \mathbf{aw}(B) &= \mathbf{au}(A) + \mathbf{ac}(A) + \mathbf{aw}(A) \\
&+ [\varepsilon u(A) + \varepsilon c(A) + \varepsilon \mathbf{w}(A)] \times (\mathbf{r}(B) - \mathbf{r}(A)) \\
&+ [\omega \mathbf{u}(A) + \omega \mathbf{w}(A)] \times [\{\omega \mathbf{u}(A) + \omega \mathbf{w}(A)\} \times (\mathbf{r}(B) - \mathbf{r}(A))]
\end{aligned} \tag{22}$$

We use the formulae (14-15) for the drift motion:

$$\begin{aligned}
\mathbf{ac}(B) + \mathbf{aw}(B) &= \mathbf{ac}(A) + \mathbf{aw}(A) + [\varepsilon c(A) + \varepsilon \mathbf{w}(A)] \times (\mathbf{r}(B) - \mathbf{r}(A)) \\
&+ [\omega \mathbf{u}(A) + \omega \mathbf{w}(A)] \times [\{\omega \mathbf{u}(A) + \omega \mathbf{w}(A)\} \times (\mathbf{r}(B) - \mathbf{r}(A))] \\
&+ \omega \mathbf{u}(A) \times [\omega \mathbf{u}(A) \times (\mathbf{r}(A) - \mathbf{r}(B))]
\end{aligned} \tag{23}$$

Comparing the formulae for the linear and angular Coriolis accelerations and Equation (18) for the relative linear velocity we observe a simplification:

$$\begin{aligned}
\mathbf{aw}(B) &= \mathbf{aw}(A) + \varepsilon \mathbf{w}(C) \times (\mathbf{r}(B) - \mathbf{r}(A)) \\
&+ \omega \mathbf{w}(A) \times [\omega \mathbf{w}(A) \times (\mathbf{r}(B) - \mathbf{r}(A))], \quad A, B \in \Omega
\end{aligned} \tag{24}$$

Similarly for the relative angular acceleration time-table in the region:

$$\varepsilon \mathbf{w}(B) = \varepsilon \mathbf{w}(A), \quad A, B \in \Omega \tag{25}$$

Changing the place B in the formulae (24-25) we can derive relative linear and angular accelerations without any determination of absolute, drift and Coriolis accelerations.

5. Rigid beam supported to moving cylinder

Let's find velocity and acceleration of the end A of the rod (Rys. 2). Angles depend on time.
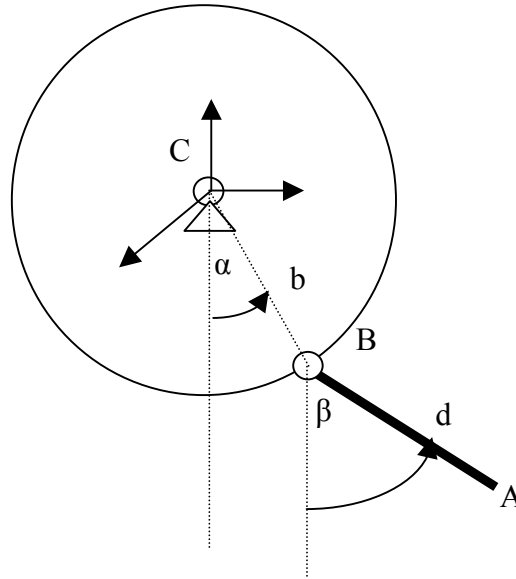
Figure. 1. The rod connecting with the moving drum by the cylindrical pin

We note that the kinematical region have to have a larger radius $b + d$ than the moving drum. Here the relative velocities of the place B are:

$$\mathbf{vw}(B) = \mathbf{0}, \quad \omega\mathbf{w}(B) = (\dot{\beta} - \dot{\alpha}, 0, 0) \tag{26}$$

The stiffness condition (18) for the relative velocities leads to the result:

$$\mathbf{vw}(A) = \omega\mathbf{w}(B) \times \mathbf{d} = d \cdot (\dot{\beta} - \dot{\alpha})(0, \cos\beta, \sin\beta) \tag{27}$$

Similarly, the relative accelerations of the place B have a shape:

$$\mathbf{aw}(B) = \mathbf{0}, \quad \varepsilon\mathbf{w}(B) = (\ddot{\beta} - \ddot{\alpha}, 0, 0) \tag{28}$$

and the formulae (24-25) allow us to determine the relative accelerations of the place A:

$$\mathbf{aw}(A) = \varepsilon\mathbf{w}(B) \times \mathbf{d} + \omega\mathbf{w}(B) \times [\omega\mathbf{w}(B) \times \mathbf{d}] = [(\ddot{\beta} - \ddot{\alpha})\mathbf{e} + (\dot{\beta} - \dot{\alpha})^2\mathbf{f}$$

$$\varepsilon\mathbf{w}(A) = (\ddot{\beta} - \ddot{\alpha}, 0, 0) \tag{29}$$

where $\mathbf{e} = (0, \cos\beta, \sin\beta)$, $\mathbf{f} = (0, -\sin\beta, \cos\beta)$.

6. Concluding remarks

The purpose of this paper is to extend the stiffness condition to be in force for the rigid body to the case of the relative motion. Consequently, the relative motion can easily be

solved for all the places of the rigid body without any absolute, drift or Coriolis components. The applications of the condition to calculate the velocities and accelerations in the relative motion similarly as for absolute motion is suggested. The elaborated model is applied to vibrations of rigid beam supported to moving cylinder.

References

1. D. J. McGill, W. W. King, Engineering *Mechanics: Statics and an Introduction to Dynamics*, PWS Engineering, Boston, 1985
2. J. Jankowski, *The equations of impulse and momentum for the rigid body*, Proc. XXI Symp. Vibrations in Physical Systems, Poznań-Kiekrz, 2004
3. S. Banach, *Mechanika*, PWN, Warszawa, 1956.

Plany prędkości i przyspieszeń w ruchu względnym

Rozważane jest zagadnienie kinematyczne w ruchu ogólnym dwu ciał sztywnych względem siebie. Przedstawiona w pracy metoda warunku sztywności dla wyznaczania ruchów względnych bryły opiera się na wzorach stosowanych w ruchu bezwzględnym. Pozwala to wyznaczać plany prędkości i przyspieszeń w sposób analogiczny jak w kinematyce bryły. Jedynie w jednym miejscu bryły należy zastosować znane wzory dla ruchów bezwzględnych, unoszenia i Coriolisa. Daje to duże możliwości zastosowań w analizie mechanizmów.

Effect of rotating during the pendulum motion

Janusz JANKOWSKI
Poznan University of Technology, Institute of Applied Mechanics
Piotrowo 3, 60-965 Poznan
janusz.jankowski@put.poznan.pl

Piotr KĘDZIA
Poznan University of Technology, Institute of Applied Mechanics
Piotrowo 3, 60-965 Poznan
piotr.m.kedzia@doctorate.put.poznan.pl

Abstract

The main contribution of this paper is to find the friction moments appear during the bar motion. The considerations are based on momentum and moment of momentum principles. The introduced friction is separated into rotating and sliding parts, where the rotating part is divided into rolling and whirling, as well.

Keywords: momentum; moment of momentum; friction; reductions pole

1. Introduction

To express the laws of rigid body dynamics with respect to both possible independence motions: translations and rotations it is necessary to connect the effect of a moment of momentum on the mathematical representation of forces and moments appearing to the motion equations. This is actually the role of an axiom stating that momentum and moment of momentum are quantities on equal terms and, in a consistent theory, the motion equations must concern the same reduction pole for the principles of momentum and moment of momentum. Note that the addition of the reduction pole to these principles leads to correct description of the rigid body motion.

2. Momentum and moment of momentum principles

Let the body model takes the region Ω in 3D Euclidean space Z with the place $A \in \Omega$ as an element. Absolute motion of the body in a frame of reference [2, p. 7] with the Cartesian coordinate system $O_1 e_2 e_3 e$ can be described with two mathematical objects: rotation matrix $\Re$ and position vector $\mathbf{x}$ connecting point O with the place A. Absolute linear velocity $\mathbf{v}(A)$ of the place $A \in \Omega$ is the time derivative of position vector. Following Chasles theorem [3, p. 329] rotation of a rigid body can be described by an absolute angular velocity $\omega(A)$. Finally, the motion can be determined locally:

$$\mathbf{v}(A) = \mathbf{g}(t; \mathbf{x}), \quad \omega(A) = \mathbf{h}(t; \mathbf{x}), \quad t \in (0, \infty) \tag{1}$$

Global properties of motion are described by the stiffness condition:

$$\mathbf{v}(B) = \mathbf{v}(A) + \omega(A) \times (\mathbf{AB}), \quad \omega(B) = \omega(A), \quad A, B \in \Omega \tag{2}$$

Inertial properties are based on the momentum-velocity relationship [4, p. 207]:

$$\mathbf{p}(t;\mathbf{0}) = \int_\Omega \rho(\mathbf{x})\mathbf{g}(t;\mathbf{x})d\mathbf{x}, \quad t \in (0,\infty) \tag{3}$$

$$\mathbf{k}(t;\mathbf{0}) = \int_\Omega \rho(\mathbf{x})\mathbf{x} \times \mathbf{g}(t;\mathbf{x})d\mathbf{x}, \quad t \in (0,\infty) \tag{4}$$

where: $\mathbf{p}$ momentum, $\mathbf{k}$ moment of momentum, ρ mass density. Dynamics can be characterized globally by the influence of all of the forces and the moments acting in an active and passive way. The definition of equipollent force systems correctly suggests that we may replace any system, by a total force $\mathbf{W}$ and a total moment $\mathbf{M}$ at any place O named the reductions pole. The force-couple pair, $\mathbf{W}$ and $\mathbf{M}$ is called a resultant of the load. The influence of all the passive and active loads on the movement is characterized by a momentum and a moment of momentum changes:

$$\dot{\mathbf{p}}(t;O) = \mathbf{W}(t;O), \qquad t \in (0,\infty)$$
$$\mathbf{p}(0;O) = \widetilde{\mathbf{p}} \tag{5}$$

$$\dot{\mathbf{k}}(t;O) = \mathbf{M}(t;O), \qquad t \in (0,\infty)$$
$$\mathbf{k}(0;O) = \widetilde{\mathbf{k}} \tag{6}$$

Here $\widetilde{\mathbf{p}}$ an initial momentum, $\widetilde{\mathbf{k}}$ an initial moment of momentum and the dot means the time derivative. The motion is specified here in the place O Ordinary differential equations, with unknown vector functions, appear as a side effect. A primary aim of the rigid body dynamics is to find the solutions for the initial value problems (5,6).

The set of points in the space Z connected with the region Ω by the stiffness condition will be denoted by $\hat{\Omega}$ and called kinematical domain.

To avoid the procedure of solving integral equations (3,4) we can use the relation (2).

Thus, we can rewrite momentum-velocity relationship in the reduction pole $C \in \hat{\Omega}$:

$$\mathbf{p}(t;C) = m\mathbf{g}(t;\widetilde{\mathbf{x}}) + \mathbf{h}(t;\widetilde{\mathbf{x}}) \times \mathbf{S}(C), \quad t \in (0,\infty) \tag{7}$$

$$\mathbf{k}(t;C) = \mathbf{S}(C) \times \mathbf{g}(t;\widetilde{\mathbf{x}}) + \Im(C) \circ \mathbf{h}(t;\widetilde{\mathbf{x}}), \quad t \in (0,\infty) \tag{8}$$

where $\widetilde{\mathbf{x}}$ is the position vector at $C \in \hat{\Omega}$. We have introduced the following denotations:

$$m = \int_\Omega \rho(\mathbf{x}) \cdot d\mathbf{x} \tag{9}$$

$$\mathbf{S}(C) = \int_\Omega \rho(\mathbf{x})(\mathbf{x} - \widetilde{\mathbf{x}})d\mathbf{x} \tag{10}$$

$$\Im(C) \circ \mathbf{h} = \int_\Omega \rho(\mathbf{x})(\mathbf{x} - \widetilde{\mathbf{x}}) \times [\mathbf{h} \times (\mathbf{x} - \widetilde{\mathbf{x}})]d\mathbf{x} \tag{11}$$

The formulae (9,10,11) define a mass m, a static moment $\mathbf{S}(C)$, and a moment of inertia $\Im(C)$ according to the reduction pole $C \in \hat{\Omega}$. It allows us to rewrite the initial value problems (5,6) into the coupled system of ordinary differential equations:

$$m \cdot \frac{d}{dt}\mathbf{g}(t;\widetilde{\mathbf{x}}) + \frac{d}{dt}[\mathbf{h}(t;\widetilde{\mathbf{x}}) \times \mathbf{S}(C)] = \mathbf{W}(t;C), \qquad t \in (0,\infty) \tag{12}$$

$$m\mathbf{g}(0;\widetilde{\mathbf{x}}) + \mathbf{h}(0;\widetilde{\mathbf{x}}) \times \mathbf{S}(C) = \widetilde{\mathbf{p}}$$

$$\frac{d}{dt}[\mathbf{S}(C) \times \mathbf{g}(t;\widetilde{\mathbf{x}}) + \Im(C) \circ \mathbf{h}(t;\widetilde{\mathbf{x}})] = \mathbf{M}(t;C), \qquad t \in (0,\infty) \tag{13}$$

$$\mathbf{S}(C) \times \mathbf{g}(0;\widetilde{\mathbf{x}}) + \Im(C) \circ \mathbf{h}(0;\widetilde{\mathbf{x}}) = \widetilde{\mathbf{k}}$$

We now fix the axes of the frame to body region so that the inertia properties become constant. It permits us to calculate the derivative of a vector by adding the cross product:

$$\widetilde{m}\mathbf{g}'(t;\hat{\mathbf{x}}) + \mathbf{h}'(t;\hat{\mathbf{x}}) \times \mathbf{S}(C)$$

$$+ \mathbf{h}(t;\hat{\mathbf{x}}) \times [\widetilde{m}\mathbf{g}(t;\hat{\mathbf{x}}) + \mathbf{h}(t;\hat{\mathbf{x}}) \times \mathbf{S}(C)] = \mathbf{W}(t;C), \qquad t \in (0,\infty) \tag{14}$$

$$\widetilde{m}\mathbf{g}(0;\hat{\mathbf{x}}) + \mathbf{h}(0;\hat{\mathbf{x}}) \times \mathbf{S}(C) = \widetilde{\mathbf{p}}(C)$$

$$\mathbf{S}(C) \times \mathbf{g}'(t;\hat{\mathbf{x}}) + \mathbf{J}(C) \circ \mathbf{h}'(t;\hat{\mathbf{x}})$$

$$+ \mathbf{h}(t;\hat{\mathbf{x}}) \times [\mathbf{S}(C) \times \mathbf{g}(t;\hat{\mathbf{x}}) + \mathbf{J}(C) \circ \mathbf{h}(t;\hat{\mathbf{x}})] = \mathbf{M}(t;C), t \in (0,\infty) \tag{15}$$

$$\mathbf{S}(C) \times \mathbf{g}(0;\hat{\mathbf{x}}) + \mathbf{J}(C) \circ \mathbf{h}(0;\hat{\mathbf{x}}) = \widetilde{\mathbf{k}}(C)$$

It is clear that the initial value problems system is lengthy and complicated. Alternatively, we have to calculate the derivative of both the static moment and moment of inertia with respect to time.

3. Friction

The equations (5,6) relate to all of the external forces acting on the body in an inertial frame of reference. Some of external forces are known before any analysis is carried out; we refer to these as loads. The external forces exerted by attaching or supporting bodies are called reactions. The free-body diagram is a figure where we show, by arrows, all of the external forces and moments of couples that act on the body. It is important to realize that each force appearing on the free-body diagram is in fact the resultant of a distributed force system. The same resultant is also transmitted when the body is in contact with a surface of surroundings, there being friction at the contact surface. We shall examine the Coulomb`s law of dry friction between a pair of surfaces. For a body in contact with surroundings the sliding friction $\mathbf{T}$ is the component of the resultant reaction force $\mathbf{R}$ that lies in the tangent plane of contact. The other (perpendicular) component $\mathbf{N}$, is called the normal force. Similarly, the rolling friction $\mathbf{V}$ is the component of the resultant fixed moment of couple $\mathbf{U}$ that lies in the tangent plane of contact. The other component, perpendicular to this tangent plane, is called the whirling friction $\mathbf{W}$. The

parallelogram law allows us to decompose both the resultant force and the resultant moment of couple into two mutually perpendicular parts:

$$\mathbf{R} = \mathbf{T} + \mathbf{N}, \quad \mathbf{U} = \mathbf{V} + \mathbf{W} \tag{16}$$

The friction will continue to balance the loads for as long as it is able:

$$T \le \mu \cdot N, \quad V \le f \cdot N, \quad W \le \nu \cdot N \tag{17}$$

where the constants μ, f, ν are the coefficients of static friction, which depend upon the types of materials in contact and upon the roughness of their surfaces. When the surfaces slide, or roll, or whirl reciprocally, the reduced values of friction coefficients $_k\mu, _k f, _k \nu$ called the coefficients of kinetic friction fulfil the kinetic Coulomb's law of dry friction:

$$T =_k \mu \cdot N, \quad V =_k f \cdot N, \quad W =_k \nu \cdot N \tag{18}$$

We should remember that usually only one, or two of relative motions may happen.

4. Rolling friction in the socket

The cantilever bar of a length b with a rectangular cross-section $c \times d$ shown in Fig. 1 supports a load $\mathbf{G}$ in the end B. The second end is hitched to the cylindrical socket. The distribution of mass in moving frames of reference is given by the function

$$\rho(x,y,z) = \rho_0 \cdot \sin\left[\pi(x/6 + c/3)/c\right] \tag{19}$$

where ρ_0 is density coefficient. The total mass of the bar reads

$$m = \int_{-d/2}^{d/2} \int_0^b \int_{-c/2}^{c/2} \rho \, dx \, dy \, dz \tag{20}$$
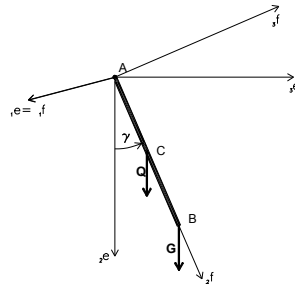
Figure. 1. Moving frame of reference

The force $\mathbf{Q} = m\mathbf{g}$ (g - gravity) acts through $C(_C x, _C y, _k z)$. We are going to find the differential equation governing the bar motion including the rolling friction moment. Firstly, we get the equation of momentum for the bar. We find that the momentum has the following form in moving coordinate system

$$\mathbf{p}(t; A) = m(\dot{\gamma}, 0, 0) \times (_C x, _C y, 0) = m(0, 0, _C y \cdot \dot{\gamma}) \tag{21}$$

According to the formula [1, p. 1165]

$$\dot{\mathbf{p}} = \mathbf{p'} + \omega \times \mathbf{p} \tag{22}$$

and the balance of momentum

$$\dot{\mathbf{p}}(t; A) = \mathbf{W}(t; A), \qquad t \in (0, \infty)$$
$$\mathbf{p}(0; A) = \mathbf{0} \tag{23}$$

we obtain the initial value problem

$$m\left(0, -_C y \cdot \dot{\gamma}^2(t), _C y \cdot \ddot{\gamma}(t)\right) = (Q + G)(0, \cos \gamma(t), \sin \gamma(t)) + \mathbf{S}, \quad t \in (0, \infty)$$
$$\gamma(0) = \frac{\pi}{6}, \quad \dot{\gamma}(0) = 0 \tag{24}$$

where $\mathbf{S}$ is the reaction force of the socket. The angular moment reads

$$\mathbf{k}(t; A) = (I_{11}, I_{21}, I_{31})\dot{\gamma} \tag{25}$$

Similarly, as for momentum, we have

$$\dot{\mathbf{k}} = \mathbf{k'} + \omega \times \mathbf{k} = \left(I_{11} \cdot \ddot{\gamma}, I_{21} \cdot \ddot{\gamma} - I_{31} \cdot \dot{\gamma}^2, I_{31} \cdot \ddot{\gamma} + I_{21} \cdot \dot{\gamma}^2\right) \tag{26}$$

Hence, we obtain the initial value problem

$$\left(I_{11} \cdot \ddot{\gamma}(t), I_{21} \cdot \ddot{\gamma}(t) - I_{31} \cdot \dot{\gamma}^2, I_{31} \cdot \ddot{\gamma}(t) + I_{21} \cdot \dot{\gamma}^2\right)$$
$$= \left(_C y \cdot Q + l \cdot G\right)(-1,0,0) + \mathbf{U}, \quad t \in (0, \infty)$$
$$\gamma(0) = \frac{\pi}{6}, \quad \dot{\gamma}(0) = 0 \tag{27}$$

There $\mathbf{U}$ is the couple of the socket. Let us take the rolling friction moment as

$$U_1 = f \cdot S_2 \cdot \text{sgn}(\dot{\gamma}) \tag{28}$$

Finally we have

$$I_{11} \cdot \ddot{\gamma}(t) = -\left(_C y \cdot Q + l \cdot G\right)(-1,0,0) + f \cdot S_2 \cdot \text{sgn}(\dot{\gamma}(t)), \quad t \in (0, \infty)$$
$$\gamma(0) = \frac{\pi}{6}, \quad \dot{\gamma}(0) = 0 \tag{29}$$

The initial value problem is not linear so we propose the following solving algorithm:

1) Set he first approximation for U_1 with

$$\text{sgn}(\dot{\gamma}(t)) = 0 \tag{30}$$

2) Solve (28) to interpolate U_1 from (27).

3) If the difference between U_1 in two successive iterations is smaller than a given value, then algorithm is finished. In other case go to *Step* 2.

the couple of the socket is derived from (26). Rolling friction is presented in Fig. 2.
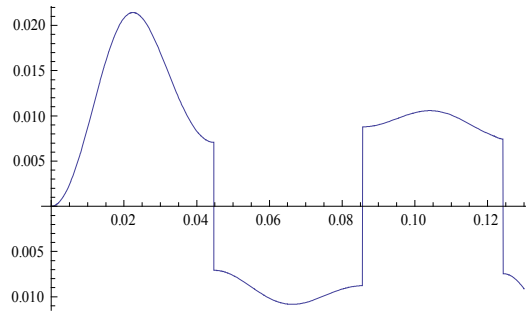
Figure. 2. The rolling friction moment acting in the socket

5. Concluding remarks

The main contribution of this study is to characterize the dynamical behaviour of the rigid body on a base of momentum- moment of momentum balance principles. These principles depend on the reduction pole. In the paper the kinematical domain was introduced. When the reduction pole is bounded with the kinematical domain of the rigid body, then it is easy to rewrite the principles into a coupled system of ordinary differential equations with coupled initial conditions. The mass moments are the coefficients in these equations and they are multiplied by the velocities (linear and angular). The introduced friction was separated into sliding and rotating parts. Additionally, the rotating friction was divided into rolling and whirling parts, as well. There are two different kinds of friction laws in both static and kinematic cases. The final part of this paper is an application of all above mathematical models to the motion of the bar hitched into a cylindrical socket.

References

1. Beer F.P., Johnston E.R. Jr., Chansen W.E., *Vector Mechanics for Engineers. Dynamics*, McGrow Hill, New York, 2007.
2. McGill D.J., King W.W., *Dynamics*, PWS Boston, 1984.
3. Banach S., *Mechanika*, PWN Warszawa, 1956.
4. Kittel C., Knight W.D., Ruderman M.A., *Mechanika*, PWN Warszawa, 1973.

Wpływ obrotu na ruch wahadła

W pracy wyznaczany jest moment tarcia podczas ruchu belki. Rozważania są oparte na zasadach pędu i krętu. Rozważane tarcie jest rozłożone na część obrotową i część postępową, przy czy w tarciu obrotowym wydzielono składniki wirowe i toczne.

Non-asymptotic modelling in elastodynamics
of periodically ribbed plate

Katarzyna JELENIEWICZ
Warsaw University of Life Sciences – SGGW
ul. Nowoursynowska 159, 02-776 Warszawa
k.jeleniewicz@tlen.pl

Wiesław NAGÓRKO
Warsaw University of Life Sciences – SGGW
ul. Nowoursynowska 159, 02-776 Warszawa
wieslaw_nagorko@sggw.pl

Abstract

In the paper we consider plates reinforced by ribs. Assuming a periodic distribution of the ribs in the plate, an averaged model is being constructed. The method used here is not asymptotic. In the modelling equations a microstructure parameter remains (basic cell size). To test out the model, a case of free vibrations is being analyzed.

Keywords: ribbed plate, elastodynamics of plates, methods of homogenization, vibrations of plates.

1. Introductory concepts

The object of considerations are rectangular elastic plates reinforced by periodically spaced ribs, (Fig. 1). A configuration of the plate will be a region $\Omega = (-L_1, L_1) \times \times (-L_2, L_2) \times (-L_3, L_3)$, $(x_1, x_2, x_3) \in \Omega$. If $L_1 \to \infty$ we will deal with a plate-band. By I we denote a known time interval, $t \in \langle t_0, t_1 \rangle \equiv I$.

The plate will be reinforced by the ribs of thickness l' and l'', spaced alternately and parallel to x_2-axis. A distances between the ribs are equal.

Let $2l$ be a length of a basic cell which we denote by $\Delta = (-l, l)$. In this case the distances between the ribs are equal $l - \dfrac{l' - l''}{2}$. It will be assumed that $l' + l'' << 2l$ and $2l << L_1$.

We denote by $w_k = w_k(x_1, x_2, x_3, t)$, $k = 1,2,3$, $(x_1, x_2, x_3) \in \Omega$, $t \in I$, components of the displacement vector field.

Let $\rho(x_1)$, $C_{klmn}(x_1)$, $x_1 \in (-L_1, L_1)$ be a mass density and the components of the plate elastic tensor, respectively. These quantities do not depend on remaining spatial variables.

The elastodynamic equations of the described plate, treated as three-dimensional body, has the form:

$$\rho(x_1)\ddot{w}_k(x_1,x_2,x_3,t) - \left[C_{klmn}(x_1)w_{m,n}(x_1,x_2,x_3,t)\right]_l = 0 \qquad (1)$$

where $k,l,m,n = 1,2,3$ and for an arbitrary function f we denote $\ddot{f} = \dfrac{\partial^2 f}{\partial t^2}$, $f_{,k} = \dfrac{\partial f}{\partial x_k}$.

In this work a summation convention holds.
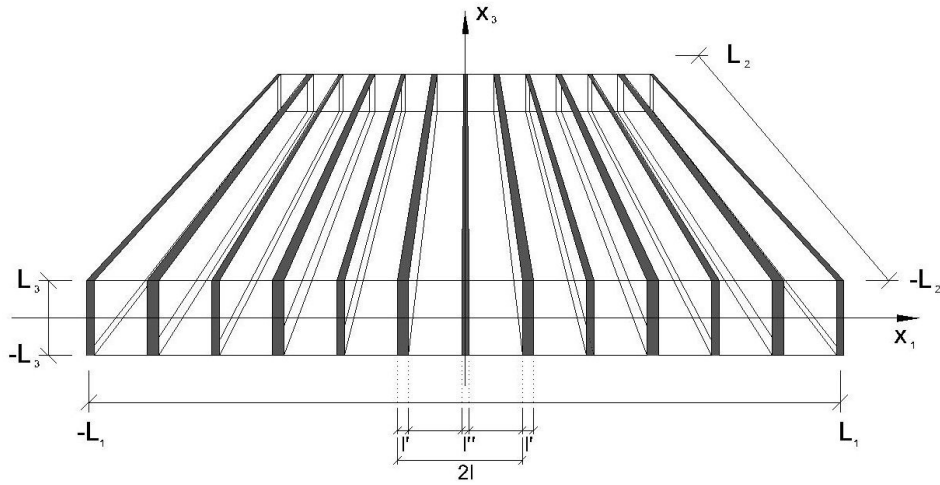
Figure 1.

The functions $\rho(\cdot)$, $C_{klmn}(\cdot)$ occurring in the equation (1) are $2l$-periodic functions, discontinuous on junction surface between the plate and the ribs. Moreover ρ^m, ρ', ρ'' and C^m, C', C'' have to be jump values of $\rho(\cdot)$, $C_{klmn}(\cdot)$ for the plate and the ribs, respectively.

If we define a functional L as

$$L = -\frac{1}{2}(\rho\ddot{w}_k\ddot{w}_k + C_{klmn}w_{k,l}w_{m,n}) \qquad (2)$$

we can rewrite the equation (1) in the form

$$\left(\frac{\partial L}{\partial w_{k,l}}\right)_{,l} - \frac{\partial L}{\partial \ddot{w}_k} - \frac{\partial L}{\partial w_k} = 0 \qquad (3)$$

Coefficients occurring in equations (1), (3) are functions. Our aim is to average them. A method which we will use here is the tolerance averaging technique, [1-3].

2. Modeling procedure

We assume the decomposition of displacement fields in a form:

$$w_k(x_1, x_2, x_3, t) = u_k(x_1, x_2, x_3, t) + h(x_1)v_k(x_1, x_2, x_3, t) \tag{4}$$

where u_k and v_k, are slowly-varying functions and the functions h are known fluctuation shape function.

According to the tolerance averaging technique, to obtain an equations for the functions u_k and v_k, at first we must substitute the displacement fields (4) to the functional (2). Then, averaging this functional, we obtain:

$$<L> = -\frac{1}{2}\left[<\rho>\ddot{u}_k\ddot{u}_k + <\rho h^2>\ddot{v}_k\ddot{v}_k + <C_{klmn}>u_{k,l}u_{m,n} + 2<C_{klmn}h'>u_{k,l}v_m\delta_{1n} + \right.$$
$$\left. + <C_{klmn}h^2>v_{k,l}v_{m,n} + <C_{klmn}(h')^2>v_kv_m\delta_{1n}\delta_{1l}\right] \tag{5}$$

where $h' = \partial h/\partial x_1$ and the averaging operator is defined as:

$$<f> \equiv \frac{1}{2l}\int_{-l}^{l} f(x_1)dx_1 .$$

Equations for the functions u_k and v_k have the form:

$$\left(\frac{\partial <L>}{\partial u_{k,l}}\right)_{,l} - \frac{\partial <L>}{\partial \ddot{u}_k} - \frac{\partial <L>}{\partial u_k} = 0$$
$$\left(\frac{\partial <L>}{\partial v_{k,\bar{a}}}\right)_{,\bar{a}} - \frac{\partial <L>}{\partial \ddot{v}_k} - \frac{\partial <L>}{\partial v_k} = 0 \tag{6}$$

where $\bar{\alpha} = 2,3$.

Substituting the functional (5) into equations (6), we obtain

$$<\rho>\ddot{u}_k - <C_{klmn}>u_{m,nl} + <C_{klm1}h'>v_{m,l} = 0 ,$$
$$<\rho h^2>\ddot{v}_k - <C_{k\bar{a}m\bar{a}}h^2>v_{m,\bar{a}\bar{a}} + <C_{k1mn}h'>u_{m,n} + <C_{k1m1}(h')^2>v_m = 0 \tag{7}$$

If the plate and the ribs are isotropic, we have:

$$C_{klmn} = \lambda\delta_{kl}\delta_{mn} + \mu(\delta_{km}\delta_{ln} + \delta_{kn}\delta_{lm})$$

where $\lambda(x_1)$, $\mu(x_1)$ are the functions.

In this case the equations (7) have the form:

$$<\rho>\ddot{u}_1 - <\lambda + \mu>u_{k,1k} - <\mu>u_{1,kk} + <(\lambda+\mu)h'>v_{1,1} + <\mu h'>v_{k,k} = 0$$

$$<\rho>\ddot{u}_{\bar{\alpha}} - <\lambda+\mu>u_{m,m\bar{\alpha}} - <\mu>u_{\bar{\alpha},mm} - <\lambda h'>v_{1,\bar{\alpha}} + <\mu h'>v_{\bar{\alpha},1} = 0$$

$$<\rho h^2>\ddot{v}_1 - <(\lambda+\mu)h^2>v_{\bar{\alpha},\bar{\alpha}1} - <\mu h^2>v_{1,\bar{\alpha}\bar{\alpha}} + <(\lambda+\mu)h'>u_{1,1} +$$
$$+ <\mu h'>u_{k,k} + <(\lambda+2\mu)(h')^2>v_1 = 0$$

$$<\rho h^2>\ddot{v}_{\bar{\alpha}} - <(\lambda+\mu)h^2>_{\bar{\beta},\bar{\beta}\bar{\alpha}} - <\mu h^2>u_{\bar{\alpha},\bar{\beta}\bar{\beta}} + <\mu h'>u_{1,\bar{\alpha}} +$$
$$+ <\mu h'>u_{\bar{\alpha},1} + <\mu(h')^2>v_{\bar{\alpha}} = 0 \qquad (8)$$

where $\bar{\alpha}, \bar{\beta} = 2,3$.

4. Example

The set of equations (7) or (8) for the unknown functions u_k and v_k will be useful only when we determine the fluctuation shape functions h. We postulate $2l$ – periodic, fluctuation shape function $h(x_1)$ in the form given in Fig. 2, where a is an arbitrary constant.
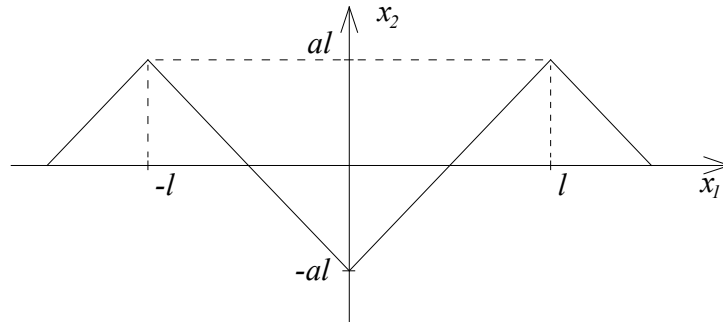
Fig. 2.

Hence all the external loads are applied only in Ox_1, x_2 - plane. The plate material is homogeneous and isotropic with Lamé module λ, μ and mass density ρ^m. Under the plane stress assumption instead of modulus λ we introduce with the reduced modulus $\lambda_0 \equiv \lambda\dfrac{2\mu}{1+2\mu}$. The ribs are assumed to be slender in Ox_1, x_2 - plane and carried out only axial stress. Hence their properties are determined by Young modulus E and mass density $\rho' = \rho'' = m$.

Denoting a Dirac function of argument $x_1 \in R$ by $\delta(\cdot)$, the functional (2) in the isotropic case take the form:

$$L = \frac{1}{2}\rho \ddot{w}_\alpha \ddot{w}_\alpha + \frac{1}{2} M\delta(x_1 + nl)\ddot{w}_\alpha(nl, x_2, t)\ddot{w}_\alpha(nl, x_2, t) - \frac{1}{2}\big[\lambda_0 \delta_{\alpha\beta}\delta_{\gamma\delta} + \mu(\delta_{\alpha\gamma}\delta_{\beta\delta} +$$

$$+ \delta_{\alpha\delta}\delta_{\beta\gamma})\big]w_{\alpha,\beta}\, w_{\gamma,\delta} - \frac{1}{2}E\delta(x_1 + nl)w_{2,2}(nl, x_2, t) \tag{9}$$

It will be shown that the analysis of the problem being under consideration can be carried out under some additional assumptions

$$u_1 = u_1(x_1, t),\ v_1 = v_1(x_1, t),\ x_1 \in [-L_1, L_1],$$
$$u_2 = u_2(x_2, t),\ v_2 = v_2(x_2, t),\ x_2 \in [-L_2, L_2] \tag{10}$$

The dynamic equations of the plates after averaging the functional (9) will be as follows:

$$\overline{m}\ddot{u}_1 - (\lambda_0 + 2\mu)u_{1,11} = 0,$$
$$ml^2\ddot{v}_1 - 4(\lambda_0 + 2\mu)v_1 = 0 \tag{11}$$

and two independent equations for $u_2(x_2, t)$, $v_2(x_2, t)$, $x_2 \in [-L_2, L_2]$

$$\overline{m}\ddot{u}_2 - (\lambda_0 + 2\mu + E)u_{2,22} = 0,$$
$$ml^2\ddot{v}_2 - \frac{l^2}{3}(\lambda_0 + 2\mu + E)v_{2,22} + 4\mu v_2 = 0 \tag{12}$$

where $\overline{m} = \rho^m + m$.

Now let us pass to analysis of the equation $(12)_2$. This equation can be rewrite in the form

$$\ddot{v}_2 - \frac{\lambda_0 + 2\mu + E}{3m}v_{2,22} + \frac{4\mu}{ml^2}v_2 = 0$$

Setting $v_2(x_2, t) = \psi(x_2)\xi(t)$ (where $\xi(t) = \cos\omega t$) we obtain

$$\frac{\lambda + 2\mu + E}{3m}\psi'' - \Big(\frac{4\mu}{ml^2} - \omega^2\Big)\psi = 0$$

We shall consider the following special cases.

If $\dfrac{4\mu}{ml^2} > \omega^2$, than $\psi'' - \kappa^2\psi = 0$, where $\kappa^2 = \dfrac{3m}{\lambda + 2\mu + E}\Big(\dfrac{4\mu}{ml^2} - \omega^2\Big)$. Hence $\psi = Ae^{-\kappa x_2}$.

If $\dfrac{4\mu}{ml^2} < \omega^2$, than denoting $\kappa^2 = \dfrac{3m}{\lambda + 2\mu + E}\Big(\omega^2 - \dfrac{4\mu}{ml^2}\Big)$ we obtain

$$\psi'' + \kappa^2 \psi = 0$$

It follows that $\psi = A_1 \cos \kappa x_2 + A_2 \sin \kappa x_2$ and

$$\psi(-L_2) = \psi(L_2) = 0$$
$$v_2(-L_2) = v_2(L_2) = 0 .$$

Since $\partial_2 w_1 + \partial_1 w_2 = \partial_1 h v_2$, we get $\psi(\pm L_2) = 0$. Taking solution of $\psi'' + \kappa^2 \psi = 0$

in form $\psi = A \cos \kappa x_2$, where $\kappa L_3 = \dfrac{\pi}{2} + n\pi$, we obtain $v_2(x_2, t) = A_n \cos \kappa_n x_2 \cos \omega t$,

where $\kappa_n = \dfrac{\pi}{2L_3} + \dfrac{n\pi}{L_3}$.

5. Conclusions

The above considerations have shown that the tolerance averaging approach constitutes an appropriate analytical tool for analyzing the dynamic problems of elastic plates reinforced by periodically spaced ribs.

The numerical analysis and selected applications of the approach proposed in this paper will be presented in the Conference.

References

1. Woźniak Cz. Wierzbicki E. (2000), *Averaging techniques in thermomechanics of composite solids. Tolerance averaging versus homogenization*, Wydawnictwo Politechniki Częstochowskiej, Częstochowa
2. *Thermomechanics of microheterogeneous solids and structures, Tolerance averaging approach*, ed. Cz. Woźniak, B. Michalak, J. Jędrysiak, Wyd. Politechniki Łódzkiej, Łódź 2008,
3. Nagórko W., Woźniak Cz. (2002), *Nonasymptotic modelling of thin plates reinforced by a system of stiffeners*, EJPAU, 5(2), #1, 2002, www.ejpau.media.pl.

Modelowanie nieasymptoytyczne płyt wzmocnionych periodycznym układem żeber

W pracy rozważa się płyty wzmocnione żebrami. Zakładając periodyczne rozmieszczenie żeber w płycie, konstruuje się model uśredniony. Metoda jaką tu zastosowano nie jest metodą asymptotyczną. W równaniach modelujących pozostaje parametr mikrostruktury (wymiar komórki periodyczności). W celu przetestowania modelu analizuje się przypadek drgań własnych.

A new method for process description of constructional materials structural degradation

Henryk KAŹMIERCZAK
Industrial Institute of Agricultural Engineering, Poland
kazmhenr@pimr.poznan.pl

Tadeusz PAWŁOWSKI
Industrial Institute of Agricultural Engineering, Poland
tadek@pimr.poznan.pl

Jacek KROMULSKI
Industrial Institute of Agricultural Engineering, Poland
kromulsk@pimr.poznan.pl

Abstract

This article presents results analysis of the structural degradation of technical materials samples. The results have been determined by the analysis of the distribution under dynamic load (a discrete model of structure dynamic load). The aim of this research is to describe the process of structural degradation of the basic technical materials. The structural changes of the constructional material samples subjected to impulsive loads have been measured. Information about the technical condition of the individual material samples have been obtained on the basis of the energy characteristics of power spectral density under degrading dynamic load. The results were presented in the form of power amplitude estimation of the dynamic stiffness forces and damping forces, changing with the ongoing samples degradation process.

Research conducted at the work station by the method of impulsive test helped to determine the initial load causing the damage in the material structure. Further analysis of the material structural changes allowed determining the limits of load, which will initiate the process of structural degradation (in. ex. cracking).

Keywords: Energetic characteristic, degradation, impulsive test, dynamic stiffness forces.

1. Introduction

This paper presents the concept of testing structural material fatigue by the method of determining spectral characteristics describing structural changes in mechanical objects. Structural changes of a mechanical object are determined by synergy of various processes (e.g. load types and amplitudes, spatial and time characteristics of such loads, corrosion and aging processes, mechanics of materials and other properties). Characteristics of structural parameter changes in materials have been determined by the powers of damping forces (internal friction) and the powers of inertial forces and dynamic stiffness forces as well as the work of forces causing degradation of material samples.

The effects of structural degradation processes taking place in an object include changes in macroscopic mechanical properties of the material caused by changes in material structure and microcracks inside the material, as well as by alteration of its structure (material ageing).

Very dangerous phenomena in the operation of machines and buildings include crack propagation within the constructional material, which usually leads to a total, catastrophic loss of structure functionality and the triggering of further degradation processes.

Cracks are accompanied by increased damping of vibration as well as changes in their spectrum composition. Cracking problem escalates together with the application of structures that are exposed to higher load and constructional materials of higher strength; their plasticity is naturally lower and so is their resistance against cracking.

In the function of time, the condition of a machine undergoes the process of evolutional degradation due to excessive load on and fatigue of constructional components, wear resulting from friction (play) etc.

2. Energy characteristics of structural degradation of a mechanical object

Assessment of constructional material efforts which amounts to analysis of their degradation process is based on the energy processor model. The concept of energy processor is the basis for identification of the degradation trend and assessment of residual durability. The method of analyzing the characteristics of constructional material efforts by hybrid, energetic method of analyzing spectral characteristics of degradation processes, as presented in this study, makes it possible to determine spectral components of structural degradation of materials. It allows for the assessment of impact of individual power spectral components of degradation forces on material life characteristics. These characteristics will facilitate the choice of materials used in building machine components exposed to intensive (including impulsing) dynamic loads. The total sum of density of dissipation energy and density of elastic strain energy causing the initiation and growth of fatigue crack has been adopted as a parameter of material destruction [16].

The work of mechanical object structural degradation forces is the sum of damping forces work (energy dissipation) and the work of forces changing dynamic rigidity of the object:

$$\int_{\Theta_0}^{\Theta_r} \mathbf{Re}\, GN_{ik}(\Theta)\mathrm{d}\Theta + \left|\int_{\Theta_0}^{\Theta_r}[\mathbf{Im}\, GN_{ik}(\Theta_0) - \mathbf{Im}\, GN_{ik}(\Theta_r)]\mathrm{d}\Theta\right| < L_{gr} \tag{1}$$

This formula permits the estimation of boundary values of the work of technical structural degradation forces in mechanical objects.
In the research of degradation process and in the assessment of technical condition of objects the method of analysis of dynamic load power distribution was used [6]. The method takes into account spatial power change in individual subsystems and the flow of energy between the subsystems. The main idea of this method is the fact that the object load condition can be represented by accumulated, dissipated and transferred energy.

The holistic model of machine load condition is described by the matrix of power spectral density of the dynamic load power in a mechanical system [6]:

$$\left\{ G_{N_{ik}} \left(j\omega, \Theta \right) \right\} = \boldsymbol{H}_{V_{ik}} \left(j\omega, \Theta \right) \cdot \boldsymbol{G}_{F_k F_k} \left(j\omega, \Theta \right) \tag{2}$$

where: $\boldsymbol{H}_{V_{ik}} \left(j\omega, \Theta \right)$ – mobility matrix of machine,

$\boldsymbol{G}_{F_k F_k} \left(j\omega, \Theta \right)$ – spectral density matrix of excitation forces.

The elements of the matrix of dynamic characteristics [6]:

$$\boldsymbol{H}_{ik} \left(j\omega, \boldsymbol{D}(r, \Theta) \right) = \left\{ \begin{matrix} H_{11}\left[j\omega, D_{11}(\Theta) \right] & \dots & H_{1n}\left[j\omega, D_{1n}(\Theta) \right] \\ H_{n1}\left[j\omega, D_{n1}(\Theta) \right] & \dots & H_{nn}\left[j\omega, D_{nn}(\Theta) \right] \end{matrix} \right\} \tag{3}$$

are the functions of spatial degradation measure D of the mechanical system.

3. Energetic modes in description of structural degradation of mechanical objects

Changes in the dynamic condition of a mechanical object, described by energetic characteristics of vibration loads on nodes of a machine, are an important indicator of differences or changes occurring in its structure.

Research into imaginary parts and real parts of the testing force powers in the frequency function, permit determination of changes (maxima) in these functions.
The shift of characteristics maxima and the occurrence of minima (anti-resonance) in energetic characteristics of dynamic rigidity constitutes key information about preliminary tentions applied to the object or information on degradation state of a mechanical object which manifests itself in dynamic rigidity changes. A growth in component frequency of testing signal power amplitude along the change in preliminary tension marks a change in the structural model of an object. Energetic modes analysis makes it possible to determine differences or changes in internal tensions in a mechanical object.

4. Structural degradation of constructional materials

Information about the technical condition and changes in structural properties of an object are obtained on the basis of energetic characteristics of power spectral densities of test dynamic loads. They are presented as the estimates of changes in dynamic stiffness and inertia forces, which change along the progressive process of object degradation. The method allows for establishing the values of changes in stiffness and inertia as a result of structural degradation. Analyses run by means of the impulse test method make it possible to determine the loads which initiate the process of structural damage of a construction.

Below are energetic characteristics of impulse loads causing structural degradation of a standard-dimension sample of constructional material. The key element of the test station was electric impact hammer (Fig. 1).
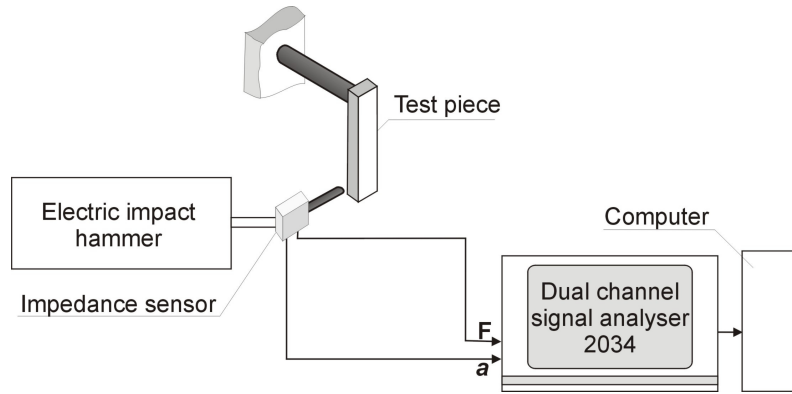
Fig. 1. The scheme of test stand to analyze dynamic degradation of constructional material samples

Torsional moment of force was applied to samples of various constructional materials (e.g. steel, cast iron) of standard measurements. The state of degradation of the presented sample manifested itself with a torsional deflexion of 9.5 degrees and changes in the frequency of energetic modes of degradation loads. Reduction of vibration frequency of the sample occured due to the reduction of its dynamic rigidity and as a result of changes in internally dissipated energy. High loads maxima characterised the process of sample cracking and breaking. The shift of characteristics extremes (Fig.2) and the occurrence of reduction (or growth) of minima frequency (anti-resonance) in energetic characteristics, serve as a confirmation of the degradation state of a mechanical object. Cracked samples are shown in Fig. 3. Based on an analysis of changes in energetic mode extremes, relative changes (reduction or growth) in dynamic rigidity of material samples were determined.

Technical degradation process of the sample resulted in either growth of mode frequency (greater rigidity) or a reduction of mode frequency. Relative change in dynamic rigidity of a mechanical object due to its structural degradation:

$$\frac{k_i - k_r}{k_i} \approx 1 - \frac{\omega_{0_r}^2}{\omega_{0_i}^2} \quad \left[\%\right] \tag{4}$$

Based on an analysis of changes in energetic modes, relative changes (reduction or growth) were determined in dynamic rigidity of the samples due to structural changes (Fig.3).
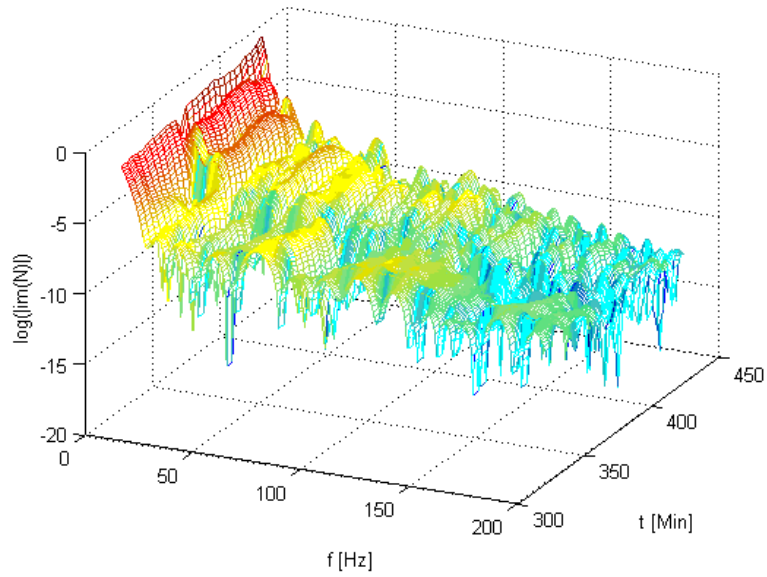
Fig. 2. The real parts of the power spectral density of the impulse loads power.
Real changes in material samples due to degrading dynamic load application
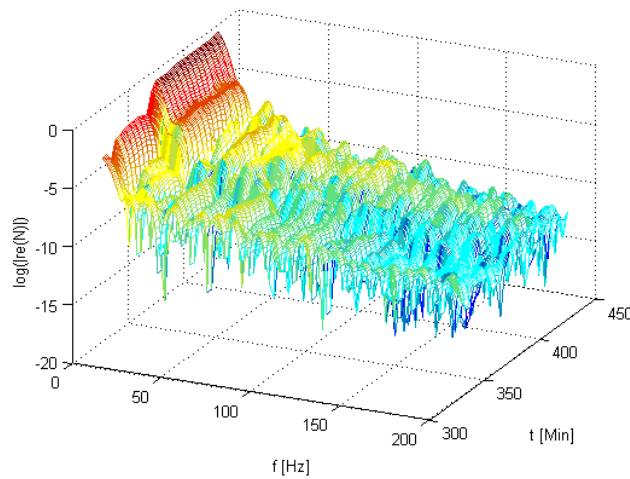
Fig. 3. The imaginary parts of the power spectral density of the impulse loads power
Rigidity changes in material samples due to degrading dynamic load application

The maximum growth of sample dynamic rigidity reached the value of approx. 4.5% while the lowering of dynamic rigidity was $1 - 10\%$ (Fig. 3).

Reduction of vibration frequency of the sample occurred due to the reduction of its dynamic rigidity and as a result of changes in internally dissipated energy. High loads maxima characterised the process of sample cracking and breaking.
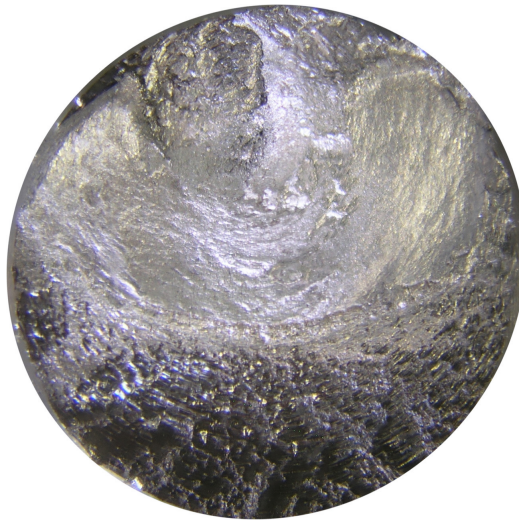
Fig. 4. Crossection of fatigue scrap

As a result of the load impact, after the completion of the work of degrading forces stepwise reduction in torsional rigidity of the sample occurred, a growth in the power of internal friction forces and periodic changes in the power of degradation forces in the analyzed sample. In the final phase of the experiment, torsional rigidity of the sample was virtually reduced to naught.

A picture of fatigue scrap is shown in Figure 4.

5. Conclusions

1. Information about the technical condition of a mechanical object is obtained on the basis of energetic characteristics of power spectral densities of dynamic loads and amplitude estimates of dynamic rigidity force power and inertia forces which change together with the progressive process of its structural changes.
2. Vibration damping, being a factor which determines mechanical energy dissipation, is a measure of the initial phase of structural degradation of a mechanical object. Changes in dynamic rigidity manifesting themselves in sample cracking, ocurr in the second, final phase of technical degradation of a mechanical object. An analysis of those changes makes it possible to determine boundary values of load powers which trigger the initiation of structural degradation processes (e.g. cracking) in a mechanical object component.

References

1. C. Cempel, *Models of Systems for Energy Process in Theory and System Engineering*. Promotion to Doctor Honoris Causa of the Szczecin University of Technology. 1995.
2. H. Kaźmierczak,. *Energetic Description of the Destruction Process of Machine Structural Nodes*, in Machine Dynamics Problem, Vol. 27, No 3, 113-123, Warszawa 2003.
3. H. Kaźmierczak, T. Pawłowski, C. Cempel, *Energy Flow Analysis of Vibration Loads of Machines*, Eleventh International Congress on Sound and Vibration (ICSV 11), St. Petersburg 2004.
4. H. Kaźmierczak,. *Energetic Characteristics of Fatigue Durability of a Machine*, in Teoria Maszyn i Mechanizmów vol. II, Polski Komitet Teorii Maszyn i Mechanizmów at KBM PAN, AGH Kraków 2004.
5. H. Kaźmierczak, *Energetic Analysis of Technical Condition of Machines*, in Inżynieria Diagnostyki Maszyn, Instytut Techn. Eksploatacji, Warszawa, Bydgoszcz, Radom 2004.
6. H. Kaźmierczak, J. Kromulski, C. Cempel, R. Barczewski, *Energetic Description of the steel concrete composite beam* in New Materials and Systems for Pre-stressed Concrete Structures, Radom2005.
7. H. Kaźmierczak, J. Kromulski, T. Pawłowski, *Energetic Characteristics of Trailer Degradation*, Diagnostyka vol.33, PTDT at Wydział Nauk Technicznych PAN, 2005.
8. H. Kaźmierczak,., J. Kromulski, C. Cempel, R. Barczewski, *Energetic Description of the Destruction Process of Steel Concrete Structures*, COST Action 534 New Materials and Systems for Pre-stressed Concrete Structures, Workshop of COST on NTD Assessment and New Systems in Pre-stressed Concrete Structures, Radom 2005.
9. H. Kaźmierczak, T. Pawłowski, J. Kromulski, R. Barczewski, *Vibration characteristics of the technical degradation process of an object*, 13 International Congress on Sound and Vibration, 2–6 July, 2006, Vienna, 2006.
10. H. Kaźmierczak,. *Energetic characteristics of dynamic loads on a machine unit*, in Teoria Maszyn i Mechanizmów, Polski Komitet Teorii Maszyn i Mechanizmów at KBM PAN, Zielona Góra 2006.
11. H. Kaźmierczak, *Energetic characteristics of system degradation*, Diagnostyka vol.38, PTDT at Wydział Nauk Technicznych PAN, 2006.
12. H. Kaźmierczak,. T. Pawłowski, J. Kromulski, *Energetic characteristics of vibration loads on a mechanical object*, 14th International Congress on Sound and Vibration, Cairns, Australia, July 2007.
13. Kaźmierczak H., Kromulski J., Barczewski R. 2007. *Structural characteristics of prestressed concrete beams*. 6th International Seminar on Technical System Degradation Problems, VI Międzynarodowe Seminarium Degradacji Systemów Technicznych, Liptowski Mikulasz 11-14 kwietnia 2007, s. 142-144.

14. Kazmierczak H., Pawlowski T., Kromulski J., Barczewski R. *Energetic. Modes in Describing the Process of Structural Degradation of Mechanical Objects*, 15th International Congress on Sound and Vibration (ICSV 15), Daejeon (Korea), 2008.

Nowa metoda opisu procesu degradacji strukturalnej materiałów konstrukcyjnych

Artykuł przedstawia analizę wyników badań procesu degradacji strukturalnej próbek materiałów technicznych, wyznaczonych metodą analizy rozkładu mocy obciążeń dynamicznych (model dyskretny obciążeń dynamicznych struktury). Celem tych badań jest opis procesu degradacji strukturalnej podstawowych materiałów technicznych. Wyznaczono miary zmian strukturalnych próbek materiałów konstrukcyjnych przy poddawaniu ich obciążeniom impulsowym. Informacje o stanie technicznym poszczególnych próbek materiałów uzyskiwane były na podstawie energetycznych charakterystyk gęstości widmowych mocy mocy degradujących obciążeń dynamicznych i przedstawione w formie estymat amplitudowych mocy sił sztywności dynamicznej i mocy sił tłumienia, zmieniających się wraz z postępującym procesem degradowania tych próbek. Badania stanowiskowe metodą testu impulsowego pozwoliły wyznaczyć obciążenia inicjujące proces uszkadzania struktury tych materiałów. Analiza zmian strukturalnych pozwala ustalić wartości graniczne mocy obciążeń, powodujących inicjację procesów degradacji strukturalnej (np. pękania) wybranych materiałów.

Analysis of Chaotic and Regular Motion of an Autoparametric System by Recurrence Plots Application

Krzysztof KĘCIK

Lublin University of Technology, Department of Apllied Mechanics
Nadbystrzycka36 St, 20-618 Lublin Poland
k.kecik@pollub.pl

Jerzy WARMIŃSKI

Lublin University of Technology, Department of Apllied Mechanics
Nadbystrzycka36 St, 20-618 Lublin, Poland
j.warminski@pollub.pl

Abstract

The purpose of this study is to use recurrence plots to investigate the dynamics of an autoparametric system with an attached pendulum. Recurrence is a fundamental property of dynamical systems, which can be exploited to characterise the system's behaviour in phase space. The Recurrence Plots method (RPs) and Recurrence Quantification Analysis (RQA) is used for analysis of relatively short time series for detection different types of behaviour including chaotic motions of the considered nonlinear system.

Keywords: Autoparametric vibrations, Chaos, Recurrence Plot, Pendulum-like System

1. Introduction

The autoparametric system represents a special class of nonlinear dynamical construction. Such a system is composed of at least two subsystems (primary and secondary), i.e. at least a two degrees of freedom model has to be considered. The secondary subsystem is coupled to the primary system in a nonlinear way, and moreover it may become a source of internal parametric excitation. However, under certain conditions the attached secondary subsystem may play a role of a dynamical absorber, as well. In a large number of problems we want to reduce vibration amplitude of the primary system and therefore, to avoid dangerous instability regions, a proper system's parameter selection is needed.

Dynamical systems with attached pendulums play significant role in many applications and posing interesting mathematical challenges. The pendulum-like structures appear in cranes, robots etc. or they can be used for vibration absorption.

Our aim is to propose an efficient method which could identify the type of motion by time history analysis and on this basis to select regions of various system's behaviours. We assumed that the time series received from an experimental set used identification are relatively short, what it is very important from control point of view. It is worth adding, that the experimental results analyzed by standard nonlinear method have been presented in the earlier work of authors [1]. Analytical and numerical verification of these results have been done there, too.

2. Equations of Motion and Experimental System

The experiment, of the two degree of freedom model presented schematically in *Fig. 1a*, has been performed on an especially prepared experimental test stand. A photo *Fig. 1b* shows a main components of real mechanical system. The pendulum which may realize full rotation is attached to an oscillator mounted to a base by a spring and a magnetorheological damper. Motion of the system is generated by a motor, and a mechanism which changes rotation of the motor into translational motion. The frequency of the vertical oscillations is controlled by inverter. Amplitude of the kinematical excitation is fixed by a pitch of a drive shaft. Detailed description and more information about experimental setup and measures apparatus are presented in [2].
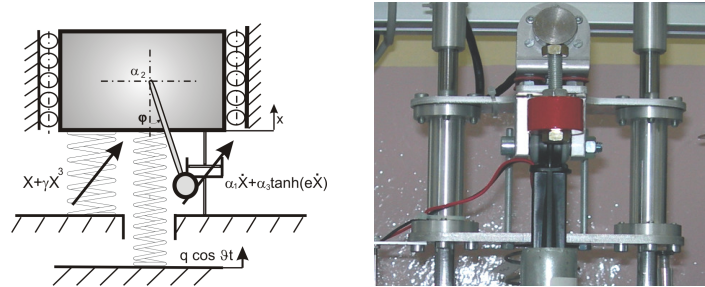
Figure 1. The autoparametric system; model with pendulum (a) and main parts of experimental system (b).

The governing equations of motions of the autoparametric system are given by non-dimensionless equations:

$$\ddot{X} + \alpha_1 \dot{X} + \alpha_3 \tanh(e\dot{X}) + X + \gamma X^3 + \mu\lambda(\ddot{\varphi}\sin\varphi + \dot{\varphi}^2\cos\varphi) = q\cos\vartheta\tau \qquad (1)$$

$$\ddot{\varphi} + \alpha_2\dot{\varphi} + \lambda(\ddot{X} + 1)\sin\varphi = 0 \qquad (2)$$

Definitions of the dimensionless parameters α_1, α_2, α_3, μ, λ, q, ϑ and analytical solutions of equations of motions (1) and (2) received by the Harmonic Balance Method (HBM) are presented in [1].

3. Recurrence Plot and Quantification Analysis

The standard procedure to perform nonlinear analysis is the phase space reconstruction. A single coordinate in nonlinear time series can be substituted by a specific vector. The corresponding vector elements are defined by the same coordinate with a certain time delay. For the scalar series x_i we construct the delay vectors

$$\mathbf{s_i} = \left(x_i, x_{i+d}, x_{i+2d}, ..., x_{i+(m-1)d}\right) \qquad (3)$$

where parameter m is the embedding dimension and parameter d is the time delay. Each unknown point of the phase space at time i is reconstructed by the delayed vector s_i in an m-dimensional space called *''the reconstructed phase space''*. This vectors (3) is useful only if parameters m and d are properly chosen by using appropriate methods. Usually

the time delay and embedding dimension can be estimated by applied average mutual information (*AMI*) [3] and false nearest neighbour method *(FNN)* [4].

The recurrence analysis is a graphical method designed to locate hidden recurring patterns, nonstationarity and structural changes, introduced in Eckmann et al. [5] in 1987. A recurrence plot *(RPs)* is a graph which shows all those time instants at which a state of the dynamical system recurs. In other words, the *RPs* method reveals all the times when the phase space trajectory visits roughly the same area in the phase space. A recurrence plot can be described by computing the matrix [6]

$$M_{ij} = \theta\left(\varepsilon - \left|\mathbf{s}_i - \mathbf{s}_j\right|\right) \tag{4}$$

where θ is the Heaviside step function, ε is a tolerance parameter (threshold), to be chosen, $\mathbf{s}_i$ is a delay vector of the embedding dimension. This matrix is symmetric by construction. If the trajectory in the reconstructed phase space returns at time i into the neighbourhood of ε where it was j then $M_{ij}=1$, otherwise $M_{ij}=0$. This results are can plot black and white dots respectively. Value of chosen parameter ε *is* very important. If ε is chosen too small, there may be almost no recurrence points and we cannot learn anything about the recurrence structure of the considered system. On the other hand, if ε is chosen too large, almost every point is a neighbour of every other point, which leads to a lot of artefacts. A too large ε includes effect called tangential motion.

In the *Fig. 2a-4a* we can see different types of responses of an autoparametric systems and it's recurrence plots. The results have been done for data: *α₁=0.261354, α₂=0.1, α₃=0, μ=17.2278, λ=0.127213, q=2.45094, γ=0* and *e=10.* All examples presented in this work were studied numerically, analytically and then verified experimentally by other methods of nonlinear dynamics [1].
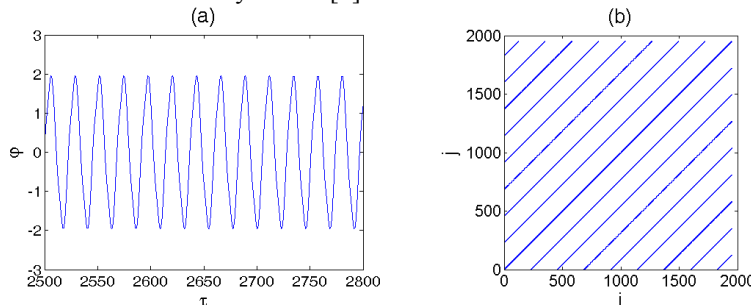
Figure 2. Time history (a) and its recurrence plot (b) of a swinging pendulum. The time delay *d=25*, the embedding dimension *m=3* and the threshold *ε=0.1*.

In the example the recurrence for swinging of the pendulum with periodic motion for *ϑ=0.55, (Fig. 2)* can be observed. The patterns of the plot are reflected by long and non-interrupted diagonals. The vertical distance between these lines corresponds to the period of the oscillation. Recurrence analysis of the rotation of the pendulum, based on the signal of angular velocity is presented in *Fig. 3a, ϑ=0.9.* For *RPs* analysis *2000* data points and angular displacement of the pendulum are used. This choice of signal makes the analysis easier because in the velocity domain the rotation of the pendulum is

eliminated. The diagonals long line are observed, but the distance between individual line is different compare to swinging of the pendulum *(Fig. 2b)*. It means that the period of the pendulum during rotation is smaller comparing to swinging.
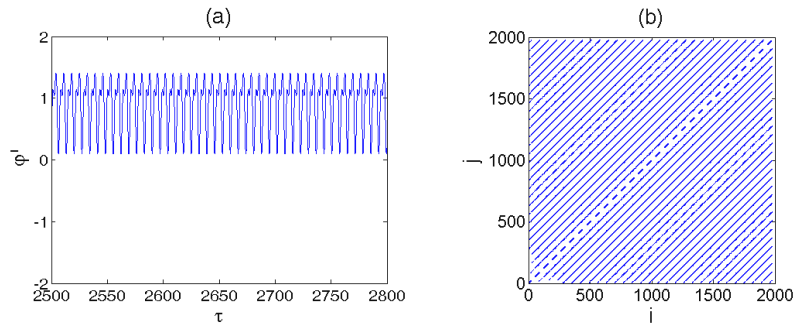
Figure 3. Time history (a) and its recurrence plot (b) of rotation of the pendulum.
The time delay d=8, embedding dimension m=4 and threshold ε=0.1
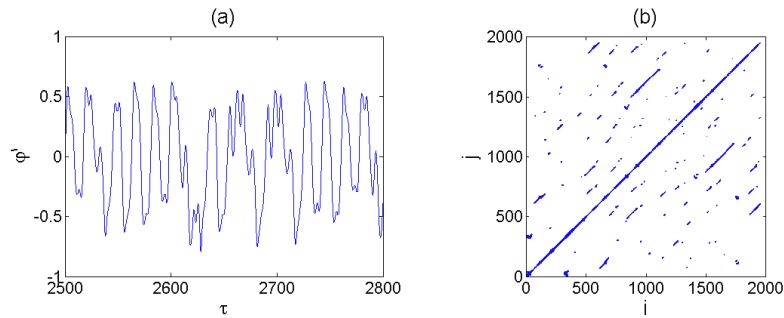
Figure 4. Time history (a) and it's recurrence plot (b) of chaotic signal.
The time delay d=15, embedding dimension m=4 and threshold ε=0.1

Next type of analyzed response is chaotic motion which consists of both swinging and rotating of the pendulum. The type of behaviour (chaotic) was established on the basis of the positive value of Lyapunov exponent and attractor reconstruction [1]. The recurrence plots of chaotic time history *(ϑ=0.7)* is presented in *Fig. 4b*. The diagram shows different line, much more shorter and dashed. The distance between diagonal lines is various because this motion include components of rotation and oscillation. In *Fig. 5* we observe the recurrence plot constructed from angular displacement of pendulum (the same experiment test as *Fig. 4a*, but another signal). In this example we used much more data points *-10 000*, therefore the time delay is changed *d=53*. We can see that time history consist of swinging, next one rotation and again swinging of the pendulum, it is clearly visible in *Fig. 5a*. This effect is observed in recurrence pattern, where areas (paths) with different length of diagonals but similar distance between them exist. The paths corresponds to *''chaotic oscillation''* of the pendulum.
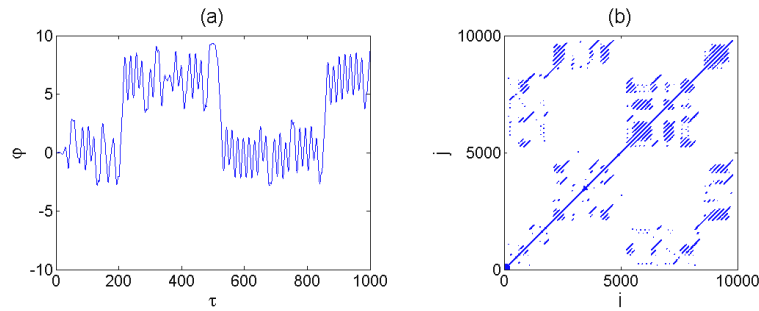
Figure 5. Time history (a) and it's recurrence plot (b) of chaotic signal of the pendulum.
The time delay d=53, embedding dimension m=4 and threshold ε=0.8

In order to go beyond the visual impression yielded by *RPs*, several measures of complexity which are know as *''Recurrence Quantification Analysis'' (RQA)* [7]. These measures are based on the recurrence point density and the diagonal and vertical line of *RPs*. The most important *RQA* measurements are: *Recurence Rate (RR), Determinism (DET), Laminarity (LAM), Trapping Time (TT), Horizontal and Vertical Diagonal Line (L_{max}, V_{max}), Entropy of Horizontal and Vertical Line Distribution (L_{ENT}, V_{ENT})*. The detailed definition and method of their calculations and more parameter quantifications one can find in papers [6, 7]. In paper [8] *RQA* method is used for classical parametric pendulum analysis. Results of calculation of recurrence quantification are presented in *Table 1*.

Table 1. Results of quantification analysis (*RQA*) for *ε=0.1* and *2000* data points.

	RR	DET	LAM	TT	L_{ENTR}	V_{ENTR}	V_{max}	L_{max}
Fig. 2b	0.0128	0.9999	0.9996	2.9273	4.5220	1.1571	5	1949
Fig. 3b	0.0334	0.9992	0.9154	2.7569	3.5358	1.0626	6	1856
Fig. 4b	0.0126	0.9994	0.9989	9.7378	3.5900	2.8793	40	1954

Different line structures can be associated with different value of parameter *RR*. Note, that parameter *RR* indicates the fraction of recurrence for the oscillating pendulum is about three times smaller comparing with rotation. However, the *DET* and *LAM* for all types of motions are very similar. The diagonal and vertical line distribution, measured entropy (referred to the Shannon entropies) are closely the same (especially for diagonal line length distribution L_{ENTR} for rotation and chaotic response). Parameters L_{max} stay also similar for all types of motions, but V_{max} and *TT* for chaotic motions are completely different comparing to other dynamic responses. This suggests that, these recurrence quantifications can be used to analyze the chaotic behaviour.

4. Conclusions

Results received from *RP* method agreed with results obtained from classical approaches to nonlinear dynamic analysis (see paper [1]). Very important advantage of this method is a possibility for a short time series application. But in a case of a rotation of the pendulum, longer time series give more precise results.

Our main objective in this work was to use *RPs* and *RQA* statistics to detect transitions to chaotic motions and to confirm their effectiveness in a real autoparametric system. *RQA* analysis showed that the best parameters to classify of kind of motion are: V_{ENTR}, V_{max} and *TT*. In future work we would like to confirmed *RQA* results for much longer time series and introduce own original quantifications.

References

1. J. Warminski, K. Kecik, *Instabilities in the main parametric resonance area of mechanical system with a pendulum*. Journal of Sound Vibration, **332** (2009) 612-628.
2. J. Warminski, K. Kecik, *Regular and chaotic motions of an autoparametric real pendulum system with the use of a MR damper*. Modeling, Simulation and Control of Nonlinear Engineering Dynamical Systems, Springer, 2009 267-276.
3. A. M. Fraser, H. L. Swinney, *Independent coordinates for strange attractors from mutual information*, Phys. Rev. A **33** (1986) 1134–40.
4. M. B. Kennel, M. Brown, H. D. I. Abarbanel, *Determining embedding dimension for phase space reconstruction using a geometrical construction*, Phys. Rev. A **45** (1992) 3403–11.
5. J. P. Eckmann, S.O. Kampshort, D. Ruelle, *Recurrence Plots of Dynamical Systems*. Europhysics Letters, **4** (1987) 973-977.
6. N. Marwan, M. C. Romano, M. Thiel, J. Kurths, *Recurrence plots for the analysis of complex systems,* Physics Reports **438** (2007) 237 – 329.
7. J. P. Zibult, C. L. Webber, *Embedding and delays as derived from quantification of Recurrence Plot,* Physic Letter A **171** (1992) 199-203.
8. G. Litak, M. Wiercigroch, B. W. Horton, X. Xu, *Transient chaotic behavior versus periodic motion of parametric pendulum by recurrence plot*. ZAMM **90** (2010) 33-41.

Analiza ruchu regularnego i chaotycznego układu autoparametryczego za pomocą metody wykresów rekurencyjnych.

W pracy przedstawiono analizę dynamiki układu autoparametrycznego z wahadłem za pomocą metody wykresów rekurencyjnych (RPs) i ich analizy ilościowej (RQA). Rekurencja jest jedną z podstawowych własności układów dynamicznych i może być wykorzystywana w celu scharakteryzowania zachowania układu w przestrzeni fazowej. Metodą wykresów analizowano "stosunkowo" krótkie przebiegi czasowe dla różnych przebiegów czasowych. Na tej podstawie wykryto różnorodne odpowiedzi układu autoparametrycznego w tym zachowania chaotycznego.

Mechanical and electromagnetic wave interaction in linear isotropic dielectrics with local mass displacement and polarization inertia

Vasyl KONDRAT

Centre of Mathematical Modelling, Ya. Pidstrigach Institute of Applied Problems of Mechanics and Mathematics, NAS of Ukraine, 15, Dudajev Str., Lviv, 79005, Ukraine
kon@cmm.lviv.ua

Olha HRYTSYNA

Centre of Mathematical Modelling, Ya. Pidstrigach Institute of Applied Problems of Mechanics and Mathematics, NAS of Ukraine, 15, Dudajev Str., Lviv, 79005, Ukraine
gryt@cmm.lviv.ua

Abstract

Using thermodynamical approach the complete set of equations of local gradient model is obtained for description of coupled mechanical, thermal and electromagnetic fields in nonferromagnetic dielectrics taking into account the local mass displacement and polarization inertia. For linear isothermal approximation the key set of equations is written for scalar and vector potentials of displacement vector and electromagnetic fields. In this case the generalization of Lorentz calibration is proposed. On this base the plane harmonic waves of displacement, electromagnetic fields and local displacement of mass in media are studied. It is shown that the process of the local mass displacement is related to the change of volume and scalar electric potential only. It is shown that the proposed model describes the dispersion of modified elastic wave in the region of high frequency.

Keywords: nonlocal model, local mass displacement, polarization inertia, mechanic and electromagnetic waves

1. Introduction

Some approaches to the construction of the gradient theory of dielectrics are known. Such theories are based on the extension of the state parameters space by gradients of the strain tensor or the polarization vector, and by gradients of the electric field vector or electric multipoles of higher order (see reviews [1, 2]). Recently the local gradient theory of dielectrics which takes into account the process of local mass displacement has been proposed [2, 3]. This work is devoted to the development of the aforementioned theory with account of polarization inertia [4]. On this base the interaction of the mechano-electromagnetic wave fields are investigated.

2. Basic set of model description

Let us consider an isotropic thermoelastic polarized nonferromagnetic solid that occupies a region (V) of Euclidean space and is bounded by a closed smooth surface (Σ). The thermomechanical and electromagnetic processes as well as the process of local mass displacement [3] proceed in the solids due to external loads of thermal, mechanical, and electromagnetic origins. The process of local mass displacement is related to the structu-

ral changes of a physically small element of a body. The mechanical and polarization processes and the process of local mass displacement are reversible.

With account of the process of local mass displacement the velocity vector $\mathbf{v}$ of the center of mass is presented as the sum of convective part $\mathbf{v}_*$ of mass transport and term $\rho^{-1}\partial\mathbf{\Pi}_m/\partial t$ caused by structure changes of a physically small element of a solid. Here $\mathbf{\Pi}_m$ is the vector of local mass displacement [3], ρ is the mass density, t is the time. Then the equation of mass balance has a typical form: $\dfrac{\partial\rho}{\partial t}+\mathbf{\nabla}\cdot(\rho\mathbf{v})=0$ [3].

Let us assume that total energy of the system "solid-electromagnetic field" is the sum of internal energy ρu, kinetic $\rho\mathbf{v}^2/2$ energy, the energy of the electromagnetic field U_e and polarization kinetic energy $\dfrac{1}{2}\rho d_E\left(\dfrac{d\mathbf{p}}{dt}\right)^2$ [4]. The total energy change is the result of the convective energy transport through the surface, the work of surface forces $\hat{\mathbf{\sigma}}\cdot\mathbf{v}$, the heat flux $\mathbf{J}_q$, the electromagnetic energy flux $\mathbf{S}_e$, the work $\mu\mathbf{J}_m$ related to the mass transport relative to the centre of the body mass, the work $\mu_\pi\,\partial\mathbf{\Pi}_m/\partial t$ related with structure change, and the action of mass forces $\mathbf{F}$ and distributed heat sources $\Re$:

$$\frac{d}{dt}\int\limits_{(V)}\left(\rho u+U_e+\frac{1}{2}\rho\mathbf{v}^2+\frac{1}{2}\rho d_E\left(\frac{d\mathbf{p}}{dt}\right)^2\right)dV=-\int\limits_{(\Sigma)}\left[\rho\left(u+\frac{1}{2}\mathbf{v}^2+\frac{1}{2}d_E\left(\frac{d\mathbf{p}}{dt}\right)^2\right)\mathbf{v}-\right.$$

$$\left.-\hat{\mathbf{\sigma}}\cdot\mathbf{v}+\mathbf{S}_e+\mathbf{J}_q+\mu\mathbf{J}_m+\mu_\pi\,\frac{\partial\mathbf{\Pi}_m}{\partial t}\right]\cdot\mathbf{n}\,d\Sigma+\int\limits_{(V)}\left(\rho\mathbf{F}\cdot\mathbf{v}+\rho\Re\right)dV. \tag{1}$$

Here $U_e=\left(\varepsilon_0\mathbf{E}^2+\mu_0\mathbf{H}^2\right)/2$; $\mathbf{S}_e=\mathbf{E}\times\mathbf{H}$; $\mathbf{E}$ and $\mathbf{H}$ are the electric and magnetic fields in the laboratory frame; $\mathbf{p}=\mathbf{P}/\rho$, $\mathbf{P}$ is the polarization vector; $\hat{\mathbf{\sigma}}$ is the Cauchy's stress tensor; ε_0,μ_0 are the electric and magnetic constants; $\mathbf{J}_m=\rho(\mathbf{v}_*-\mathbf{v})$; μ is the chemical potential; μ_π is the energy measure of the influence of the mass displacement on the internal energy [3]; d_E is the scalar related with inertia of the polarization process [4]; $\mathbf{n}$ is the unit outward normal vector to the surface (Σ); $d/dt=\partial/\partial t+\mathbf{v}\cdot\mathbf{\nabla}$.

Taking into account the formula $\mathbf{J}_m=-\partial\mathbf{\Pi}_m/\partial t$ and the balance equations of electromagnetic field energy [3], mass and entropy [3, 5] from integral equation (1) we obtain the following local form of balance equation for the internal energy:

$$\rho\frac{du}{dt}=\rho T\frac{ds}{dt}+\hat{\mathbf{\sigma}}_*:\frac{d\hat{\mathbf{e}}}{dt}+\rho\mathbf{E}_*\cdot\frac{d\mathbf{p}}{dt}+\rho\mu_\pi'\frac{d\rho_m}{dt}-\rho\mathbf{\nabla}\mu_\pi'\cdot\frac{d\mathbf{\pi}_m}{dt}-\rho d_E\frac{d^2\mathbf{p}}{dt^2}\cdot\frac{d\mathbf{p}}{dt}+$$

$$+ \mathbf{J}_{e*} \cdot \mathbf{E}_* - \mathbf{J}_q \cdot \frac{\nabla T}{T} - T\sigma_s + \mathbf{v} \cdot \left(-\rho \frac{d\mathbf{v}}{dt} + \nabla \cdot \hat{\boldsymbol{\sigma}}_* + \rho \mathbf{F}_* + \mathbf{F}_e \right). \tag{2}$$

Here s is the specific entropy; T is the absolute temperature; σ_s is the strength of the entropy source; $\mu'_\pi = \mu_\pi - \mu$; $\hat{\mathbf{e}}$ is the strain tensor, $\boldsymbol{\pi}_m = \boldsymbol{\Pi}_m / \rho$; $\rho_m = -(\nabla \cdot \boldsymbol{\Pi}_m)/\rho$ is the specific value of density of induced mass [3]; $\mathbf{E}_*$ and $\mathbf{J}_{e*}$ are the vectors of the electric field and density of electric current in the reference frame of the centre of mass moving with speed $\mathbf{v}$ relatively to the laboratory reference frame ($\mathbf{E}_* = \mathbf{E} + \mathbf{v} \times \mathbf{B}$, $\mathbf{J}_{e*} = \mathbf{J}_e - \rho_e \mathbf{v}$ [6]); $\mathbf{B}$ and $\mathbf{J}_e$ are the vectors of magnetic induction and the density of electric current in the laboratory frame; ρ_e is the density of free electric charge; $\hat{\boldsymbol{\sigma}}_* = = \hat{\boldsymbol{\sigma}} - \rho \left(\mathbf{E}_* \cdot \mathbf{p} - \rho_m \mu'_\pi - \boldsymbol{\pi}_m \cdot \nabla \mu'_\pi \right) \hat{\mathbf{I}}$; $\mathbf{F}_* = \mathbf{F} + \rho_m \nabla \mu'_\pi - \boldsymbol{\pi}_m \cdot \nabla \nabla \mu'_\pi$, $\mathbf{F}_e = \rho_e \mathbf{E}_* + \left(\mathbf{J}_{e*} + + \frac{\partial(\rho\mathbf{p})}{\partial t} \right) \times \mathbf{B} + \rho (\nabla \mathbf{E}_*) \cdot \mathbf{p}$, $\hat{\mathbf{I}}$ is the unit tensor. For nonferromagnetic medium $\mathbf{B} = \mu_0 \mathbf{H}$.

Now let us assume that the body state depends on a local electric field vector $\mathbf{E}^L$ [4]. Introduce the generalized Helmholtz free energy $f = u - Ts - \mathbf{E}^L \cdot \mathbf{p} + \nabla \mu'_\pi \cdot \boldsymbol{\pi}_m - \mu'_\pi \rho_m$ and rewrite formula (2) as:

$$\rho \frac{df}{dt} = -\rho s \frac{dT}{dt} + \hat{\boldsymbol{\sigma}}_* : \frac{d\hat{\mathbf{e}}}{dt} - \rho \mathbf{p} \cdot \frac{d\mathbf{E}^L}{dt} - \rho \rho_m \frac{d\mu'_\pi}{dt} + \rho \boldsymbol{\pi}_m \cdot \frac{d\nabla \mu'_\pi}{dt} + \rho \left(\mathbf{E}_* - \mathbf{E}^L - \right.$$

$$\left. -d_E \frac{d^2\mathbf{p}}{dt^2} \right) \cdot \frac{d\mathbf{p}}{dt} + + \mathbf{J}_{e*} \cdot \mathbf{E}_* - \mathbf{J}_q \cdot \frac{\nabla T}{T} - T\sigma_s + \mathbf{v} \cdot \left(-\rho \frac{d\mathbf{v}}{dt} + \nabla \cdot \hat{\boldsymbol{\sigma}}_* + \rho \mathbf{F}_* + \mathbf{F}_e \right). \tag{3}$$

From the requirement that equation (3) is invariant with respect to translations [7] and assuming that $f = f\left(T, \mu'_\pi, \mathbf{E}^L, \nabla \mu'_\pi, \hat{\mathbf{e}} \right)$ (all of these parameters are independent), we obtain the generalized Gibbs equation, the conservation law of momentum, a relation for the entropy production and a balance relation for polarization vector

$$df = -s\, dT + \rho^{-1} \hat{\boldsymbol{\sigma}}_* : d\hat{\mathbf{e}} - \mathbf{p} \cdot d\mathbf{E}^L - \rho_m d\mu'_\pi + \boldsymbol{\pi}_m \cdot d\nabla \mu'_\pi \ , \qquad \rho \frac{d\mathbf{v}}{dt} = \nabla \cdot \hat{\boldsymbol{\sigma}}_* + \rho \mathbf{F}_* + \mathbf{F}_e \ ,$$

$$\sigma_s = \mathbf{J}_{e*} \cdot \frac{\mathbf{E}_*}{T} - \mathbf{J}_q \cdot \frac{\nabla T}{T^2} \ , \qquad \mathbf{E}_* - \mathbf{E}^L = d_E \frac{d^2\mathbf{p}}{dt^2} \ . \tag{4}$$

The Gibbs equation and relation for the entropy production are the base for the formulation of constitutive equations. In particular, from (4_1) we obtain the next state equations:

$$s = -\frac{\partial f}{\partial T} , \quad \hat{\boldsymbol{\sigma}}_* = \rho \frac{\partial f}{\partial \hat{\mathbf{e}}} , \quad \rho_m = -\frac{\partial f}{\partial \mu'_\pi} , \quad \mathbf{p} = -\frac{\partial f}{\partial \mathbf{E}^L} , \quad \boldsymbol{\pi}_m = \frac{\partial f}{\partial (\nabla \mu'_\pi)} . \quad (5)$$

Taking into account the equation (4_4) the last two formulas in (5) in linear approximation can be written as

$$\mathbf{p} + \chi_E d_E \frac{d^2\mathbf{p}}{dt^2} = \chi_E \mathbf{E}_* - \chi_{Em} \nabla \tilde{\mu}'_\pi , \quad \boldsymbol{\pi}_m + \chi_{Em} d_E \frac{d^2\mathbf{p}}{dt^2} = -\chi_m \nabla \tilde{\mu}'_\pi + \chi_{Em} \mathbf{E}_* . \quad (6)$$

Here $\tilde{\mu}'_\pi = \mu'_\pi - \mu'_{\pi 0}$, $\mu'_{\pi 0}$ is the reduced potential μ'_π in the reference state; χ_E, χ_{Em} and χ_m are the material constants. Note that the occurrence in these relations of the value $\nabla \tilde{\mu}'_\pi$ exhibits the space non-locality of the state equations.

Assuming that thermodynamic fluxes are the linear functions of thermodynamic forces and using the Onsager principle from equation (4_3) for the entropy production, one finds such kinematic relations [3]

$$\mathbf{J}_{e*} = \sigma_e \mathbf{E}_* + \sigma_e \eta \nabla T , \qquad \mathbf{J}_q = -\lambda \nabla T + \pi_t \mathbf{J}_{e*} . \quad (7)$$

Here σ_e, λ, η and π_t are kinetic coefficients [3].

The obtained here constitutive relations (5) and (7), equation (4_4), the conservation laws of momentum, masses, and entropy, the equations of electrodynamics, geometrical relations $\hat{\mathbf{e}} = \left[\nabla \mathbf{u} + (\nabla \mathbf{u})^T \right] / 2$ and formula $\rho_m = -(\nabla \cdot \mathbf{\Pi}_m) / \rho$ form a complete set of equations of electromagneto-thermo-mechanics of the polarized nonferromagnetic iso-tropic solids taking into account the local displacement of the mass and polarization inertia. Note that since for determination of the vectors of polarization and local mass displacement the differential equations, which contain the second time derivative of the polarization vector were found, the equations obtained here can be effective for study of acceleration waves, high-frequency processes and behaviour of solids under the impact loading.

3. The interaction of mechanic and electromagnetic fields

Using the model equations let us investigate the interaction of mechanic and electromagnetic fields in dielectric isotropic medium. Further for simplicity let us neglect the polarization inertia ($d_E = 0$) and accept the isothermal approximation.

Represent the displacement vector $\mathbf{u}$, electric field $\mathbf{E}$, magnetic induction $\mathbf{B}$ and body force vector $\mathbf{F}$ by scalar and vector potentials: $\mathbf{u} = \nabla \varphi_m + \nabla \times \boldsymbol{\psi}$, $\mathbf{E} = -\nabla \varphi_e - \frac{\partial \mathbf{A}}{\partial t}$, $\mathbf{B} = \nabla \times \mathbf{A}$, $\mathbf{F} = \nabla \Phi + \nabla \times \boldsymbol{\Psi}$, $(\nabla \cdot \boldsymbol{\psi} = 0, \nabla \cdot \boldsymbol{\Psi} = 0, \nabla \cdot \mathbf{A} = 0)$. Introduce also the general scalar potential $\varphi_{e\mu} = \varphi_e + \rho_0 \chi_{Em} \varepsilon^{-1} \tilde{\mu}'_\pi$ [8], where $\varepsilon = \varepsilon_0 + \rho_0 \chi_E$ is the electric permittivity of the medium. Then the key set of equations with respect to potentials φ_m, $\varphi_{e\mu}$, $\tilde{\mu}'_\pi$, $\boldsymbol{\psi}$ and $\mathbf{A}$ can be written in the following form

$$\left(K + \frac{2}{3}G\right)\Delta\varphi_m - \rho_0\frac{\partial^2\varphi_m}{\partial t^2} + \rho_0\Phi = K\alpha_\mu\tilde{\mu}'_\pi,$$

$$\Delta\varphi_{e\mu} - \mu_0\varepsilon\frac{\partial^2\varphi_{e\mu}}{\partial t^2} = 0, \qquad \left(1 - \frac{\rho_0\chi_{Em}^2}{\varepsilon\chi_m}\right)\Delta\tilde{\mu}'_\pi - \frac{D_\mu}{\chi_m}\tilde{\mu}'_\pi = \frac{K\alpha_\mu}{\rho_0\chi_m}\Delta\varphi_m, \qquad (8)$$

$$G\Delta\boldsymbol{\psi} - \rho_0\frac{\partial^2\boldsymbol{\psi}}{\partial t^2} + \rho_0\boldsymbol{\Psi} = 0, \qquad \Delta\mathbf{A} - \mu_0\varepsilon\frac{\partial^2\mathbf{A}}{\partial t^2} = 0. \qquad (9)$$

Here newly introduced values are the material constants [3]. Note that for obtaining equation (9$_2$) we used a condition $\nabla\cdot\mathbf{A} + \mu_0\varepsilon\frac{\partial\varphi_{e\mu}}{\partial t} = 0$, which generalized the known condition of Lorentz calibration in case of account of the process of local displacement of mass. From equations (8) it is obvious that within the framework of the considered model in the linearized approximation the fields of scalar potentials φ_m, φ_e and value $\tilde{\mu}'_\pi$ are coupled. From equations (9) it is clear that the fields of vector potentials $\boldsymbol{\psi}$ and $\mathbf{A}$ are related neither between themselves nor with the scalar fields. Thus the process of the local mass displacement is related to the change of the volume and scalar electric potential only. In particular, the modification of parameters of longitudinal elastic wave manifests such coupling. A velocity of such a wave propagation becomes dependent on the frequency (see figure).

Figure. The dependence of the normalized velocity of modify longitudinal elastic wave

on the normalized frequency Ω [8]
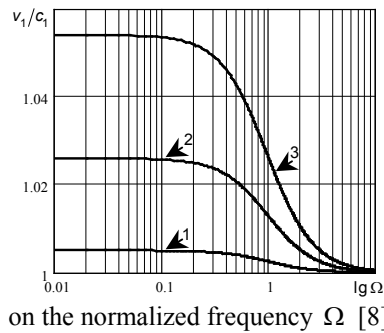
It is noted that similar results have been obtained also in [9] where the Mindlin's gradient theory of piezoelectrics has been used.

4. Conclusions

The complete set of equations of local gradient theory of electro-magneto-thermomechanics of nonferromagnetic dielectrics has been obtained with account of the local displacements of mass and polarization inertia. It is shown that for the polarization

vector and vector of local mass displacement the non-stationary and non-local state equations which contain the second time derivative of the polarization vector have been obtained due to the polarization inertia accounting. Such a set of equations can be effective for investigation of quick-change processes. The coupling of mechanical and electromagnetic fields in isotropic solids has been analyzed. It has been shown that the model describes the dispersion of the modified elastic longitudinal wave in the high frequency range. These results agree well with those obtained using the gradient theories of piezoelectrics.

References

1. J. Yang, *Review of a Few Topics in Piezoelectricity,* Appl. Mech. Rev., 59 (2006) 335-345.
2. V. Kondrat, O. Hrytsyna, *Linear theories of electromagnetomechanics of dielectrics,* Physico-Mathematical Modelling and Inform. Techn., 9 (2009) 7-46 (In Ukrainian).
3. Ya. Burak, V. Kondrat, O. Hrytsyna, *An introduction of the local displacements of mass and electric charge phenomena into the model of the mechanics of polarized electromagnetic solids,* J. Mech. Mat. and Struct., 3, No 6 (2008) 1037-1046.
4. G. A. Maugin, *Continuum mechanics of electromagnetic solids,* North-Holland, Amsterdam, 1988.
5. S. R. de Groot, P. Mazur, *Non-equilibrium thermodynamics,* Noth-Holland, Amsterdam, 1962.
6. L. D. Landau, E. M. Lifshits, *Electrodynamics of continuous media,* Pergamon, Oxford, 1984.
7. M. M. Bredov, V. V. Rumjantsev, I. N. Toptyhin, *Classic electrodynamics,* Moscow, Nauka, 1985 (In Russian).
8. V. F. Kondrat, O. R. Hrytsyna, *Mechano-electro-magnetic interaction in isotropic dielectrics taking into account a local mass displacement,* Mathematical Methods and Physicomechanical Fields, 52, № 1 (2009) 150-158 (In Ukrainian).
9. X. Yang, Y. Hu, J. Yang, *Electric field gradient effects in anti-plane problems of polarized ceramics,* Int. J. of Solids and Structures, 41 (2004) 6801-6811.

Mechano-elektromagnetyczne falowe oddziaływanie w liniowych izotropowych dielektrykach uwzględniające lokalne przemieszczenie masy oraz bezwładność polaryzacji

Korzystanie termodynamicznego podejścia otrzymano kompletny układ równań gradientnego modelu dla opisu pól mechanotermoelektromagnetycznych w nieferromagnetycznych dielektrycznych ośrodkach, biorąc pod uwagę proces lokalnego przemieszczenia masy i bezwładności polaryzacji. W aproksymacji liniowej izotermicznej system podstawowych równań modelu przedstawiony stosunkowo potencjałów wektorowych i skalarnych wektora przemieszczeń i pola elektromagnetycznego. Zaproponovana uogólniona kalibracja Lorentza. Na tej podstawie prowadzono badania oddziaływania płaskich fal harmonicznych przemieszczenia, pola elektromagnetycznego i lokalnego przemieszczenia masy w ośrodku nieskończonym. Wykazano, że proces lokalnego przemeszczenia masy związane tylko ze zmianą objętości i skalarnego potencjału elektrycznego. Wykazano tez, że zaproponowany model opisuje rozpraszanie sprężystej fali, zmodyfikowanej oddziaływaniem mechanoelektrycznym i lokalnym przemieszczeniem masy w zakresie wysokich częstotliwości, zgodnie z wynikami znanych z literatury.

Love waves in pre-stressed Yeoh materials

Anna KOSIŃSKA

Łódź University of Technology, 90-924 Łódź, al. Politechniki 6
annakos@p.lodz.pl

Sławomir KOSIŃSKI

Łódź University of Technology, 90-924 Łódź, al. Politechniki 6
kosislaw@p.lodz.pl

Abstract

The paper is concerned with the effect of pre-stress on the propagation of Love waves in incompressible nonlinear rubberlike materials with the representation for the strain energy function derived by Yeoh. The special initial deformations in the form of the large static homogeneous pure strains are assumed in the half-space and in the layer of the waveguide. It is considered the wave propagation along a principal axis and the dispersion equation for Love waves along a principal axis of the underlying deformation in respect of a selected strain energy function is analyzed in details. For two types of homogeneous equibiaxial deformations the numerical results are obtained. They are quite different as in linear theory, because the equibiaxial static deformations can lead to reduction or increase of the cut-off frequency of the waveguide. The standard procedure for the linearization of equations of motion was used. This approach bases on the assumption that, small time depending motions are superimposed on large static deformation.

Keywords: Love waves, Yeoh material, small motion superimposed on large elastic deformations

1. Basic equations

We consider a layer and a half-space referred to a Cartesian coordinate system. Both the layer and the supporting half-space are made of different pre-stressed incompressible nonlinear rubberlike materials and they are rigidly coupled along the plane $X_2 = 0$. The half-space is defined by $X_2 < 0$ and the layer of thickness h, has boundaries $X_2 = 0$ and $X_2 = h$. The initial static deformations in both material regions, the layer and the half-space are the same. Here and below all quantities with the mark "-"are valid for the half-space. It is assumed that the material has been subjected to an initial static homogeneous deformation with constant principal stretches and to a different superimposed small motions $u_3 = u_3(X_1, X_2, t)$ and $\overline{u}_3 = \overline{u}_3(X_1, X_2, t)$ characterized by a small displacement field which is time dependent:

$$x_1 = \lambda_1 X_1, \quad x_2 = \lambda_2 X_2, \quad x_3 = \lambda_3 X_3 + u_3(X_1, X_2, t),$$
$$\overline{x}_1 = \lambda_1 X_1, \quad \overline{x}_2 = \lambda_2 X_2, \quad \overline{x}_3 = \lambda_3 X_3 + \overline{u}_3(X_1, X_2, t) \tag{1}$$

where the incompressibility condition imposes the constraint $\lambda_1 \lambda_2 \lambda_3 = 1$. For an incompressible isotropic hyperelastic material there exists a strain energy function denoted $W = W(\mathbf{F})$, defined on the space of deformation gradients such that, the nominal stress tensor $\mathbf{S}$ (the transpose of the first Piola-Kirchhoff tensor) is defined as

$$\mathbf{S} = \left[\partial(W(\mathbf{F}))/\partial\mathbf{F}\right] = 2W_1\mathbf{F}^T + 2W_2\left(I_1\mathbf{F}^T - \mathbf{C}\mathbf{F}^T\right) - \pi\mathbf{F}^{-1}, \tag{2}$$

where $\mathbf{F}$ is the deformation gradient, I_i are invariants of the deformation tensor $\mathbf{C} = \mathbf{F}^T\mathbf{F}$, $W_i = \partial W / \partial I_i$, i= 1, 2, and π is the hydrostatic pressure. The linearization of the constitutive relations gives the following result

$$\widetilde{\mathbf{S}} = \mathbf{S}^0 + \hat{\mathbf{S}}, \quad \widetilde{\pi} = \pi^0 + \hat{\pi}, \tag{3}$$

where the first term in both equations is connected with the static deformation and the second one with the small wave motion $u_3 = u_3(X_1, X_2, t)$. Substitution of (1) and (4) into the differential equations of motion of finite elasticity gives two nontrivial systems of equations of motion for the superimposed infinitesimal displacement in the layer u_3 and in the half-space $\overline{u}_3$:

$$\hat{\pi},_1 = \hat{\pi},_2 = 0, \qquad\qquad \hat{\overline{\pi}},_1 = \hat{\overline{\pi}},_2 = 0,$$

$$A_{33}^{11}(\mathbf{F}_0)u_{3,11} + A_{33}^{22}(\mathbf{F}_0)u_{3,22} = \rho_R\ddot{u}_3, \quad \overline{A}_{33}^{11}(\overline{\mathbf{F}}_0)\overline{u}_{3,11} + \overline{A}_{33}^{22}(\overline{\mathbf{F}}_0)\overline{u}_{3,22} = \overline{\rho}_R\ddot{\overline{u}}_3 \tag{4}$$

where $A_{ik}^{\alpha\beta}(\mathbf{F}) = (\partial S_{\alpha i} / \partial F_{k\beta})$ and by $A_{ik}^{\alpha\beta}(\mathbf{F}_0)$ are denoted the values of these derivatives calculated at $\mathbf{F}=\mathbf{F}_0$, and $\hat{\pi}$, $\hat{\overline{\pi}}$ are the corresponding increments in $\pi, \overline{\pi}$. Assuming now the solutions for infinitesimal motions in both parts of the waveguide in the form

$$u_3(X_1, X_2, t) = w(X_2)u(X_1, t), \quad \overline{u}_3(X_1, X_2, t) = \overline{w}(X_2)\overline{u}(X_1, t). \tag{5}$$

The nontrivial equation of motion in the layer takes the form

$$c_{T//}^2 w(X_2)[u(X_1, t)]_{,11} + c_{T\perp}^2 u(X_1, t)[w(X_2)]_{,22} = w(X_2)\ddot{u}(X_1, t), \tag{6}$$

where $c_{T//}^2 = 2(\breve{W}_1 + \breve{W}_2\lambda_2^2)/\rho_R$ and $c_{T\perp}^2 = 2(\breve{W}_1 + \breve{W}_2\lambda_1^2)/\rho_R$ can be interpreted as propagation speed of the shear plane waves in initially deformed layer in the direction parallel and normal to the interface $X_2 = 0$ and $\breve{W}_i = W_i(\mathbf{F}_0)$, $i = 1, 2$.

Suppose now that the displacements in the layer and in the half-space are given by

$$u_3 = w(X_2)\exp[i(kX_1 - \omega t)], \quad \overline{u}_3 = \overline{w}(X_2)\exp[i(\overline{k}X_1 - \overline{\omega}t)]. \tag{7}$$

where $\omega, \overline{\omega}$ are the frequencies and k, $\overline{k}$ the wave numbers.

Substituting of $(7)_{1,2}$ into (6) gives two equations for two unknown functions $w(X_2)$, $\overline{w}(X_2)$

$$[w(X_2)]_{,22} + k^2 p^2 w(X_2) = 0, \quad [\overline{w}(X_2)]_{,22} + \overline{k}^2\overline{p}^2\overline{w}(X_2) = 0, \tag{8}$$

where $p^2 = (\omega^2/(k^2 c_{T\perp}^2) - (c_{T//}/c_{T\perp})^2)$, $\overline{p}^2 = (\overline{\omega}^2/(\overline{k}^2\overline{c}_{T\perp}^2) - (\overline{c}_{T//}/\overline{c}_{T\perp})^2)$, and the displacements (7) take the forms

$$u_3 = \exp[i(kX_1 - \omega t \pm kpX_2)], \quad \overline{u}_3 = \exp[i(\overline{k}X_1 - \overline{\omega}t \pm \overline{k}\overline{p}X_2)]. \tag{9}$$

2. Love waves

Combining the four basic solutions (9) obtained earlier, we are able to compose all wave configurations characteristic for the Love waves. It is easy to see that in the case when the propagation speed of Love waves c = ω/k satisfied the condition $c > (c_{2//}, \overline{c}_{2//})$,

both p, $\overline{p}$ are real. The wave motion characteristic for the Love waves is practically confined to the thin layer h adjacent to the boundary. The solution $\overline{u}_3$ in the half-space $X_2 \leq 0$ should decreases rapidly with the distance from the interface, when $X_2 \rightarrow -\infty$. The last condition can be satisfied when we assume that $\overline{p}$ is an imaginary number i.e.

$$c < \overline{c}_{2//} \quad \Rightarrow \quad \overline{p} = -i\overline{v}, \qquad \overline{v} = \left(\left(\overline{c}_{T//} / \overline{c}_{T\perp} \right)^2 - c^2 / \overline{c}_{T\perp}^2 \right)^{1/2}, \tag{10}$$

The linearized solution of the Love waves problem can be found immediately when the expressions for the displacements in the layer and in the half-space will become completed with boundary conditions at the interface $X_2 = 0$ $\hat{S}_{23} = \hat{\overline{S}}_{23}$, $u_3 = \overline{u}_3$ and at the free surface $X_2 = h$, $\hat{S}_{23} = 0$. The possible combination of solutions (9) and the boundary conditions determine the dispersion relation for Love waves (comp. [1])

$$\tan(kph) = \frac{\overline{\rho}_R \overline{c}_{T\perp}^2}{\rho_R c_{T\perp}^2} \frac{\overline{v}}{p} = \frac{\overline{\rho}_R \overline{c}_{T\perp} \overline{c}_{T//}}{\rho_R c_{T\perp} c_{T//}} \left(\frac{1 - c^2 / \overline{c}_{T//}^2}{c^2 / c_{T//}^2 - 1} \right)^{1/2}, \tag{11}$$

It is easy to see that in the case when the initial deformations vanish, the equation (11) is the same as in the linear theory.

The strain energy function $W = W(I_1, I_2)$ for many models of nonlinear elastic incompressible materials is independent on the second strain invariant I_2 of the deformation tensor i.e. $W = W(I_1)$, $W_2 = \overline{W}_2 = 0$ and the expressions for both propagation speeds (6) in the layer and in the half-space and also the dispersion relation (11) take the simple forms

$$c_T^2 = c_{T//}^2 = c_{T\perp}^2 = 2\breve{W}_1 \rho_R^{-1}, \qquad \overline{c}_T^2 = \overline{c}_{T//}^2 = \overline{c}_{T\perp}^2 = 2\breve{\overline{W}}_1 \overline{\rho}_R^{-1}, \tag{12}$$

$$\tan(khp) = \frac{1}{M} \frac{\overline{\rho}_R}{\rho_R} \left(\frac{M^{-2} - 1}{p^2} - 1 \right)^{1/2}, \tag{13}$$

where the function p has now the form $p^2 = c^2 / c_T^2 - 1$ and $M = c_T / \overline{c}_T$. The right hand side of (13) must be real, it should be also satisfied the condition known from the linear theory i. e. $c_T^2 < c^2 < \overline{c}_T^2$.

3. Yeoh constitutive model

The constitutive modeling of incompressible hyperelastic materials such as vulcanized rubbers, carbon filled reinforced rubber, polymers and human arterial wall tissues involves strain energy functions that depend on the first two invariants of the deformation tensor. The most well known of these is the Mooney-Rivlin model and its special form the neo-Hookean. In recent years, several constitutive models that capture the effects of limiting chain extensibility and crystallization have been proposed. The

Yeoh hyperelastic material is a cubic in I_1 and involves three material parameters. Conceptually, the strain energy function proposed by Yeoh is a material model with a shear modulus that varies with deformation and for this reason the proposed model is applicable over a wide range of strain. Assuming that $\partial W / \partial I_2 = 0$ and that $\partial W / \partial I_1$ is independent on I_2 we obtain now strain energy function (comp.[2])

$$W(I_1) = C_{10}(I_1 - 3) + C_{20}(I_1 - 3)^2 + C_{30}(I_1 - 3)^3 \quad , \tag{14}$$

which is cubic equation in $(I_1 - 3)$ and C_{10}, C_{20}, C_{30} are material parameters. The ratio $M = c_T / \overline{c}_T < 1$ (comp. (13)) of the propagation speeds of transverse waves is the basic variable parameter in our analysis. Assuming, that the half-space and overlying layer are filled with different Yeoh materials and for the assumed initial deformation (1) which is identical in both material regions we obtain the following condition for the parameter M

$$M = \frac{c_T}{\overline{c}_T} = m \left(\frac{1 + 2c_{20}c_{10}^{-1}(I_1 - 3) + 3c_{30}c_{10}^{-1}(I_1 - 3)^2}{1 + 2\overline{c}_{20}\overline{c}_{10}^{-1}(\overline{I}_1 - 3) + 3\overline{c}_{30}\overline{c}_{10}^{-1}(\overline{I}_1 - 3)^2} \right)^{1/2} < 1 \tag{15}$$

where $m = c_{0T} / \overline{c}_{0T} = ((c_{10}\rho_R^{-1})(\overline{c}_{10}\overline{\rho}_R^{-1}))^{1/2}$ and if $\lambda = 1$ then $M = m$.

4. Numerical analysis

The dispersion relation for Love waves (13) discussed in the previous section is now examined numerically. Some experimental results for three kinds of silicon rubber (soft, medium, hard) by utilizing Yeoh constitutive relation were presented in [3]. The greatest differences for the values of the ratio $M(\lambda)$ occur in the case when the layer of soft silicone rubber is supporting by the half-space made of hard silicone rubber ($m=0.629$) and only this case is presented on both figures below.

Table 1. Yeoh material parameters

Silicone rubber	C_{10} [MPa]	C_{20} [MPa]	C_{30} [MPa]
Soft	0.0231	- 0.0000314	0.000195
Medium	0.0335	- 0.0019100	0.000937
Hard	0.0583	- 0.0036600	0.001780

Three kinds of initial static deformation are considered:

a) $\lambda_1 = \lambda_3 = \lambda$, $\lambda_2 = \lambda^{-2}$, $I_1^a = 2\lambda^2 + \lambda^{-4}$

b) $\lambda_1 = \lambda_3 = \lambda^{-1/2}$, $\lambda_2 = \lambda$, $I_1^b = 2\lambda + \lambda^2$ $\tag{16}$

c) $\lambda_1 = 1$, $\lambda_3 = \lambda^{-1}$, $\lambda_2 = \lambda$, $I_1^c = 1 + \lambda^2 + \lambda^{-2}$.

Fig. 1 presents the ratios $M(\lambda)$ of the speeds of propagation as functions of the initial deformation parameter λ for three kinds of initial deformations (16). The function $M(\lambda)$ in every case has one local minimum $M_{min}(1) = m$ and two local maximums $M_{1,2\ max} > m$.

The dispersion equation for the value $m = 0.629$ and for deformations $(16)_{a,b}$ is solved graphically on Fig 2. The right hand side of (13) depends only on the ratio $M(\lambda)$ and on the density ratio. The solid lines on this Fig. 1 describe the function on the right hand side of (13) for two values of the deformation parameter $\lambda=2$ and $\lambda=0.5$ and for two kinds of initial deformations described with invariants I_1^a and I_1^b. The dropped line represents the solution known from the linear theory.
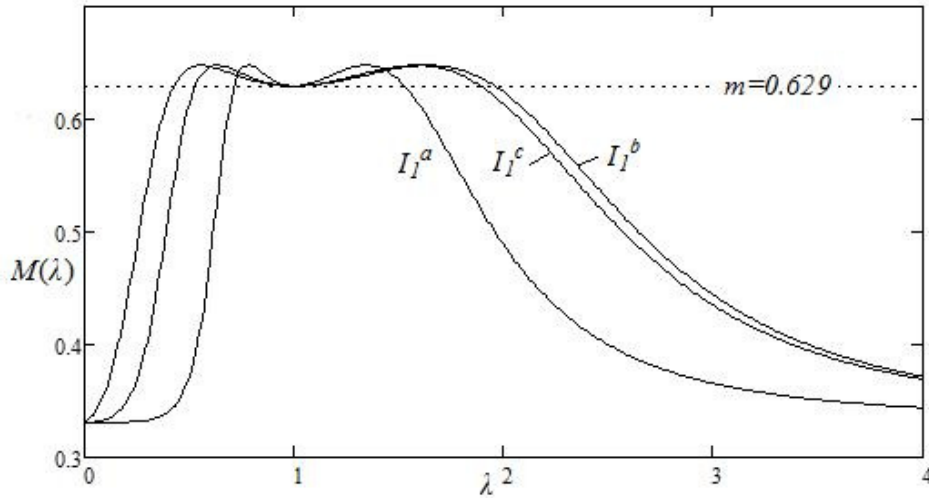
Figure 1. The speeds ratio M as function of the parameter λ

The branches of the function $\tan(khp)$ for the value $kh=1.76$ are described with hatches lines. The function of the right hand side of (13) takes the value zero for $p^* = \sqrt{M^{-2} - 1} > 0$. All coordinates $p_{(i)}$ of the points of intersection of this curve with the n branches of the function $\tan(1.76p) > 0$ belong to the interval $0 < p_{(i)} < p^*$. Assuming now that the wave number k can change and that the sequence of n values $p_{(i)}$ in the interval $(0, p^*)$ exists, then n particular modes of propagation of the waves in the layer to a given wave number are possible.
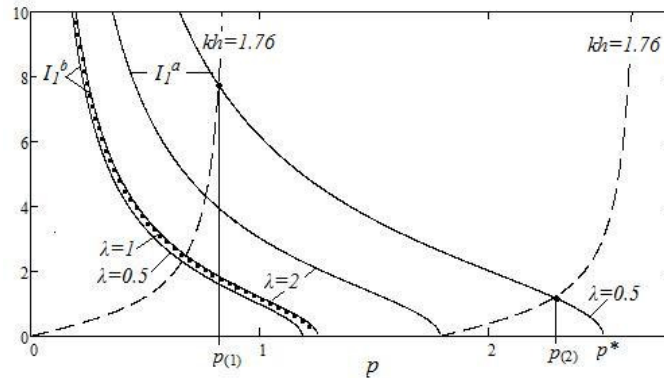
Figure 2. Solutions of the dispersion equation

There are intervals of the values of λ for which the graphs on Fig. 1 for I_1^a and I_1^b differ considerable and run away from $m = 0.629$. This means that the adequate functions on the right hand side of (13) for I_1^a diverge also remarkable in shapes and contrast with the standard shape for $\lambda = 1$. Opposite for the invariant I_1^b and the in same range of values of λ these functions deviate negligibly from the shape for $\lambda = 1$.

References

1. M. A. Dowaikh, *On SH waves in a pre-stressed layered half-space for an incompressible elastic material*, Mech. Res. Comm., **26**, (1999), 665-672.
2. O. H. Yeoh, *Characterization of elastic properties of carbon-black-filled rubber*, Rubber Chem. &Technol., **63**, (1990), 792-805.
3. T.V. Korochkina and all, *Experimental and numerical investigation into nonlinear deformation of silicone rubber pads during ink transfer process*, Polymer Testing, **27**, (2008), 778-791.

Fale Love'a we wstępnie odkształconym materiale Yeoha

W pracy rozpatrzono zlinearyzowane zagadnienie brzegowe dla fal Love'a. Założono, że półprzestrzeń sprężysta i spoczywająca na niej cienka warstwa o grubości h wykonane są z różnych materiałów Yeoha i poddane są jednorodnej statycznej deformacji wstępnej, identycznej w obu obszarach. Dla materiału Yeoha funkcja energii odkształcenia W zależy jedynie od pierwszego niezmiennika tensora deformacji tj. $W = W(I_1)$. Ta szczególna zależność może powodować w zależności od typu deformacji wstępnej występowanie dużych lub nieistotnych różnic jakościowych między liniowym i zlinearyzowanym podejściem do propagacji fal Love'a w nieściśliwych materiałach sprężystych

Built-in implementation of some boundary conditions for vibrating systems in the SDQ method

Artur KROWIAK

Cracow University of Technology, Institute of Computing Science
Al. Jana Pawła II 37, 31-864 Kraków, Poland
krowiak@mech.pk.edu.pl

Abstract

The paper presents an efficient way of the application of the spline-based differential quadrature method for solving equations of chosen vibrating systems. The efficiency relies on the implementation of some types of boundary conditions at the stage of the determination of weighting coefficients that approximate the derivatives in the governing equation. The weights determined in such a way contain information about the boundary conditions and the discretization of these conditions is not further carried out. In the paper, the spline interpolation applied to differential quadrature method as well as the procedure for the determination of the weighting coefficients with built-in boundary conditions are described. The accuracy and the convergence of the approach is studied on the example of the free vibration of the conical shell.

Keywords: spline interpolation, differential quadrature, free vibration analysis, conical shells

1. Introduction

Many works [1] that use the differential quadrature method (DQM) to solve problems with computational mechanics have been appeared in recent years. The increase of interest in the method is caused by its simple formulation, high rate of convergence and high accuracy. These advantages follows from the way of the approximation of the solution. The solution is approximated by the interpolation polynomial which uses all the nodes from the entire domain with respect to appropriate coordinate. On this basis the weighting coefficients that approximate spatial derivatives are determined. Using these coefficients the differential equation is reduced to the system of algebraic equations. This system is completed by the equations arising from boundary conditions.

This approach allows to obtain very accurate results using few sampling points, however DQM has some limitations. Due to its formulation the method requires a regular node distribution and therefore it cannot be easily applied to problems with irregular domains. Further, the method is sensitive to the number of nodes, distribution pattern and in some applications shows computational instability. To overcome some of mentioned drawbacks, the spline interpolation has been used to approximate the solution [2]. The method is referred to spline-based differential quadrature (SDQM) or symbolic spline-based differential quadrature. The SDQM has been successfully applied to chosen problems of linear and nonlinear mechanics [2,3]. It turns out that the idea presented in [2] allows to introduce some types of boundary conditions at the stage when the weighting coefficients for derivatives appearing in the equation are determined. This approach facilitates the discretization of boundary-value problem. The details are

presented in section 3, while the practical application is shown on the example of free vibration of conical shell demonstrated in section 4.

2. Spline-based differential quadrature method

The idea of the DQM relies on the approximation of the derivatives in the governing equation by the linear weighted sum of unknown function values from entire domain, what can be put as

$$\frac{d^r f(x)}{dx^r}\Big|_{x=x_i} = \sum_{j=1}^{N} a_j^{(r)}(x_i)f(x_j) = \sum_{j=1}^{N} a_{ij}^{(r)}f_j \quad i=1,...,N \tag{1}$$

where N denotes the number of grid points and $a_{ij}^{(r)}$ are the weighting coefficients for the rth order derivative. The key stage of the method is to determine these weights. The values of $a_{ij}^{(r)}$ depend on the approximation of the sought function $f(x)$ and influence the accuracy, convergence and stability of the method.

According to [2], the function $f(x)$ is approximated using spline interpolation. If spline degree is assumed to be odd then the interpolation has the form

$$f(x) \approx \left\{ s_i(x), \ x \in [x_i, x_{i+1}], \ i=1,..,N-1 \right\} \tag{2}$$

where the ith spline section is defined as n degree polynomial

$$s_i(x) = \sum_{j=0}^{n} c_{ij}x^j \tag{3}$$

The coefficients c_{ij} in Eq. (3) are determined from the interpolation conditions, the derivative continuity conditions and the so-called natural end conditions [2]. Since the latter are important for further studies they are listed below

$$s_1^{(k)}(x_1) = 0, \ s_{N-1}^{(k)}(x_N) = 0, \ k = \frac{n+1}{2},..,n-1 \tag{4}$$

The unknown function values f_i in the interpolation conditions are marked by symbols. With the aid of symbolic-numeric computations the coefficients c_{ij} can be obtained. They depend on nodes distribution and unknown function values, what can be generally written as

$$c_{ij} = \sum_{k=1}^{N} C_{ijk}(x_1,...,x_N)f_k, \quad i=1,...,N-1, j=0,...,n \tag{5}$$

Using the values of (5) in Eq. (3) and calculating appropriate derivatives of polynomial piecewise function (2) at the nodes, one can determine the weighting coefficients $a_{ij}^{(r)}$ by separating the numbers standing next to appropriate symbols f_i. The weighting coefficients are described by the following formulas

$$a_{ik}^{(r)} = \sum_{j=r}^{n}\left(C_{ijk}\, x_i^{j-r} \prod_{l=j-r+1}^{j} l \right), \quad i=1,...,N-1, \ a_{Nk}^{(r)} = \sum_{j=r}^{n}\left(C_{N-1jk}\, x_N^{j-r} \prod_{l=j-r+1}^{j} l \right) \tag{6}$$

If the spline degree is assumed to be even the auxiliary knots are imposed in order to meet conditions for the spline interpolation and the further procedure for determining the weighting coefficients is similar. The details are described in [2].

3. Implementation of boundary conditions in SDQM

General way to introduce derivative boundary conditions in the DQM is based on the discretization of these conditions using rules of the method. The obtained equations are used to calculate function values at the boundary points. In higher order equation, when more than one condition is defined at a boundary, remaining conditions are used to determine function values at the points adjacent to the boundary. This approach is described in [4] and is referred to the general approach. It has been also applied in the SDQM [2].

It turns out that in the SDQM some types of derivative boundary conditions can be introduce during computing the weighting coefficients. To this end a part of natural end conditions (4) is replaced with these boundary conditions. For the sake of one-dimensional approximation of the sought function in the method, such boundary conditions have to fulfill some criterions. They have to be homogeneous with respect to the considered function and should contain derivatives with respect to only one independent variable. It means that the boundary conditions should have the general form

$$G\{f(x)\}_{|x=x_b} = 0 \qquad (7)$$

where G is linear differential operator of the form $G = \sum_{r=0}^{R-1} b_r \dfrac{d^r}{dx^r}$, imposed on the function at a boundary point $x = x_b$, where, in turn R denotes the order of the governing equation and b_r are the constant coefficients but one at least of these coefficients for $r > 0$ must not be equal zero.

Assuming that N_B^L is the number of the boundary conditions in the form of (7), imposed at one edge and N_B^R is their number at the other edge, the modified end conditions (4) take the form

$$\sum_{r=0}^{R-1} b_r^{(i)} s_1^{(r)}(x_1) = 0, \quad i = 1,..,N_B^L, \quad s_1^{(k)}(x_1) = 0, \ k = \frac{n+1}{2} + N_B^L,..,n-1 \qquad (8a)$$

$$\sum_{r=0}^{R-1} \overline{b}_r^{(i)} s_{N-1}^{(r)}(x_N) = 0, \quad i = 1,..,N_B^R, \quad s_{N-1}^{(k)}(x_N) = 0, \ k = \frac{n+1}{2} + N_B^R,..,n-1 \qquad (8b)$$

where $b_r^{(i)}$ and $\overline{b}_r^{(i)}$ denote the constants standing next to appropriate derivatives at the ith boundary condition defined at one and the opposite edge, respectively.

Using the algorithm described in previous section, where Eqs. (8a) and (8b) are used instead of Eq. (4), one obtains weights $a_{ij}^{(r)}$ with the built-in boundary conditions. Further discretization of boundary-value problem is carried out without these conditions,

what facilitates the discretization procedure and sometimes reduces it to discretizing governing equation only.

The presented idea is shown on the example of free vibration of isotropic conical shell.

4. Free vibration of the truncated conical shell

Conical shells are construction elements that are widely used in civil, mechanical and aeronautical engineering. Therefore the free vibration analysis of these elements has been the subject of many works, e.g. [5,6]. To solve this problem several approximate methods have been used. Among them the DQM has been also applied [5]. In the present work, the method described in previous sections is used to solve free vibration problem of thin, truncated conical shell. The aim of the work is to examine the possibility of using the presented approach in the application to this construction elements and some boundary conditions encountered in the problem. The special attention is focused on the accuracy and the rate of convergence of the method.

In Fig. 1 the analyzed conical shell with the reference coordinate system (x, θ, z) and the components of the displacement field in appropriate directions (u, v, w) are shown.
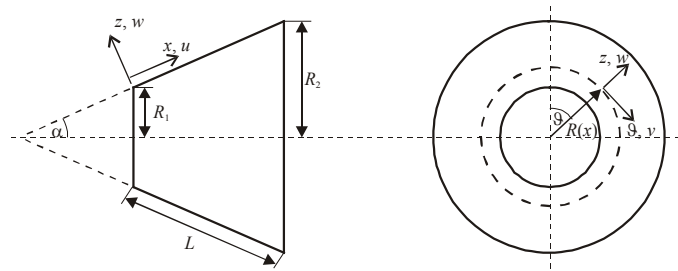
Figure 1. Geometry of truncated conical shell

General relations for displacements in the case of free vibration of the system are assumed as [5]

$$u = U(x)\cos(m\theta)\cos(\omega t), \ v = V(x)\sin(m\theta)\cos(\omega t), \ w = W(x)\cos(m\theta)\cos(\omega t) \quad (9)$$

where m is the wave number in the circumferential direction and ω is the circular frequency.

Thus, the equation of motion based on Love's first approximation theory can be written as

$$\begin{bmatrix} L_{11} & L_{12} & L_{13} \\ L_{21} & L_{22} & L_{23} \\ L_{31} & L_{32} & L_{33} \end{bmatrix} \begin{bmatrix} U \\ V \\ W \end{bmatrix} = -\rho h \omega^2 \begin{bmatrix} U \\ V \\ W \end{bmatrix} \quad (10)$$

where L_{ij} are differential operators, e.g.

$$L_{11} = A_{11}\frac{d^2}{dx^2} + \frac{A_{11}\sin(\alpha)}{R}\frac{d}{dx} - \frac{A_{22}\sin^2(\alpha)+A_{66}m^2}{R^2}$$, that contain the extensional (A_{ij})

and bending (D_{ij}) stiffnesses. The details can be found in [5].

For the isotropic conical shell the boundary conditions are given by the formulas

$$V = 0,\ W = 0,\ \frac{A_{12}\sin(\alpha)}{R}U + A_{11}U^{(1)} = 0,\ \frac{D_{12}\sin(\alpha)}{R}W^{(1)} + A_{11}W^{(2)} = 0 \qquad (11)$$

for simply supported edge and

$$U = 0,\ V = 0,\ W = 0,\ W^{(1)} = 0 \qquad (12)$$

for clamped edge.

Derivative conditions in (11) or (12) fulfill the requirements described in section 3, what allows to introduce this conditions during determining the weighting coefficients. For example, when both edges of the shell are simply supported, Eqs. (8a) and (8b), written for function U, take the form

$$\frac{A_{12}\sin(\alpha)}{R_1}s_1(x_1) + A_{11}s_1^{(1)}(x_1) = 0,\ s_1^{(k)}(x_1) = 0,\ k = \frac{n+1}{2}+1,..,n-1 \qquad (13a)$$

$$\frac{A_{12}\sin(\alpha)}{R_2}s_{N-1}(x_N) + A_{11}s_{N-1}^{(1)}(x_N) = 0,\ s_{N-1}^{(k)}(x_N) = 0,\ k = \frac{n+1}{2}+1,..,n-1 \qquad (13b)$$

Similarly the derivative conditions for function W are implemented and appropriate weights are determined. As a result Eq. (10) is reduced to algebraic eigenvalue problem in the following form

$$\begin{bmatrix} \mathbf{P}_{11} & \mathbf{P}_{12} & \mathbf{P}_{13} \\ \mathbf{P}_{21} & \mathbf{P}_{22} & \mathbf{P}_{23} \\ \mathbf{P}_{31} & \mathbf{P}_{32} & \mathbf{P}_{33} \end{bmatrix}\begin{bmatrix} \mathbf{U} \\ \mathbf{V} \\ \mathbf{W} \end{bmatrix} = -\rho h\omega^2\begin{bmatrix} \mathbf{U} \\ \mathbf{V} \\ \mathbf{W} \end{bmatrix} \qquad (14)$$

where e.g. elements of matrix $\mathbf{P}_{11}$ are as follows

$$P_{11_{ij}} = A_{11}a_{u\,ij}^{(2)} + \frac{A_{11}\sin(\alpha)}{R}a_{u\,ij}^{(1)} - \frac{A_{22}\sin^2(\alpha)+A_{66}m^2}{R^2},\ i,j = 1,...,N,\ a_{u\,ij}^{(r)}$$ denote the

weighting coefficients for rth order derivative of function U. Vectors $\mathbf{U}$, $\mathbf{V}$, $\mathbf{W}$ contain node function values. The system (14) is modified by deleting appropriate rows and columns in order to meet remaining boundary conditions. The solution of eigenproblem (14) is displayed in Table 1 by the non-dimensional frequency parameter $\lambda = R_2\omega\sqrt{\rho h / A_{11}}$. The computations are carried out using several numbers of nodes N, assuming $n = 9$ spline degree. For the comparison, the table contains also results obtained with the use of general approach to implement boundary conditions as well as the results from another work.

The results show that the presented method leads to rapid convergence. Great accuracy is achieved using fewer nodes than for the general approach.

5. Conclusions

The paper shows the possibility of the implementation of some boundary conditions at the stage of the determination of the weighting coefficients in the SDQM. The approach has been tested in the vibration analysis of the conical shell. The results show that the method has higher rate of convergence and higher accuracy comparing with the general approach in implementation of boundary conditions. Furthermore, due to the buit-in method, the discretization procedure is simplified.

Table 1. Frequency parameter λ for axisymmetric vibration ($m = 0$) of conical shell
(h/R_2=0.01, ν=0.3, α=60°, $L\sin(\alpha)/R_2 = 0.25$)

	simply supported at both edges		simply supported R_1 and clamped R_2	
	built-in approach	general approach	built-in approach	general approach
$N = 7$	0.3630	0.3858	0.7853	0.7674
$N = 10$	0.3629	0.3721	0.7853	0.7798
$N = 13$	0.3628	0.3671	0.7853	0.7831
$N = 16$	0.3628	0.3651	0.7853	0.7842
[5]	0.3628		0.7853	

References

1. C.W. Bert, M. Malik, *Differential quadrature method in computational mechanics*, Applied Mechanics Review, **49** (1996) 1-28.

2. A. Krowiak, *Symbolic computing in spline-based differential quadrature method*, Commun. Numer. Meth. Engng, **22** (2006) 1097-1107.

3. A. Krowiak, *The application of the differential quadrature method based on a piecewise polynomial to the vibration analysis of geometrically nonlinear beams,* Comp. Assisted Mech. Eng. Sci., **15** (2008) 1-13.

4. C. Shu, H. Du, *A generalized approach for implementing general boundary conditions in the GDQ free vibration analysis of plates*, Int. J. Solids Structures, **34** (1997) 837-846.

5. C. Shu, *An efficien approach for free vibration analysis of conical shells*, Int. J. Mech. Sci., **38** (1996) 935-949.

6. T. Irie, G. Yamada, Y. Kaneko, *Natural frequencies of truncated conical shells*, J. Sound Vib., 92 (1984) 447-453.

Wbudowany sposób wprowadzenia pewnych warunków brzegowych dla układów drgających w metodzie SDQ

W pracy przedstawiono efektywny sposób użycia metody kwadratur różniczkowych opartej na funkcjach sklejanych do rozwiązywania równań opisujących drgania wybranych układów. Wspomniana efektywność polega na wprowadzeniu niektórych typów warunków brzegowych na etapie wyznaczania współczynników wagowych, które przybliżają pochodne funkcji w równaniu. Wagi wyznaczone w ten sposób zawierają informacje o warunkach brzegowych i warunki te nie są brane pod uwagę w dalszej części procesu dyskretyzacji zagadnienia. W pracy przedstawiono zastosowanie interpolacji typu spline w metodzie kwadratur różniczkowych, jak również sposób wyznaczania współczynników wagowych z wbudowanymi warunkami brzegowymi. Dokładność i zbieżność metody zbadano na przykładzie drgań własnych powłoki stożkowej.

A Wobblestone Modelling with Coupled Model of Sliding Friction and Rolling Resistance

Grzegorz KUDRA

Department of Automation and Biomechanics, Technical University of Lodz
1/15 Stefanowski St., 90-924 Łódź, Poland
grekudra@p.lodz.pl

Jan AWREJCEWICZ

Department of Automation and Biomechanics, Technical University of Lodz
1/15 Stefanowski St., 90-924 Łódź, Poland
awrejcew@p.lodz.pl

Abstract

A wobblestone also known as the Celtic stone or rattleback is usually a semi-ellipsoidal solid with the special asymmetry in the mass distribution. For most celts, when it lays on a flat horizontal surface, it rotates around its horizontal axis in a preferred direction, i.e. if it spins in the opposite direction, it becomes unstable, and reverses its spin to the preferred direction. In this paper we try to model wobblestone as realistically as possible taking into account the frictional coupling between the translational and rotational motion of the contact patch and the rolling resistance as well but with simplifying assumption of circular contact patch. The Coulomb-Contensou-Zhuravlev model of friction is used with the use of the first order Padé approximants.

Keywords: wobblestone, celt, friction modelling, rolling resistance, Coulomb-Contensou friction model, Padé approximation.

1. Introduction

Since the times of ancient culture of Celts there is known some kind of solid (stone) which exhibits (seemingly) curious dynamic behaviour. The Celtic stone also known as wobblestone or rattleback is usually a semi-ellipsoidal solid (or a other kind of body with smoothly curved oblong lower surface) with the special mass distribution. Most celts lied on a flat horizontal surface and set in rotational motion about the vertical axis can rotate in only one direction. The imposition of an initial spin in the opposite direction leads to transverse wobbling and then to spinning in the "preferred" direction. The Celtic stone with its special dynamical properties was an object of investigation of many researchers and the first scientific publication on this subject appeared in the end of the 19th century [1].

One of the widely used assumptions in modelling of the celt is that of dissipation-free rolling without slip [1-4]. In the work [1] the non-coincidence of the principal axes of inertia and the principal directions of curvature at the equilibrium contact point was pointed out as essential in explanation of the wobblestone properties.

In work [5] an attempt of analysis of the linearized equations of the model assuming continuous slipping (quasi-viscous relation between the friction force and the velocity of the contact point) is performed. Another model taking into account dissipation but being far from reality is analyzed by the use of asymptotic perturbation theory [6]. The model

assuming rolling without slip and viscous damping (torque about all three axes) is proposed in paper [7]. More realistic modelling with aerodynamic dissipation and slip with dry friction force, with addition of experimental validation of the model are presented in work [8]. In the other paper [9] the perturbation analysis of local dynamics around the equilibrium points of the model assuming absence of friction as well as the experimental verification are performed. The closest to reality modelling of the celt is proposed in work [10], where the possibility of the slip is assumed, but in contrast to all the earlier works, the Coulomb-Contensou-Zhuravlev (CCZ) friction model is applied, that is the frictional coupling between the translational and rotational motion of the contact patch is taken into account. However, since the friction force is the only way of dissipation in the proposed model, the time of the wobblestone motion (until rest) is unrealistically long.

In the present work we extend the model [10] by adding the rolling resistance as well as the friction torque. The coupled model of sliding and rolling friction proposed in the work [11] is applied to the celt with simplifying assumption of circular contact patch between bodies. Additionally a constant radius of the contact area is assumed. We also propose the method of smoothing the governing equations, allowing to avoid numerical problems.

2. Celt modelling and numerical example

The wobblestone as a semi-ellipsoid rigid body with the mass centre at the point C, touching a rigid, flat and immovable horizontal surface π (parallel to the XY plane of the global immovable co-ordinate system $X_1 X_2 X_3$) at point A is presented in Fig. 1.
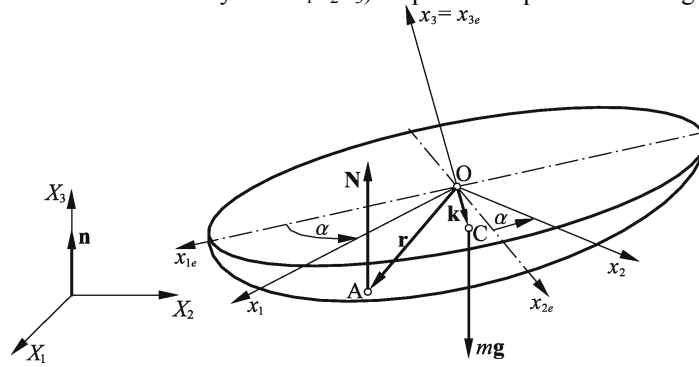
Figure 1. The wobblestone on a horizontal plane π.

The equations of motion in the movable co-ordinate system $0x_1 x_2 x_3$ (with axes parallel to the central principal axes of inertia – we assume that geometrical axis x_{3e} of the ellipsoid is parallel to one of them) are as follows

$$m\frac{d\mathbf{v}}{dt} + \boldsymbol{\omega} \times (m\mathbf{v}) = -mg\mathbf{n} + N\mathbf{n} + \mathbf{T},$$

$$\mathbf{B}\frac{d\boldsymbol{\omega}}{dt}+\boldsymbol{\omega}\times(\mathbf{B}\mathbf{v})=(\mathbf{r}-\mathbf{k})\times(N\mathbf{n}+\mathbf{T})+\mathbf{M}_t+\mathbf{M}_r\,, \tag{1}$$

$$\frac{d\mathbf{n}}{dt}+\boldsymbol{\omega}\times\mathbf{n}=0\,,$$

where m is the mass of the celt, $\mathbf{B}=\mathrm{diag}(B_1,B_2,B_3)$ is the tensor of inertia of the solid, $\mathbf{v}$ is the absolute velocity of the mass centre C, $\boldsymbol{\omega}$ is the absolute angular velocity of the body, N is the value of the normal reaction of the horizontal plane, $\mathbf{n}$ is the unit vector normal to the plane XY, $\mathbf{T}$ (ignored in Fig. 1) is the sliding friction force in the point of contact A, $\mathbf{M}_t$ and $\mathbf{M}_r$ (ignored in Fig. 1) are the dry friction and the rolling resistance torques applied to the body respectively. Vector $\mathbf{r}$ indicates the actual contact point position and the vector $\mathbf{k}$ determines the mass centre position.

The reaction of the horizontal plane due to the dry friction and the rolling resistance is given by

$$\mathbf{T}=\mathbf{T}_0+\mathbf{T}_{r\pi}+\mathbf{T}_{r\beta}\,,$$

$$\mathbf{M}_t=-\mu\rho N\frac{3\pi}{16}\frac{\boldsymbol{\omega}\cdot\mathbf{n}-k_r\dfrac{|\mathbf{v}_A|}{\rho}s_\beta}{\dfrac{15\pi}{16}\dfrac{|\mathbf{v}_A|}{\rho}+|\boldsymbol{\omega}\cdot\mathbf{n}|+\varepsilon}\mathbf{n}\,, \tag{2}$$

$$\mathbf{M}_r=-\frac{f_r N\boldsymbol{\omega}_\pi}{|\boldsymbol{\omega}_\pi|+\varepsilon}\,,$$

where

$$\mathbf{T}_0=-\mu N\frac{\dfrac{\mathbf{v}_A}{\rho}}{\dfrac{|\mathbf{v}_A|}{\rho}+\dfrac{8}{3\pi}|\boldsymbol{\omega}\cdot\mathbf{n}|+\varepsilon}\,,$$

$$\mathbf{T}_{r\beta}=\left(T_{r\parallel}c_\beta+T_{r\perp}s_\beta\right)\frac{\boldsymbol{\omega}_\beta}{|\boldsymbol{\omega}_\beta|+\varepsilon}\,,\quad \mathbf{T}_{r\pi}=\left(-T_{r\parallel}s_\beta+T_{r\perp}s_\beta\right)\frac{\boldsymbol{\omega}_\pi}{|\boldsymbol{\omega}_\pi|+\varepsilon}\,,$$

$$T_{r\parallel}=\frac{1}{4}\mu N\frac{\boldsymbol{\omega}\cdot\mathbf{n}\,k_r s_\beta}{\dfrac{|\mathbf{v}_A|}{\rho}+\dfrac{8}{3\pi}|\boldsymbol{\omega}\cdot\mathbf{n}|+\varepsilon}\,,\quad T_{r\perp}=-\frac{1}{5}\mu N\frac{\boldsymbol{\omega}\cdot\mathbf{n}\,k_r c_\beta}{\dfrac{|\mathbf{v}_A|}{\rho}+\dfrac{32}{15\pi}|\boldsymbol{\omega}\cdot\mathbf{n}|+\varepsilon}\,,$$

where μ is the dry friction coefficient, ρ is the radius of the contact patch (with simplifying assumption of the constant-size circular contact patch between bodies), $f_r=\rho k_r/5$ is the rolling resistance coefficient (where $0\le k_r\le1$ is the coefficient describing the asymmetry in the normal stress distribution due to the rolling resistance), $\mathbf{v}_A$ is the velocity of the body point being in contact with the horizontal surface, $\boldsymbol{\omega}_0$ is the component of angular velocity parallel to the X_3 axis, $\boldsymbol{\omega}_\pi$ is the component of angular velocity lying in the π plane, $\boldsymbol{\omega}_\beta$ is the vector lying in the π plane of the same length as

$\boldsymbol{\omega}_\pi$ but perpendicular to $\boldsymbol{\omega}_\pi$, c_β and s_β are approximated sine and cosine functions of the angle β (angle between the sliding and rolling direction):

$$\mathbf{v}_A = \mathbf{v} + \boldsymbol{\omega} \times (\mathbf{r} - \mathbf{k}) \ , \boldsymbol{\omega}_0 = (\boldsymbol{\omega} \cdot \mathbf{n})\mathbf{n} , \ \boldsymbol{\omega}_\pi = \boldsymbol{\omega} - \boldsymbol{\omega}_0 , \ \boldsymbol{\omega}_\beta = \boldsymbol{\omega}_\pi \times \mathbf{n} , \tag{3}$$

$$c_\beta = \frac{v_\beta}{\sqrt{v_\beta^2 + v_\pi^2}} , \ s_\beta = \frac{v_\pi}{\sqrt{v_\beta^2 + v_\pi^2}} , v_\beta = \frac{\mathbf{v}_A}{\rho} \cdot \boldsymbol{\omega}_\beta + \varepsilon \ , v_\pi = -\frac{\mathbf{v}_A}{\rho} \cdot \boldsymbol{\omega}_\pi .$$

The **T** and $\mathbf{M}_t$ vectors in Eqs (2) follow the CCZ friction model with assumption of normal stresses (in the contact domain) satisfying the Hertz law and applying the Padé approximation in calculating some kind of integrals [11]. The $\mathbf{M}_r$ vector is constructed with assumption that the rolling resistance torque opposes the angular velocity component lying in the π plane (it is equivalent to assumption of rigid π plane and deformable wobblestone). The parameter ε is introduced in order to smooth the equations and avoid numerical problems around some singularities.

The differential equations of motion (1) are supplemented with the following algebraic equation

$$(\mathbf{v} + \boldsymbol{\omega} \times (\mathbf{r} - \mathbf{k})) \cdot \mathbf{n} = 0 , \tag{4}$$

which follows the fact that the velocity $\mathbf{v}_A$ lies in the plane π. Equations (1) and (3) form now the differential-algebraic equation set. One way to solve them is to differentiate the condition (3) with respect to time and then treat it as an additional equation during solving the governing equations algebraically with respect to the corresponding derivatives and the normal reaction N.

To complete the model the relation between the vectors **r** and **n** should be given. Taking the ellipsoid equation

$$\frac{r_{1e}^2}{a^2} + \frac{r_{2e}^2}{b^2} + \frac{r_{3e}^2}{c^2} = 1 , , \tag{5}$$

(where a, b and c are the semi-axes of the ellipsoid) and the condition of tangent contact between the ellipsoid and the horizontal plane

$$n_{1e} = \frac{\lambda r_{1e}}{a^2} , \ n_{2e} = \frac{\lambda r_{2e}}{b^2} , \ n_{3e} = \frac{\lambda r_{3e}}{c^2} , \tag{6}$$

we can find the relation between the components of vectors **r** and **n** in the $0x_{1e}x_{2e}x_{3e}$ co-ordinate system. Since the $0x_1x_2x_3$ co-ordinate system is obtained by rotation of the $0x_{1e}x_{2e}x_{3e}$ system around the x_{3e} axis by the angle α, the corresponding relation in the $0x_1x_2x_3$ co-ordinate system can be found easily.

The results presented in Figs 2-3 correspond to the typical behaviour of the celt and have been obtained for the following parameters and initial conditions: $m = 0.25$ kg, $g = 10$ m/s^2, $\alpha = \ \square\ 0.3$ rad, $B_1 = 10^{-4}$ kg·m^2, $B_2 = 8 \cdot 10^{-4}$ kg·m^2, $B_3 = 10^{-3}$ kg·m^2, $a = 0.08$ m, $b = 0.016$ m, $c = 0.012$ m, $k_1 = k_2 = 0$, $k_3 = \ \square\ 0.002$ m, $\mu = 0.5$, $\rho = 6 \cdot 10^{-4}$ m, $k_r = 1$, $\varepsilon = 10^{-3}$ rad/s, $v_{10} = v_{20} = v_{30} = 0$ m/s, $n_{10} = n_{20} = 0$, $n_{30} = 1$.
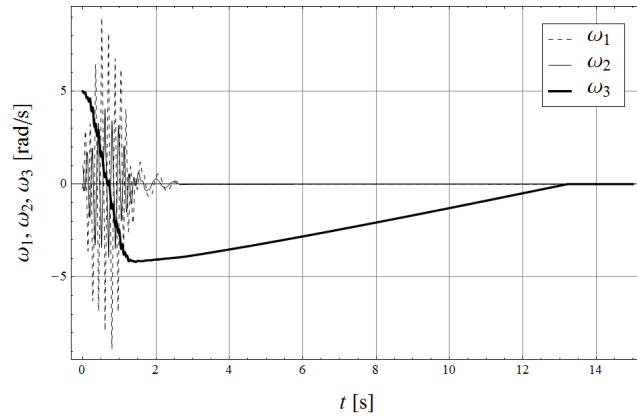
Figure 2. The wobblestone response with initial conditions $\omega_{10}=0$, $\omega_{20}=1$, $\omega_{30}=5$ (rad/s).
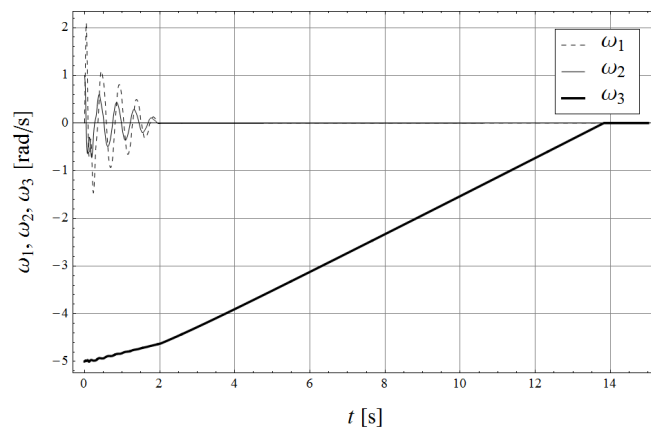
Figure 3. The wobblestone response with initial conditions $\omega_{10}=0$, $\omega_{20}=1$, $\omega_{30}=-5$ (rad/s).

4. Concluding remarks

In the paper the extension of the model introduced in the work [10] is proposed. Both presented model and its simulations are very realistic, when compared with most earlier works on the celt, since the correct friction models for both the translational and rotational motion of the contact patch as well as the rolling resistance torque have been taken into account. The most significant simplification assumed in the presented modeling is probably that of circular constant-radius contact patch between bodies.

More systematic research of the presented model of the celt is required as well as the careful experimental validation of the model should be performed. The proposed smoothing of the governing equations should be treated as temporary and substitute

method of avoiding numerical problems, but certain extension of the model should be made in order to join different modes of dynamics (for example stick and slip). In the next future we are also going to extend presented modeling to elliptical shapes of the contact patch.

Acknowledgments

References

1. G.T. Walker, *On a dynamical top.* Q. J. Pure App. Math., **28** (1896) 175-184.
2. Sir Hermann Bondi, *The rigid body dynamics of unidirectional spin*. Proc. Roy. Soc. Lond., **A 405** (1986) 265-279.
3. R.E. Lindberg, R.W. Longman, *On the dynamic behavior of the wobblestone*. Acta Mechanica, **49** (1983) 81-94.
4. A.V. Borisov, A.A. Kilin, I.S. Mamaev, *New effects of rattlebacks*. Doklady Physics, **51(5)** (2006) 272-275.
5. K. Magnus, *Zur Theorie der keltischen Wackelsteine*. Zeitschrift für Angewandte Mathematik und Mechanik, **5** (1974) 54-55.
6. T.K. Caughey, *A mathematical model of the rattleback*. Int. J. Non-linear Mechanics, **15** (1980) 293-302.
7. T.R. Kane, D.A. Levinson, *Realistic mathematical modeling of a rattleback*. Int. J. Non-linear Mech. **17** (1982) 175-186.
8. Garcia, M. Hubbard, *Spin reversal of the rattleback: theory and experiment*. Proc. Roy. Soc. Lond. **A 418** (1988) 165-197.
9. A.P. Markeev, *On the dynamics of a solid on an absolutely rough plane*. Regular and Chaotic Dynamics, **7(2)** (2002) 153-160.
10. V.Ph. Zhuravlev, D.M. Klimov, *Global motion of the celt*. Mechanics of Solids, **43(3)** (2008) 320-327.
11. A. A. Kireenkov, *Combined model of sliding and rolling friction in dynamics of bodies on a rough surface,* Mechanics of Solids **43(3)** (2008) 116-131.

Modelowanie dynamiki kamienia celtyckiego ze sprzężonym modelem tarcia poślizgowego i oporu toczenia

Kamień celtycki jest przedmiotem o kształcie zazwyczaj zbliżonym do półelipsoidy ze specjalnym asymetrycznym rozkładem masy. Położony na poziomej płaszczyźnie łatwo może zostać wprawiony w ruch obrotowy dokoła swojej pionowej osi w jedną, ściśle określoną stronę. Wprawiony w ruch obrotowy w przeciwną stronę staje się niestabilny, wpada w poprzeczne drgania i zmienia zwrot obrotu na przeciwny. W pracy podjęta została próba modelowania dynamiki kamienia celtyckiego w sposób możliwie najbardziej realistyczny ze szczególnym uwzględnieniem modelu tarcia, gdzie uwzględniono sprzężenie cierne pomiędzy ruchem postępowym i obrotowym obszary styku ciał oraz oporem toczenia. Przyjęto założenie upraszczające kołowego obszaru styku o stałym w czasie promieniu pomiędzy kamieniem i podłożem oraz zastosowano model tarcia CZZ z aproksymacją Padé'go pierwszego rzędu.

The meaning of the piezoelectric and streaming potential in bone remodeling

Łukasz LECH

AGH University of Science and Technology, Mickiewicz 30 av, 30-059 Cracow
llech@agh.edu.pl

Marek IWANIEC

AGH University of Science and Technology, Mickiewicz 30 av, 30-059 Cracow
iwaniec@agh.edu.pl

Abstract

In this paper authors include the most important information about piezoelectric effect and streaming potential occurring in bone. In their opinion these phenomena play important role during bone remodeling, so that model binding them together was proposed. Model describes mechanisms responsible for "sensing" by osteocytes local changes in stresses and strains and for signal transmissions from sensors to effectors i.e. osteoblasts.

Keywords: bone remodelling; piezoelectric effect in bone; streaming potential in bone

1. Introduction

These days one can notice very fast technological progress, which to a large extent, facilitates the   development of a wide range disciplines of science. In bioengineering, which is quite relatively young field of science, this rapid progress is exceptionally noticeable. Scientists and engineers have possibilities to use reach selection of tools and methods in order to improve already existing solutions or to invent other. However, lots of phenomena that occur in human organism have not been yet recognized. Those hinder and in certain cases prevent the process of modeling the mechanisms that regulate human body functions. For example a remodeling of bone structure, that actuates when bone experiences stresses and strains. Implantation brings changes to a stress and strain distribution, which accordingly entails the necessity of adjustment to diversified conditions of load applied along with the stress distribution. Therefore, a suitable theory describing bone remodeling with respect to phenomena occurring during this process is crucial**.** Otherwise, the process of designing an appropriate shape and properties implant, of which load actions are transmitted similarly to a healthy bone, becomes complex. Previous theories do not bring a full explanation to that mechanism and many questions remain unanswered e.g. how does bone "sense" different types of stress such as bending, compression or torsion. Authors of the following work introduce the approach, according to which mechanisms responsible for bone remodeling can be explained.

2. Piezoelectric effect inducing in bone.

Fukada and Yasuda, who in 1957 published the results of their investigations in the article titled: "*On the piezoelectric effect of bone*" are treated as the discoverers of the

piezoelectric effect occurring in bone. They demonstrated that in a dry bone under the proper load applied, charges are induced on the surface of a sample. Basset and Becker continued their research and in 1962 claimed that charges inducing on the surface of the specimen during bending are proportional to stresses produced [9]. They stuck when returning to its normal shape. Moreover, they showed that the polarization sign is dependent on the type of stresses produced, i.e. negative in case of compression charges generated on the surfaces and positive in case of tension.

In 1964 Becker proposed a theory that nature of piezoelectric effects induced in bone does not resemble a classic piezoelectric effect [8]. He claimed that bone is a double-element consisting of hydroxyapatite crystals and highly directional collagen fibrils. According to Becker it was similar to P-N junction known from semiconductors and used in diodes. In subsequent researches he demonstrated that bone has such properties as e.g. photoconductivity, thus he could claim that apatite-collagen junction has properties of semiconducting diode.

Becker theory was questioned by Shamos, who declared that he was unable to observe photoconductivity in bone [7]. The hypothesis he propounded says that induced charges have influence on the collagen fibrils orientation and ions or polarized molecules deposition. Its magnitude might depend on the direction of force applied. It was supposed to identify, that piezoelectric effect occurs only due to presence of directional collagen fibrils while generated electric field linearly correlates with the stresses produced.

Subsequent investigations were conducted in an environment highly saturated with moisture (as it naturally occurs in a human organism). Unfortunately, it did not bring optimistic results like those obtained of dry specimens. However, hydroxyapatite in spite of the important role of transmitting external loads also, to a large extent, limits the access of water to collagen fibrils. These in turn, as first experiments demonstrated exhibit piezoelectric properties. With respect to piezoelectric effect in moist environment, stress generated voltage is expressed by the following equations [13]:

$$V = \left(\frac{d_{ijk} \cdot L}{\varepsilon} \right) \cdot B \cdot e^{\left(\frac{\sigma \cdot t}{\varepsilon} \right)} \tag{1}$$

where:
d_{ijk} – third rank piezoelectric tensor,
L – sample thickness,
ε - dielectric permittivity,
B – load applied to the sample,
t – time
σ - solution conductivity.
Looking on hydroxyapatite-collagen structure one can notice, that under forces applied externally, collagen fibrils exhibit more strains because they are more compliant. That causes charge generation on their surfaces.

3. Presence of the streaming potential in porous media.

In porous media when saturated with fluid, a forced fluid streaming potential is created as a result. The negative charge capillary surface affects the opposite charge ions and in consequence becomes covered with layer of counter ions. This layer is composed of two parts: absorptive and diffusive and is called the electrical double layer (EDL) (Fig 1.). The potential between two contiguous layers (absorptive and diffusive) is called the electro kinetic potential or zeta potential. In that area also a shear plane exists. Its role is to separate the movement of ions bound through to the solid surface from other ions that show normal viscous behavior under the applied pressure. Ions located the closest to the charged surface remain immovable, and in turn bulk the ions flow laminarly with parabolic profile. It results in the streaming potential occurring in capillary which is dependent on electro kinetic potential zeta. It can be mathematically expressed as [12]:

$$V = \frac{\zeta \cdot \varepsilon \cdot \Delta P}{\sigma \cdot \eta} \tag{2}$$

Where:

ζ - zeta potential,

ε - dielectric permittivity ,

ΔP – pressure gradient acting on sample,

σ - solution conductivity,

η - solution viscosity.

Fluid flow or in this case ions flow is stated as the streaming current, whereas potential made in such manner is stated as the streaming potential. It affects directly the hydraulic permeability and conditions the ion transports within porous media.
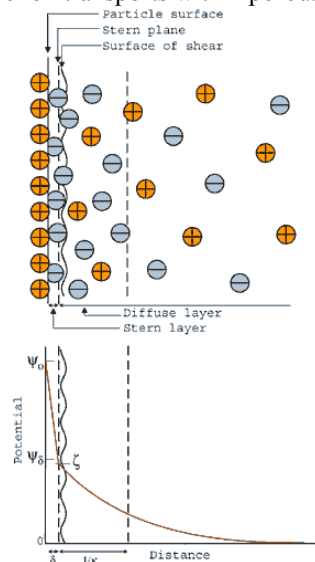
Figure 1. Double layer view and corresponding zeta potential.

4. Bone structure in microscopic picture.

The following three types of cells take part in remodeling process i.e. osteoblasts, osteocytes and osteoclasts. Osteocytes are the most frequent group of cells in bone tissue. They are located inside of bone tissue precisely inside of osteocytic lacuna, and have numerous cytoplasmic extensions placed in canaliculus used to exchange nutrients and waste. (Fig. 2). Scientists suppose that osteocytes play significant role in the process of bone remodeling for the fact they have the ability of communicating each other due to gap junctions. Hence the received information concerning the stress level is transmitted through the three-dimensional network on to the second group of cells – osteoblasts. These are responsible for the bone formation, synthesizing collagen and controlling its calcification. They receive signals from osteocytes, and by that means, are able to manage the deposition of successive collagen layers. Placed on internal surfaces of bone they create a consistent barrier, which limits the access for the third cells group i.e. osteoclasts. That type of cells is responsible for removing the bone tissue by purging mineralized matrix and breaking up the organic bone. When the signals from osteocytes are too weak to activate mineralization, the osteoclasts start resorption processes in bone tissue.
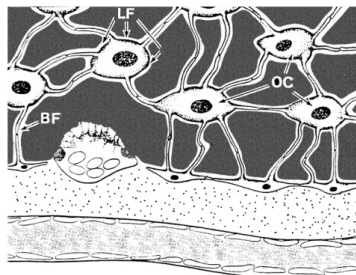
Figure 2. Osteocytes Network (OC) placed in osteocytic lacuna (LF), and cytoplasmic extension located inside canaliculus (BF). Bone surface is lined with longitudal osteoblasts and one big osteoclast.

5. Relation piezoelectric effect with streaming potential.

The two co-existing phenomena, suspected by scientists to play an important role in the state of stress information transmission should, in a way, influence each other. If so, signals could be differentiated with respect to stress and strain distribution. In 1984, Pollack conducted and developed investigations which showed that strain-generated potential (SGP) present in bone has a twofold nature (Fig. 3). In the Fig. 3B one can notice that the relaxation time is significantly shorter than in the other cases while spikes can be observed only in the Fig. 3B and C. These spikes probably can be ascribed to piezoelectric properties of bone, where relaxation time is smaller approximately of order of magnitude than in case of electrokinetic phenomena. In Fig. 3 B the absence of waveform typical for streaming potential can be explained by recording electrode placed off the axis of fluid flow (normally fluid flow occurs along the axis of osteons). In such

way streaming potential activity can be easily missed and recorded measurement is attributed only to piezoelectric effect.
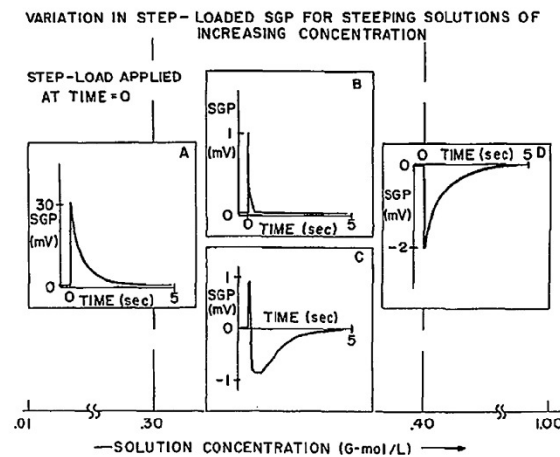
Figure 3. Different forms of bone SGP as a function of KCL concentration. [11]

Higher magnitude of stress results in higher surface polarization and that basically has influence on the magnitude of zeta potential. It entails more ionic concentration in the bone-fluid interface. In effect, it decreases the amount of available agents in fluid, which are used to transmit information between adjacent osteocytes (Fig. 4). Taking into account, that canaliculus are turned to many different directions (each osteocyte has approximately 40 cytoplasmic extensions), charges induced on solid surfaces vary since piezoelectric properties of bone are determined by piezoelectric coefficient d_{ij} describing generated charges to an external force applied.

Researches show that bone remodeling starts when loads applied to the osseous system are dynamic. Following this idea one can conclude that osteoblasts are activated by signals changed in time which emanate from osteocytes. However, they must exceed some threshold activation which can be achieved by accumulating appropriate ions in osteoblasts.

Another case to be considered is how the structure of bone adjusts to different states of stress e.g. torsion, compression, bending etc. It can be achieved again by certain threshold activation i.e. accumulation of proper ions by which synthesized collagen fibrils are directed in some specific manner, so that structure of bone tissue corresponds to the actual state of stress. In effect, successive collagen lamellae will be oriented parallel to the osteon axis (Type L), alternating (Type A) and perpendicular to the osteon axis (Type T) (Fig.5).
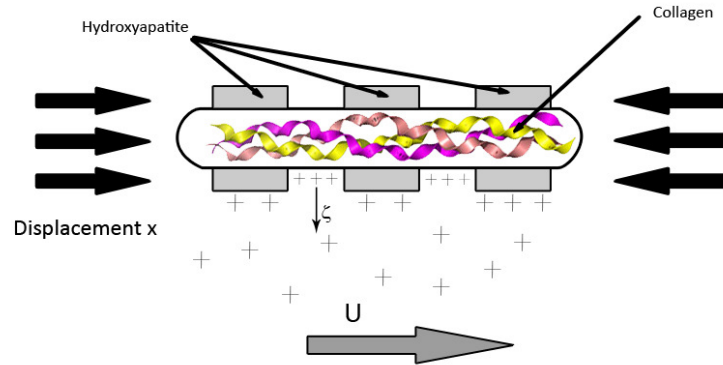
Figure 4. Theoretical relation between piezoelectric effect and streaking potential.
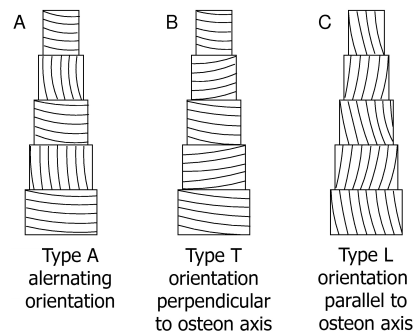
Figure 5. Types of collage fibrils orientations in successive lamellae [1].

6. Model based on cell interactions.

Having defined a signal induced by externally applied force, it has to be considered on how a signal sensed by osteocytes is being transmitted to cells that are responsible for bone formation or resorption. It is known, that during the process of forming subsequent lamellae, part of the osteoblasts are converted into osteocytes. In this way the newly-born "cell-sensors" are connected to each other by means of cytoplasmic extensions, which form three-dimensional network. As a result, it allows transmitting signals towards executive cells. It is also highly probable, that osteoblastic cells receive signals from group of osteocytes which are located in its neighborhood. (Fig. 6). Eventually, the transmitted signal is decayed in correlation to distance between osteocyte and target cell – osteoblast.
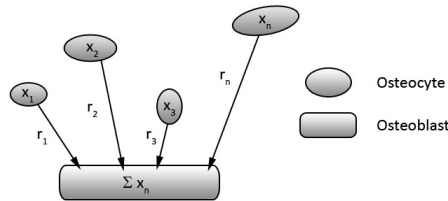
Figure 6. Chart showing singal transmittance from osteocytes with different coordinates to osteoblast.

In overview, these mathematical relationships illustrating the influence function advance as follows:

$$\phi(r_n(x)) = \frac{D}{r_n(x)} \tag{3}$$

Where:

$r_n(x)$ – distance from n osteocyte located in x,
D – characteristic dimension.

Therefore, the signal received by osteoblasts will be correlated with the influence function, i.e.:

$$S(x, x_n, t) = [S_n(x_n, t) - S_0]\phi(r_n(x)) \tag{4}$$

where:

$S_n(x_n,t)$ – signal value, which is received by n osteocyte which has x_n coordinate,
S_0 – value of the reference signal, which determines threshold activation,
t – time.

Signals developed from N located osteocytes reach the osteoblast where they are summed up. In other words, transmitted ions are accumulated. Thus, when signals exceed defined threshold that determines the state of biological equilibrium S_0, cells responsible for the bone formation are activated, and processes of bone matrix synthesis are started.

7. Conclusions.

The aim of the discussed article was to explain the principles of mechanisms responsible for the stress state signal transmission back from osteocytes to osteoblasts. Unfortunately, many processes that occur in bone have not been yet revealed, hence the hypothesis remains full of gaps until further development. This model is based on specialized cells interactions whereby remodeling of bone structure is local process based on signals received from osteocytes located in the specified region. Such system of signal transmission and reception more closely corresponds to the real biological system.

The conception introduced in this work provides a solid foundation for a bigger and more complex system of liaison which is to be developed in future works. This approach is going to be correlated with the hypothesis of Bone adaptation based on the optimal response proposed by Lekszycki [1] in order to perform numeric simulations. This will help to verify the current of thoughts and to move on by extending the model to suit best in real processes occurring during bone remodeling.

References

1. Lekszycki, T. *Wybrane zagadnienia modelowania w biomechanice kości.* Warszawa : IPPT, 6 (2007).
2. C.Ahn, Andrew and Grodzinsky, Alan J. *Relevance of collagen piezoelectricity to "Wolff's Law": A critical review.* Medical Engineering & Phisics. (2009) 733-741.
3. P., Dechadilok and D., William M. *Electrostatic and electrokinetic effects on hindered convection in pores.* Journal of Colloid and Interface Science. (2009) 135-144.
4. Hung, C. T., et al. *Intracellular Ca2+ stores and extracellular Ca2+ are required in the real-time Ca2+ response of bone cells experiencing fluid flow.* J. Biomechanics. **29**(11) (1996) 1411-1417.
5. Telega, J. J. and Wojnar, R. *Piezoelectric effects in biological tissues. Journal of Theoretical and Applied Mechanics.* **40**(3) (2002).
6. Telega, J. J. and Wojnar, R. *Flow of conductive fluids through poroelastic media with piezoelectric properties.* Journal of Theoretical and Applied Mechanics. 3, **36** (3) (1998).
7. Shamos, M. H., Lavine, L. S. and Shamos, M. I. *Piezoelectric Effect in Bone.* Nature 81 (1963).
8. Becker, R. O., Bassett, C. A. and Bachman, C. H. *Bioelectrical factors controlling bone structre.* Bone Biodynamics. **175** (1964) 209-232.
9. Bassett, C. A. L. *Electrical effects in bone. Scient.* Am., **213** (4) (1965) 18-25.
10. Basset, C.A.L. and Becker, R. A. *Generation of electrical potentials by bone in response to mechanical stress. Science*, **137** (1962) 1063-1064.
11. Pollack, S. R., Salzstein, R. and Pienkowski, D. *The electric double layer in bone and its influence on stress-generated potentials.* Calcif Tissue Int. **36** (1984) 77-81.
12. Pienkowski D., Pollack SR. *The origin of stress-generated potentials In fluid-saturated bone.* J Orthop Res 1 (1983) 30-41.
13. Petrov N. *On the electromechanical interaction In physiologically wet bone.* Biomechanics 2 (1975) 43-52

Znaczenie zjawisk: piezoelektrycznego oraz potencjału przepływu podczas przebudowy struktur kostnych.

W pracy tej zawarto najważniejsze informacje dotyczące występowania efektu piezoelektrycznego oraz potencjału przepływu w strukturach kostnych, które zdaniem autorów tego tekstu, ma odgrywa ważną rolę przy przebudowie tkanki kostnej. Dlatego został zaproponowany model odbierania sygnałów o stanie mechanicznym kości przez osteocyty i powiązany z modelem oddziaływań międzykomórkowych opisującym przekazywanie informacji z osteocytów do osteoblastów.

Identification of parameters of the fractional rheological model of viscoelastic dampers

Roman LEWANDOWSKI
Poznan University of Technology, 60-965 Poznan, ul. Piotrowo 5
roman.lewandowski@put.poznan.pl

Bartosz CHORĄŻYCZEWSKI
Poznan University of Technology, 60-965 Poznan, ul. Piotrowo 5
bartosz.chorazyczewski@prometplast.com.pl

Abstract

An identification method for determination of parameters of the rheological model of damper made of viscoelastic material is presented in this paper. The rheological model of damper has four parameters and the model equation of motion contains derivatives of the fractional order. The identification procedure has two main parts. Results of dynamical experiments are approximated using the trigonometric function in the first part of the procedure while the model parameters are determined in the second part of the procedure as the solution to an optimization problem. The particle swarm optimization method is used to solve the optimization problem. Efficiency and accuracy of the proposed method are proof on an example where the parameters of the rheological model are determined on the basis of artificially generated experimental data with measured noises.

Keywords: viscoelastic dampers, fractional rheological model, identification procedure

1. Introduction

Fractional rheological models of viscoelastic (VE) dampers are becoming more and more popular. The reason is their ability to correctly describe the behavior of VE dampers using a small number of parameters. A single equation is enough to describe the VE damper dynamics. An important problem, connected with the fractional models, is the estimation of model parameters using experimental data. The process of parameter identification is an inverse problem which can be ill conditioned. The identification procedures for the three parameters fractional Kelvin-Voigt model and the fractional Maxwell model are proposed in [1]. The problem of parameters identification of rheological models with fractional derivatives is also discussed by Pritz in [2].

A new method for identification of the parameters of the fractional model of VE dampers with four parameters is presented in this paper. The results of static and dynamical test are used to identify the parameters of a damper model. The identification procedure comprises two main steps. The experimental results are approximated by a simple harmonic function in the time domain in the first step while model parameters are determined in the second stage of the identification procedure. The validity, accuracy and effectiveness of the procedures have been tested using artificial experimental data.

2. Description of the rheological model and a steady state vibration of the model

The equation of motion of the considered rheological model is in the following form:

$$u(t) + \tau^\alpha D_t^\alpha u(t) = k_0 q(t) + k_\infty \tau^\alpha D_t^\alpha q(t) \tag{1}$$

where $u(t)$ denotes the dampers force, $q(t)$ is the dampers displacement, k_0, k_∞, τ and α are models parameters. Moreover, a symbol such as $D_t^\alpha q(t)$, is the Riemann-Liouville fractional derivative of the order α of consecutive function, here $q(t)$, with respect to time t (please, consult [3] for details concerning fractional derivatives).

Based on the results presented by Lion in [4], it can be demonstrated that this model fulfils the second law of thermodynamics for $0 \leq \alpha \leq 1$, $\tau > 0$ and $k_\infty > k_0 > 0$.

Equation (1) can be understood as the equation of motion of two mechanical models shown in Figures 1 and 2. These models consists of springs and springpot elements connected in parallel or in series. The springpot element can be seen as an interpolation between the spring ($\alpha = 0$) and the dashpot ($\alpha = 1$). The springpot element satisfies the following constitutive equation (see [1] for details):

$$u(t) = c\, D_t^\alpha q(t) \ . \tag{3}$$

The parameters of mechanical models are related to parameters of the considered fractional model in the following way:

$$k_0 = k_1 \ , \qquad k_\infty = k_1 + k_2 \ , \qquad \tau^\alpha = c_2 / k_2 \ , \tag{3}$$

$$k_0 = k_1 k_2 /(k_1 + k_2) \ , \qquad k_\infty = k_1 \ , \qquad \tau^\alpha = c_2 /(k_1 + k_2) \ , \tag{4}$$

for the first and the second mechanical model, respectively.
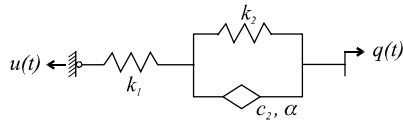
Figure 1. The first mechanical models of VE dampers
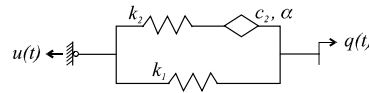
Figure 2. The second mechanical models of VE dampers

If the damper executes harmonic oscillations then the damper's steady state vibration is described by

$$u(t) = u_c \cos \lambda t + u_s \sin \lambda t \ , \qquad q(t) = q_c \cos \lambda t + q_s \sin \lambda t \ , \tag{5}$$

and the parameters shown above fulfil the following relationships

$$u_c = z_1 q_c + z_2 q_s \ , \qquad u_s = -z_2 q_c + z_1 q_s \ , \tag{6}$$

where

$$z_1 = \frac{k_0 + (k_0 + k_\infty)(\tau\lambda)^\alpha \cos(\alpha\pi/2) + k_\infty (\tau\lambda)^{2\alpha}}{1 + 2(\tau\lambda)^\alpha \cos(\alpha\pi/2) + (\tau\lambda)^{2\alpha}} \ , \tag{7}$$

$$z_2 = \frac{(k_\infty - k_0)(\tau\lambda)^\alpha \sin(\alpha\pi/2)}{1 + 2(\tau\lambda)^\alpha \cos(\alpha\pi/2) + (\tau\lambda)^{2\alpha}} \ . \tag{8}$$

3. Description of identification method

The identification procedure consists of two main steps. In the first step the experimental results are approximated by a simple harmonic function in the time domain while the model parameters are determined in the second stage of the identification procedure.

In the first step, experimentally measured displacements $q_e(t)$ of the damper are approximated using the function:

$$\widetilde{q}(t) = \widetilde{q}_c \cos \lambda t + \widetilde{q}_s \sin \lambda t \; , \tag{9}$$

The least-square method is used to determine parameters $\widetilde{q}_c$ and $\widetilde{q}_s$ of function (9). This method requires minimization of the following functional:

$$J_1(\widetilde{q}_c, \widetilde{q}_s) = \frac{1}{t_2 - t_1} \int_{t_1}^{t_2} [q_e(t) - \widetilde{q}(t)]^2 \, dt \; , \tag{10}$$

where the symbols t_1 and t_2 denote the beginning and the end of the time range in which the damper's displacements were measured. Part of the measuring results relating to a steady state vibration is used as data in this step. From the stationary conditions of the functional (10), the following system of equations is obtained:

$$I_{cc}\widetilde{q}_c + I_{sc}\widetilde{q}_s = I_{cq} \; , \qquad I_{sc}\widetilde{q}_c + I_{ss}\widetilde{q}_s = I_{sq} \tag{11}$$

from which the parameters $\widetilde{q}_c$ and $\widetilde{q}_s$ are obtained and where:

$$I_{cc} = \int_{t_1}^{t_2} \cos^2 \lambda t dt \; , \qquad I_{ss} = \int_{t_1}^{t_2} \sin^2 \lambda t dt \; , \qquad I_{cs} = I_{sc} = \int_{t_1}^{t_2} \sin \lambda t \cos \lambda t dt \tag{12}$$

$$I_{cq} = \int_{t_1}^{t_2} q_e(t) \cos \lambda t \, dt \; , \qquad I_{sq} = \int_{t_1}^{t_2} q_e(t) \sin \lambda t \, dt \; . \tag{13}$$

Similarly, the experimentally measured dampers force $u_e(t)$ is approximated by

$$\widetilde{u}(t) = \widetilde{u}_c \cos \lambda t + \widetilde{u}_s \sin \lambda t \; . \tag{14}$$

Proceeding to a description of the second step of identification method, it is assumed that a set of results of the above-described first step of procedure given by $\widetilde{u}_i(t)$, $\widetilde{u}_{ci}$, $\widetilde{u}_{si}$ $\widetilde{q}_i(t)$, $\widetilde{q}_{ci}$ and $\widetilde{q}_{si}$ and relating to the different excitation frequencies λ_i $(i = 1,2,...,n)$ is known. If the considered rheological model is able to correctly simulate the VE damper behavior then the relationships (6) must approximately be fulfilled by the above-mentioned results of the first step identification procedure, i.e.:

$$\widetilde{u}_{ci} = \widetilde{z}_{1i}\widetilde{q}_{ci} + \widetilde{z}_{2i}\widetilde{q}_{si} \; , \qquad \widetilde{u}_{si} = -\widetilde{z}_{2i}\widetilde{q}_{ci} + \widetilde{z}_{1i}\widetilde{q}_{si} \; , \qquad i = 1,2,...,n \; . \tag{15}$$

Solving Equations (15) with respect to $\widetilde{z}_{1i}$ and $\widetilde{z}_{2i}$ the following is obtained:

$$\widetilde{z}_{1i} = \frac{\widetilde{u}_{ci}\widetilde{q}_{ci} + \widetilde{u}_{si}\widetilde{q}_{si}}{\widetilde{q}_{ci}^2 + \widetilde{q}_{si}^2} \; , \qquad \widetilde{z}_{2i} = \frac{\widetilde{u}_{ci}\widetilde{q}_{si} - \widetilde{u}_{si}\widetilde{q}_{ci}}{\widetilde{q}_{ci}^2 + \widetilde{q}_{si}^2} \; . \tag{16}$$

If the rheological model perfectly fits the experimental data then $z_{1i} - \widetilde{z}_{1i} = 0$ and $z_{2i} - \widetilde{z}_{2i} = 0$ for $i = 1,2,...,n$, where $z_{1i} = z_1(\lambda_i)$, $z_{2i} = z_2(\lambda_i)$ are calculated using formulas (7) and (8). In practice some differences usually exist and parameters, k_0, k_∞, τ and α of the rheological model are determined as the solution of the appropriately defined optimization problem. However, here it is assumed that the parameter k_0 is known and determined previously using the experimental data taken from the static tests.

In the paper the optimization problem mentioned above is formulated as follows.

Find the values of k_∞, τ and α which minimize the functional

$$J(k_\infty, \tau, \alpha) = \sum_{i=1}^{n} \left\{ [z_{1i}(k_\infty, \tau, \alpha) - \widetilde{z}_{1i}]^2 + [z_{2i}(k_\infty, \tau, \alpha) - \widetilde{z}_{2i}]^2 \right\} , \qquad (17)$$

and fulfil the following constraints:

$$0 < \alpha \le 1 , \quad \tau > 0 , \quad k_\infty > k_0 > 0 . \qquad (18)$$

The above optimization problem is solved with the help of the particle swarm optimization method described, for example in [5] and briefly in the following Section.

4. Description of the adopted version of the particle swarm optimization method

The particle swarm optimization (PSO) method is a population based optimization technique inspired by the social behaviour of animals. The populations consist of possible solutions (referred to as particles) and the search for optimal solutions is performed by updating the subsequent positions of particles. Each particle explores the problem space being drawn to current optimal solutions. Moreover, each particle keeps its best values of functional (17) achieved so far (along with the associated solution $\mathbf{p}^{(j)}(k) = col(p_1^{(j)}(k), p_2^{(j)}(k), p_3^{(j)}(k))$, where k is the number of the current time instance, the superscript j is the number of the current particle; ($j = 1,2,...,m$)) and the best fitness and corresponding solution achieved in the particle's neighbourhood $\mathbf{p}^{(b)}(k) = col(p_1^{(b)}(k), p_2^{(b)}(k), p_3^{(b)}(k))$. It was shown that using global neighbourhood (all particles are fully aware of other particles' fitness) minimizes the median number of iterations needed to converge. On the other hand, the neighbourhood of size 2 gives the highest resistance to local minima.

At each time instances k of the PSO, the velocities of the particles are changed (accelerated) towards the $\mathbf{p}^{(j)}(k)$ and the $\mathbf{p}^{(b)}(k)$ and the particles are moved to new positions according to the following formulas:

$$v_i^{(j)}(k+1) = w(k+1)v_i^{(j)}(k) + c_1 r_{1i}^{(j)}(k+1)\left[p_i^{(j)}(k) - x_i^{(j)}(k)\right]/\Delta t + \\ c_2 r_{2i}^{(j)}(k+1)\left[p_i^{(g)}(k) - x_i^{(j)}(k)\right]/\Delta t \qquad , \qquad (19)$$

$$x_i^{(j)}(k+1) = x_i^{(j)}(k) + v_i^{(j)}(k+1)\Delta t . \qquad (20)$$

where $\Delta t = 1$, $v_i^{(j)}(k)$ vj and $x_i^{(j)}(k)$ are the i-th element of the velocity and the position vectors of the j-th particle, respectively; $w(k+1)$ is the inertia factor providing balance between exploration and exploitation, c_1 is the individuality constant, and c_2 is the sociality constant. To speed up convergence, the inertia weight was linearly reduced from $w_{max} = 0.9$ to $w_{min} = 0.1$. In our experiments we have used $m = 10$ particles, a maximum number of iterations $i_{max} = 400$ and $c_1 = c_2 = 2.0$. A size 4 neighbourhood was used as a tradeoff between fast convergence and resistance to local minima. Moreover, $r_{1i}^{(j)}$ and $r_{2i}^{(j)}$ are random numbers taken from the range from 0 to 1. More information on the selection of the algorithm parameters, constraints handling and selecting the starting vectors $\mathbf{x}^{(j)}(0)$ and $\mathbf{v}^{(j)}(0)$ can be found in [5].

5. Results of demonstration applications of identification method

A typical calculation is performed using the artificially generated data. At the beginning, the artificial data without noises for the second mechanical model are calculated using formulas (3) and (6) and assuming that: $n = 14$, $k_1 = 600.0 \, \text{kN/m}$, $k_2 = 400.0 \, \text{kN/m}$, $c = 150.0 \, \text{kNs/m}$, $q_{si} = 0.01 \, \text{m}$, $q_{ci} = 0.005 \, \text{m}$ and $\alpha = 0.6$. The chosen values of the excitation frequency are taken from the range $0.5 - 13.5 \, \text{Hz}$ with the frequency increment $\Delta\lambda = 1.0 \, \text{Hz}$. After applying the identification procedure and assuming that $k_0 = 240.0 \, \text{kN/m}$ is known from the static test, the following results, very close to the exact ones, are obtained: $k_{1,iden} = 601.5 \, \text{kN/m}$, $k_{2,iden} = 399.3 \, \text{kN/m}$, $c_{iden} = 149.9 \, \text{kNs/m}$, $\alpha_{iden} = 0.5968$.

Moreover, the random noises are added to the artificial data using the formulas:
$$\hat{u}_{ci} = (1 + \tilde{r}_{1i}\varepsilon)\,\tilde{u}_{ci}, \quad \hat{u}_{si} = (1 + \tilde{r}_{2i}\varepsilon)\,\tilde{u}_{si}, \quad \hat{q}_{ci} = (1 + \tilde{r}_{3i}\varepsilon)\,\tilde{q}_{ci}, \quad \hat{q}_{si} = (1 + \tilde{r}_{4i}\varepsilon)\,\tilde{q}_{si} \qquad (20)$$
where ε is the noise level, $\tilde{r}_{1i}$, $\tilde{r}_{2i}$, $\tilde{r}_{3i}$ and $\tilde{r}_{4i}$ are random numbers taken from the range from 0 to 1.

The calculation is made for $\varepsilon = 0.02$. After several runs of the identification procedure the following median solution is obtained: $k_{1,iden} = 608.7 \, \text{kN/m}$, $k_{2,iden} = 396.2 \, \text{kN/m}$, $c_{iden} = 151.6 \, \text{kNs/m}$ and $\alpha_{iden} = 0.5866$. It is easy to find that the accuracy of the obtained values of model parameters is of the order of noises introduced.

A comparison of the storage modulus resulting from the artificially generated data with noises (small crosses) and from the rheological model (solid curve) is presented in Fig. 3. It is evident that both approaches are in good agreement.

6. Concluding remarks

The proposed identification method can be effectively used to determine parameters of the rheological model with the fractional derivatives. The mentioned rheological model can be used to modelling the dynamic behaviour of VE dampers. The identification

problem is reduced to the nonlinear optimization problem which is solved by means of the particle swarm optimization method. Based on the demonstration calculation, it was found that the proposed method is not sensitive to any noises introduced during the measurements.
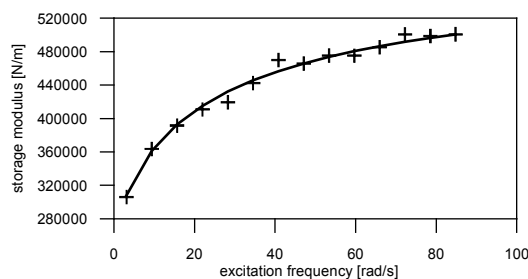
Figure 3. Comparison of the storage modulus

Acknowledgments

References

1. Lewandowski R., Chorążyczewski B., *Identification of the parameters of the Kelvin-Voigt and the Maxwell fractional models, used to the modeling of viscoelastic dampers,* Comp. Struct., **88**, (2010) 1 - 17.
2. Pritz T., *Five-parameter fractional derivative model for polymeric damping materials*. J Sound Vib **265** (2003) 935–952
3. Podlubny I., *Fractional differential equations,* Academic Press, 1999
4. A. Lion, *Thermomechanically consistent formulations of the standard linear solid using fractional derivatives*, Arch. Mech*.*, **53**, (2001) 253 – 273.
5. Perez R.E., Behdinan K., *Particle swarm approach for structural design optimization,* Comp. Struct., **85**, (2007) 1579 – 1588.

Identyfikacja parametrów ułamkowego modelu reologicznego modelującego zachowanie tłumika lepkosprężystego

W pracy omawia się metodę identyfikacji parametrów modelu reologicznego tłumika wykonanego z materiału o właściwościach lepkosprężystych. Model reologiczny tłumika ma cztery parametry, a równanie ruchu modelu zawiera pochodne ułamkowego rzędu. Procedura identyfikacji składa się z dwóch części. W pierwszej części aproksymuje się wyniki badań doświadczalnych za pomocą funkcji trygonometrycznych, a w drugiej części wyznacza się parametry modelu jako rozwiązanie pewnego zadania optymalizacji. Do rozwiązania zadania optymalizacji użyto metody roju cząstek. Efektywność i dokładność zaproponowanej metody identyfikacji wykazano wyznaczając parametry ułamkowego modelu reologicznego na podstawie sztucznie wygenerowanych danych doświadczalnych z szumami pomiarowymi.

Substitutional transmittance function of helicoidal resonator

Wojciech ŁAPKA

Poznań University of Technology, Institute of Applied Mechanics
ul. Piotrowo 3, 60-965 Poznań, Poland
wojciech.lapka@put.poznan.pl

Abstract

An analytical and computational characteristics of transmission losses of the helicoidal resonator are compared in this paper. The substitutional transmittance function of helicoidal resonator was proposed based on amplitude characteristic of electrical band-stop filter. At first approach the analytical model can be considered as valid for practical silencing systems design calculations in ducted systems.

Keywords: helicoidal resonator, spiral duct, transmittance, acoustical filter, sound attenuation.

1. Introduction

There are several papers about spiral ducts [2-8] where are developed theirs acoustic attenuation properties in ducted acoustical systems. There is also developed that the acoustic attenuation for spiral (helicoidal) ducts exists in consequence of an acoustical resonance [2-7]. Hence, in this paper a helicoidal resonator is considered.

Acoustical properties, mainly attenuation of sound due to an acoustical resonance, of helicoidal resonators can be modified by doing a change in relations between its basic geometrical parameters [3], which are shown in Figure 1.

l_{Tz} - outer length of helicoidal profile

l_{Tw} - inner length of helicoidal profile
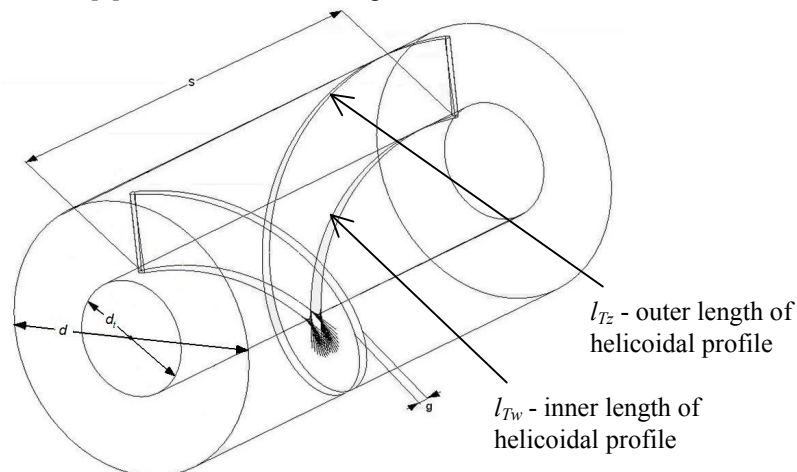
Figure 1. Basic geometrical parameters of helicoidal resonator.

Very important parameter of helicoidal resonator is the number of helicoidal turns n, which strongly determines the character of acoustical resonance [3]. This work describes

a substitutional transmittance function of helicoidal resonator as a first approach for this question based on computational results in COMSOL Multiphysics [3].

2. Determination of a resonance frequency based on geometrical relationships

To define the substitutional transmittance function of helicoidal resonator placed inside an infinite long cylindrical duct (Figure 2) of diameter d, there was chosen a case of helicoidal resonator,

Cylindrical duct

Helicoidal resonator
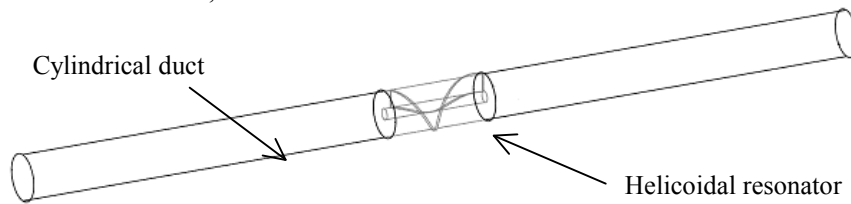
Figure 2. Cylindrical duct with helicoidal resonator.

where predominates only one component of transmission loss (TL) [2, 3, 5, 6, 10] in the resonance frequency and remaining components are almost symmetrically distributed in the frequency domain, as it is shown in Figure 3.
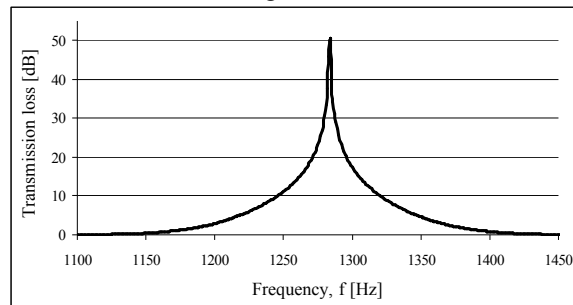
Figure 3. Transmission loss of helicoidal resonator with only one resonance frequency f_r=1281Hz and almost symmetrically distributed other attenuated frequencies in the range from 1200Hz to 1365Hz – TL characteristic obtained computationally [3].

In that case there are satisfied relations (1) between basic geometrical parameters of investigated helicoidal resonator, according to Figure 1, as follows [3]:

$$\frac{s}{d} = 1,976, \qquad \frac{d_t}{d} = 0,24, \qquad \frac{g}{d} = 0,04, \, n=1. \tag{1}$$

It is the case of full spread of helicoidal surface of one helicoidal turn, where attenuated components of a sound in a frequency domain are almost symmetrically distributed in relation to the resonance frequency of the helicoidal resonator.

To write the equation for a resonance frequency f_r of that helicoidal resonator, there was used undermentioned relation (2) to obtain frequency f [Hz], which depends on the length of a sound wave λ [m] and a speed of sound in air c_a (343m/s), in form:

$$f = \frac{c_a}{\lambda}, [Hz] \tag{2}$$

By making precise numerical computations (calculation step 0,01Hz) there was determined exact resonance frequency, which equals f_r=1281,17Hz, of the helicoidal resonator with ratio s/d=1,976, and other dimensions: thickness of the helicoidal profile g=0,005m, diameter of the mandrel d_t=0,03m placed inside infinite long cylindrical duct (as it is presented in Figure 2.) of diameter d=0,125m. On this basis there can be written a relation (3) between diameter of a cylindrical duct d and the length of a sound wave in resonance frequency λ_r of helicoidal resonator with one full spread of the helicoidal turn, in form:

$$\frac{\lambda_r}{d} = 2,141792268 \cdot \tag{3}$$

Which means, that the diameter of the cylindrical duct represents a 46,69% of a resonance wavelength of the helicoidal resonator.

Substituting the previously obtained dimensional relationship s/d=1,976 to the model (3) we obtain the wavelength dependence for the acoustic resonance frequency of the helicoidal resonator based on its turn s, in form:

$$\lambda_r = s \cdot 1,08390297 \quad [m]. \tag{4}$$

So in this case optimal dimensions of the helicoidal resonator in terms of a sound attenuation performance is that for which the helicoidal turn s is slightly larger than the resonant wavelength. Relations (3) and (4) can be expressed in conjunction with the following dependences [1]:

- to calculate the outer length of the helicoidal profile:

$$l_{T_z} = \frac{\pi d n}{\cos \psi_{T_z}}, \qquad \psi_{T_z} = \arctan\left(\frac{s}{\pi d}\right), \tag{5}$$

- to calculate the inner length of the helicoidal profile:

$$l_{T_w} = \frac{\pi d_t n}{\cos \psi_{T_w}}, \qquad \psi_{T_w} = \arctan\left(\frac{s}{\pi d_t}\right), \tag{6}$$

On the basis of dependences (5) and (6) we learn that the angle of the helicoid lift lines (inner and outer) ψ_T in this case is constant and independent of the dimensions, and it equals as follows:

$$\psi_{T_w} = 69,11464814°, \ \psi_{T_z} = 32,16908553°$$
$$\psi_{T_w} = 69°06'52''73''', \ \psi_{T_w} = 32°10'08''70''' \tag{7}$$

Next, we can specify the inner and outer lengths of the helicoidal profile, as below:

$$l_{T_w} = \frac{\pi d_t n}{\cos \psi_{T_w}} = \frac{\pi 0,24 d n}{\cos \psi_{T_w}} = \frac{\pi 0,24 s n}{1,976 \cos \psi_{T_w}} = s \cdot 1,070325[m]$$

$$l_{T_z} = \frac{\pi d n}{\cos \psi_{T_z}} = \frac{\pi s n}{1,976 \cos \psi_{T_z}} = s \cdot 1,8782177[m] \tag{8}$$

Taking under attention above mentioned relationship (4), it can be assumed that the inner length of helicoid profile corresponds to the resonance wavelength:

$$\lambda_r \cong l_{T_w}. \tag{9}$$

The formula for the resonant frequency f_r of the helicoidal resonator shown in relations (1) by taking into account relations (9) has the form:

$$f_r = \frac{c}{\lambda_r}, [Hz]. \tag{10}$$

2. Substitutional transmittance function

To obtain a substitutional transmittance function of the helicoidal resonator there have been made an analysis of different equations of the transfer functions and amplitude characteristics K_u of different band-stop filter [9]. The greatest similarity of the analytical characteristics and the simulation is obtained as a result of the transformation for the amplitude characteristics of a band-stop filter of second order [3, 9] in the form:

$$|K_u| = \frac{k_{u0}|1 - \Omega^2|}{\sqrt{1 + \Omega^2\left(\frac{1}{Q^2} - 2\right) + \Omega^4}} \tag{11}$$

where $\Omega = f/f_r$ is an normalized pulsation, $k_{u0}=1$ is an excitation signal, and $Q=1/\Delta f$ is a quality factor, whereas Δf [Hz] is a frequency range, in which the sound is attenuated.

To determine the substitutional transmittance function of the helicoidal resonator the resonant frequency formula (10) was placed into the formula (11). Then, by squaring such formula (11) we obtain the most similar to simulation the substitutional transmittance function $T_{S,hr}$ of the helicoidal resonator, in the form:

$$|T_{S,hr}| = \frac{\left|1 - \left(\frac{f \cdot \lambda_r}{c}\right)^2\right|^2}{1 + \left(\frac{f \cdot \lambda_r}{c}\right)^2 \left(\frac{1}{Q^2} - 2\right) + \left(\frac{f \cdot \lambda_r}{c}\right)^4}. \tag{12}$$

Based on transmittance function (12) below can be shown the transmission loss characteristic of the helicoidal resonator with determined relationships (1), by the use of equation [10, p. 462]:

$$TL = 10 \log\left(\frac{1}{|T_{S,hr}|}\right), [dB]. \tag{13}$$

A graphical interpretation of the formula (13) together with the simulation results in a COMSOL Multiphysics computational environment in accordance to the dimensional relationships (1) and the quality factor $Q=8$ and difference between these two characteristics are shown in Figure 4.
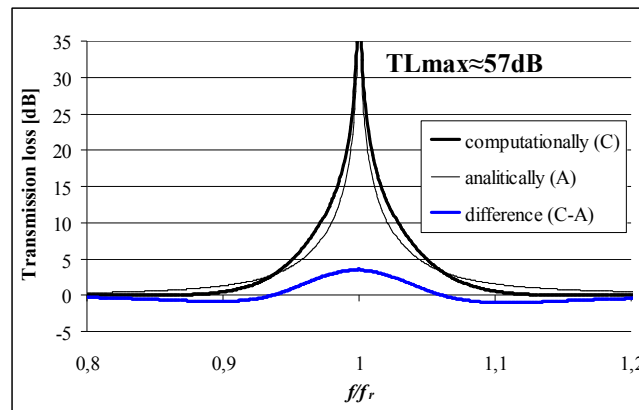
Figure 4. Transmission loss characteristics of: (C) helicoidal resonator computed by the use of finite element method (FEM) in COMSOL Multiphysics, (A) band-stop filter from equation (13) of quality factor Q=8 and (C-A) difference between these two characteristics.

As shown in Figure 4 the TL characteristics of the helicoidal resonator calculated analytically using the formula (13) and computed by the use of finite element method (FEM) in the COMSOL Multiphysics environment is quite similar. Maximum TL differences occur near the resonant frequency, which reach a value of less than 3.5 dB. The range of attenuated frequencies is closely identical for both characteristics (A and C), when we look on 3dB level of TL.

3. Conclusions

An analytical model of the substitutional transmittance function of helicoidal resonator was proposed in this paper. The inner length of helicoidal profile corresponds to the resonance wavelength and it can be used to calculate the resonance frequency of this acoustical filter. Transmission loss characteristics of the helicoidal resonator calculated analytically and computed by the use of the finite element method (FEM) in the COMSOL Multiphysics environment are quite similar. Maximum TL differences occur near the resonance frequency. However, at first approach of transmittance function of helicoidal resonator, the analytical model can be considered as valid for practical silencing systems design calculations in ducted systems.

Acknowledgments

References

1. Branowski B. K., *Sprężyny metalowe*, Wydawnictwo Naukowe PWN, Warszawa, s.196, 1997.
2. Łapka W., *Acoustic attenuation performance of a round silencer with the spiral duct at the inlet,* Archives of Acoustics, Vol. 32, No 4 (Supplement), 2007, pp. 247-252.
3. Łapka W., *Acoustical properties of helicoid as an element of silencers*, doctoral thesis, Poznań University of Technology, Faculty of Mechanical Engineering and Management, Poznań, 2009.
4. Łapka W., *Insertion loss of spiral ducts - measurements and computations*, Archives of Acoustics, Vol. 34, No. 4, 2009, pp. 537-545.
5. Łapka W., *Sound propagation through circular duct with spiral element inside*, European COMSOL Conference 2008, Hannover, Germany, 4–6 November 2008, Proceedings CD - 5 pages.
6. Łapka W., Cempel C., *Acoustic attenuation performance of Helmholtz resonator and spiral duct*, Vibrations in Physical Systems, Vol. 23, 2008, pp. 247-252.
7. Łapka W., Cempel C., *Computational and experimental investigations of a sound pressure level distribution at the outlet of the spiral duct*, Archives of Acoustics, Vol. 33, No. 4 (Supplement), 2008, pp. 65-70.
8. Łapka W., Cempel C., *Noise reduction of spiral ducts*, International Journal of Occupational Safety and Ergonomics (JOSE), Vol. 13, No. 4, 2007, pp. 419-426.
9. Tietze U., Schenk Ch., *Układy półprzewodnikowe*, wyd. 3 zmienione, WNT Warszawa, s. 1014, 1996.
10. Ver Istvan L., Beranek Leo L., *Noise and vibration control engineering*, 2nd edition, John Wiley & Sons, Inc., Hoboken, New Jersey, USA, s. 966, 2005.

Zastępcza funkcja transmitancji rezonatora helikoidalnego

W niniejszym artykule dokonano porównania charakterystyk tłumienia przenoszenia rezonatora helikoidalnego uzyskanych na drodze obliczeń analitycznych i numerycznych. Zaproponowana została zastępcza funkcja transmitancji rezonatora helikoidalnego na podstawie charakterystyki amplitudowej elektrycznego filtru pasmowo-zaporowego. Tak wykonany analityczny model transmitancji w pierwszym przybliżeniu może być uznany za poprawny dla celów obliczeniowych praktycznego projektowania systemów wyciszeniowych w instalacjach kanałowych.

Modelling and control of semi-active seat suspension with magneto-rheological damper

Igor MACIEJEWSKI

Koszalin University of Technology, 75-620 Koszalin, Racławicka 15-17
igor.maciejewski@tu.koszalin.pl

Abstract

The paper deals with modelling and control of a semi-active seat suspension with magneto-rheological damper. In order to protect the working machines operators against harmful vibration, the vibro-isolation properties of conventional seat suspension are improved by using the magneto-rheological damper. In this paper the vibration isolation characteristics of semi-active damping control strategy are studied, that are based on the inverse dynamics of magneto-rheological damper and the primary controller. The dynamic behaviour of passive and semi-active seat suspension is compared on the basis of a seat effective amplitude transmissibility factor and suspension travel. As results of computer simulation, the power spectral densities of seat acceleration and the transmissibility functions are presented for random excitation.

Keywords: vibration damping, semi-active system, seat suspension, magneto-rheological damper

1. Introduction

Full active suspensions require large power supply and this is the main disadvantage of using such the systems extensively in practice. Semi-active suspensions consume much less power than active suspensions, therefore they have received much attention in the literature [1]. The desirable performance of suspension systems can be achieved using semi-active control, especially when some controllable dampers: electro- rheological (ER) or magneto-rheological (MR) are utilized. In particular, MR dampers are often used in vibration reduction of the seat suspensions, vehicle suspensions, vibration isolators, etc. Many control strategies such as sky-hook, ground-hook or hybrid control, H-inf control and model-following sliding mode control have been evaluated in terms of their applicability in practice. However, the practical use of the MR dampers for control is relatively difficult by its inherently hysteretic and highly non-linear dynamics. This makes the modelling of MR dampers very important for its application. In order to characterize the performance of MR dampers, several models have been proposed to describe their behaviour [2], [3], [4]. Active and semi-active suspension systems provide more effective vibration isolation performance, but their control systems have to be formulated. The ongoing development of control algorithms indicates that improved methods of controlling active and semi-active suspension systems is an effective way to deal with the suspension system performance problem [3].

2. Physical and mathematical model of the semi-active seat suspension

In Fig. 1 a physical model of the semi-active seat suspension system containing a passive air-spring and a controllable magneto-rheological damper is shown. The magneto-rheological fluid inside a damper changes its properties (mainly its viscosity) with the

application of a magnetic field [4]. A magnetic filed is produced by the solenoids which are placed around the orifices between chambers of the damper. A controllable current, that supplies solenoids, changes the properties of a fluid flow and in consequence force of the damper is regulated.
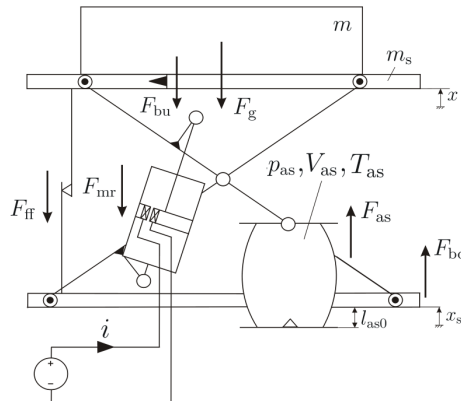
Figure 1. Physical model of the semi-active seat suspension
with magneto-rheological damper

Equation of motion of the semi-active seat suspension takes a similar form as in the case of the passive seat suspension model, that have been presented in the paper [5]. The mathematical models of basic forces in the system: the air-spring force F_{as}, the forces from end-stop buffers: bottom F_{bd} and top F_{bu}, the overall friction force of suspension system F_{ff} and the gravity force of suspended mass F_g are adequate to the models of forces in the passive system. However, a description of the damping force F_{mr} is different from the passive seat suspension model (F_d), because the conventional shock-absorber has been replaced in the magneto-rheological damper (F_{mr}). The damping force is controlled by the electric input signal i.

The Bingham model described in the paper [2] is adopted in this study for the magneto-rheological damper using the obtained experimental data. In this simplified model, the hysteresis loop of the MR damper is neglected and a description of the MR damper force contains components from the viscous damper and friction only (c.f. Fig. 2). The force equation is given by:

$$F_{mr} = d_{mr}\left(\frac{\dot{x} - \dot{x}_s}{\delta_d}\right) + \alpha_{mr}\, \text{sgn}\left(\frac{\dot{x} - \dot{x}_s}{\delta_d}\right) \qquad (1)$$

where: d_{mr} is the viscous damping coefficients, α_{mr} is the scale factor of the damper friction.
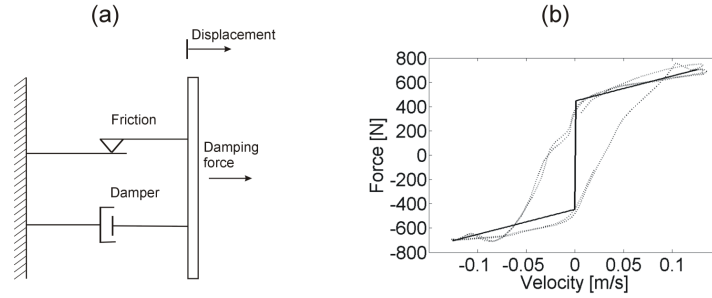
Figure 2. Bingham model of the magneto-rheological damper (a), force of the magneto-rheological damper (b): simulation (solid line), measurement (dashed line)

Based on the experimental data, a least-square approximation method is employed to determine the appropriate parameters d_{mr} and α_{mr} for the analytical model:

$$d_{mr} = a_{mr}i + b_{mr}, \quad \alpha_{mr} = e_{mr}i^2 + f_{mr}i + g_{mr} \tag{2}$$

where: a_{mr}, b_{mr}, e_{mr}, f_{mr} and g_{mr} are the polynominal coefficients expressed with respect to the input current. These coefficients are evaluated based on additional MR damper measurements that have been presented in the paper [6].

3. Reverse model of the magneto-rheological damper

If the Bingham model is determined than the desirable force F_a can be realized by injecting an appropriate current into the MR damper in accordance with actual piston velocity of the damper $i = f(F_a, \dot{x} - \dot{x}_s)$. This input current i is calculated from Eqs. (1), (2) with measurable velocity $\dot{x} - \dot{x}_s$ and is given by:

$$i = \frac{f_{mr}\,\mathrm{sgn}\!\left(\dfrac{\dot{x} - \dot{x}_s}{\delta_d}\right) - a_{mr}\!\left(\dfrac{\dot{x} - \dot{x}_s}{\delta_d}\right) + \mathrm{sgn}\!\left(\dfrac{\dot{x} - \dot{x}_s}{\delta_d}\right)\sqrt{\Delta}}{2 f_{mr}\,\mathrm{sgn}\!\left(\dfrac{\dot{x} - \dot{x}_s}{\delta_d}\right)} \tag{3}$$

with function Δ that is calculated as:

$$\Delta = \left(f_{mr}\,\mathrm{sgn}\!\left(\frac{\dot{x} - \dot{x}_s}{\delta_d}\right) + a_{mr}\!\left(\frac{\dot{x} - \dot{x}_s}{\delta_d}\right) \right)^2 - \ldots$$
$$4 e_{mr}\,\mathrm{sgn}\!\left(\frac{\dot{x} - \dot{x}_s}{\delta_d}\right)\!\left(g_{mr}\,\mathrm{sgn}\!\left(\frac{\dot{x} - \dot{x}_s}{\delta_d}\right) + b_{mr}\!\left(\frac{\dot{x} - \dot{x}_s}{\delta_d}\right) - \delta_d F_a \right) \tag{4}$$

Graphical representation of the MR damper reverse model is shown in Fig. 3. It should be noted that the MR damper is a passive device and the desired force F_a can be realized only if this force and damper velocity have the same sign. Than the calculated input current of the MR damper varies in the range of 0 A (minimum value) and 1 A

(maximum value) and depends on the actual value of desired MR damper force and its actual velocity (c.f. 3). If the desired force and damper velocity have opposite sign than the input current is settled to zero.
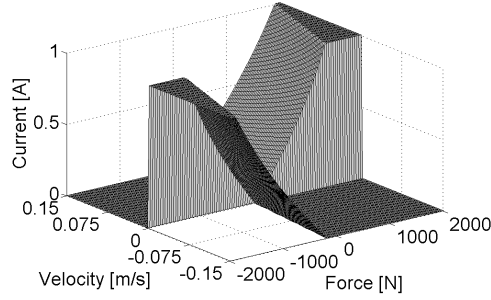
Figure 3. Reverse model of the magneto-rheological damper $i = f(F_a, \dot{x} - \dot{x}_s)$

4. Desired damper force

A proper design of the vibration isolation systems implies a lot of difficulties for the designers, because conflicted objectives are involved in this case [3]. Forces transmitted to the isolated body should be reduced by the suspension system, but this is only the first objective of a system evaluation. The second objective is that the suspension travel has to be minimized as well.

On the one hand, the suspended mass velocity $\dot{x}$ should approach zero, in order to protect the isolated body against a harmful vibration. On the other hand, the relative displacement of suspension system $x - x_s$ should approach zero as well, in order to minimize the suspension travel. The desired damper force that deals with conflicted objectives can be defined as follows:

$$F_a = K_{\dot{x}}\dot{x} + K_{x-x_s}(x - x_s)$$ (5)

where: $K_{\dot{x}}$ is the proportionality factor of absolute velocity feedback loop and K_{x-x_s} is the proportionality factor of relative displacement feedback loop. A different selection of the controller settings allows decreasing the forces transmitted to suspended mass at the simultaneous increase of suspension travel and vice versa.

In order to check the elaborated control system, the desired active force and the predicted MR damper force obtained from the reverse model are compared as shown in Fig. 4. To check the effectiveness of the reverse model under various operating conditions, the excitation signal has the random wave form within the frequency range 1-5 Hz. The results are obtained at first estimation of the controller settings $K_{\dot{x}} = 2 \times 10^3$ Ns/m and $K_{x-x_s} = 20 \times 10^3$ N/m. In the Fig. 4 is clearly observed that the desired force is well predicted by the reverse model. Highest discrepancy between the desired force and the predicted MR damper force are shown while these forces are in opposite signs. In

this situation the MR damper cannot generate such desired force therefore the input current is settled to zero and minimum MR damper force is provided into the system.
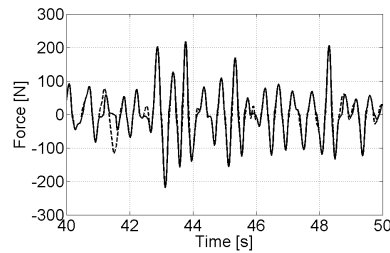
Figure 4. Desired damper force F_a (solid line)
and realized MR damper force F_{mr} (dashed line)

5. Simulation results

The MR damper control is realized by algorithm presented in Eqs. (3), (4) and (5). In Fig. 5 the simulation results obtained for the semi-active seat suspension (variable input) in comparison with the passive system (constant input $i = 0,3$ A) are presented.
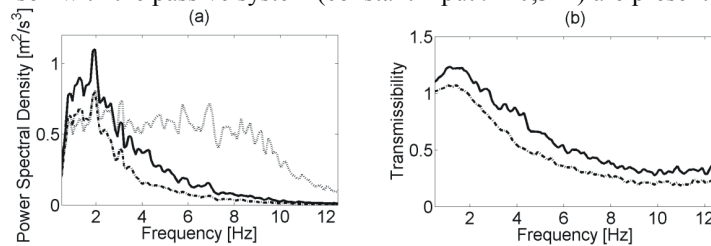
Figure 5. Simulated power spectral densities (a) and transmissibility curves (b)
of the semi-active suspension with MR damper control (dash-dotted line) and of the
passive suspension (solid line), power spectral density of excitation signal (dotted line)

The advantage of the semi-active suspension system with continuous damping control is the attenuation of resonant frequency vibration without the amplification of high frequency vibration. Simulated Seat Effective Amplitude Transmissibility factors (SEAT) [7] of the passive and semi-active suspension systems are: 0,618 and 0,462, respectively. The maximum relative displacements of the passive and semi-active suspension systems are: 112 mm and 86 mm, respectively.

6. Conclusions

The semi-active seat suspension with magneto-rheological damper effectively reduces vibration amplitudes in whole frequency range considered. The amplification of vibration amplitudes for the low frequency range is achieved by means of damping control using the MR damper device. The reduction of vibration amplitudes is also

obtained for the higher frequency range. Such effect of vibration isolation is required in order to improve the seat suspension performance.

Acknowledgments

References

1. Ballo I.: *Comparison of the properties of active and semiactive suspension*, Vehicle System Dynamics, Vol. 45, No. 11 (2007), 1065-1073
2. Spencer Jr. B. F., Dyke S. J., Carlson J. D.: *Phenomenological Model for Magnetorheological Dampers*, Journal of Engineering Mechanics 123(3) (1997), 230-238
3. He Y., McPhee J.: *Multidisciplinary design optimization of mechatronic vehicles with active suspensions*, Journal of Sound and Vibration 283 (2005), 217-241
4. Kromulski J., Kazmierczak H.: *Damping of vibrations with using magnetorheological fluid devices*, Journal of Research and Applications in Agricultural Engineering, Vol. 51(3) (2006), 47-49
5. Maciejewski I.: *On modelling of working machines seat suspension (in Polish)*, Logistyka No. 3/2009 (CD publication)
6. Maciejewski I.: *Vibro-isolation properties of semi-active seat suspension with the magneto-rheological damper (in Polish)*, Pomiary, Automatyka, Kontrola, No. 9/2009, 727-730
7. ISO 7096, *Earth-moving machinery – Laboratory evaluation of operator seat vibration*, Geneva 2000

**Modelowanie i sterowanie semi-aktywnym systemem zawieszenia siedziska
z tłumikiem magneto-reologicznym**

W pracy zawarto zagadnienia związane z modelowaniem i sterowaniem semi-aktywnego układu zawieszenia siedziska z tłumikiem magneto-reologicznym. W celu zwiększenia ochrony operatorów maszyn roboczych przed szkodliwym działaniem drgań mechanicznych, właściwości wibroizolacyjne konwencjonalnego systemu zawieszenia siedziska zostały poprawione poprzez zastosowanie tłumika magneto-reologicznego. W pracy analizowano charakterystyki wibroizolacyjne semi-aktywnego układu tłumienia drgań, dla którego opracowano algorytm sterowania bazujący na modelu odwrotnym tłumika magneto-reologicznego i kontrolerze głównym. Właściwości dynamiczne układu pasywnego oraz semi-aktywnego porównano wykorzystując współczynnik przenoszenia drgań siedziska oraz maksymalne przemieszczenia względne systemu zawieszenia. Jako wyniki symulacji komputerowej zaprezentowano gęstości widmowe przyspieszenia drgań na siedzisku oraz funkcje przenoszenia systemu zawieszenia dla wymuszenia jego ruchu sygnałem losowym.

Natural Frequencies and Mode Shapes
of a Composite Annular Membrane

Adam MARCINIEC

Faculty of Mechanical Engineering and Aeronautics, Rzeszów University of Technology
ul. W. Pola 2, 35 – 959 Rzeszów, Poland
amarc@prz.edu.pl

Stanisław NOGA

Faculty of Mechanical Engineering and Aeronautics, Rzeszów University of Technology
ul. W. Pola 2, 35 – 959 Rzeszów, Poland
noga@prz.edu.pl

Abstract

In the paper the transversal vibrations of a system of composite annular membrane is studied using analytical methods and numerical simulation. The two mathematical models are analyzed. At first the motion of the system is described by two homogeneous partial differential equations. The general solution of the free vibrations are derived by the Bernoulli – Fourier method and the boundary problem is solved. The second model is formulated by using finite element representations. The natural frequencies and natural mode shapes of vibration of the system are determined. The FE model is manually tuned to reduce the difference between the natural frequencies of the analytical solution and the natural frequencies of the FE model calculations, respectively. It is important to note that the data presented in the paper have the practical meaning for design engineers.

Keywords: composite annular membranes, transverse vibration, natural frequencies, mode shapes

1. Introduction

The free transverse vibration analysis of membranes with discontinuously varying material properties is the subject of many recent investigations. The majority of previous work in the field present solutions for the free vibrations of the circular, annular and rectangular membrane systems. Fundamental theory of vibration of simple two – dimensional continuous systems is elaborated in [3]. Free transverse vibrations of composite rectangular membranes are studied in the work [1]. In the paper [4] exact solution for the vibration frequencies of a composite annular membranes with discontinuously varying density is given by using theory of membrane. In this paper the free transverse vibrations of a composite annular membrane system with discontinuously varying density and thickness are analyzed using classical membrane theory and finite element technique. The analytical solution is used to manual tuning the finite element model of the system. This work continues the recent author's investigations concerning vibrations of membrane systems [2].

2. Formulation of the problem

The objective of this work is formulation of a dynamic model of an annular composite membrane. It is assumed that the membrane is thin and it is composed of two concentric portion of the homogeneous regions. Each region has the constant thickness. The membrane is uniformly tense by adequate constant tensions applied at the edges. Making use of the classical theory of vibrating membranes, the partial differential equations of motion for the free transversal vibrations are

$$\frac{1}{r}\frac{\partial}{\partial r}\left(r\frac{\partial w_i}{\partial r}\right)+\frac{1}{r^2}\frac{\partial^2 w_i}{\partial\varphi^2}-\frac{1}{a_i^2}\frac{\partial^2 w_i}{\partial t^2}=0, \qquad i=1,2 \tag{1}$$
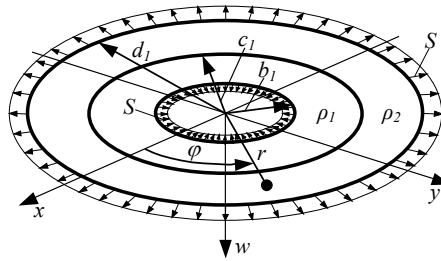
Figure 1. Vibrating system under study

where $w_i = w_i(r,\varphi,t)$ is the transverse membrane displacement, r,φ,t are the polar coordinates and the time, b_1,c_1,d_1,h_1,h_2 are the membrane dimensions, ρ_i is the mass density, S is the uniform constant tension per unit length and

$$a_1^2 = S/(\rho_1 h_1), \qquad a_2^2 = S/(\rho_2 h_2) \tag{2}$$

The boundary and the compatibility conditions are

$$w_1(b_1,\varphi,t)=0, \quad w_2(d_1,\varphi,t)=0, \quad w_i(r,\varphi,t)=w_i(r,\varphi+2\pi,t), \quad i=1,2$$
$$w_1(c_1,\varphi,t)=w_2(c_1,\varphi,t), \qquad \frac{\partial w_1(c_1,\varphi,t)}{\partial r}=\frac{\partial w_2(c_1,\varphi,t)}{\partial r} \tag{3}$$

3. Free vibration analysis

Now using the separation of variables method, one writes [3, 4]

$$w_i(r,\varphi,t)=R_i(r)U(\varphi)T(t), \qquad T(t)=L\cos\omega t+M\sin\omega t, \quad i=1,2 \tag{4a, b}$$

where ω is the natural frequency of the system. The boundary and compatibility conditions in terms of $R_i(r)$ become

$$R_1(b_1)=R_2(d_1)=0, \qquad R_1(c_1)=R_2(c_1), \quad \frac{dR_1(c_1)}{dr}=\frac{dR_2(c_1)}{dr} \tag{5}$$

Substituting solution (4a) into (1) yields

$$R_{in}(r) = A_{in}J_n(r\,\omega/a_i) + B_{in}Y_n(r\,\omega/a_i), \quad U_n(\varphi) = C_n\sin(n\varphi) + D_n\cos(n\varphi), \quad i = 1,2 \qquad (6)$$

where J_n and Y_n are the Bessel functions of the first and second kinds, respectively. The constants A_{in}, B_{in} are determined from the boundary and compatibility conditions. Conditions (5) yields a system of four linear, homogeneous equations in the constants A_{1n}, A_{2n} and B_{1n}, B_{2n}, respectively. Finally, a determinantal equation in the natural frequencies is obtained from the non–triviality condition. It yields the secular determinant

$$\begin{vmatrix} J_n(b_1\omega/a_1) & Y_n(b_1\omega/a_1) & 0 & 0 \\ J_n(c_1\omega/a_1) & Y_n(c_1\omega/a_1) & -J_n(c_1\omega/a_2) & -Y_n(c_1\omega/a_2) \\ -m_{31} & -m_{32} & m_{33} & m_{34} \\ 0 & 0 & J_n(d_1\omega/a_2) & Y_n(d_1\omega/a_2) \end{vmatrix} = 0 \qquad (7)$$

where the roots of the determinantal equation (7) $\omega = \omega_{mn}\ (m = 1,2,3,\dots)$ are the free frequencies of the membrane and

$$m_{31} = \frac{n}{c_1}J_n(c_1\omega/a_1) - \frac{\omega}{a_1}J_{n+1}(c_1\omega/a_1), \quad m_{32} = \frac{n}{c_1}Y_n(c_1\omega/a_1) - \frac{\omega}{a_1}Y_{n+1}(c_1\omega/a_1)$$

$$m_{33} = \frac{n}{c_1}J_n(c_1\omega/a_2) - \frac{\omega}{a_2}J_{n+1}(c_1\omega/a_2), \quad m_{34} = \frac{n}{c_1}Y_n(c_1\omega/a_2) - \frac{\omega}{a_2}Y_{n+1}(c_1\omega/a_2) \qquad (8)$$

The general solution of equation (1) takes the form

$$w_1(r,\varphi,t) = \sum_{m=1}^{\infty}\sum_{n=0}^{\infty} R_{1mn}(r)U_n(\varphi)T_{mn}(t) = \sum_{m=1}^{\infty}\sum_{n=0}^{\infty}\left(\left(K_{1mn}^{(1)}\cos(\omega_{mn}t) + N_{1mn}^{(1)}\sin(\omega_{mn}t)\right)\times\right.$$
$$\left.\times W_{1mn}^{(1)}(r,\varphi) + \left(K_{1mn}^{(2)}\cos(\omega_{mn}t) + N_{1mn}^{(2)}\sin(\omega_{mn}t)\right)W_{1mn}^{(2)}(r,\varphi)\right)$$

$$w_2(r,\varphi,t) = \sum_{m=1}^{\infty}\sum_{n=0}^{\infty} R_{2mn}(r)U_n(\varphi)T_{mn}(t) = \sum_{m=1}^{\infty}\sum_{n=0}^{\infty}\left(\left(K_{2mn}^{(1)}\cos(\omega_{mn}t) + N_{2mn}^{(1)}\times\right.\right.$$
$$\left.\left.\times\sin(\omega_{mn}t)\right)W_{2mn}^{(1)}(r,\varphi) + \left(K_{2mn}^{(2)}\cos(\omega_{mn}t) + N_{2mn}^{(2)}\sin(\omega_{mn}t)\right)W_{2mn}^{(2)}(r,\varphi)\right) \qquad (9)$$

where

$$W_{1mn}^{(1)}(r,\varphi) = \left(e_{1mn}J_n(r\omega_{mn}/a_1) + Y_n(r\omega_{mn}/a_1)\right)\sin(n\varphi)$$
$$W_{1mn}^{(2)}(r,\varphi) = \left(e_{1mn}J_n(r\omega_{mn}/a_1) + Y_n(r\omega_{mn}/a_1)\right)\cos(n\varphi)$$
$$W_{2mn}^{(1)}(r,\varphi) = \left(e_{2mn}J_n(r\omega_{mn}/a_2) + Y_n(r\omega_{mn}/a_2)\right)\sin(n\varphi)$$
$$W_{2mn}^{(2)}(r,\varphi) = \left(e_{2mn}J_n(r\omega_{mn}/a_2) + Y_n(r\omega_{mn}/a_2)\right)\cos(n\varphi) \qquad (10)$$

are the eigenfunctions and

$$e_{1mn} = -Y_n\left(b_1\omega_{mn}/a_1\right)\!/J_n\left(b_1\omega_{mn}/a_1\right), \quad e_{2mn} = -Y_n\left(d_1\omega_{mn}/a_2\right)\!/J_n\left(d_1\omega_{mn}/a_2\right) \qquad (11)$$

Each natural frequency ω_{mn} correspond two linear – independent mode shapes which may be plotted from relations

$$W_{1mn}^{*} = W_{1mn}^{(1)}, \quad W_{2mn}^{*} = W_{2mn}^{(1)}; \qquad\qquad W_{1mn}^{**} = W_{1mn}^{(2)}, \quad W_{2mn}^{**} = W_{2mn}^{(2)} \qquad (12a, b)$$

4. The finite element representations

In this section the finite element (FE) models are formulated to discretize the continuous models given by the equations (1). To find the eigenpairs (eigenvalue, eigenvector) connected with the natural frequencies and natural mode shapes of the system, the block Lanczos method is employed [5]. As mentioned earlier, the FE models are treated as an approximation of the exact systems. In this work the impact of the manner of the membranes tensile forces application in the FE models on the quality of the accurate model approximation is analysed. In order to make a comparison of the continuous system analysis results with the FE models solutions, two finite element models are prepared and discussed.

The first FE model consists of the composite annular membrane divided into 8964 finite elements. The four node quadrilateral membrane element with six degree of freedom in each node is used to solve the problem. The uniform constant tension per unit length is applied to the outer edge by using the ANSYS code system standard procedure. The prepared model is shown in Fig. 2.
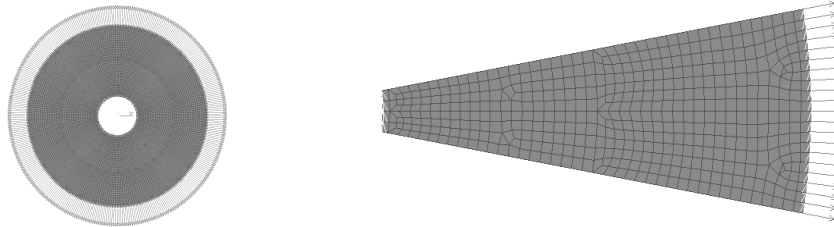
Figure 2. Finite element model

The second FE model of the system taken into consideration is the same as the first, but the application of the constant tension is different. To each node lying on the outer edge is imposed a concentrated tensile force S_j in the radial direction. The proper value of the force is selected experimentally to minimize the frequency error [5]

$$\varepsilon_{mn} = \left(\omega_{mn}^{f} - \omega_{mn}^{c}\right)\!/\omega_{mn}^{c} \cdot 100\% \qquad (13)$$

where ω_{mn}^{f} and ω_{mn}^{c} are the natural frequencies of the FE and exact models, respectively.

5. Numerical analysis

Numerical analysis results of the composite annular membrane free vibration are obtained using the models suggested earlier. For each approach, only the first ten natural frequencies and mode shapes are discussed and compared for these two models. The parameters characterizing the system used in calculations are shown in Table 1.

Table 1. Parameters characterizing the composite membrane

b_1 [m]	c_1 [m]	d_1 [m]	h_1 [m]	h_2 [m]	ρ_1 [kg/m^3]	ρ_2 [kg/m^3]	E_1 [Pa]	E_2 [Pa]	v_1	v_2	S *[N/m]*
0.1	0.3	0.5	0.001	0.002	$7.85 \cdot 10^3$	$2.7 \cdot 10^3$	$2.05 \cdot 10^{11}$	$7 \cdot 10^{10}$	0.29	0.32	*1000*

In the table, E_i and v_i $(i=1,2)$ are, the Young's modulus of elasticity and Poisson ratio, respectively. In this paper the continuous model is considered as exact, compared to the FE models, which are treated as approximation of the precise model.

For the continuous model the natural frequencies are determined from numerical solution of the equation (7). The results of the calculation of the natural frequencies are shown in Table 2.

Table 2. Natural frequencies of the composite membrane system ω_{mn} [Hz] (exact model)

		n					
		0	1	2	3	4	5
m	1	14.8413	16.5576	20.6931	25.7996	31.1661	36.553
	2	30.8524	31.8401	34.5752	38.5114		

The natural frequencies and the frequency errors (see eq. (13)) obtained by using the first FE model of the system under investigation are presented in Tables 3 – 4, respectively.

Table 3. Natural frequencies of the composite membrane system ω_{mn} [Hz]

		n					
		0	1	2	3	4	5
m	1	15.849	17.227	20.717	25.247	30.141	35.099
	2	32.751	33.498	35.636	38.898		

Table 4. Frequency error ε_{mn} [%]

		n					
		0	1	2	3	4	5
m	1	6.7898	4.0429	0.1155	-2.1419	-3.2892	-3.9778
	2	6.1538	5.207	3.068	1.0039		

In the second FE model case the results presented in Tables 5 – 6 are achieved for $S_j = 8.7 [N]$.

Table 5. Natural frequencies of the composite membrane system ω_{mn} [Hz]

		n					
		0	1	2	3	4	5
m	1	15.825	17.201	20.686	25.21	30.096	35.046
	2	32.702	33.448	35.583	38.839		

Table 6. Frequency error ε_{mn} [%]

		n					
		0	1	2	3	4	5
m	1	6.6281	3.8858	-0.0343	-2.2853	-3.4335	-4.1227
	2	5.995	5.0499	2.9148	0.8507		

For both FE model cases the largest difference between the analytical results and the FE solutions can be visible for the frequencies ω_{10}, ω_{20} and ω_{21}, respectively. In the second FE model case only for the frequencies ω_{13}, ω_{14} and ω_{15}, the frequency error increased.

6. Conclusions

The present work deals with the transverse vibrations of a composite annular membrane. The free vibrations are determined by using the separation of variables method and finite element technique. Due to space limitation the mode shapes are not presented. The exact solution is utilized to manually tune the FE model. At this stage of search it seems that the second FE model would be better to simulate the analyzed system. The main advantage of using the second FE model is the knowledge regarding the value of the concentrated tensile force applied to all the nodes lying on the outer edge.

References

1. S. Kang,, *Free vibration analysis of composite rectangular membranes with a bent interface*, J. of Sound and Vibration, **272** (2004) 39 – 53.
2. S. Noga,, *Free transverse vibration analysis of an annular membrane*, Vibrations in Physical Systems, vol. XXIII (2008) 283 – 288.
3. S. Rao, *Vibration of continuous systems*, Wiley, New Jersey 2007
4. C. Rossit, S. Malfa, P. Laura,, *Antisymmetric modes of vibrations of composite, doubly – connected membranes*, J. of Sound and Vibration, **217** (1998) 191 – 195.
5. C. Silva, *Vibration and shock handbook*, Taylor & Francis, Boca Raton, 2005

Częstości własne i postacie drgań własnych kompozytowej membrany pierścieniowej

Przedmiotem rozważań niniejszej pracy jest analiza drgań poprzecznych kompozytowej membrany pierścieniowej. Omawiane w pracy modele matematyczne układu opracowano wykorzystując klasyczną teorię drgań poprzecznych membran oraz metodę elementów skończonych. Ścisłe rozwiązanie drgań układu otrzymano stosując metodę rozdzielenia zmiennych (metodę Bernoulliego – Fouriera). W oparciu o uzyskane rozwiązanie, wyznaczono częstości własne i odpowiadające im postacie drgań własnych układu. Wyniki rozwiązania analitycznego wykorzystano do dostrajania zaproponowanych modeli elementów skończonych układu.

Dynamics of a rotor of asynchronous motor loaded with magnetic tension and axial force

Waldemar MORZUCH

Wrocław University of Technology, 50-372 Wrocław, ul. Smoluchowskiego 25
waldemar.morzuch@pwr.wroc.pl

Abstract

Purpose of research work represented in the said paper consisted in fulfilment of analysis of dynamic stability of a rotor of asynchronous motor. The rotor model of continuous mass distribution and variable rigidity was assumed for analysis. On the ground of motion equations differential equations binding dynamic deflections of the rotor with space and time have been obtained. Finally, there have been obtained partial differential equations, heterogeneous and of variable coefficients which have been solved by application of the variables separation method. Then the ordinary differential equation describing the vibration of the rotor in time function have been solved. On the basis of the above mentioned, the characteristic equation have been derived. The critical values of magnetic tension and axial force have been determined.

Keywords: rotor, dynamic stability, deflection, vibration

1. Introduction

Among in electric machines, the squirrel-cage asynchronous motors occupy a particular space. These motors have small value of the magnetic gap. For this reason, the basic problem encountered in the phase of construction of such machines is to estimate the stability of the rotors. The problem of stability rotors is in relation to the problem of vibration. On certain values of some quantities, such as rotational speed, magnetic tension rigidity etc., the effect of unstability can take place. The assesment of the stability is of particular importance in the case of long rotors loaded by axial force, for example rotors of motors of deep-well pumps. Such pumps works in deep waters. It follows that the rotors of such motors are loaded by large forces. In this paper the influence of axial force and magnetic tension on the frequency of free vibration has been determined. Estimation, of the stability of transverse motion of rotors is presented in works [3]÷[5]. In these works, the influence of the axial force was not considered. After analyzing a number of positions of the professional literature (for example [1], [2]) relative to this problem, one can state that the considerations presented there are based on a simple model of the rotor, reduced to a point mass with spring. The force of magnetic tension is (assumptioned) as a concentrationed force. This assumption is not consistent with the reality, because the force is continuously distributed on the surface of the packet. Influence of axial force and magnetic tension on the free vibration frequency has been determined in the paper.

2. The dynamic stability of the rotor

In order to estimate the dynamic stability of the rotor, it is necessary to formulate differential equations, expressing the relation between the dynamic deflections of the

rotor with space and time. These equations have been derived in a similar way as in the paper [3]. The force of magnetic tension is continuous load on the surface of rotor and is acting in direction of a rotor's centre deflection. A load intensity of the magnetic tension (Fig.1) can be described by following formula [2]:

$$q(x) = Cy(x) \tag{1}$$

where: C – coefficient of the magnetic tension, y(x) – deflection of the rotor

The rotor shown in Fig. 1 is loaded with magnetic tension and axial force. In order to simplify the considerations a vertical position of the rotor has been assumed (position of rotors in deep-well pumps).
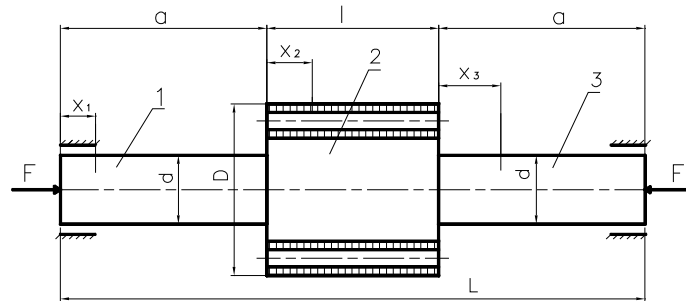
Fig. 1. The rotor loaded by magnetic tension and axial force

The differential equations of dynamic deflections of the rotor can be obtained on the basic of the differential equation of a centre line of a beam.
This equation can be introduced in the form:

$$S\frac{\partial^2 y}{\partial x^2} = -M \tag{2}$$

where: S – flexural rigidity of the section on which acts the magnetic tension (section 2), M – bending moment.
The bending moment M can be expressed as M = Fy and equation (2) in the form:

$$S\frac{\partial^4 y}{\partial x^4} = -q_x \tag{3}$$

where q_x is load intensity in the section 2 which can be introduced in the form:

$$q_x = q_{1x} + q_{2x} + q_{3x} \tag{4}$$

where: q_{1x} – load intensity taking into account influence of a compressive force F, q_{2x} – load intensity taking into account influence of forces of inertia, q_{3x} - load intensity taking into account influence of the magnetic tension.

The equation (3) can be then introduced in the form:

$$\beta^2 \frac{\partial^4 y}{\partial x^4} + \alpha \frac{\partial^2 y}{\partial x^2} - \gamma y + \frac{\partial^2 y}{\partial t^2} = 0 \tag{5}$$

where:

$$\beta^2 = \frac{S}{\mu} \qquad \alpha = \frac{F}{\mu} \qquad \gamma = \frac{C}{\mu} \tag{6}$$

μ – unit mass (per unit length) of the section 2, t - time

Equation (5) is a partial differential equation with constant coefficients. It can be solved by means of Fourier's method and presented in form of infinite series

$$y = \sum_{n=1}^{\infty} X_n(x)T_n(t) \tag{7}$$

After a separation of variables and definion of parameter k_n the following equations have been obtained:

$$\beta^2 \overset{IV}{X}_n + \alpha \overset{II}{X}_n - k_n^4 X_n = 0 \tag{8}$$

$$\overset{\bullet\bullet}{T}_n + \omega_n^2 T_n = 0 \tag{9}$$

where ω_n denotes the n – order frequency of free vibrations of rotor.

On the basis of above equations the following formula has been obtained:

$$\omega_n^2 = k_n^4 - \gamma \tag{10}$$

The equation (8) can be introduced in the form

$$\overset{IV}{X}_n + a \overset{II}{X}_n - bX_n = 0 \tag{11}$$

The solution of the equation (11) can be introduced in the form

$$X_n = C_{1n}shmx + C_{2n}chmx + C_{3n}\sin nx + C_{4n}\cos nx \tag{12}$$

where

$$m = \sqrt{\frac{-a + \sqrt{a^2 + 4b}}{2}} \; , \; n = \sqrt{\frac{a + \sqrt{a^2 + 4b}}{2}} \tag{13}$$

The constants in solution (12) can be determined on the basis of the boundary conditions. The equations describing the boundary conditions can be written in the following form:

$$f(k_n) = 0 \tag{14}$$

Is results from the above considerations that equation (14) has an infinite quantity of solutions. This way, the next frequency of the rotor can be determined. The equation (14) was solved with an microcomputer.

3. Example of calculations

This chapter presents calculations of a rotor for following data: L=0,7m , l=0,375m , d=0,05m ,D=0,08m. Calculations were done for different values of the coefficient of the magnetic tension C. Fig. 2 shows the diagram of the frequency ω_n (the formula 10) against the axial force F, with different values of magnetic tension coefficients C.

The point of intersection of the curve with the axis of abscissae determines the value of the so-called critical force. In the presence of this force instability of the rotor occurs.
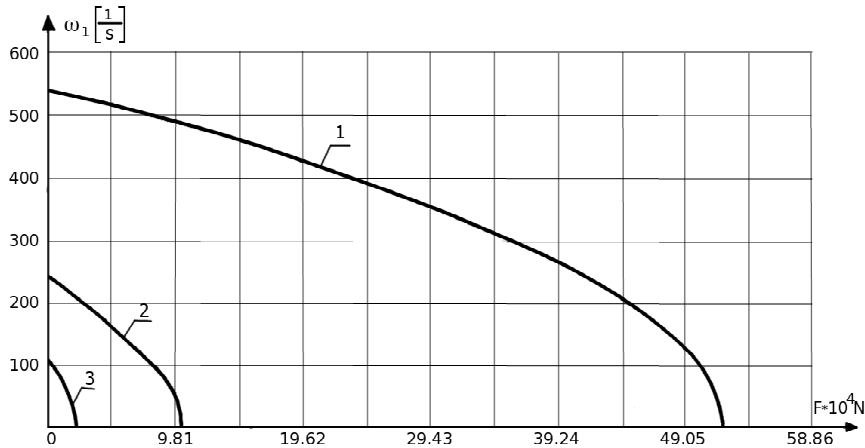
Fig. 2. The relations between rotor's natural frequency ω_1 and axial force F: 1 – C=19,62 MPa, 2 – C=29,43 MPa, 3 – C=31,39 MPa

On the basis of the diagram shown in Fig. 2 one can state that with the value of the coefficient C=19,62 MPa, the critical force has a value of about $F=5{,}4 \cdot 10^{-5}$ N. If C=29,43 MPa, the critical force has a value of about $F=10^5$ N. However, if C=31.39 MPa, F has a value of about $0{,}23 \cdot 10^5$ N. The diagram shown in Fig. 2 demonstrate that there exist such a magnetic tension called the critical one, at which the frequency of free vibrations of the rotor is equal to zero. On the basic of the above example of calculations, the critical magnetic tension has a value of C_{cr}=31,98 MPa.

4. Conclusions

The increase of magnetic tension as well as the increase of the axial force causes the decrease of the frequency of free vibrations of the rotor. The diagram describing the dependence of the free vibrations frequency of the rotor on the axial force is a decreasing function. The diagram of this function remind a parabola with horizontal axis of symmetry. There exist a critical magnetic tension and a critical force at which the rotor loses stability of the transverse motion.

References

1. Aleksiejev A.E.: *Konstrukcja maszyn elektrycznych   (Design of electric machines – in Polish)*. Warszawa, PWT, 1953.
2. Dąbrowski M.: *Konstrukcja maszyn elektrycznych (Design of electrical machines – in Polish)*. Warszawa, WNT, 1977.
3. Gabryszewski Z., Morzuch W.: *Analiza dynamiczna wirników silników asynchronicznych klatkowych (Dynamic analysis of squirrel-cage asynchronous motors – in Polish)*. Archiwum Elektrotechniki, Vol. XXX, No. 1, 1981.

4. M o r z u c h W .: *Statecznośc dynamiczna wirników dwubiegunowych silników asynchronicznych (Dynamic stability of rotors of two-pole asynchronous motors – in Polish)*. Archiwum Elektortechniki, Vol. XXXII, No. 3-4, 1983.

5. M o r z u c h W .: *Obszary niestateczności wirników klatkowych dwubiegunowych silników asynchronicznych (Instability areas of squirrel-cage rotors of two-pole asynchronous motors – in Polish)*. Archiwum Budowy Maszyn, Vol. XXXIII, No. 2, 1986.

Dynamika wirnika silnika asynchronicznego obciążonego naciągiem magnetycznym i siłą osiową

Celem pracy przedstawionej w artykule było dokonanie analizy stateczności dynamicznej wirnika silnika asynchronicznego. Do analizy przyjęto model wirnika o ciągłym rozłożeniu masy i zmiennej sztywności. Na podstawie równań ruchu otrzymano równania różniczkowe wiążące ugięcia dynamiczne wirnika z przestrzenią i czasem. Ostatecznie otrzymano równania różniczkowe, cząstkowe niejednorodne i o zmiennych współczynnikach, które rozwiązano stosując metodę rozdzielenia zmiennych. Następnie rozwiązano równanie zwyczajne opisujące drgania wirnika w funkcji czasu.

Na podstawie powyższego rozwiązano równanie charakterystyczne. Wyznaczono krytyczne wartości naciągu magnetycznego i siły osiowej.

Dynamics of a rotor of two-pole asynchronous motor with damping

Waldemar MORZUCH

Wrocław University of Technology, 50-372 Wrocław, ul. Smoluchowskiego 25
waldemar.morzuch@pwr.wroc.pl

Abstract

The paper presents an analysis of dynamic stability of a rotor in two-pole asynchronous motor. A model of the rotor with continuous mass distribution, with changeable rigidity and with damping have been applied in the analysis. In order to determine the stability of the rotor transverse motion equations of its transverse vibration have been formulated. From the equations of motion, differential equations interrelating of the rotor dynamic deflection with space and time have been derived. Eventually, homogeneous, partial, differential equations have been obtained and solved by the Fourier's method. Then an ordinary differential equation (Hill's equation) describing the rotor vibration have been solved. An analysis of the solution became the basis for determining the regions of rotor motion instability. Finally, the critical damping coefficient values at which parametric resonance occurs have been determined.

Keywords: rotor, dynamic stability, deflection, damping coefficient, vibration

1. Introduction

Among in electric machines, the two-pole asynchronous motors occupy a particular space. These motors have small value of the magnetic gap. For this reason, the basic problem encountered in the phase of construction of such machines is to estimate the stability of the rotors. The problem of stability of rotors is in relation to the problem of vibration. On certain values of some quantities, such a rotational speed, magnetic tension, rigidity, etc. the effect of unstability can take place. The assessment of the stability is of particular importance in the case of long rotors, for example rotors of motors of deep-well pumps.

Problem of estimation of stability of transverse motion of rotors without damping are presented in the works [4,6,7]. In this paper the influence of damping in rotors on the dynamic stability of its rotors in two-pole asynchronous motors have been determined.

2. Dynamic stability of rotor

The model of rotor accepted for calculations is shown in Fig.1.
In order to simplify the considerations a vertical position of the rotor have been assumed. The basis for describing the dynamic stability of the rotor is the differential equation of the centre line of the beam. The equation can be written as:

$$S\frac{\partial^4 y}{\partial x^4} = -q_x \tag{1}$$

where: S – flexural rigidity of the section 2
　　　 y – deflection of the rotor
　　　 q_x – load intensity
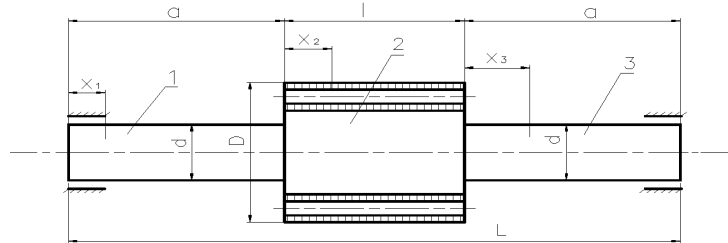
Fig.1. The model of rotor accepted for calculations

The load intensity q_x can be introduced in the form:

$$q_x = q_{1x} + q_{2x} + q_{3x} \tag{2}$$

where: q_{1x} – load intensity related to the influence of the forces of inertia,

q_{2x} – load intensity related to the influence of the magnetic tension,

q_{3x} – load intensity related to the influence of the damping.

The load intensity q_{1x} can be expressed as:

$$q_{1x} = -\mu \frac{\partial^2 y}{\partial t^2} \tag{3}$$

where: μ – mass of the unit of length of the section 2

t – time

The load intensity q_{2x} can be expressed as [1,2]:

$$q_{2x} = (A_1 + A_2 \cos pt)y \tag{4}$$

where: A_1, A_2, p – parameters of magnetic tension [2,6,7].

The load intensity q_{3x} can be expressed as:

$$q_{3x} = -\eta_r \frac{\partial y}{\partial t} \tag{5}$$

where: η_r – damping coefficient on the rotor

After substituting (2) in (1), the following differential equation in obtained:

$$\beta^2 \frac{\partial^4 y}{\partial x^4} + \frac{\partial^2 y}{\partial t^2} + 2h\frac{\partial y}{\partial t} - (\gamma + \vartheta \cos pt)y = 0 \tag{6}$$

where: $\qquad \beta^2 = \dfrac{S}{\mu} \;, \; 2h = \dfrac{\eta}{\mu} \;,\; \gamma = \dfrac{A_1}{\mu}, \;\; \vartheta = \dfrac{A_2}{\mu} \tag{7}$

The above equation is a fourth – order homogeneous equation with time – dependent coefficients. It was solved by the Fourier's method. The solution can be presented in the form of an infinite series:

$$y = \sum_{n=1}^{\infty} X_n(x)T_n(t) \tag{8}$$

After a separation of variables and definion of parameter k_n the following equations have been obtained:

$$\overset{IV}{X_n}(x) - k_n^4 \overset{II}{X_n}(x) = 0 \tag{9}$$

$$\ddot{T}_n + 2h\,\dot{T}_n + (\omega_n^2 - \vartheta \cos pt)T_n = 0 \tag{10}$$

where: ω_n denotes the n – order frequency of free vibrations of rotor when $\vartheta = 0$,

$\eta_r = 0$

The equation (10) can be expressed as follows:

$$\ddot{T}_n + 2h\,\dot{T}_n + \omega_n^2(1 - 2\psi_n \cos pt)T_n = 0 \tag{11}$$

where:

$$2\psi_n = \frac{\vartheta}{\omega_n^2} \tag{12}$$

Differential equation (11) is Hill's equation in the form [3,5]:

$$\ddot{T}_n + 2h\,\dot{T}_n + \Omega_n^2[1 - f(t)]T_n = 0 \tag{13}$$

If there is no damping in the rotor (h=0) and assuming $f(t) = 2\psi_n \cos pt$, one gets the following classical Mathieu equation:

$$\ddot{T}_n + \omega_{on}^2(1 - 2\psi_n \cos pt)T_n = 0 \tag{14}$$

Let us now analyse the stability solutions of the differential equation (13) limiting the analysis to the first (most important) region of instability. By solving of this equation the boundary lines of the first region of instability has been obtained (Fig.2.).
The relations for the first region of instability are obtained:

$$\frac{P}{\Omega_n} < 2\sqrt{\frac{(1 - \xi_n)^2 - \psi_n^2}{1 - 3\xi_n - \sqrt{\psi_n^2 - 4\xi_n + 8\xi_n^2}}} \tag{15}$$

$$\frac{P}{\Omega_n} > 2\sqrt{\frac{(1 - \xi_n)^2 - \psi_n^2}{1 - 3\xi_n + \sqrt{\psi_n^2 - 4\xi_n + 8\xi_n^2}}} \tag{16}$$

where:

$$\xi_n = (\frac{h}{\Omega_n})^2 \tag{17}$$
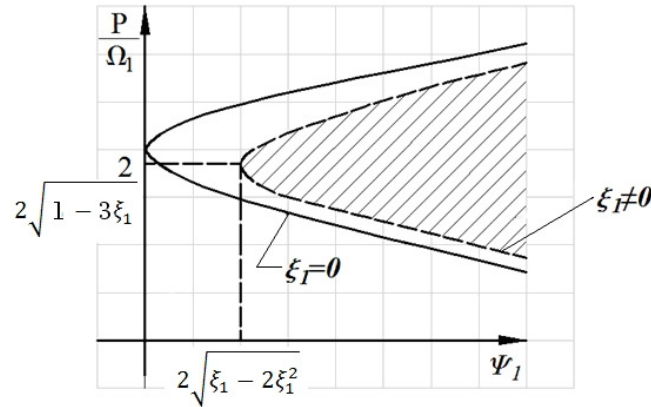
Fig.2. First region of instability ($\xi_1 = 0$, without damping, $\xi_1 \neq 0$, with damping)

Vertex of the first region instability has the coordinates:

$$\psi_{1gr} = 2\sqrt{\xi_1 - 2\xi_1^2} \ , \quad \frac{P}{\Omega_1} = 2\sqrt{1 - 3\xi_1} \tag{18}$$

Relation (15) and (16) describe the upper and lower boundary line, respectively. From formula (18) the boundary value of coefficient ψ_1 at which parametric resonance occurs has been obtained. If $\psi_1 < \psi_{1gr}$, no parametric resonance arises. It follows from the above that there exist coefficient A_2 of magnetic tension and coefficient of damping ξ_1 at which the rotor does not lose stability.

3. Conclusions

The magnetic field (described by the coefficients A_1, A_2 and frequency p) in two – pole asynchronous motor and damping in rotor have a great influence on the rotor stability. Damping reduces the areas of instability of rotor. Owing to damping, there are certain values of coefficients of magnetic field at which the rotor does not stability.

References

1. A l e k s i e j e v A . E .: *Konstrukcja maszyn elektrycznych (Design of electric machines – in Polish)*. Warszawa, PWT, 1953.
2. D ą b r o w s k i M .: *Konstrukcja maszyn elektrycznych (Design of electrical machines – in Polish)*. Warszawa, WNT, 1977.
3. D ż y g a d ł o Z ., K a l i s k i S ., S o l a r z L ., W ł o d a r c z y k E .: *Vibrations and vaves*, WAT, Warsaw 1965
4. G a b r y s z e w s k i Z ., M o r z u c h W .: *Analiza dynamiczna wirników silników asynchronicznych klatkowych (Dynamic analysis of squirrel-cage asynchronous motors – in Polish)*. Archiwum Elektrotechniki, Vol. XXX, No. 1, 1981.
5. M c L a c h l a n N . W .: *Theory and application of Mathieu Functions*, Oxford 1947.

6. M o r z u c h W .: *Stateczność dynamiczna wirników dwubiegunowych silników asynchronicznych (Dynamic stability of rotors of two-pole asynchronous motors – in Polish)*. Archiwum Elektrotechniki, Vol. XXXII, No. 3-4, 1983.

7. M o r z u c h W .: *Obszary niestateczności wirników klatkowych dwubiegunowych silników asynchronicznych (Instability areas of squirrel-cage rotors of two-pole asynchronous motors – in Polish)*. Archiwum Budowy Maszyn, Vol. XXXIII, No. 2, 1986.

Dynamika wirnika silnika asynchronicznego, dwubiegunowego z tłumieniem.

Artykuł przedstawia analizę stateczności dynamicznej wirnika dwubiegunowego silnika asynchronicznego. Przyjęto model wirnika z ciągłym rozłożeniem masy, o zmiennej sztywności z tłumieniem. W celu określenia stateczności wirnika ułożono równania opisujące jego drgania gięte. Na podstawie równań ruchu otrzymano równania różniczkowe opisujące ugięcia dynamiczne wirnika w funkcji przestrzeni i czasu. Ostatecznie otrzymano równanie różniczkowe cząstkowe, które rozwiązano metodą Fouriera. Następnie rozwiązano równania różniczkowe Hilla opisujące drgania poprzeczne wirnika. Analiza rozwiązania powyższego równania była podstawą do wyznaczenia obszarów niestateczności wirnika.

Ostatecznie wyznaczono krytyczną wartość współczynnika tłumienia przy której ma miejsce rezonans parametryczny.

Free Vibrations of an Annular Membrane Attached to Winkler Foundation

Stanisław NOGA

*Faculty of Mechanical Engineering and Aeronautics, Rzeszów University of Technology
ul. W. Pola 2, 35 – 959 Rzeszów, Poland
noga@prz.edu.pl*

Abstract

In this study the free transverse vibration analysis of the annular membrane resting on elastic foundation with fixed boundary conditions at the inner and outer edges of the annular membrane is presented on the basis of the analytical method and numerical simulation. The elastic foundation is described by the Winkler model. At first the general solution of the free vibrations are derived by the Bernoulli – Fourier method. The natural frequencies and natural mode shapes of vibrations of system under consideration are determined. Then the model of the system formulated by using finite element representations is prepared and eigenvalue problem is solved. Obtained results of calculation are discussed and compared for these two models. It is important to note that the data presented in the paper is brought the practical advice to design engineers.

Keywords: annular membrane, transverse vibration, natural frequencies, Winkler foundation

1. Introduction

Annular membranes have wide applications in various fields of engineering [3]. Sometimes, they are used as structural elements attached to foundations, such as parts of pharmaceutical, chemical and biomedical devices [3, 4]. Firstly, the fundamental vibration theory of two – dimensional continuous systems resting on foundation are mainly investigated for plates attached to elastic foundation. In work [1] a three – dimensional free vibration analysis of thick annular plates resting on elastic foundation of a Pasternak type is presented on the basis of the polynominals – Ritz method. Paper [5] describes a study of the three – dimensional vibration characteristics of thick circular plates resting on Pasternak foundation. This paper describes an investigation of the free vibration of annular membrane resting on Winkler foundation. The complete analytical solution of undamped free vibrations of this system is derived by using the Bernoulli – Fourier method. Then the studies focused on the preparation of the appropriate FE models of the system under study are provided. Some results known for the first time are reported.

2. Theoretical formulation

Mechanical model of the system taking into account consists of annular membrane resting on massless, linear, elastic foundation of a Winkler type. It is assumed that the membrane is thin, homogeneous and perfectly elastic, and it has constant thickness. The membrane is uniformly tense by adequate constant tensions applied at the edges of membrane (see Fig. 1). The small vibrations with no damping are considered. The partial

differential equation of motion for the free transversal vibrations can be written in the form [2, 3]

$$m_0 \ddot{w} - S\, \Delta w + k\, w = 0 \tag{1}$$
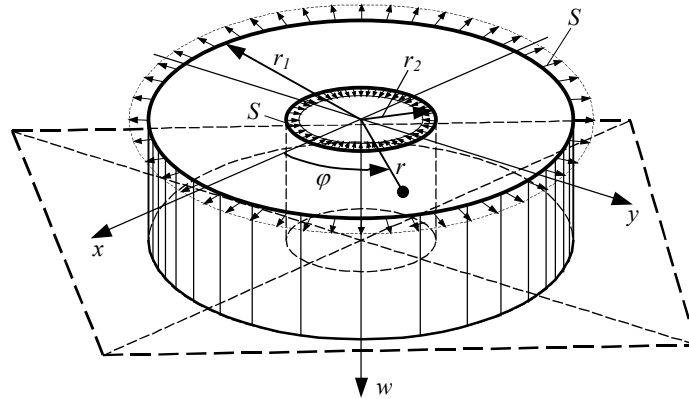
Figure 1. Physical model of the system

where $w = w(r,\varphi,t)$ is the transverse membrane displacement, r,φ,t are the polar coordinates and the time, r_1, r_2, h are the membrane dimensions, ρ is the mass density, S is the uniform constant tension per unit length, k is the stiffness modulus of a Winkler elastic foundation and

$$m_0 = \rho\, h, \quad \dot{w} = \frac{\partial w}{\partial t}, \quad \Delta w = \frac{\partial^2 w}{\partial r^2} + \frac{1}{r}\frac{\partial w}{\partial r} + \frac{1}{r^2}\frac{\partial^2 w}{\partial \varphi^2} \tag{2}$$

The boundary and periodicity conditions are

$$w(r_1,\varphi,t) = w(r_2,\varphi,t) = 0, \quad w(r,\varphi,t) = w(r,\varphi + 2\pi, t) \tag{3}$$

Making use of the classical method of separation of variables [2] one writes

$$w(r,\varphi,t) = W(r,\varphi)T(t), \qquad T(t) = C\sin(\omega t) + D\cos(\omega t) \tag{4a, b}$$

where ω is the circular frequency of the system. Introducing solutions (4) into (1) gives the following expression

$$\Delta W + k_1^2\, W = 0 \tag{5}$$

where

$$k_1^2 = \left(m\omega^2 - k\right)/S \tag{6}$$

The coefficient k_1^2 is positive when $\omega^2 > k/m$. This condition guarantees the harmonic type of free vibrations [3]. Assuming the solution of equation (5) in the form

$$W(r,\varphi) = R(r)U(\varphi) \tag{7}$$

and introducing it into (5) yields

$$r^2 \frac{d^2 R(r)}{dr^2} + r \frac{dR(r)}{dr} - \left(n^2 - \left(k_1^2 r\right)^2 \right) R(r) = 0, \quad \frac{d^2 U(\varphi)}{d\varphi^2} + n^2 U(\varphi) = 0, \, n = 0,1,2,\ldots \tag{8}$$

The boundary and periodicity conditions takes the form

$$R(r_1) = R(r_2) = 0, \qquad U(\varphi) = U(\varphi + 2\pi) \tag{9}$$

The general solutions of equations (8) can be easily obtained as

$$R_n(r) = A_n J_n(k_1 r) + B_n Y_n(k_1 r), \; U_n(\varphi) = L_n \sin(n\varphi) + M_n \cos(n\varphi), \; n = 0,1,2,\ldots \tag{10}$$

where A_n, B_n, L_n, M_n are unknown coefficient and $J_n(\cdot)$, and $Y(\cdot)$ are the first and second kinds of Bessel functions of order n. Conditions (9) yields a system of two linear, homogeneous equations in the constants A_n, B_n. Finally, a determinantal equation in the natural frequencies is obtained from the non – triviality condition. It leads to the following secular equation

$$J_n(k_1 r_1) Y_n(k_1 r_2) - J_n(k_1 r_2) Y_n(k_1 r_1) = 0 \tag{11}$$

From the relation (11) it is shown that $k_1 = k_{mn}$ $(m = 1,2,3,\ldots)$ are the roots of the above equation. Then taking into account equation (6), the natural frequencies of the system under study are determined from the relation

$$\omega^2 = \omega_{mn}^2 = \left(k_{mn}^2 S + k\right)/m_0 \tag{12}$$

Finally the general solution of the free vibrations of the system under consideration can be written in the following form

$$w(r,\varphi,t) = \sum_{m=1}^{\infty}\sum_{n=0}^{\infty} W_{mn}(r,\varphi) T_{mn}(t) = \sum_{m=1}^{\infty}\sum_{n=0}^{\infty} \left(\left(C_{mn}^{(1)} \sin(\omega_{mn} t) + D_{mn}^{(1)} \cos(\omega_{mn} t)\right) \times \right.$$
$$\left. \times W_{mn}^{(1)}(r,\varphi) + \left(C_{mn}^{(2)} \sin(\omega_{mn} t) + D_{mn}^{(2)} \cos(\omega_{mn} t)\right) W_{mn}^{(2)}(r,\varphi) \right) \tag{13}$$

where

$$W_{mn}^{(1)}(r,\varphi) = \left(e_{mn} J_n(k_{mn} r) + Y_n(k_{mn} r)\right) \sin(n\varphi)$$
$$W_{mn}^{(2)}(r,\varphi) = \left(e_{mn} J_n(k_{mn} r) + Y_n(k_{mn} r)\right) \cos(n\varphi) \tag{14}$$

are a two linear – independent mode shapes, and

$$e_{mn} = -Y_n(k_{mn} r_1)/J_n(k_{mn} r_1) \tag{15}$$

3. The finite element formulation

The discrete models of the system under investigation are formulated using the finite element technique (ANSYS code). These FE models are treated as an approximation of the analytical solution of the continuous system given by the equations (12), (13) and (14), respectively. To find the natural frequencies and natural mode shapes, the block Lanczos method is employed [4]. The essential problem of this section is built the FE model of the elastic foundation.

The first FE model is realized as follows. The foundation is modeled by a finite number of parallel massless springs. The stiffness modulus k_S of each spring can be obtained from the relation [3]

$$k_S = (k \, p_0)/b \tag{16}$$

where p_0 is the area of the membrane large face and b is the number of the springs. The spring – damper (combin) element defined by two nodes is used to realize the elastic layer. The damping capability of the element are neglected. The four – node quadrilateral (shell) element is used to realize the membrane. Application of the constant tension is realized as follows. To each node lying on the outer edge is imposed a concentrated tensile force S_0 in the radial direction. The proper value of the force is selected experimentally by numerical simulation [3]. The prepared model consists of 9540 shell elements, and 9324 combin elements, respectively.

elastic layer
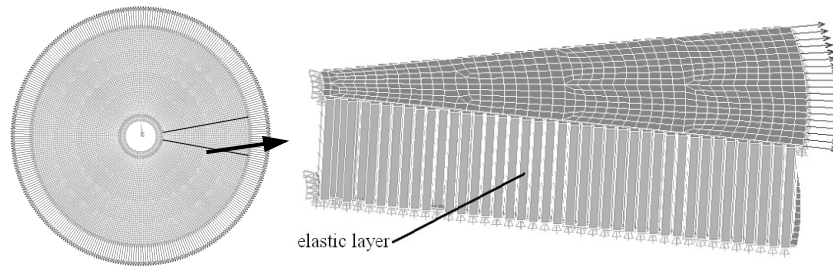
Figure 2. Finite element model

The second FE model is the same as the first, but the realization of the Wikler elastic foundation is different. Each massless spring is modeled by using bar (link) element. The values of the bar dimension parameters are fixed a priori. The proper value of the Young's modulus E_f of each bar is selected experimentally to minimize the frequency error defined by [4]

$$\varepsilon_{mn} = (\omega_{mn}^f - \omega_{mn}^c)/\omega_{mn}^c \cdot 100\% \tag{17}$$

where ω_{mn}^f and ω_{mn}^c are the natural frequencies of the FE and analytical models, respectively.

4. Numerical computations

Numerical solutions for free vibration analysis of the annular membrane resting on elastic foundation models suggested earlier, are computed. For all results presented here, only the first ten natural frequencies and mode shapes are discussed. Table 1 demonstrates the parameters characterizing the system under study.

Table 1. Parameters characterizing the annular membrane

r_1 [m]	r_2 [m]	h [m]	ρ [kg/m^3]	E [Pa]	ν	S [N/m]
0.5	0.1	0.002	$2.7 \cdot 10^3$	$7 \cdot 10^{10}$	0.32	500

In the table, E and ν are, the Young's modulus and Poisson ratio, respectively. In this work the analytical solution is considered as exact, compared to the finite element results, which are treated as approximation of the precise solution.

For the analytical model the natural frequencies are determined from numerical solution of the equations (11) and (12). The results of the calculation are shown in Table 2.

Table 2. Natural frequencies of the system under study ω_{mn} [Hz] (analytical solution)

		n					
		0	1	2	3	4	5
m	1	12.0828	13.3304	16.2846	19.8242	23.4497	27.0413
	2	24.0425	24.8625	27.1393	30.3978		

Results presented in Tables 3 – 4 are connected with the first FE model and are obtained for $S_0 = 4.8 [N]$.

Table 3. Natural frequencies of the system under study ω_{mn} [Hz]

		n					
		0	1	2	3	4	5
m	1	12.486	13.516	16.094	19.377	22.861	26.359
	2	24.85	25.486	27.302	30.046		

Table 4. Frequency error ε_{mn} [%]

		n					
		0	1	2	3	4	5
m	1	3.337	1.3923	-1.1704	-2.2558	-2.5105	-2.5232
	2	3.3586	2.5078	0.5995	-1.1573		

Tables 5 – 6 show the results connected with the second FE model and are achieved for $S_0 = 4.8 [N]$ and $E_f = 265 [Pa]$.

Table 5. Natural frequencies of the system under study ω_{mn} [Hz]

		n					
		0	1	2	3	4	5
m	1	12.485	13.515	16.093	19.376	22.86	26.358
	2	24.849	25.485	27.301	30.045		

Table 6. Frequency error ε_{mn} [%]

		n					
		0	1	2	3	4	5
m	1	3.3287	1.3848	-1.1766	-2.2609	-2.5147	-2.5269
	2	3.3545	2.5038	0.5958	-1.1606		

For both FE model cases the biggest difference between the analytical computations and the FE solutions may be visible for the frequencies ω_{10} and ω_{20}, respectively.

3. Conclusions

Based on the classical theory of membranes, a comprehensive study of the vibration analysis of annular membranes resting on Winkler elastic foundation is investigated. The separation of variables method is applied to derive the eigenvalue problem. Two FE models of the system under study are investigated. The numerical solution results demonstrated that the second FE model would be better to simulate the free vibration of the system under investigation.

References

1. S. Hashemi, H. Taher, M. Omidi,, *3 – D free vibration analysis of annular plates on Pasternak elastic foundation via p – Ritz method*, J. of Sound and Vibration, **311** (2008) 1114 – 1140.
2. S. Kaliski, *Vibrations and waves in solids*, IPPT PAN, Warsaw, 1966 (in Polish)
3. S. Noga,, *Free transverse vibration analysis of an elastically connected annular and circular double – membrane compound system*, J. of Sound and Vibration, **329** (2010) 1507 – 1522.
4. C. Silva, *Vibration and shock handbook*, Taylor & Francis, Boca Raton, 2005
5. D. Zhou, S. Lo, F. Au, Y. Cheung,, *Three – dimensional free vibration of thick circular plates on Pasternak foundation*, J. of Sound and Vibration, **292** (2006) 726 – 741.

Analiza drgań własnych membrany pierścieniowej osadzonej na podłożu typu Winklera

W pracy analizowane są drgania własne poprzeczne membrany pierścieniowej osadzonej na podłożu sprężystym typu Winklera. Prezentowane modele matematyczne układu opracowano w oparciu o klasyczną teorię drgań membran pierścieniowych oraz metodę elementów skończonych. Rozwiązanie ścisłe drgań własnych układu wyprowadzono stosując metodę Bernoulliego – Fouriera (metoda rozdzielenia zmiennych). Uzyskane z rozwiązania ścisłego wyniki (częstości własne i odpowiadające im formy własne) porównano z rezultatami otrzymanymi z metody elementów skończonych.

Magnetic Levitation of a Light Cylindrical-Shape Mass with Control of Damping of the Transition-State Vibrations

Paweł OLEJNIK

Department of Automation and Biomechanics, Faculty of Mechanical Engineering of the Technical University of Łódź, 1/15 Stefanowski St., 90-924 Łódź, Poland
olejnikp@p.lodz.pl

Jan AWREJCEWICZ

Department of Automation and Biomechanics, Faculty of Mechanical Engineering of the Technical University of Łódź, 1/15 Stefanowski St., 90-924 Łódź, Poland
awrejcew@p.lodz.pl

Abstract

Development in the direction of future applications of fast and accurate position control systems used in optoelectronics, computer hardware, precision machining, robotics and automobile industry stimulates high engagement in creation of non-conventional implementations [1, 2]. The work presents a numerical analysis devoted to that domain basing on a non-contact (frictionless) fixing of some cylindrical-shape's mass in an alternating magnetic field. These considerations precede identification of electromagnet parameter and created by it magnetic field in the real experimental realisation of the problem shown on a photo in Fig 1. The mass levitates in field generated by the electromagnet's system sourced by voltage of 12V. Next to the numerical algorithm of voltage feedback there has been even used a modified PID control [2] of transition state's oscillations of the levitated light mass that are recorded until it reaches the stable equilibrium position. Results of the experiments have been presented on time-history charts of $h(t)$ displacement measured between themselves faced surfaces of the electromagnet's core and surface of the levitated mass.

Keywords: decaying vibrations, magnetic levitation, numerical control, experimental rig

1. Introduction

Magnetic levitation is a known topic and can be realised in some ways [3, 4] but the most visual effects can be observed after utilization of an electromagnet made of superconductor.
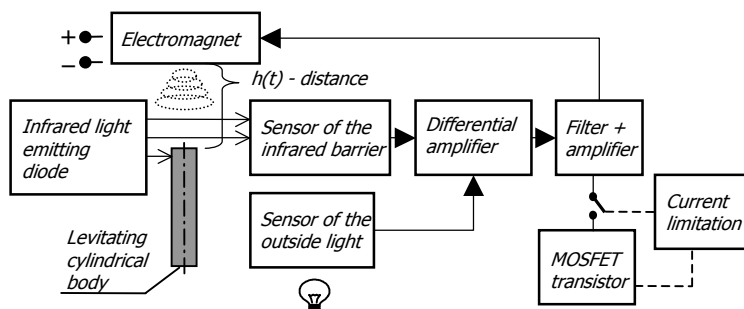
Figure 1. A schematic block diagram of the hardware, signal connections and the levitating solid body.

In a simpler way of creation of a system for examination of levitation's phenomenon one can use a system with infrared light's sensor that traces position of the levitated mass (barrier) placed in the magnetic field generated by the electromagnet.

For the purpose of the experiment presented here the role of sensor is played by the infrared light barrier that monitors actual position of the cylindrical mass. A schematic view of the experiment is shown in Fig. 1.

2. The Analysed System

Electronic part of the system uses two light-sensitive resistors of which the first one acts together with infrared light-emitting diode as a simple barrier tracing the cylindrical solid body's position. Because of existence, in the surrounding space, of many infrared light emitting sources like sun or light bulbs (producing disturbance signals to the barrier) the second one measures the amount of light coming into the system from surrounding space. When the barrier's sensor is partially illuminated (a result of covering of it by the levitating body) then a voltage difference appears and is inputted to the differential amplifier for generation of another value of voltage sourcing the electromagnet's circuit. Experimental realisation of the diagram presented in Fig. 1 has been shown in Fig. 2.
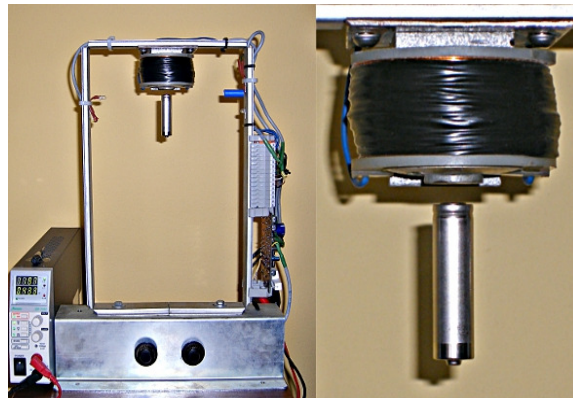
Figure 2. Experimental setup of the control system of the levitating cylindrical light mass (constructed by Piotr Jędrzejczyk, student of the second degree studies at the Faculty of Mechanical Engineering).

The system shown in Fig. 2 can be modelled (in a simplified dimension) by the dynamical system of three first-order differential equations (1) describing motion of the mass levitating in magnetic and gravitational fields and the voltage equation for the electric circuit with alternating current. One distinguishes the following meaning of the system state's vector x: $x_1 \rightarrow h$ displacement of the levitating mass measured downward from the electromagnet's surface, $x_2 \rightarrow dh/dt$ corresponding velocity of the displacement, $x_3 \rightarrow i$ electric current in the electromagnet's electric circuit.

$$\dot{x}_1(t) = x_2(t),$$

$$\dot{x}_2(t) = g - \frac{k}{m}\left(\frac{x_3(t)}{x_1(t)}\right)^2 + u(t)\,|_{1case},$$

$$\dot{x}_3(t) = \frac{1}{L}\Big(v(t)\,|_{2case} - Rx_3(t)\Big),$$

(1)

where electrical and physical constants are as follows: $L = 0.002$H is the coefficient of inductance, $R = 0.29\ \Omega$ – the coefficient of resistance, $k = 10^{-4}$ kg·m^2/C^2, C – the magnetic flux, $m = 0.0226$ kg – mass of the levitating body.

3. Two Cases of the Numerical Control

Voltage $v(t)$ and force excitation $u(t)$ are the two control signals. They are considered in two separate cases, namely: 1) $u(t)$ is a feedback from position h in the system with *PID* controller having the transfer function $PID(s) = k_P + (s+k_I)/s + k_D s$ inserted to the first axis of the block diagram shown in Fig. 3, while $v(t)$, a voltage source remaining constant at 12V; 2) the time-dependent control input voltage in Laplace representation $V(s) = -((k_1 + k_2 s + k_3 s^2)H(s) - k_1 h_0)$ to the analysed dynamical system working as the plant in the closed-loop control system with feedback from full state-vector (numerical model of the control strategy has been shown in Fig. 4). Disturbances coming from any external light sources have been neglected.

   Both presented numerical models include characteristics of operation of the infrared light barrier $IRR(t) = 1 - b_{IRR} h(t)^{-2}$. This approximation with b_{IRR} dumping (sensitivity) constant measures the amount of the infrared light transferred from the emitting diode to the light-sensitive resistor with presence of the levitating body working as the barrier.
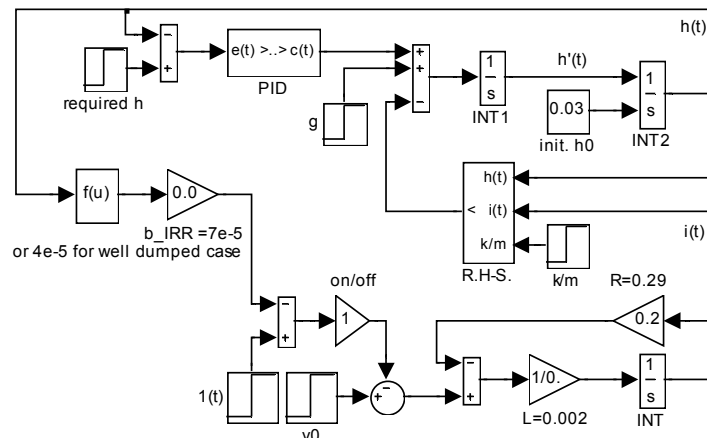
Figure 3. Feedback from displacement of the levitating mass in *PID* control
for $k_P = 250$, $k_I = 800$, $k_D = 13$.
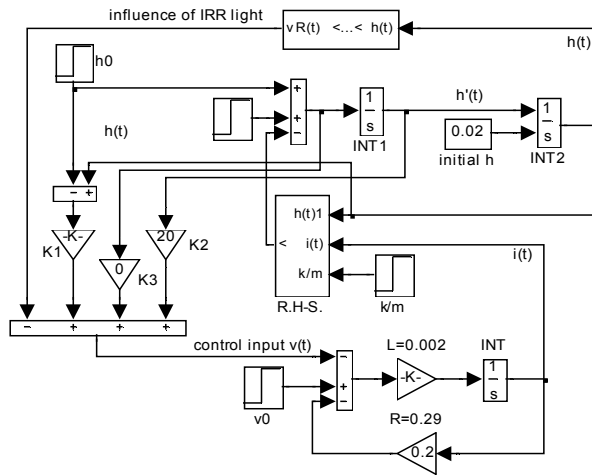
Figure 4. Closed-loop input voltage control with a usage of full state-vector feedback for $k_1 = 10^3$, $k_2 = 20$, $k_3 = \{0.0, 0.2\}$ in a model made in Simulink.
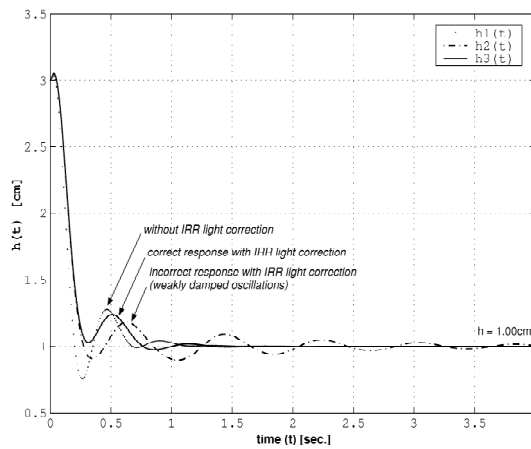
Figure 5. Time-histories of $h(t)$ obtained from the diagram shown in Fig. 3 for different values of the infrared light's barrier factor $b_{IRR\{1,2,3\}} = \{IRR\ off, 0.7 \cdot 10^{-4}, 0.4 \cdot 10^{-4}\}$ in the closed-loop position feedback control and for $h_0 = 3$cm.

In Fig. 5 there is visible a well-founded effect of introduction of the infrared light barrier. The case, for a short interval of values of the IRR factor has been described as the correct one being more realistic in relation to the motion of mass m observed on the experimental rig. Conducting this experiment one tries to hang the mass at height $h_f =$

1cm with the initial condition $h_0 = 3$cm. It is visible that the mass is quickly attracted to the steady-state position but it is achieved in a different manner.
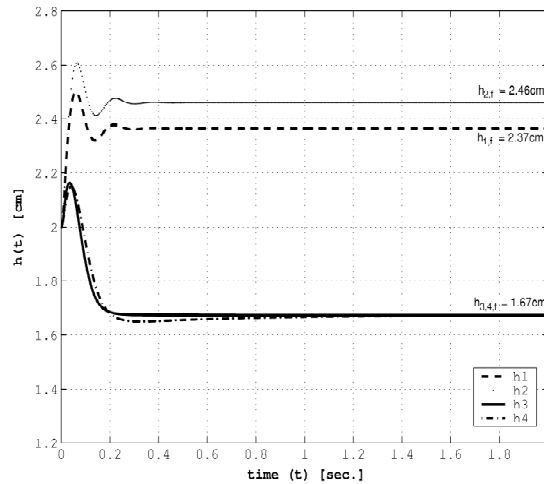
Figure 6. Time-histories of $h(t)$ evaluated from the diagram visible in Fig. 4 for different values $b_{IRR\{1,2,3\}} = \{7, 0.7, 22.2\}\cdot10^{-4}$ corresponding to $h_{\{1,2,3\}}$ (for $k_3 = 0$), respectively. Infrared light's sensitivity factor $b_{IRR\{4\}} = b_{IRR\{3\}}$ (for $k_3 = 0.2$), and $h_0 = 2$cm.

Frictionless oscillations in the transition to stable position can be pretty damped (see Fig. 6) with the use of the second case of the control strategy that bases on a feedback from the full state's vector as it has been shown in Fig. 4. For a different initial position ($h_0 = 2$cm) of mass m there is visible a quicker (because of voltage but not external force feedback as examined in the first approach) and better dumped attraction of the mass to the steady-state position. With respect to application of a different method of control (with a control with feedback to the voltage time variable input v) the whole system is characterized by a slightly different dynamics so the position of convergence changes with assumption of bigger values of $b_{IRR\{1,2,3\}} = \{7, 0.7, 22.2\}\cdot10^{-4}$. Factor $b_{IRR\{3\}}$ is the highest available here and the control nicely fixes the levitating mass at $h_3 = 1.67$cm. At this position the stabilized voltage sourcing the electromagnet equals 13.66V. Time-history of h_4 in Fig. 6 is the unnatural effect of the non-zero coefficient of feedback from acceleration ($k_3 = 0.2$, see Fig. 4). Desired position is achieved in about 1.2 sec., and it confirms, the vector component of feedback from acceleration is not necessary in this application.

4. Conclusions

Dependently on the presence of IRR light's barrier and values of its sensitivity factor (b_{IRR}) there can be distinguished various shapes of the step response. The convergence is quite fast and well-damped when the IRR light's correction exists, and moreover, takes a correct value of its significance. A choice of the incorrect value of b_{IRR} reflects in bringing the mass into a small-amplitude weakly-dumped oscillations around its desired

steady-state position. At some conditions such effect of oscillations is observable on the real laboratory rig and is undesirable when one needs to fix the levitating mass at a constant height. Therefore, the introduced feedback from the infrared light barrier with mass *m* working as the armature of the electromagnet makes sense. Better shapes of characteristics of the transition to steady-state responses have been confirmed by the second strategy. They are faster, more stable, and no oscillations have been reported after examination of system parameters. Magnetic field has allowed for elimination of any kinds of friction that are usually necessary in various realisations of fixings. Our experimental investigations will turn to identification of electro-magnetic parameters of the whole mechatronic system and the associated magnetic field. It should help in improvement of numerical adequateness of the presented approach as well as improvement of the tested strategy of control.

Acknowledgments

References

1. J. Ackermann, *Robust control,* Springer-Verlag, 1993.
2. M. Aliasghary, et al., *Sliding mode control of magnetic levitation system using radial basis function neural networks,* IEE XPlore, RAM (2008), 467-470.
3. A. Green, K.C. Craig, *Robust, design, nonlinear control of magnetic-levitation systems*, Journal of Dynamics, Measurement and Control **120**(4), (1998), 488-495.
4. A. Piłat, *Active magnetic suspension and bearing. Modeling and simulation*, InTech Education and Publishing, Vienna, (2008), 453-470.

Lewitacja Magnetyczna Lekkiej Masy o Kształcie Cylindrycznym z Kontrolą Tłumienia Oscylacji Stanu Przejściowego

Rozwój w kierunku przyszłych aplikacji szybkich i dokładnych układów pozycjonujących stosowanych w optoelektronice, sprzęcie komputerowym, obróbce precyzyjnej, robotyce czy też przemyśle samochodowym wzmaga wysokie zaangażowanie w tworzenie implementacji niekonwencjonalnych. Praca przedstawia analizę numeryczną dotyczącą tego obszaru zastosowań bazującą na bezkontaktowym podwieszeniu pewnej przewodzącej masy o kształcie cylindrycznym w zmiennym polu magnetycznym. Rozważania te poprzedzają identyfikację parametrów elektromagnesu oraz wytworzonego przez niego pola elektromagnetycznego na rzeczywistym stanowisku doświadczalnym pokazanym na fotografii na rysunku 1. Masa lewituje w polu magnetycznym generowanym przez układ elektromagnesu zasilany napięciem 12V. Algorytm numeryczny obok sprzężenia napięciowego zawiera także zmodyfikowaną kontrolę typu *PID* oscylacji w stanie przejściowym lewitującej masy o mały ciężarze poprzedzającym osiągnięcie przez nią stabilnego położenia równowagi. Wyniki tych doświadczeń pokazano na wykresach czasowych przemieszczenia $h(t)$ zmierzonego pomiędzy skierowanymi do siebie powierzchnią rdzenia elektromagnesu i powierzchnią lewitującej masy.

Eigenvalue problem for multi-degree-of-freedom systems with repeated frequencies

Rafał PALEJ

Cracow University of Technology, Institute of Computing Science
Al. Jana Pawła II 37, 31-864 Kraków
palej@mech.pk.edu.pl

Abstract

The paper deals with the eigenvalue problem related with discrete systems, consisting of *n* identical masses connected with springs in such a way that the stiffness matrix has the form of a multiband symmetric matrix. The eigenvalue problem formulated for such systems is characterized by repeated eigenvalues to which linearly independent eigenvectors correspond. The solution of the eigenvalue problem has been found for an arbitrary, finite number of degrees of freedom for the fully coupled systems and the systems in which masses are connected exclusively with the nearest neighbours.

Keywords: repeated eigenvalues, linearly independent eigenvectors

1. Introduction

For undamped natural systems possessing distinct eigenvalues, to every eigenvalue corresponds one unique eigenvector. The eigenvalues determine, by a suitable formula, natural frequencies while the eigenvectors determine directly the modes of vibration. Repeated eigenvalues can appear in discreet systems, consisting of identical masses and springs – arranged in such a way that every mass is constrained in the same manner. It turns out, that depending on the degree of coupling, the number of frequencies and their multiplicity may be different. The eigenvalue problem formulated for such systems is characterized by repeated eigenvalues to which linearly independent eigenvectors correspond. Since such systems have regular structure, there is a possibility of deriving analytical formulae for natural frequencies and modes of vibration for an arbitrary, finite number of degrees of freedom.

2. System with double frequency

One of the simplest system which possesses natural frequency with multiplicity 2 consists of three identical masses, connected with one another with the use of identical springs. The schematic diagram of such a system is presented in Fig.1.
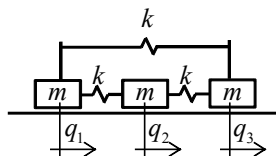
Figure 1. Schematic diagram of the system possessing a double frequency

The mass matrix **M** and the stiffness matrix **K** of the system have the following form

$$\mathbf{M} = \begin{bmatrix} m & 0 & 0 \\ 0 & m & 0 \\ 0 & 0 & m \end{bmatrix}, \quad \mathbf{K} = \begin{bmatrix} 2k & -k & -k \\ -k & 2k & -k \\ -k & -k & 2k \end{bmatrix} \tag{1}$$

Seeking the solution of equation $\mathbf{M\ddot{q} + Kq = 0}$ in trigonometrical form $\mathbf{q = u}\sin\omega\,t$ we obtain the eigenvalue problem in the standard form

$$\mathbf{Au} = \alpha\mathbf{u} \tag{2}$$

where

$$\mathbf{A = M^{-1}K} = \frac{k}{m}\begin{bmatrix} 2 & -1 & -1 \\ -1 & 2 & -1 \\ -1 & -1 & 2 \end{bmatrix}, \quad \alpha = \omega^2 \tag{3}$$

The eigenvalues and eigenvectors of **A** are as follows

$$\begin{aligned} \alpha_1 &= 0, & \mathbf{u}_1 &= \begin{bmatrix} 1 & 1 & 1 \end{bmatrix}^T \\ \alpha_2 &= \frac{3k}{m}, & \mathbf{u}_2 &= \begin{bmatrix} -1 & 1 & 0 \end{bmatrix}^T \\ \alpha_3 &= \frac{3k}{m}, & \mathbf{u}_3 &= \begin{bmatrix} -1 & 0 & 1 \end{bmatrix}^T \end{aligned} \tag{4}$$

The second eigenvalue has multiplicity 2. The eigenvectors $\mathbf{u}_2$ and $\mathbf{u}_3$ are linearly independent and any linear combination of them is also an eigenvector corresponding to the double eigenvalue so, the system presented in Fig.1 can perform vibration with double frequency in infinite ways.

3. Multi-degree-of-freedom system with double frequencies

The system presented in Fig.1 is a special case of the system composed of identical masses connected exclusively with the nearest neighbours where the first mass is connected with the second one and the last one. The schematic diagram of such a system is presented in Fig.2.

Figure 2. Schematic diagram of regular system possessing double frequencies

Now, matrix **A** has the following form

$$
\mathbf{A} = \frac{k}{m}
\begin{bmatrix}
2 & -1 & 0 & \dots & 0 & 0 & -1 \\
-1 & 2 & -1 & \dots & 0 & 0 & 0 \\
0 & -1 & 2 & \dots & 0 & 0 & 0 \\
\vdots & \vdots & \vdots & \ddots & \vdots & \vdots & \vdots \\
0 & 0 & 0 & \dots & 2 & -1 & 0 \\
0 & 0 & 0 & \dots & -1 & 2 & -1 \\
-1 & 0 & 0 & \dots & 0 & -1 & 2
\end{bmatrix}_{n \times n}
\tag{5}
$$

The location of the eigenvalues of **A** can be done making use of Gerschgorin's theorem which states in this case that all eigenvalues lies within the segment on real axis with center at $2\frac{k}{m}$ and of length $4\frac{k}{m}$. To compute their exact values, natural frequencies of the regular system will be calculated first. The system shown in Fig. 2 has its continuous counterpart in the form of unrestrained prismatic bar with the ends connected with each other by a rigid weightless link. The natural frequencies and eigenfunctions of such system have the form

$$
\nu_j = \frac{2\pi(j-1)}{l}\sqrt{\frac{E}{\rho}}, \ \ j = 1,2,\dots
\tag{6}
$$

$$
X_j(x) = C_j \sin\frac{2\pi(j-1)}{l}x + D_j \cos\frac{2\pi(j-1)}{l}x, \ j = 1,2,\dots
\tag{7}
$$

where l denotes the length of the rod, ρ – density and E –Young's modulus. Making use of the relation between amplitude of three subsequent masses, the relation between length of the rod and relative distance between masses in the regular system and the formula determining location of masses in a rod frame of reference, one can obtain formulae on frequencies and modes of vibration in the form [1]

$$
\omega_j = 2\sqrt{\frac{k}{m}}\sin\frac{\pi(j-1)}{n}, \ \ j = 1,2,\dots,n
\tag{8}
$$

$$
u_{ij} = X_j(x_i) =
\begin{cases}
\cos\dfrac{2\pi i(j-1)}{n}, \ \text{dla } j \leq j_{sep} \\[4mm]
\sin\dfrac{2\pi i(j-1)}{n}, \ \text{dla } j_{sep} < j \leq n
\end{cases}
, \ i = 1,2,\dots,n
\tag{9}
$$

where

$$j_{sep} = \begin{cases} \dfrac{n+1}{2}, & n \text{ odd} \\[2mm] \dfrac{n}{2}+1, & n \text{ even} \end{cases} \tag{10}$$

Taking under consideration the second relation of Eq. (3), the eigenvalues of **A** take the form

$$\alpha_j = 4\frac{k}{m}\sin^2\frac{\pi(j-1)}{n}, \quad j = 1, 2, ..., n \tag{11}$$

It appears from Eq. (11) that the smallest eigenvalue α_1 is single, while the remaining eigenvalues, in the case when n is odd, are double. In the case when n is even, the smallest eigenvalue α_1 as well as the biggest one $\alpha_{n/2+1}$ are single, while the remaining eigenvalues are double. The matrix **U** composed of elements u_{ij} diagonalizes matrix **A** [2], i.e.:

$$\mathbf{U}^{-1}\mathbf{AU} = \text{diag}(\alpha_1, \alpha_2, ..., \alpha_n) \tag{12}$$

4. Multi-degree-of-freedom system with one repeated frequency

Let us consider a mechanical system consisting of n identical elements of mass m, connected – each one with each one – through springs of stiffness k and, additionally connected with the base through springs of stiffness p. The potential energy of such system has the form

$$U = \frac{1}{2}k\sum_{i=1}^{n}\sum_{j=i+1}^{n}(q_j - q_i)^2 + \frac{1}{2}p\sum_{i=1}^{n}q_i^2 \tag{13}$$

Matrix **A** for such system is the symmetric Toeplitz matrix of the form

$$\mathbf{A} = \begin{bmatrix} (n-1)\dfrac{k}{m}+\dfrac{p}{m} & -\dfrac{k}{m} & \cdots & -\dfrac{k}{m} & -\dfrac{k}{m} \\[2mm] -\dfrac{k}{m} & (n-1)\dfrac{k}{m}+\dfrac{p}{m} & \cdots & -\dfrac{k}{m} & -\dfrac{k}{m} \\[2mm] \vdots & \vdots & \ddots & \vdots & \vdots \\[2mm] -\dfrac{k}{m} & -\dfrac{k}{m} & \cdots & (n-1)\dfrac{k}{m}+\dfrac{p}{m} & -\dfrac{k}{m} \\[2mm] -\dfrac{k}{m} & -\dfrac{k}{m} & \cdots & -\dfrac{k}{m} & (n-1)\dfrac{k}{m}+\dfrac{p}{m} \end{bmatrix}_{n\times n} \tag{14}$$

The determinant of **A** can be written as [3]

$$\det \mathbf{A} = \frac{p}{m}\left(n\frac{k}{m}+\frac{p}{m}\right)^{n-1} \tag{15}$$

Since the determinant of the matrix is equal to the product of its eigenvalues, one can suppose that eigenvalues of $\mathbf{A}$ will have the form

$$\begin{cases} \alpha_1 = \dfrac{p}{m} \\[2mm] \alpha_j = n\dfrac{k}{m}+\dfrac{p}{m}, \quad j = 2,3,...,n \end{cases} \tag{16}$$

As can be seen α_1 is a single eigenvalue while α_2 is repeated $n-1$ times. Analyzing Eq. (2) for $\alpha = \alpha_1$ and $\alpha = \alpha_2$ one can demonstrate that matrix $\mathbf{U}$ composed of eigenvectors of $\mathbf{A}$ has the form

$$\mathbf{U} = \begin{bmatrix} 1 & -1 & \cdots & -1 & -1 \\ 1 & 1 & \cdots & 0 & 0 \\ \vdots & \vdots & \ddots & \vdots & \vdots \\ 1 & 0 & \cdots & 1 & 0 \\ 1 & 0 & \cdots & 0 & 1 \end{bmatrix}_{n\times n} \tag{17}$$

and the inverse of $\mathbf{U}$ can be written as follows

$$\mathbf{U}^{-1} = \begin{bmatrix} \frac{1}{n} & \frac{1}{n} & \cdots & \frac{1}{n} & \frac{1}{n} \\ -\frac{1}{n} & \frac{n-1}{n} & \cdots & -\frac{1}{n} & -\frac{1}{n} \\ \vdots & \vdots & \ddots & \vdots & \vdots \\ -\frac{1}{n} & -\frac{1}{n} & \cdots & \frac{n-1}{n} & -\frac{1}{n} \\ -\frac{1}{n} & -\frac{1}{n} & \cdots & -\frac{1}{n} & \frac{n-1}{n} \end{bmatrix}_{n\times n} \tag{18}$$

The matrix $\mathbf{U}$ plays the part of transformation matrix in similarity transformation of matrix $\mathbf{A}$, determined by Eq. (14), i.e.:

$$\mathbf{U}^{-1}\mathbf{A}\mathbf{U} = \mathrm{diag}\left(\alpha_1,\alpha_2,...,\alpha_n\right) \tag{19}$$

The system presented in Fig.1 can be recognized as a special case of the system defined by Eq. (13), for $n = 3$ i $p = 0$ and in consequence the eigenvalues calculated from

Eq. (16) will be identical with the roots of characteristic equation, presented in Eq. (4) and the eigenvalues calculated from Eq. (11).

5. Conclusions

The eigenvalues determine, by a suitable formula, natural frequencies while the eigenvectors determine directly the modes of vibration for undamped natural systems. Repeated eigenvalues can appear in discreet systems, consisting of identical masses and springs – arranged in such a way that every mass is constrained in the same manner. In such systems, to repeated eigenvalue corresponds the set of linearly independent eigenvectors which determine the modes of vibration. Since any linear combination of linearly independent eigenvectors corresponding to the repeated eigenvalue is also an eigenvector, therefore, an infinite number of modes of vibration correspond to repeated eigenvalue.

References

1. T. Goik, *Dynamika liniowych układów regularnych w ujęciu analitycznym*, Ph.D. Thesis, Politechnika Krakowska, 2008.
2. L. Meirovitch, *Principles and Techniques of Vibrations*, Prentice Hall, Upper Saddle River, New Jersey 1997.
3. D. S. Bernstein, *Matrix Mathematics*, Princeton University Press, New Jersey 2005.

Zagadnienie własne w układach o dowolnej liczbie stopni swobody z wielokrotnymi częstościami drgań

Praca dotyczy zagadnienia własnego macierzy związanych z układami dyskretnymi, zbudowanymi z *n* identycznych mas połączonych sprężynami w taki sposób, by macierz sztywności miała budowę wielopasmowej macierzy symetrycznej. Zagadnienie własne tego typu macierzy charakteryzuje się wielokrotnymi wartościami własnymi, którym odpowiadają układy liniowo niezależnych wektorów własnych. W pracy podano analityczne rozwiązanie zagadnienia własnego macierzy dla układu w pełni sprzężonego i układu, w którym każda masa połączona jest wyłącznie z dwiema sąsiednimi.

Identification of the elasto-damping properties of long bones on a basis of the degenerate models

Maciej PANEK

Wrocław University of Technology, Smoluchowskiego25 str,50-370 Wrocław, Poland
maciej.panek@pwr.wroc.pl

Abstract

The dynamic load is essential for proper working of the skeletal system. The loads affecting skeleton during practising different kinds of sports and when accidents occur (for example resulting with bone injuries) have dynamic character, often with periodical or pulse shape. Therefore, from the scientific and clinical point of view, assignment of the dynamical properties of bone tissues is necessary. In this paper two degenerate models for description of the bovine bones dynamic properties are presented. The whole femur bone supported as a cantilever beam with additional mass on the free end is subject of investigations. The excitation is applied by electro-dynamic shaker. The force sensor is situated between shaker and the bone, and the reaction of the system is measured by acceleration sensor. On the basis the energy balance and the power balance equations the models parameters are identified. In this paper is presented a set of parameters describing chosen models for two cases. In the first case, it is assumed that a value of the additional mass is not known, and in the second case calculations are performed for known value of the substitutional mass. In the first case for both models (built on a basis of the *Zener* model I and the system basing on the general model of viscoelastic body II), a majority of identified parameters are negative. For a given mass value, in model I every parameter had positive value whereas in model II only the damping parameter was negative. The obtained results indicate that the model I is more suitable to describe of the bone dynamical properties.

Keywords: Dynamic properties, bone, degenerate model, identification.

1. Introduction

In human organism the osseous skeleton is acting as a load-bearing structure which assure possibility of maintaining an appropriate posture. Additionally, the skeleton as a passive motion apparatus together with the other motion system elements assures possibility of efficient motion. The loads affecting the osseous elements during body motion, have key meaning as well from the bone biology as the mechanical point of view. For the osseous correct system functioning, an appropriate physical activity is essential to assure occurrence of the dynamic loads (in peculiarity with periodic shape oscillations) [I, II, IV]. During practising different kinds of sports, forces acting on the human bones have also a dynamic character. Damages of the osseous tissues are rarely caused by static load, usually they are a result of working of the external forces which have pulse shape or are originating from the material fatigue. Therefore from the scientific as well as the clinical point of view, the recognition of dynamic properties of osseous tissues is crucial.

As it is shown in literature, there is still lack of models describing dynamic behaviour of bones. Their properties under static loading are rather well known, but behaviour under dynamic excitations is still not well recognized. Therefore models describing bones behaviour in conditions of dynamic loads are still searched.

2. Material and Method

In this paper two degenerate models are presented which are going to describe the dynamic properties of bovine bone. Model I is built on a basis of tde *Zener* model (parallel configuration of a *Maxwell* body and a *Hooke* body - nonlinear in this case) with a *Saint-Venant* body connected in parallel (Figure 1a). Elasticity function for the nonlinear element is taken as follows:

$$F_c(x) = c_1 x + c_3 x^3 \tag{1}$$

Dynamic system II (Figure 1b) is created by parallel connection of the general model of springy-viscous medium (*Hooke's* and *Kelvin-Voight* body in serial configuration) with *Saint-Venant* body.

The purpose of using the models described above is to describe mechanical properties of the examined osseous element under dynamic loadings.
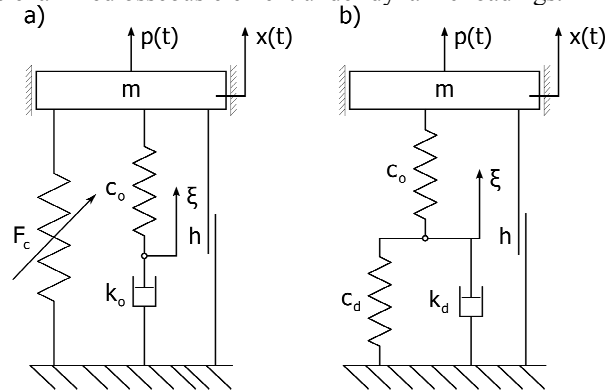
Figure 1. Models used to the dynamic properties of bones description:

a) model I, b) model II.

The bovine femoral bone is the examined material, because one of the biggest forces acting on elements of the human skeleton are located in lower limbs. Moreover injuries of the lower limbs bones are frequent consequence of dynamic loads which occur for example in road accidents. Also the lack of human bone material decided about taking the bovine bone for examinations.

The experimental examinations are conducted on constructed research stand, which is shown in Figure 2. Osseous specimen is examined in a cantilever beam with additional mass configuration. To restrain investigated object one end of the bone is placed in the handle and flooded in epoxy resin, whereas at the second end an additional mass m is fastened. For better restraining examined specimen, some steel elements are put between the bone and handle walls (also flooded in resin), which partially transfer the load from bone to the handle and relieve a resin.

During bone examinations the excitation is realized with the help of electro-dynamic shaker. Between the shaker and specimen a force sensor is placed, which detect a real load acting on the examined element. The load is applied to the free end in sagittal plane

of femur, perpendicularly to its long axis. Bone vibrations are measured by the acceleration sensor seized to the additional mass *m* (Figure 2). Information about force and acceleration changes are gathered by HP Analyzer and next sent to PC computer which collected and stored information obtained from the experiment. These data, are analyzed in order to determine the parameters describing models I and II.
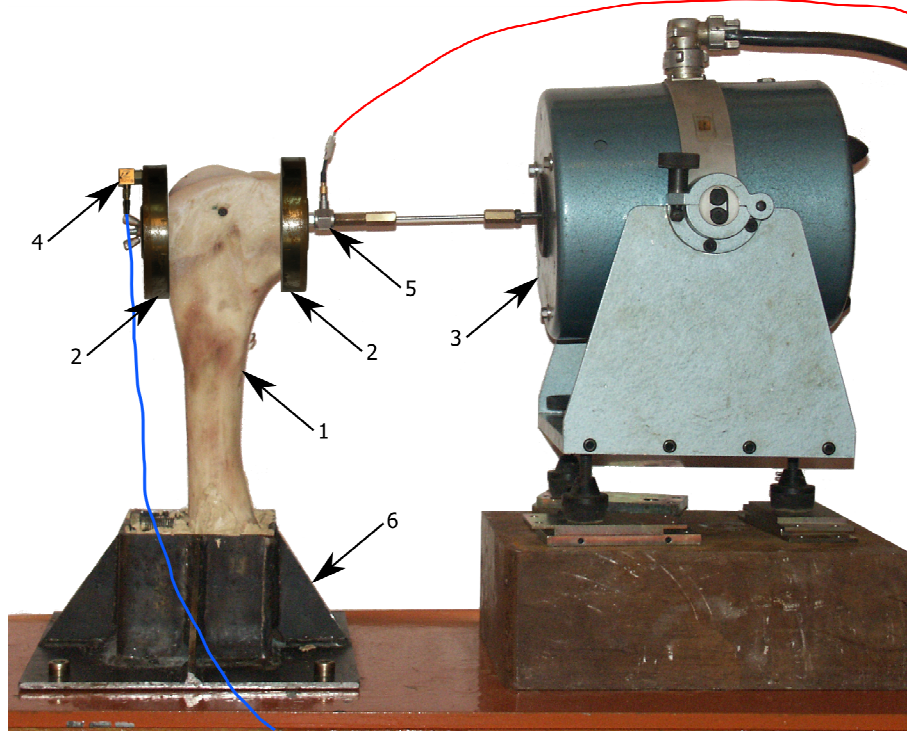
Figure 2. Scheme of investigation stand, 1- restrained bone, 2- additional mass,
3- shaker, 4- accelerometer, 5- force sensor, 6- handle.

The motion of additional mass fastened on the free end of bone is considered as a mass vibration in one degree of freedom system (see Figure 1). An identification algorithm basing on the energy balance and the power balance equations [V, III, VI] is used to determine the models parameters. For each of the chosen model an equation of dynamic equilibrium of mass *m* is derived. On this basis the equation of energy balance is obtained by multiplying both sides of the mentioned equation by elementary displacement and integrating it with period *T*. Similarly, the power balance equation is received i.e. equation of mass *m* motion is multiplied by elementary velocity and integrated in limits of a full period *T* of the observed vibrations.

For example, an equation of dynamic equilibrium of model II can be described by formulae (2) and (3), whereas energy balance and the power balance equations take form (4) and (5), i.e.:

$$c_0(x - \xi) = c_d\xi + k_d\dot{\xi} \tag{2}$$

$$m\ddot{x} = -c_0(x - \xi) - h\,\text{sgn}(\dot{x}) + p(t) \tag{3}$$

$$\frac{k_d}{c_0}m\alpha_a^v + k_d\alpha_x^v + h\alpha_v^{\text{sgn}\,v} + \frac{k_d}{c_0}\alpha_v^p - \frac{c_d}{c_0}\alpha_x^p = \alpha_x^p \tag{4}$$

$$m\left(1 + \frac{c_d}{c_0}\right)\alpha_v^a + c_d\alpha_v^x - \frac{k_d}{c_0}h\alpha_a^{\text{sgn}\,v} + \frac{k_d}{c_0}\alpha_a^p - \frac{c_d}{c_0}\alpha_v^p = \alpha_v^p \tag{5}$$

Symbols α denote variables which examples are presented below:

$$\alpha_x^p = \int_0^T p\dot{x}\,dt = \int_{x(0)}^{x(T)} p\,dx \tag{6}$$

$$\alpha_v^a = \int_0^T \dddot{x}\ddot{x}\,dt = \int_{x(0)}^{x(T)} a\,dv \tag{7}$$

where p means force (excitation signal) whereas x, v, a, adequately represent displacement, velocity and acceleration of additional mass m. The values of these integrals are equal to the areas bounded by appropriate closed curves (loops), see Fig 3.
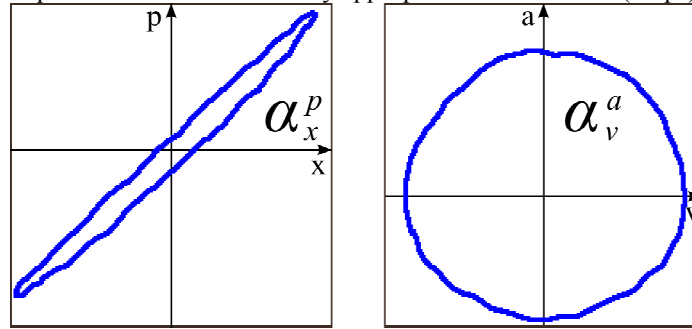
Figure 3. Examples of loops for the system investigated.

The obtained formulae (4) and (5) are algebraic equations which are convenient to identification of material constants: m, c_0, c_d, k_d, and h. In the case of application periodic excitations during experimental investigation, these constants can be calculated by help of the linear regression method.

3. Results

On the basis of the data obtained from the experiment, parameters of model I and II are evaluated. Values of parameters describing these models, for two cases, are presented in Table 1. In the first approach, it is assumed that the size of an additional mass in unknown and this value is calculated in the same way as for the other parameters. For this case most of the appointed parameters have negative values. In the second approach after appropriate modification of identification procedure, calculations were performed for a given value of the concentrated mass. In this case all of the evaluated parameters (except k_d in model II) have positive values see Tab. 1.

Table 1. Results of the identification process for model I and II. *- model parameters
are appointed for set mass value.

Parameter	Unit	*Model I*	Model I*	Model II	Model II*
c_1	N/m	$-332\cdot10^3$	$345\cdot10^3$	—	—
c_3	N/m^3	0	0	—	—
c_0	N/m	$-207\cdot10^3$	$457\cdot10^3$	$-1,9\cdot10^{-10}$	$557\cdot10^3$
c_d	kN/m	—	—	$1,9\cdot10^{-10}$	$380\cdot10^3$
k_0	N·s/m	76	360	—	—
k_d	N·s/m	—	—	$1,94\cdot10^{-7}$	$-5,2\cdot10^9$
h	N	-1,1	1,27	$-3,8\cdot10^{-1}$	16,1
m	kg	-4,55	2	-0,21	2

4. Conclusions

In the case of unknown mass *m*, most of the identified parameters values are negative for model I and for model II reasonable doubts occur regarding the order of magnitude of the appointed parameters. Therefore the assumption of a given magnitude of the concentrated mass *m,* is well-founded.

In model I parameter c_3 takes "0" value in both unmodified and modified procedures. It seems that using the non-linear elastic element, in the case of modeling of the osseous elements dynamic properties, is not necessary. Taking into account that in model II the k_d parameter has a negative value (for set mass *m*) while in osseous elements a clear viscous effects occurs [IV, IX, VII, VIII], it seems that this model is not suitable to describe of the bone dynamic properties.

Further examinations under dynamic loads are necessary for the ultimate determination of usefulness of presented models. In order to obtain a description of the bone dynamic properties further studies in the degenerate models domain are needed.

The identification method of elasto-dissipative properties of long bones, presented in this paper, does not currently allow for fully automatic evaluation of the models parameters used to describe the dynamic properties of the bone elements. Further studies of the models describing the dynamic behaviour of osseous elements are necessary.

It seems that the examined material behaves itself in a more complex manner than model II proposed and investigated in this paper.

References

1. Będziński R., *Biomechanika inżynierska, Zagadnienia wybrane.* Oficyna wydawnicza Politechniki Wrocławskiej, Wrocław 1997.
2. Bocian M., Kulisiewicz M., Piesiak St., *Wykorzystanie nieliniowych modeli zdegenerowanych w Identyfikacji elementów sprężysto-tłumiących maszyn.* XIV Konferencja Naukowa pt. "Problemy Rozwoju Maszyn Roboczych", Zakopane, 2001.

3. Cowin S.C., *Bone Mechanics Handbook*. Informa Health Care, 2001.

4. Currey J.D., *Bones: Structure and Mechanics*. Princeton University Press, 2002.

5. Garner E., Lakes R.S., Lee T., Swan C., Brand R., *Viscoelastic dissipation in compact bone: implications for stress-induced fluid flow in bone*. J. Biomech. Engineering, 2000; 122:166–172.

6. Iyo T., Maki Y., Sasaki N., Nakata M., *Anisotropic viscoelastic properties of cortical bone*. Journal of Biomechanics, 2004; 37:1433–1437.

7. Kulisiewicz M., Modeling and identyfication of nonlinear mechanical systems under dynamic complex loads. Oficyna wydawnicza Politechniki Wrocławskiej, Wrocław 2005

8. Piesiak St., Identyfikacja układów mechanicznych w dziedzinie nieliniowych i zdegenerowanych modeli dynamicznych. Oficyna wydawnicza Politechniki Wrocławskiej, Wrocław 2003.

9. Sasaki N., Enyo A., *Viscoelastic properties of bone as a function of water content*. Journal of Biomechanics, 1995; 28:809–815.

Identyfikacja właściwości dysypatywno-sprężystych kości długich na bazie modeli zdegenerowanych.

Do prawidłowego funkcjonowania układu kostnego niezbędne jest działanie obciążeń o charakterze dynamicznym. Siły działające na kościec podczas uprawiania różnych rodzajów sportu oraz podczas wypadków, np. prowadzących do uszkodzenia kości, także mają charakter dynamiczny, w tym często o przebiegu impulsowym lub okresowym. Dlatego tez z naukowego oraz klinicznego punktu widzenia, istotne jest poznanie własności dynamicznych tkanek kostnych. W niniejszej pracy przedstawiono dwa modele zdegenerowane, mające opisać własności dynamiczne kości wołowych. Badaniom poddano całą kość udową, która mocowana była w układzie belki wspornikowej z dodatkową masą. Wymuszenie realizowane było za pomocą wzbudnika elektro-dynamicznego. Pomiędzy nim a kością umieszczony był czujnik siły, natomiast odpowiedź układu rejestrowana była za pomocą czujnika przyspieszenia. Na tej podstawie za pomocą metody bilansu energii i bilansu mocy identyfikowano wartości parametrów występujących w modelach. Ruch masy dodatkowej zamocowanej na wolnym końcu kości, rozpatrywano jako drgania masy w układzie o jednym stopniu swobody. W pracy przedstawiono zestaw parametrów opisujących wybrane modele dla dwóch przypadków. W pierwszym założono, że wielkość masy dodatkowej nie jest znana, a w drugim obliczenia przeprowadzono dla zadanej wielkości masy zastępczej. W pierwszym przypadku, zarówno układzie w bazującym na modelu Zenera I jak i powstałym na bazie ogólnego modelu ośrodka sprężysto-lepkiego II, większość identyfikowanych parametrów przyjmowała wartości ujemne. Przy zadanej wielkości masy, w modelu I wszystkie parametry przyjmowały wartości dodatnie, natomiast w modelu II tylko parametr tłumienia był ujemny. Na tej podstawie wydaje się, że model I lepiej nadaje się do opisu właściwości dynamicznych kości.

Modelling and control optimization of the electromagnetic motor using genetic algorithm

Sebastian PECOLT
Koszalin University of Technology
Department of Mechatronics and Applied Mechanics, PL 75-620 Koszalin
sebastian.pecolt@tu.koszalin.pl

Tomasz KRZYŻYŃSKI
Koszalin University of Technology
Department of Mechatronics and Applied Mechanics, PL 75-620 Koszalin
tomasz.krzyzynski@tu.koszalin.pl

Abstract

The paper deals with the problem of implementing a genetic algorithm GA to calculate a pareto-optimal function of voltage powering solenoids, used for controlling a linear electromagnetic motor. The process assumes two conflicted criteria: minimizing the time of motion of the linear electromagnetic motor (l.e.m.) and minimizing the energy input. The results have been obtained for a set position with a narrow range of power supply. The work of electromagnetic motor is based on a electromagnetic repulsion. The device consists of a two solenoids and a slide control with neodymium magnet bars placed on its end. The paper discusses also static characteristics of l.e.m., i.e. a current density vs. force, a dependence of a force on displacement of the slide control and magnetic flux density. There are also dynamic characteristics of l.e.m. presented and compared to the results of simulations obtained in the Matlab-simulink program.

Keywords: electromagnetic motor, electromagnetic repulsion, control, genetic algorithm, optimization

1. Introduction

The device consists of two solenoids and a slide control with neodymium magnet bars placed on its end (Fig.1). The work of the electromagnetic motor is based on the phenomenon of a electromagnetic repulsion. One can steer the position of the slider by changing the force created by the solenoids. The mathematical model of the electromagnetic motor is non-linear, so we can't apply conventional controlling systems with a feedback. By applying a genetic algorithm GA, it is possible to designate pareto-optimal solutions as control functions of a voltage and current in time domain, with the criteria of time the movement and absorbed energy defined and then applying the control functions to the device. This paper focuses on the simulations of the electromagnetic motor in the Matlab-Simulink environment.
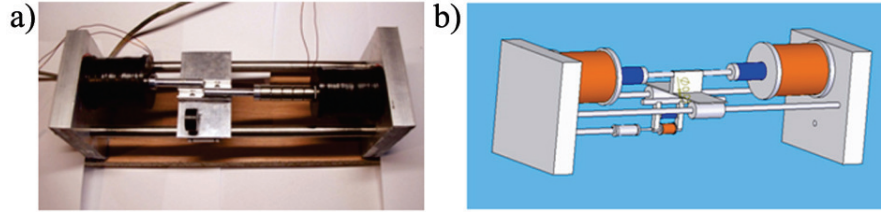
Figure 1. Physical model of electromagnetic motor (a),
3D model of the electromagnetic motor (b)

2. Modelling of electromagnetic motor

The mathematical model of the electromagnetic motor is described by the equation of motion of the slider (1), the forces F1 and F2 result from the finite element analysis that has been carried out for the magnet bar and coil system [2]:

$$\ddot{x} = \frac{1}{m}(F_1(x) - F_2(x) + F_{tm}) \tag{1}$$

$$F_n = ki_n weight_n(x) - Fi_n(x) \tag{2}$$

$$F_{in} = k_i i_{in} weight_n(x) \tag{3}$$

$$\dot{i}_n = \frac{1}{L_n}(U_n - i_n R_n) \tag{4}$$

$$\dot{i}_{in} = \frac{1}{L_n}(U_{in} - i_{in} R_n) \tag{5}$$

$$U_{in} = -\dot{x}\, sign(\dot{x}) weight_n(x) k_{vn} \tag{6}$$

$$P = i_n^2 R_n \tag{7}$$

$$F = \frac{T + E}{2} \mapsto \min \tag{8}$$

In equations (1) ÷ (8): m is the mass of the slider, $n = 1;\ 2$ (left or right coil), F_1 and F_2 are forces acting on the slider, F_{tm} is the damping force, k and k_v are constants resulting from the researched simulation , i_n describes the behaviour of current in both coils, i_{in} is inducted current in coil, $weight_n(x)$ is a function describing dependence of a force acting on the magnet and electromagnetic induction on the position of the slider in the coil, L_n is an inductance in coil, U_n is a voltage, U_{in} is inducted voltage in coil, R_n is resistance, T is normalized time of movement, E is normalized absorbed energy, P is an absorbed energy.

By carrying out calculations by means of the Finite Element Method (FEM) we can observe changes in the magnetic potential and magnetic flux density in the coil and magnet bar. As a result (Fig.2), we can calculate the forces between the magnet bar and the coil (2) by using Maxwell Stress Tensor analysis (Fig.3).
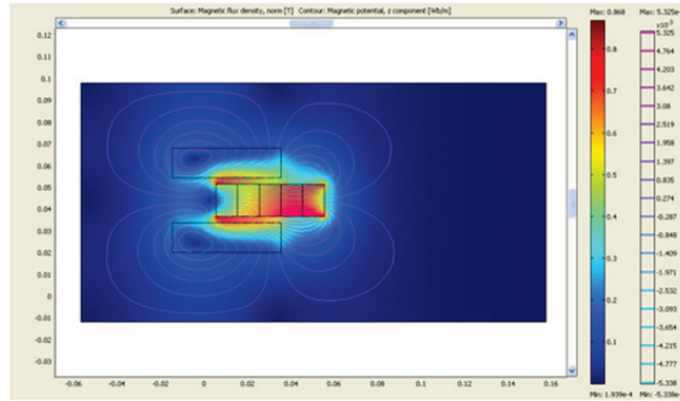
Figure 2. Magnetic potential and magnetic flux density in the coil and the magnet bar

The model, based on the one in the FEM environment was built in Matlab-Simulink. On the basis of the model device built in FEM environment with transient analyses, electromagnetic induction was found to be dependent on the magnet velocity in a coil (6). The model device in the Matlab-Simulink environment was created and based on the data resulting from the FEM analyses. Its accuracy was found to match the FEM model. The control system for the model is open, thus there is not a feedback loop to control its output. Input signals are only time-dependent functions of voltage powering the coils.
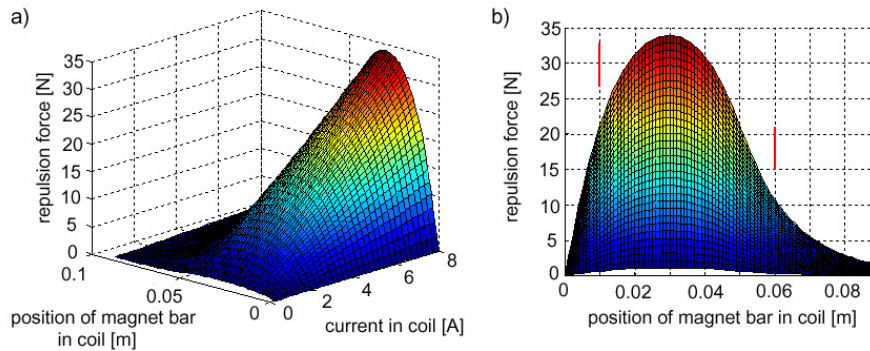
Figure 3. a) Dependance between the force acting on the magnet bar, the position of the magnet in coil and current value, b) dependance between the force acting on the magnet bar, the position of the magnet in coil

The objective of the slider is to move from the starting point (marked in Fig.3b as first red line) to the final point (marked in Fig.3b as the second red line) and stop there with a required accuracy i.e. 10^{-3}m. Time of movement has to be below 0.1s, and the absorbed energy has to be low one [1].

3. Formulation of the control problem

The main problem is to find the minimum of two conflicted the local criteria - the normalized time of movement and normalized absorbed energy (8). The voltage and current as time-dependent functions are searched for. The genetic algorithm selects parameters, for the left coil and for the right one, as points of the voltage in starting and final points of the slider positions. Each of the points may take values from zero to fifty volts with accuracy to one volt. There are only four parameters necessary to create two voltage functions dependent on the slider position of the coils. The numeric model calculates time-dependent functions of voltage on the basis of the four parameters mentioned above. On the basis of the selected points the interpolated function, i.e. the voltage from the slider position, is created. The voltage function determines the current value in the coils (4) and (3).

4. Comparison of the full survey method and genetic algorithm

By applying the method of full survey, where the number of solutions to analyse is over 6,7 million, only 689 solutions fulfil the required constrains. All these solutions are illustrated in Fig.4. Thus, only 0,0102 percent of all the solutions is acceptable. The best solutions, marked as blue star, are pareto-optimal (global) solutions. The time used to analyse all the solutions was 310 hours. As a result of implementing genetic algorithms, three solutions, marked in the chart as red round points (Fig.4), are obtained after 2 000 iterations with initial population of 50. The time needed to find these solutions is only 2 hours and 48 minutes. Figure 5 shows the position-dependent voltage functions built for the results marked as the blue star with the arrow pointing at it (Fig.4). The time-dependent functions used for controlling the electromagnetic motor results from the position-dependent voltage functions.
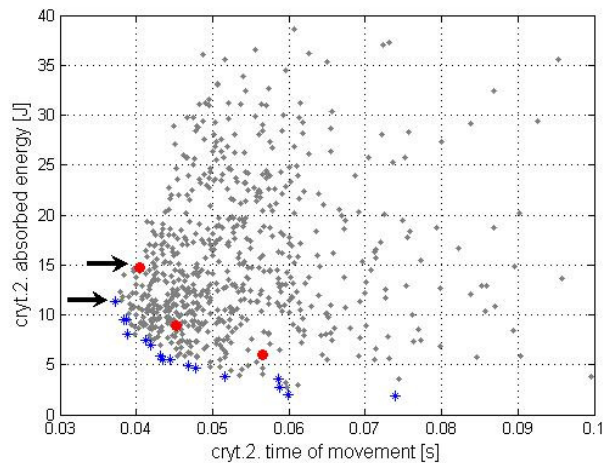
Figure 4. Results from full survey method compared with GA
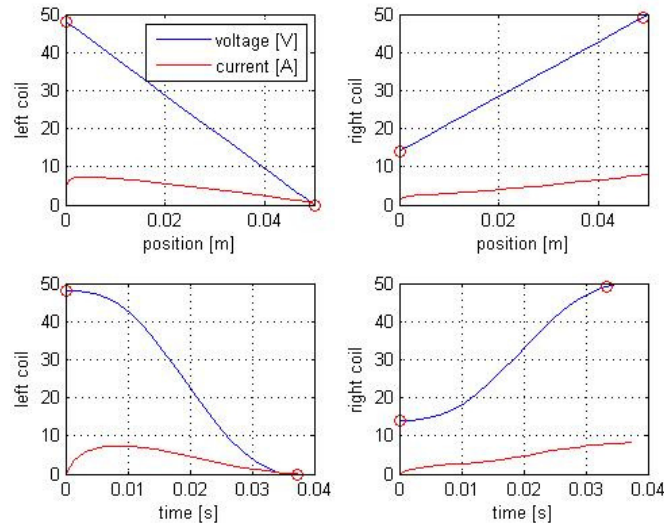
Figure 5. Control functions for the one global pareto-optimal solution marked in Fig.4 as blue star with arrow pointed
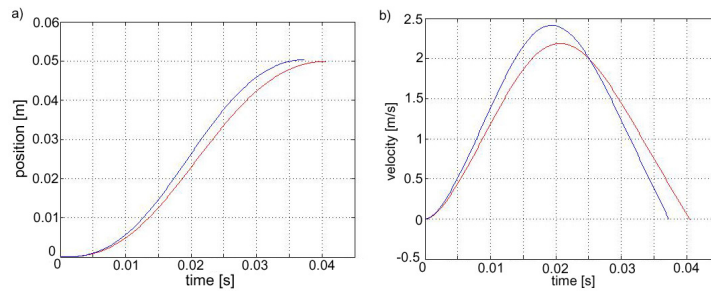
Figure 6. Compared two results marked in Fig. 4 by arrows. Red curves are from GA optimization, blue one are from full survey method. Positions (a) and velocity (b) of the slider in time domain.

5. Results and conclusions

If we compare the obtained result with the time necessary to implement the full survey method, we notice that it is only 0,9 percent of the time spent on calculations. The locations of the solutions found by the genetic algorithm are close to pareto-optimal solutions (marked as blue stars). In Fig.6a and 6b the two solutions are compared, the first resulting from using the genetic algorithm and the second one obtained using the full survey method (the red line corresponds to the red colour points in Fig.4). The red curve represents the solution where GA selects four parameters, two for the left coil and two for

the right one, as points of voltage. The blue curve represents the best solution obtained from the full survey method for the same constraints (Fig.6).

In this case, the movement time equals 37 miliseconds and the absorbed energy is over 11 Joules. For the red curve, the time of movement equals 40,4 miliseconds and the absorbed energy is less then 15 Joules. The genetic algorithm is able to calculate a solution that is similar to the global optimum in a short period of time. Using the genetic algorithm one can designate pareto-optimal solutions as control functions of the voltage and current in time domain, with the two conflicted criteria defined: minimizing the time of motion and minimizing absorbed energy.

References

1. Popov A., *Genetic algorithms for optimization, Programs for MATLAB, User manual*, Hamburg (2005).
2. Chee-Mun Ong, *Dynamic simulation of electric machinery*, Prentice-Hall, Inc. (1998).
3. Tarnowski W., *Modeling Systems (in Polish),* Publishing House of Koszalin University of Technology, Koszalin (2004).

Modelowanie i optymalizacja sterowania siłownikiem elektromagnetycznym z wykorzystaniem algorytmów genetycznych

W pracy przedstawiono sposób implementacji algorytmów genetycznych do wyznaczania pareto-optymalnych funkcji sterujących, służących do sterowania pozycją suwaka siłownika elektromagnetycznego. Proces zakłada minimalizację dwóch przeciwstawnych kryteriów, tj. czasu ruchu tłoka siłownika i energii pobranej przez urządzenie. Praca siłownika elektromagnetycznego oparta jest o zasadę wypychania magnesów stałych z pola magnetycznego solenoidów. Urządzenie składa się z dwóch solenoidów i suwaka na którego końcach są umieszczone magnesy stałe. W pracy przedstawiono charakterystyki statyczne jak i dynamiczne urządzenia, m.in. zależność prądu od siły wypychającej magnes, zależność siły od pozycji magnesu w solenoidzie.

On the semi-active control of carrying structures under a moving load

Dominik PISARSKI

Institute of Fundamental Technological Research, IPPT PAN
Pawińskiego 5b, 02-106 Warsaw
dpisar@ippt.gov.pl

Czesław I. BAJER

Institute of Fundamental Technological Research, IPPT PAN
Pawińskiego 5b, 02-106 Warsaw
cbajer@ippt.gov.pl

Abstract

In this paper we address a group of recent research focused on the semi active control problems in carrying structures systems subjected to a travelling load. The magnitude of the moving force is assumed to be constant by neglecting inertial forces. The response of the system is solved in modal space. The optimal control problem is stated and it is solved by using of Pontryagin Maximum Principle. Switching control method is verified by numerical examples. The controlled system widely outperforms passive solutions. Due to its simplicity in practical design, the presented solution should be interesting to engineers.

Keywords: Semi-active control, structural control, optimization, moving load

1. Introduction

An increasing speed requirements in transport and technological processes forces engineers to apply new and unique solutions for the carrying structures design. From the last few decades the main role in such a design play an integrated systems of control. Semi-active methods superiority over active result from its reliability and low power consumption.

Figure 1. Semi-active controlled guideways.

In this paper we propose two fields of applications of semi-active controlled systems. The first one is dedicated to technological processes such as cutting or bonding, where the straight passage of a moving load is essential. The second one is directed to large-

scale engineering structures like bridges that span gaps or beams that must resist loads due to heavy and fast vehicles.

Technical difficulties with the rigid support of the bottom parts of the dampers require new, more practical solutions. One of them is presented in Fig 1.

A good number of semi-active control methods have spread widely and some of them have been put into practice recently. They are usually based on sky-hook and ground-hook ideas. These strategies are used for the active suspension of a moving oscillator in [3, 4]. The idea of a beam vibrations control by dampers and preliminary results were presented in [5]. The early papers deal with the problem of active control of a beam vibrations [6]. An active constrained layer is applied in [7].

In this paper we propose an open loop switching control method. The optimal solution is based on the Maximum Principle [8]. The form of cost integrand depends on the aim of control.

2. Mathematical background

In this section we present a control method and its optimal solution in a short. The aim of the proposed strategy is to provide a straight passage for the moving load. We consider the double-beam system as shown in Fig. 1. The solution scheme for a single-beam system is analogous.
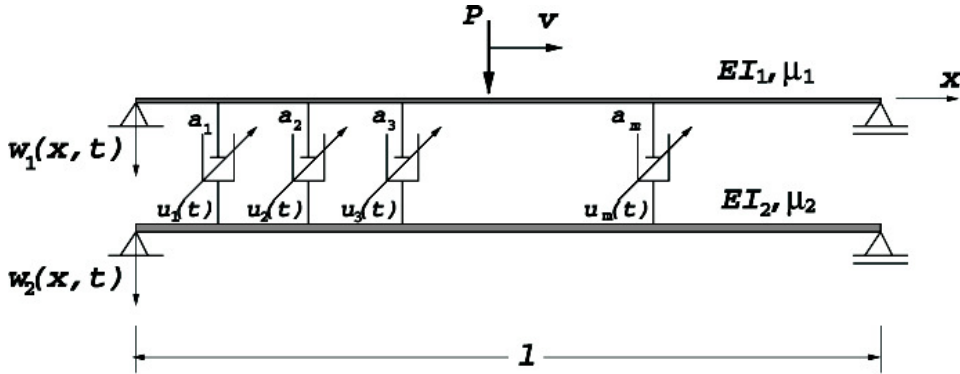
Figure 2. Double Euler-Bernoulli beam system coupled by a set of semi-active dampers.

We can write the governing equation for the considered system as follows:

$$EI_1 \frac{\partial^4 w_1(x,t)}{\partial x^4} + \mu_1 \frac{\partial^2 w_1(x,t)}{\partial t^2} = -\sum_{i=1}^{m} u_i \left[\frac{\partial w_1(a_i,t)}{\partial t} - \frac{\partial w_2(a_i,t)}{\partial t} \right] \delta(x - a_i) +$$

$$+ P\delta(x - vt), \tag{1}$$

$$EI_2 \frac{\partial^4 w_2(x,t)}{\partial x^4} + \mu_2 \frac{\partial^2 w_2(x,t)}{\partial t^2} = -\sum_{i=1}^{m} u_i \left[\frac{\partial w_2(a_i,t)}{\partial t} - \frac{\partial w_1(a_i,t)}{\partial t} \right] \delta(x - a_i),$$

together with the boundary and initial conditions:

$$w_1(0,t) = 0, w_1(l,t) = 0, w_1(x,0) = 0, \dot{w}_1(x,0) = 0,$$
$$w_2(0,t) = 0, w_2(l,t) = 0, w_2(x,0) = 0, \dot{w}_2(x,0) = 0. \tag{2}$$

Here, $w_1(x,t)$ and $w_2(x,t)$ are the transverse deflections of the beams at point (x,t), $u_i(t)$ is the i-th damping coefficient as a function of time, m is the number of viscous supports and P is the concentrated force passing the upper beam at constant velocity v and δ is the Dirac delta function. For the control design we use a representation of the system in modal space. Respecting the boundary conditions we look for the solution expressed upon the sine serie base.

$$V_{1(2)}(j,t) = \int_0^l w_{1(2)}(x,t)\sin\frac{j\pi x}{l}\,dx \,, w_{1(2)}(x,t) = \frac{2}{l}\sum_{j=1}^{\infty}V_{1(2)}(j,t)\sin\frac{j\pi x}{l}. \tag{3}$$

Furthermore, we consider only approximate solutions of Eq. 1 by using a finite-dimensional modal space, i.e. $j, k = 1,2,\ldots, M$. The transformation (3) yelds the following system of ODEs

$$\mu_1\ddot{V}_1(j,t) + \frac{2}{l}\sum_{i=1}^{m}\sum_{k=1}^{\infty}u_i(t)\left[\dot{V}_1(k,t) - \dot{V}_2(k,t)\right]\sin\frac{k\pi a_i}{l}\sin\frac{j\pi a_i}{l} + EI_1\frac{j^4\pi^4}{l^4}V_1(j,t) = P\sin\frac{j\pi vt}{l},$$
$$\tag{4}$$
$$\mu_2\ddot{V}_2(j,t) + \frac{2}{l}\sum_{i=1}^{m}\sum_{k=1}^{\infty}u_i(t)\left[\dot{V}_2(k,t) - \dot{V}_1(k,t)\right]\sin\frac{k\pi a_i}{l}\sin\frac{j\pi a_i}{l} + EI_2\frac{j^4\pi^4}{l^4}V_2(j,t) = 0.$$

Entering the generalized state vector $y(t) \in R^n$, where $y_{4k-3}(t) = V_1(k,t)$, $y_{4k-2}(t) = \dot{V}_1(k,t)$, $y_{4k-1}(t) = V_2(k,t)$, $y_{4k}(t) = \dot{V}_2(k,t)$, $k = 1,2,\ldots,n/4 = M$, we can formulate the optimal control problem:

$$\text{Minimize} \quad J = \int_0^{t_f = (v/l)}\left[\sum_{k=1}^{n/4}y_{4k-3}(t)\sin\frac{k\pi vt}{l}\right]^2 dt, \tag{5}$$

$$\text{subject to} \quad \dot{y}(t) = \mathbf{A}y(t) + \sum_{i=1}^{m}\mathbf{B_i}\,y(t)u_i(t) + \mathbf{f}(t), \tag{6}$$

$$y_{4k-3}(0) = V_1(k,0), \quad y_{4k-2}(0) = \dot{V}_1(k,0),$$
$$y_{4k-1}(0) = V_2(k,0), \quad y_{4k}(0) = \dot{V}_2(k,0), \quad k = 1,2,\ldots,n/4 , \tag{7}$$

$$u_i(t) \in [0,u_{max}], \quad \forall t \in [0,t_f], \quad i = 1,2,\ldots,m . \tag{8}$$

Introducing a new state variable $\dot{y}_{n+1}(t) = 1$, $y_{n+1}(0) = 0$ and rebuilding $A \to \hat{A}$, $B_i \to \hat{B}_i$, $f(t) \to \hat{f}(y)$ in such a way they respect a new variable, we replace (5)-(8) with the autonomous optimal control problem so Maximum Principle can be applied directly. The Hamiltonian function is given by

$$H(\mathbf{y}, \mathbf{u}, \boldsymbol{\eta}) = \langle \boldsymbol{\eta}, \hat{\mathbf{A}}\mathbf{y} \rangle + \sum_{i=1}^{m} \langle \boldsymbol{\eta}, \hat{\mathbf{B}}_i \mathbf{y} \rangle u_i + \langle \boldsymbol{\eta}, \hat{\mathbf{f}} \rangle - \left[\sum_{k=1}^{n/4} y_{4k-3} \sin \frac{k\pi vt}{l} \right]^2 . \tag{9}$$

The adjoint differential equation and the transversality conditions are as follows:

$$\dot{\boldsymbol{\eta}}(t) = -\frac{\partial H}{\partial \mathbf{y}}, \qquad \boldsymbol{\eta}(t_f) = 0 \ . \tag{10}$$

The Hamiltonian (9) takes the maximum value when the controls equal:

$$u_i(t) = \begin{cases} u_{max}, & \langle \boldsymbol{\eta}(t), \hat{\mathbf{B}}_i \mathbf{y}(t) \rangle > 0 \\ 0, & \langle \boldsymbol{\eta}(t), \hat{\mathbf{B}}_i \mathbf{y}(t) \rangle < 0 \end{cases} . \tag{11}$$

However Maximum Principle is only a nessesary condition for the optimal solution. We suppose the most efficient control method is generated by switching controls.

The implicit solution of stated problem can be solved numerically by the shooting method for instance. However, it can be extremely difficult due to high dimensional problem. For the alternate method we assume a priori a number of switchings for every control and then transform the problem into mathematical programming.

3. Numerical examples

Here, we present a few numerical solutions of optimal control problem stated in the previous section. We use Hooke-Jeeves Direct Search Method, where we consider at least 3 different starting points with 3 reducing step size schemes for each case. The number of switchings was first assumed as 3, then 2, and finally 1 for every control. Reduced number of switching actions is a great advantage from the practical point of view while the cost (Eq. 5) is comparable.
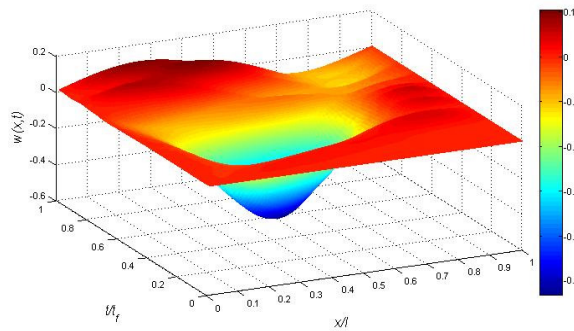
Figure 3. Transverse vibration of controlled beam in space-time domain.

The idea of straight-line passage is based on the principle of a two-sided lever. The first part of the beam which is subjected to a moving load is supported by an active damper placed on the rigid base. The first damper is active while the second one is passive. At this stage, a part of the beam is turned around its centre of gravity, levering the right hand part with a passive damper attached. The temporal increment of displacements on

the right hand part of the beam enables us to exploit it during the second stage of the passage. This phenomenon can be observed in the space time-domain (Fig 3).

Below, we present the exemplary optimal deflection trajectories under a moving load in two different cases. In the first one (Fig. 4), we consider a single beam with two active dampers placed in the positions $0.25l$, $0.75l$. In the second one (Fig. 5), four dampers placed in positions $0.2l$, $0.4l$, $0.6l$, $0.8l$ are attached to the double beam system. Trajectories for passive cases (all dampers are on) are added for comparison.
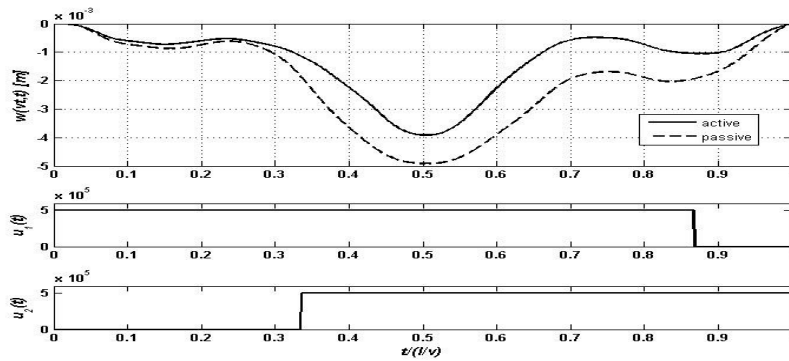
Figure 4. Optimal deflection trajectory and switching controls.

While the cost integrand is calculated with respect to velocities or accelerations of vibrations we do not observe a significant efficiency of the proposed method. High-frequency harmonics included in those trajectories can be reduced by high-frequency switching controls. This is the ongoing research topic of the authors.
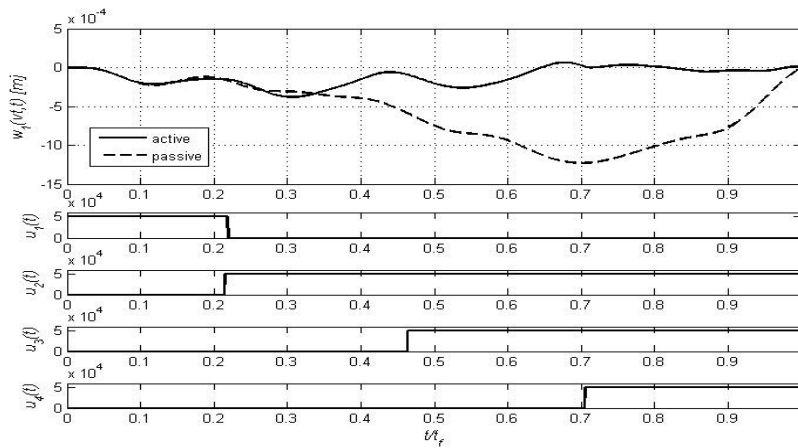
Figure 5. Optimal deflection trajectory and switching controls.

4. Conclusions

In this paper, a semi-active control method for linear carrying structures has been presented. A bang-bang control method has been proposed and its performance has been verified by numerical examples. The best efficiency is obtained at high travel speeds. The controlled system can efficiently decrease the mass of the guideway. The control strategy is simple for practical design. It can be implemented by creating an optimal control map in the memory of the controller. Integration of a neural network with the system will be addressed in future works.

References

1. D. Pisarski, C.I. Bajer, *Semi-active control of 1D continuum vibrations under a travelling load,* J. Sound and Vibration, **329(2)** (2010) 140 – 149.
2. L. Fryba, *Vibrations of solids and structures under moving loads*, Thomas Telford House, 1999.
3. D. Giraldo, Sh. J. Dyke, *Control of an elastic continuum when transverse by a moving oscillator,* J. of Structural Control and Health Monitoring, **14** (2002), 197-217.
4. Y. Chen, C. A .Tan, L. A Bergman, T. C, Tsao, *Smart suspension system for bridge-friendly vehicles*. SPIE Proceedings Series, **4696** (2002), 52-61.
5. R. Bogacz, Cz. I. Bajer, *Active control of beams under moving load.* Journal of Theoretical and Applied Mechanics, **38(3)** (2000), 523-530.
6. T. Frischgesel, K. Popp, H. Reckmann, O. Schutte, *Regelung eines elastischen Fahrwegs inter Verwendung eines variablen Beobachters*. Technische Mechanik, **18(1)** (1998), 44-55.
7. A. Baz, *Dynamic boundary control of beams using active constrained layer damping*. Mechanical Systems and Signal Processing **11(6)** (1997), 811-825.
8. L. S. Pontryagin, V. G. Bolytanskii, R. V. Gamkrelidze, E. F. Mishchenko, *The mathematical theory of optimal processes*. Fizmatgiz, Moscow, 1961.

O semi-aktywnym sterowaniu układów nośnych pod ruchomym obciążeniem.

W pracy przedstawiono wyniki badań półaktywnego sterowania w układach nośnych poddanym obciążeniom ruchomym. Obciążenie zostało przedstawione jako bezinercyjne. Odpowiedź układu została wyznaczona w reprezentacji modalnej. Sformułowano zadanie sterowania optymalnego. Uzasadniono zastosowanie sterowań typu bang-bang opierając się na Twierdzeniu o Maksimum Pontryagina. Proponowana metoda sterowania została zweryfikowana na podstawie przykładów numerycznych. Wykazano przewagę układów sterowanych nad układami tłumienia pasywnego. Opracowana strategia sterowania jest prosta w implementacji i może być atrakcyjnym rozwiązaniem dla inżynierów.

Instability and free vibrations of a column with imperfection subjected to load by the force directed towards the positive pole

Iwona PODGÓRSKA-BRZDĘKIEWICZ

Technical University of Częstochowa, Institute of Mechanics and Machine Design Foundations, ul. Dąbrowskiego 73, 42-200 Częstochowa
iwonapb@imipkm.pcz.czest.pl

Abstract

The work refers to the problem of free vibrations and global instability of slender system with imperfections subjected to load by the force directed towards the positive pole. The inaccuracies in the systems are modelled assuming an initial curvature and the introduction of the eccentricity of an external load. On the basis of total mechanical energy, equations of motion and boundary conditions are determined. The relationship between the introduced inaccuracies for which the bending of the free end of the column has a finite value at load approaching critical load is determined. Curve courses of longitudinal bending are presented. The results of numerical calculations of the course of the natural frequency against external load for given geometry and physical constants of the column are presented.

Keywords: elastic column, free vibrations, initial imperfections

1. Introduction

The influence of initial imperfections on the stability and longitudinal bending of columns loaded by conservative loads was considered in works [1-4]. The initial geometrical imperfection of the system in the form of the initial curvature was analysed or the eccentric external load was taken into account separately. The systems subjected to the Euler's load or to a force directed towards the positive pole (realised on linear elements) were examined in [5]. Imperfections in shape and applied external load were taken into consideration in the systems mentioned above. Mutual interactions between the introduced imperfections were revealed and proved. The relationships between the imperfections in shape and load, for which the bending of characteristic points has a finite value at load P approaching critical load P_c, were determined. The static criterion of stability is insufficient for the evaluation of the system behaviour. The discussed phenomenon was illustrated by diagrams showing the courses of longitudinal bending and was confirmed by experimental research**.**

2. Physical model of the column

In this paper the column loaded by the force directed towards the positive pole [compare 6], realised by loading head built from circular elements is considered. The imperfections resulting from an initial curvature of the system, described by $W_0(x) = \alpha x$ function, and from eccentricity of external force P (e – the value of eccentric) are taken into account.Total transverse displacement of the system was denoted as $Wc(x,t)$, where: $Wc(x,t) = W_0(x) - W(x,t)$.

The direction of external force P is crossing the constant point O (Fig. 1). The point O is lying at R distance from the point of application of the force and is displaced by the value e in relation to non-deformed axis of the system. The following relationships are fulfilled:

$$\beta_0 = \frac{W_0(l)}{R-r}, \ \beta = \frac{W_c(l,t)}{R-r} \tag{1}$$

where β_0 and β are the angles created by the direction of external force P and non-deformed axis of the system for the initial state (the initial bending) and state of strain, respectively.
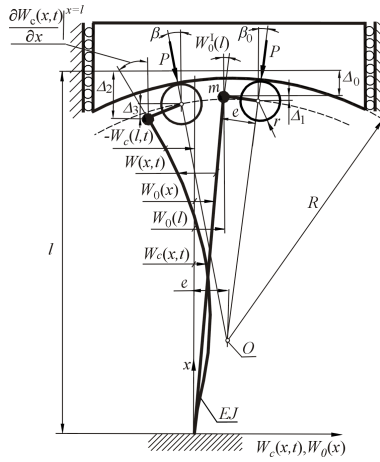
Figure 1. Physical model of the considered column

Individual longitudinal displacements of the systems are determined by relations:

$$\Delta_0 = \frac{1}{2}\int_0^l \left[W_0^I(x)\right]^2 dx, \ \Delta_1 = eW_0^I(l), \ \Delta_2 = \frac{1}{2}\int_0^l \left[W_c^I(x,t)\right]^2 dx, \ \Delta_3 = eW_c^I(l,t) \tag{2}$$

3. Mechanical energy of the system, formulation of the boundary problem

The boundary problem is formulated on the basis of the Hamilton's principle described for conservative system by the relationship:

$$\delta\int_{t_1}^{t_2}(T-V)dt = 0 \tag{3}$$

The kinetic energy T is sum of the column's kinetic energy and mass m placed at the end of the column:

$$T = \frac{1}{2}\int_0^l (\rho_0 A)\left[\frac{\partial W(x,t)}{\partial t}\right]^2 dx + \frac{1}{2}m\left[\frac{\partial W(l,t)}{\partial t}\right]^2 \tag{4}$$

Total potential energy V of the system is described by the formula:

$$V = \frac{1}{2} EJ \int_0^l \left[\frac{\partial^2 W_c(x,t)}{\partial x^2} \right]^2 dx - P(\Delta_2 - \Delta_0) - Pe(\Delta_3 - \Delta_1) - \frac{1}{2} P(\beta_0 + \beta) W(l,t) \tag{5}$$

Equations (4) and (5) after taking into account relationships (1), (2) are considered in Hamilton's principle (3).

The equation of motion and boundary conditions for the considered system, after taking into account the commutation of variation and differentiation operators and after integrating kinetic (4) and potential energies (5) of the system are obtained. Using of the expansion function $W(x,t)$ in the form:

$$W(x,t) = y_0(x) + y(x)\cos(\omega t) \tag{6}$$

then, by grouping the components of series connected to expressions $\cos^0(\omega t)$ and $\cos^1(\omega t)$, the equation of displacement and boundary conditions necessary to solution of the longitudinal bending problem was obtained:

$$\cos^0(\omega t): \qquad y_0^{IV}(x) + k^2 y_0^{II}(x) = 0, \ k^2 = \frac{P}{EJ} \tag{7}$$

$$y_0(0) = 0, \ y_0^I(0) = 0, \ y_0^{II}(l) + k^2 e = 0 \tag{8}$$

$$y_0^{III}(l) + k^2 \left\{ \left[y_0^I(l) - \alpha \right] - \frac{1}{R-r} \left[y_0(l) - \alpha \right] \right\} = 0 \tag{9}$$

and formulation of dynamic's problem:

$$\cos^1(\omega t): \qquad y^{IV}(x) + k^2 y^{II}(x) - \Omega^2 y(x) = 0 \tag{10}$$

$$y(0) = 0, \ y^I(0) = 0, \ y^{II}(l) = 0 \ \ y^{III}(l) + k^2 \left[y^I(l) - \frac{1}{R-r} y(l) \right] = 0 \tag{11}$$

4. The solution of longitudinal bending problem, results of numerical computation

The general solution to equation (7), which fulfils adequate boundary conditions in the form of function described by:

$$y_0(x) = C_1 \sin(kx) + C_2 \cos(kx) + C_3 x + C_4 \tag{12}$$

is being searched. Substituting solution (12) into boundary conditions (8) and (9) equation for $y_0(x)$ expressing total displacement for considered system is obtained:

$$y_0(x) = e \frac{k\{x[1-\cos(kl)] - (l-R+r)[1-\cos(kx)]\} - \sin[k(l-x)] - \sin(kx) + \sin(kl)}{k(l-R+r)\cos(kl) - \sin(kl)} +$$
$$+ \alpha(l-R+r) \frac{kx\cos(kl) - \sin(kl) + \sin[k(l-x)]}{k(l-R+r)\cos(kl) - \sin(kl)} \tag{13}$$

Based on dependency (13) between displacement of the column's end $y_0(l)$ and load parameter k^2 was determined:

$$y_0(l) = \frac{\alpha(l-R+r)[kl\cos(kl) - \sin(kl)] + ek(R-r)[\cos(kl) - 1]}{k(l-R+r)\cos(kl) - \sin(kl)} \tag{14}$$

The condition describing interactions of imperfections in form and load of the column (15) is determined considering relationship (14) as well as the transcendental equation for the value of critical force for the column loaded by the force directed towards the positive pole in the form $k(l - l_B)\cos(kl) - \sin(kl) = 0$:

$$\alpha[1 - (R - r)]\cos(kl) - e[\cos(kl) - 1] = 0 \tag{15}$$

The graphical interpretation of form and load imperfections, for the several value of the Δr^* parameter is presented in Fig. 2.
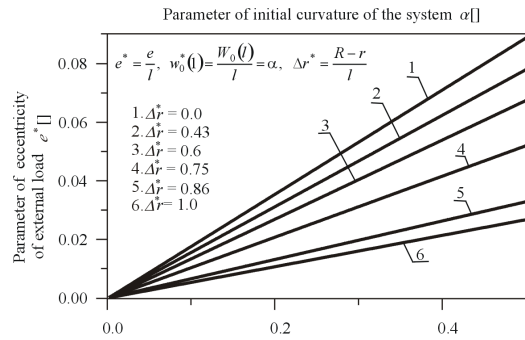
Figure 2. Curve courses of the interactions of imperfections in shape and load

Exemplary courses of transversal displacements of the end of system $y_c(l) = W_0(l) - y_0(l)$ in relation to the external load were determined (Fig. 3) on the basis of relationship (14) describing displacement $y_0(l)$ of the systems, where:

$$\lambda^* = k^2 l^2 = \frac{P l^2}{EJ}, \quad y_c^*(1) = \frac{y_c(l)}{l}, \quad \lambda_c^* = \frac{P_c l^2}{EJ} \tag{16}$$
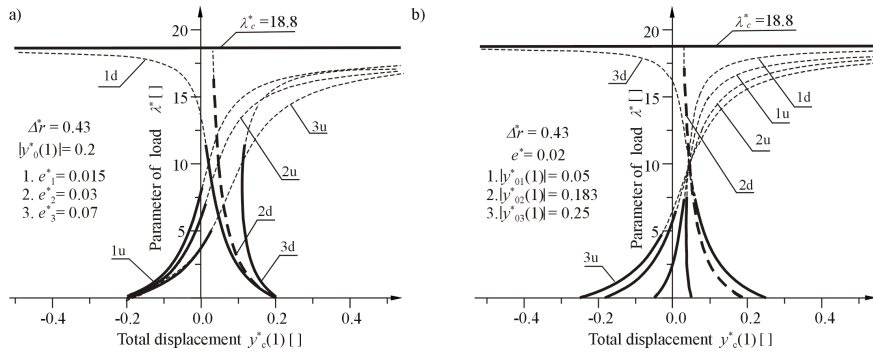
Figure 3. Curve courses of longitudinal bending on the plane: $\lambda^* - y_c^*(1)$

5. The solution of the vibration problem, results of numerical computation

A general solution of equation (10) is:

$$y(x) = D_1 \cosh(\alpha x) + D_2 \sinh(\alpha x) + D_3 \cos(\beta x) + D_4 \sin(\beta x) \tag{17}$$

where D_n are integration constants ($n = 1, 2, 3, 4$) and:

$$\alpha^2 = -0.5k^2 + \left(0.25k^4 + \Omega^2\right)^{\frac{1}{2}}, \ \beta^2 = 0.5k^2 + \left(0.25k^4 + \Omega^2\right)^{\frac{1}{2}}, \ \Omega^2 = \frac{(\rho_0 A)\omega^2}{(EJ)} \tag{18}$$

Substitution of solution (17) into boundary conditions (11) yields a transcendental equation to eigenvalues of the considered system.

Numerical computations for the change of natural frequencies in relation to the external load for several values of the parameter Δr^*, with the constant length l and constant value of concentrated mass m has been performed. In Fig. 4 the courses of two basic natural frequencies change Ω^* and additional frequencies Ω^*_s characterized by symmetry of vibrations against dimensionless parameter of load λ^* are presented, where:

$$\Omega^* = \Omega^2 l_1^4 = \frac{\rho_0 A \omega^2 l_1^4}{EJ}, \quad m^* = \frac{m}{\rho_0 A l_1} \tag{19}$$
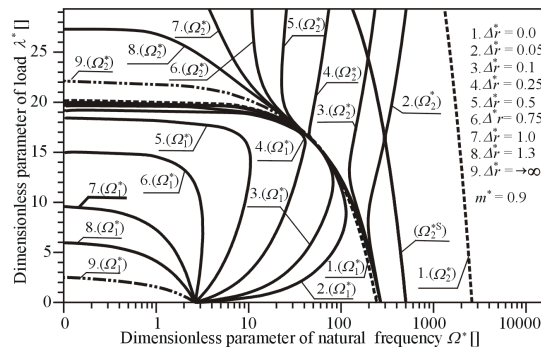
Figure 4. Curves in the plane: loading parameter λ^* – natural frequency parameter Ω^*

The courses of free vibration frequencies in relation to external load, typical for divergence (curves 1, 7 – 9) or divergence pseudoflatter (curves 2 – 6) type system were obtained.

5. Conclusions

Based on theoretical considerations and results of numerical simulations related to the influence of introduced inaccuracy on the longitudinal bending and free vibrations of considered system, one can state that:

– the interaction of the imperfections in shape and load was revealed and proved,
– the relationships between the introduced inaccuracies for which the bending of the column's end has a finite value at load P approaching critical load P_c were determined,
– the system depending of the course eigenvalues curves can be classified as one of the two types: divergence or divergence pseudoflatter system. Obtained curves allowing

classify considered column to system realising specific load (L. Tomski) in divergence pseudoflatter range.

Acknowledgments

References

1. L. Tomski, J. Szmidla, *Wprowadzenie do problematyki stateczności i drgań swobodnych kolumn*, rozdział 1.4*, Drgania i stateczność układów smukłych*, Praca zbiorowa wykonana pod kierunkiem naukowym i redakcją L. Tomskiego, WNT, Fundacja „Książka Naukowo-Techniczna", Warszawa (2004) 31 – 39.
2. L. Tomski , I. Podgórska-Brzdękiewicz, *Drgania swobodne i stateczność kolumn poddanych obciążeniu Eulera*, rozdział 3.5, *Drgania swobodne i stateczność obiektów smukłych jako układów liniowych lub nieliniowych*, Praca zbiorowa wykonana pod kierunkiem naukowym i redakcją L. Tomskiego, WNT, Fundacja „Książka Naukowo-Techniczna", Warszawa (2007) 81 – 92.
3. G. J. Simitses, D. H. Hodges, *Fundamentals of Structural Stability* (2006) 19 – 47.
4. A. S., Wolmir, *Stability of deformable systems*, Publishing House „Nauka", Moskwa 1967.
5. L. Tomski, I. Podgórska-Brzdękiewicz, *Wyboczenie globalne oraz interakcja imperfekcji kształtu i obciążenia słupa przy obciążeniu eulerowskim lub siłą skierowaną do bieguna dodatniego*, XII Sympozjum Stateczności Konstrukcji, Zakopane (2009) 443 – 450.
6. L. Tomski, J. Szmidla, *Drgania swobodne i stateczność układów poddanych działaniu obciążenia swoistego*, rozdział 4, *Drgania swobodne i stateczność obiektów smukłych jako układów liniowych lub nieliniowych*, Praca zbiorowa wykonana pod kierunkiem naukowym i redakcją L. Tomskiego, WNT, Fundacja „Książka Naukowo-Techniczna", Warszawa (2007) 114 – 121.

Niestateczność i drgania kolumny z imperfekcjami poddanej obciążeniu siłą skierowaną do bieguna dodatniego

W pracy rozważa się zagadnienie drgań własnych i niestateczności globalnej układu smukłego z imperfekcjami, poddanego obciążeniu siłą skierowaną do bieguna dodatniego. Niedokładności układu modeluje się zakładając wstępną jego krzywiznę oraz wprowadzając mimośrodowe przyłożenie obciążenia zewnętrznego. Na podstawie całkowitej energii układu wyznacza się równania ruchu oraz warunki brzegowe rozpatrywanego układu. Określa się relację między wprowadzonymi niedokładnościami, dla których ugięcie swobodnego końca kolumny ma wartość skończoną przy obciążeniu dążącym do obciążenia krytycznego. Prezentuje się wykresy przebiegu krzywych podłużnego zginania. Przedstawia się wyniki obliczeń numerycznych dotyczące przebiegu krzywych częstości drgań własnych w funkcji obciążenia zewnętrznego, dla zadanej geometrii i stałych fizycznych kolumny.

System for automatic rotor balancing using a continuous change of the correction mass distribution

Rafał RUMIN

AGH - University of Science and Technology, Dept. of Robotics and Mechatronics
Al. Mickiewicza 30, 30-059 Kraków, rafal.rumin@agh.edu.pl

Jacek CIEŚLIK

AGH - University of Science and Technology, Dept. of Robotics and Mechatronics
Al. Mickiewicza 30, 30-059 Kraków, cieslik@agh.edu.pl

Abstract

This paper presents the proposal design of the active balancing of rotors with correction mass (liquid), whose relative position to the rotor is changed continuously. Two design versions are adopted for the implementation - the mechanical models of the system. Proposed models consisted of rings with internal chambers, filled with fluid in sequence. It has been described a mathematical model of the equivalent correction mass allocation. There are presented concepts of supply and control of the fluid flow into the selected chamber. There were elaborated the algorithms of start-up and run-out the rotor. It has been presented the scheme of supplementary hydraulic manual control. Paper presents the potential scope of use of method for industrial applications.

Keywords: balancing rotor, unbalance, rotor dynamics, balance disc

1. Introduction

Most of rotating machines operate at rotational speeds out of the resonance conditions. Vibrations of rotor can be amplified by the unbalanced mass. Unbalance is caused by the rotor deflection or change in mass distribution due to work conditions e.g. dust adhesion to blower's blades. Vibrations of rotors with unbalanced masses lead to damage of the bearings, the rotor fatigue effects and shorten the life of the entire system. The methods of the unbalance reduction apply electro-magnetic bearings, active dampers and systems for correction masses motion. Research focuses on the active vibration reduction in rotor systems, as it was described in the literature [1, 5, 6, 7, 8, 9, 13, 14].

In purpose of rotor balance it was proposed the use of a balancing disks dedicated for balancing, with channels and various valves separating the liquid storage chambers. Replacement and storage of fluid in the chambers corresponds to the correction mass motion within the shaft. By the application of the control system a desired quantity of fluid can be allocated in each of single chambers. System should actively respond to changes of unbalance without the need to retain the rotor to adjust the distribution of the correction mass. The conducted research develops also an algorithm for safe start-up and run-out of the rotor with a balancing discs and supplementary manual control system.

2. Previous automatic balancing methods

The one of next steps in the development of rotors dynamics was application of automatic balancing methods. Adverse effect on the rotor machines was making

substantial changes to the balanced device, which greatly complicated their installation in existing structures. Selection of balancing technologies of rotating systems derived from the literature review [4, 13, 14] is presented as follows:

Van de Vegte and Lake 1978 - proposed a procedure for balancing rigid shafts during their normal work. The system includes a mechanical device with at least two correction masses. The electric drives were mounted on the disk and provided the change of the position of correction masses: Majewski 1976, 1994 – the theoretical background to the automatic balancing of rotors; Bishop 1982 – made a system for flexible shafts balancing; similar system to the Van de Vegte; Furman 1982 – an additional special metal disc was placed into the rotor. Locally heated disc undergoes a plastic deformation leading to the creation of a centrifugal force; Gosiewski 1985 – concept of rotated mass with electric drive. Instead of single mass numerous elements are used - automatic continuous balancing; Smalley, Baldwin, Schick 1998, and Smalley, Baldwin, Yuhas 1989 – study about balancing by synchronous projection of metal particles; Jenkins 1996 – active balancing device for machine with large size rotor. The disk with containers including the liquid was placed to balanced shaft. In the process of balancing the liquid has been moved from one chamber to the another through the procedure of temperature gradient generation; Alauze, Der Hagopian, Gaudiller, Voinis 2001 – an active balancing system consisted of two satellites with own drives (correction masses), located on round track, specially prepared for this purpose; Felis J, Mańka M., Uhl T. 2004 – device for dynamic balancing of rotors – angular motion of constant masses, external drives.

Currently used automatic balancing systems have various disadvantages that restrict their use. This is the main reason for further development of automatic balance system for rotary machines [2]. Current research investigate a new, efficient and less expensive mechanical balancing systems for use in specific environmental conditions.

3. Equivalent of correction mass

According the theoretical assumptions of automatic balancing system is equipped with additional discs placed onto the rotor. Each disc includes hydraulic system supplying the small amount of fluid (correction mass) to the proper chambers.
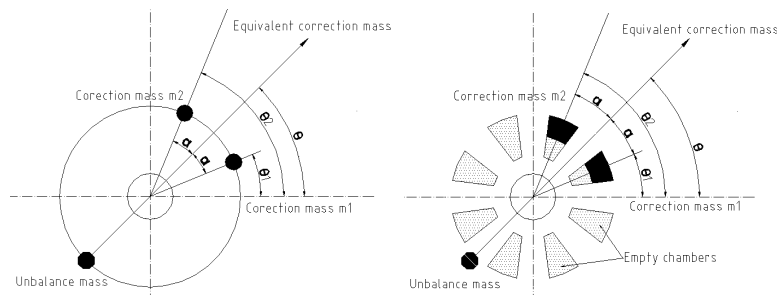
Figure 1 Principle of equivalent correction force generation through two mass components: a) constant mass motion; b) fluid filling the appropriate single chamber.

The mechanism allows the use combination of at least two correction masses (liquid), placed concentrically with respect to the axis of rotation of the system. The entire balancing ring with several chambers may be filled in the same time. Each chamber can be filled partly or in full in order to obtain the exact effective balancing mass.

Balancing is performed in several steps: by measuring the shaft vibration at the synchronous speed of the system (actual work of system), then by calculating which chamber should be filled by fluid (new position of equivalent correction mass) and controlling valve which determine the flow of the fluid from starting position to correction position. The automatic balance process changes the fulfillment of the chambers to gain the angular position of the partial mass (correction masses m_1, m_2) and thus the position of equivalent correction mass. This causes the corrective force of equal magnitude but opposite in phase (relative angular position with respect to an axis of rotation) relatively to unbalanced force identified in the system.

4. Active balancing theory

Previously there were developed a lot of methods for rotor's active balancing e.g.: modal method, method of influence coefficients (IC) and the combination of these two. The method of influence coefficients is widely used active balancing method in industrial applications [10]. This method describes change of response of the unbalance in function of rotating speed and point out the dynamic characteristics. The response to the unbalance for k-th iteration is expressed by the formula [11]:

$$\{V\}_k = [A(\omega)]\{U\}_k + \{D(\omega)\} \tag{1}$$

where:

$\{V\}_k$ – measured signal of vibrations for k^{th} iteration,
$[A(\omega)]$ – matrix of influence coefficients determined for the rotating speed ω,
$\{U\}_k$ – vector of unbalance for the kth iteration,
$\{D(\omega)\}$ – vibration signal for the initial unbalance at speed ω.

Response to unbalance system for $k+1^{th}$ iteration is represented by the formula:

$$\{V\}_{k+1} = [A(\omega)]\{U\}_{k+1} + \{D(\omega)\} \tag{2}$$

Subtracting the equation (1) from the equation (2) we obtain:

$$\{V\}_{k+1} - \{V\}_k = [A(\omega)]\{ \{U\}_{k+1} - \{U\}_k \} \tag{3}$$

In order to balance it is necessary to find a vector of correction mass $\{U\}_{k+1}$ such the response of vibration will be minimized after the completing of control sequences.

Correction vector take the form:

$$\{U\}_{k+1} = \{U\}_{k+} - [A(\omega)]^{-1}\{V\}_k \tag{4}$$

Equation (4) may be used only if the number of measurement planes is equal to the number of balancing planes. This condition is satisfied when the matrix of influence coefficients is a square matrix and the inverse matrix exists.

If the number of measurement planes is larger than the balancing planes, the solution is related to the optimization problem. Correction vector should minimize the system response to the unbalance.

Cost function is defined in following form:

$$J_{k+1} = \{V\}^T_{k+1} \{V\}_{k+1} \tag{5}$$

The correction vector can be written as follows to minimize the cost function:

$$\{U\}_{k+1} = \{U\}_k - ([A(\omega)]^T [A(\omega)])^{-1} [A(\omega)]^T \{V\}_k = \{U\}_k - [K(\omega)]\{V\}_k \qquad (6)$$

where: $[K(\omega)]$ – is the control gain.

The correction vector as the result of IC method determining the location of the correction mass and minimizing the vibration amplitude can be obtained from equation (6) when the current vibrations signal and the rotor's position are known. The influence coefficients matrix of the rotation speed is obtained by additional run the rotor with trial mass. The value of the correction mass is acquired by re-launching of the rotor.

Any influence coefficients which are used to create a influence coefficients matrix for active rotor balancing may be calculated by the following equation:

$$a_{ii} = [(V_i)_k - (V_i)_{k-1}] / [(U_i)_k - (U_i)_{k-1}] \qquad (7)$$

where: A_{ij} - means a change of the vibration signal of i plane to unbalance of j balancing plane.

If the predicted influence coefficients are more closer to the currently calculated, the vibration responses are increasingly minimized. An important element of active balancing is the choice of appropriate minimizing method. In the literature is reported the use of the following methods: LAD - Least Absolute Deviation, LS - Least-squares (LS), Chebyshev, or minmax - minimization of the maximum vibration amplitude. Previous studies have shown that using the plain least-squares method does not always bring the optimal solution [12].

5. Measurement and computational rules of IC

In the IC method we can distinguish two main parts [3, 4]: the measurement and the consecutive computation. During the measurement part are performed three measurements of vibration amplitude and phase. The first measurement is made in the natural state of the rotor. The measured vibrations at the chosen points must be linearly dependent on the unbalance. In order to perform the dynamic balancing of rotating machines is necessary to use at least two correction planes. It is necessary to measure vibrations in the bearings 1 and 2, which are generated by the action of an unbalance. Then at the first correction plane is positioned trial mass and measurements of vibrations are made again. At the next step the trial mass is removed from the first correction plane, and then it is positioned in the second correction plane to make consecutive vibration measurements. In case the measured vibrations in the system are caused by an unbalance, the location and size of the correction mass could be calculated through the use of influence coefficients method. Obtained influence coefficients are vectors and determine the impact of trial masses placed in the correction planes on the amplitude and phase of vibrations measured at the measuring points.

The method is based on the impact factors determining the sensitivity of the vibration amplitude to balancing mass placement in the correction plane. The amplitude of vibration is measured at the point of sensors attachment. Using this method requires the following conditions to be fulfilled: (1) vibration amplitude measured at the chosen points are linearly dependent on the unbalance present in the rotor; (2) distribution of the

masses in the system during the measurement does not change, including the changed position of the trial masses; (3) balanced object is considered as a rigid body.

Among described methods of calculating the location of the correction mass the best results gives modal method allowing to precise rotor balancing, regardless of its speed of work. In most cases it is sufficient to balance on one speed – speed of the system. The most suitable method seems to be the method of influence coefficients.

6. Draft of balancing system with fluid as correction mass

The proposed solution is based on the concept of modification of existing with minimization of rebuilding of rotor systems. In this model balancing the rotor element is done by continuously changing of correction mass distribution. Proposed system gives the possibility of shaft balancing at arbitrary chosen plain. Main mechanical element is the balancing ring. Inside this element are specially designed and arranged chambers (slots, cells). The fluid will flow through them and concentrate in special correction volumes.
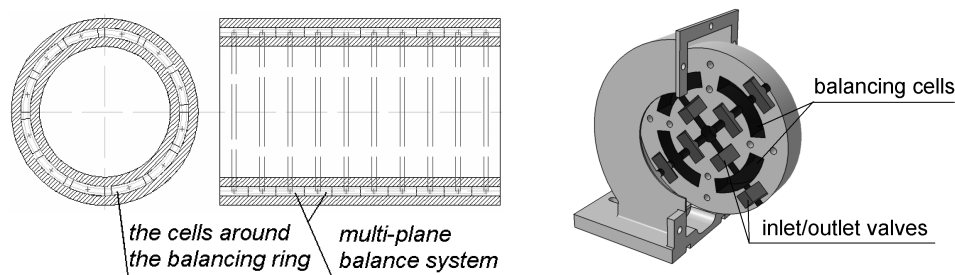
Figure 2. Concept of balancing system: (a) I-st version: The hollow shaft with cells,
(b) II-nd version: The balancing disc connected with rotor

Distribution of cells at the periphery of the balanced shaft should be symmetric so the flow of the liquid can be controlled into each tributary cell independently. This will enable the unbalance reduction by change of concentrated correction mass location. Authors bring up that the particular design of system is the patent pending.

Conclusion

The main target of presented study and research was to find opportunities for active shaft balancing at an arbitrary chosen plains, possible to apply in existing unbalanced rotors. Innovative approach was use to elaborate of the concept of system with liquid medium as a correction mass for system balancing. There was considered the concept of rotors balancing method with continuous gaining mass. The use of this concept will take full advantage of control of balancing of rotating systems in industrial application e.g. rotors of ventilation system, laboratory centrifuges, and water or wind turbines.

References

1. C. Alauze, J. Der Hagopian, L. Gaudiller, Ph. Voinis, *Active Balancing of turbo-machinery: Aplication to large shaft lines,* J. of Vibration and Control, 7, 249-278, 2001.
2. J. Felis, H. Jaworowski, J. Cieślik, *Teoria maszyn i mechanizmów. Cz 1: Analiza mechanizmów,* Kraków: Publishing House AGH, 2008.
3. J. Felis, M. Mańka, T. Uhl, *Urządzenie do dynamicznego wyważania wirujących elementów maszynowych,* Patent proposal P – 370466, 2004.
4. M. Mańka, *Automatyczne wyrównoważanie maszyn wirujących*, Doctoral Thesis, AGH, Kraków, 2005.
5. P. M. Frank, *Fault diagnosis in dynamic systems using analytical and knowledge based redundancy – a survey and some new results,* Automatica 26, 459-474. 1990.
6. L. S. Jenkins, *Vibration perfomance of a Westinghouse RCP during continuous changes in mass umbalance at the pump coupling,* EPRI Eighth Intern. Workshop on Main Collant Pumps, Pittsburgh, 20. 1996.
7. J. Kiciński, *Dynamika wirników i łożysk ślizgowych,* Publ. House. IMP, PAN. 2005.
8. Z. Walczyk, J. Kiciński, *Dynamika turbozespołów energetycznych: wybrane zagadnienia drgań prostych i sprzężonych*, Publishing House Pol. Gdańska, 2001.
9. J. Van De Vegte, R. T. Lake, *Balancing of rotating systems during operation,* Journal of Sound and Vibration, 2, 57, 225-235. 1978.
10. M. S. Darlow, *Balancing of High-Speed Machinery*, New York: Springer, 1989.
11. Soo-Hun Lee, Bong-Suk Kim, Jong-Duck Moon, Do-Hyung Kim, *A study on active balancing for rotating machinery using influence coefficient method*, Computational Intelligence in Robotics and Automation, 659–664, 2005, CIRA 2005.
12. Guoxin Li, Zongli Lin, C. Untaroiu, P.E. Allaire*, Balancing of high-speed rotating machinery using convex optimization*, Decision and Control,4351-4356 vol.4, 2003.
13. T. Majewski, *Samoczynne wyważanie wirnika podpartego sprężyście w jednym kierunku,* The Archive of Mechanical Engineering, 23 (3), 377-390, Warsaw 1976.
14. T. Majewski, *Synchronous Elimination of Mechanical Vibration*, Publishing House Warsaw University of Technology, Warsaw 1994.

Układ do automatycznego wyważania wirników przy pomocy ciągłej zmiany rozkładu masy korekcyjnej

Artykuł przedstawia projekt układu do aktywnego wyważania wirników za pomocą masy korekcyjnej (płynu), którego położenie względem osi wirnika zmieniane jest w sposób ciągły. Dla realizacji układu przyjęto dwie konstrukcje – dwa modele układu. Zaproponowano modele złożone z pierścieni z wewnętrznymi komorami, wypełnianymi sekwencyjnie przez płyn. Przedstawiono matematyczny opis zastępczej masy korekcyjnej. Opracowano koncepcje układu sterowania dostarczaniem i przepływem płynu do wybranej komory. Opracowano algorytmy rozbiegu i wybiegu wirnika. Przedstawiono schemat hydrauliczny dla rezerwowego układu sterowania ręcznego. Przedstawiono potencjalny zakres wykorzystania układu w zastosowaniach przemysłowych.

Analysis of Human Ear Ossicles Vibrations

Rafal RUSINEK

Department of Applied Mechanics, Lublin University of Technology
Nadbystrzycka36 St, 20-618 Lublin, Poland
r.rusinek@pollub.pl

Jerzy WARMINSKI

Department of Applied Mechanics, Lublin University of Technology
Nadbystrzycka36 St, 20-618 Lublin, Poland
j.warminski@pollub.pl

Marcin SZYMANSKI

Department of Otolaryngology, Head and Neck Surgery, Medical University of Lublin
Jaczewskiego 8 St, 20-854 Lublin, Poland
marcinszym@poczta.onet.pl

Marek ZADROZNIAK

Department of Otolaryngology, Head and Neck Surgery, Medical University of Lublin
Jaczewskiego 8 St, 20-854 Lublin, Poland
mzadrozniak@interia.pl

Abstract

The paper focuses on experimental investigations of ossicular chain vibrations using Laser Doppler Vibrometer. Measurement of stapes velocity in case of intact, damaged and reconstructed with Partial Ossicular Replacement Prosthesis ossicular chain is presented. A typical transfer function between an input and an output signal is completed by other methods applied in dynamics such as Lyapunov and Hurst exponent. The main aim of the study is to find the most efficient method of ossicles reconstruction and measurements analysis. Apart from a classical approach based on the transfer function which gives an information about vibrations amplitude also analysis of vibration types exhibiting nonlinear behaviours is presented.

Keywords: ossicles vibrations, middle ear prosthesis, middle ear mechanics

1. Introduction

Middle ear surgery techniques, known since middle of the last century, can improve hearing destroyed by a disease. There is a huge number of ossiculoplasty prostheses to choose from. Additionally, each of them has several factors that a surgeon can vary during prosthesis placement. On the other hand, also prosthesis designers are able to decide about prosthesis shape, size or length. Recently, the study which examines another key variable – the size of the prosthesis head has been published [3]. The results point out no essential difference in vibration transmission from the eardrum to the stapes footplate. Generally all prosthesis head size exhibit worse transmission properties than intact ear that is quite obvious and should motivate to improve existing prostheses. In case of damaged incus reconstruction of the ossicular chain can be done using the incus

replacement prosthesis (IRP). The main problem that must be solved is proper prosthesis length which provides optimal tension between the tympanic membrane or malleus and stapes. Different types of a cement incus replacement prosthesis (CIRP) in temporal bone were tested in [1]. The best tension and an acoustical efficient as well give the narrow Y-CIRP. Similar problem of optimum tension for partial ossicular replacement prosthesis (PORP) reconstruction is presented in [6]. Tension has a very significant effect on stapes vibration. Loose prosthesis result in the best overall vibration transmission, especially for lower frequencies. While tight prosthesis has a slight advantage in the higher than 2 kHz frequencies. The same conclusions are shown for adjustable-length titanium ossicular prosthesis [10]. Some authors report that an anatomically shaped incus prosthesis used for reconstruction of the ossicular chain is better than PORP [5]. The important decision for surgeon during prosthesis placement is to choose the best site on a stapes footplate that is discussed in [2]. The results prove that the centre site is the best location on the footplate. A separate problem is prosthesis material which must fulfill a lot of requirements such as: stiffness or force transfer function. In publication [9] teflon, polyetheretherketone, polysulfone, gold, Al_2O_3 ceramics, carbon and titanium were examined. Finally, titanium prosthesis with open head was chosen.

Most researchers (presented above and others) use Laser Doppler Vibrometer (LDV) as a tool to measure vibrations of human middle ear ossicles [4;7;8]. Usually, results of measurements are provided as a transfer function which most often is stapes velocity or displacement response to the sound stimuli. It gives us information about ossicles vibrations amplitude but not about the type of motion or regularity. Therefore, this study is an attempt to find another way of signal analysis engaging Lyapunov and Hurst exponent. The objective of the paper is to assess an effectiveness of middle ear prosthesis with various length compared to other method of hearing defects treatment and to the intact middle ear.

2. Material and measurement methods

Measurements are performed on fresh human temporal bone specimens. The specimens are subjected to extended procedure to visualise ossicular chain and to attach the microphone (ER-7C Etymotic Reserch) and the sound source (ER2 Etymotic Reserch) to external ear canal. The artificial canal is closed with a glass plate to create a sound seal chamber. Pieces of a retroleflective tape (0,5 mm2 squares) weighing less than 0,05 mg, are placed on the footplate of the stapes Detailed preparation of the temporal bone are described in [8]

The measurements are performed on a antivibration table inside a sound booth. Sound stimuli are frequency sweeps from 0,2 to 8 kHz at 80-120 dB signal pressure level (SPL). The sound source is connected to power amplifier to produce an adequate signal output. The measurements have been recorded using processing board (National Instrument) and DasyLab software and the experimental data analyzed with the MatLab package.

Stapes footplate velocity is measured with Laser Doppler Vibrometer (LDV) system composed of OFV-5000 controller with VD-06 velocity decoder (Polytec). OFV-534 sensor head is connected to a joystick operated micromanipulator, which is mounted on the operating microscope. The helium-neon laser beam is directed with the micromanipulator onto retroreflective targets on the stapes footplate through the artificial ear canal or on the stapes through the posterior tympanotomy approach.

After baseline measurements of stapes in the intact ossicular chain the incus was removed and series of trials were made. Then, titanium PORP prosthesis (Kurz Vario) was placed, instead of the original incus, between the stapes head and the eardrum. Three lengths of the prostheses are tested. Optimum length (3mm) set by experienced surgeon then 0.5mm lengthen and 0.5mm shorter prostheses are introduced.

3. Results

The difference in vibrations velocity, measured at the stapes footplate, between the intact middle ear, incus removed and titanium prosthesis for three various length (3mm - optimum, +0.5mm and -0.5mm) is presented in Figure 1 as velocity normalized to SPL of the input signal.
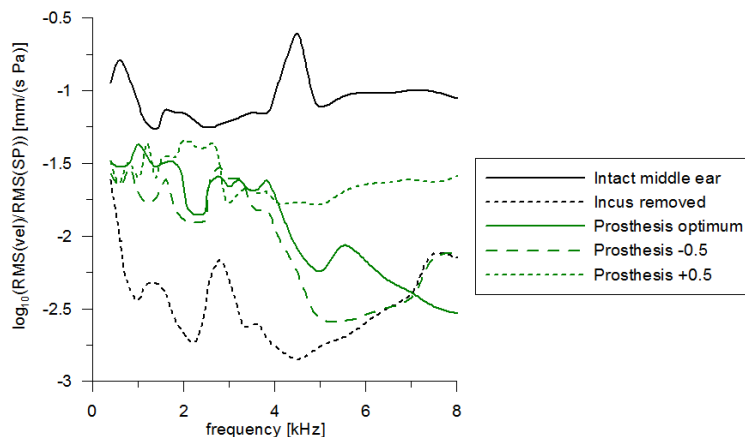
Figure 1. Velocity response in case of intact middle ear, incus removed and titanium prosthesis

The acoustic transfer function of the optimum length prosthesis is of course not as good as the baseline intact middle ear particularly above 4 kHz. Higher frequencies are important, especially for understanding speech in noise. Generally, using this type of prosthesis causes a meaningful improvement compared to situation with incus completely removed or destroyed. Interestingly, tight mounted prosthesis (length optimum +0.5mm) gives better results for higher frequencies (>2kHz) then optimum length. For frequencies below 2 kHz optimal prosthesis length is the most appropriate.

Looking at the problem in details, it must be noticed that the transfer function say only about vibrations amplitude but nothing about regularity and possible motions which stapes perform. Some symptoms of regular or irregular behaviour can be obtained just from time series of velocity (Table 1) made for chosen frequencies.

Table 1. Time series of the stapes velocity

	0.6kHz	1kHz	2kHz
Intact ear			
Incus removed			
Prosthesis opt.			
Prosthesis +0.5			
Prosthesis -0.5			
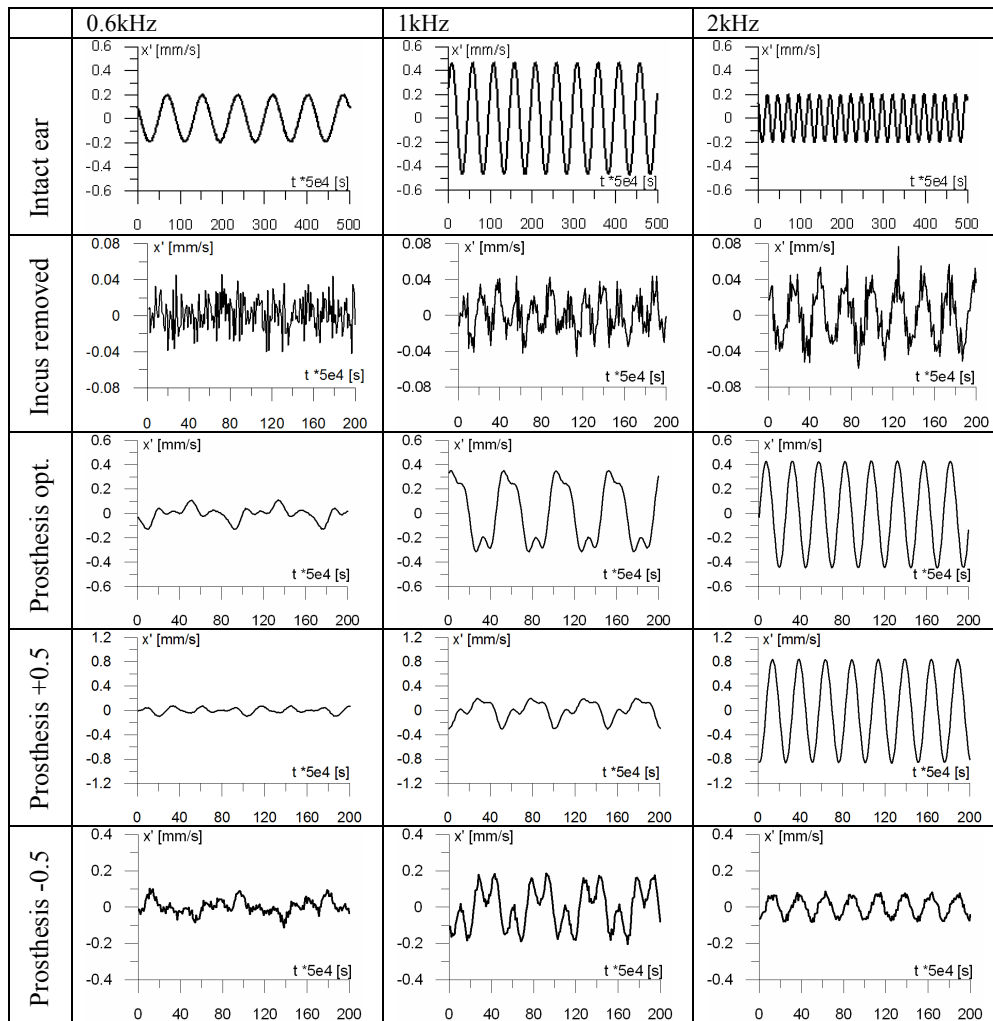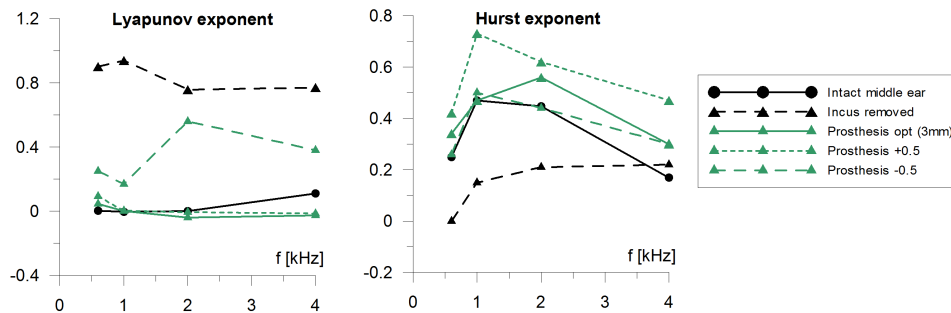
Figure 2 Lyapunov and Hurst exponent versus frequencies for intact middle ear, incus removed and three length of Kurz prosthesis

All prostheses show subhrmonical nature for lower frequencies (0.6 and 1kHz) while the intact ossicular chain is characterized by harmonic motion. Additionally, the loose placement of prosthesis seems to work worse than optimal (3mm) and longer (3.5mm) assembly. Middle ear vibrations without incus are irregular specially below 2kHz. It suggests that another tools like Lyapunov and Hurst exponent (Figure 2) should be used to estimate hearing results after various kind of treatment including PORP reconstruction. Both the intact middle ear and the ear with optimal and long (+0.5mm) prosthesis can be easily distinguishable from the damaged ossicles chain, when Lyapunov exponent is bigger that 0.7. Only the loose fitted prosthesis (-0.5mm) gives higher Lyapunov exponent, what is consistent with Figure 1 and speaks volumes for worse features of short prostheses. Similarly, Hurst exponent shows that the time series of reconstructed ear with prosthesis are more predictable (persistent) because the exponent is distinctly bigger.

3. Conclusions

Proper prosthesis tension is essential for excellent reconstructed middle ear sound transmission. The best tension is produced by prosthesis length of 3mm although, for higher frequencies 3.5mm length seems to be better. General conclusion obtained on the basis of the transfer function can be completed by time series of vibrations or replaced with Lyapunov exponent analysis.

Interestingly subharmonic vibrations for low frequencies are observable when PORP prosthesis is applied. This effect cannot be shown looking only at transfer function therefore, further analysis of phase space should be helpful to disease diagnosis and specially to estimate method of reconstruction.

Acknowledgments

References

1. M. Asai, K.E. Heiland, A.M. Huber, R.L. Goode, *Evaluation of a Cement Incus Replacement Prosthesis in a Temporal Bone Model*. Acta Otolaryngol, **119** (1999) 573-576.

2. M. Asai, A.M. Huber, R.L. Goode, *Analysis of the Best Site on the Stapes Footplate for Ossicular Chain Reconstruction*, Acta Otolaryngol, **119** (1999) 355-361.

3. M. Bance, A. Campos, L. Wong, D.P.Morris, R.G.van Wijhe, *How does prosthesis head size affect vibration transmission in ossiculoplasty?* Otolaryngology–Head and Neck Surgery, **137** (2007) 70-73.

4. A.M. Huber, F. Ma, H. Felix, T. Linder, *Stapes Prosthesis Attachement: The Effect of Crimping on Sound Transfer in Otosclerosis Surgery*. The Laryngoscope **113** (2003) 853-858.

5. R.M. Lord, R.P. Mills, E.W. Abel, *An anatomically shaped incus prosthesis for reconstruction of the ossicular chain*. Hearing Research, **145** (2000) 141-148.

6. D.P. Morris, M. Bance, R.G. van Wijhe, M. Kiefte, R. Smith, *Optimum Tension for Partial Ossicular Replacement Prosthesis Reconstruction in the Human Middle Ear*. The Laryngoscope, **114** (2004) 305-308.

7. M. Szymański, R. Mills, *Ruchy kosteczek słuchowych podczas zmian ciśnienia statycznego*. Otolaryngol Polska, **58** (2004) 593-597.

8. M. Szymański, R. Rusinek, M. Zadrożniak, J. Warmiński, K. Morshed, *Drgania błony bębenkowej oceniane Dopplerowskim wibrometrem laserowym*. Otolaryngologia Polska **63**(2) (2009) 180-183.

9. H.P. Zenner, H.-G. Freitag, C. Linti, U. Steinhardt, J.R. Jorge, S. Preyer et al, *Acoustomechanical properties of open TTP titanium middle ear prostheses*. Hearing Research, **192** (2004) 36-46.

10. S. Zhao, N. Hato, R.L. Goode, *Experimental study of an adjustable-length titanium ossicular prosthesis in a temporal bone model*. Acta Oto-Laryngologica, **125** (2005) 33-37.

Analiza drgań kosteczek słuchowych człowieka

Praca przedstawia wyniki pomiarów drgań kosteczek ucha środkowego wykonane Dopplerowskim wibrometrem laserowym w przypadku zdrowego łańcucha kosteczek, uszkodzonego i naprawionego z użyciem protezy tytanowej Kurz. Przeanalizowano drgania kosteczek słuchowych w przypadku trzech różnych długości protezy i oceniono ich skuteczność klasycznie stosując funkcję przejścia oraz z zastosowaniem wykładnika Lyapunowa i Hursta do oceny zastosowanych protez.

Identification of model parameters of a sandwich beam incorporating magnetorheological fluid

Bogdan SAPIŃSKI

AGH University of Science and Technology, al. Mickiewicza 30, 30-059 Kraków
deep@agh.edu.pl

Jacek SNAMINA

AGH University of Science and Technology, al. Mickiewicza 30, 30-059 Kraków
snamina@agh.edu.pl

Mateusz ROMASZKO

AGH University of Science and Technology, al. Mickiewicza 30, 30-059 Kraków
matek@agh.edu.pl

Abstract

The study covers the *identification* of model parameters of a sandwich (three-layered) cantilever beam incorporating magnetorheological (MR) fluid. The beam comprises two outer layers made of aluminium and a *MR fluid* layer in between, sealed with silicone rubber. The beam finite element (FE) model is created using the ANSYS software. Interactions of the magnetic field are taken into account by varying the FE model parameters. Data required for *identification* are collected from results of measurement of the beam's free *vibration*. The *identification* procedure assumes the good agreement between the frequencies of the beam's free *vibrations* and dimensionless *damping* factors obtained from research and computation data.

Keywords: MR fluid, beam, vibrations, damping, identification

1. Introduction

Control of *vibration* of flexible structures using smart fluids has received a great deal of attention since the early 1990s. The literature on the subjects abounds in reports on adaptive features of *beam* and plate structures incorporating electrorheological (ER) fluid. Fewer reports are available that explore similar applications of *MR fluids* [3, 4, 5, 6, 7].

The distinctive feature of such structure is that their structural behaviour can be controlled by the magnetic/electric field which activates the smart fluids present in them. Interactions of the magnetic/electric field cause the stiffens and *damping* characteristics to change, hence enabling *vibration* reduction.

At this stage of the research programs, the authors focus on a three-layered cantilever *beam*, incorporating *MR fluid* layer of 140CG type of Lord Corporation [8] in between two flexible layers. The purpose of the research program is to reduce the free transverse *vibration* of the *beam* under the applied magnetic field.

The paper is concerned with *identification* of model parameters of a *beam* incorporating *MR fluid*, assuming the fluid is represented by finite elements in the form of a rheological structure of the Voigt-Kelvin type and of the modified Bingham structure. The model is intended to be used for testing the control algorithms of *beam vibration*.

2. Model

The structure of the *beam* with a *MR fluid* layer, is shown in Figure 1. Development of the *beam* model involves three stages. The *beam* considered in the first stage is made of a single layer of aluminium 400 mm in length, 30 mm in width and 2 mm in thickness (Beam1). The *beam* modelled in the second stage comprises two aluminium layers and a silicone rubber sealing 2 mm in thickness (Beam2). Finally, the *beam* modelled in the third stage has a *MR fluid* layer in between the aluminium layers (Beam3).

The *beam* is modelled using the finite elements readily available in the ANSYS library: solid45 (aluminium layer), solid185 (silicone rubber sealing), combin40 and mass21 (*MR fluid*). The schematic diagram of the finite element combin40 is shown in Figure 2a. The *MR fluid* layer is modelled by the rheological Voigt-Kelvin structure (Figure 2b) and the modified Bingham structure (Figure 2c) assuming shear mode of *MR fluid* operation.

In order to assure the shearing mode operation it is required that vertical displacements of relevant cross-sections of the upper and lower aluminium layers should be the same [2]. Thus the relative displacement of modes of the element combin40 is confined to direction coinciding with the *beam*'s axis.
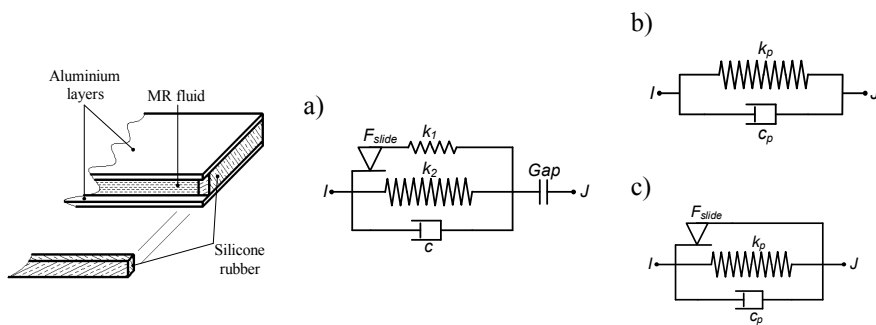
Figure 1. Beam structure   Figure 2. combin40 element and its modifications

3. Identification experiment

Experiments were performed in the set-up shown schematically in Figure 3. Data for *identification* were collected by testing the *beam's* free *vibration* and recording the displacement z of the point P.

Experiments were performed on the *beams*: Beam1, Beam2 and Beam3. Experiments were performed in the absence of magnetic field and under the applied field. The free end of the *beam* was deflected from the equilibrium state and displacement z of the point P was registered with the laser vibrometer. The height of the slit between the poles of an electromagnet was 20 mm.

Of particular interest is the relationship between the electromagnet's position and dimensionless damping coefficient. The electromagnet position was measured by the

distance y_m between the *beam* attachment point and the slit centre. The following values of y_m were assumed: 43, 50, 60, 70, 80, 90, 100, 110, 120, 130, 140 mm.
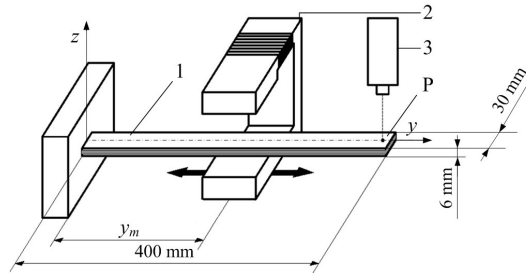
Figure 3. Experimental set-up: 1— beam; 2— electromagnet; 3— laser vibrometer

In each position of the electromagnet, it was supplied with current $I=5$ A. The current induced the magnetic field with flux density 0.16 T. Figure 4 shows time histories of displacement of the point P for the Beam1 and Beam3 with no magnetic field and under the applied field, for y_m=80 mm.
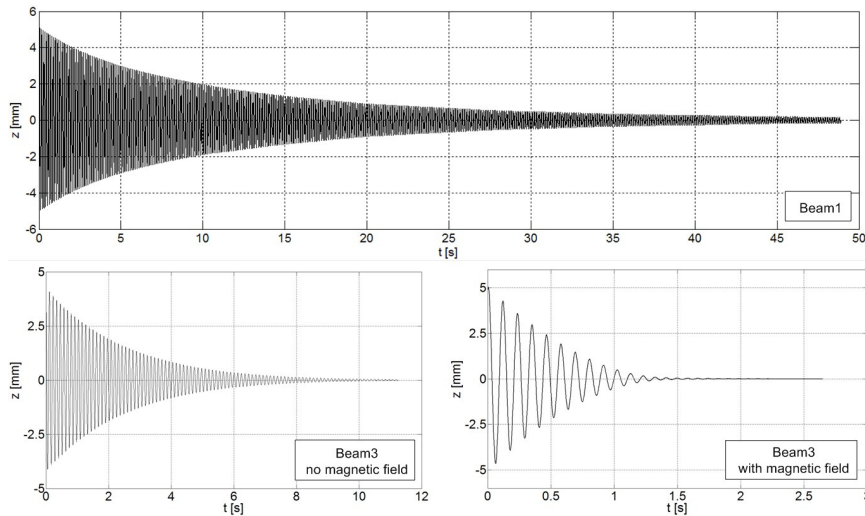
Figure 4. Displacement of the point P

Thus obtained time histories yield natural frequencies f and dimensionless *damping* coefficient ζ of the *beam's vibration*, depending on the position of the electromagnet for the current $I=5$ A. Computation data, obtained for selected positions of the electromagnet, are compiled in Table 1. Frequency and the dimensionless *damping* coefficient for Beam3 with no activated magnetic field become 8.63 Hz and 0.0075, respectively.

Table 1. Frequency and dimensionless damping coefficient

y_m [mm]	43	60	80	100	120	140
f [Hz]	8.82	8.90	8.98	9.02	9.07	8.94
ζ [−]	0.016	0.018	0.023	0.030	0.041	0.049

4. Identification procedure

The main purpose of *identification* was to find the values of major model parameters: the internal *damping* factor for aluminium and the rubber sealing, Young modulus for aluminium and the rubber sealing and, most importantly, of model parameters of the *MR fluid* layer.

Identification of parameters of the MR fluid layers involved two procedures. In accordance with the procedure 1, parameter values of the Voigt-Kelvin structure c_p, k_p (Figure 2b) are determined basing on the equality between experimental and calculated values of natural frequencies and dimensionless *damping* coefficients obtained for the electromagnet position y_m=80 mm. In the procedure 2 we sought such values of parameters c_p, k_p that the error defined by the formula (1) takes minimum value:

$$\min_{c_p,k_p}\left[\sum_{j=1}^{11}\left(\zeta_j\left(c_p,k_p\right)-\zeta_j^*\right)^2 + W\cdot\sum_{j=1}^{11}\left(f_j\left(c_p,k_p\right)-f_j^*\right)^2\right] \tag{1}$$

where: f_j^*, f_j − natural frequency, experimental and theoretical; ζ_j^*, ζ_j − dimensionless *damping* coefficient, experimental and theoretical; j=1, 2, ... ,11 − index corresponding to successive positions of the electromagnet; W=0.001 − weighting coefficient.

Values of c_p and k_p obtained in the first procedure are equal to c_p=19.2 [N·s/m], k_p=2544 [N/m] and in the second procedure are equal to c_p=21.1 [N·s/m], k_p=2162 [N/m]. These values yield the relationship between frequency and the dimensionless *damping* coefficient and the electromagnet's position, shown in Figures 5 and 6.

The values of c_p and k_p calculated for various current levels are compiled in Tables 2 and 3.
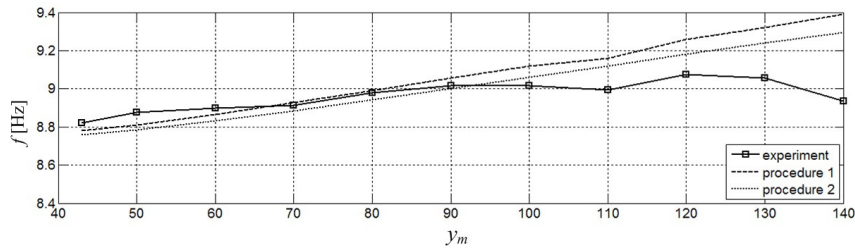
Figure 5. Frequency as the function of electromagnet's position
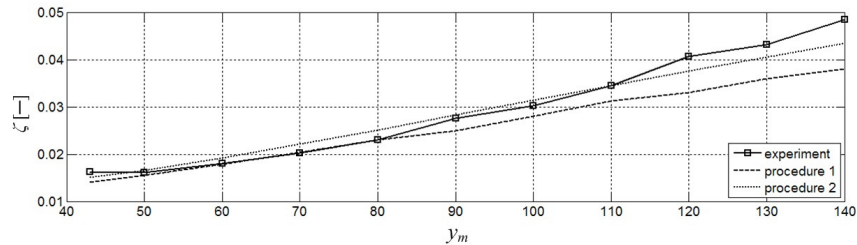
Figure 6. Dimensionless damping coefficient as the function of electromagnet's position

<table>
<tr><td colspan="4">Table 2. Values of c_p and k_p in accordance with the procedure 1</td></tr>
</table>

	I=3 A	I=5 A	I=9 A
c_p[N·s/m]	7.9	19.2	32.6
k_p [N/m]	1000	2544	3670

Table 3. Values of c_p and k_p in accordance with the procedure 2

	I=3 A	I=5 A	I=9 A
c_p[N·s/m]	8.7	21.1	35.9
k_p [N/m]	900	2162	3303

The proposed model correctly predicts the changes of parameters ζ and f for successive position of the electromagnet along the *beam* axis. A good approximation of the dimensionless *damping* coefficient is achieved for all electromagnet's positions. Frequencies are well predicted for the electromagnet in the position y_m<100 mm, which might be associated with enhanced interactions of a non-homogenous magnetic field at the edges of the space between the poles of an electromagnet [1]. The influence of non-homogeneity of the field on the *beam's* motion enhances with amplitude increase. It was observed at points of the *beam* at a larger distance from the attachment point. At higher amplitudes of *vibration*, points of the *beam* are temporarily placed in the space where concentration of magnetic field lines is so high that attraction of ferromagnetic particles causes the natural frequency to be vastly reduced.

5. Summary

A model of a sandwich *beam* incorporating *MR fluid* is proposed and its parameters are identified. The model enables us to accurately predict the *vibration damping* capability over the entire range of electromagnet's positions. Natural frequencies of *beam vibration* are established with sufficient accuracy for the electromagnet in the position given as y_m<100 mm. Phenomena due to non-homogeneity of the magnetic field in the slit of the electromagnet can be neglected for the electromagnet positions y_m< 100 mm. In the light of the assumptions made, the predictions of the *beam's* motion are sufficiently accurate, enabling us to the test the control algorithms of *beam's vibration*.

Acknowledgments

References

1. B. Sapiński, J. Snamina: *Vibration of a beam with magnetorheological fluid in non-homogenous magnetic field*. Engineering Modeling, **6**, 241−48, 2009
2. B. Sapiński, J. Snamina: *Modeling of an adaptive beam with MR fluid*. Solid State Phenomena **147−149,** 831−838, 2009
3. M. Yalcinitas, H. Dai: *Vibration suppression capabilities of magneto-rheological materials based adaptive structures*. Smart Materials and Structures, **13**, 1−11, 2004
4. Q. Sun, J. X. Zhou, L. Zhang: *An adaptive beam model and dynamic characteristics of magnetorheological materials*. Journal of Sound and Vibration, **261**, 465−81, 2003
5. Z. F. Yeh, Y. S. Shih: *Dynamic characteristics and dynamic instability of magnetorheological based adaptive beams*. Journal of Composite Materials, **40**, 1333−59, 2006
6. V. Lara-Prieto, R. Parkin, M. Jackson, V. Siberschmidt, Z. Kęsy: *Vibration characteristics of MR cantilever sandwich beams experimental study*. Smart Materials and Structures, **19**, 1−9, 2010
7. US Patent 5547049 *Magnetorheological Fluid Composite Structure*
8. http://www.lord.com

Identyfikacja parametrów modelu trójwarstwowej belki z cieczą magnetoreologiczną

W pracy dokonano *identyfikacji* parametrów modelu trójwarstwowej *belki* wspornikowej z *cieczą magnetoreologiczną* (*MR*). *Belka* składa się z dwóch zewnętrznych warstw aluminiowych, pomiędzy którymi znajduje się warstwa *cieczy MR* uszczelniona gumą silikonową. Model *belki* zbudowano przy wykorzystaniu elementów skończonych dostępnych w programie ANSYS. Oddziaływanie pola magnetycznego na *belkę* uwzględniono przez zmianę wartości parametrów użytych w modelu elementów skończonych. Dane do *identyfikacji* pozyskano z badań drgań własnych *belki*. W procedurze *identyfikacji* kierowano się zgodnością wartości częstotliwości drgań własnych *belki* oraz bezwymiarowych współczynników tłumienia uzyskanych z badań i obliczeń.

Assessing the wear of friction pads in disc braking system of rail vehicle by using selected amplitude characteristics of vibration signal

Wojciech SAWCZU

Faculty of Working Machines and Transportation, Poznan University of Technology
Piotrowo 3, 60-965 Poznan, Poland
wojciech.sawczuk@put.poznan.pl

Franciszek TOMASZEWSKI

Faculty of Working Machines and Transportation, Poznan University of Technology
Piotrowo 3, 60-965 Poznan, Poland
franciszek.tomaszewski@put.poznan.pl

Abstract

In rail vehicles, because of higher and higher ride speeds, there are works carried out to upgrade braking systems to stop the vehicle at shortest possible braking distance. It is required that in braking systems the condition of friction set is periodically controlled and the wear of braking system parts is constantly monitored. The purpose of this article is to present possibility to diagnose the friction set of disc brake by using selected amplitude characteristics of vibration signal generated by brake holder with friction pads.

Keywords: wear, friction pad, railway disc brake, point parameters, amplitude characteristics

1. Introduction

In rail vehicle, because of constantly rising ride speed and to obtain required braking distance, disc brakes are used as primary brake. Additionally, according to UIC 546, speed of passenger trains of over 160km/h triggers application of disc brake. Few disadvantages of disc brake include a lack of possibility of controlling the condition of the friction set: brake and pad in the whole operation time. It is particularly observable in rail cars, where disc brakes are mounted on the axle of the axle set between the wheels [3]. To check the wear of friction pads and brake discs it is necessary to apply specialistic station e.g. inspection channel to carry out inspections, and to carry out replacement of friction parts in case they reach their terminal wear.

In rail technique, rail track stations are used to diagnose the wear of friction pad. At these stations friction set consisting of disc brake and friction pad is photograhed during train ride. However is not a very precise metho because, on the basis of registered pictures the thickness of frction pads of disc brake is only assessed. When pads' thickness amounts to approx. 10mm tram driver receives information that terminal acceptable wear of pads on a certain axle of axle set has been reached. Rail track stations to diagnose the wear of friction pads are used by German, British and French railways.

In railway vehicles, systems signaling braking process and easing process, visible for the service from the inside and outside of the vehicle, are the most often applied. Those systems enable to check during train ride in which car braking system is bloked.

Nevertheless, rail technique lacks an objective method of quantitive assessment of the wear of friction pads.

The purpose of this research is to apply vibration signal of pad calipers to assess the wear of friction pads of disc brake.

2. Methodology research

The research was carried out at inertial station for tests of railway brakes. A brake disc type 610×110 with ventilation fans made by Kovis and three sets of pads type 200 FR20H.2 made by Frenoplast constitute the research object. One set was new - 35 mm thick and two sets were worn to thickness of 25 mm and 15 mm.

A reasearch program C (fast ride) according to instructions of UIC 541-3 was applied. The brakings were carried out from speed of 50, 80, 120, 160 and 200 km/h. During the research pad's pressures to disc N of 28 and 44kN were realized as well as braking masses per one disc of M=4.4T and 7.5T [5]. Vibration converters were mounted on pad calipers with a mounting clip, which is presented in Figure 1a [6].
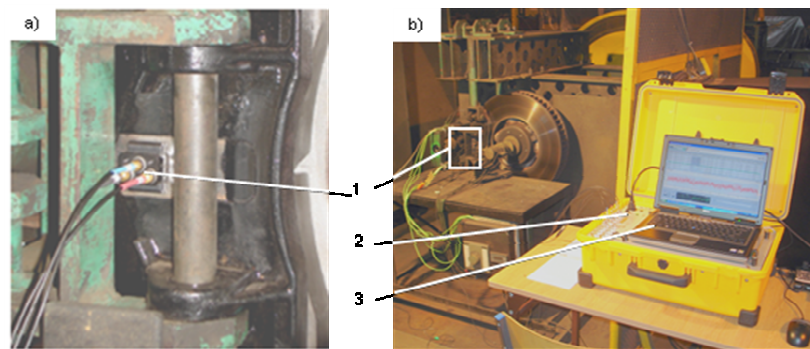
Figure 1. Interial station for tests of railway brakes; a) pad calliper with accelerometer,
b) view of measurement set of vibrations generated by calliper with pads;
1-accelerometer, 2-measuring case type B&K 3560 C , 3- System software PULSE 12.5

During the research signals of vibration accelerations were registered in three reciprocally orthogonal directions. To acquire vibration signal a measuring system consisting of piezoelectric vibration accelerations converter and measuring case type B&K 3560 C with system software PULSE 12.5. was used. Figure 1b presents the view of the measuring track.

Vibration converters type 4504 made by Brüel&Kjær were selected on the basis of instructions included in papers [1], the linear frequency of converters transit amounted to 13 kHz. During diagnostic tests signals in frequency from 0.7 Hz to 9 kHz [1] were registered. Sampling frequency was set at 32 kHz. This means that the frequency that was subject of the analysis in accordance with Nyquist relation amounted to 16 kHz.

This research was carried out in accordance with principles of active experiment. After carrying out a series of brakings at set speeds at the beginning of braking, pads'

pressures to the disc and braking masses, the friction pads were changed and values of instantenuous vibration accelerations were registered.

3. Research results

In domain of amplitudes, the most common are the point parameters [2], which are used to describe displacement signals, speed signals and signals of vibration accelerations. Characterizing vibration signal with one number is an advantage of point parameters, thanks to which it is easy to define changes in vibroacoustic signal resulting from changes in technical condition of the tested object.

To diagnose the wear of friction pads of railway brake the following dimensional point parameters are applied:

- average amplitude, described with dependence:

$$S_{AVERAGE} = \frac{1}{T} \int_0^T |s(t)| dt \tag{1}$$

where: T　-　means average time [s],

　　　$s(t)$　-　means instantaneous value of vibration accelerations [m/s^2].

- RMS amplitude, described with equation:

$$S_{RMS} = \sqrt{\frac{1}{T} \int_0^T [s(t)]^2 dt} \tag{2}$$

- square amplitude, describe with dependence:

$$S_{SQuARE} = \left[\frac{1}{T} \int_0^T |s(t)|^{\frac{1}{2}} dt \right]^2 \tag{3}$$

- peak amplitude, described with equation:

$$S_{PEAK} = \left[\frac{1}{T} \int_0^T |s(t)|^\infty dt \right]^{\frac{1}{n}} \; dla \; n \to \infty \tag{4}$$

Before calculating point parameters from signals of vibration accelerations in program Matlab 7.0, a preliminary processing of signal in time domain was carried out. The reason of this processing was to select from the whole registered signal a part connected only with braking process. This process was also carried out to obtain required dynamics of changes essential for diagnostic purposes. Defining dependence of friction pad's thickness on selected point parameters was carried out through determining dynamics of changes for a certain parameter, which is presented in dependence (5) [4]:

$$D = 20 \lg \left(\frac{s_2}{s_1} \right) \tag{5}$$

where: s_1　-　means the value of point parameter determined for pad G_3 or G_2 [m/s^2],

s_2 -   means the value of point parameter determined for pad G_1 [m/s^2].

The analysis of results of vibration tests showed that obtaining dependence of friction pads' thickness on the value of point parameters is possible by measuring vibration in directions Y_2 and Z_2 on a sensor mounted from the side of brake cylinder's case. Diagnostic tests with application of point parameters showed that inference about the wear of friction pads is dependant on type of braking with pressure N to the disc and on braking mass M. Realizing pressure N=44kN on the disk with M=4.4T enables determining dependence of the wear of friction pads on the value of point parameters in the whole speed range at the beginning of braking i.e. from 50 to 200km/h. Moreover vibration tests showed that combinations of brakings with N=44kN and M=7.5T, N=28kN and M=4.4T, N=28kN and M=7.5T preclude assessment of pad wear on the basis of values of point parameters for considered speeds at the beginning of braking.

The greatest values of dynamics of changes were noticed by using from point parameters the RMS value and square value. Figure 2 present dependence of (RMS) value of vibration accelerations in direction Z_2 on braking speed for various values of pad wear G with N=44kN and M=4,4t.
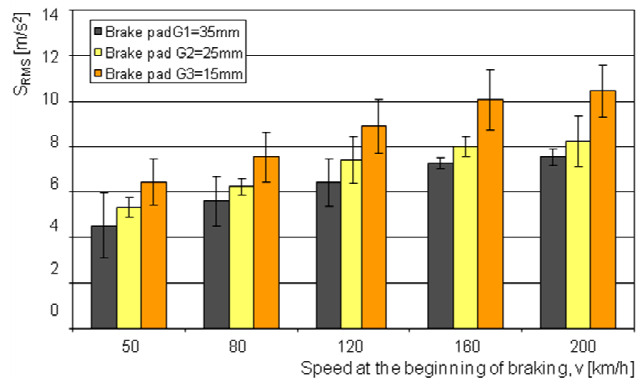
Figure 2. Dependence of (RMS) value of vibration accelerations in direction *Z2* on braking speed for various values of pad wear *G* with N=44kN and M=4,4t

Because of increasing values of selected point parameters in the speed function at the beginning of braking, which was found out for each tested friction set, in the further analysis calculated point parameters were approximated against three friction pads' thicknesses. Dependences were approximated with the polynomial function or the linear function (depending on the speed at the beginning of braking) receiving the largest values of correlation coefficient R^2. As a result of approximation mathematical models were obtained, which enable to calculate value of selected point parameters in the function of friction pad's thickness. In the measurement's orthogonal direction to the friction surface of the disc (Y_2) and tangential direction (Z_2), approximation was carried out for RMS value, average value and square value, which resulted from the greatest dynamics of changes in enumerated point parameters.

In case of measurement of instantaneous values of vibration accelerations in direction Y_2, it was found out that for lower speeds at the beginning of braking (to 80km/h), approximation of point parameters can be effected with linear functions, which was confirmed for each calculated parameter i.e. for, RMS value, average value, square value and peak value. Higher braking speeds cause that the value of point parameters should be approximated with the polynomial function. In direction Z_2 of measurement of vibration accelerations of calipers with pads, average value should be approximated with the polynomial function in the whole range of speeds at the beginning of braking.

During station research, dynamics of changes of analyzed values of point parameters according to dependence (5) was defined, which is presented in table 1. On this basis it was found out that RMS value of vibration accelerations shows the best sensitivity towards change of pad's thickness against other point parameters at vibration measurement in directions Y_2 and Z_2.

Table 1. Dynamics of changes of selected point parameters in direction Y_2 and Z_2

Point paramiters	Symbol	Unit	Value of dynamics of changes	
			Measurement direction Y_2	Measurement direction Z_2
RMS value	S_{RMS}	m/s^2	4.8	5.3
Average value	$S_{AVERAGE}$	m/s^2	4.3	4.5
Square value	S_{SQUARE}	m/s^2	4.1	5.1
Peak value	S_{PEAK}	m/s^2	3.9	4.4

Fundamental aim of station research of diagnostic character is to determine the wear of friction pads on the basis of values of vibration accelerations by applying approximating functions, on the basis of which, measured value of point parameter enables to define the wear of brake's friction pad. The wear of pads determinates pads' thickness, which in the carried out tests were diversified. Calculations were carried out for RMS value obtained in measurement direction Z_2. For RMS value of point parameter, also obtained from measurement in direction Z_2 by using linear approximating functions described with dependences (6-10) for five speeds at the beginning of braking, the following equations defining friction pads' thickness were introduced:

$$G_{RMS,(v=50)} = -10{,}312 \cdot S_{RMS,(v=50)} + 80{,}974 \tag{6}$$

$$G_{RMS,(v=80)} = -9{,}9328 \cdot S_{RMS,(v=80)} + 89{,}157 \tag{7}$$

$$G_{RMS,(v=120)} = -8{,}0383 \cdot S_{RMS,(v=120)} + 85{,}929 \tag{8}$$

$$G_{RMS,(v=160)} = -6{,}68 \cdot S_{RMS,(v=160)} + 89{,}416 \tag{9}$$

$$G_{RMS,(v=200)} = -6{,}3409 \cdot S_{RMS,(v=200)} + 80{,}448 \tag{10}$$

where: $G_{RMS,(...)}$ - means pad's thickness calculated on the basis of RMS value of vibration accelerations S_{RMS} [mm]

4. Conclusions

In the diagnostics of the wear of friction pad of disc brake, point parameters obtained from amplitude flows of vibration accelerations are easier to interpret. Analyzing results in the range of applying point parameters of signals of vibration accelerations to determine friction pads' wear determinated by current pads' thickness in the moment of measurement, it can be found out that selected parameters allow to determine friction pads' thickness..

Measurement of vibration accelerations in direction Z_2 tangential direction to friction surface of the disc and mounting vibration converter from the side of brake cylinder's case, is characterized as the most sensitive towards direction Y and X, which is confirmed by values of coefficient of dynamics of changes defined with dependence (5). During verification of regression diagnostic models determined on the basis of point parameters of signals coming from pad caliper, differences in determining pads' thickness did not exceed 14% for RMS value in direction Z_2.

References

1. Brüel & Kjær, *Piezoelectric Accelerometer Miniature Triaxial Delta Tron Accelerometer – Type 4504A*, oferta firmy Brüel & Kjær
2. C. Cempel, *Podstawy wibroakustycznej diagnostyki maszyn*, WNT Warszawa 1982
3. M. Gruszewski, *Wybrane zagadnienia eksploatacji hamulca tarczowego*, Technika Transportu Szynowego 1995, nr **6-7**, s. 84-86
4. R. Gryboś, *Drgania maszyn*, Wydawnictwo Politechniki Śląskiej, Gliwice 2009, s. 214
5. Kodeks UIC 541-3, *Hamulec-Hamulec tarczowy i jego zastosowanie. Warunki dopuszczenia okładzin hamulcowych,* Wydanie 6, listopad 2006
6. W. Sawczuk, *Badanie tarczowego układu hamulcowego pojazdu szynowego w aspekcie możliwości jego diagnozowania*, Rozprawa doktorska Politechnika Poznańska, Poznań 2010

Szacowanie zużycia okładzin ciernych tarczowego układu hamulcowego pojazdu szynowego przy wykorzystaniu wybranych charakterystyk amplitudowych sygnału drganiowego

W pojazdach szynowych ze względu na coraz to większe prędkości jazdy prowadzi się prace nad udoskonalaniem układów hamulcowych tak, aby zatrzymanie pojazdu odbyło się na możliwie najkrótszej drodze hamowania. Większe wymagania stawiane układom hamulcowym wymusza nie tylko okresowe kontrolowanie stanu pary ciernej, ale również stałego monitorowania zużycia elementów układu hamulcowego.

Celem artykułu jest przedstawienie możliwości diagnozowania pary ciernej hamulca tarczowego wykorzystując wybrane charakterystyki amplitudowe sygnału drganiowego generowanego przez obsadę hamulcową z okładzinami ciernymi.

Active vibroisolation system with magnetic springs

Jacek SNAMINA
AGH University of Science and Technology, Department of Process Control
Mickiewicz Avenue 30, Cracow
snamina@agh.edu.pl

Andrzej PODSIADŁO
AGH University of Science and Technology, Department of Process Control
Mickiewicz Avenue 30, Cracow
apod@agh.edu.pl

Piotr HABEL
AGH University of Science and Technology, Department of Process Control
Mickiewicz Avenue 30, Cracow
habel@agh.edu.pl

Abstract

The paper presents an active vibroisolation system with two magnetic springs. Force exerted by the *magnetic spring* is a result of interaction of magnetic fields formed by magnets and coils. The stiffness of the spring can be modified by changing the current in coils. Static characteristic of the spring were determined using results of calculations and experiments. *Magnetic springs* were applied in two degrees of freedom system.

Keywords: vibration control, switching stiffness, magnetic suspension, controlled magnetic spring

1. Introduction

Magnetic springs are very useful elements in design of vibroisolation systems. The principle of operation of *magnetic spring* consists in automatic control of spring force by the current in coils. The current modifies the magnetic flux and simultaneously the spring force.

Recently the active vibroisolation systems with *magnetic springs* are used in many applications for instance in vehicle suspensions [1], [2]. Traditional suspension systems are often replaced by active *magnetic suspension* systems. Operating principle of *magnetic suspension* were discussed in [3], [4] and [5], where authors considered mathematical models and result of experiments.

Paper presents the new design of *controlled magnetic spring*. The assumed characteristic of spring was obtained by the appropriate arrangement of magnets and coils.

2. Operating principle of magnetic spring

Schematic sketch of *magnetic spring* is shown in Figure 4. Main parts of the *magnetic spring* are: magnetic core, magnets, coils, shaft and covers. Two upper neodymium magnets are fixed to the end of the shaft and the next two magnets are fixed to the lower

magnetic core in the spring axis. Four coils are used to change the magnetic field in the space between magnets.
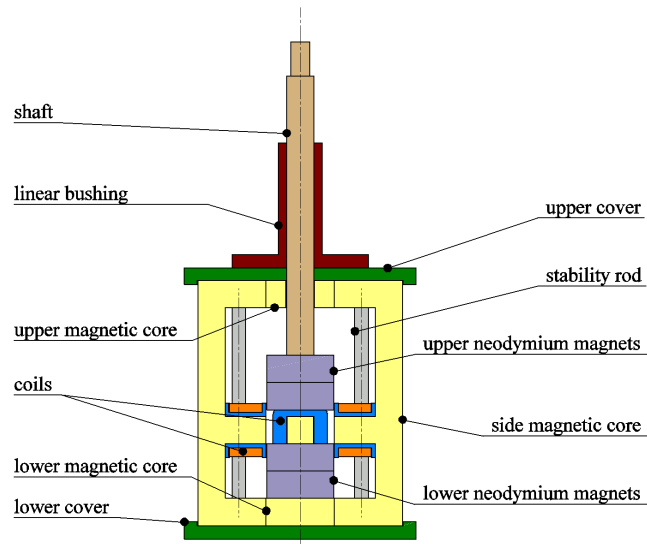
Figure 2. Axis section of magnetic spring

3. Spring characteristics

In order to determine the magnetic field distribution and spring forces the finite element (FE) model was prepared using ANSYS 11.0. The FE model of spring and its section are shown in Figures 2 and 3.
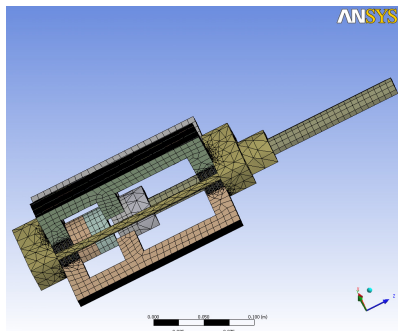
Figure 3. FE model of magnetic spring   Figure 4. XZ section of FE model
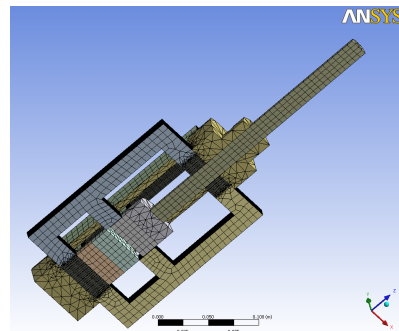
Calculations were done for various positions of the shaft. The result of calculations of spring force is presented in Figure 4.
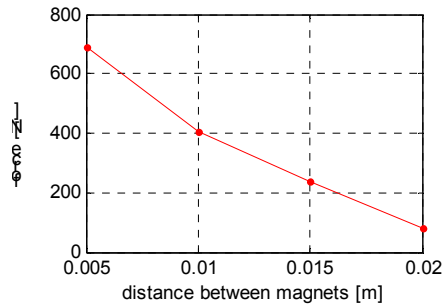
Figure 5. Force vs distance between magnets

The force is a non-linear function of distance between magnets. As it was expected the force decreases for larger distances between magnets. The force tends to very large values if the distance tends to zero.

The prototype of *magnetic spring* was made and using this prototype the series experiments were conducted in the Laboratory of Dynamic Structures and Systems in Department of Mechanical Engineering and Robotics AGH. Displacements and forces, measured for various sequences of active coils, were the base for determination of *magnetic spring* characteristics..

Results of calculation and results of experiments are shown Figure 8. Both relations between force and distance were approximated by third degree polynomials.
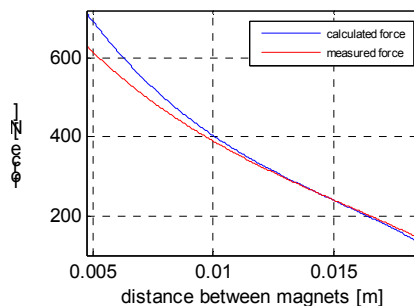
Figure 6. Calculated and measured forces

The relative error between calculation and experiments results does not exceed 13 %. The highest value of error is attained for small value of displacement between magnets.

4. Vibroisolation systems with controlled magnetic springs

The system considered in this study is a simple two-degree of freedom system. It is shown in Figures 6 and 7. For instance such system can be used as a model of truck and cabin suspension system.
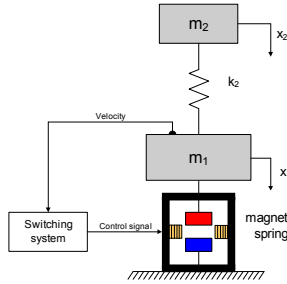
Figure 7. First version of the system   Figure 8. Second version of the system
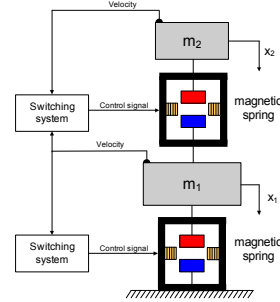
The coordinate system introduced previously, for the presentation of the force as a function of distance between magnets (Figure 5), is replaced with a new, more convenient coordinate system as shown in Figure 8.
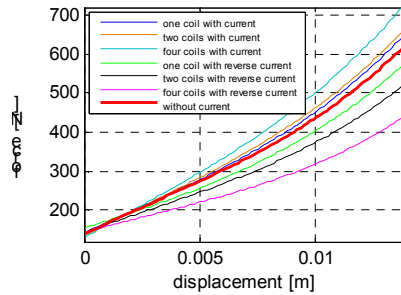
Figure 9. Force vs. displacement for various configuration of active coils

The principle of operation of vibroisolation system reduces to adequate switching between two characteristic of the spring. In each period of oscillation the energy of the system decreases. Two versions of vibroisolation system are considered. In the first version, the system consists of only one *controlled magnetic spring* (Figure 6) and in the second version, the system contains two *controlled magnetic springs* (Figure 7). Depending on the velocity sign the switching system selects the appropriate characteristic of *magnetic spring*.

In the system with one *magnetic spring* the magnetic force $F_1(x_1, \dot{x}_1)$ depends on switching function $f_1(\dot{x}_1)$ which takes the value 1 (when $\dot{x}_1 < 0$) or 0 (when $\dot{x}_1 > 0$). The force can be calculated from the following formula:

$$F_1 = f_1(\dot{x}_1) \cdot F_1^{(1)}(x_1) + (1 - f_1(\dot{x}_1)) \cdot F_1^{(2)}(x_1) \tag{1}$$

Functions $F_1^{(1)}(x_1)$ and $F_1^{(2)}(x_1)$ describe spring forces for assumed combinations of active coils. In the system with two *magnetic springs* the first force $F_1(x_1, \dot{x}_1)$ depends on switching function $f_1(\dot{x}_1)$ as it was described in (1) and the second force

$F_2(x_2 - x_1, \dot{x}_2 - \dot{x}_1)$ depends on switching function $f_2(\dot{x}_2 - \dot{x}_1)$ which takes the value 1 (when $\dot{x}_2 - \dot{x}_1 < 0$) or 0 (when $\dot{x}_2 - \dot{x}_1 > 0$). The second force can be written in the form:

$$F_2 = f_2(\dot{x}_2 - \dot{x}_1) \cdot F_2^{(1)}(x_2 - x_1) + (1 - f_2(\dot{x}_2 - \dot{x}_1)) \cdot F_2^{(2)}(x_2 - x_1) \qquad (2)$$

Forces $F_1(x_1, \dot{x}_1)$ and $F_2(x_2 - x_1, \dot{x}_2 - \dot{x}_1)$ are independent. As a result of spring action, the energy is reduced in each cycle of vibration. The implementation of control algorithms in Matlab environment enables us the simulation of vibrations decrease.

The following parameters of the system are assumed in numerical calculations: the lower mass m_1=30 kg, the upper mass m_2= 10 kg, stiffness coefficient k_2= 10^5 N/m.

Results of calculations are shown in Figures 9 and 10. All displacements of masses are related to equilibrium positions.
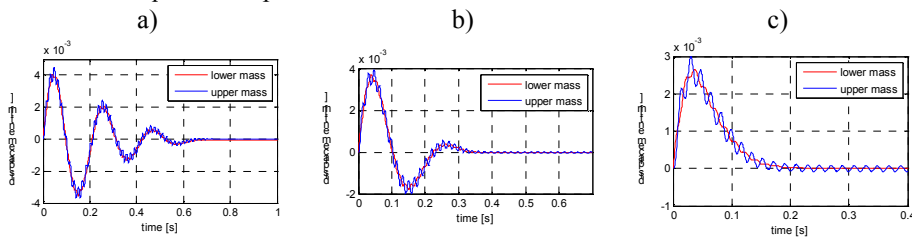
Figure 10. Displacements: a) one active coil, b) two active coils, c) four active coils.

As long as the lower mass is not in equilibrium state the energy of the system is dissipated. Amplitudes of displacements of each mass decrease. When the lower mass is near equilibrium position the amplitude of displacement of the upper mass is almost constant.
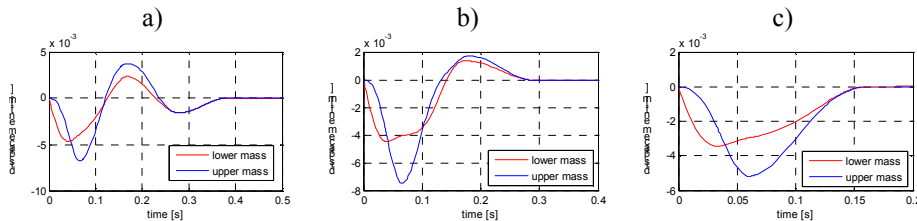
Figure 11. Displacements: a) one active coil, b) two active coils, c) four active coils.

In the second version of vibroisolation system both mass attain equilibrium positions at almost the same time. Dissipation of energy is more effective than in the first version of vibroisolation system.

8. Conclusions

In the paper the new design of *magnetic spring* was proposed. Active vibroisolation systems with *magnetic springs* were studied analytically and experimentally. Vibrations

of two degrees of freedom system were reduced by vibroisolation systems with one and two *magnetic springs*. Various configurations of active coils were used in applied algorithms of vibroisolation. Numerical and experimental studies can be reassumed as follows:

1. *Magnetic spring* characteristics are nonlinear. Difference between spring characteristics obtained by measurement and FE calculations is very small.

2. The variation of the current in coils allows for modification of the spring force up to 33%. The force changing in this range can be exploited by control algorithms.

3. The number of active coils is the base for more effective damping of the upper mass in both versions of vibroisolation system,

4. Due to the range of effective force the *magnetic springs* should be designed for definite masses constituting the system.

Acknowledgments

References

1. B. Gysen, J. Paulides, J. Janssen, E. Lomonova, *Active electromagnetic suspension system for improved vehicle,* Vehicle Power and Propulsion Conference (VPPC), China, Harbin 2008.

2. J. Paulides, L. Encica, E. Lomonova, A. Vandenput, *Design considerations for a semi-active electromagnetic suspension system*, IEEE Transactions on magnetic, Vol. 42, No. 10 (2006), 3446-3448.

3. T. Mizuno, M. Takasaki, D. Kishita, K. Hirakawa, *Vibration isolation system combining zero-power magnetic suspension with springs*, Control Engineering Practice, Vol. 15, No. 2 (2007), 187-196.

4. W. Robertson, *Design of a non-contact magnetic spring for vibration isolation*, Research proposal, Australia, Adelaide 2003.

5. B. Gysen, J. Janssen, J. Paulides, E. Lomonova, *Design aspects of an active electromagnetic suspension system for automotive applications,* IEEE Transactions on Industry Applications, Vol. 45, No. 5 (2009), 1589-1597

Sprężyna magnetyczna, jako element aktywnego układu wibroizolacji

W pracy przedstawiono badania symulacyjne układu wibroizolacji z wykorzystaniem sprężyny magnetycznej ze sterowalnym polem magnetycznym. Analizę pola magnetycznego sprężyny magnetycznej wykonano metodą elementów skończonych wykorzystując pakiet ANSYS. W pracy przedstawiono symulację układu wibroizolacji z zaprojektowaną sprężyną przy zastosowaniu odpowiedniego algorytmu przełączającego. Wyniki symulacji przedstawiono na wykresach. Proponowany układ wibroizolacji może być wykorzystany w układach zawieszenia kabin pojazdów roboczych, foteli operatorów maszyn oraz w układach mocowania stabilizowanych platform.

Dynamic stability of beams with harmonic oscillator

Wojciech SOCHACKI
Instytut Mechaniki i PKM, Politechnika Częstochowska
ul. Dąbrowskiego 73, 42-200 Częstochowa
sochacki@imipkm.pcz.czest.pl

Abstract

The problem of the dynamic stability of a beam with different boundary conditions and with undamped oscillator is formulated and solved in this work. Oscillator can be mounted at any chosen place along the beam length. The beam is axially loaded by a force in the form $P(t)= P_0+S\cos v t$. The problem of dynamic stability is solved by applying the mode summation method. The obtained Mathieu equation allows the influence of oscillator on the position of solutions on a stability chart to be analysed. This analysis relies on testing the influence of oscillator on the value of coefficient b in the Mathieu equation. The considered beams were treated as Euler- Bernoulli columns.

Keywords: Dynamic stability, beam, harmonic oscillator

1. Introduction

A lot of works dealing with the dynamic stability of beams with additional discrete elements can we find in the literature. Evensen and Evan-Iwanowski [1] carried out analytical and experimental research on the influence of a mass mounted at the end of a beam on the dynamic stability of this beam. Sato *et al*. [2] investigated the parametric vibrations of a horizontal beam loaded by a concentrated mass, which showed the influence of the beam weight and the inertia of a rotational mass on the beam vibrations. Gürgöze [3] analysed the influence of a mass mounted at the end of an elastically supported beam along its axis. The dynamic stability of an elastic beam was analysed by Cederbaum and Mond [4]. Majorana and Pellegrino [5] analysed the dynamic stability of an elastically supported beam (rotation and translation springs at the ends). In [6] Sochacki has investigated a simply supported beam axially loaded by a harmonic force, showing the destabilising effect of the concentrated mass, spring and harmonic oscillator.

This paper takes into account beams at different types of boundary conditions (clamped-free C-F, clamped-sliding C-S, clamped-clamped C-C and clamped-pinned C-P). An undamped harmonic oscillator was connected to the beams at a chosen position between the supports. The considered beams are treated as Bernoulli-Euler beams and solved according to the small bending theory. The dynamic of the system was described with the use of the Mathieu equation. The problem of dynamic stability was solved using the mode summation method. The influence of additional an undamped harmonic oscillator (its values and positions) on the value of coefficient b in the Mathieu equation was investigated. In this way the possibility of a loss in dynamic stability by the investigated system was determined.

2. Mathematical model

A scheme of the considered C-F beam is presented in Fig. 1.
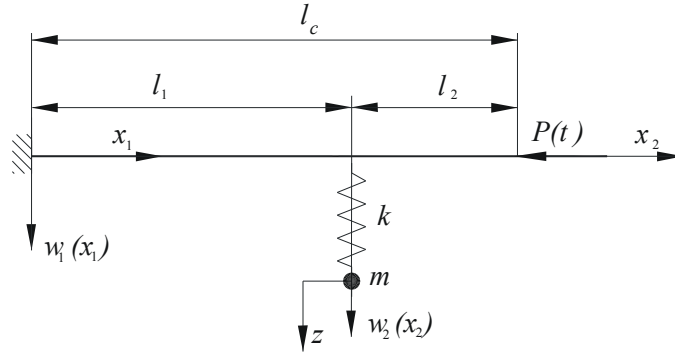
Figure 1. Model of the C-F beam with additional undamped harmonic oscillator
mounted in selected positions along the beam length.

The equations of vibrations:

$$E_i J_i \frac{\partial w_i^4(x_i,t)}{\partial x_i^4} + P(t)\frac{\partial w_i^2(x_i,t)}{\partial x_i^2} + \rho_i A_i \frac{\partial^2 w_i(x_i,t)}{\partial t^2} = 0 \qquad (1a,b)$$

where : $P(t) = P_0 + S\cos\nu t$, ν - forcing frequency, $E_i J_i$ – flexural rigidity of beam,
ρ_i – density, A_i – cross-section area, $i = 1,2$ ith part of the beam
together with the boundary and matching conditions:

$$w_1(0,t) = 0, \qquad w_1^I(0,t) = 0 \qquad (2a\text{-}b)$$

$$E_2 J_2 w_2^{III}(l_2,t) + P(t)w_2^I(l_2,t) = 0, \qquad w_2^{II}(l_2,t) = 0 \qquad (2c\text{-}d)$$

$$E_1 J_1 w_1^{III}(l_1,t) + P(t)w_1^I(l_1,t) + $$
$$- m_2 \ddot{z} - E_2 J_2 w_2^{III}(0,t) - P(t)w_2^I(0,t) = 0 \qquad (2e)$$

$$w_1(l_1,t) = w_2(0,t), \quad w_1^I(l_1,t) = w_2^I(0,t), \quad E_1 J_1 w_1^{II}(l_1,t) = E_2 J_2 w_2^{II}(0,t) \qquad (2f\text{-}h)$$

$$m\ddot{z} + k(z - w_1(l_1,t)) = 0 \qquad (2i)$$

where: the Roman numerals denote differentiation with respect to x, and dots denote
differentiation with respect to time t,
made the formulation of the boundary value problem of the investigated beam.
During the vibrations the displacement of the beam and oscillator mass take the form:

$$w_i(x_i,t) = W_i(x_i)\cos(\omega t), \quad (i = 1,2) \qquad (3)$$

$$\text{and} \qquad z = Z\cos(\omega t) \qquad (4)$$

where $W_i(x_i)$ and Z are displacement amplitudes w_i and z, while ω is the natural
frequency of the beam with discrete elements.

For the nth mode the natural frequency ω_n and eigenfunctions of the beam $W_{in}(x_i)$ are determined by solving the boundary value problem.

Analogical procedure in case of remaining beams C-C, C-P and C-S after introducing the appropriate boundary conditions, leads to determination of the natural frequency and eigenfunction of these beams.

2. Solution of the dynamic stability

The solution of equation (1a,b) is assumed to be in the form of eigenfunction series [7].

$$w_i(x_i,t) = \sum_{n=1}^{\infty} W_{in}(x_i)T_n(t) \qquad (i=1,2) \qquad (5a,b)$$

where: $T_n(t)$ are unknown time functions and $W_{in}(x_i)$ are normalized eigenfunctions of free frequencies of ith parts of the beams.

Substituting solution (5a,b) into equation (1a,b) one can obtain:

$$\sum_{n=1}^{\infty}\left[E_i J_i W_{in}^{IV}(x_i)T_n(t) + (P_0 + S\cos\nu t)W_{in}^{II}(x_i)T_n(t) + \rho_i A_i W_{in}(x_i)\ddot{T}_n(t)\right] = 0$$

(6)

After multiplying by $W_{im}(x_i)$, one can receive from equation (6):

$$\sum_{n=1}^{\infty}\left[E_i J_i W_{in}^{IV}(x_i)W_{im}(x_i)\,T_n(t) + P_0 W_{in}^{II}(x_i)W_{im}(x_i)T_n(t) + \right.$$
$$\left. + S\cos\nu t\, W_{in}^{II}(x_i)W_{im}(x_i)T_n(t) + \rho_i A_i W_{in}(x_i)W_{im}(x_i)\ddot{T}_n(t)\right] = 0$$

(7)

From equations (1a,b) for the nth eigenfunction $W_{in}(x_i)$, for free vibrations of the beam, after separate variables and multiplying by $W_{im}(x_i)$, one can obtain:

$$E_i J_i W_{in}^{IV}(x_i)W_{im}(x_i) + P_0 W_{in}^{II}(x_i)W_{im}(x_i) = \rho_i A_i \omega_n^2 W_{in}(x_i)W_{im}(x_i) \qquad (i=1,2) \qquad (8)$$

Then (7) takes the following form:

$$\sum_{n=1}^{\infty}\left[\rho_i A_i \omega_n^2 W_{in}(x_i)W_{im}(x_i)T_n(t) + S\cos\nu t\, W_{in}^{II}(x_i)W_{im}(x_i)T_n(t) + \right.$$
$$\rho_i A_i W_{in}(x_i)W_{im}(x_i)\ddot{T}_n(t)\Big] = 0$$

(9)

After integrating equations (9), the following form was obtained for the whole beam and the first term:

$$T_1(t)\left(\omega_1^2 \rho_i A_i \int_0^l W_{i1}^2(x_i)dx_i + S\cos\nu t \int_0^l W_{i1}^{II}(x_i)W_{i1}(x_i)dx_i\right) + \ddot{T}_1(t)\rho_i A_i \int_0^l W_{i1}^2(x_i)dx_i = 0 \quad (10)$$

Appropriate transformations of equation (10) and the substitution of t by a new variable $\tau = \nu t$ lead to the following form of Mathieu equation.

$$\ddot{T}(\tau) + (a + b\cos\tau)T(\tau) = 0 \qquad (11)$$

where: $a = \dfrac{\omega_1^2}{\nu^2}$, $b = \dfrac{S}{\nu^2}\dfrac{\sum\limits_{i=1}^{2}\int\limits_0^l W_{i1}^{II}(x_i)W_{i1}(x_i)dx_i}{\sum\limits_{i=1}^{2}\rho_i A_i \int\limits_0^l W_{i1}^2(x_i)dx_i}$ (12a,b)

The periodical solutions to the Mathieu equation (11) are known (e.g. [8]). These solutions allow us to determine the stable and unstable regions of solutions. The numerical values of a and b each time decide the position of solution in the stable or unstable region. However, it must be stated that the probability of obtaining stable solution is higher in case of lower value of coefficient b, at the determined value of a.

4. The results of numerical computations and discussion

The solution to the problem of dynamic stability of the tested beams allowed to determine the values of coefficient b in the Mathieu equation at changeable values of the elasticity coefficient of oscillator K (Fig. 2) and mass of oscillator M (Fig.3).
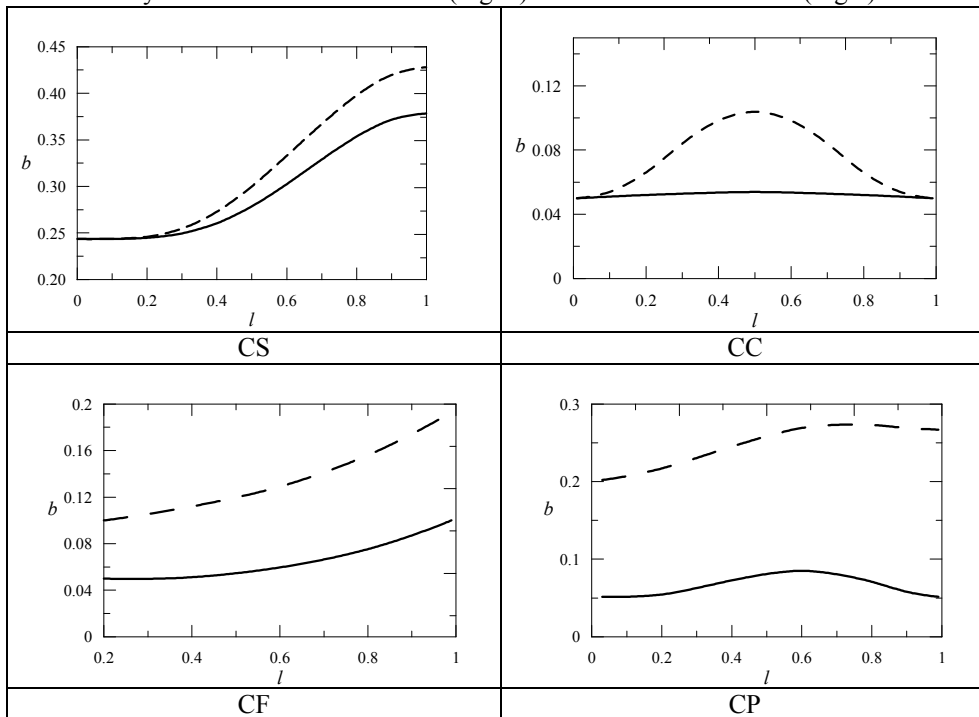
Figure 2. The influence of oscillator mounting location on the beams and the value of the elasticity coefficient of oscillator K on the value of coefficient b for $a = 1$ and $M = 0.2$: $K = 10$ $-----$; $K = 100$ ———,
(for CF beam $K = 1$ $-----$; $K = 10$ ———)

Calculations were carried out assuming the following dimensionless quantities:

$$K = \frac{k l_c^3}{E_1 J_1}, \quad M = \frac{m}{\sum_{i=1}^{2} \rho_i A_i l_i}, \quad (13)$$
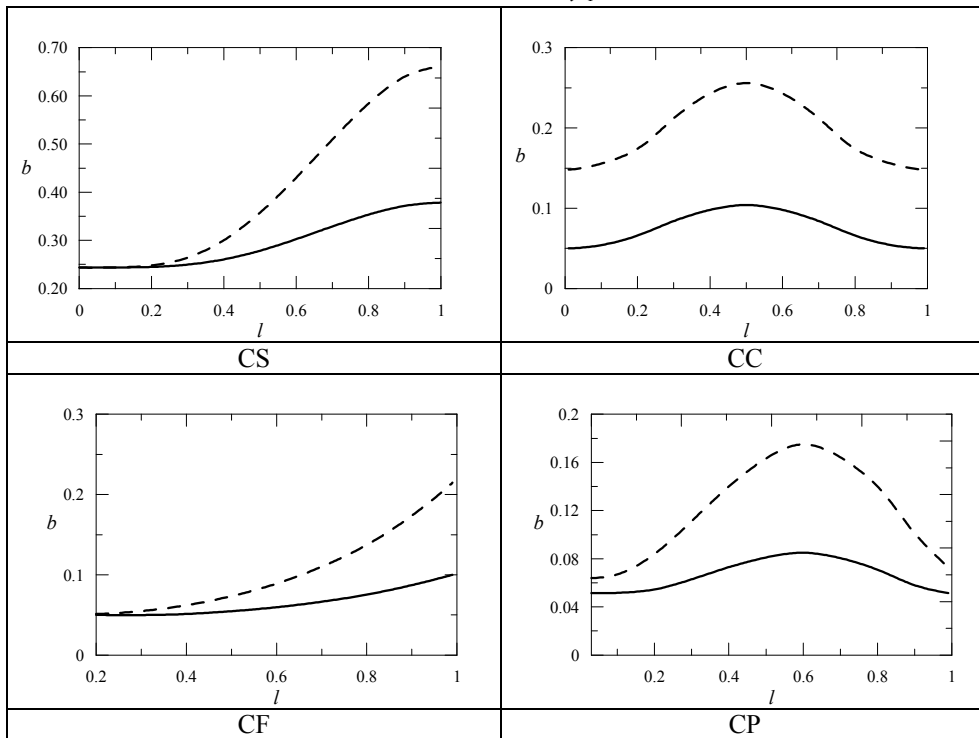
Figure 3. The influence of the oscillator mounting location on the beams and its mass *M* on the value of coefficient *b* for *a* =1 and *K* = 100 (for CF beam *K* = 10): *M* = 0.2 ――――― , *M* = 0.6 ― ― ― ―.

Analysis of the research results of the influence of the oscillator (*K* and *M*) and its placement on the beams on the value of coefficient *b* allows the following conclusions to be drawn: an increase in the elasticity coefficient *K* of the oscillator leads to a decrease in coefficient *b* (Fig.2), while an increase in oscillator mass *M* leads to an increase in the value of coefficient *b* (Fig. 3).

Analysing the influence of the oscillator placement on the beams it can be stated that, independently of the values *K* and *M*, the closer oscillator mounting in places for which the amplitudes of first modes are the highest leads to an increase in the value of coefficient *b*.

References

1. H. A. Evensen i R. M. Evan-Iwanowski, *Effects of Longitudinal Inertia Upon the Parametric Response of Elastic Columns*, ASME Journal of Applied Mechanics **33** (1966) 141-148.
2. K. Sato, H. Saito, K. Otomi, *The Parametric Response of a Horizontal Beam Carrying a Concetrated Mass Under Gravity*, ASME Journal of Applied Mechanics **45** (1978) 643-648.
3. M. Gürgöze, *Parametric vibrations of restrained beam with an and mass under displacement excitation,* Journal of Sound and Vibration **108(1)** (1986) 73-84.
4. G. Cederbaum, M. Mond, *Stability Properties of a Viscoelastic Column Under a Periodic Force,* Journal of Applied Mechanics **59** (1992)16-19.
5. C. E. Majorana, C. Pellegrino, *Dynamic stability of elastically constrained beams: an exact approach,* Engineering Computations, **14(7)** (1997) 792-805.
6. W. Sochacki, *The dynamic stability of a simply supported beam with additional discrete elements,* Journal of Sound and Vibration, **314** (2008), 180-193.
7. Craig Jr., R. R., *Structural Dynamics*, New York, Wiley (1981).
8. S. P. Timoshenko, J. E. Gere, *Theory of Elastic Stability*, Mc Graw–Hill – INC. (1961).

Stateczność dynamiczna belek z oscylatorem harmonicznym

W niniejszej pracy rozważa się belki o różnych warunkach brzegowych, obciążonych siłą wzdłużną postaci $P(t) = P_0 + S\cos \nu t$. Dodatkowo w dowolnym miejscu pomiędzy podporami do belek dołączono liniowy oscylator harmoniczny bez tłumienia. Badane belki traktuje się zgodnie z teorią Bernouliego – Eulera i rozwiązuje zgodnie z teorią małych ugięć. Zagadnienie stateczności dynamicznej rozwiązano, stosując metodę sumowania funkcji własnych i opisano za pomocą równania Mathieu. Zbadano wpływ oscylatora harmonicznego na stateczność drgań belek. Badania polegały na określeniu wpływu oscylatora dołączonego do belki zarówno co do jego wartości jak i miejsca mocowania na belce na wartość współczynnika b w równaniu Mathieu. W ten sposób określono możliwość utraty stateczności dynamicznej przez badane układy.

Localization of Increased Vibroreactivity Sources Based on S-Discriminant Analysis and Exemplified on Gas Turbine Unit

Asja SOKOLOVA

Machinery Engineering Research Institute, Russian Academy of Science
M.Kharitonievskiy, 4, Moscow, 101990, Russia
agsokolova@gmail.com

Feliks BALITSKIY

Machinery Engineering Research Institute, Russian Academy of Science
M.Kharitonievskiy, 4, Moscow, 101990, Russia
fbalitsky@gmail.com

Abstract

The paper describes some new vibration features which had been successfully applied and could be recommended for more effective vibration monitoring and incipient fault detection. These features known as the vibration non-dimensional S-discriminants are now calculated in parallel way for a set of narrow frequency bands and represented in format convenient for interpretation and documentation. This cartography kind of vibration data visualization enables localization of increased vibroreactivity sources, an early fault detection and prompt estimation of the machinery degradation speed in a very sensitive manner, in contrast with other current methods. The point is that this approach allows to emphasize not only common used changes (growth) of powerful vibration signal components (event of vibroactivity), but also variability of weak, though just informative vibration components (event, called "vibroreactivity"). One of the practical example of successful application of this method is given for incipient burn-out of turbine nozzle.

Keywords: machinery, sources localization, incipient fault detection, vibration non-dimensional discriminant.

1. Introduction

Generally, most of machinery monitoring and protection system algorithms are based on estimation of vibration velocity RMS (root mean square) values within 10 to 1000 Hz frequency band, or of current amplitude divergences (for specific narrow frequency bands) from baseline meanings collected under the good machinery condition [1]. There are well-known conventions accordingly to which RMS level increase by a factor greater than 10 (20 dB) is classified as "not permissible", which suggests the crash condition.

This approach is based on an assumption that rotary machines, having similar power, axes location height, shaft rotation speed, foundation and amortization types may be unified in a particular class with the same alarm thresholds of vibration RMS levels: for its good, allowable and not permissible status, without taking into account some difference in their operation, excitation of oscillation, fault symptoms in the vibration signal. The conventional frequency band for such high-speed machinery as gas turbine units (GTU) contains only several first shaft rotation frequency harmonics which are affected only by rough machinery malfunctions like an unbalance, a part breakage, and so on). Meanwhile, technique of an incipient fault detection (such as erosion, pitting and so on) bases on some other principles, because their symptoms lie in higher frequency

range. Obviously, an application of common vibration monitoring technique for high-speed machinery is not effective. This is the reason to address to more effective methods. The proposed one is the fresh machinery vibration monitoring technique, which is built upon usage of parallel narrowband S-discriminant analysis of clipped vibration signals [2-3]. This method provides localization of machinery heightened "vibroreactivity" sources in bands with signal dispersion dramatically grown in comparison with reference measurement data due to arising and then developing defects [4]. An example of this novel vibration monitoring technique practical application is given for an early detection of gas turbine engine part damage.

2. A new approach to the vibration monitoring of high-speed machinery

There are several well-known common laws of vibration waveform changes along machine operational time. Firstly, the amplitude and amount of signal overshoots are increasing; secondly, noise level is growing; and at last, waveform changes become irregular, unstable and non-linear. The specific signal changes depend on an operational damage nature, but a mandatory feature of an incipient fault influence is appearance of single or multiple signal overshoots deriving from interaction conjugate parts format changes due to erosion, corrosion, pitting, contact surfaces local welding and so on.

As a matter of fact, the informative components of vibration signal changes that really describe a process of machine deterioration, especially at its early stage, are too weak. So, these negligible amplitude changes are masked by vibration background, making the detection of any fault very difficult. To properly realize the "critical" machine condition monitoring and incipient fault detection it is suggested to use the algorithm of estimation of some dimensionless S-discriminant magnitude declining from the value equal to unit which corresponds to machinery normal (reference) condition:

$$I_C = \frac{\frac{1}{N}\sum_{i=1}^{N}\left[(x_i)_{(t)} - P\right]^C}{\frac{1}{N}\sum_{j=1}^{N}\left[(x_j)_{(n)} - P\right]^C} \cdot \left(\frac{K_{(t)}}{K_{(n)}}\right)$$

Here $(x_i)_{(t)}$ and $(x_i)_{(n)}$ are values of vibration amplitude components, calculated for current and reference machine conditions, correspondingly; $P = \lambda\,\sigma_n$, ($\lambda = 0.5 - 3.0$) – amplitude clip-threshold, σ_n - standard deviation (RMS) of vibration signal for normal machinery condition; C – power (equal to 2 for dispersion index I_d of threshold exceedings); $K_{(t)}$ and $K_{(n)}$ - are numbers of spikes above the threshold P for current and normal vibration signals. Thus, it is dimensionless amplitude S-discriminants, featuring high sensitivity to instability, caused by machinery operational imbalance, resulted from any fault, and noise immunity to internal machinery masking interference.

For normal condition, discriminant meanings are equal to 1, and become much bigger than 1, if amplitude overshoots (spikes) and their amount increase due to deterioration process development. These properties permit to use them in machinery condition monitoring systems not only for emergency protection aim, but for heightened

vibroreactivity sources localization, caused by incipient faults influence, and hence, for early machinery operational damages detection.

3. GTU condition monitoring technique based on multidimensional visualization of vibration S-discriminants

The method was used for condition monitoring of avia derivative gas turbine engine PS-90 of gas transportation compressor stations. GTU case measurement points disposition is presented on figure 1. Further only results for point 5 are considered.
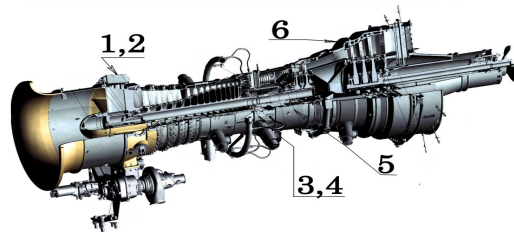
Figure 1. Vibration sensor locations on engine PS-90 case were as follows: 1, 2 –input compressor flange; 3, 4 – combustion chamber area; 5 – high pressure turbine (HPT) of gas-generator (GG) area (measuring point is TGG-H); 6 – power turbine area.

GTU condition monitoring results are known to depend on some factors that reduce degree of diagnosis accuracy. Remoteness of case sensors from vibration sources; instability of load and high speed of rotor revolution; anisotropic construction and temperature deformation susceptibility; using for monitoring aim vibration velocity information, contained in 0-4.0 kHz, - are the factors which make the standard vibration monitoring methods ineffective. For example, Figure 2 shows the case vibration velocity spectrum for damaged inner race of HPT roller bearing with relative frequency BPFI=15.2 Fr. This spectrum includes only first harmonics of shaft rotation frequency.

Figure 2. Case vibration velocity spectrum of PS-90 for HPT roller bearing damage.

The proposed machinery vibration monitoring technique is based on parallel narrowband S-discriminant analysis of clipped vibration signals for the machinery heightened "vibroreactivity" sources localization, i.e. definition of the frequency bands with significant growth (in comparison with reference measurement data) of signal dispersion and overshoots amount originated from arising and then developing defects. Presentation of the multidimensional information in a table form, where array colour cells are S-discriminant meanings (in accordance with coloured bargraph), which is convenient for further interpretation, provides a good tool for incipient fault detection, primary identification of flaws and on-the-fly estimation of its development rate. An example of this technique usage is shown on Table 1 (in reduced form).

Table 1. The trend of vibration velocity S-discriminant values calculated within several frequency bands: a broad one (0…4.0 kHz) and eight narrow (0.5 kHz) ones, as for GTU case horizontal vibration under the HTP nozzle set burn-out development.

| (1-2) | (3-4) | (5-8) | (9-16) | (17-32) | (33-64) | (65-128) | (129-256) | (257-512) | 513-1024 |

Frequency band	ΔF= 4.0 kHz	ΔF ≈0.5 kHz							
Dates	0 – 4.0	0.1-0.5	0.5-1.0	1.0-1.5	1.5-2.0	2.0-2.5	2.5-3.0	3.0-3.5	3.5-4.0
26.12.06_18.02 - Reference	1	1	1	1	1	1	1	1	1
Out of operation (13.02-15.04.07)									
16.04.07_18.00 – Defect arise	2	2	1	2	3	1	1	45	2
17.04.07_18.02	1	4	2	1	1	1	1	382	2
18.04.07_18.00	1	2	1	2	2	1	2	106	1
27.04.07_18.00	1	2	1	2	4	1	2	428	2
10.05.07_06.00 – Full-blown defect	1	2	1	2	1	1	1	742	1
13.05.07_06.00	1	2	1	3	1	1	1	350	1
13.05.07_18.00 – Max defect	2	3	1	2	2	1	1	802	1
14.05.07_06.00	2	3	1	3	1	1	1	249	1
14.05.07_18.00	2	4	1	2	4	1	1	560	1
20.05.07_18.00– Secondary damages	1	10	1	2	2	1	1	282	5
24.05.07_06.00	1	2	1	1	1	1	1	150	2
Out of operation (25.5- 27. 05.07)									
28.05.07_08.32– Secondary damages	1	5	1	2	2	1	1	107	17
29.05.07_06.00	1	2	1	3	3	1	1	122	33
31.05.07_18.00	2	4	1	2	3	1	1	20	39
06.06.07_18.00	1	1	1	3	1	1	1	465	1
12.06.07_06.00	1	1	1	3	1	1	1	16	2
12.06.07_18.00	1	1	1	2	1	1	1	195	1
14.06.07_18.00	1	3	1	2	1	1	1	598	3
Out of operation (19.06 - 24.06.07)									
25.06.07_18.00	1	1	1	4	1	2	1	29	9
07.07.07_18.00	1	1	1	3	1	1	1	278	1
11.07.07_06.00	1	1	1	2	1	1	1	6	1
11.07.07_18.00	1	1	1	2	1	1	1	240	1
18.07.07_18.00 – Multiple faults	1	1	1	1	1	1	1	4	1
Out of operation (19.07- 23.07.07)									
27.07.07_18.00 – Engine shutdown	1	1	1	1	1	1	1	1	1

Table 1 with vibration velocity S-discriminants peak values colour presentation for case measurement point TGG-H (in narrow frequency bands) within operational dates Dec 26, 2006 through Jul 27, 2007, when the nozzle set of HPT was burning up, demonstrates case vibroreactivity changes during the nozzle degradation. Given vibroreactivity table allows visual estimating of current machinery condition and malfunction development rate to promptly make decision about further machine exploitation. As it could be seen from the table a nozzle burn-out (the stationary part of HPT) essentially affects 3.0-3.5 kHz frequency band vibration features with maximum discriminant value I_d=802 as early as on May 13, 2007, i.e. 2.5 months beforehand the engine final breakage. Obviously, neither wide frequency band (0-4.0 kHz), nor rotation frequencies narrow band (0.1-0.5 kHz) show any reaction to this machinery damage.

Figure 3 represents a narrowband (3.0-3.5 kHz) S-discriminant trend. To understand the origin of its changes, see Figure 4.
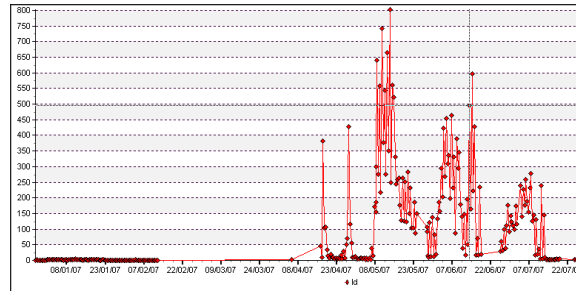
Figure 3. Dependence of narrowband (3.0-3.5 kHz) S-discriminants on operational time when the nozzle set of HPT was burning up, with max Id=802.2 of 13.05.07.
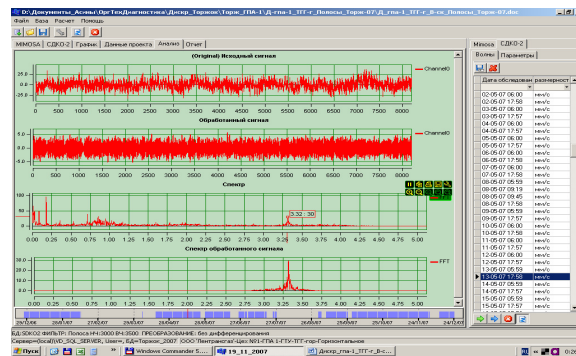
Figure 4. Waveforms and corresponding spectrums in wide (top) and narrow (bottom) bands) for date 13.05.07, when the second stage HPT nozzle set of engine PS-90 is burning up. (Max I_d =802.2).

It could be well seen at the bottom part of Figure 4 where spectra for wide frequency band (0…4.0 kHz) – upper, and for narrow frequency band (3…3.5 kHz) – lower, respectively, are presented. It is significant that the high frequency component is not synchronous with rotation frequency. Presumably, with regard to the other vibration spectrum data, the real source of the vibration is self-excitation oscillations generated by high pressure flow going by reach-through holes due to whirls arising at their edges and producing something similar to a whistle. The positive results of the novel vibration monitoring technique practical application were also obtained for some other parts operational damages (bearing faults, damages of compressor and turbine blade set) of avia- and navy-derivative gas turbine engines.

Conclusions

The paper shows that in order to effectively monitor machinery condition, detect incipient faults and localize heightened vibroreactivity sources, the condition monitoring procedure has to deal with the vibration features susceptible to vibration signal overshoots and even slight changes of its amplitude. These requirements are met by the proposed vibration condition monitoring algorithm based on conception of dimensionless vibration S-discriminants presentation such as multidimensional trend plot which is convenient tool for fulfillment of different tasks: organization of automatic machinery condition monitoring; incipient fault detection; preliminary faults identification and definition of cause-and-effect relations along the operational time.

As it is seen from practice, the more complicated a machine unit is, the bigger is the dispersion of measured parameters within general scope of similar machines. Thus, it is important to use the individual approach when the vibration monitoring is on.

References

1. ISO 13373-1:2002. Condition monitoring and diagnostics of machines. Vibration condition monitoring. Part 1: General procedures.
2. Соколова А.Г. Алгоритм вибромониторинга машинного оборудования с адаптацией к базовому состоянию /Контроль. Диагностика №11, 2005, с.30-40.
3. Asja Sokolova, Felix Balitsky. On some critical machinery vibration monitoring algorithm and its application for incipient fault detection and localization / Diagnostyka Nr 3(47)/2008, PTDT (Polskie Towarzystwo Diagnostyki Technicznej) Wydziale Nauk Technicznych Polskiej Akademii Nauk/ISSN 1641-6414/P.121-124.
4. Соколова А.Г. Метод локализации источников повышенной вибр* реактивности машинного оборудования по данным дискриминантного анализа в задачах вибромониторинга и диагностики неисправностей / Вестник научно-технического развития (www.vntr.ru) No 1 (29), 2010. C. 26-42.

Multiple Scale Analysis of a Nonlinear Kinematically Driven System with Pendulum

Roman STAROSTA
Poznan University of Technology, Institute of Applied Mechanics
ul. Piotrowo 3, 60-965 Poznań
roman.starosta@put.poznan.pl

Grażyna SYPNIEWSKA-KAMIŃSKA
Poznan University of Technology, Institute of Applied Mechanics
ul. Piotrowo 3, 60-965 Poznań
grazyna.sypniewska-kaminska@put.poznan.pl

Jan AWREJCEWICZ
Technical University of Łódź, Department of Automatics and Biomechanics
ul. Stefanowskiego 1/15, 90-924 Łódź
awrejcew@p.lodz.pl

Abstract

The nonlinear spring pendulum externally and parametrically excited has been tested. The approximate analytical method was adopted to solve the equations of motion. Dimensionless variables are introduced into the equations of motion. The conditions for all the third order resonances were detected. The modulation equations and the frequency response functions for chosen cases of resonances have been derived and presented graphically. Calculations were made in the computer algebra system *Mathematica*. The elaborated procedures are in a general form and can be used to investigate the other systems in the similar way.

Keywords: nonlinear dynamics, asymptotic analysis, resonances

1. Introduction

Nonlinear dynamics of mechanical system with two degrees of freedom near the resonance is the subject of the paper. This system is the pendulum with changing length moving on circular path (Fig.1). There are many papers investigating various kinds of single, multiple or spring pendulums [2, 3, 5], because they can simulate the dynamics of various engineering systems and machine parts.

The coupling in the equations describes energy exchange between modes of vibrations and possibility of autoparametric excitation. Energy transfer in nonlinear systems is well known in nonlinear dynamics of multi degree-of-freedom and is widely discussed by many authors [1, 4].

In our work we introduce the equations of motion of the pendulum in the dimensionless form. The asymptotic method of multiple scales was applied both to solving equations of motion and to determine resonances conditions. All calculations were performed with the help of the computer algebra system *Mathematica,* in which several procedures were elaborated in order to automatize most operations. The procedures have general form and enable researching other nonlinear systems.
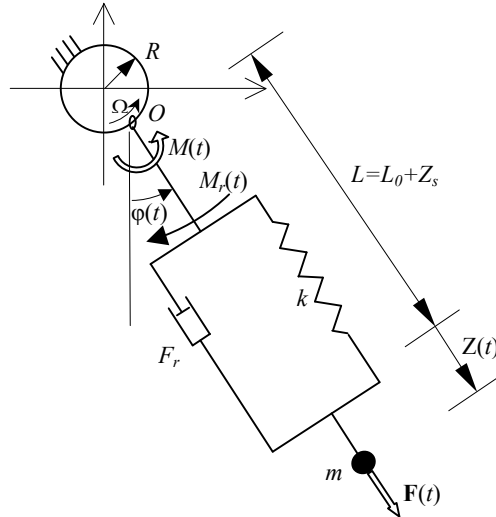
Fig. 1. Spring pendulum moving on circular path

2. Formulation of the problem

The studied system is presented in Fig. 1. The motion is planar and X and φ are the generalized co-ordinates. The pendulum is loaded by external force $F(t) = F_0 \cos \Omega_1 t$ and moment $M(t) = M_0 \cos \Omega_2 t$. Moreover, linear viscous damping is assumed.

The governing equations of the system in non-dimensional form are as follows:

$$\ddot{z}(\tau) + c_1 \dot{z}(\tau) - (1 + z(\tau))(\dot{\varphi}(\tau))^2 + z(\tau) +$$
$$+ w^2(1 - \cos(\varphi(\tau))) - r\,p^2 \cos(\tau\,p - \varphi(\tau)) = f_1 \cos(p_1\tau) \tag{1}$$

$$(1 + z(\tau))^2 \ddot{\varphi}(\tau) + (c_2 + 2(1 + z(\tau))\dot{z}(\tau))\dot{\varphi}(\tau) +$$
$$+ w^2 \sin(\varphi(\tau))(1 + z(\tau)) - r\,p^2(1 + z(\tau))\sin(\tau\,p - \varphi(\tau)) = f_2 \cos(p_2\tau) \tag{2}$$

where $L = L_0 + \dfrac{mg}{k}$, $z = \dfrac{Z}{L}$, $r = \dfrac{R}{L}$, $\omega_1^2 = \dfrac{k}{m}$, $w = \dfrac{\omega_2}{\omega_1}$, $\omega_2^2 = \dfrac{g}{L}$,

$c_1 = \dfrac{B_1}{m\omega_1}$, $c_2 = \dfrac{B_2}{mL^2\omega_1}$, $f_1 = \dfrac{F_0}{mL\omega_1^2}$, $f_2 = \dfrac{M_0}{mL^2\omega_1^2}$, $p_1 = \dfrac{\Omega_1}{\omega_1}$, $p_2 = \dfrac{\Omega_2}{\omega_1}$, $p = \dfrac{\Omega}{\omega_1}$, $\tau = \omega_1 t$.

L denotes length of the statically stretched pendulum at $\varphi = 0$, m is its mass, k denotes stiffness of the spring, g is the Earth acceleration, B_1 and B_2 are the viscous coefficients. The equations (1) – (2) should be supplemented by adequate initial conditions.

3. Solution Method

The asymptotic method of multiple scales is used to obtain the solution and to determine resonances conditions. Trigonometric functions in Eqs. (1)–(2) are approximated by the power series of 3rd order. The amplitudes of vibrations are assumed to be of the order of a small parameter ε, where $0 < \varepsilon << 1$, and hence $z = \varepsilon x, \varphi = \varepsilon \phi$. The generalized forces, damping coefficients and radius of the path are assumed in the form: $c_i = \varepsilon^2 \tilde{c}_i, f_i = \varepsilon^3 \tilde{f}_i, r = \varepsilon^2 \tilde{r}$, $i=1,2$. The parameters $\tilde{f}_i, \tilde{c}_i, \tilde{r}$ are of the order of 1.
The functions x and ϕ, are sought in the form

$$x(t;\varepsilon) = \sum_{k=1}^{k=3} \varepsilon^k x_k(T_0,T_1,T_2) + O(\varepsilon^4), \phi(t;\varepsilon) = \sum_{k=1}^{k=3} \varepsilon^k \phi_k(T_0,T_1,T_2) + O(\varepsilon^4), \quad (3)$$

where $T_0 = \tau$, $T_1 = \varepsilon\tau$ and $T_2 = \varepsilon^2\tau$ are various time scales.

Substituting the definitions (3) into Eqs. (1)-(2) and then arranging them according to the powers of the small parameter, we obtain the set of the partial linear differential equations. First order solutions have a form

$$x_1 = A_1 e^{iT_0} + \overline{A}_1 e^{-iT_0}, \quad \phi_1 = A_2 e^{iT_0 w} + \overline{A}_2 e^{-iT_0 w}, \quad (4)$$

where A_1 and A_2 are unknown complex functions of slow time scales.
After eliminating secular terms we get the following second and third order solutions

$$x_2 = w^2 A_2 \overline{A}_2 - \frac{e^{iT_0 p} \tilde{r}\Omega^2}{2(p^2-1)} + \frac{3e^{2iT_0 w} A_2^2}{2(4w^2-1)} + CC \quad (5)$$

$$\phi_2 = \frac{ie^{iT_0 p} \tilde{r} p^2}{2(p^2-w^2)} - \frac{e^{iT_0(1+w)} w(2+w)A_1 A_2}{1+2w} + \frac{e^{iT_0(1-w)} w(2-w)A_1 \overline{A}_2}{1-2w} + CC, \quad (6)$$

where CC stands for the complex conjugates of the preceding terms.

The third order approximation is given by

$$x_3 = \frac{ie^{iT_0 p} \tilde{r} p^4 A_2}{2(p^2-w^2)((p+w)^2-1)} + \frac{ie^{iT_0(p-w)} \tilde{r} p^4 \overline{A}_2}{2(p^2-w^2)((p-w)^2-1)}$$
$$+ \frac{e^{iT_0(1-2w)}(1-w)wA_1 A_2^2}{4(2w+1)} + \frac{e^{iT_0(1-2w)}(1+w)wA_1 \overline{A}_2^2}{4(2w-1)} - \frac{e^{iT_0 p_1} \tilde{f}_1}{2(p_1^2-1)} + CC \quad (7)$$

$$\phi_3 = + \frac{ie^{iT_0(p+1)} \tilde{r} p^4 A_1}{2(p^2-w^2)((p+1)^2-w^2)} + \frac{ie^{iT_0(p-1)} \tilde{r} p^4 \overline{A}_1}{2(p^2-w^2)((p-1)^2-w^2)} + \frac{3e^{3iT_0 w} w^2 A_2^3}{16(1-4w^2)} +$$
$$\frac{e^{iT_0(p+w)} \tilde{r} p(p^2-1+w^2)A_2}{2(p^2-1)(p+2w)} + \frac{e^{iT_0(p-w)} \tilde{r} p(p^2-1+w^2)\overline{A}_2}{2(p^2-1)(p-2w)} - \frac{e^{iT_0 p_2} \tilde{f}_2}{2(p_2^2-w^2)} +$$
$$+ \frac{e^{iT_0(2+w)} w(2+3w+w^2)A_2 A_1^2}{4(2w+1)} - \frac{e^{iT_0(2-w)} w(2-3w+w^2)\overline{A}_2 A_1^2}{4(2w-1)} + CC \quad (8)$$

The functions A_1 and A_2 can be calculated from secular terms and initial conditions related to Eqs. (1)–(2). In the further part of the work we make the polar representation

of the complex amplitudes

$$A_1(T_1,T_2) = \frac{\tilde{a}_1(T_1,T_2)}{2}e^{i\psi_1(T_1,T_2)}, \qquad A_2(T_1,T_2) = \frac{\tilde{a}_2(T_1,T_2)}{2}e^{i\psi_2(T_1,T_2)} \quad, \text{ where } a_i = \varepsilon\tilde{a}_i.$$

4. Parametric and External Resonances

The resonances detected from the solutions (5)–(8) can be classified as: primary external $p_1 = 1$, $p_2 = w$, parametric $p=1$, $p=w$, internal $1 = 2w$ and combined $p = \pm(1-w)$, $p = \pm(1+w)$. Two cases of simultaneously occurring resonances are discussed below and then solved for chosen parameters.

   Case 1 − Parametric spring resonance $p \approx 1$ and external resonance with pendulum $p_2 \approx w$. Resonance conditions are reflected in the secular terms when we introduce the detuning parameters σ_1 and σ_2 in the following way $p = 1 + \varepsilon\tilde{\sigma}_1$, $p_2 = w + \varepsilon\tilde{\sigma}_2$, where $\sigma_i = \varepsilon\tilde{\sigma}_i$. Using above substitutions into equations of motion and eliminating the secular terms we can obtain the modulation equations. After labor−consuming transformations we get autonomous modulation system

$$i\frac{da_1}{dt} + a_1\left(-\sigma_1 + \frac{d\theta_1}{dt}\right) = -\frac{1}{2}ia_1c_1 + \frac{1-7w^2}{4(1-4w^2)}w^2a_1a_2^2$$
$$+\frac{rp^2}{2}\left(1-\frac{\sigma_1}{2}\right)(\cos\theta_1 + i\sin\theta_1),$$

(9)

$$i\frac{da_2}{dt} + a_2\left(-\sigma_2 + \frac{d\theta_2}{dt}\right) = -\frac{1}{2}ia_2c_2 + \frac{1-7w^2}{4(1-4w^2)}wa_2a_1^2$$
$$-\frac{a_2^3w^3}{16}\frac{1+8w^2}{(1-4w^2)} + \frac{f_2}{2w}(\cos\theta_2 + i\sin\theta_2).$$

(10)

where $\theta_1(T_1,T_2) = T_1\tilde{\sigma}_1 - \psi_1(T_1,T_2)$, $\theta_2(T_1,T_2) = T_1\tilde{\sigma}_2 - \psi_2(T_1,T_2)$.

   Amplitude modulations according to (9, 10) and time history obtained numerically from eq. (1) are presented in Fig 2.
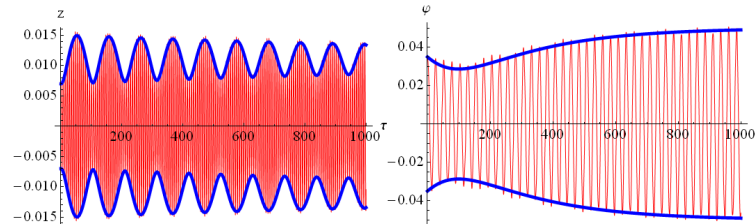
Fig 2. Amplitude modulations (thick line) and time history (thin) obtained from (1).

Considering steady state motion, frequency response functions can be obtained

(i)   for parametric resonance

$$\left(-\sigma_1 a_1 + \frac{w^2\left(7w^2 - 1\right)a_1 a_2^2}{4\left(1 - 4w^2\right)}\right)^2 + \frac{c_1^2}{4}a_1^2 = \frac{r^2 p^4}{4} ; \qquad (11)$$

(ii)   for external resonance

$$\left(-\sigma_2 a_2 - \frac{w\left(1 - 7w^2\right)a_2 a_1^2}{4\left(1 - 4w^2\right)} + \frac{w^3\left(1 + 8w^2\right)a_2^3}{16\left(1 - 4w^2\right)}\right)^2 + \frac{c_2^2}{4}a_2^2 = \frac{f_2^2}{4w^2} . \qquad (12)$$

Some families of resonance curves are shown in Figs. 3 and 4.
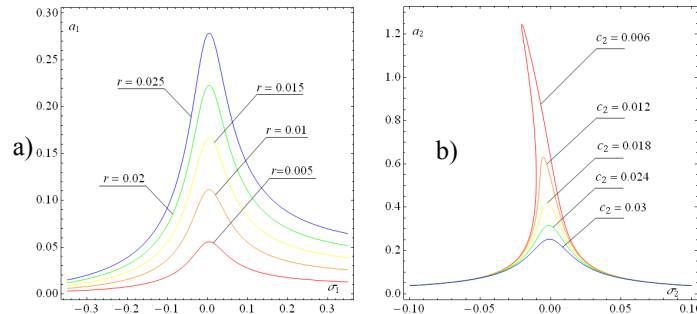
Fig. 3 a) Amplitudes a_1 vs. detuning parameter for different r .b) Amplitudes a_2 vs. detuning parameter for different c_2.
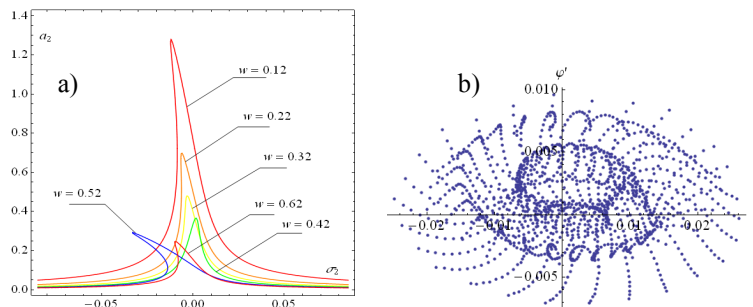
Fig. 4 a) Amplitudes a_2 against detuning parameter (effects of natural frequency w variation) b)Poincare map in resonance.

The change of character of resonance from "hard" to "soft" (Fig. 4a) is a consequence of changing sign of the coefficient standing at a^6 in Eq. (12). For some parameters the motion is very complicated (see Fig. 4b).

Case 2 – Parametric spring resonance $p_1 \approx 1$ and external resonance with pendulum $p \approx w$. In order to consider that case we introduce the detuning parameters σ_1 and σ_2 in the following way $p_1 = 1 + \varepsilon\widetilde{\sigma}_1$, $p = w + \varepsilon\widetilde{\sigma}_2$, where $\sigma_i = \varepsilon\widetilde{\sigma}_i$.
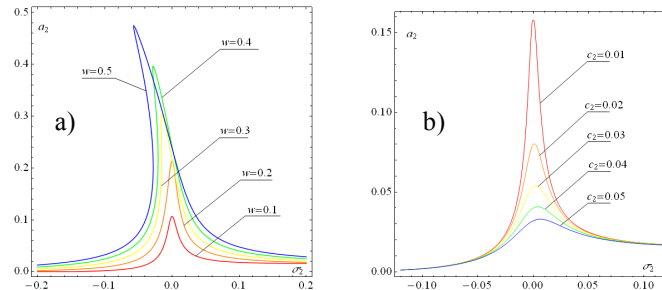
Fig. 5. a) Amplitudes a_2 vs. detuning parameter (effects of natural frequency w variation) b) Amplitudes a_2 vs. detuning parameter for different c_2

6. Conclusions

The dimensionless equations of motion were introduced and successfully solved with the multiple scale method. General solutions, including the third order of approximation, were achieved in analytical form. Dimensionless solutions are universal and valid for many systems of the same scale of similarity. The amplitude modulations presented in Fig. 2 well agreed with time history obtained numerically. Frequency response functions for the chosen resonances are presented graphically. The complicated motion of the pendulum near resonance is illustrated in the Poincare map. Most operations were performed with the help of procedures elaborated by authors in *Mathematica*.

References

1. O.V. Gendelman, D.V. Gorlov, L.I. Manevitch, A.I. Musienko, *Dynamics of coupled linear and essentially nonlinear oscillators with substantially different Masses*, J. Sound Vib*.,* **286** (2005), 1-19.
2. R. Starosta, J. Awrejcewicz, *Asymptotic analysis of parametrically excited spring pendulum*, Proc. of SYROM 2009, Brasov, Romania, Springer (2009).
3. A. Tondl, R. Nabergoj, *Dynamic absorbers for an externally excited pendulum*, J. Sound Vib. **234**(4) (2000) 611– 624.
4. A.F. Vakakis, L.I. Manevitch, O. Gendelman, L. Bergman, *Dynamics of linear discrete systems connected to local, essentially non-linear attachments,*" J. Sound Vib. **264**(3) (2003) 559–577.
5. S. J. Zhu, Y.F. Zheng, Y.M. Fu, *Analysis of non-linear dynamics of a two-degree-of-freedom vibration system with nonlinear damping and non-linear spring*, J. Sound Vib. **271** (2004) 15 – 24.

Metoda wielu skal dla wymuszanego kinematycznie nieliniowego układu z wahadłem

Badana jest dynamika wahadła sprężystego z zewnętrznym i kinematycznym wymuszeniem. Do rozwiązania równań ruchu zastosowano metodę wielu skal. Określono warunki pojawienia się rezonansu i przedstawiono wykresy krzywych rezonansowych oraz funkcje modulacji dla wybranych parametrów. Obliczenia przeprowadzono w systemie algebry komputerowej *Mathematica*.

Stability of rotor operating in cylindrical 3-pocket journal bearings

Stanisław STRZELECKI

Lodz University of Technology, Stefanowskiego 1/15, 90-924 Lodz, Poland
stanislaw.strzelecki@p.lodz.pl

Zygmunt TOWAREK

Lodz University of Technology, Stefanowskiego 1/15, 90-924 Lodz, Poland
zygtow@p.lodz.pl

Abstract

Multilobe journal bearings with 3 operating lobes of cylindrical profile and 3 oil pockets are applied in different types of rotating machinery. The design of 3-lobe journal bearings, the number of lobes and oil grooves improves thermal state of bearing at higher speeds and the stability of operation.

The paper describes the results of the calculations of dynamic characteristics and determination of stability ranges of simple symmetric rotor operating in 3-lobe journal bearings of cylindrical profile. The dynamic characteristics of supporting bearings are defined by four stiffness and damping coefficients of oil film. The iterative solution of Reynolds, energy and viscosity equations allows the obtaining of the load capacity of bearings and the required coefficients of oil film. Adiabatic, laminar oil film and the static equilibrium position of journal were assumed. The oil film pressure, temperature, viscosity fields and the oil film forces were the basis of the bearing dynamic characteristics and stability determination.

Keywords: multilobe journal bearings, stability of rotor

1. Introduction

The 3-lobe journal bearings [1-4] applied in the turbines and turbo generators should assure long and reliable operation of this responsible rotating machinery. They are characterised by good stability in the range of higher rotational speeds assuring very good cooling conditions for the oil film. Any failure occurring during operation of these bearings can cause very high power losses. The static and dynamic characteristics of the journal bearings are the basis for the determination of the stability of rotor operating in the journal bearings.

In the turbogenerators, the lemon bearings are very often applied. The „half-lemon" bearing (Fig. 1a) has been used with success in the bearing systems of rotating machinery, too [4]. This has a lower half with the normal radial clearance, the bearing and the shaft centres coincide if the shaft spins centrally. The top half has a difference in radii between shaft and bearing surface, about 2,5 to 3 times that of the bottom part. Its centre is however dropped, so the actual top clearance equals the bottom clearance, but that of the side is larger. This ensures that the shaft is always running eccentric to the top half, which therefore exerts a downward force on it. Some unpublished experiments at Imperial College have shown that this puts up the vibration frequency by some 20 per cent [4].

The design that is mentioned in [4] can be applied for the 3-lobe journal bearings (cylindrical profile, Fig. 1b), i.e. the bottom lobe as the cylindrical and both upper lobes

with the difference in radii between shaft and bearing surface (multilobe profile, Fig. 1c). For such solution there are no publications and this situation generates the need for more results to obtain better knowledge on this type of bearing. However, for the cylindrical 3-pockets bearing little publication are known, only. Hence, more investigation on the static and dynamic properties of this type of bearings can be useful.

The 3-lobe bearings are represented by the 3-lobe cylindrical bearing [1-4] (Fig. 1b), classic bearing [1-4] and with the pericycloid profile [3]. All these types of bearings have three lubricating grooves placed each 120^0. The 3-lobe bearing is designed as three parts bearing of cylindrical non-continuous profile [1-4]. The single lobes of this bearing are designed as the arc of the circle with the centre points placed on the symmetry line of the single lobe. In the symmetric multilobe bearing the circle inscribed in the bearing profile is tangent to the lobe exactly at the middle point of each lobe.

The paper introduces theoretical investigation into the stability of rotor operating in 3-lobe cylindrical journal bearings (3-pocket). The Reynolds, energy and viscosity equations were solved numerically on the assumption of incompressible lubricant, the laminar and adiabatic flow of oil in the lubricating gap of finite length bearing. The static equilibrium position of the journal was assumed in the calculations. Finite difference method was applied for the solution of all hydrodynamic equations.

The stability of rotor running in considered journal bearings is investigated on the basis of bearing dynamic characteristics [5]. On the assumption of very small displacement of journal centre from its static equilibrium position, the oil film forces were linearized. Characteristic equation of the system rotor-bearings obtained in the form of an algebraic polynomial of 6-th order with the coefficients, which are functions of oil film stiffness and damping coefficients, was applied. Application of the Routh-Hurwitz criteria has allowed knowing whether or not; the characteristic equation has a positive root with positive real part.

2. Oil film pressure and temperature distributions

The geometry of multilobe journal bearing (Fig. 1) describes Eqn. (1) on the assumption of the parallel axis of journal and bearing sleeve. In this equation, the first member gives the geometry of multilobe bearing [1,3] and the second member describes the geometry of cylindrical bearing.

$$\overline{H}(\varphi) = \overline{H}_{Li}(\varphi) - \varepsilon \cdot \cos(\varphi - \alpha) \tag{1}$$

where: α - attitude angle, $(^0)$, ε - relative eccentricity, φ - peripheral co-ordinate, $(^0)$

The first member of the right side of Eqn. (1) determines the gap geometry of 3-lobe journal bearing, at the concentric position of journal and bearing axis. It has the following form [1, 3]:

$$\overline{H}_{Li}(\varphi) = \psi_{si} + (\psi_{si} - 1) \cdot \cos(\varphi - \gamma_i) \tag{2}$$

where: γ_i - angle of lobe centre point, $(^0)$, ψ_{si} - lobe relative clearance.
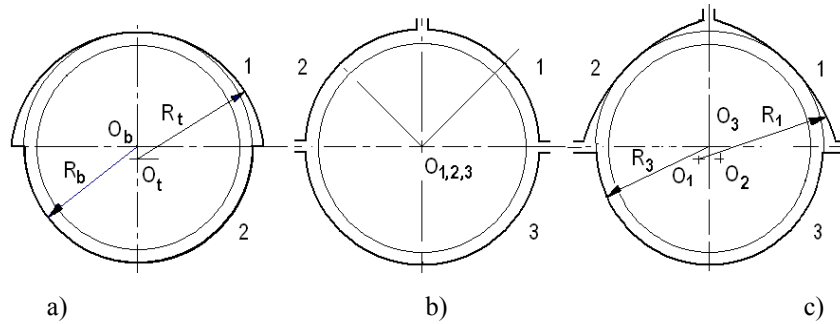
Fig. 1 Examples of multilobe journal bearings: a) half-lemon, b) cylindrical 3-pockets, c) 3-lobe asymmetrical (combined profile)

The journal bearing performances for laminar, adiabatic model of oil film can be determined by the numerical solution of the oil film geometry, Reynolds, energy and viscosity equations on the assumption of static equilibrium position of the journal [6-9]. The oil film pressure distribution was defined from the following, transformed Reynolds equation:

$$\frac{\partial}{\partial \varphi}\left(\frac{\overline{H}^3}{\overline{\eta}} \frac{\partial \overline{p}}{\partial \varphi}\right) + \left(\frac{D}{L}\right)^2 \frac{\partial}{\partial \overline{z}}\left(\frac{\overline{H}^3}{\overline{\eta}} \frac{\partial \overline{p}}{\partial \overline{z}}\right) = 6\frac{\partial \overline{H}}{\partial \varphi} + 12\frac{\partial \overline{H}}{\partial \phi} \qquad (3)$$

where: D, L - bearing diameter and length (m), $\overline{H} = h/(R\text{-}r)$ - dimensionless oil film thickness, h - oil film thickness (μm), $\overline{p}$ - dimensionless oil film pressure, $\overline{p} = p\psi^2/(\eta\omega)$, p - oil film pressure (MPa), r, R - journal and sleeve radius (m), t – time (sec), φ, $\overline{z}$ - peripheral and axial co-ordinates, $\phi = \omega t$ - dimensionless time, ω - angular velocity, $\overline{\eta}$ - dimensionless viscosity, ψ - bearing relative clearance, $\psi = \Delta R/R$ (‰), ΔR - bearing clearance, $\Delta R = R\text{-}r$ (m).

It has been assumed for the pressure region that on the bearing edges the oil film pressure $p(\varphi, z) = 0$ and in the regions of negative pressure, $p(\varphi, z) = 0$. The oil film pressure distribution computed from Eqn. (3) has been introduced in the transformed energy equation [6-9]. The boundary conditions for the oil film pressure and temperature take into account the inlet pressure and temperature. Temperature values $T(\varphi, z)$ on the boundaries $(z = \pm L/2)$ were determined by means of the parabolic approximation [6]. Temperature and viscosity distributions were found by the iterative solution of equations (1) through (3) and energy one [6-9].

The equations of motion for the journal and the centre of elastic shaft are given in matrix form by Eqn. (4). All the stiffness and damping coefficients were calculated by means of perturbation method [1-3].

The motion of simple symmetric rotor can be described by the following equation [5]:

$$M \cdot \ddot{x} + B \cdot \dot{x} + C \cdot x = \hat{a} \cos \omega t + \hat{b} \sin \omega t \tag{4}$$

where: M, B, C –matrices of mass, damping and stiffness, $\hat{a}, \hat{b}$ - coefficients of dynamic constraints.

After transformations of Eqn. (4) the real and imaginary part was obtained [5]. The stability of elastic rotor-bearing system is analysed on the basis of the following characteristic frequency equation of 6-th order with regard to (λ/ω) [5]:

$$c_6(\lambda / \omega)^6 + c_5(\lambda / \omega)^5 + c_4 (\lambda / \omega)^4 + c_3 (\lambda / \omega)^3 + c_2 (\lambda / \omega)^2 + c_1 (\lambda / \omega) + c_0 = 0. \tag{5}$$

The coefficients c_0 through to c_6 of Eqn. (5) are given by the Eqn. (6):

$$\begin{aligned}
c_0 &= A_0 & c_1 &= A_1 & c_2 &= A_2 + a_0 (2 A_0 + b_0 A_4) \\
c_3 &= a_0 (2 A_1 + b_0 A_3) & c_4 &= 2 a_0 A_2 + a_0^2 (b_0^2 + A_0 + b_0 \cdot A_4) \\
c_5 &= a_0^2 (A_1 + b_0 \cdot A_3) & c_6 &= a_0^2 A_2
\end{aligned} \tag{6}$$

where: a_0 - ratio of angular velocity to the angular self-frequency of stiff shaft, $a_0 = \omega^2 / \omega_{cr}^2$, b_0 - ratio of Sommerfeld number to the relative elasticity of shaft, So/c_s, c^* – shaft stiffness, (Nm^{-1}), c_s – relative elasticity of shaft, $c_s = f/\Delta R = g /(\omega_{cr}^2 \cdot \Delta R)$, f- static deflection of shaft, (m), F - resultant force of oil film (N), F_{stat} - static load of bearing, (N), g - acceleration of gravity, (ms^{-2}), m - mass of the rotor, (kg), So - Sommerfeld number, $So = F \cdot \psi^2 /(L \cdot D \cdot \eta \cdot \omega)$, S_{ok} - critical Sommerfeld number, So ω/ω_{cr}, τ - angle determining stability range, $(^0)$, ω_{cr} - angular self frequency of stiff rotor, $\omega_{cr} = \sqrt{c^*/m}$.

As the result of the transformations of Eqn. (6), the expression that determines the ratio of boundary angular speed ω_b to the critical ω_c one, and determines the stability of rotor, has the form [3, 5]:

$$\left(\frac{\omega_b}{\omega_c} \right) = \frac{1}{1 + b_0 \cdot \dfrac{A_3}{A_1}} \cdot \frac{A_2 \cdot A_3^2}{A_1^2 + A_1 \cdot A_3 \cdot A_4 + A_0 \cdot A_3^2} \tag{7}$$

where: $A_0 \div A_4$ are the combination of eight coefficients (four stiffness g_{ik} and four damping b_{ik}).

3.   Results of calculations

The stability of simple elastic, symmetric rotor was determined based on the calculated dynamic characteristics. These calculations included the non-dimensional load capacity S_0 and journal displacement ε as well as the static equilibrium position angles α_{eq}, too. The 3-lobe cylindrical journal bearings under consideration have the length to diameter ratio L/D=0.5 and L/D=0,8. The rotational speed of journal was n=3000 rpm. The feeding oil temperature was 40^0C and the corresponding thermal coefficients K_T [1,6] were 0,014 at the bearing relative clearances ψ = 2,7‰. Exemplary results of the calculations of journal displacement ε versus Sommerfeld number S_0 and the static equilibrium position angles α_{eq} are showed in Fig. 2 and Fig. 3.

The journal displacements ε that were obtained at different Sommerfeld numbers of bearings with different operating surfaces can be observed in Fig. 2. The values of these displacements are different for the bearings under considerations. In case of bearing with the operating surfaces having the lobe relative clearance ψ_s =1 (cylindrical 3-pocket bearing) the displacements are larger at larger Sommerfeld number as compared to the bearing with the lobe relative clearance ψ_s =1,5 or ψ_s =3,0 (Fig. 2; denotations in this figure are: 3LC – three lobe cylindrical profile, 3LM – multilobe profile). An increase in the lobe relative clearance and at assumed journal eccentricity ε, causes the decrease in the Sommerfeld number (Fig. 2). The static equilibrium position angles α_{eq} for all types of operating surfaces (i.e. at ψ_s =1 and ψ_s =1,5 and ψ_s =3,0) shows Fig. 3; the difference between these angles results from the profiles of considered bearings.
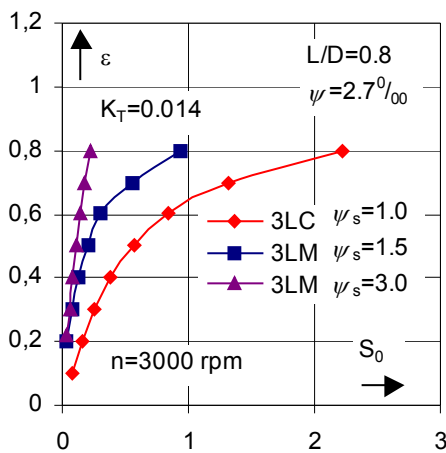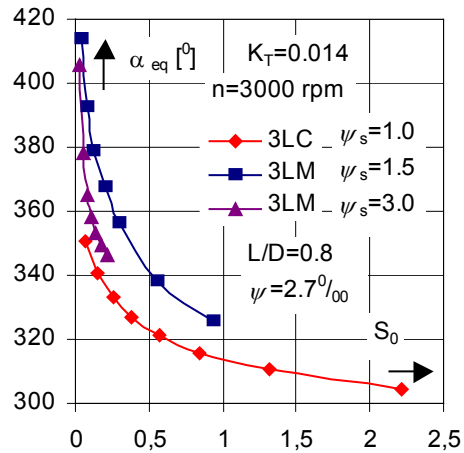

Fig. 2 Load capacity versus Sommerfeld number

Fig. 3 Static equilibrium position angles versus Sommerfeld number

Exemplary results of the calculated stiffness g_{ik} and damping b_{ik} coefficients are showed in Fig. 4 and Fig. 5.

The run of all coefficients is similar for the considered values of the bearing length to diameter ratios L/D. Among the stiffness coefficients that were obtained at L/D=0.8, the coefficient g_{21} shows the largest values in the range of Sommerfeld numbers from 0 through 0,8 (Fig. 4). However, at higher values of Sommerfeld numbers, the coefficient g_{22} has the largest values (Fig. 4 – see the range of S_0 over the value 0,8). The smallest values show the stiffness coefficients g_{12} (e.g. Fig. 4). The values of stiffness coefficient g_{11} are placed between the values of the coefficient g_{22} (they are smaller than the values of this coefficient) and g_{12} (the values greater than the values of g_{12}) (Fig. 4).

Among the damping coefficients, the coefficient b_{22} has the largest values (Fig. 5). In the range of Sommerfeld numbers from 0 through about 0,75 the smallest values have the coupled damping coefficients b_{12} and b_{21} (Fig. 5). However, for the Sommerfeld numbers larger than 0,75 the coefficient b_{11} shows the smallest values (see the curve of b_{11} in Fig. 5). The coupled damping coefficients have very close values with the values of coefficient b_{12} larger than coefficient b_{21} in the range of Sommerfeld numbers over 0,75 (Fig. 5).
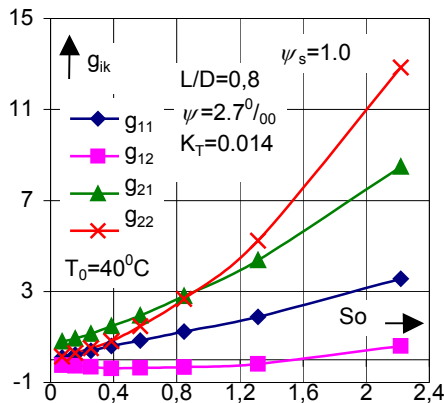
Fig. 6 Stiffness coefficients of the oil of 3-lobe cylindrical journal bearing
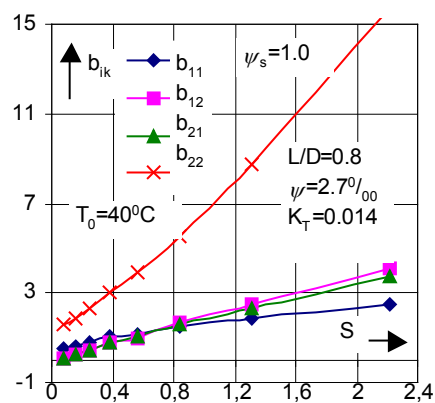
Fig. 7 Damping coefficients of the oil film of 3-lobe cylindrical journal bearing

The stability charts of rotor operating in the 3-lobe cylindrical journal bearings at different relative stiffness of rotor can be observed in Fig. 6 and Fig. 7 for two considered bearing length to diameter ratios. The stability properties of rotor are characterized by the angle τ that is different for different types of journal bearings [2]; better stability occurs at larger angle τ. Very small values of the relative elasticity correspond to very stiff rotor and very high values of relative elasticity c_s correspond to the very elastic rotor.

There is a difference in the stability of symmetric rotor operating in the bearings with the bearing length tot diameter ratio L/D=0.5 and L/D=0.8 (Fig. 8 and Fig. 9). The rotor running in the bearings that are characterized by the value of L/D=0.8 (Fig. 9, τ =

63^{0}27') shows better stability then for the bearings with *L/D*=0.5 (Fig. 8, $\tau = 26^030'$).
The ranges below the curves are the stability ranges and the ranges over the curves are
the ranges of instability (e.g. Fig. 7 the curve for $c_s = 0.5$). An increase in the relative
elasticity of rotor causes the increase in the stability – better stability for the rotor with
larger relative elasticity.
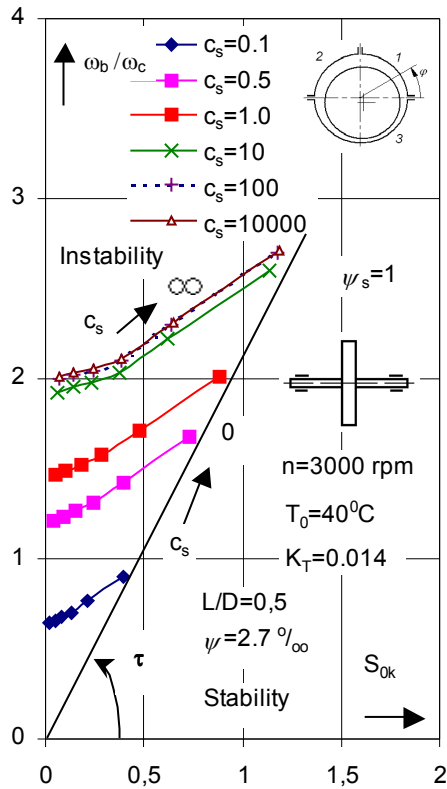
Fig. 8 Stability chart of rotor operating in
3-lobe cylindrical journal bearings at
different relative stiffness of rotor
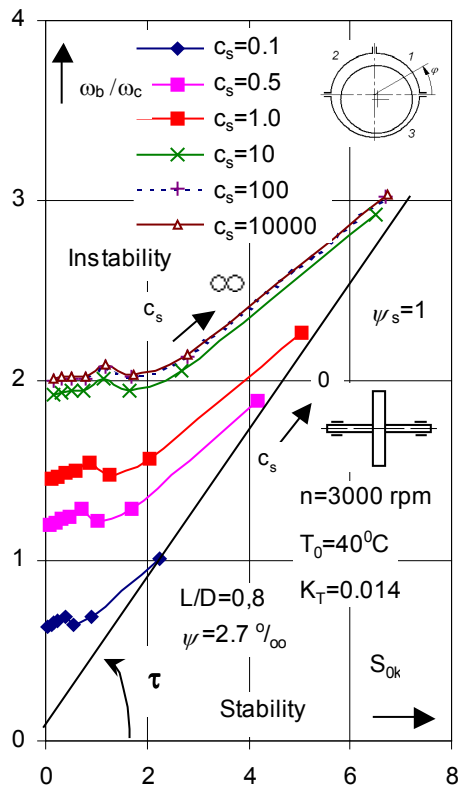
Fig. 9 Stability chart of rotor operating in
3-lobe cylindrical journal bearing at
different relative stiffness of rotor

4. Conclusions

The calculations of the dynamic characteristics of 3-lobe cylindrical journal bearings
with three lubricating pockets and the determination of stability ranges of simple
symmetric, elastic rotor allow to present the conclusions given below.
1. At assumed value of Sommerfeld number an increase in the lobe relative clearance
   causes the increase in the journal displacement.

2. The static equilibrium position angles show the increase at the increase in the lobe relative clearance.
3. The runs of stiffness and damping coefficients that were obtained in this investigation are typical for the multilobe type of bearings with the coupled damping coefficients having very close values.
4. In case of considered journal bearings, an increase in the bearing length to diameter ratio causes the increase in the stability of rotor.

References

1. E. Pollmann, *Das Mehrgleitflächenlager unter Berücksichtigung der veränderlichen Ölviskosität*. Konstruktion **21** H.3, (1969). 85-97
2. J. Glienicke, *Feder- und Dämpfungskonstanten von Gleitlagern für Turbomaschinen und deren Einfluß auf das Schwingungsverhalten eines einfachen Rotors*. Ph. D. Thesis. Technische Universität Karlsruhe 1962.
3. S. Strzelecki, *Stability of elastic rotor operating in 3-lobe journal bearings of different sleeves profile*. 7th IFToMM- Conference on Rotor Dynamics, Vienna, Austria, September 25-28, 2006. CD. ISBN 3-200-00689-7.
4. A. Cameron, *The Principles of Lubrication*. Longmans 1966.
5. R. Gasch, H. Pfützner, *Rotordynamik*. Springer-Verlag 1975.
6. S. Strzelecki, Z. Towarek, *Thermal Effects on Dynamic Characteristics of Tilting 5-Pad Journal Bearing*. Proceedings of 2nd International Symposium on Stability Control of Rotating Machinery. 4 – 8 August 2003, Gdansk, Poland (2003) 372 – 380.
7. S. Strzelecki, Z. Socha, *Effect of Load Direction on the Oil Film Temperature Distribution of 3-Lobe Pericycloid Journal Bearing*. Technical University Ostrava. PIME2009. Transactions of Technical University. Ostrava. Metallurg. Ser. (2009) R.**52** No. 3. 211-216.
8. S. M. Ghoneam, S. Strzelecki, *Thermal Problems of Multilobe Journal Bearings*. Meccanica DO1 10.1007/s 11012-006-9004-z. Meccanica (2006) **41**. Springer. 571-579.
9. S. Strzelecki, Z. Towarek, *Oil film temperature of high-speed cylindrical journal bearing*. Proc. of the International Conference SLAVYANTRIBO'7a, 2006. Vol. 2. Sankt Petersburg. Russia. (2006) 22-29.

Stateczność wirnika łożyskowanego w łożyskach cylindrycznych z trzema kieszeniami smarowymi

Przedstawiono wyniki obliczeń charakterystyk dynamicznych oraz wyznaczenie obszarów stateczności prostego wirnika symetrycznego pracującego w łożyskach cylindrycznych z trzema kieszeniami smarowymi. Charakterystyki dynamiczne łożysk wirnika określone są przez 4 współczynniki sztywności i 4 współczynniki tłumienia filmu smarowego. Podstawowe równania hydrodynamicznej teorii smarowania, równanie Reynoldsa, energii i lepkości rozwiązano numerycznie otrzymując nośność oraz wymagane współczynniki filmu smarowego. Założono laminarny, adiabatyczny film smarowy oraz statyczne położenie równowagi czopa. Obszary statecznej pracy wirnika wyznaczono w oparciu o równanie charakterystyczne 6-go rzędu.

Liquid sloshing in baffled tanks

Ryszard SYGULSKI

Institute of Structural Engineering, Poznan University of Technology
Piotrowo 5, 60-965 Poznań, Poland
ryszard.sygulski@put.poznan.pl

Abstract

The paper concerns the natural frequencies and mode shapes of a liquid sloshing in three dimensional baffled tanks with arbitrary geometries. The hydrodynamic pressure of the liquid is described by the boundary integral equation. The boundary element method is used to solve it. In the present formulation the baffles are treated as double layers. Numerical results are presented.

Keywords: sloshing, tanks with baffles, BEM

1. Introduction

The liquid sloshing phenomenon in a tank is an important field of the fluid dynamic research. Liquid tanks are considered as important parts of municipal facilities systems, oil industry, naval and aerospace systems. Hydrodynamic forces acting on walls of the tank as a result of sloshing of the liquid inside may damage the whole system. The baffles in tanks are used to increase the damping of the liquid sloshing and usually cause changes of sloshing frequencies and can be treated as a passive control system.

This paper presents the application of the boundary element method to determine the natural frequencies and mode shapes of a liquid sloshing in three dimensional baffled tanks with arbitrary geometries. Triangular curvilinear 6-node boundary elements are applied. In the present formulation the baffles are treated as double layers. A similar problem of liquid sloshing in tanks with baffles was considered in the papers [1, 2, 3], in which the zoning method was introduced. The domain of the liquid was divided into zones. The baffles were than located at boundaries of the zones and compatibility conditions between zones were applied. In the present formulation such an approach is not necessary.

2. Problem formulation

Let us consider a tank of an arbitrary shape with a liquid free surface S_1, a bottom surface S_2 and baffle S' (Fig.1). It is assumed that the fluid is incompressible and inviscid. The perturbation fluid velocity potential $\Phi(x, y, z, t)$ satisfies the Laplace's equation:

$$\nabla^2 \Phi(x, y, z, t) = 0 \tag{1}$$

The solution of the Eq. (1) may be expressed as a single-layer and a double-layer potential:

$$C(P)\Phi(P,t) = \int_S \frac{\partial \Phi(Q,t)}{\partial n(Q)} \Phi^*(P,Q)dS(Q) - \int_S \Phi(Q,t)\frac{\partial \Phi^*(P,Q)}{\partial n(Q)}dS(Q) +$$

$$+ \int_{S'} \Phi'(Q',t)\frac{\partial \Phi^*(P,Q')}{\partial n(Q')}dS'(Q') \qquad (2)$$

where $C(P)$ is a coefficient defined as:

$$C(P) = \begin{cases} 1 & P \text{ inside the domain,} \\ \frac{1}{2} & P \text{ on the smooth part of the boundary liquid,} \end{cases}$$

$\Phi'(Q',t)$ is the resultant velocity potential at a point Q' on the surface S', $\Phi^*(P,Q) = \frac{1}{4\pi}\frac{1}{r(P,Q)}$ is the fundamental solution, $r(P,Q)$ is a distance between an arbitrary point P and a point Q on the surface, t is the time.
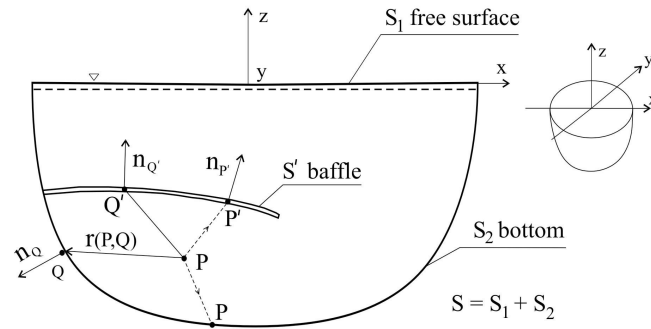
Figure 1. A tank of an arbitrary shape with a baffle.

The last part of Eq. (2) represents a double-layer potential of the open surface S' immersed in liquid. Boundary conditions on the surface S and S' are of the Neumann type:

- bottom condition: $\quad \dfrac{\partial \Phi}{\partial n} = 0 \;$ on $\; S_2$ $\hfill (3)$

- free-surface condition: $\quad \dfrac{\partial \Phi}{\partial z} = -\dfrac{1}{g}\dfrac{\partial^2 \Phi}{\partial t^2} \;$ on $\; S_1$ $\hfill (4)$

- baffle-surface condition: $\quad \dfrac{\partial \Phi}{\partial n} = 0 \;$ on $\; S'$ $\hfill (5)$

where g is the gravity acceleration.

The boundary condition (4) is known as the linearized surface wave condition. Coming with the point P onto the surface S' (see point P', Fig.1) and calculating the

derivative of the velocity potential in the direction normal to the surface at this point, Eq. (2) with the boundary condition (5) can be rewritten as:

$$\frac{\partial \Phi(P',t)}{\partial n(P')} = \int_S \frac{\partial \Phi(Q,t)}{\partial n(Q)} \frac{\partial \Phi^*(P',Q)}{\partial n(P')} dS(Q) - \int_S \Phi(Q,t) \frac{\partial^2 \Phi^*(P',Q)}{\partial n(Q)\partial n(P')} dS(Q) +$$

$$+ \int_{S'} \Phi'(Q',t) \frac{\partial^2 \Phi^*(P',Q')}{\partial n(Q')\partial n(P')} dS'(Q') = 0 \qquad (6)$$

The boundary integral equation (2) with the boundary conditions (3) and (4) and the boundary integral equation (6) allow us to solve the sloshing problem of any tank with baffles.

The hydrodynamic pressure is expressed as:

$$p = -\rho \frac{\partial \Phi}{\partial t} \qquad (7)$$

where ρ is the fluid density, $p = \widetilde{p}e^{i\omega t}$, ω is the circular frequency.

Differentiating (2) and (6) with respect to time and using (7) we can rewrite (2) and (6) in the form:

$$C(P)p(P,t) = \int_S \frac{\partial p(Q,t)}{\partial n(Q)} \Phi^*(P,Q) dS(Q) - \int_S p(Q,t) \frac{\partial \Phi^*(P,Q)}{\partial n(Q)} dS(Q) +$$

$$+ \int_{S'} p'(Q',t) \frac{\partial \Phi^*(P,Q')}{\partial n(Q')} dS'(Q'), \qquad (8)$$

$$\int_S \frac{\partial p(Q,t)}{\partial n(Q)} \frac{\partial \Phi^*(P',Q)}{\partial n(P')} dsS(Q) - \int_S p(Q,t) \frac{\partial^2 \Phi^*(P',Q)}{\partial n(Q)\partial n(P')} dS(Q) +$$

$$+ \int_{S'} p'(Q',t) \frac{\partial^2 \Phi^*(P',Q')}{\partial n(Q')\partial n(P')} dS'(Q') = 0 \qquad (9)$$

Using (7) the boundary conditions (3) and (4) can be expressed in the form:

- $$\frac{\partial \widetilde{p}_2}{\partial n} = 0 \text{ on } S_2 \qquad (10)$$

- $$\frac{\partial \widetilde{p}_1}{\partial z} = \frac{\omega^2}{g} \widetilde{p}_1 \text{ on } S_1 \qquad (11)$$

On the free surface the hydrodynamic pressure p_1 can be approximated by assuming the actual surface to be at an elevation w_1 relatively to the mean surface.

Using (4), (7) and the relation $\frac{\partial \Phi}{\partial z} = \frac{\partial w_1}{\partial t}$ on S_1 we can write down:

$$p_1 = \rho g w_1 \qquad (12)$$

3. Solution of the problem

The surface of the liquid boundary and the baffle surface were discretized using 6-node isoparametric curvilinear triangular boundary elements. The curvilinear elements located at the baffle were subdivided into four planar triangular constant type elements. The collocation points were the centroids of the planar triangles. It was necessary because the last part of Eq. (9) contains the hypersingular integral. The boundary element discretization of Eqs. (8) and (9) results in the following matrix equations:

$$\mathbf{C}\widetilde{\mathbf{p}} = \mathbf{A}\widetilde{\mathbf{f}} - \mathbf{B}\widetilde{\mathbf{p}} + \mathbf{D}_1\widetilde{\mathbf{p}}' \tag{13}$$

$$\mathbf{A}_1\widetilde{\mathbf{f}} - \mathbf{D}_2\widetilde{\mathbf{p}} + \mathbf{D}_3\widetilde{\mathbf{p}}' = \mathbf{0} \tag{14}$$

where $\widetilde{\mathbf{p}}, \widetilde{\mathbf{p}}'$ and $\widetilde{\mathbf{f}}$ are the amplitudes of nodal vectors, $\mathbf{p} = \widetilde{\mathbf{p}}e^{i\omega t}$, $\mathbf{f} = \widetilde{\mathbf{f}}e^{i\omega t}$, $\mathbf{f} = \dfrac{\partial \mathbf{p}}{\partial n}$, $\mathbf{C}$ is the diagonal matrix of coefficients $C(P)$.

The majority of the elements of the matrices $\mathbf{A}$, $\mathbf{B}$, $\mathbf{D}_1$, $\mathbf{A}_1$, $\mathbf{D}_2$, and $\mathbf{D}_3$, is computed numerically using Gaussian integration formulae. The exception is with the diagonal elements of matrices $\mathbf{A}$ and $\mathbf{D}_3$, which have the singularity of $1/r$ and $1/r^3$ types, respectively. Calculations of such integrals are discussed in the papers [4] and [5], respectively. Using Eq. (13) and (14) we get:

$$\mathbf{B}_s\widetilde{\mathbf{p}} = \mathbf{A}_s\widetilde{\mathbf{f}}, \tag{15}$$

where $\mathbf{B}_s = \mathbf{B}_1 - \mathbf{D}_1\mathbf{D}_3^{-1}\mathbf{D}_2$, $\mathbf{A}_s = \mathbf{A} - \mathbf{D}_1\mathbf{D}_3^{-1}\mathbf{A}_1$, $\mathbf{B}_1 = \mathbf{C} + \mathbf{B}$.

From Eq. (15) we obtain:

$$\widetilde{\mathbf{p}} = \mathbf{B}_s^+\mathbf{A}_s\widetilde{\mathbf{f}}, \tag{16}$$

where $\mathbf{B}_s^+$ is the pseudoinverse of $\mathbf{B}_s$. The matrix $\mathbf{B}_s$ is singular, so we calculate the Moore-Penrose pseudoinverse matrix using the SVD procedure [6]. After the substitution of (10) and (11) into Eq. (16) we get:

$$\begin{Bmatrix} \widetilde{\mathbf{p}}_1 \\ \widetilde{\mathbf{p}}_2 \end{Bmatrix} = \frac{\omega^2}{g}\mathbf{E}\begin{Bmatrix} \widetilde{\mathbf{p}}_1 \\ \mathbf{0} \end{Bmatrix}, \tag{17}$$

or:

$$\widetilde{\mathbf{p}}_1 = \frac{\omega^2}{g}\mathbf{E}_{11}\widetilde{\mathbf{p}}_1, \tag{18}$$

where $\mathbf{E} = \mathbf{B}_s^+\mathbf{A}_s$, $\mathbf{E}_{11}$ is the MxM submatrix of the matrix $\mathbf{E}$, M is the number of free surface nodal points.

Substituting of Eq. (12) into Eq. (18) gives the standard eigenvalue problem:

$$(\mathbf{D} - \lambda\mathbf{I})\widetilde{\mathbf{w}}_1 = \mathbf{0}, \tag{19}$$

where $\mathbf{D} = \dfrac{1}{g}\mathbf{E}_{11}$, $\lambda = \dfrac{1}{\omega^2}$, $\mathbf{I}$ is the unit matrix.

The eigenvalues and eigenvectors of Eq. (19) allow us to determine the sloshing frequencies and their corresponding modes. The eigenproblem is reduced to the free surface degrees of freedom only.

4. Numerical examples

Basing on the problem formulation given in Sections 2 and 3, computer programs were developed. The calculations were performed for several types of tanks.

4.1. Example 1. The cylindrical tank

The calculations are performed for the cylindrical tank with $H/R = 1.0$ and $H/R = 0.5$, where R and H are the cylinder radius and the liquid depth, respectively. The boundary element mesh is as follows: 60 curvilinear elements on full domain, 18 curvilinear elements and 43 DOF on the free surface.

Table 1 presents the first three dimensionless sloshing frequencies in comparison with the exact values.

Table 1. The first three dimensionless sloshing frequencies in the cylindrical tank
$$(\overline{\omega} = \omega\sqrt{R/g})$$

mode	$H/R = 1.0$		$H/R = 0.5$	
	present BEM	analytical	present BEM	analytical
$\overline{\omega}_1$	1.318	1.323	1.152	1.156
$\overline{\omega}_2$	1.740	1.744	1.665	1.667
$\overline{\omega}_3$	1.941	1.957	1.901	1.915

4.2. Example 2. The cylindrical tank with the ring baffle

We consider the cylindrical tank with the ring baffle [2]. The geometry of the tank and the baffle position is shown in Figure 2.
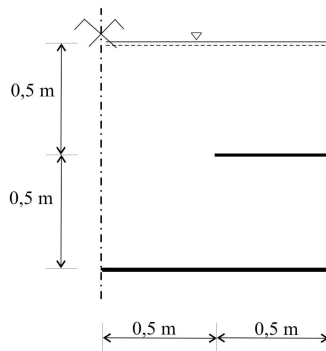

Figure 2. Cross-section of the cylindrical tank with the ring baffle.

The boundary element mesh of the fluid domain is similar as in Example 1. The baffle surface is discretized by 18 curvilinear elements.

The first natural frequency of the liquid is: present BEM - $f_1 = 0.613 Hz$; Reference [2] - $f_1 = 0.605 Hz$. The agreement of results is good.

3. Conclusions

The method of calculation the natural frequencies and mode shapes of liquid sloshing in three dimensional baffled tanks with arbitrary geometries is presented in the paper. The hydrodynamic pressure of the liquid is described by the boundary integral equation and the boundary element method is applied to solve it. The triangular curvilinear 6-node boundary elements are used. In the present formulation the baffles are treated as double layers and it is not necessary to introduce the zoning method. Some examples demonstrate the effectiveness and efficiency of the proposed method.

References

1. A. Gedikli, M. E. Ergüven, *Seismic analysis of a liquid storage tank with a baffle,* Int. J. Sound Vib., **223** (1999) 141 – 155.
2. A. Gedikli, M. E. Ergüven, *Evaluation of sloshing problem by variational boundary element method,* Engng Anal. Bound. Elem., **27** (2003) 935 – 943.
3. R. D. Firouz-Abadi, H. Haddadpour, M. A. Noorian, M. Ghasemi, *A 3D BEM model for liquid sloshing in baffled tanks,* Int. J. Numer. Meth. Engng, **76** (2008) 1419 – 1433.
4. R. Sygulski, *Vibrations of pneumatic structures interacting with air,* Comput. Struct., **Vol. 49, No. 5** (1993) 867 – 876.
5. R. Sygulski, *Dynamic analysis of open membrane structures interacting with air,* Int. J. Numer. Meth. Engng., **37** (1994) 1807 – 1823.
6. G. E. Forsythe, M. A. Malcolm, C. B. Moler, *Computer Methods for Mathematical Computations,* Prentice-Hall, Englewood Cliffs, NJ (1977).

Drgania swobodne cieczy w zbiornikach z przegrodami

W pracy zaprezentowano metodę obliczania drgań swobodnych cieczy w zbiornikach z zainstalowanymi przegrodami. Przegrody w zbiornikach stosuje się w celu zmniejszenia dynamicznego oddziaływania cieczy na ściany zbiornika. Do rozwiązania problemu zastosowano metodę elementów brzegowych. Do dyskretyzacji brzegu obszaru cieczy wykorzystano trójkątne 6-cio węzłowe krzywoliniowe elementy brzegowe. Sztywną przegrodę w zbiorniku traktuje się jako warstwę podwójną. Pozwoliło to zrezygnować z podziału obszaru cieczy na strefy w celu uwzględnienia obecności przegrody. Zamieszczono przykłady liczbowe.

Free vibrations of a column with an optimum shape with regard to the value of the critical load loaded by a follower force directed towards the positive pole

Janusz SZMIDLA

Technical University of Częstochowa, Institute of Mechanics and Machine Design
Foundations, ul. Dabrowskiego 73, 42-200 Częstochowa
szmidla@imipkm.pcz.czest.pl

Abstract

The results of numerical computations and experimental research into the free vibrations of a column loaded by a follower force directed towards the positive pole – the case of the specific load – are presented in this paper. The total mechanical energy of the column was formulated by taking into account the physical model of the system and constructional solution of the loading head. The curve courses of changes in the eigenvalues in the plane: load – natural frequency are shown on the basis of the solution to boundary problem which is obtained by considering kinetic criterion of the stability. The changes in natural frequencies were determined for the chosen values of the geometrical parameters of the loading head. The distribution of bending rigidity of the column, accepted for the numerical computations, corresponds to the systems with maximum values of the critical load at the assumed constant volume of the structure.

Keywords: column, specific load, free vibrations

1. Introduction

Many scientific publications have been dedicated to analysis of free transverse vibrations of columns and beams with jumping changeable cross-section. There are works where the problems of free vibrations of systems consisting of segments with changeable cross-sectional area [1-3] or works where the cross-section was changed continuously along the length [4, 5] were considered. Additional discrete elements, such as translational and rotational springs and bodies of concentrated masses, were taken into account in the models of beams and columns. The added discrete elements were mounted at the ends of the system [3, 5] or at points marking changes in the cross-section [1, 2, 4]. The solution to the vibration problem is also considered in research into the optimisation of slender system forms [3, 6].

2. The physical model of the column

The physical model of the column for the chosen specific load which was first formulated by L. Tomski [7] is presented in Fig. 1a. Column 3 is loaded by the follower force directed towards the positive in constructional solution [7 - 9] of the loading head 1 and receiving head 2 with circular profile (constant curvature). Direction of force P passes through the constant point O, place at distance R from the end of the column. The column is rigidly mounted from one side ($x_1 = 0$) and is connected to receiving head at the free end ($x_n = l$) by rigid element of l_0 in length (elements of the loading head are infinitely rigid). The system is divided into smaller segments (Fig. 1b) with flexural

rigidity (EJ_i) (indexes $i = 1.. n$), where J_i is a moment of inertia of the cross section of the i – th segment of the column in relation to neutral bending axis. Segments are described by the length l and by transverse displacement $W_i(x_i, t)$. The following assumptions and denotations are applied in work [9, 10]:
- constant total length of column L and constant length of its elements $l_i = l$ ($L = n l$),
- constant value of Young's modulus E and material density ρ of all segments of the column,
- constant total volume of all segments describing form of the column.
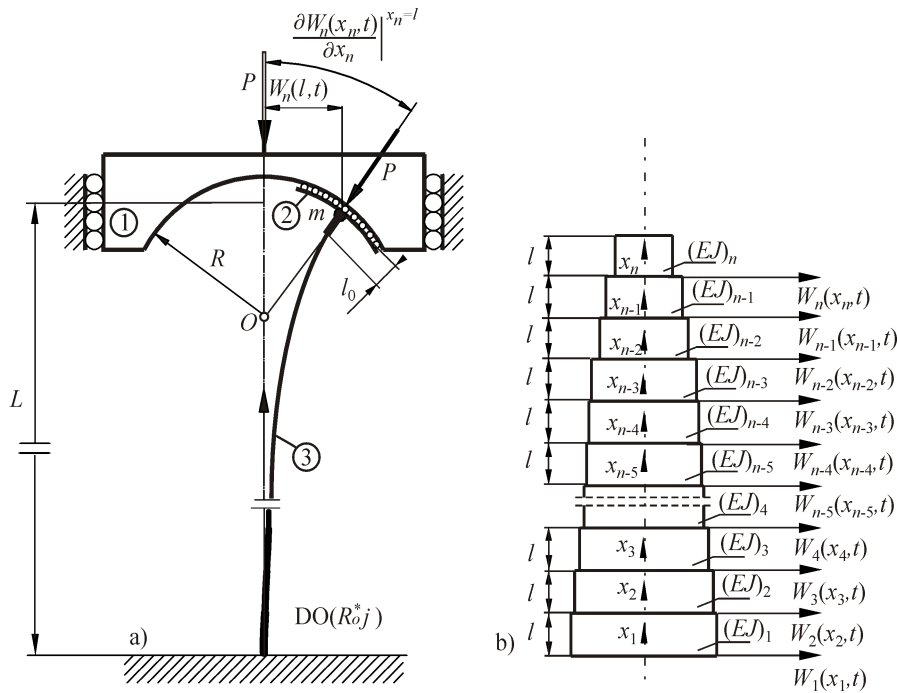
Figure 1. The physical model of the column: a) loaded by the follower force directed towards the positive pole, b) division of the columns into segments

Exemplary denotations of the columns considered in this paper are introduced:
- $DO(R_o^* 0.3)$ – optimized column with changeable bending rigidity at the parameter of the loading and receiving head $R_o^* = 0.3$,
- $DP(R_o^* 0.2)$ – comparative column with bending rigidity constant along the length of the system at the parameter of the loading and receiving head $R_o^* = 0.2$, while:

$$R_o^* = \frac{R}{L} \tag{1}$$

Volume of the column $DP(R_o^* j)$ is identical to the total volume of all segments describing the form of the system $DO(R_o^* j)$.

3. Formulation of and solution to the boundary problem

The boundary problem is formulated on the basis of the Hamilton's principle which for conservative systems takes the form:

$$\delta \int_{t_1}^{t_2} (T - V) dt = 0 \tag{2}$$

where: δ is operator of variation.

Kinetic energy T of the considered column $DO(R_o^* j)$ is a sum of kinetic energy of its individual segments and kinetic energy of a body with mass m.

$$T = \sum_{i=1}^{n} \frac{(\rho A_i)}{2} \int_0^l \left[\frac{\partial W_i(x_i, t)}{\partial t} \right]^2 dx_i + \frac{m}{2} \left[\frac{\partial W_n(l, t)}{\partial t} \right]^2 \tag{3}$$

The total potential energy V is described by the relationship :

$$V = \sum_{i=1}^{n} \frac{(EJ_i)}{2} \int_0^l \left[\frac{\partial^2 W_i(x_i, t)}{\partial x_i^2} \right]^2 dx_i - \frac{P}{2} \sum_{i=1}^{n} \int_0^l \left[\frac{\partial W_i(x_i, t)}{\partial x_i} \right]^2 dx_i +$$

$$+ \frac{P(R - l_0)}{2} \left[\frac{\partial W_n(x_n, t)}{\partial x_n} \bigg|^{x_n = l} \right]^2 \tag{4}$$

Commutation of integration (in relation to space coordinates x_i and time t) and computation of variation is used in Hamilton's principle (2). After computing variation of kinetic energy (3), variation of potential energy (4) and separation of variables of function $W_i(x_i, t)$ in relation to variables x_i and t :

$$W_i(x_i, t) = y_i(x_i) \cos(\omega t) \tag{5}$$

one can obtain:
- equations of motion for the considered system:

$$y_i^{IV}(x_i) + k_i^2 \, y_i^{II}(x_i) - \Omega_i^2 y_i(x_i) = 0, \quad i = 1 \ldots n \tag{6}$$

- boundary conditions for the column in relation to mounting point ($x_0 = 0$), at the free end ($x_n = l$) and continuity conditions between individual segments:

$$y_1(0) = y_1^I(0) = 0, \; y_j(l) = y_{j+1}(0), \; y_j^I(l) = y_{j+1}^I(0) \tag{7a-d}$$

$$y_j^{II}(l) = \chi_{j+1} y_{j+1}^{II}(0), \;\; y_j^{III}(l) = \chi_{j+1} y_{j+1}^{III}(0) \tag{7e-f}$$

$$y_n(l) = (R - l_0) y_n^I(l), \;\; y_n^{III}(l) - \frac{1}{R - l_0} y_n^{II}(l) + \frac{m \omega^2}{(EJ_n)} y_n(l) = 0 \tag{7g-h}$$

where: $j = 1, \ldots, (n-1)$, $k_i^2 = P/(EJ_i)$, $\Omega_i^2 = (\rho A_i) \omega^2 / (EJ_i)$, $\chi_{j+1} = (EJ_{j+1})/(EJ_j)$.

Substitution of equation solutions (6) into the boundary conditions (7a-h) leads into transcendental equation for natural frequency ω.

4. Results of numerical computations and experimental research

Results of experimental research and numerical computations applied to the values of natural frequency of optimized system [9] for chosen geometry of the receiving head (R = 0.059 [m], l_0 = 0.051 [m]) are presented [8, 9]). Physical and geometrical parameters of the tested column are given in Table 1.

Table 1. Geometrical and physical parameters of the column $DO(R_o^* 0.0125)$

Quantity	Symbol	Unit	Value
Young's modulus of column material	E	N/m^2	$7.5*10^{10}$
Density of column material	ρ	kg/m^3	2790
Length of optimized column	L	m	0.6
Concentrated mass	m	kg	0.39
Dimension of the cross-section	b	m	0.008

The results of computations concerning optimization of the column $DO(R_o^* j)$ are presented in works [9, 10]. The rectangular cross-section of the tested column with a and b in dimensions was assumed in research by taking into account static criterion of the stability and modified algorithm of simulated annealing. The width of the cross-section a (a_i – decision variables of optimization) was optimized at its constant thickness.
The following condition was additionally considered in computations:

$$a_i \geq b + 0.001 \ [\text{m}] \quad i = 1,...,n \tag{8}$$

Geometrical inequality limitations (8) of the optimized column were justified due to buckling plane of the system assumed in numerical computations and experimental research. This plane is described by the minimal moment of inertia in terms of neutral axis in the bending plane. The form of the optimized column $DO(R_o^* 0.0125)$ (full lines), at division of the system into n = 128 segments is presented in Fig. 2. The profile of adequate comparative column $DP(R_o^* 0.0125)$ is shown by broken line.
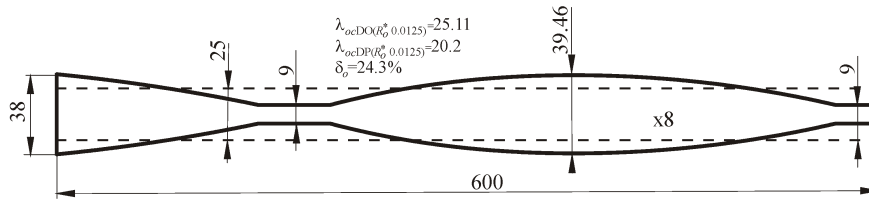
Figure 2. Form of the column $DO(R_o^* 0.0125)$, $DP(R_o^* 0.0125)$

Experimental research was carried out at the test stand designed and built in the Institute of Mechanics and Machine Design Foundations of Czestochowa University of Technology [11]. The results of numerical computations (full lines - system $DO(R_o^* 0.0125)$) and experimental research (points) in relation to changes in natural frequency are presented in Fig. 3. The course of changes in the eigenvalues of the comparative column $DP(R_o^* 0.0125)$ are marked by broken line. Range of changes in the

first three natural frequencies f in relation to the external load P was given. It was stated that the results stay in good agreement after comparison of numerical computations and experimental research of the column DO(R_o^* 0.0125). At the basic natural frequency, maximal relative error between experimental results f^e and frequencies obtained theoretically f^t is equal to 7.24%.
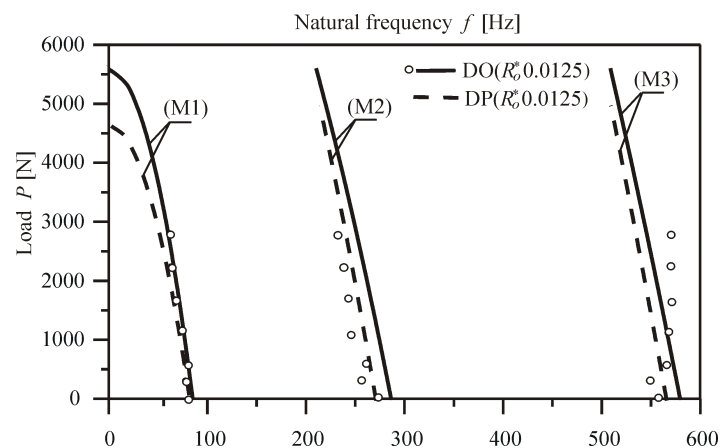
Figure 3. The curves in the plane: load P –natural frequency f
(system DO(R_o^* 0.0125))

5. Conclusions

Regarding the influence of the external load and the geometrical parameters of the loading and receiving heads on the changes in natural frequencies, the considered column was rated as a divergence or divergence pseudo-flutter type of the systems. The accuracy of the assumed mathematical model of the system was confirmed by the results of original experimental research.

Acknowledgments

References

1. S. Kukla, I. Zamojska, *Frequency analysis of axially loaded stepped beams by Green's function method*, Journal of Sound and Vibration, **300** (2007) 1034-1041.
2. S. Naguleswaran, *Natural frequencies, sensitivity and mode shape details of an Euler-Bernoulli beam with one-step change in cross-section and with ends on classical supports*, Journal of Sound and Vibration, **252** (2002) 751-767.

3. J. Szmidla, A. Wawszczak, *Drgania swobodne kolumn o optymalnym kształcie ze względu na wartość obciążenia krytycznego poddanych obciążeniu eulerowskiemu*, Modelowanie Inżynierskie **38** (2009) 205 - 212.

4. S. Abrate, *Vibration of non-uniform rods and beams*, Journal of Sound and Vibration, **185** (1995) 703-716.

5. N. Auciello, *Transverse vibrations of a linearly tapered cantilever beam with tip mass of rotary inertia and eccentricity*, Journal of Sound and Vibration, **194(1)** (1996) 25- 34.

6. R. Bogacz, H. Irretier, O. Mahrenholtz, *Optimal design of structures subjected to follower forces*, Ingenieur – Archive, **49** (1980) 63 -71.

7. L. Tomski, *Obciążenia układów oraz układy swoiste. Rozdział 1: Drgania swobodne i stateczność obiektów smukłych jako układów liniowych lub nieliniowych.* Praca zbiorowa wykonana pod kierunkiem naukowym i redakcją L. Tomskiego, WNT, Fundacja „Książka Naukowo-Techniczna", Warszawa (2007) 17 – 46.

8. A. Kasprzycki, *Opis techniczny struktur obciążających kolumny*, rozdział 2, *Drgania swobodne i stateczność obiektów smukłych jako układów liniowych lub nieliniowych*, Praca zbiorowa wykonana pod kierunkiem naukowym i redakcją L. Tomskiego, WNT, Fundacja „Książka Naukowo-Techniczna", Warszawa, (2007) 47 – 60.

9. J. Szmidla, *Drgania swobodne i stateczność układów smukłych poddanych obciążeniu swoistemu*, Seria Monografie, Nr 165, Wydawnictwo Politechniki Częstochowskiej, Częstochowa (2009).

10. J. Szmidla, *Optymalny kształt kolumny obciążonej siłą śledzącą skierowaną do bieguna dodatniego*, Stability of Structures XII-th Symposium – Zakopane (2009) 387–394.

11. L. Tomski, M. Gołębiowska – Rozanow, A. Kasprzycki, *Rozdział 3.5: Stanowiska do badań drgań własnych kolumn*, Drgania i stateczność układów smukłych, Praca zbiorowa wykonana pod kierunkiem naukowym i redakcją L. Tomskiego, WNT, Fundacja „Książka Naukowo-Techniczna", Warszawa, (2004) 75 - 78.

Drgania swobodne kolumny o optymalnym kształcie ze względu na wartość obciążenia krytycznego poddanej obciążeniu siłą śledzącą skierowaną do bieguna dodatniego

W pracy przedstawia się wyniki obliczeń numerycznych i badań eksperymentalnych dotyczących drgań swobodnych kolumny realizującej obciążenie siłą śledzącą skierowaną do bieguna dodatniego - przypadek obciążenia swoistego. Biorąc pod uwagę model fizyczny układu oraz rozwiązanie konstrukcyjne głowicy realizującej obciążenie, formułuje się całkowitą energię mechaniczną kolumny. Na podstawie rozwiązania zagadnienia brzegowego, które uzyskuje się przy uwzględnieniu kinetycznego kryterium stateczności, prezentuje się przebieg krzywych zmian wartości własnych na płaszczyźnie: obciążenie – częstotliwość drgań własnych. Zakres zmian częstości drgań własnych wyznacza się przy wybranych wartościach parametrów geometrycznych głowicy realizującej obciążenie. Przyjęty do obliczeń numerycznych rozkład sztywności na zginanie kolumny odpowiada układom, dla których uzyskano maksymalne wartości obciążenia krytycznego, przy przyjętym warunku optymalizacyjnym stałej objętości struktury.

Free vibrations of a Γ type planar frame loaded by a follower force directed towards the positive pole

Janusz SZMIDLA

Technical University of Czestochowa, Institute of Mechanics and Machine Design
Foundations, ul. Dąbrowskiego 73, 42-200 Czestochowa
szmidla@imipkm.pcz.czest.pl

Abstract

Theoretical research into and numerical computations of free vibrations of a rectangular two rod frame for the chosen case of a specific load are presented in this paper. A column of the frame is loaded by a follower force directed towards the positive pole. The equations of motion and boundary conditions of the considered system are determined by taking into account the total mechanical energy and Hamilton's principle. The solution to the boundary problem leads to adequate relationships in changes in natural frequency in relation to the external load. The results of numerical computations are presented for the chosen physical and geometrical parameters of the system. The obtained results were verified on the basis of original experimental research.

Keywords: frame, specific load, free vibrations

1. Introduction

The free vibration problems of slender systems including planar frames are very significant from the point of view of mechanical structural designs. Theoretical and numerical research into the stability of planar frames was carried out for different types of loads. The determined values of critical load (comp. [1 − 4, 6]) and the course of changes in natural frequencies in relation to the external load (comp. [3 − 6]) at the accepted structural solutions of the systems were the results of the above research. The structures of frames in square form (Γ type) (comp. [1, 2, 5, 6]), three rod frames (**T** type) (comp. [1, 4]), or systems built up from a certain number of straight frames – portal frames (comp. [7]) have been considered in many scientific publications. The results of theoretical research into and numerical simulations of changes in natural frequency for the chosen cases of the conservative load for the planar frame were confirmed by experimental research in works [4, 6].

2. The physical model, mechanical energy of the system

Loading and mounting method of the considered system of Γ type is presented in Fig. 1. The frame consists of two rods with flexural rigidities (EJ_1), (EJ_2) and mass (ρA_1), (ρA_2) per unit length. A frame bolt with flexural rigidity (EJ_2) and a frame column with flexural rigidity (EJ_1) were mounted in rigid way. Additionally, the frame bolt is able to displace in longitudinal direction. The frame column is subjected to the one of specific load types formulated by L. Tomski (comp. [8]). In the considered case of the load by the follower force directed towards the positive pole (comp. [6, 8]), the rods of column and bolt were connected to a head, which received the load by a rigid element ③ with l_0

in length ensuring equality of the bending angles of the frame two elements. Direction of the loading force action crosses the constant point O − the centre of curvature of the loading ① and receiving ② heads, described by radius R. In the body of concentrated mass m, the total reduced mass of receiving head elements ②, ③ was taken into account.

Figure 1. The physical model of the system

Kinetic energy T of the considered flat frames is a sum of kinetic energy of individual rods of the frame and kinetic energy of element with concentrated mass m (transverse inertia towards the frame column) :

$$T = \sum_{i=1}^{2} \frac{(\rho A_i)}{2} \int_0^{l_i} \left[\frac{\partial W_i(x_i,t)}{\partial t} \right]^2 dx_i + \frac{m}{2} \left[\frac{\partial W_1(l_1,t)}{\partial t} \right]^2 \tag{1}$$

Bending elasticity of the individual rods of the system and the direction of the external load are taking into account in potential energy V :

$$V = \sum_{i=1}^{2} \frac{(EJ_i)}{2} \int_0^{l_i} \left[\frac{\partial^2 W_i(x_i,t)}{\partial x_i^2} \right]^2 dx_i - \frac{P}{2} \int_0^{l_1} \left[\frac{\partial W_1(x_1,t)}{\partial x_1} \right]^2 dx_1 + \frac{P(R-l_0)}{2} \left[\frac{\partial W_1(x_1,t)}{\partial x_1} \bigg|^{x_1=l_1} \right]^2 \tag{2}$$

3. Formulation of the problem, equations of motion, boundary conditions

The boundary problem is formulated on the basis of the kinetic criterion of the stability. This criterion relies on finding such a load at which free motion of the system stopped being restricted. Hamilton's principle is taken into consideration :

$$\delta \int_{t_1}^{t_2} (T - V)dt = 0 \tag{3}$$

Geometrical boundary conditions and continuity conditions are as follows :

$$W_1(0,t) = W_2(0,t) = \left.\frac{\partial W_1(x_1,t)}{\partial x_1}\right|_{x_1=0} = \left.\frac{\partial W_2(x_2,t)}{\partial x_2}\right|_{x_2=0} = 0, \tag{4a-d}$$

$$\left.\frac{\partial W_1(x_1,t)}{\partial x_1}\right|^{x_1=l_1} = \left.\frac{\partial W_2(x_2,t)}{\partial x_2}\right|^{x_2=l_2}, \; W_1(l_1,t) - (R-l_0)\left.\frac{\partial W_1(x_1,t)}{\partial x_1}\right|^{x_1=l_1} = 0 \tag{4e-f}$$

Geometrical relationship between elements of the loading head ① and receiving head ②, ③ (comp. Fig. 1) is given by equation 4f. After substituting equations (1), (2) into the Hamilton's principle (3), using adequate boundary conditions (4a-f), one can obtain :
- equations of motion

$$(EJ_1)\frac{\partial^4 W_1(x_1,t)}{\partial x_1^4} + P\frac{\partial^2 W_1(x_1,t)}{\partial x_1^2} + (\rho A_1)\frac{\partial^2 W_1(x_1,t)}{\partial t^2} = 0$$

$$(EJ_2)\frac{\partial^4 W_2(x_2,t)}{\partial x_2^4} + (\rho A_2)\frac{\partial^2 W_2(x_2,t)}{\partial t^2} = 0, \tag{5a-b}$$

- natural boundary conditions in the connection point of the column and the frame bolt $(x_1 = l_1, x_2 = l_2)$

$$\left.\frac{\partial^3 W_1(x_1,t)}{\partial x_1^3}\right|^{x_1=l_1} +$$

$$-\frac{1}{R-l_0}\left[\left.\frac{\partial^2 W_1(x_1,t)}{\partial x_1^2}\right|^{x_1=l_1} + \frac{(EJ_2)}{(EJ_1)}\left.\frac{\partial^2 W_2(x_2,t)}{\partial x_2^2}\right|^{x_2=l_2}\right] - \frac{m}{(EJ_1)}\frac{\partial^2 W_1(x_1,t)}{\partial t^2} = 0 \tag{6a}$$

$$\left.\frac{\partial^3 W_2(x_2,t)}{\partial x_2^3}\right|^{x_2=l_2} = 0 \tag{6b}$$

4. The results of numerical computations and experimental research

The constructional solution to the frame (comp. [6, 10]) loaded by the follower force directed towards the positive pole is presented in Fig. 2. Experimental research into the course of changes in natural frequency in relation to the external load was carried out by taking into account geometrical and physical parameters of the applied head realising the

load (R = 0.059 [m], l_0= 0.019 [m], m = 2.24 [kg]). The research was carried out on a stand designed and built in the Institute of Mechanics and Machine Design Foundations at Czestochowa University of Technology (comp. [9]). The frame is composed of bolts 6(3), 6(4) and columns 6(1), 6(2). The loading head (comp [11]) consists of an element (1) with mounted external ball race 9(1). An internal ball race 9(2) is mounted in enclosure (2) and attached to a rigid beam (10). The elements of receiving head are assumed to be infinitely rigid with regard to construction. The ends of the bolts 6(3), 6(4) and columns 6(1), 6(2) are attached to the beam (10) in such a way that bending angles of the frame rods are identical. Rigid support of the frame column is realized by element 5(1). Support structure of the frame bolt 5(2) is built of the beam (7) with mounted pivots of rolling bearings (8). The beam (7) can be shifted in guides (8) of mounting (4). Measurement of the loading force is realised by the dynamometer (3).
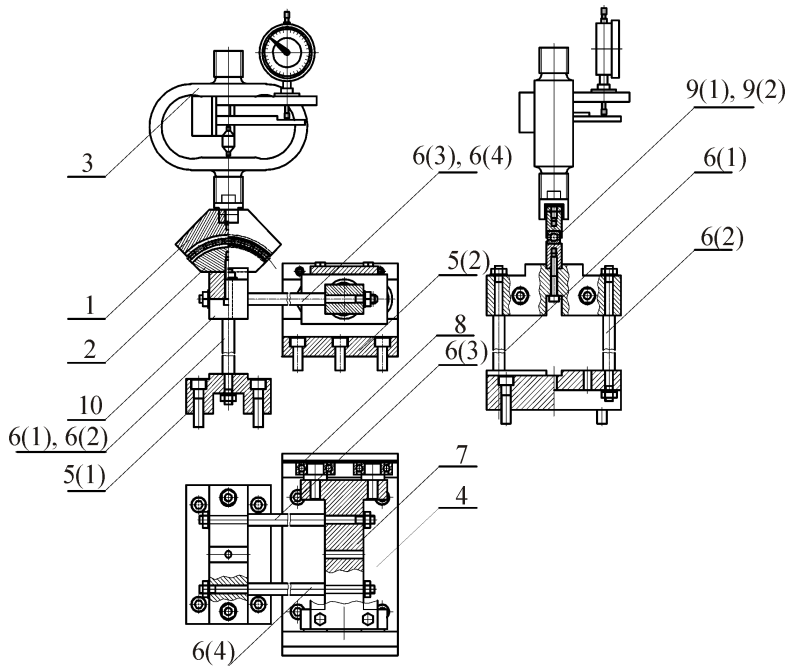

Figure 2. The constructional solution to the tested system

The results of numerical calculations (lines) and experimental research (points) are presented in Fig. 3 at the given geometrical and physical parameters of the frame elements (table 1). The range of the first three M1, M2, M3 natural frequencies f in relation to the external load P is also presented. The course of two additional natural frequencies for the column M2s[e] and the frame bolt M2r[e] was determined. The presence of additional natural frequencies, characterised by symmetrical form of the vibrations, is

connected to slender systems which component elements are built of even number of identical rods (comp. Fig. 2).

Table 1. Geometrical and physical parameters of the flat frame

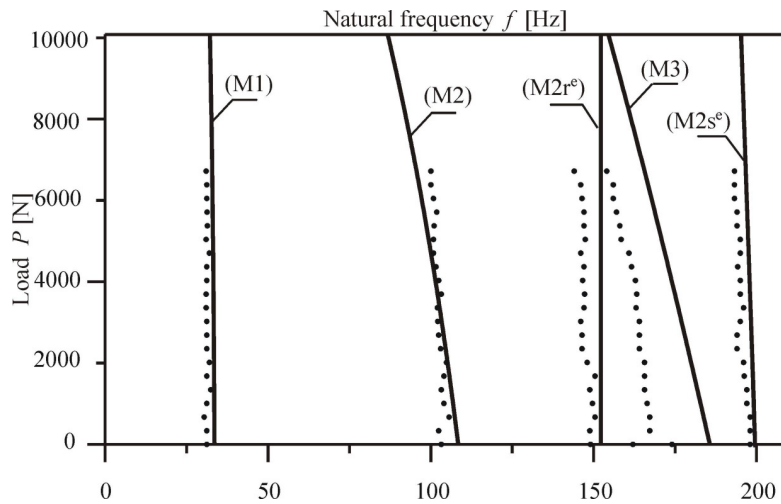| Quantity	Symbol	Unit	Value
Bending rigidity of the column	(EJ_1)	Nm^2	282.26
Bending rigidity of the bolt	(EJ_2)	Nm^2	152.68
Mass per unit length of the column	(ρA_1)	kg/m	0.859
Mass per unit length of the bolt	(ρA_2)	kg/m	0.631
The length of the column	l_1	m	0.59
The length of the bolt	l_2	m	0.61

Figure 3. Curves in the plane: load P – natural frequency of the system f

Conclusions

The flat frame, considered in this paper, is one of the two types of systems: a divergence or divergence pseudo-flutter, depending on the parameters of the loading head. The conducted experimental research confirmed the correctness of the assumed mathematical model of the system.

Acknowledgments

References

1. A. N. Kounadis, *Static stability analysis of elastically restrained structures under follower forces*, Amer., Inst. Aeron. Astr. J., **18(4)** (1980) 473 – 476.
2. N. S. Rallis, A. N. Kounadis, *Nonlinear sway – bucking of geometrically imperfect rectangular frames*, Ing. Arch., **55** (1985) 90 – 97.
3. L. Tomski, J. Przybylski, J. Szmidla, *Stability and vibrations of a two – bar frame under a follower force*, Zeit. Ang. Math, Mech., **S5(76)** (1996) 521 – 522.
4. J. Szmidla, *Vibrations and stability of T – type frame loaded by longitudinal force in relation to its bolt*. Thin Walled Structures **45** (2007) 931 – 935.
5. M.C. Albarraccin, R.O. Grossi, *Vibrations of elastically restrained frames*, Journal of Sound and Vibration **285** (2005) 467–476.
6. J. Szmidla, *Drgania swobodne i stateczność układów smukłych poddanych obciążeniu swoistemu*, Seria Monografie, Nr 165, Wydawnictwo Politechniki Częstochowskiej, Częstochowa (2009).
7. G. J. Simitses,. D. H. Hodges, *Fundamentals of Structural Stability, chapter 4: Buckling of frames*, Butterworth – Heinemann, Elsevier Inc., (2006).103-144.
8. L. Tomski, *Obciążenia układów oraz układy swoiste. Rozdział 1: Drgania swobodne i stateczność obiektów smukłych jako układów liniowych lub nieliniowych.* Praca zbiorowa wykonana pod kierunkiem naukowym i redakcją L. Tomskiego, Wydawnictwa Naukowo Techniczne, Fundacja „Książka Naukowo-Techniczna”, Warszawa (2007) 17 – 46.
9. L. Tomski, M. Gołębiowska – Rozanow, A. Kasprzycki, *Rozdział 3.5: Stanowiska do badań drgań własnych kolumn*, Drgania i stateczność układów smukłych, Praca zbiorowa wykonana pod kierunkiem naukowym i redakcją L. Tomskiego, Wydawnictwa Naukowo Techniczne, Fundacja „Książka Naukowo-Techniczna”, Warszawa, (2004) 75 - 78.
10. L. Tomski, J. Szmidla, A. Kasprzycki, *Wybrane rozwiązania konstrukcyjne ram płaskich poddanych obciążeniu konserwatywnemu*, XXIII Sympozjon Podstaw Konstrukcji Maszyn, Rzeszów – Przemyśl, (2007) 527 – 536.
11. A. Kasprzycki, *Opis techniczny struktur obciążających kolumny*, rozdział 2, *Drgania swobodne i stateczność obiektów smukłych jako układów liniowych lub nieliniowych*, Praca zbiorowa wykonana pod kierunkiem naukowym i redakcją L. Tomskiego, Wydawnictwa Naukowo Techniczne, Fundacja „Książka Naukowo-Techniczna”, Warszawa, (2007) 47 – 60.

Drgania swobodne ramy typu Γ obciążonej siłą śledzącą skierowaną do bieguna dodatniego
W pracy prezentuje się badania teoretyczne oraz obliczenia numeryczne dotyczące drgań swobodnych prostokątnej dwuprętowej ramy przy wybranym przypadku obciążenia swoistego. Słup ramy realizuje obciążenie siłą śledzącą skierowaną do bieguna dodatniego. Biorąc pod uwagę całkowitą energię mechaniczną układu oraz zasadę Hamiltona wyznacza się równania ruchu i warunki brzegowe rozpatrywanego układu. Rozwiązanie zagadnienia brzegowego prowadzi do odpowiednich zależności na zakres zmian wartości częstości drgań własnych w funkcji obciążenia zewnętrznego. Wyniki obliczeń numerycznych prezentuje się przy wybranych parametrach fizycznych i geometrycznych układu. Otrzymane rezultaty weryfikuje się na podstawie przeprowadzonych badań eksperymentalnych.

Transient and steady-state coupled electromechanical vibration analysis of the micro-drive system

Tomasz SZOLC

Institute of Fundamental Technological Research of the Polish Academy of Sciences
ul. Pawińskiego 5B, 02-106 Warsaw
tszolc@ippt.gov.pl
Faculty of Mechatronics of the Warsaw University of Technology
ul. Św. Andrzeja Boboli 8, 02-525 Warsaw
t.szolc@mchtr.pw.edu.pl

Andrzej POCHANKE

Faculty of Electrical Engineering of the Warsaw University of Technology
Pl. Politechniki 1, 00-661 Warsaw
andrzej.pochanke@ee.pw.edu.pl

Abstract

In the paper there is performed an analysis of transient and steady-state electro-mechanical vibrations of the laboratory micro-drive system driven by the stepping motor. The main purpose of these studies is to indicate significant differences between the dynamic responses obtained for the considered object regarded respectively as electro-mechanically coupled and uncoupled. These theoretical investigations are based on a hybrid structural model of the mechanical system as well as on the classical circuit model of the stepping motor. From the computational results it follows that these differences are qualitatively and quantitatively essential from the viewpoint of possibly precise and reliable operation of the micro-drive systems.

Keywords: Electro-mechanical vibrations, micro-drive system, stepping motor, hybrid model

1. Introduction

The drive systems of machines, vehicles as well as of precise micro-mechanisms are commonly driven by electric motors of various types, e.g. asynchronous motors, synchronous motors, direct-current motors or stepping motors. During nominal and steady-state operating conditions these motors generate more or less significant variable components of the electromagnetic torques which are sources of severe torsional vibrations of the entire mechanical drive system. The torsional vibrations of the drive system usually result in significant fluctuation of rotational speed of the rotor of the driving electric motor. Such oscillation of the angular velocity superimposed on the average rotor rotational speed cause more or less severe perturbation of the magnetic flux and thus additional oscillation of the electric currents in the motor windings. Then, the generated electromagnetic torque is also characterized by additional variable in time components which induce torsional vibrations of the drive system. According to the above, the mechanical vibrations of the drive system become coupled with the electrical vibrations of the currents in the motor windings. An importance of the electromechanical coupling effects taken into consideration is particularly severe when possibly very exact

simulation results are required for investigation of extremely responsible drive systems or for analyses of their sufficiently precise motions, realized by e.g. micro-drive systems, as well as in order to elaborate for them proper active vibration control algorithms.

In the presented paper there is studied an influence of electro-mechanical coupling effects on dynamic responses of the laboratory precise micro-drive system driven by the stepping motor. Since in such case a possibly exact rotational motion of the micro-mechanism must be assured, it is necessary to introduce sufficiently accurate models of the micro-drive system and of the electric motor, where dynamic electro-mechanical coupling effects are going to be taken into consideration. The fundamental purpose of this study is realized by investigation of dynamic interaction between the stepping motor and the micro-drive system during its start-ups, run-downs and steady-state operation.

2. Assumptions for the electromechanical model.

In the paper there is considered the laboratory micro-drive system driven by means of the stepping motor shown in Fig. 1. This system consists of the driving motor, direct-current micro-generator, rotational angle encoder, three elastic couplings of the Oldham-type, inertial disk representing a rotor of the power receiver (impeller), one-stage rubber teethed-belt gear and of the connecting shaft segments properly supported by the roll-bearings.
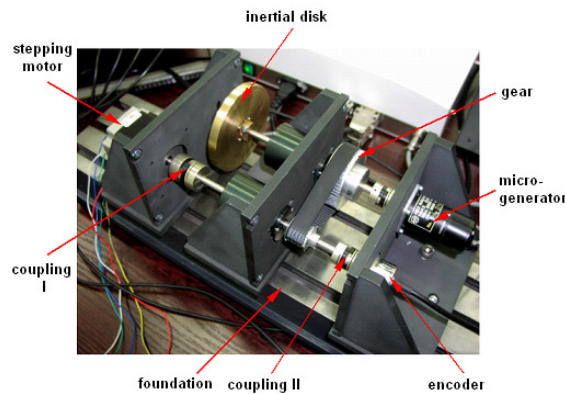

Figure 1. Laboratory micro-drive system

Since the fundamental excitations generated by the driving motor as well as the retarding torques produced by the power receivers are torsional in character, the torsional vibrations of the micro-drive system are going to be regarded as predominant. In order to perform a theoretical investigation of the electro-mechanical coupling effects in this system, a reliable and computationally efficient simulation model is required. In this paper dynamic investigations of the entire micro-drive system are performed by means of the one-dimensional hybrid structural model consisting of continuous visco-elastic macro-elements and rigid bodies. In this model by the torsionally deformable cylindrical macro-elements of continuously distributed inertial-visco-elastic properties

there are substituted successive cylindrical segments of the stepped shafts. The rigid bodies represent gear wheels as well as the rotors of the of the power receiver, micro-generator and of the rotational angle encoder, as presented in Fig. 2. Apart of numerical simulations of coupled electro-mechanical vibrations, this model is employed here also for torsional eigenvalue analysis of the drive train.
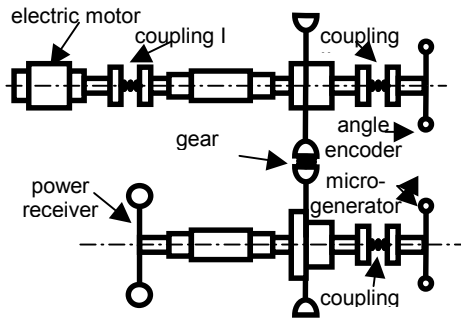

Figure 2. Hybrid mechanical model of the laboratory micro-drive system

Torsional motion of cross-sections of each visco-elastic macro-element is governed by the hyperbolic partial differential equations of the wave type. Mutual connections of the successive macro-elements creating the stepped shaft as well as their interactions with the rigid bodies are described by equations of boundary conditions. These equations enclose geometrical conditions of conformity for rotational displacements of the macro-element extreme cross-sections as well as linear conditions of equilibrium for external torques and for inertial, elastic and external damping moments. The solution for the forced vibration analysis has been obtained using the analytical-computational approach demonstrated in details e.g. in [1]. Solving the differential eigenvalue problem for the orthogonal system and an application of the Fourier solutions in the form of series lead to the set of modal equations in the Lagrange co-ordinates $\xi_m(t)$:

$$\ddot{\xi}_m(t) + (\beta + \tau\omega_m^2)\dot{\xi}_m(t) + \omega_m^2\xi_m(t) = \frac{1}{\gamma_m^2}Q_m(t), \quad m = 0,1,2,\dots , \quad (1)$$

where ω_m are the successive natural frequencies of the drive system, β denotes the coefficient of external damping assumed here as proportional one to the modal masses γ_m^2, τ is the shaft material retardation time and $Q_m(t)$ are the modal external excitations.

In the considered micro-drive system there is applied a quite typical four-cycle, double-phase stepping motor with the fundamental step angle 1.8 deg, which means that its rotor is characterized by Z_r=50 poles. According e.g. to [2], the mathematical model of such stepping motor is described by two voltage equations:

$$L_0\frac{di_1(t)}{dt} + Ri_1(t) - K_U\Omega(t)\cdot\sin\left(\Theta_E(t)\right) = -U(t)\cdot\mathrm{sgn}\left\{\sin\left(\Theta_E(t)\right)\right\},$$

$$L_0\frac{di_2(t)}{dt} + Ri_2(t) + K_U\Omega(t)\cdot\cos\left(\Theta_E(t)\right) = U(t)\cdot\mathrm{sgn}\left\{\cos\left(\Theta_E(t)\right)\right\}, \quad (2)$$

where $i_1(t)$, $i_2(t)$ denote the electric currents in both motor phases, L_0 is the phase inductance, R denotes the resistance of each phase, K_U is the motor voltage constant, $\Omega(t)$ denotes the instantaneous angular velocity of the rotor, $U(t)$ is the slowly varying control voltage and $\Theta_E(t)$ denotes the rotor electric angle. The electromagnetic torque generated by the double-phase stepping motor is expressed by the following formula

$$T_E(t) = K_T\left[-i_1(t)\cdot\sin\left(\Theta_E(t)\right)+i_2(t)\cdot\cos\left(\Theta_E(t)\right)\right], \qquad (3)$$

where K_T denotes the stepping motor torque constant. Assuming a uniform distribution of the motor electromagnetic torque along the rotor, by the use of the virtual work principle the modal external excitations for the hybrid discrete-continuous model of the considered micro-drive system have been determined in the following form

$$Q_m(t) = \frac{T_E(t)}{l_2}\cdot\int_0^{l_2} X_{2m}(x)\,\mathrm{d}x - M_{18}(t)\cdot X_{18,m}(0) - M_{28}(t)\cdot X_{28,m}(l_{28}), m = 0,1,2,\ldots, (4)$$

where $X_{2m}(x)$ denotes the local m-th eigenfunction of the macro-element (2) corresponding to the electric motor rotor, $X_{18,m}(0)$, $X_{28,m}(l_{28})$ are the m-th eigenfunction values for the model cross-sections to which there are imposed the retarding torques $M_{18}(t)$ and $M_{28}(t)$ generated by the power receiver and the micro-generator, respectively.

By substituting expression (3) into (4) and (1) and upon a proper combinations of the modal equations (1) with the voltage equations (2) one obtains the coupled set the parametric ordinary differential equations

$$\mathbf{M}\ddot{\mathbf{r}}(t) + \mathbf{C}\left(\Theta_E(t)\right)\cdot\dot{\mathbf{r}}(t) + \mathbf{K}\left(\Theta_E(t)\right)\cdot\mathbf{r}(t) = \mathbf{F}(t,\dot{\mathbf{r}}(t)), \qquad (5)$$

where: $\mathbf{C}\left(\Theta_E(t)\right) = \mathbf{C}_0 + \mathbf{C}_E\left(\Theta_E(t)\right)$, $\qquad \mathbf{K}\left(\Theta_E(t)\right) = \mathbf{K}_0 + \mathbf{K}_E\left(\Theta_E(t)\right)$,

$$\mathbf{r}(t) = \mathrm{col}\left[i_1(t),i_2(t),\xi_0(t),\xi_1(t),\xi_2(t),\ldots\right],$$

$$\mathbf{F}(t,\dot{\mathbf{r}}(t)) = \begin{bmatrix} -U(t)\cdot\mathrm{sgn}\left\{\sin\left(\Theta_E(t)\right)\right\} \\ U(t)\cdot\mathrm{sgn}\left\{\cos\left(\Theta_E(t)\right)\right\} \\ -\kappa\left(M_{18}(t)+M_{28}(\dot{\mathbf{r}}(t))\right) \\ -X_{18,1}(0)\cdot M_{18}(t)-X_{28,1}(l_{28})\cdot M_{28}(\dot{\mathbf{r}}(t)) \\ -X_{18,2}(0)\cdot M_{18}(t)-X_{28,2}(l_{28})\cdot M_{28}(\dot{\mathbf{r}}(t)) \\ \ldots \end{bmatrix}.$$

The symbols $\mathbf{M}$, $\mathbf{C}_0$ and $\mathbf{K}_0$ denote respectively the constant diagonal modal mass, damping and stiffness matrices, $\mathbf{C}_E(\Theta_E(t))$ is the band matrix of the inductant-electro-magnetic effects and $\mathbf{K}_E(\Theta_E(t))$ denotes the band matrix of the resistant-electro-magnetic effects, both of periodically variable coefficients with the electric rotation frequency $Z_r\Omega(t)$. The symbol $\mathbf{F}(t, \mathbf{r}'(t))$ denotes the external excitation vector due to the control input voltage and the retarding torques. The unknown co-ordinate vector $\mathbf{r}(t)$ consists of the electric currents in both motor phases and of the unknown time functions $\xi_m(t)$ in the Fourier solutions. In order to obtain the system's dynamic response Eqs. (5) are solved

by means of a direct integration. The number of equations (5) corresponds to the number of eigenmodes taken into consideration in the range of frequency of interest. These equations are mutually coupled by the parametric terms corresponding to the electromagnetic interaction with the stepping motor. A fast convergence of the applied Fourier solutions enables us to reduce the appropriate number of the modal equations to solve, in order to obtain a sufficient accuracy of results in the given range of frequency.

3. Computational example

In the computational example there is performed a simulation of the run-up, steady state operation and run-down of the considered geared micro-drive system shown in Fig.1 and driven by means of the stepping motor of the nominal voltage and current 4.8 V and 1.5 A, respectively, and the maximal braking torque 0.8 Nm, where the reduction gear ratio is equal to 1:3. This mechanical system of the entire mass moment of inertia reduced to the motor axis $9.34 \cdot 10^{-5}$ kgm^2 has been uniformly accelerated from its standstill to the constant average rotational speed 300 rpm within 3 s in order to operate for next 1 s under the constant retarding torque 0.35 Nm generated by the micro-generator. Then, within successive 3 s the micro-drive was uniformly stopped back to the standstill.

In order to study the influence of electro-mechanical coupling effects on the considered system dynamic response, the numerical simulation of the assumed above motion has been carried out in the form of two modes: For the coupled electro-mechanical mode the full system of equations (5) was solved. In the case of the uncoupled mode only the first three equations (5) have been solved, i.e. two electrical equations coupled with the third one describing the rigid body motion of the drive train. Then, using (3) the electromagnetic torque 'a priori' determined and substituted into the modal equations (1) in the form of an external excitation of the mechanical system torsional vibrations. In Fig. 3 by the black and grey lines, respectively for the coupled and uncoupled mode, there are presented time history plots of the stepping motor electro-magnetic torques. From this figure it follows that in the case of coupled mode the driving torque generated by the motor is characterized by greater fluctuation during run-up and run-down phase than in the case of the uncoupled mode. However, during the steady-state operation the latter has greater amplitudes of predominant frequency close to the first system natural frequency equal103.4 Hz. In Fig. 4 there are shown plots of
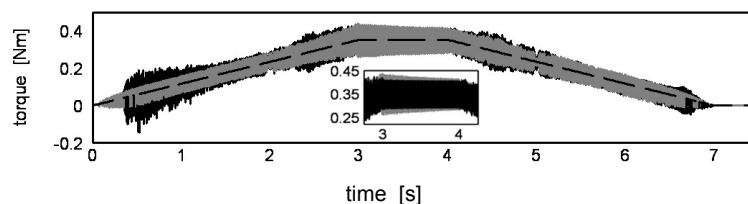

Figure 3. The retarding (dashed line) and electro-magnetic torque in the coupled (black line) and uncoupled (grey line) electro-mechanical system
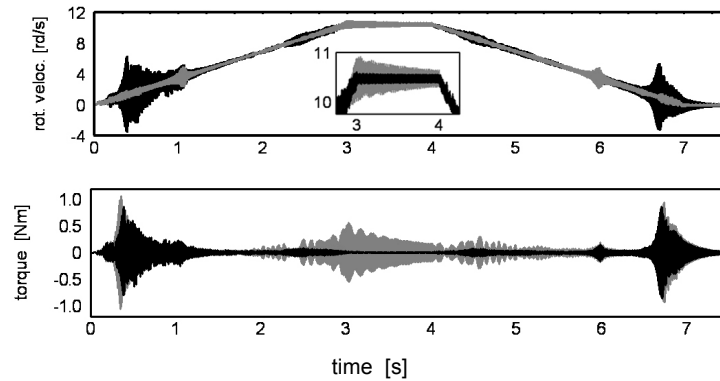
Figure 4. The rotational velocity and the dynamic torque in the coupled (black line) and uncoupled (grey line) electro-mechanical system

the system dynamic response corresponding appropriately, i.e. by the black and grey lines, to both compared modes of the problem solutions. In this figure the time histories of the angular velocity and of the dynamic torque in the shaft at the input to the power receiver are depicted. Here, the significant differences of the transient fluctuations of the velocity and of the steady-state oscillations of the dynamic torque are worth noting.

4. Conclusions

The performed investigations enabled us to indicate essential qualitative and quantitative differences between the computational results obtained using the coupled and uncoupled modes of the vibrating electro-mechanical micro-drive system. The electromagnetic torque generated by the stepping motor is characterized by more regular time history in the case of the traditional uncoupled mode. Then, the induced resonant effects during steady-state operation are artificially more severe than in the case of the much realistic coupled mode, where the velocity dependent parametric coupling terms result in significantly greater transient states and weaker or even negligible resonant responses.

References

1. T. Szolc, *On the discrete-continuous modeling of rotor systems for the analysis of coupled lateral-torsional vibrations,* Int. J. of Rot. Machinery. **6**(2), (2000) 135–149
2. R. Sochocki, *Mikromaszyny electryczne,* Warsaw Univ. Techn. Eds., Warsaw 1996

Analiza przejściowych i ustalonych sprzężonych drgań elektro-mechanicznych w układzie mikro-napędu

W pracy przeprowadzono analizę przejściowych i ustalonych elektro-mechanicznych drgań laboratoryjnego układu mikro-napędowego napędzanego silnikiem skokowym. Głównym celem badań było wykazanie różnic odpowiedzi dynamicznych układu potraktowanego jako elektro-mechanicznie sprzężonego i rozsprzężonego. Rozważań teoretycznych dokonano dzięki zastosowaniu hybrydowego modelu układu mechanicznego oraz klasycznego obwodowego modelu silnika skokowego. Uzyskane jakościowe i ilościowe znaczące różnice badanych odpowiedzi są istotne z punktu widzenia precyzyjnego działania układów mikro-napędowych.

Instability and free vibrations of a geometrically non-linear cantilever column with imperfections subjected to Euler's load

Lech TOMSKI

Technical University of Częstochowa, Institute of Mechanics and Machine Design
Foundations, ul. Dąbrowskiego 73, 42–200 Częstochowa
sekr@imipkm.pcz.czest.pl

Iwona PODGÓRSKA-BRZDĘKIEWICZ

Technical University of Częstochowa, Institute of Mechanics and Machine Design
Foundations, ul. Dąbrowskiego 73, 42–200 Częstochowa
iwonapb@imipkm.pcz.czest.pl

Abstract

The paper deals with the stability problem, longitudinal bending and free vibrations of a geometrically non-linear cantilever column loaded by Euler's load. Imperfections, resulting from the omission of the assumption that the external load is perfectly axially applied, were taken into account in the physical model of the column. An initial curvature of the rods was introduced. The problem of free vibrations and stability was formulated on the basis of Hamilton's principle and then solved by applying the small parameter method. Local or global instability of the system specified by free vibrations (the plane: load – natural frequency) is presented in the first part of the paper. The second part concerns the influence of imperfections in shape and load on the stability of the system. The interactions between the introduced imperfections were analysed.

Keywords: column, free vibrations, initial imperfections, local and global instability

1. Introduction

Theoretical considerations and solutions of numerical computations referring to stability and transverse free vibration geometrically non-linear columns, subjected to Euler's load are included in many scientific publications [1-9]. Distinguished are to be works dealt with:
− rectilinear form of static equilibrium (determination of bifurcation force) [1-7, 9],
− curvilinear form of static equilibrium (determination of critical force) [3, 7, 8, 9],
− local and global non-stability [5-7],
− pre-stressing of the system [3, 4, 6, 7],
− course of characteristic curves in the plane: load – natural frequency [3, 4, 6, 7, 9],
− influence of eccentrically fixed external loads [8, 9].
In works [6, 7] are presented results of experimental research dealing with the vibration frequencies in relation to the external load, which confirms local and global non-stability of geometrically nonlinear column.

2. The physical model of the column

A geometrically non-linear column N and linear column L, subjected to Euler's load are considered in this paper. The physical models of these columns are presented in Fig. 1.

The initial curvature of the system described by function $W_0(x)$ was introduced. Innacuracy in the external load application was modelled by introducing the eccentric action of a force with value dentoted as e. The geometrically non-linear column was built of three rods with a symmetrical distribution of flexural rigidity $(EJ)_i$, compression rigidity $(EA)_i$ and mass per unit length $(\rho A)_i$ (for $i = 1\div3$),while:

$$(EJ)_1 = (EJ)_2, \ (EA)_1 = (EA)_2, \ (\rho A)_1 = (\rho A)_2 \tag{1}$$

Rods of the system are rigidly mounted for $x = 0$ and connected to each other in point $x = l$ with the help of the body with mass m in such a way that transverse and longitudinal displacements and bending angles of every rods are identical. Linear column L was only built of two rods with total bending rigidity $(EJ)_1+(EJ)_2$ compression rigidity $(EA)_1+(EA)_2$ (without the middle rod). Flexural rigidity asymmetry factor μ is defined during description of the stability of a geometrically non-linear column N assuming that sum of flexural rigidity of rods is constant:

$$\mu = \frac{(EJ)_3}{(EJ)_1 + (EJ)_2}, \ \sum_{i=1}^{3}(EJ)_i = const \tag{2}$$

The rigidity of rods of column L is the same as for rods with indexes 1, 2 of column N at the assumed flexural rigidity asymmetry of the geometrically non-linear column described by coefficient μ.
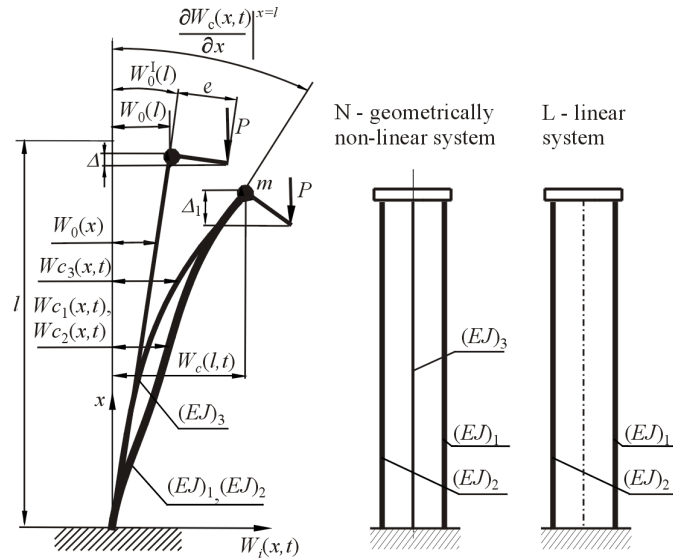

Figure 1. The physical model of geometrically non-linear column N

Total transverse deflection of the i–th rod of the system was denoted as: $Wc_i(x,t) = W_0(x) + W_i(x,t)$, while function of the initial deflection was accepted in the form: $W_0(x) = \alpha x$. Longitudinal displacements of the system were determined by relationships: $\Delta = e \ W_0^1(l)$, $\Delta_1 = e \ Wc_1^1(l,t)$.

3. Mechanical energy of the system, equations of motion, boundary conditions

The problem of stability and vibrations is formulated on the basis of Hamilton's principle. Kinetic energy T is a sum of kinetic energy of its individual rods and kinetic energy of mass m:

$$T = \frac{1}{2}\sum_{i=1}^{3}\int_0^l (\rho_0 A)_i \left[\frac{\partial Wc_i(x,t)}{\partial t}\right]^2 dx_i + \frac{1}{2}m\left[\frac{\partial Wc_1(l,t)}{\partial t}\right]^2 \tag{3}$$

The total potential energy V consists of energies of: internal forces, bending elasticity and action of the external load components:

$$V = \frac{1}{2}\sum_{i=1}^{3}(EJ)_i\int_0^l\left[\frac{\partial^2 Wc_i(x,t)}{\partial x^2}\right]^2 dx + PU_1(l) +$$

$$+ \frac{1}{2}\sum_{i=1}^{3}(EA)_i\int_0^l\left[\frac{\partial U_i(x)}{\partial x} + \frac{1}{2}\left(\frac{\partial Wc_i(x)}{\partial x}\right)^2\right]^2 - P(\Delta_1 - \Delta) \tag{4}$$

Taking into account equations (3) and (4) in Hamilton's principle, using commutation of integration (over x and t) and variation computation, the equations of motion of the considered system in transverse (5a) and longitudinal (5b) directions were obtained:

$$(EJ)_i\frac{\partial^4 Wc_i(x,t)}{\partial x^4} + S_i(t)\frac{\partial^2 Wc_i(x,t)}{\partial x^2} + (\rho A)_i\frac{\partial^2 Wc_i(x,t)}{\partial t^2} = 0, \tag{5a}$$

$$\frac{\partial}{\partial x}\left[\frac{\partial U_i(x)}{\partial x} + \frac{1}{2}\left(\frac{\partial Wc_i(x)}{\partial x}\right)^2\right] = 0, \quad i = 1, 2, 3 \tag{5b}$$

Known geometrical boundary conditions of the considered system, after taking into account relationships describing function $W_0(x)$ and its adequate derivatives:

$$W_1(0,t) = W_2(0,t) = W_3(0,t) = U_1(0,t) = U_2(0,t) = U_3(0,t) = 0,$$

$$\left.\frac{\partial W_1(x,t)}{\partial x}\right|_{x=0} = \left.\frac{\partial W_2(x,t)}{\partial x}\right|_{x=0} = \left.\frac{\partial W_3(x,t)}{\partial x}\right|_{x=0} = 0,$$

$$W_1(l,t) = W_2(l,t) = W_3(l,t), U_1(l,t) = U_2(l,t) = U_3(l,t),$$

$$\left.\frac{\partial W_1(x,t)}{\partial x}\right|^{x=l} = \left.\frac{\partial W_2(x,t)}{\partial x}\right|^{x=l} = \left.\frac{\partial W_3(x,t)}{\partial x}\right|^{x=l} \tag{6}$$

considered in the Hamilton's principle, make it possible to obtain the remaining conditions necessary to solve the problem:

$$\sum_{i=1}^{3}(EJ)_i\frac{\partial^2 W_i(x,t)}{\partial x^2}\Bigg|^{x=l} - Pe = 0 \ , \quad \sum_{i=1}^{3}S_i(t) - P = 0$$

$$\sum_{i=1}^{3}(EJ)_i\frac{\partial^3 W_i(x,t)}{\partial x^3}\Bigg|^{x=l} + P\left[\frac{\partial W_1(x,t)}{\partial x}\Bigg|^{x=l} + \alpha\right] - m\frac{\partial^2 W_1(l,t)}{\partial t^2} = 0$$

(7)

The problem of stability and free vibrations of a geometrically non-linear column L was solved by applying the small parameter method. The values of bifurcation force were determined on the basis of solution to equations of displacements. Transcendental equation for natural frequency ω was obtained substituting the solutions to motion equations into boundary conditions after previous separation of variables in terms of time and displacement.

4. Results of numerical computations and experimental research

The results of research into the stability were partly worked out on the basis of work [7]. Diagram of changes in bifurcation load of column N and in critical load parameter of column L in relation to flexural rigidity asymmetry function μ is presented in Fig. 2. The value of external load, concentrated mass and obtained values of bifurcation load and natural frequencies are expressed in dimensionless way:

$$\lambda_c^* = \frac{P_C l^2}{\sum_{i=1}^{3}(EJ)_i}, \ \lambda^* = \frac{Pl^2}{\sum_{i=1}^{3}(EJ)_i}, \ \Omega^* = \frac{\sum_{i=1}^{3}(\rho A)_i \omega_0^2 l^4}{\sum_{i=1}^{3}(EJ)_i}, \ m^* = \frac{m}{l\sum_{i=1}^{3}(\rho A)_i}$$

(8)

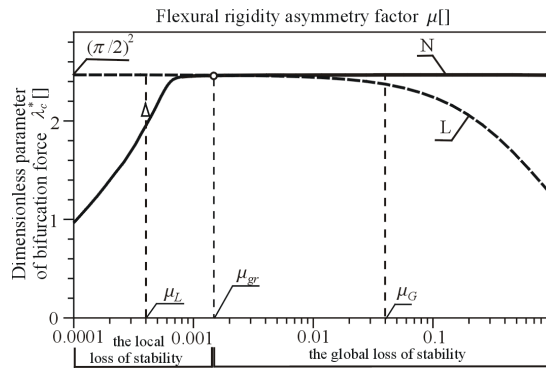Figure 2. The value of dimensionless parameter of bifurcation force λ_c^* in relation to flexural rigidity asymmetry factor μ

For coefficient value μ_L in the range of changes from 0 to μ_{gr}, parameter of bifurcation force λ_c^* for geometrically non-linear column N is lowest than for linear column L. Increase in parameter λ_c^* is obtained by removal of the rod with flexural rigidity $(EJ)_3$ from the system. The global loss of stability takes place at the coefficient value $\mu > \mu_{gr}$.

Numerical computations of changes in value of natural frequency in relation to the external load was carried out for the geometrically non-linear system characterised by the local stability loss and corresponded to it linear system. The results of numerical computations are presented in Fig. 3.

Table 1. Geometrical and physical parameters of the column

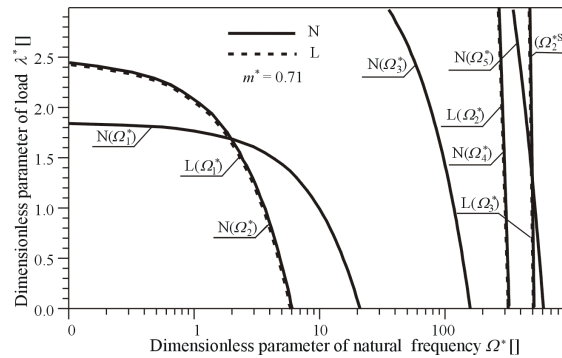| Quantity	Symbol	Unit	Value for $i= 1,2$	Value for $i= 3$
Flexural rigidity of the i–th rod	$(EJ)_i$	Nm^2	792.4	0.568
Mass per unit length	$(\rho A)_i$	kg/m	0.598	0.012
Flexural rigidity asymmetry factor	μ	/	0.00036	

Figure 3. The curves in the plane: loading parameter λ^* – natural frequency parameter Ω^*

The results of numerical computations and experimental research into the stability and natural vibrations as well as influence of imperfection in form and load on instability of the system will be presented during Symposium.

5. Conclusions

The considered system, being dependent on the value of the distribution of flexural rigidity asymmetry factor, is characterised by a local or global loss of stability. The term with lower flexural rigidity is responsible for the local loss of stability.

Acknowledgments

References

1. M. H. R, Godley, A. H Chilver: *Elastic Buckling of Overbraced Frames*, J. Mech. Eng. Sci. **12(4)** (1970) 238 – 247.
2. L. Tomski, *Prebuckling Behaviour of Compound Column – Direct Nonlinear Analysis*, ZAMM, Z. Angew. Math. U. Mech. **65(1)** (1985) 59 – 61.
3. J. Przybylski, L. Tomski, *Vibration of an Initially Prestressed Compound Column under Axial Compression*, Elsevier Science Publishers B.V. (1992), 263 – 268.
4. J. Przybylski, L. Tomski, M. Gołębiowska – RozanowM, *Free Vibration of an Axially Loaded Prestressed PlanarFrame*, J. of Sound and Vibration 89(5) (1996) 609 – 624.
5. L. Tomski, J. Szmidla, *Stateczność lokalna i globalna oraz drgania przesztywnionej kolumny Eulera*, IX Sympozjum Stateczności Konstrukcji, Zakopane 25-29.09. (2000) 299 – 304.
6. L. Tomski, J. Szmidla, *Local and global instability and vibration of overbraced Euler's column*, J. of Theoretical and Applied Mechanics **41(1)** (2003) 137 – 154.
7. L. Tomski, J. Przybylski, J. Szmidla, S. Uzny, *Drgania i stateczność układów smukłych geometrycznie nieliniowych*, rozdział 9.3, *Drgania i stateczność układów smukłych*, Praca zbiorowa wykonana pod kierunkiem naukowym i redakcją L. Tomskiego, Wydawnictwa Naukowo Techniczne, Fundacja „Książka Naukowo-Techniczna", Warszawa (2004) 288 – 306.
8. L. Tomski, S. Kukla, *Free Vibrations of a Certain Geometrically Nonlinear System with Iniital Imperfection*. AIAA, **28(7)** (1990) 1240 – 1245.
9. J. Przybylski, *Stateczność i drgania kolumny złożonej jako układu geometrycznie nieliniowego* (praca doktorska – promotor L. Tomski), Politechnika Częstochowska, Częstochowa 1987.
10. L. Tomski, I. Podgórska-Brzdękiewicz, *Wyboczenie globalne oraz interakcja imperfekcji kształtu i obciążenia słupa przy obciążeniu eulerowskim lub siłą skierowaną do bieguna dodatniego*, XII Sympozjum Stateczności Konstrukcji, Zakopane (2009) 443 – 450.

**Niestateczność i drgania kolumny wspornikowej, geometrycznie nieliniowej
z imperfekcjami poddanej obciążeniu eulerowskiemu**

Praca dotyczy zagadnienia stateczności, podłużnego zginania i drgań swobodnych wspornikowej, geometrycznie nieliniowej kolumny poddanej obciążeniu eulerowskiemu. W modelu fizycznym kolumny uwzględniono niedokładność wynikającą z pominięcia założenia idealnie osiowego przyłożenia obciążenia zewnętrznego oraz wprowadzono wstępną krzywiznę prętów. Zagadnienie drgań własnych i stateczności sformułowano na podstawie zasady Hamiltona, a następnie rozwiązano wykorzystując metodę małego parametru. W pierwszej części pracy, poprzez drgania swobodne (płaszczyzna: obciążenie – częstość drgań własnych) opisana jest niestateczność lokalna lub globalna układu. Druga część pracy dotyczy wpływu imperfekcji kształtu i obciążenia na stateczność układu. Analizuje się interakcje wprowadzonych imperfekcji.

Divergence and flutter instability of a column subjected to Reut's generalized load with regard to rotational elasticity

Lech TOMSKI

Częstochowa University of Technology, Institute of Mechanics and Machine Design Foundations, ul. Dąbrowskiego 73, 42-200 Częstochowa
sekr@imipkm.pcz.czest.pl

Janusz SZMIDLA

Częstochowa University of Technology, Institute of Mechanics and Machine Design Foundations, ul. Dąbrowskiego 73, 42-200 Częstochowa
szmidla@imipkm.pcz.czest.pl

Sebastian UZNY

Częstochowa University of Technology, Institute of Mechanics and Machine Design Foundations, ul. Dąbrowskiego 73, 42-200 Częstochowa
uzny@imipkm.pcz.czest.pl

Abstract

Boundary problem of free vibrations of an elastically mounted slender system subjected to Reut's generalized load is formulated in the paper. A finite elasticity of kinematic pair connecting column to beam was considered. The beam was directly affected by external load. On the basis of the kinetic stability criterion, critical load of divergence and flutter type was determined for different rigidities of the kinematic pair connecting the column to the beam. The boundary value of the rigidity dividing the divergence and flutter instability area and the characteristics curves in the plane load – natural frequency were also determined. Computations were carried out using different parameters of the considered system including: coefficient describing the place of external force application, rigidity of mounting, and rigidity of the kinematic pair connecting the column to the beam.

Keywords: Flutter instability, divergence instability, column,

1. Introduction

All systems, loosing stability due to divergence instability or flutter instability in dependence on values of parameters were called hybrid systems by Leipholz [1]. Parameters, having influence on the method of stability loss, are as follows: structural parameters and parameters connected to application of the load. Translational springs [2, 3, 4, 5, 6], rotational springs (comp.[2, 3]), systems of viscoelastic and elastoplastic dumpers [7, 8], and the concentrated mass [9] are the structural parameters. Flexural rigidity asymmetry factor [10] and initial pre-stressing [11, 12] are the structural parameters in the case of complex slender systems. Major parameter defining character of load is a load following factor [4, 10, 13] (Beck's generalized load) and coefficient describing the place of load application (Reut's generalized load) [10]. Reut's generalized load is coupled with Beck's generalized load [14].

2. Formulation of boundary problem

The considered system is presented in fig. 1. The column is elastically mounted (rigidity of mounting C_o) and subjected to Reut's generalized load . The place of external force application is determined by η coefficient. Additionally, the finite rigidity of kinematic pair connecting the column to the beam was considered in the system, while the beam was directly affected by the external load. Rigidity of the kinematic pair connecting the column to the beam was modelled by the rotational spring with rigidity C.
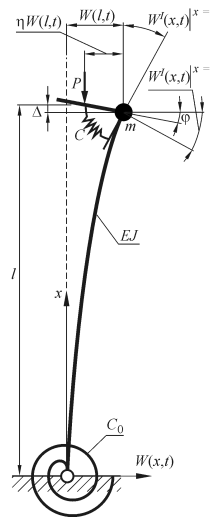

Fig. 1. Diagram of the considered system

The described above system is a hybrid system and the kinetic criterion of stability was used to determine the critical load. The boundary problem regarded free vibrations of the system was formulated on the basis of Hamilton's principle:

$$\delta \int_{t_1}^{t_2} \left(T - V + L_n \right) dt = 0 \tag{1}$$

where: T – kinetic energy, V – potential energy, L_n – work of non-conservative forces.

$$T = \frac{1}{2} \rho A \int_0^l \left(\frac{\partial W(x,t)}{\partial t} \right)^2 dx + \frac{1}{2} m \left(\frac{\partial W(x,t)}{\partial t} \bigg|^{x=l} \right)^2 \tag{2}$$

$$V = \frac{1}{2} EJ \int_0^l \left(\frac{\partial^2 W(x,t)}{\partial x^2} \right)^2 dx - \frac{1}{2} P \int_0^l \left(\frac{\partial W(x,t)}{\partial x} \right)^2 dx +$$

$$+ \frac{1}{2} C \left(\frac{\partial W(x,t)}{\partial x} \bigg|^{x=l} - \varphi \right)^2 + \frac{1}{2} C_0 \left(\frac{\partial W(x,t)}{\partial x} \bigg|_{x=0} \right)^2 \tag{3}$$

$$L_n = -P\eta W(l,t)\varphi \tag{4}$$

Equations describing the kinetic (2) and potential (3) energies and work of non-conservative forces (4) were substituted into Hamilton's principle (1). After application of geometrical boundary conditions:

$$W(0,t) = 0 \tag{5}$$

the following was obtained:
− angle φ equation

$$\varphi = \left.\frac{\partial W(x,t)}{\partial x}\right|^{x=l} - \frac{P\eta}{c}W(l,t) \tag{6}$$

− the natural boundary conditions

$$EJ\left.\frac{\partial^2 W(x,t)}{\partial x^2}\right|_{x=0} - C_0\left.\frac{\partial W(x,t)}{\partial x}\right|_{x=0} = 0 \tag{7}$$

$$EJ\left.\frac{\partial^2 W(x,t)}{\partial x^2}\right|^{x=l} + P\eta W(l,t) = 0 \tag{8}$$

$$EJ\left.\frac{\partial^3 W(x,t)}{\partial x^3}\right|^{x=l} + P\left.\frac{\partial W(x,t)}{\partial x}\right|^{x=l} + \frac{P^2\eta^2}{C}W(l,t) - m\left.\frac{\partial^2 W(x,t)}{\partial t^2}\right|^{x=l} = 0 \tag{9}$$

− differential equation of motion

$$EJ\frac{\partial^4 W(x,t)}{\partial x^4} + P\frac{\partial^2 W(x,t)}{\partial x^2} + \rho A\frac{\partial^2 W(x,t)}{\partial t^2} = 0 \tag{10}$$

By separating the variables using the relationship:

$$W(x,t) = Y(x)\cos(\omega t) \tag{11}$$

the differential equation was obtained, which must be fulfilled in the range $x \in (0, l)$ and at every time of interval t:

$$\frac{d^4 Y(x)}{dx^4} + k^2\frac{d^2 Y(x)}{dx^2} - \Omega^2 Y(x) = 0 \tag{12}$$

where: $\qquad k^2 = P/EJ \;;\; \Omega^2 = \rho A\omega^2/EJ$

Substituted formula (11) into the equations (5) and (7-9) the boundary conditions were obtained, which must be fulfilled by solution to equation (12).

The solution to equation (12) is as follows:

$$Y(x) = D_1\cosh(\alpha x) + D_2\sinh(\alpha x) + D_3\cos(\beta x) + D_4\sin(\beta x) \tag{13}$$

where: $\qquad \alpha = \sqrt{-0.5k^2 + \sqrt{0.25k^4 + \Omega^2}} \;,\; \beta = \sqrt{0.5k^2 + \sqrt{0.25k^4 + \Omega^2}}$

Taking into account solution (13) in the boundary conditions, the system of equations is obtained where determinant of matrix coefficient equated to zero is a transcendental equation for natural frequency:

$$\left|a_{ij}\right| = 0 \tag{14}$$

On the basis of equation (14) one can determine the relationships between the load and natural frequency. The critical divergence load takes place when the first natural frequency equals zero ($\omega_1 = 0$). The critical flutter load is when the first natural frequency equals the second natural frequency ($\omega_1 = \omega_2$).

3. Results of numerical computations

Figure 2 presents dimensionless parameter of the critical load in dependence on dimensionless parameter of the rigidity of rotational spring. This spring is present in kinematic pair connecting the column to the beam. If coefficient η is in the range $\eta \in (0.5 - 1.0)$ for spring rigidity values $c = c_{gr}$, "snap through" occurs - from critical divergence force to critical flutter force.
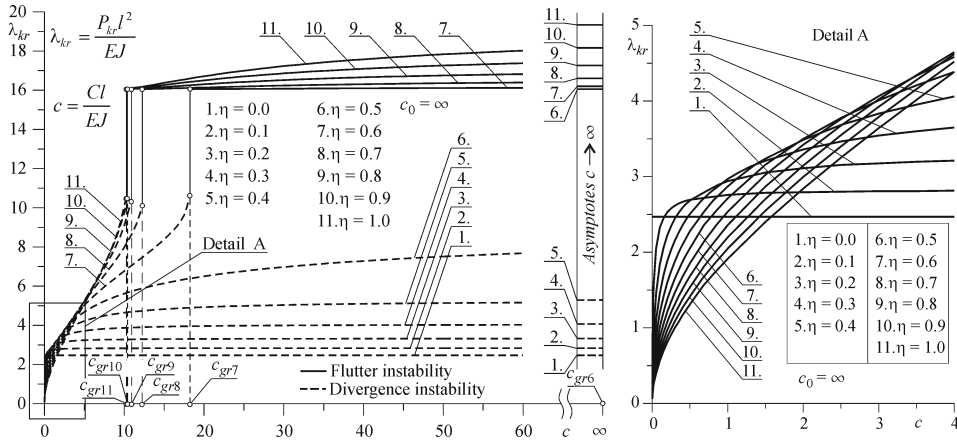

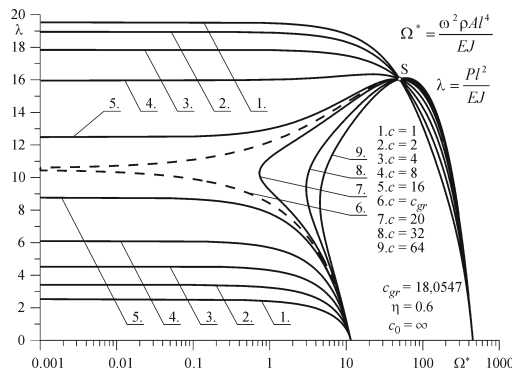Fig. 2. The critical load in dependence on rigidity C

Fig. 3. The characteristics curves in the plane: load – natural frequency.

Exemplary characteristic curves in the plane: load − natural frequency are presented in figure 3. The characteristic curves, independent on the rigidity value of rotational spring *C,* are intersecting in the one point (fig. 3 − point S).

4. Summary

In the paper the critical load of a column subjected to Reut's generalized load was determined on the basis of the kinetic criterion of stability. The finite rigidity of kinematic pair connecting the column to the beam was considered. Divergence and flutter instability areas were dependent on rigidity of kinematic pair connecting the column to the beam, rigidity of system mounting and on coefficient describing the place of load application. The characteristic curves in the plane: load − natural frequency were determined. Numerical computations were carried out for different values of the parameters characterizing the considered system.

Acknowledgments

References

1. Leipholz H.: *Aspects of Dynamic Stability of Structures*, Journal of the Engineering Mechanics Division, April 1975, EM2, 109−124.
2. Kounadis A.N.: *Divergence and flutter instability of elastically restrained structures under follower forces*, Int. J. Engng. Sci. 19(4), 1981, 553-562.
3. Kounadis A.N.: *The existence of regions of divergence instability for nonconservative systems under follower forces*, Int. Journal Solids Structures 19(8), 1983, 725−733.
4. Ryu J.B., Sugiyama Y., Yim K.B., Lee G.S.: *Dynamic stability of an elastically restrained column subjected to triangulary distributed subtangential forces*, Computers & Structures 76, 2000, 611−619.
5. Sundararajan C.: *Influence of an elastic end support on the vibration and stability of Beck's column*, Int. J. Mech. Sci. 18, 1976, 239−241.
6. Tomski L., Przybylski J.: *Static Instability of an Elastically Restrained Cantilever Under a Partial Follower Force*. AIAA Journal 23(10), 1985, 1637−1639.
7. Bogacz R., Mahrenholtz O.: *Modal analysis in application to design of inelastic structures subjected to circulatory loading*, Proc. of EUROMECH 174, Colloq. on „Inelastic structures under variable loads", Palermo, 1983, 378−388.
8. Bogacz R., Mahrenholtz O.: *Multi-Modal Analysis of Critical Forces on Tangentially Loaded Structures*, ZAMM, Vol. 64, 1984, 34−36.

9. Leipholz H., Piche R.: *Stability of follower-force rods with weight*, J. Eng. Mech. Div., ASCE, 110(3), 1984, 367-379.

10. Przybylski J.: *Vibrations and stability of initially prestressed two-member rod systems under nonconservative load*, Publishing House of Częstochowa University of Technology, series Monographs, Nr 92, Częstochowa, 2002, (in Polish).

11. Przybylski J.: *Instability regions of a prestressed compound column subjected to a follower force*, Journal of Theoretical and Applied Mechanics, 37(1), 1999, 147-162.

12. Przybylski J.: *The role of prestressing in establishing regions of instability for a compound column under conservative or nonconservative load*, Journal of Sound and Vibration, 231(2), 2000, 291-305.

13. Tomski L., Kukla S., Posiadała B., Przybylski J., Sochacki W.: *Divergence and Flutter Instability of the Column Supported by a Nonlinear Spring and Loaded by a Partially Follower Force*, Akademiai Kiado, Publishing House of Hungarian Academy of Science, Budapest, 1990, 1227–1234.

14. Nemat-Nasser S., Herrmann G.: *Adjoint Systems in Nonconservative Problems of Elastic Stability*, AIAA Journal 4(12), 1966, 2221-2222.

Niestateczność dywergencyjna i flatterowa kolumny poddanej uogólnionemu obciążeniu Reuta z uwzględnieniem sprężystości rotacyjnej

W pracy sformułowano zagadnienie brzegowe dotyczące drgań własnych sprężyście zamocowanego smukłego układu poddanego obciążeniu uogólnionemu Reuta. Uwzględniono skończoną sprężystość węzła łączącego kolumnę z belką, na którą oddziałuje bezpośrednio siła zewnętrzna. Na podstawie kinetycznego kryterium stateczności wyznaczono obciążenie krytyczne zarówno dywergencyjne jak i flatterowe rozważanego układu przy różnych sztywnościach węzła łączącego kolumnę i belkę. Wyznaczono również graniczną wartość sztywności rozdzielającą obszary niestateczności dywergencyjnej i flatterowej oraz krzywe charakterystyczne na płaszczyźnie obciążenie − częstość drgań własnych. Badania numeryczne wykonano przy różnych parametrach rozważanego układu. Parametrami układu są: współczynnik określający miejsce przyłożenia siły zewnętrznej, sztywność zamocowania oraz sztywność węzła łączącego kolumnę z belką.

Chosen slender systems in aspect of possibility of specific load realization

Lech TOMSKI

Częstochowa University of Technology, Institute of Mechanics and Machine Design Foundations, ul. Dąbrowskiego 73, 42-200 Częstochowa, sekr@imipkm.pcz.czest.pl

Sebastian UZNY

Częstochowa University of Technology, Institute of Mechanics and Machine Design Foundations, ul. Dąbrowskiego 73, 42-200 Częstochowa, uzny@imipkm.pcz.czest.pl

Abstract

Slender system is considered in the paper. While using this system two cases of specific load (generalized load with the force directed toward the positive pole and load by follower force directed toward the positive pole) occur at the same realization of the load. These two cases of the specific load exist at determined values of rigidity of rotational spring which is mounted in the considered system. The rotational spring generating adequate case of the specific load is mounted in kinetic pair connected infinite rigid elements. Infinite rigid elements create loading system. Constructional diagram of the considered system is presented in this work and theoretical and numerical research into free vibrations and stability in dependence on geometrical and physical parameters as well as on a location of kinetic pair with the rotational spring was carried out.

Keywords: divergence instability, column, free vibration, specific load

1. Introduction

Specific load for the first time was formulated and introduced to literature by L. Tomski in 1994 (comp. [1]). Two basic kind of specific load are presented: generalized load with the force directed toward the pole (comp. [1, 2, 3]) (positive or negative) and load by follower force directed toward the pole (comp. [4, 5, 6]) (positive or negative). Realization of the considered load is possible by usage of appropriately designed loading heads built of linear or circular elements. Geometrical parameters of heads loading the specific load have an influence on a critical force as well as on natural frequency. One can obtain new course of characteristic curves in the plane: load – natural frequency appropriately selecting mentioned above parameters. These curves have been called by L. Tomski and R. Bogacz as the curves of divergence pseudoflutter type (comp. [7]).

2. Formulation of the boundary problem

The system, considered in this work, is presented in fig. 1b. This system is loaded by properly designed loading heads built of linear elements. Additionally, rotational spring, with the rigidity C modelling the finite rigidity of the considered kinetic pair, is placed in kinetic pair which joins rigid elements with l_D and l_C in length respectively. At limiting value of rigidity of spring C ($C = 0$ and $1/C = 0$), two classical cases of the specific load

are obtained. If $C = 0$, the slender system is subjected to generalized load with the force directed toward the positive pole (fig. 1a). If $1/C = 0$ (infinite rigid element with $l_D + l_C$ in length), the slender system is subjected to a load by follower force directed toward the positive pole (fig. 1c).
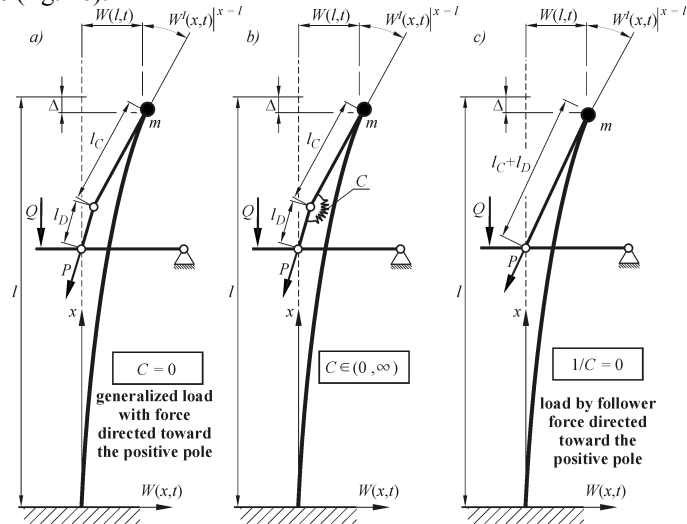

Fig. 1. Diagram of the considered system

Boundary problem of free vibrations of the considered system is formulated on the basis of the Hamilton's principle:

$$\delta \int_{t_1}^{t_2} (T - V) dt = 0 \tag{1}$$

where: T – kinetic energy, V – potential energy.

$$T = \frac{1}{2} \rho A \int_0^l \left(\frac{\partial W(x,t)}{\partial t} \right)^2 dx + \frac{1}{2} m \left(\frac{\partial W(x,t)}{\partial t} \bigg|^{x=l} \right)^2 \tag{2}$$

$$V = \frac{1}{2} EJ \int_0^l \left(\frac{\partial^2 W(x,t)}{\partial x^2} \right)^2 dx - \frac{1}{2} P \int_0^l \left(\frac{\partial W(x,t)}{\partial x} \right)^2 dx +$$

$$+ \frac{1}{2} P l_C \left(\frac{\partial W(x,t)}{\partial x} \bigg|^{x=l} \right)^2 + \frac{1}{2} P \frac{1}{l_D} \left(W(l,t) - \frac{\partial W(x,t)}{\partial x} \bigg|^{x=l} \right)^2 + \tag{3}$$

$$+ \frac{1}{2} C \left(\frac{\partial W(x,t)}{\partial x} \bigg|^{x=l} - \frac{1}{l_D} \left(W(l,t) - \frac{\partial W(x,t)}{\partial x} \bigg|^{x=l} l_C \right) \right)^2$$

The equations determining kinetic energy (2) and potential energy (3) are substituted into the Hamilton's principle (1). After giving consideration to the geometrical boundary conditions:

$$W(0,t) = \frac{\partial W(x,t)}{\partial x}\bigg|_{x=0} = 0 \tag{4}$$

the following equations were obtained:
− differential equation of motion

$$EJ\frac{\partial^4 W(x,t)}{\partial x^4} + P\frac{\partial^2 W(x,t)}{\partial x^2} + \rho A\frac{\partial^2 W(x,t)}{\partial t^2} = 0 \tag{5}$$

− natural boundary conditions

$$EJ\frac{\partial^2 W(x,t)}{\partial x^2}\bigg|^{x=l} + \left(P\frac{l_C}{l_D} - C\frac{l_C + l_D}{l_D^2}\right)\left((l_C + l_D)\frac{\partial W(x,t)}{\partial x}\bigg|^{x=l} - W(l,t)\right) = 0 \tag{6}$$

$$EJ\frac{\partial^3 W(x,t)}{\partial x^3}\bigg|^{x=l} + \left(P\frac{1}{l_D} + C\frac{1}{l_D^2}\right)\left((l_C + l_D)\frac{\partial W(x,t)}{\partial x}\bigg|^{x=l} - W(l,t)\right) - $$

$$- m\frac{\partial^2 W(x,t)}{\partial t^2}\bigg|^{x=l} = 0 \tag{7}$$

Separation of variables with the help of relationship:

$$W(x,t) = Y(x)\cos(\omega t) \tag{8}$$

leads into differential equation, which must be fulfilled in the range $x \in (0, l)$:

$$\frac{d^4 Y(x)}{dx^4} + k^2\frac{d^2 Y(x)}{dx^2} - \Omega^2 Y(x) = 0 \tag{9}$$

where: $k^2 = P/EJ$; $\Omega^2 = \rho A\omega^2/EJ$

Substituting formulae (8) into the equations (4), (6, 7), the boundary conditions were obtained, which must fulfil the solution to equation (9).

The solution to equation (9) is presented as follows:

$$Y(x) = D_1\cosh(\alpha x) + D_2\sinh(\alpha x) + D_3\cos(\beta x) + D_4\sin(\beta x) \tag{10}$$

where: $\alpha = \sqrt{-0.5k^2 + \sqrt{0.25k^4 + \Omega^2}}$, $\beta = \sqrt{0.5k^2 + \sqrt{0.25k^4 + \Omega^2}}$

After considering the solution (10) in the boundary conditions, the system of equations was obtained where determinant of matrix of coefficient was equated to zero. This is the transcendental equation for natural frequency:

$$|a_{ij}| = 0 \tag{11}$$

Relationships between the load and natural frequency was determined on the basis of the equation (11). The critical load occurs when the first natural frequency is equal to zero (the kinetic criterion of stability $\omega_1 = 0$).

3. The results of numerical computations

Dimensionless parameter of the critical load in dependence on a rigidity of spring C was presented in fig. 2. Numerical calculations was carried out for different values of the parameter ζ_B (ζ_B = 0.01; 0.25; 0.5; 0.75; 0.9) and for parameter ζ_A = 0.5. The parameters ζ_A i ζ_B were defined in a way presented in Fig. 2.
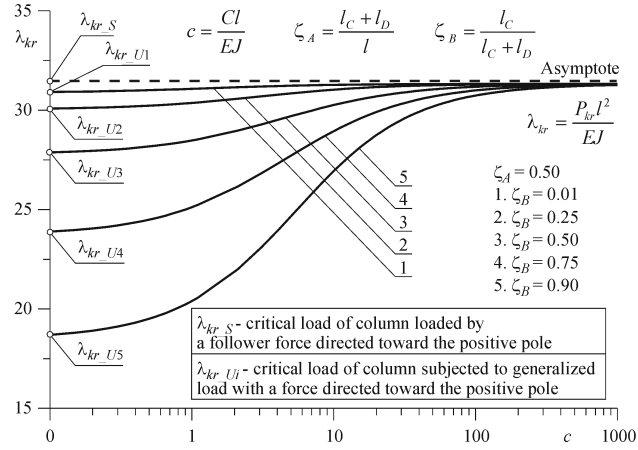

Fig 2. Dimensionless parameter of the critical load λ_{kr} in dependence on dimensionless parameter of the rigidity of spring c
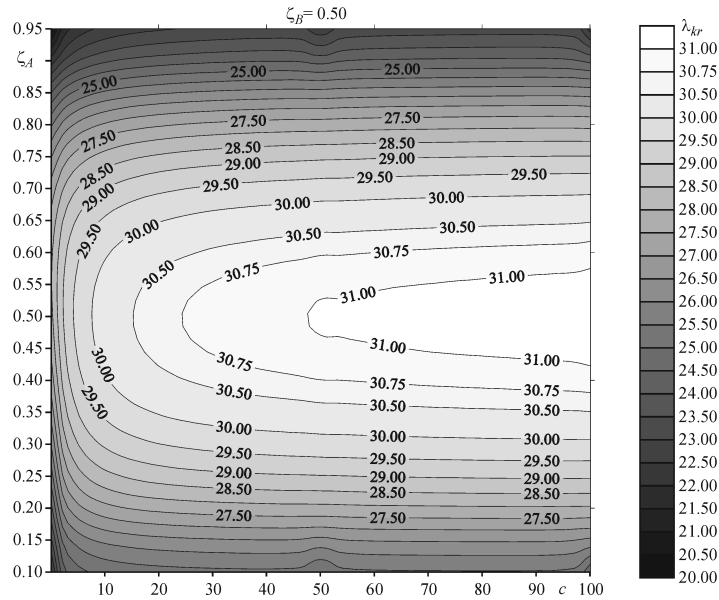

Fig. 3. Parameter of the critical load λ_{kr} in relation to parameters c and ζ_A at ζ_B = 0.5

Maximum differences in the value of critical force with changes in the spring rigidity was observed at higher value of parameter ζ_B. Dimensionless parameter of the critical load in dependence on rigidity parameter of spring c and parameter ζ_A was presented in fig. 3. In computations it was assumed that length l_C and l_D were identical. Maximum critical load was when sum of length $l_C + l_D$ was equal to a half of the column length ($\zeta_A = 0.5$) (independently on rigidity of spring C).
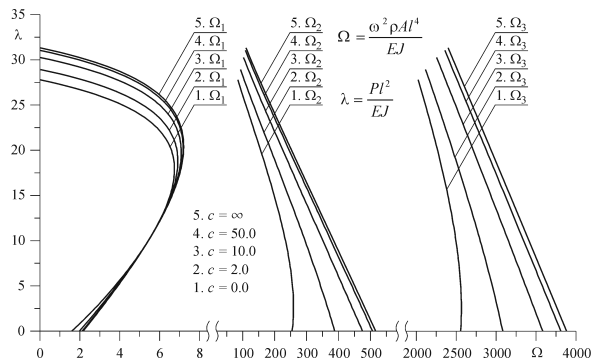

Fig. 4. The characteristic curves in the plane: load − natural frequency

Exemplary characteristic curves in the plane: load − natural frequency were presented in fig. 4.

4. Summary

The critical load of a column subjected to compression load generated by adequately constructed system built of linear elements was determined in this paper. Rigidity of kinetic pair, in which rigid bolts were connected, was taken into consideration. The rigid bolts made loading system. The rigidity of the kinetic pair was modelled by a rotational spring with rigidity C. Generalized load with the force directed toward the positive pole and load by follower force directed toward the positive pole was obtained by selecting boundary values of the spring rigidity ($C = 0$ and $1/C = 0$, respectively). The characteristic curves in the plane: load − natural frequency were also determined in this work. Numerical computations were carried out at different parameters of the considered system.

Acknowledgments

References

1. Tomski L., Gołębiowska-Rozanow M., Szmidla J.: *Free Vibration of a Column Loaded by a Force and Bending Moment*, XVI Symposium „Vibrations in Physical Systems", Poznań - Błażejewko, May 26-28, 1994, 317-319.

2. Tomski L., Szmidla J.: *Vibration and Stability of Column Subjected to Generalised Load by a Force Directed Towards a Pole*, Journal of Theoretical and Applied Mechanics, 2004, 163-193.

3. Tomski L., Uzny S., *Vibration and stability of geometrically non-linear column subjected to a force directed towards the positive pole*, International Journal of Structural Stability and Dynamics, 8, 1, 2008,

4. Tomski L., Przybylski J., Gołębiowska-Rozanow M., Szmidla J.: *Vibration and stability of a cantilever column subject to a follower force passing through a fixed point*, Journal of Sound and Vibration, 214, 1, 1998, 67-81

5. Tomski L., Szmidla J., Gołębiowska-Rozanow M.: *Vibrations and Stability of a Two-Rod Column Loaded by A Sector of a Rolling Bearing*, Journal of Theoretical and Applied Mechanics 42, 4, Warsaw 2004, 905-926.

6. Tomski L., Uzny S., *Free vibration and the stability of a geometrically non-linear column loaded by a follower force directed towards the positive pole*, International Journal of Solids and Structures, 45, 2008, 87-112.

7. Bogacz R., Imiełowski Sz., Tomski L.: *Stability and Vibration of Column Structures Subjected to Generalized Concentrated Load*, Theoretical and Experimental Study, Dynamics of Continua – International Symposium, Physikzentrum Bad Honnef, 9 - 13 September 1996, 45-54.

Wybrane układy smukłe w aspekcie możliwości realizacji obciążenia swoistego

W pracy rozważaniom poddano pewien układ smukły, za pomocą którego przy tej samej realizacji obciążenia generuje się dwa przypadki obciążenia swoistego (obciążenie uogólnione z siłą skierowaną do bieguna dodatniego oraz obciążenie siłą śledzącą skierowaną do bieguna dodatniego). Te dwa typy obciążenia swoistego występują przy określonych wartościach sztywności sprężyny rotacyjnej umiejscowionej w rozważanym układzie. Sprężyna rotacyjna, za pomocą której generuje się odpowiedni przypadek obciążenia swoistego znajduje się węźle łączącym nieskończenie sztywne rygle wchodzące w skład układu wywołującego obciążenie. W pracy zaprezentowany zostanie schemat konstrukcyjny rozpatrywanego układu oraz przeprowadzone zostaną badania teoretyczne i numeryczne dotyczące drgań swobodnych i stateczności w zależności od parametrów geometrycznych i fizycznych oraz w zależności od położenia przegubu ze sprężyną rotacyjną.

An investigation of functionally graded material parameters effects on free torsional vibrations of a bar using meshfree methods

Anita USCILOWSKA

Institute of Applied Mechanics, Poznan University of Technology
ul Piotrowo 3, 60-965 Poznan, POLAND
anita.uscilowska@put.poznan.pl

Agnieszka FRASKA

Institute of Applied Mechanics, Poznan University of Technology
ul Piotrowo 3, 60-965 Poznan, POLAND
agnieszka.fraska@put.poznan.pl

Abstract

This paper describes the application of the method of fundamental solutions to the solution of the initial-boundary value problems of the dynamic torsion of functionally graded rods. The time derivation is approximated by finite differences method. For the obtained by this way boundary value problem the interpolation of an inhomogeneous term in governing equation is done by the radial basis function. The very basic step of the calculations of dynamics of rod torsion is solution of boundary value problem with the method of fundamental solutions.

Keywords: Method of fundamental solutions; Radial basis functions; Functionally graded materials

1. Introduction

Functionally graded materials (FGMs) are materials with continuously varying material properties designed for specific engineering applications. FGMs have recently been applied in variety of fields, including aircraft, aerospace and automobile technologies.

Although the torsion problem for homogeneous linearly elastic bars is a classical one in the elasticity, there has been relatively little attention for case when material is inhomogeneous. Recently, research activity on functionally graded materials has stimulated investigation also on the torsion problem for inhomogeneous material. In 1964 Chen presented a study on torsion of inhomogeneous bars [1]. He presented governing equations and boundary conditions of the torsion problem of inhomogeneous bars in terms of stress function. Then, he applied a semi-inverse method and found a specific distribution for shear modulus of rigidity in a specific geometry of cross section. By this method, he could find simple solutions for stress function and torsional stiffness of circular and elliptical shafts. An analytical formulation for torsional analysis of functionally graded elastic bars with circular cross sections was presented by Horgan and Chan [3]. They supposed the shear modulus of rigidity to be a function of radius, just as in [2]. Using the axisymmetric geometry of the cross section of the circular bar, they found an exact analytical solution. The Saint-Venant's torsion problem of linearly elastic, isotropic, non-homogeneous cylindrical bars was considered in paper [4]. The novelty of this paper is that the shear modulus of the investigated non-homogeneous bar

is a given function of the Prandtl's stress function of a homogeneous bar, which has the same cross-sections as considered non-homogeneous bar.

In paper [5] an analytical formulation was presented for torsion of functionally graded hollow tubes of arbitrary shape. Authors assumed that thicknesses of all segments of the cross section are the same and shear modulus of rigidity changes continuously across the thickness. In this way the simple but relatively accurate formulas for stresses and torsional stiffness were obtained on the base of analytical integration of governing equation for stress function.

As the above short review shows, by far, the uniform torsion problem of functionally graded materials has been solved by analytical methods and traditional mesh methods such as FEM [5], and FED [6]. The purpose of this paper is the application of Method of Fundamental Solutions (MFS) to the dynamic torsion problem of functionally graded materials. This method belongs to so-called meshless methods which have been more and more popular in the two last decades. The MFS was first proposed by the Georgian researchers Kupradze and Aleksidze [7]. Its numerical implementation was carried out by Mathon and Johnston [8]. The comprehensive reviews of the MFS for various applications can be found in [9-10].

2. Formulation of the problem

We consider an infinitely long cylinder with a solid circular cross-section of radius a. The displacement components in the cylindrical coordinates are u_r, u_θ, u_z and the components of stress are σ_{rr}, $\sigma_{r\theta}$, σ_{rz}, etc. The torsional waves propagating in a cylinder involve only a u_θ - circumferential displacement which is independent of θ.

The dynamical torsions of cylinder made with functionally graded materials in the axi-symmetric case is described by the equation (given in [12]):

$$G(r)\left(\frac{\partial^2}{\partial r^2} + \frac{1}{r}\frac{\partial}{\partial r} - \frac{1}{r^2} + \frac{\partial^2}{\partial z^2}\right)u_\theta + \frac{\partial G(r)}{\partial r}\left(\frac{\partial}{\partial r} - \frac{1}{r}\right)u_\theta = \rho\frac{\partial^2 u_\theta}{\partial t^2} \tag{1}$$

for $(r,z)\in\Omega$ and $t\geq 0$, where $\Omega = \{(r,z): 0\leq r\leq a,\ z\in\Re\}$, $G(r)$ is a shear modulus of functionally graded material.

The initial conditions are defined as:

$$u_\theta(r,z,t_0) = u_o(r,z) \tag{2}$$

and

$$\left.\frac{\partial u_\theta(r,z,t)}{\partial t}\right|_{t=t_0} = \dot{u}_0(r,z) \tag{3}$$

for $(r,z)\in\Omega$.

The cylindrical surface is free of tractions which gives boundary condition:

$$\sigma_{r\theta}(a,z,t) = \left(G(r)\left(\frac{\partial}{\partial r} - \frac{1}{r}\right)u_\theta(r,z,t)\right)\Bigg|_{r=a} = 0 \text{ for } (r,z)\in\partial\Omega \tag{4}$$

where $\partial\Omega$ is the boundary of the region Ω.

Also we assume that the displacement at $r = 0$ is finite.

3. Numerical approach

The considered problem is solved in the time period (t_0, t_{MAX}), which is descretized. And the solution is obtained in chosen time steps t_i, where $i = 0,1,2,...,N$ and $t_N = t_{MAX}$. The time subinterval has length $h = t_i - t_{i-1}$ for $i = 1,2,...,N$. For every time step the time derivation is approximated by finite difference (see [11]) as

$$\left.\frac{\partial^2 u_\theta(r,z,t)}{\partial t^2}\right|_{t=t_i} = \frac{u_\theta(r,z,t_{i-2}) - 2u_\theta(r,z,t_{i-1}) + u_\theta(r,z,t_i)}{h^2} \text{ for } i = 2,3,...N. \tag{5}$$

So, the initial-boundary problem (1-4) is written as a boundary value problem in axi-symmetric case

$$G(r)\left(\frac{\partial^2}{\partial r^2} + \frac{1}{r}\frac{\partial}{\partial r} - \frac{1}{r^2} + \frac{\partial^2}{\partial z^2}\right)u_\theta(r,z,t_i) + \frac{\partial G(r)}{\partial r}\left(\frac{\partial}{\partial r} - \frac{1}{r}\right)u_\theta(r,z,t_i) - \rho\frac{u_\theta(r,z,t_i)}{h^2} =$$
$$= \rho\frac{u_\theta(r,z,t_{i-2}) - 2u_\theta(r,z,t_{i-1})}{h^2} \tag{6}$$

for $(r,z) \in \Omega$, and

$$\left.\left(G(r)\left(\frac{\partial}{\partial r} - \frac{1}{r}\right)u_\theta(r,z,t_i)\right)\right|_{r=a} = 0 \text{ for } (r,z) \in \partial\Omega \tag{7}$$

for $i = 2,3,...N$.

To start the calculations, the solution of the boundary value problem (6, 7) for $t = t_2$ has to be obtained. The equation for this case is:

$$G(r)\left(\frac{\partial^2}{\partial r^2} + \frac{1}{r}\frac{\partial}{\partial r} - \frac{1}{r^2} + \frac{\partial^2}{\partial z^2}\right)u_\theta(r,z,t_2) + \frac{\partial G(r)}{\partial r}\left(\frac{\partial}{\partial r} - \frac{1}{r}\right)u_\theta(r,z,t_2) - \rho\frac{u_\theta(r,z,t_2)}{h^2} =$$
$$= \rho\frac{u_\theta(r,z,t_0) - 2u_\theta(r,z,t_1)}{h^2} \tag{8}$$

for $(r,z) \in \Omega$.

The quantities $u_\theta(r,z,t_0)$, $u_\theta(r,z,t_1)$ are described by the initial conditions. So, $u_\theta(r,z,t_0)$ is directly given by equation (2). To obtain $u_\theta(r,z,t_1)$ the finite difference of first order is applied as:

$$\left.\frac{\partial u_\theta(r,z,t)}{\partial t}\right|_{t=t_0} = \frac{u_\theta(r,z,t_1) - u_\theta(r,z,t_0)}{h} \tag{9}$$

and finally from equation (3) and (9) the solution for t_1 is given by

$$u_\theta(r,z,t_1) = h\dot{u}_\theta(r,z) + u_\theta(r,z,t_0). \tag{10}$$

For the next time step i.e. $t = t_3$ the governing equation (6) has the form

$$G(r)\left(\frac{\partial^2}{\partial r^2}+\frac{1}{r}\frac{\partial}{\partial r}-\frac{1}{r^2}+\frac{\partial^2}{\partial z^2}\right)u_\theta(r,z,t_3)+\frac{\partial G(r)}{\partial r}\left(\frac{\partial}{\partial r}-\frac{1}{r}\right)u_\theta(r,z,t_3)-\rho\frac{u_\theta(r,z,t_3)}{h^2}=$$

$$=\rho\frac{u_\theta(r,z,t_1)-2u_\theta(r,z,t_2)}{h^2}$$

(11)

for $(r,z)\in\Omega$.

The $u_\theta(r,z,t_1)$ is defined by formula (10) and $u_\theta(r,z,t_2)$ is the solution of the boundary value problem (8, 7).

The equation (6) is the linear one with variable coefficient. The proposal of this paper is to solve the equation in an iterative procedure. The equation (6) is rewritten in the iterative fashion as

$$G(r)\left(\frac{\partial^2}{\partial r^2}+\frac{1}{r}\frac{\partial}{\partial r}-\frac{1}{r^2}+\frac{\partial^2}{\partial z^2}\right)u_\theta^{(j)}(r,z,t_i)-\rho\frac{u_\theta^{(j)}(r,z,t_i)}{h^2}=$$

$$=\rho\frac{u_\theta(r,z,t_{i-2})-2u_\theta(r,z,t_{i-1})}{h^2}-\frac{\partial G(r)}{\partial r}\left(\frac{\partial}{\partial r}-\frac{1}{r}\right)u_\theta^{(j-1)}(r,z,t_i)$$

for $(r,z)\in\Omega$ (12)

which is the modified Helmholtz equation in axi-symmetric case.

For the equation (12) the boundary condition (7) has form:

$$\left(G(r)\left(\frac{\partial}{\partial r}-\frac{1}{r}\right)u_\theta^{(j)}(r,z,t_i)\right)\Bigg|_{r=a}=0 \text{ for } (r,z)\in\partial\Omega .$$

(13)

So, at each iteration at every time step the boundary value problem is to solve. The problem is described by inhomogeneous modified Helmholtz equation in axi-symmetric case and the boundary condition. This problem is solved by the Method of Fundamental Solutions (MFS) supported by the approximation with Radial Basis Functions (RBF) (see Ref. [13]).

Lets write the equation (12) in a general form

$$Lu(r,z)=f(r,z) \text{ for } (r,z)\in\Omega$$

(14)

where L is a linear operator, which can be modified Helmholtz one, as well.

The boundary condition (13) is rewritten as:

$$Bu(r,z)=g(r,z) \text{ for } (r,z)\in\partial\Omega$$

(15)

where B can describe Dirichlet, Newman or Robin boundary condition.

The approximation of the right-hand side function is done by

$$f(r,z)=\sum_{i=1}^{Nw}a_i\varphi_i(r,z)+\sum_{i=1}^{Nl}b_ip_i(r,z)$$

(16)

where $\varphi_i(r,z)=\varphi\left(\left\|r-r_i^a,z-z_i^a\right\|\right)$ is a Radial Basis Function and $\left\{\left(r_i^a,z_i^a\right)\right\}_{i=1}^{Nw}$ is a set of points of the region Ω (see Fig. 1) and $p_i(r,z)$ for $i=1,2,\ldots,N_l$ are monomials.

The approximation given by (16) is written for each point chosen in the region as

$$f(r_j^a,z_j^a)=\sum_{i=1}^{Nw}a_i\varphi_i(r_j^a,z_j^a)+\sum_{i=1}^{Nl}b_ip_i(r_j^a,z_j^a) \text{ for } j=1,2,\ldots,N_w$$

(17)

Additionally, the condition is to fulfill

$$\sum_{i=1}^{Nw} a_i p_j\left(r_i^a, z_i^a\right) = 0 \text{ for } j = 1, 2, \ldots, N_l. \tag{18}$$

The solution $\{a_i\}_{i=1}^{Nw}$ of system of the linear algebraic equations (17, 18) gives the particular solution of the boundary value problem (14, 15) as

$$u_p(r,z) = \sum_{i=1}^{Nw} a_i \phi_i(r,z) + \sum_{i=1}^{Nl} b_i P_i(r,z) \text{ for } (r,z) \in \Omega \tag{19}$$

where

$$L\phi_i(r,z) = \varphi_i(r,z) \text{ for } (r,z) \in \Omega \text{ and } i = 1, 2, \ldots, N_w \tag{20}$$

$$LP_i(r,z) = p_i(r,z) \text{ for } (r,z) \in \Omega \text{ and } i = 1, 2, \ldots, N_l. \tag{21}$$

The implementation of the Method of Fundamental Solutions is based on assumption that the solution of the boundary value problem is a sum of particular solution given by (19) and homogeneous one written as

$$u_h(r,z) = \sum_{i=1}^{Ns} c_i fs_i(r,z), \tag{22}$$

where $fs_i(r,z) = fs\left(\left\| \left(r - r_i^s, z - z_i^s\right) \right\|\right)$ is the fundamental solution of the equation $Lu(r,z) = 0$ and $\left\{\left(r_i^s, z_i^s\right)\right\}_{i=1}^{Ns}$ is a set of points outside the region Ω. The points $\left\{\left(r_i^s, z_i^s\right)\right\}_{i=1}^{Ns}$ called source points are presented in Figure 2.
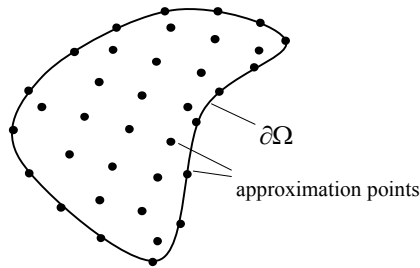
Figure 1. The set of approximation points   Figure 2. The sets of boundary and source points
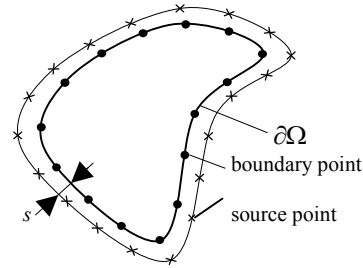
The set of boundary points $\left\{\left(r_i^b, z_i^b\right)\right\}_{i=1}^{Nb}$ is chosen (see Fig. 2). The boundary condition (15) is written at every boundary point, which gives the system of linear algebraic equations:

$$\sum_{i=1}^{Ns} c_i Bfs_i\left(r_j^b, z_j^b\right) = g\left(r_j^b, z_j^b\right) - Bu_p\left(r_j^b, z_j^b\right) \text{ for } j = 1, 2, \ldots, N_b. \tag{23}$$

The solution of the system (23) gives the homogeneous solution of the boundary value problem (14, 15). Therefore, the numerical procedure of solution of the initial-boundary value problem (1-4) is completed.

4. Summary

The numerical experiment has been performed to check the convergence of the proposed algorithm of numerical calculations. The influence of the method parameters on the convergence is investigated. Due to complexity of the proposed combined numerical procedure the very strong and complicated dependence of the accuracy and convergence of the calculations on the method parameters is observed.

References

1. Y. Chen *Torsion of nonhomogeneous bars*. J Franklin Institute 1964;277:50-54.
2. F. J. Rooney, M. Ferrari, *Torsion and flexure of inhomogeneous elements.* Composites Engineering, 5 (1995) 901-911.
3. C. O. Horgan, A. M. Chan, *Torsion of functionally graded isotropic linearly elastic bars.* Journal of Elasticity, 52 (1999)181-199.
4. I. Ecsedi, Some analytical solutions for Saint-Venant torsion of non-homogeneous cylindrical bars. European Journal of Mechanics A/Solids, 28 (2009) 985-990.
5. S. Arghavan, M. R. Hematiyan, *Torsion of functionally graded hollow tubes.* European Journal of Mechanics A/Solids , 28 (2009) 551-559.
6. J. F. Ely, O. C. Zienkiewicz, *Torsion of compound bars – a relaxation solution.* International Journal of Mechanical Science, 1 (1960) 356-365.
7. V. D. Kupradze, M. A. Aleksidze, The method of functional equations for the approximate solution of certain boundary-value problems (in Rusian). Zurnal Vycislennoj Matematiki i Matetyczeskoj Fizyki, 4 (1964) 683-715.
8. R. Mathon, R. L. Johnston, The approximate solution of elliptic boundary-value problems by fundamental solutions. SIAM Journal on Numerical Analysis, 14 (1977) 638-650.
9. G. Fairweather, A. Karageorghis, *The method of fundamental solutions for elliptic boundary value problems.* Advances in Computational Mathematics, 9 (1998) 69-95.
10. M. A. Golberg, C. S. Chen, *The method of fundamental solutions for potential, Helmholtz and diffusion problems.* In: Golberg MA, editor. Boundary integral methods - numerical and mathematical aspects. Boston, Computational Mechanics Publications, 1998, 103-176.
11. A. Uscilowska, J. A. Kolodziej, *Solution of the non linear equation for isothermal gas flow in porous medium by Trefftz method.* Computer Assisted Mechanics and Engineering Sciences, 13 (2006) 445-456.
12. W. Nowacki, *Teoria sprężystośc*, PWN, Warszawa 1970
13. A. Uscilowska, *The Method of Fundamental Solutions for Solving Axi-symmetric Isothermal Gas Flow in Porous Medium*. In: Chen C. S., Karageorghis A., Y. S. Smyrlis, editors. The Method of Fundamental Solutions – A Meshless Method. Dynamics Publishers, Inc. Atlanta, 2008, 165-180.

Local and global instability and vibrations of a geometrically nonlinear cantilever column with regard to the finite elasticity of element connecting individual rods

Sebastian UZNY
Częstochowa University of Technology
Institute of Mechanics and Machine Design Foundations
ul. Dąbrowskiego 73, 42-200 Częstochowa
uzny@imipkm.pcz.czest.pl

Abstract

A boundary problem concerning the stability and free vibrations of a geometrically nonlinear cantilever column subjected to Euler's load (one end of column is free) was formulated in the paper. The boundary problem was formulated on the basis of the Hamilton's principle and the small parameter method due to nonlinearity. Internal forces in the individual elements of a system (both in the case of rectilinear and curvilinear form of a static equilibrium), the regions of local and global instability, bifurcation load and characteristic curves in the plane: load – natural frequency were determined in this work. Numerical calculations were carried out for different values of parameters of the considered system. These parameters are: flexural rigidity asymmetry factor and the rigidity of element connecting the rods of the column .

Keywords: divergence instability, column, free vibration, Euler load, nonlinear system

1. Introduction

Geometrically nonlinear slender systems are the systems where mathematical description of the stability and free vibrations problem relies on nonlinear differential equations (nonlinearity is connected with geometrical parameters). Nonlinear differential equations are obtained by applying theory of moderately large deflections to formulate the boundary problem. Complete solution to the stability of slender system consisting of two different elements was presented for the first time by L. Tomski in work [1]. The presented solution concerned a behaviour of the considered system after attaining the bifurcation load. Research into geometrically nonlinear systems included the different cases of the load: both conservative [1-6] and non-conservative [7] as well as local and global instability [2, 3] and the initial prestressing [4-6].

2. Boundary problem – formulation and solution

Complex geometrically nonlinear system considered in the paper is presented in Fig.1. This system consists of three symmetrically placed rods of the flexural rigidities $(EJ)_1$, $(EJ)_2$ and $(EJ)_3$ $((EJ)_2 = (EJ)_3)$, compression rigidity $(EA)_1$, $(EA)_2$ i $(EA)_3$ $((EA)_2 = (EA)_3)$ and mass per the unit length $(\rho A)_1$, $(\rho A)_2$ and $(\rho A)_3$ $((\rho A)_2 = (\rho A)_3)$. The finite rigidity of element connecting the individual rods of the column at $x = l$ was modelled with the use of rotational spring of rigidity C. The system was subjected to Euler's compressed load and was rigidly fastened. The boundary problem was formulated on the basis of

Hamilton's principle and the small parameter method. Kinetic energy T and potential energy V of the considered system are as follows:

$$T = \frac{1}{2}\sum_i (\rho A)_i \int_0^l \left(\frac{\partial W_i(x,t)}{\partial t}\right)^2 dx + \frac{1}{2}m\left(\frac{\partial W_1(x,t)}{\partial t}\bigg|^{x=l}\right)^2 \tag{1}$$

$$V = \frac{1}{2}\left(\sum_i (EJ)_i \int_0^l \left(\frac{\partial^2 W_i(x,t)}{\partial x^2}\right)^2 dx + \sum_i (EA)_i \int_0^l \left(\frac{\partial U_i(x,t)}{\partial x} + \frac{1}{2}\left(\frac{\partial W_i(x,t)}{\partial x}\right)^2\right)^2 dx\right) +$$

$$PU_1(l,t) - \frac{1}{2}C\left(\frac{\partial W_1(x,t)}{\partial x}\bigg|^{x=l} - \frac{\partial W_2(x,t)}{\partial x}\bigg|^{x=l}\right) \tag{2}$$
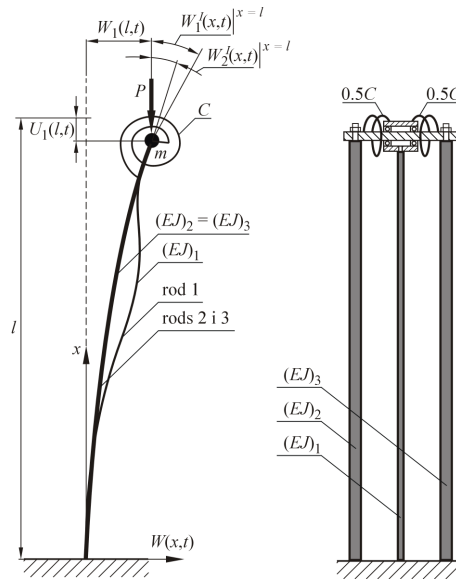
Fig. 1. Diagram of the considered nonlinear system

The internal force in the *i-th* rod is defined by formula:

$$S_i(t) = -(EA)_i\left(\frac{\partial U_i(x,t)}{\partial x} + \frac{1}{2}\left(\frac{\partial W_i(x,t)}{\partial x}\right)^2\right) \tag{3}$$

Further discussion into the boundary problem was carried out with the use of dimensionless quantities:

$$\xi = \frac{x}{l};\ w_i(\xi,\tau) = \frac{W_i(x,\tau)}{l};\ u_i(\xi,\tau) = \frac{U_i(x,\tau)}{l};\ k_i^2(\tau) = \frac{S_i(t)l^2}{(EJ)_i};\ \tau = \omega t \tag{4}$$

where: $S_i(\tau)$ – internal force of *i-th* rod of the column, ω – natural frequency

The geometrical boundary conditions of the column are written in the following form:

$$w_1(0,\tau) = w_2(0,\tau) = w_3(0,\tau) = 0 \; ; \; \frac{\partial w_1(\xi,\tau)}{\partial \xi}\bigg|_{\xi=0} = \frac{\partial w_2(\xi,\tau)}{\partial \xi}\bigg|_{\xi=0} = \frac{\partial w_3(\xi,\tau)}{\partial \xi}\bigg|_{\xi=0} = 0 \quad (5)$$

$$w_1(1,\tau) = w_2(1,\tau) = w_3(1,\tau); \; \frac{\partial w_2(\xi,\tau)}{\partial \xi}\bigg|^{\xi=1} = \frac{\partial w_3(\xi,\tau)}{\partial \xi}\bigg|^{\xi=1} \quad (6)$$

$$u_1(0,\tau) = u_2(0,\tau) = u_3(0,\tau) = u_4(0,\tau) = 0 \quad (7)$$

$$u_1(1,\tau) = u_2(1,\tau) = u_3(1,\tau) = u_4(1,\tau) \quad (8)$$

Using Hamilton's principle and considering the geometrical boundary conditions (5-8) one can obtain:

− differential equations of motion in the transversal direction to axis of the column

$$\frac{\partial^4 w_i(\xi,\tau)}{\partial \xi^4} + k_i^2(\tau)\frac{\partial^2 w_i(\xi,\tau)}{\partial \xi^2} + \frac{(\rho A)_i \omega^2 l^4}{(EJ)_i}\frac{\partial^2 w_i(\xi,\tau)}{\partial \tau^2} = 0 \quad (9)$$

− differential equations of longitudinal displacement

$$\frac{\partial}{\partial \xi}\left[\frac{\partial u_i(\xi,\tau)}{\partial \xi} + \frac{1}{2}\left(\frac{\partial w_i(\xi,\tau)}{\partial \xi}\right)^2\right] = 0 \quad (10)$$

− natural boundary conditions

$$\frac{(EJ)_1}{l}\frac{\partial^2 w_1(\xi,\tau)}{\partial \xi^2}\bigg|^{\xi=1} + C\left(\frac{\partial w_1(\xi,\tau)}{\partial \xi}\bigg|^{\xi=1} - \frac{\partial w_2(\xi,\tau)}{\partial \xi}\bigg|^{\xi=1}\right) = 0 \quad (11)$$

$$\sum_{j=2}^{3}\frac{(EJ)_j}{l}\frac{\partial^2 w_j(\xi,\tau)}{\partial \xi^2}\bigg|^{\xi=1} - C\left(\frac{\partial w_1(\xi,\tau)}{\partial \xi}\bigg|^{\xi=1} - \frac{\partial w_2(\xi,\tau)}{\partial \xi}\bigg|^{\xi=1}\right) = 0 \quad (12)$$

$$\sum_{i}\frac{(EJ)_i}{l^2}\frac{\partial^3 w_i(\xi,\tau)}{\partial \xi^3}\bigg|^{\xi=1} + S_1(\tau)\frac{\partial w_1(\xi,\tau)}{\partial \xi}\bigg|^{\xi=1} + S_2(\tau)\frac{\partial w_1(\xi,\tau)}{\partial \xi}\bigg|^{\xi=1} +$$

$$+ S_3(\tau)\frac{\partial w_3(\xi,\tau)}{\partial \xi}\bigg|^{\xi=1} - m\frac{\partial^2 w(\xi,\tau)}{\partial \tau^2}\bigg|^{\xi=1} = 0 \quad (13)$$

$$S_1(\tau) + S_2(\tau) + S_3(\tau) - P = 0 \quad (14)$$

Equations of longitudinal displacement after double integration and application of the boundary conditions (7) were written as follows:

$$u_i(\xi,\tau) = -\frac{S_i(\tau)}{(EA)_i}\xi - \int_0^{\xi}\left(\frac{\partial w_i(\xi,\tau)}{\partial \xi}\right)^2 d\xi \quad (15)$$

Equations (15) are nonlinear. The small parameter method was used to finally formulate the boundary problem. This method relies on expansion of all nonlinear components of differential equations into the power series of small parameter. Nonlinear

components of differential equations are: transversal displacements $w_i(\xi, \tau)$, longitudinal displacement $u_i(\xi, \tau)$, internal forces of individual rods $S_i(\tau)$ and natural frequency ω. Complex geometrically nonlinear column is characterized by two form of static equilibrium: rectilinear and curvilinear. The component of transversal displacement independent on time occurs in the case of curvilinear form of static equilibrium in expansion into power series of small parameter. This component is characterized by static displacement around which free vibrations appeared for curvilinear form of static equilibrium. Expansions into the power series of small parameter are substituted into differential equations and the boundary conditions. Thus, the differential equations and boundary conditions connected to appropriate power of the small parameter were obtained. On the basis of the solution to the formulated boundary problem, the distribution of internal forces in the individual rods of system, bifurcation and critical load and natural frequency were determined.

3. The results of numerical computations

The dimensionless parameter of bifurcation load in dependence on flexural rigidity asymmetry factor μ for different values of parameter c defining the rigidity of rotational spring is shown in Fig. 2. The results of numerical computations concern geometrically nonlinear λ_b and linear λ_{bL} system. Geometrically linear system is built only of two rods denoted by indexes 2 and 3 (Fig. 1). At a certain value of flexural rigidity asymmetry factor μ, the relationship $\lambda_b < \lambda_{bL}$ took place. In this case system is characterized by local instability. The global instability $\lambda_b > \lambda_{bL}$ occurs in the remaining range of flexural rigidity asymmetry factor.
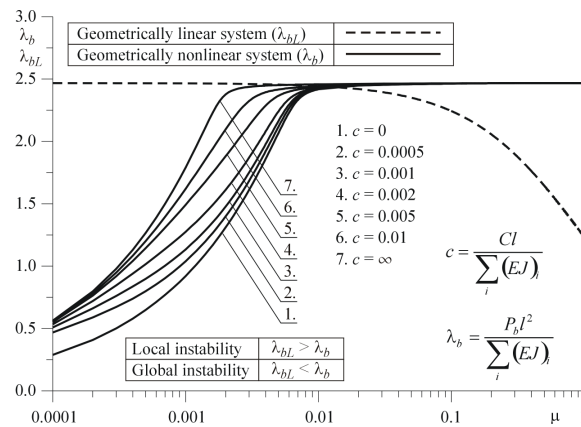

Fig. 2. Dimensionless parameter of bifurcation load λ_b in dependence of coefficient of asymmetry flexural rigidity μ at different value of parameter rigidity of spring c

The initial prestressing is a way of increase in bifurcation load of geometrically nonlinear system which is characterized by local instability. The initial prestressing

relies on the initial stretching and compressing rods of the column. The influence of the initial prestressing on bifurcation load was presented in Fig. 3.
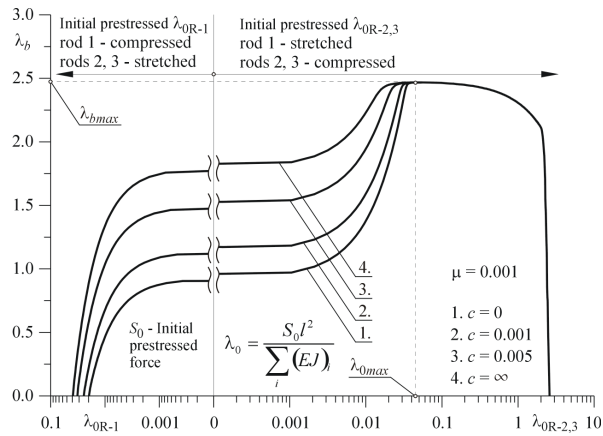
Fig. 3. Parameter of bifurcation load λ_b in relation to parameters c and ζ_A at $\zeta_B = 0.5$

Characteristic curves in the plane: load – natural frequency were presented in figure 4. Numerical computations were conducted for different parameters of the considered system.
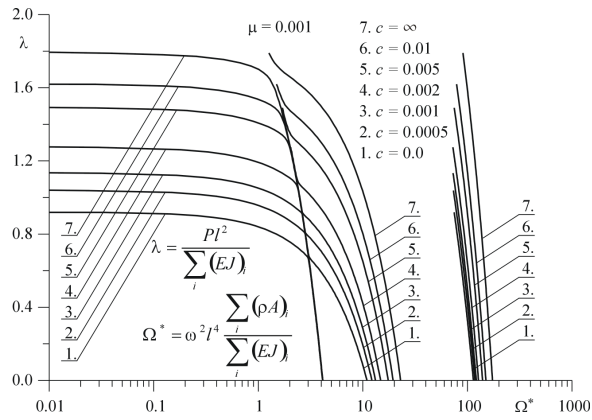
Fig. 4. Characteristic curves in the plane: load – natural frequency

4. Summary

The boundary problem concerning free vibrations of a geometrically nonlinear system subjected to Euler's load was formulated in the paper. The bifurcation load, influence of the initial prestressing on value of the bifurcation load and characteristic curves in the plane: load – natural frequency were determined. Numerical computations were conducted for different values of parameters of the system (such as flexural rigidity

asymmetry factor, torsional rigidity of element connecting individual rods of the column and the initial prestressing of the system). On the basis of numerical calculations was found that the increase of the stiffness of rotational spring causes the increase of bifurcational force at smaller value of parameters μ and $\lambda_{0R-2,3}$. First free vibration frequency is not depended on the stiffness of rotational spring at smaller value of external force.

Acknowledgments

References

1. Tomski L.: *Prebuckling Behaviour of Compound Column – Direct Nonlinear Analysis*, ZAMM, Z. Angew. Math. U. Mech. 65, 1985, 1, 59-61.
2. Tomski L., Szmidla J.: *Local and global instability and vibration of overbraced Euler's column*, Journal of Theoretical and Applied Mechanics 41, 1, 2003, 137-154.
3. Tomski L., Uzny S.: *Free vibration and the stability of a geometrically non-linear column loaded by a follower force directed towards the positive pole*, International Journal of Solids and Structures, 45, 1, 2008, 87-112.
4. Godley M.H.R., Chilver A. H.: *Elastic Buckling of overbraced frame*, Journal Mechanical Engineering Science, 1970, 12(4), 238-246.
5. Mead D. J.: *Free vibrations of self-strained assemlies of beam*, Journal of Sound and Vibration, 249(1), 2002,101-126.
6. Przybylski J.: *The role of prestressing in establishing regions of instability for a compound column under conservative or nonconservative load*, Journal of Sound and Vibration, 231(2), 2000, 291-305.
7. Nayfeh A., *Perturbation Methods*, John Wille, New York 1973. (46)

Niestateczność lokalna i globalna oraz drgania wspornikowej kolumny geometrycznie nieliniowej z uwzględnieniem skończonej sprężystości elementu łączącego poszczególne człony kolumny

W pracy sformułowano zagadnienie brzegowe dotyczące stateczności i drgań własnych wspornikowej kolumny geometrycznie nieliniowej poddanej obciążeniu Eulera (jeden koniec swobodny). Do sformułowania zagadnienia brzegowego wykorzystano zasadę Hamiltona oraz ze względu na występującą nieliniowość metodę małego parametru. W pracy wyznaczono siły wewnętrzne w poszczególnych członach układu (zarówno w przypadku prostoliniowej jak i krzywoliniowej postaci równowagi statycznej), obszary niestateczności lokalnej i globalnej, obciążenie bifurkacyjne oraz krzywe charakterystyczne na płaszczyźnie obciążenie – częstość drgań własnych. Obliczenia numeryczne przeprowadzono przy różnych wartościach parametrów rozważanego układu do których zalicza się współczynnik asymetrii sztywności na zginanie oraz sztywność elementu łączącego człony układu.

Application of Fundamental Solution Method in Cervical Spine Biomechanics

Tomasz WALCZAK
Institute of Applied Mechanics, Poznan University of Technology
3 Piotrowo Street, 60-965 Poznan, Poland
tomasz.walczak@put.poznan.pl

Bogdan MARUSZEWSKI
Institute of Applied Mechanics, Poznan University of Technology
3 Piotrowo Street, 60-965 Poznan, Poland
bogdan.maruszewski@put.poznan.pl

Roman JANKOWSKI
Clinic of Neurosurgery and Neurotraumatology
Poznan University of Medical Sciences
49Przybyszewskiego Street, 60-355 Poznan, Poland
klinikanch@op.pl

Marta CHUDZICKA-ADAMCZAK
Polytechnic Institute, Higher Vocational State School in Piła
10 Podchorążych Street, 64-920 Piła
martachudzicka@wp.pl

Abstract

Thanks to great progress that has occurred in technology in the past twenty years many engineering issues which were difficult or even impossible to solve in the past, now are worked out with use of the modern numerical technology tools. Such tools consist of systems supporting calculations with Finite Element Method. This method is currently the main tool used to solve many mechanical problems. What is more, dominates among all the calculations performed in the field of biomechanics. In the paper, the alternative methods of solving differential equations was presented – Method of Fundamental Solutions (MFS). It is a meshfree method which in the last years is becoming more and more popular as it is very effective and easy to determine solutions of the differential equations of many engineering solutions [1-6]. However, it is not as commonly used in three-dimensional issues of theory of elasticity or heat conduction. The aim of the paper is to show that the method can be successfully implemented in order to determine the spatial stress pattern or displacement distribution in case of biomechanics.

Keywords: Biomechanics, Method of Fundamental Solutions, Spine, Cervical Segment, Stresses

1. Introduction

Method of Fundamental Solutions belongs to the meshfree numerical methods serving to solve the differential equations describing many engineering issues. It has already been used in problems of heat conduction, theory of elasticity, plasticity and fluid mechanics. Its main advantage is its relatively easy computer implementation and in comparison to other methods very little complexity of calculations.

In MFS the solution of problem (differential equation + boundary condition) is approximated with help of linear combination of fundamental solutions of governing equation. The fundamental solutions are the functions of the source points occurring outside the examined area.

In order to obtain the solution of examined problem in the given area, it is enough to define one algebraic linear equations system in which the coefficients standing before the fundamental solutions in their linear combination are the unknown. These linear coefficients are determined based on boundary conditions. It allows to estimate easily the calculation error and approximation thanks to the standard tools of linear algebra.

Determining stress patterns in the model implant of the intervertebral disc is an example of the method's use. The chosen object has a homogeneous structure, therefore the classical equations of Cauchy-Navier were used to describe the fundamental mechanical parameters (stresses, displacements, strains).

2. Governing equations

On the basis of linear theory of elasticity for a homogeneous body with constant material parameters in three-dimensional area Ω, the Cauchy-Navier equations for displacements u_1, u_2, u_3 have form:

$$\left(\frac{2-2\nu}{1-2\nu}\right)\frac{\partial^2 u_1}{\partial x_1^2} + \frac{\partial^2 u_1}{\partial x_2^2} + \frac{\partial^2 u_1}{\partial x_3^2} + \left(\frac{1}{1-2\nu}\right)\frac{\partial^2 u_2}{\partial x_1 \partial x_2} + \left(\frac{1}{1-2\nu}\right)\frac{\partial^2 u_3}{\partial x_1 \partial x_3} = 0 \tag{1}$$

with the boundary conditions defined on $\partial\Omega$ form:

$$B_i[u_1, u_2, u_3, t_1, t_2, t_3] = f_i \quad for \quad i = 1,2,3, \tag{2}$$

where $\partial\Omega$ is the boundary for the Ω area and an operator B_i for i-1,2,3 defines boundary condition by Dirichlet, Neumann or Robin. Defining a stress ε_{ij} as:

$$\varepsilon_{ij} = \frac{1}{2}\left(\frac{\partial u_i}{\partial x_j} + \frac{\partial u_j}{\partial x_i}\right) \quad for \quad i,j = 1,2,3, \tag{3}$$

stresses can be obtained from the Hook's law:

$$\sigma_{ij} = \lambda \delta_{ij} u_{k,k} + 2\mu \varepsilon_{ij} \quad for \quad i,j = 1,2,3. \tag{4}$$

And thanks to them, interacting forces t_i can be expressed in the form:

$$t_i = \sigma_{ij} n_j \quad for \quad i = 1,2,3. \tag{5}$$

In the above formulae the Lame constants λ and μ are determined with relations:

$$\lambda = \frac{\nu E}{(1+\nu)(1-2\nu)}, \tag{6}$$

$$\mu = \frac{E}{2(1+v)}, \tag{7}$$

where E is the module of elasticity and v is the Poisson coefficient. For a source point Z placed outside the examined boundary acting on a point $P \in \partial\Omega$, the fundamental solutions of system of equations Cauchy-Navier have a form:

$$G_{11}(P,Z) = \frac{1}{16\pi\mu(1-v)}\left[\frac{(3-4v)r_{PZ}^2 + (x_{1_P} - x_{1_Z})^2}{r_{PZ}^3}\right], \tag{8}$$

$$G_{12}(P,Z) = G_{21}(P,Z) = \frac{1}{16\pi\mu(1-v)}\left[\frac{(x_{1_P} - x_{1_Z})(x_{2_P} - x_{2_Z})}{r_{PZ}^3}\right], \tag{9}$$

$$G_{13}(P,Z) = G_{31}(P,Z) = \frac{1}{16\pi\mu(1-v)}\left[\frac{(x_{1_P} - x_{1_Z})(x_{3_P} - x_{3_Z})}{r_{PZ}^3}\right], \tag{10}$$

$$G_{22}(P,Z) = \frac{1}{16\pi\mu(1-v)}\left[\frac{(3-4v)r_{PZ}^2 + (x_{2_P} - x_{2_Z})^2}{r_{PZ}^3}\right], \tag{11}$$

$$G_{23}(P,Z) = G_{32}(P,Z) = \frac{1}{16\pi\mu(1-v)}\left[\frac{(x_{2_P} - x_{2_Z})(x_{3_P} - x_{3_Z})}{r_{PZ}^3}\right], \tag{12}$$

$$G_{33}(P,Z) = \frac{1}{16\pi\mu(1-v)}\left[\frac{(3-4v)r_{PZ}^2 + (x_{3_P} - x_{3_Z})^2}{r_{PZ}^3}\right], \tag{13}$$

where:

$$r_{PZ} = \sqrt{(x_{1_P} - x_{1_Z})^2 + (x_{2_P} - x_{2_Z})^2 + (x_{3_P} - x_{3_Z})^2} \tag{14}$$

The solution (the searched displacements) is obtained as the linear combination of fundamental forms' solutions:

$$u_{1_N}(\boldsymbol{a},\boldsymbol{b},\boldsymbol{c},Z;P) = \sum_{i=1}^{N} a_i G_{11}(P,Z_i) + \sum_{i=1}^{N} b_i G_{12}(P,Z_i) + \sum_{i=1}^{N} c_i G_{13}(P,Z_i), \tag{15}$$

$$u_{2_N}(\boldsymbol{a},\boldsymbol{b},\boldsymbol{c},Z;P) = \sum_{i=1}^{N} a_i G_{21}(P,Z_i) + \sum_{i=1}^{N} b_i G_{22}(P,Z_i) + \sum_{i=1}^{N} c_i G_{23}(P,Z_i), \tag{16}$$

$$u_{3_N}(\boldsymbol{a},\boldsymbol{b},\boldsymbol{c},Z;P) = \sum_{i=1}^{N} a_i G_{31}(P,Z_i) + \sum_{i=1}^{N} b_i G_{32}(P,Z_i) + \sum_{i=1}^{N} c_i G_{33}(P,Z_i), \tag{17}$$

where $3N$-dimensional vector $\boldsymbol{S}$ contains the coordinates of the source points Z_i, however N-dimensional vectors $\boldsymbol{a}$, $\boldsymbol{b}$, $\boldsymbol{c}$ contain the unknown coefficients. After solving the above system of linear equations with 3N unknown coefficients, the stresses, displacements and strains in any point of the considered area can be determined according to the formulae presented above.

3. Example and conclusions

In the paper, the problem of determining the stress pattern in the corpus vertebrae of cervical spine of human was used as an example of the application of the Fundamental

Solution Method. In the Figure 1 the outline of the structure of the spinal vertebra (C_3-C_6) is shown.
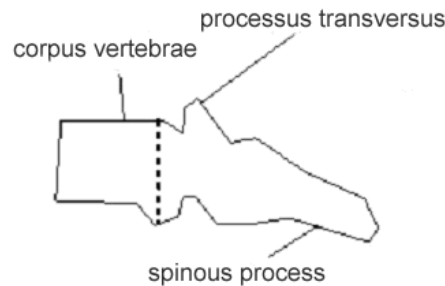

Figure 1. The structure of the spinal vertebra (C_3-C_6)

The maximum strains in the corpus vertebrae of a patient with a degenerative disease of the segment of cervical spine were examined. They were determined for two conformations of a spine: before and after surgery. The load consisted only of the mass forces and the geometry of the corpuses was determined based on the X-ray photography of a patient. The examined patient was 170 cm high and his mass was 78 kg. Material parameters of the bone tissue was taken from literature [8]. In the below Table 1 the maximum stresses in the C_3 to C_6 corpuses vertebrae are presented.

Table 1. The maximum stresses [MPa] in the sagittal section in the corpuses vertebrae

spinal vertebra	C3	C4	C5	C6
after surgery	1.84	2.10	2.64	2.97
before surgery	1.80	2.15	3.13	3.59

A minor improvement can be observed – the decrease in the maximum stresses especially for C5 and C6 vertebrae. It is caused by the change in the conformation of a cervical spine. As a result of placing the implant between the vertebrae C5 and C6, the geometry of the cervical segment has changed which leaded to different stress pattern. The increased stresses present in the vertebrae as a result of improper conformation are the reason for the deformation of the bone tissue which contributes to pain complaints and demands surgery.

Acknowledgments

References

1. J.R. Berger, A. Karageorghis, *The method of fundamental solutions for layered elastic materials*, Engineering Analysis with Boundary Elements, **25** (2001), 877-86.

2. G. Fairweather, A. Karageorghis, *The method of fundamental solutions for elliptic boundary value problems*, Advances in Computational Mathematics, **9** (1998), 69-95.

3. A. Poullikas, A. Karageorghis, G. Georgiou, *The method of fundamental solutions for three dimensional elastostatics problems*, Computers & Structures, **80** (2002), 365-370.

4. D. Redekop, R. S. W. Cheung, *Fundamental solutions for the collocation method in three-dimensional elastostatics*, Computers & Structures, **26** (1987), 703-707.

5. D. Redekop, J. C. Thompson, *Use of fundamental solutions in the collocation method in axisymmetric elastostatics*, Computers & Structures, **17** (1983), 485-490.

6. C. C. Tsai, *The method of fundamental solutions for Three-dimensional elastostatic problems of transversely isotropic solids*, Engineering Analysis with Boundary Elements, **31** (2007), 586-594.

7. J. Mrozowski, J. Awrejcewicz, *Fundamentals of Biomechanics* [in Polish], Wydawnictwo Politechniki Łódzkiej, Łódź 2004.

8. M. Gzik, *Biomechanics of Human Spine* [in Polish], Wydawnictwo Politechniki Śląskiej, Gliwice 2007.

9. Q. H. Zhang, E. C. Teo, *Finite element application in implant research for treatment of lumbar degenerative disc disease*, Medical Engineering & Physics, **30** (2008) 1246–1256.

Zastosowanie metody rozwiązań podstawowych w biomechanice kręgosłupa szyjnego

Duży postęp jaki dokonał się w informatyce w przeciągu ostatnich dwóch dekad spowodował, że wiele zagadnień inżynierskich trudnych bądź wręcz niemożliwych niedawno do rozwiązania, zostało opracowanych za pomocą nowoczesnych narzędzi numerycznych. Do takich narzędzi zaliczyć można wszelkie systemy wspierające obliczenia metodą elementów skończonych (MES). Metoda ta jest w tej chwili głównym narzędziem rozwiązywania wielu problemów mechaniki, a szczególnie dominuje we wszelkich obliczeniach prowadzonych w dziedzinie biomechaniki. W pracy zaprezentowano alternatywną metodę rozwiązywania równań różniczkowych - metodę rozwiązań podstawowych (Method of Fundamental Solutions MFS). Jest to metoda bezsiatkowa, która w ostatnich latach zyskuje coraz większą popularność jako wyjątkowo skuteczna i prosta do wyznaczania rozwiązań równań różniczkowych wielu zagadnień inżynierskich [1-6]. Metoda ta, nie jest jednak powszechnie stosowana w trójwymiarowych zagadnieniach teorii sprężystości czy przewodzenia ciepła. Celem pracy jest pokazanie, że można ją skutecznie zastosować do wyznaczania przestrzennego rozkładu naprężeń czy przemieszczeń w zagadnieniach biomechaniki.

Model of the Cervical Segment of the Spine
based on the Theory of Strongly Curved Beams

Tomasz WALCZAK
Institute of Applied Mechanics, Poznan University of Technology
3 Piotrowo Street, 60-965 Poznan, Poland
tomasz.walczak@put.poznan.pl

Bogdan MARUSZEWSKI
Institute of Applied Mechanics, Poznan University of Technology
3 Piotrowo Street, 60-965 Poznan, Poland
bogdan.maruszewski@put.poznan.pl

Roman JANKOWSKI
Clinic of Neurosurgery and Neurotraumatology
Poznan University of Medical Sciences,
49Przybyszewskiego Street, 60-355 Poznan, Poland
klinikanch@op.pl

Marta CHUDZICKA-ADAMCZAK
Polytechnic Institute, Higher Vocational State School in Piła
10 Podchorążych Street, 64-920 Piła
martachudzicka@wp.pl

Abstract

In the paper the model of the cervical segment of the human's spine based on the theory of strongly curved beams was proposed. Suggested model was used to biomechanical analysis of cervical segment of the spine before and after its stabilization by cage. The stress patterns in centra around stabilizer among chosen patients suffering from discopathy in the cervical segment were described.

Keywords: Biomechanics, Spine, Cervical Segment, Stresses

1. Introduction

Degenerative changes in the spine develop in case of every human. They intensify with the age and very often may lead to the deformation of the vertebrae and of intervertebral discs, to the narrowing of the vertebral canal as well as of the intervertebral openings and even to the instability of the spine. The spine which is distorted with disease can not fulfill the basic functions correctly as the organ protecting the spinal cord, responsible for the movement or as the support for the body. The degenerative changes which significantly disrupt the basic functions of a spine may contain different changes of the physiological curvatures, scoliosis, twists and improper positions if vertebrae. In the paper, the cervical spine segment is analyzed, where the physiological lordosis has changed as the result of degenerative disease. The method for determining stresses present between the vertebrae was presented and it was used to compare the stresses for

the certain vertebrae for the patients who were operated on. The treatment considered the remove of the degenerated intervertebral disc and substituting it with the implant. As the result of the surgery, the spine conformation and the stress pattern change.

2. Mechanical model of the cervical spine segment

The cervical spine segment consists of seven vertebrae (from C_1 to C_7) where each of them has different characteristic dimensions. The vertebrae from C_2 to C_7 have a similar structure presented schematically in the Figure 2.
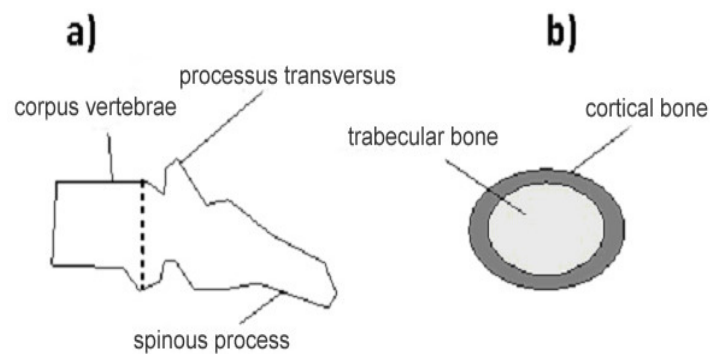

Figure 1. The scheme of the structure of cervical vertebrae C2- C7: a) section of vertebrae in sagittal plane, b) section of vertebrae in cross-section

The vertebrae C_1 and C_2 belong to the upper part of a cervical spine and have different structure from the other vertebrae. The links with the scale of the occipital bones are called the cranial-spinal junction and their structure and compound system of the ligaments assure the proper motion of head. The corpus vertebrae for C_2 to C_7 are responsible for the transfer of stresses such as the force caused by the contraction of muscles or by the weight of the head. In order to determine the stresses, there are possible different approaches because the corpuses are made of different substances [1] (Figure 2b). The assumption that the corpus is a homogenous body consisting of substance with averaged properties of the cortical bone and the trabecular bone is frequently used and is the approach which most simplifies a model. In the paper, the model illustrates the reality as much as it is possible, which means treating every corpus as the heterogeneous body made of the two different substances. Some simplifications were also introduced, such as omitting the trabecular bone as the one which transfers a minor part of stresses in comparison to the cortical layer of corpus. The stresses determined for the posterior and anterior planes of the corpuses vertebrae for C_2 to C_7 are the field of the examinations in the paper. This is why, every vertebra is treated as the elliptical beam with the elliptical hollow.
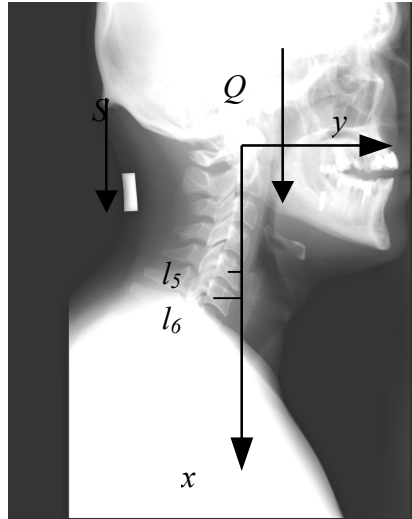
Figure 2. The scheme of the loads of cervical spine

The forces causing stresses in the corpuses vertebrae are the weight of head and the vertical component of the net force of the muscles acting on its posterior part (Figure 3). The data considering the forces and the arm of the forces on which they act and the geometry of the cervical spine segment as well as the dimensions of the characteristic vertebrae were taken from literature [2]. For every examined case, the centre of the coordinate system was chosen in the centre of vertebra C_1 (as in Figure 3). Furthermore, the coordinates of the centre of corpuses of every vertebrae from C_2 to C_7 were used as the bends of interpolations. In order to obtain a curve $y(x)$ representing the conformation of cervical spine segment the method of the interpolation with the spline functions [7] was used. The value of an axial force F acting on the system is the sum of the weight of head and the force originated in neck muscles

$$F = Q + S . \tag{1}$$

While, the bending moment derived from these forces is determined from formula

$$M_i = l_i(Q + S), \quad i = 2,...,7 , \tag{2}$$

where M_i –bending moment acting on i^{th} vertebra, l_i – y-coordinate of the centre of the corpus of ith vertebra. Moment acting on the vertebra C_1 is equal to 0. Knowing the loads on every vertebra the stresses which are the field of interest can be determined. In order to do this, the radius of the curvature in every x point of $y(x)$ curve must be defined, in which the stresses are to be known. It is determined from the formula:

$$r_0(x) = \frac{\left[1 + \left(\dfrac{dy}{dx}\right)^2\right]^{\frac{3}{2}}}{\left|\dfrac{d^2 y}{dx^2}\right|}. \tag{3}$$

Having a radius of the curve r_0, the position of the neutral axis e is determined (on which the stresses coming from the bending moment are equal to zero) [3]:

$$e(x) = r_0(x) - \frac{A_i}{\displaystyle\int_{A_i} \frac{dA_i}{r(x)}}, \tag{4}$$

where A_i – the fields of the cross-section of the ith vertebra and the integral in the above expression is on the cross-section area of the ith vertebra, $r(x)$ – distance from fiber to the centre of the curve $y(x)$ (Figure 3).
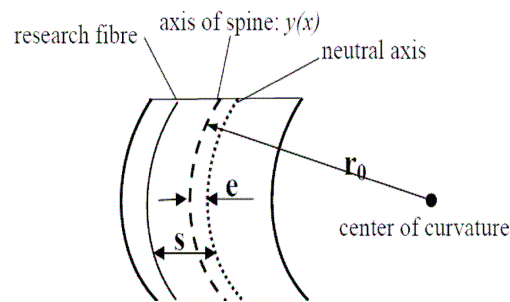

Figure 3. Basic geometric parameters in sagittal section.

For such defined parameters, normal stresses σ_i in the ith section of vertebra in the distance s from the neutral axis of vertebra can be derived from the formula:

$$\sigma_i = -\frac{F}{A_i} + \frac{M_i}{A_i e} \frac{s}{r} \quad for \quad i = 1,2,3, \tag{5}$$

where $r = r_0 - e + s$ is the distance between the examined fiber and the centre of the of the curvature of curve $y(x)$ [3].

3. Conclusions

In the paper, the two conformations of cervical spine before and after surgery on a patient were studied. Parameters such as the coordinates of the centers of corpuses vertebrae, the diameters (characteristic dimensions) of corpuses vertebrae were read from patient's X-Ray photography, the value of the force S was derived based on the data considering the moment of neck's muscles' force [4,5,6,9,10,11]. The mass of the patient was 68 kg, however, the material parameters of bone tissue were taken from literature.

In Table 1, the values of normal stresses for the anterior and posterior plane of corpuses vertebrae from C_2 to C_7 measured in the middle of corpuses' heights are presented. The normal stresses were determined for the conformation of cervical segment before and after surgery which was characterized by placing between C_5 and C_6 vertebrae an implant substituting the intervertebral disc. As the result of the geometrical change, the stress pattern has changed.

Table 1. Normal stresses determined for anterior and posteriori C_2-C_7 vertebral margins

	place of determining stresses	Normal stresses σ_i [MPa]					
		C_2	C_3	C_4	C_5	C_6	C_7
before burgery	anterior body margin	-0.45	0.83	0.96	1.33	0.39	-1.55
	Posterior body margin	-1.79	-2.64	-2.90	-3.14	-2.47	-0.64
after surgery	anterior body margin	-0.48	0.84	1.27	2.00	1.04	-1.40
	Posterior body margin	-1.85	-2.53	-2.97	-2.79	-2.22	0.03

Based on the results shown in the Table 1, it can be observed that the biggest stresses in the corpuses vertebrae occur in C_4, C_5, C_6 vertebrae before as well as after operation. Even a minor change of the relative distribution of cervical vertebrae after the surgery caused change in stress pattern. It can be noticed that the reduction in the absolute value of stresses in the operated segment is connected to increased stresses in the neighbouring segments. X-Ray photographies are usually taken a few weeks after operation. In order to have a full picture of the situation, the measurements should be repeated after a longer period of time e.g. after a year. After such a time, as the result of the introduction of implant, the conformation of the cervical spine segment can differ significantly from the original conformation.

Data about the stresses occurring in cervical vertebrae can provide valuable information specifying the assessment of the deformations of spinal axis. In the presented method, determining the geometrical parameters as well as the loads of the segment of cervical spine cause that the model is individualized. Additionally, the calculations can be implemented to the common use and processing big amount of data. What is more, this method of determining stresses is very fast and easy, which is a great advantage of such an approach.

Acknowledgments

References

1. J. Mrozowski, J. Awrejcewicz, *Fundamentals of Biomechanics* [in Polish], Wydawnictwo Politechniki Łódzkiej, Łódź 2004.
2. M. Gzik, *Biomechanics of Human Spine* [in Polish], Wydawnictwo Politechniki Śląskiej, Gliwice 2007.
3. J. Zielnica, *Strength of Materials* [in Polish], Wydawnictwo Politechniki Poznańskiej, Poznań 1996.
4. D. E. Harrison, D. D. Harrison, T. J. Janik, E. W. Jones, R. Cailliet, M. Normand, *Comparison of axial and flexural stress in lordosis and three buckled configurations of the cervical spine,* Clinical Biomechanics, **16** (2001), 276-284.
5. M. de Zee, D. Falla, D. Farina, J. Rasmussen, *A detailed rigid-body cervical spine model based on inverse dynamics*, Journal of Biomechanics, **40** (2007).
6. A. N. Vasavada, S. Li, S. L. Delp, *Influence of muscle morphometry and moment arms on the moment-generating capacity of human neck muscle*, Spine, **23** (1998), 412-422.
7. R. L. Burden, J. D. Aires, *Numerical Analysis*, PWS-KENT Publishing Company, Boston, 1988 .
8. Y. Ogawa, K. Chiba, M. Matsumoto, M. Nakamura, H. Takaishi, Y. Toyama, *Postoperative factors affecting neurological recovery after surgery for cervical spondylotic myelophaty*, Journal of Neurosurgery Spine, **5** (2006), 483-487.
9. D. E. Harrison, D. D. Harrison, T. J. Janik, E. W. Jones, R. Cailliet, M. Normand, *Evaluation of axial and flexural stresses in the vertebral body cortex and trabecular bone in lordosis and two sagittal cervical translation configurations with an elliptical shell model*, Journal of Manipulative and Physiological Therapeutics, **16** (2001), 276-284.
10. D. E. Harrison, E. W. Jones, T. J. Janik, D. D. Harrison, *Evaluation of axial and flexural stresses in the vertebral body cortex and trabecular bone in lordosis and two sagittal cervical translation configurations with an elliptical shell model,* Journal of Manipulative and Physiological Therapeutics, **25** (2002), 391-401.
11. D. Harrison, D. Harrison, J. Haas, T. Janik, *Evaluation of axial and flexural stresses in the vertebral body cortex and trabecular bone in lordosis and two sagittal cervical translation configurations with an elliptical shell model*, Journal of Manipulative and Physiological Therapeutics, **26** (2003), 608-612.

Model odcinka szyjnego kręgosłupa oparty na teorii silnie zakrzywionego pręta

W pracy zaproponowano model odcinka szyjnego kręgosłupa człowieka oparty na teorii mocno zakrzywionego pręta. Opracowany model został wykorzystany do biomechanicznej analizy kręgosłupa szyjnego przed i po jego stabilizacji cage'em. Opisano panujące rozkłady naprężeń w trzonach kręgowych wokół stabilizatora u wybranych pacjentów cierpiących na dyskopatię w odcinku szyjnym.

Simulation of controlled drug release
from biomaterial delivery systems

Iwona WANAT

AGH University of Science and Technology, Mickiewicz 30 av, 30-059 Cracov
wanat@agh.edu.pl

Marek IWANIEC

AGH University of Science and Technology, Mickiewicz 30 av, 30-059 Cracov
iwaniec@agh.edu.pl

Abstract

The aim of this paper was to develop and validate a model of controlled drug release from hydroxyapatite in the form of a cylinder, using cellular automata. In the course of working there were analyzed many main parameters of shapes and medicine, as well as various models of the inflow buffer, diffusion and dissolution of particles.

Keywords: Cellular Automata; Controlled drug delivery; Model FHP; drunk random walker;

1. Introduction

Hydroxyapatite belongs to a group of so-called biomaterials. In a biological environment material this degrades into biocompatible substances. However, the time of this process is longer than the time of the release of the drug and it is a reason why the model assumes that the structure of delivery does not change during the simulation.

In the study a cylindrical shape with a hole in the shape of a smaller cylinder was analyzed. In this hole there was a drug (heterogeneous model). The device was secured at the top with wax to prevent the escape of the medicament (Figure 1).
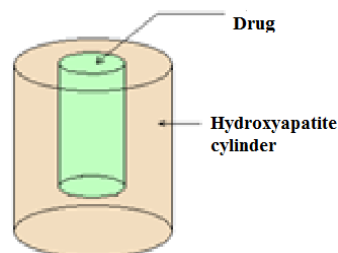

Figure 1 The model of hydroxyapatite device in cylindrical shape

2. Cellular automata

Cellular automata are a tool for modeling changing in time the various physical, chemical, and biological phenomena, in which many systems interact together [1].

Using this simple model it can be simulated a lot of complex processes taking advantage of a simple algorithm. A cellular automaton is a dynamic mathematical model, in which time, space and states are discrete values

At each step, a cellular automaton changes the state of its cells. A step is called a system's evolution. Each cell is assigned a state from a finite set of states. In order to make the cellular automaton reflect the simulated phenomenon correctly, it should:

- define initial states of all cells at t = 0,
- designate a set of rules by which the automaton can evolve.

3. Model of dissolution

Dissolution is a complex process, which is influenced by physicochemical properties of drug and solvent. The first step is to contact the solvent with the surface of solid substances. The next step is to break the molecular bonds (merger) and salvation (impact created after dissolving ions with solvent's molecules). The last stage is a transfer molecules within the solvent (diffusion) [2].

The process of dissolution, although quite complex in terms of physico-chemical properties, is usually presented in a simple way of simulation. In work [3] [4] the authors applied a simple rule of transition, describing the process of dissolving the drug, which lies in the fact that the cell can alter the state of permanent drug to dissolved drug if it has at least one neighbor with solvent state.

In created application each cell with permanent drug's state is assigned a "solubility" parameter, which determines the life span of such cells. In subsequent iterations, in which at least one of the neighbors is in the buffer state this parameter is able to decrement. At the time when it will be zero, the state of the cell changes to the drug dissolved. Thus, the smaller the parameter value, the quicker the drug is soluble.

4. Model of diffusion

Diffusion is a process by which matter is transported from one part of the system to another, due to the random motion of molecules [5].

The description of the basic laws of diffusion was developed by Adolf Fick. Fick's first law describes the relationship between the quantity of substance released per unit time from the unit area of the media and the gradient of the concentration of this substance. When the system is heterogeneous, Fick's law takes the form [8]:

$$J = \frac{DK\varepsilon\Delta c}{\tau l} \tag{1}$$

where J – the change of the quantity of drug in time, D – the diffusion coefficient, Δc - the difference in concentration, τ – the tortuosity of pores, ε – the porosity, l – the thickness of the material, K – the coefficient of medicine distribution between the liquid surrounding and contained in the pores of delivery system.

Fick's second law, assuming that the diffusion coefficient does not depend on the concentration, can be written:

$$\frac{\partial c}{\partial t} = D\left(\frac{\partial^2 c}{\partial x^2} + \frac{\partial^2 c}{\partial y^2} + \frac{\partial^2 c}{\partial z^2}\right) \tag{2}$$

Molecules in the medium move in an irregular manner. These movements are referred to as Brownian motion [6]. Although Brownian motion is really complicated process, often it is simulated using simple models. One of them is called a random drunk walker [2]. In each iteration, the transfer of molecule is the same (regardless of direction) and after each step a new direction (all are equivalent) is chosen. If all particles are in one agglomeration at the initial moment, after several iterations the area of molecule occurrence will be much greater. It turns out that the spatial distribution of particles in this model corresponds to the Gaussian decomposition. Also calculated that the average displacement at time t is proportional to .

The Block rotation method bases on Margolus's neighborhood. In the model there is a separation of iterations into odd and even, for which the transition rule is the same. It consists in the fact that the 2x2 block of cells can be rotated clockwise or counterclockwise. The probability of rotation in both directions is the same [9]. It required numerous modifications to apply the block rotation algorithm to simulate a diffusion, where obstacles may get in the way of particles (eg. hydroxyapatite). After entering the appropriate changes, in some cases, a cell in the dissolved drug's state does not change its position. This happens when in the block is not a single cell in the buffer state, which the drug molecule could switch places. If in the block there are two cells representing the moving drug molecules and one obstacle, it may happen that only one drug molecule changes the position. The examples of rules used in the method of Block rotation are shown in Figure 2.
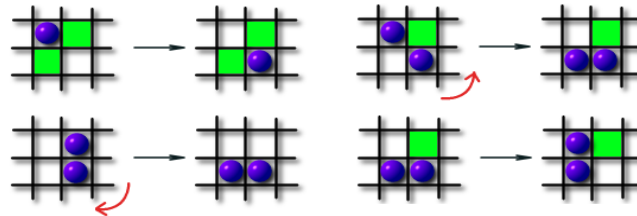

Figure 2. Samples of transition rules in modified algorithm for Block rotation. Symbols: green cells - cells which are an obstacle for moving medicine, violet - a cell capable of dissolving drug, the red arrow points the direction of rotation.

5. Model of flow buffer

The problem of simulating the flow of buffer through a porous material is not a new issue. Using the Navier-Stokes's equations [10] the principle of conservation of mass and momentum of a moving fluid was described. According to them, changes of the element of fluid momentum depend only on external pressure and internal viscosity in

fluid. The first Navier-Stokes's equation for incompressible fluid compares acceleration to the vector sum of forces acting on the particle:

$$\frac{\partial \mathbf{V}}{\partial t} + (\mathbf{V} \cdot \nabla)\mathbf{V} = -\frac{1}{\rho}\nabla p + \nu\nabla^2\mathbf{V} + f \qquad (3)$$

where ρ – the fluid(liquid) density, V – the flow speed, p – the pressure, ν – kinetic viscosity, f – main force acting on the particle, e.g. gravity and $\square$ - the del operator.

The second Navier-Stokes's equation looks as follows:

$$\frac{1}{\rho}\frac{\partial p}{\partial t} + \nabla \cdot \mathbf{V} = 0 \qquad (4)$$

However, it should be noted that these equations apply to an incompressible fluid and the time derivative of the density is equal to zero, so the equation will reduce to the form:

$$\nabla \cdot \mathbf{V} = 0 \qquad (5)$$

The above equation (5) is the law of conservation of mass. As a result, there are additional restrictions on the equation of motion of the first Navier-Stokes (3). Therefore, three components of velocity are closely linked. By identifying two components of speed, it can clearly identify the third component.

With the advent of the gas lattice model's cellular automata [11], there has been a huge breakthrough in simulating the flow of water in the pores. The main method of this group of models is a Lattice-Boltzmann method (LBM) [12]. In gas lattice models space and time are discrete. Particles can move on two or more dimensional grid with the nodes located in the same distance from each other. Time steps are equally divided. The location of particles is represented by the coordinates $x = (x_1, x_2,\ldots, x_n)$, where n is the dimension of the space grid. Number of particles in a given node is presented by n's,
$s = (s_0, s_1,\ldots,s_n)$, where s_0 is the number of fixed particles, while $s_1,\ldots,s_n \square \{0,1\}$, where 0 - presence or 1- lack of particles moving in the direction of the velocity vector $\square_1$, $\square_2$, $\square_3, \ldots, \square_n$.

If algorithm based on the model of the gas lattice is implemented, a defect should be taken into consideration, namely, a defect consisting in that the time, the position and velocity of particles are natural numbers. The advantages of this model are the speed and the slow accumulation of numerical error.

6. Results

The measure of successful simulation is the best match between the results obtained and their experimental results. For this purpose the criterion was introduce, the so-called index differences [7]:

$$I_c = \frac{\sqrt{\sum\limits_{t=1}^{N}(E_t - S_t)^2 / N}}{\sqrt{\sum\limits_{t=1}^{N}(E_t)^2 / N}} \tag{6}$$

where: E_t - experimental result at t, S_t – simulation results at t, t - time, N – number of points.

This index is a number ranging from 0 to 1. The better the fit of simulation results to the experimental data, the smaller is the number. In [7] the authors suggest that Ic < 0.2 means a good fit. Figure 3 shows the release profiles for different drugs together with examples of simulation results after calibration. The values of the index differences for each pair of curves are provided. Apparently the match is on a very good level, since indexes are much lower than 0.2 and are in the range of 0.1040 to 0.0577.
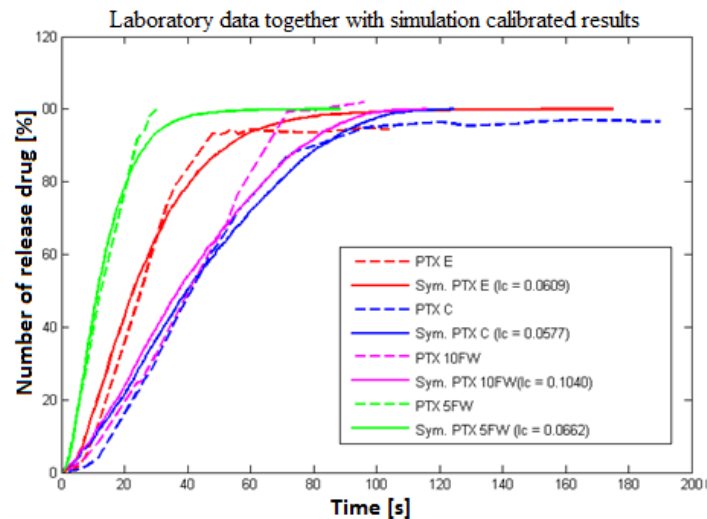

Figure 3. Laboratory data, together with simulation calibrated results. Next to simulation results are index values differences.

7. Conclusions

For each model of the diffusion the relationship between the parameter of solubility and the speed of release have been determined. Each time it had the exponential character, but it differed in scope adopted values. For the diffusion based on Brownian motion it was examined how the number of changes in position of diffusive molecule decreased the rate of drug release. In the work it was found that models using Margolus's neighborhood are characterized by several adverse features such as a very slow process

algorithm, the ability to block the drug inside pores and unpredictable results on the basis of preset parameters.

Thanks to these tests, the choice a particular model of diffusion can be consciously made on the basis of the advantages and disadvantages of the different methods presented in the work.

References

1. K. Malarz. *Automaty komórkowe. Notatki do wykładu*, WFiIS AGH.

2. M. Grassi, G. Grassi, R. Lapasin, and I. Colombo. *Understanding Drug Release and Absorption Mechanisms: a physical and mathematical approach*. CRC Press, 2006.

3. N. Bertrand, G. Leclair, and P. Hildgen. *Modeling drug release from bioerodible microspheres using a cellular automaton*. International Journal of Pharmaceutics, 2007.

4. A. Barat, J. Heather, and M. C. Ruskin. *Probabilistic methods for drug dissolution. part 2. Modeling a soluble binary drug delivery system dissolving in vitro.* Elsevier Science B.V., 2006.

5. J. Crank. *The mathematics of diffusion*. Oxford University Press, 1979.

6. R. M. Mazo. *Brownian motion: fluctuations, dynamics and applications.* Oxford University Press, 2002.

7. N. Bertrand, G. Leclair, and P. Hildgen. *Modeling drug release from bioerodible microspheres using a cellular automaton*. International Journal of Pharmaceutics, 2007.

8. L. Zhang, C. Long, J. Pan, and Y. Qian. *A dissolution-diffusion model and quantitative analysis of drug controlled release from biodegradable polymer microspheres.* The Canadian Journal of Chemical Engineering, 2006.

9. O. B. Bandman. *Experimental study of cellular-automata diffusion models.* Russian Academy of Science, 2006.

10. J. V. Iribarne and H.-R. Cho. *Fizyka atmosfery*. Państ. Wydaw. Naukowe, Warszawa, 1988.

11. M.Sahimi *Flow phenomena In rocks:from continuum models to tractals, percolation, cellular automata and simulated annealing.* Rev. in Modem Physics, 1993.

12. S.Sucii *The lattice Boltzmann equation for fluid dynamics and beyond.* Oxford University Press, 2001

Symulacja uwalniania leków z hydroksyapatytowych kształtek przy użyciu automatów komórkowych

Celem pracy było opracowanie oraz walidacja modelu kontrolowanego uwalniania leków z hydroksyapatytowego nośnika w formie walca, przy użyciu automatów komórkowych. W toku pracy dokonano analizy najważniejszych parametrów kształtki oraz leku, a także różnych modeli napływu buforu, dyfuzji oraz rozpuszczania cząsteczek.

Continuous connection method in dynamic analysis of composite tall building structures

Jacek WDOWICKI

Institute of Structural Engineering, Poznan University of Technolog
Piotrowo 5, 60-965 Poznan, Poland

Abstract

The continuous connection method has been extended for the dynamic analysis of composite tall buildings structures, which contain substructures of different materials. The example of free vibration analysis of 79-storey building has been included. The results obtained by the present method have been compared with those of the finite element method program and field measurements, given in the literature, and a good match has been observed.

Keywords: dynamic analysis, tall buildings, coupled shear walls, continuous connection method

1. Introduction

In tall buildings the lateral loads that arise from effects of wind and earthquakes are often resisted by a system of coupled shear walls acting as vertical cantilevers. It is possible to perform the analysis of shear wall structures using either the discrete method or the continuous one [5]. In the continuous approach, the horizontal connecting beams, floor slabs, and vertical joints are substituted by continuous connections. In recent years the use of continuum models in structural analysis has received considerable attention. These models offer an attractive, low cost method for analysing large structures and they represent the useful tool for the design analysis.

For the dynamic analysis it is convenient to use a hybrid approach based on the analysis of an equivalent continuous medium and a discrete lumped mass system [1, 3, 6]. This paper presents the extension of the method and the computer program based on it allowing for computations of the tall buildings constructed from different materials. The description of a structure and loads applied to it is made with the use of the global coordinate system, OXYZ, with axes X and Y assumed arbitrarily on the level of fixing shear walls, and with vertical Z axis (Fig.1).

2. Equations of equilibrium

An equation of equilibrium of resultant shear forces and torsional moment in the cross-section of a shear wall system $\mathbf{t_k}$, with shear forces and flexure-torsional moments acting in the cross-sections of shear walls $\mathbf{t_E}$ can be presented in a matrix form ($\mathbf{L}$ is matrix defining the transformation from the global coordinate system of the structure to local coordinate systems of shear walls):

$$\hat{\mathbf{t}}_\mathbf{k}(z) = \mathbf{L^T}\,\mathbf{t_E}(z) \tag{1}$$

An equation of equilibrium of normal forces in shear walls $\mathbf{n_E}$ with forces in continuous connections $\mathbf{n_N}$ and vertical loads acting on those elements $\mathbf{n_R}$ is expressed

by a matrix relation (S_E - matrix related to the interaction between the continuous connection and the adjoining shear walls; S_R - matrix related to the action of vertical loads on shear walls)

$$\mathbf{n_E}(z) \;=\; \mathbf{S_E} \int_z^H \mathbf{n_N}(z)\,dr \;+\; \mathbf{S_R} \int_z^H \hat{\mathbf{n}}_R(z)\,dr \tag{2}$$

A differential relation in bending constitutes an equation of equilibrium of bending moments and bimoments $\mathbf{m_E}$ for segments dz of shear walls. After taking into account the forces $\mathbf{n_N}$ in continuous connections and loads $\mathbf{n_R}$ acting on the shear walls with eccentricities of those forces described by coordinates collected in matrices $\mathbf{C_N}$ and $\mathbf{C_R}$, the equation in a matrix notation takes the following form:

$$\mathbf{t_E}(z) - \mathbf{C_N}\mathbf{n_N}(z) - \mathbf{C_R}\hat{\mathbf{n}}_R(z) \;=\; \mathbf{m}_E'(z) \tag{3}$$
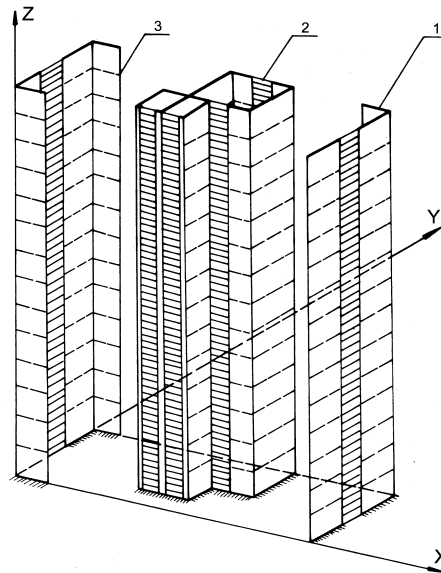

Figure 1. Three-dimensional shear wall structure: 1 – three-dimensional shear wall, 2 – continuous connections which substitute connecting beam bands, 3 – floor slabs

3. Compatibility equations

The equation of compatibility of horizontal displacements of shear walls $\mathbf{v_L}$ (on the assumption that floors are undeformable in their planes) is expressed by the following relation ($\mathbf{v_G}$ - vector of global horizontal displacements of the structure)

$$\mathbf{v_L}(z) \;=\; \mathbf{L}\,\mathbf{v_G}(z) \tag{4}$$

The equation of compatibility of vertical displacements of connecting beams (Fig. 2) has the following form:

$$\mathbf{d_1}(z) + \mathbf{d_2}(z) + \mathbf{d_3}(z) \;=\; \mathbf{0} \tag{5}$$

where the following relation expresses components of those displacements resulting from bending and torsion of stiffening elements

$$\mathbf{d_1}(z) = -\mathbf{C_N^T}\, \mathbf{v_L'}(z) \tag{6}$$

and components resulting from vertical displacements of stiffening elements due to shortenings and settlement are presented as follows

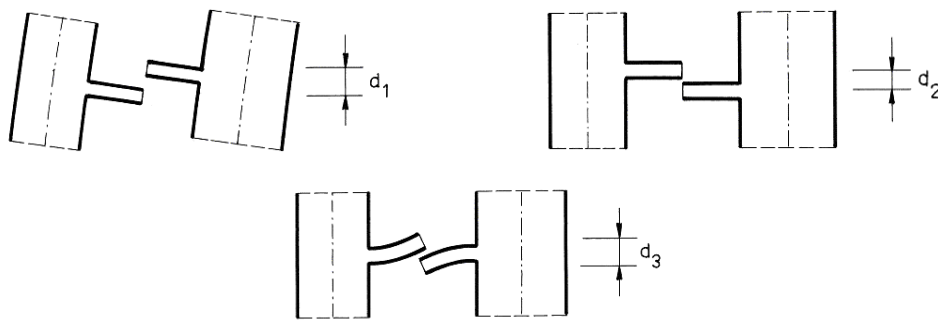$$\mathbf{d_2}(z) = \mathbf{S_E^T}\, \mathbf{v_Z}(z) \tag{7}$$

Figure 2. Components of a vertical displacement of connecting beams:
d1 – from bending of walls,   d2 – from vertical displacement of walls,
d3 – from bending of connecting beams

The relation between shortenings of shear walls $\mathbf{u}$, assumed foundation settlements $\mathbf{z_0}$ and vertical displacements of shear walls $\mathbf{v_Z}$ is expressed by the following equation

$$\mathbf{v_Z}(z) = \mathbf{u}(z) + \mathbf{\hat{z}_0} \tag{8}$$

4. Physical relations

A differential equation of deformations in bending of stiffening elements has the following form

$$\mathbf{m_E}(z) = \mathbf{K_Z}\, \mathbf{v_L''}(z) \tag{9}$$

and an equation linking normal forces $\mathbf{n_E}$ with axial shortenings of shear walls $\mathbf{u}$ can be presented as follows

$$\int_0^z \mathbf{n_E}(w)\, dw = \mathbf{K_S^{-1}}\, \mathbf{u}(z) \tag{10}$$

The relation defining bending stiffness of connecting beams $\mathbf{K_W}$ (the remaining stiffnesses, i.e. compression and torsion stiffness, are of no importance due to the assumption of floors undeformable in their planes) is as follows

$$\mathbf{n_N}(z) = \mathbf{K_W}\, \mathbf{d_3}(z) \tag{11}$$

5. Boundary conditions

The assumption of fixing the stiffening elements at the base, on one level, directly yields the boundary conditions:

$$\mathbf{v_L}(0) = \mathbf{0}, \quad \mathbf{v'_L}(0) = \mathbf{0}, \quad \mathbf{v_z}(0) = \mathbf{\hat{z}_0} \; . \tag{12}$$

The assumption of free ends of stiffening elements at the top of a building allows us to write the following relations

$$\mathbf{n_E}(h_b) = \mathbf{0}, \quad \mathbf{m_E}(h_b) = \mathbf{0}, \tag{13}$$

where: h_b - height of the shear wall system.

6. Equations of motion and computer program

Dynamic solutions have been obtained by treating the structure as a lumped parameter system with discrete masses in the form of rigid floor slabs arbitrary located along the height, having flexural and torsional inertia [6]. A dynamic model with masses in the form of rigid floor slabs has been adopted since over a half of building total mass is concentrated on the floor levels. The coupled torsional-flexural vibrations have been considered because torsional response of buildings during ambient and earthquake response is significant. For shear wall multi-storey structure it is more natural to determine the flexibility matrix D than stiffness matrix K. The vibration of a structure is described by the following relation [2]:

$$\mathbf{D\,M\,\ddot{x}} + \mathbf{D\,C\,\dot{x}} + \mathbf{x} = \mathbf{D\,f} \tag{14}$$

where: $\mathbf{D}$ - flexibility matrix, $\mathbf{M}$ - mass matrix, $\mathbf{C}$ - damping matrix, $\mathbf{x}$ - d-element vector of generalised coordinates (d - number of dynamic degrees of freedom of the calculated structure), $\mathbf{f}$ - d-element vector of generalised excitation forces, corresponding to generalised coordinates.

Calculations were made using DAMB program (Dynamic Analysis of Multistorey Buildings) [7], which gives a possibility to carry out linear dynamic analysis of three-dimensional shear wall structures.

The involved stages are as follows: (1) Determination of natural frequencies and mode shapes, (2) Evaluation of modal participation factors and calculation of modal loading on the structure (using an appropriate design spectrum), (3) Determination of response estimate taking into account the contribution from the given number of modes for various parameters of interest.

7. Numerical example

Di Wang Tower (Shun Hing Square) is a 79-storey office building, built in Shenzen City, China in 1996 year. The main structure of Di Wang Tower is about 325 m high and now it is the eighth tallest building in the world. The aspect ratio of height to transverse width is about 9. This example has been chosen in order to demonstrate the potential of the presented method in the free vibration analysis of non-planar composite shear wall structures.

The plan of standard floors in this tower (Fig.3) includes a rectangular section (53.5m x 35.5 m) and two semi-circles (12.5 m radius) [4]. The composite structural system consists of central reinforced concrete core wall and perimeter frames connected by rigid steel outriggers.
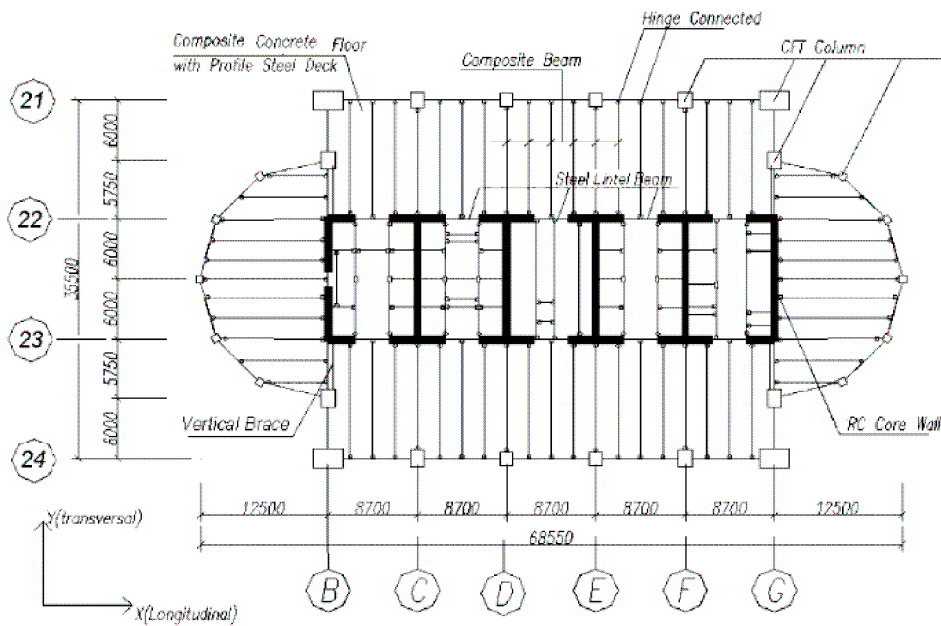

Figure 3. The floor plan of Di Wang Tower [4]

The results of the free vibration analysis obtained by finite element method and by presented method are listed in Table 1. The field measurements results given by Li [4] and Xu [8] are also presented for comparison purposes.

8. Conclusions

In the present paper the continuous-discrete approach to the free vibration analysis of non-planar coupled shear walls has been extended to composite structures.

The results obtained by the present method have been compared with those of the finite element method program and field measurements, given in the literature, and a good match has been observed.

Table 1.   The first two translational natural frequencies (Hz)
in each direction obtained using FEM software [4],
from the field measurements and by the presented method (CCM)

	The 1st mode in longitudinal direction X	The 2nd mode in longitudinal direction X	The 1st mode in transverse direction Y	The 2nd mode in transverse direction Y
SATWE (FEM)	0.201	0.676	0.159	0.592
Field measurements:				
Li [4]	0.208	0.688	0.173	0.540
Xu [8]	0.203	0.660	0.171	0.682
Present method (CCM)	0.190	0.636	0.166	0.636

References

1. O. Aksogan, H.M. Arslan, B.S. Choo, *Forced vibration analysis of stiffened coupled shear walls using continuous connection method*, Engineering Structures, **25** (2003) 499-506.

2. R.W. Clough, J. Penzien, *Dynamics of Structures*, McGraw-Hill, New York 1993.

3. G.-Q. Li, B.S. Choo, *A continuous-discrete approach to the free vibration analysis of stiffened pierced walls on flexible foundations*, Int. J. Solids and Structures. **33** (1996) 249-263.

4. Q.S. Li, J.R. Wu, *Correlation of dynamic characteristics of a super-tall building from full-scale measurements and numerical analysis with various finite element models*, Earthquake Engng & Struct. Dyn., **33** (2004) 1311-1336.

5. B. Stafford-Smith, A. Coull, *Tall Building Structures: Analysis and Design*, Wiley, New York 1991.

6. J. Wdowicki, E. Wdowicka, *Integrated system for analysis of three-dimensional shear wall structures*, Comp. Meth. in Civil Engineering, **1** (1991) 53-60.

7. J. Wdowicki, E. Wdowicka, T. Błaszczyński, *System of programs for dynamic analysis of shear wall tall buildings*, in: Proc. of the Int. Conf. on "Lightweight Structures in Civil Engineering". Warsaw Univ. of Technology, Warsaw, Poland, 440-445.

8. Y.L. Xu, S.W. Chen, R.C. Zhang, *Modal identification of Di Wang Building under Typhoon York using the Hilbert-Huang transform method*, The Structural Design of Tall and Special Buildings, **12** (2003) 21-47

Metoda ciągłych połączeń w obliczeniach dynamicznych konstrukcji budynków wysokich z różnych materiałów

Przedstawiono rozszerzenie metody ciągłych połączeń umożliwiające analizowanie budynków wysokich, których konstrukcje zawierają podukłady z różnych materiałów. Zawarto przykład liczbowy analizy dynamicznej budynku o 79 kondygnacjach. Uzyskane przy użyciu zaproponowanej metody wyniki wykazują dobrą zgodność z wynikami metody elementów skończonych oraz wynikami eksperymentu na rzeczywistym obiekcie.

Identification research on a demolition hammer

Małgorzata WOJSZNIS
Institute of Applied Mechanics, Poznań University of Technology
3 Piotrowo Street, PL-60-965 Poznań
malgorzata.wojsznis@put.poznan.pl

Marian Witalis DOBRY
Institute of Applied Mechanics, Poznań University of Technology
3 Piotrowo Street, PL-60-965 Poznań
marian.dobry@put.poznan.pl

Abstract

The paper presents results of preliminary experimental tests carried out on a demolition hammer. The hammer has a T-shape symmetric handle to be operated with two hands. [1], which forces an operator to assume a symmetric and vertically erect position. The measurements were performed using standard equipment at the Laboratory of Dynamics and Ergonomics of the Metasystem: Human Being – Technical Object – Environment of the Department of Vibroacoustics and Bio-Dynamics of Systems of Poznań University of Technology. Values of vibration acceleration in three directions x, y and z were measured on the tool handle. The tests have shown, that the tool generates impulse forces during work. It concerns particularly the 'z' direction along the axis of symmetry of the tool, which is simultaneously the main direction of motion of the tool.. The identification research on the tool are to be used for verification of the model of a Human Being – Demolition Hammer system [3].

Keywords: vibrations, a biomechanical model

1. Introduction

The paper presents results of experimental tests carried out at the Laboratory of Dynamics and Ergonomics of the Metasystem: Human Being – Technical Object – Environment of the Department of Vibroacoustics and Bio-Dynamics of Systems of Poznan University of Technology. The research is part of a research project funded by the Ministry of Science and Higher Education.

The main goal of the research conducted within the confines of the project mentioned above is to adapt a vibroisolation system to a tool with a T-shape handle and to achieve in this way a reduction in vibration energy flow from the tool into a human operator. A demolition hammer with mass of 15.5 kg with a stiff symmetric handle for two hands was bought for the received means. At an earlier stage of the project was built a spatial dynamic model of a Human Being – Demolition Hammer system [3]. The conducted identification research have been used to verify the developed model as to the correctness of its dynamic structure and the forces exciting the hammer to vibrations during work. The correctness of the model will allow wide-ranging analysis of dynamics, power distribution and energy flow in the investigated structure, which is planned as the next stage of the research project.

2. Demolition hammer

A tool with mass of above 15 kg with a T-shape symmetric handle to be operated with two hands (Fig. 1) was used for identification research. It is a heavy pneumatic hammer with a monolithic casing, a built-in lubricator, and an outlet air silencer.

TECHNICAL DATA OF THE PNEUMATIC HAMMER:
Tool grip: 25x108 mm
Mass: 15.5 kg
Air consumption: 1.5 m^3/min
Length: 590 mm
Number of strokes per minute: 1470 strokes/min.

Standard demolition hammers are used for such works as crushing of asphalt, concrete, frozen soil, driving posts, consolidation of subgrade etc.

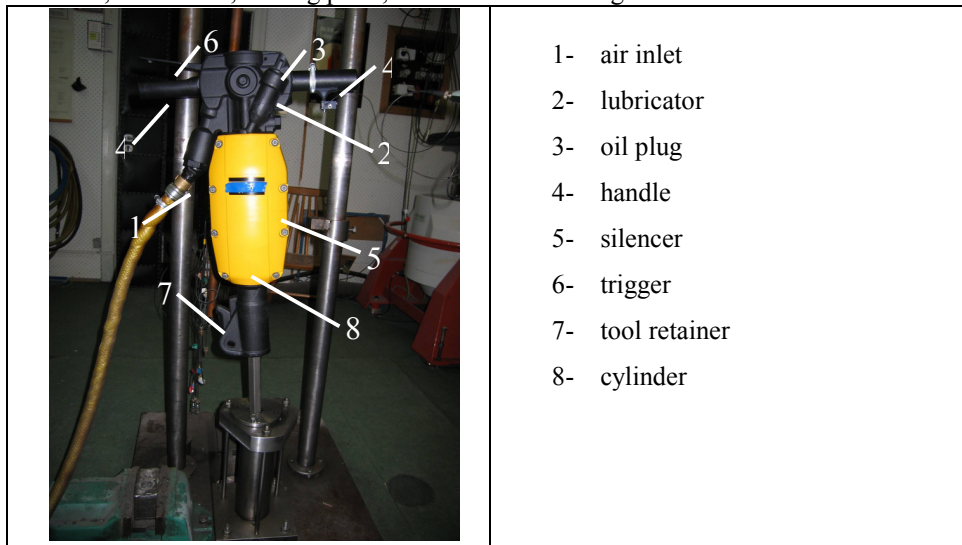|	
1-	air inlet
2-	lubricator
3-	oil plug
4-	handle
5-	silencer
6-	trigger
7-	tool retainer
8-	cylinder

Figure 1. Demolition hammer used for identification research

The investigated tool is not equipped with any vibroisolation system. It is a pneumatic tool with 1470 strokes of the ram per minute.

3. Test stand

Experiments were carried out on a test stand for hand-held impact tools with use of a variant for measurements performed with participation of a human operator [1] (Fig. 2).

Figure 2. Test stand for hand-held impact tools

Conditions of interaction of a hammer with a substrate are defined precisely by international standard ISO 8662 [4]. A standard substrate in the form of an impact energy absorber was introduced – Fig. 2. The substrate consists of a 150 mm high pile of four-millimeter steel balls closed in a thick-walled casing with the internal diameter of 60 mm. The energy absorber is fixed to a concrete foundation with mass of about 500 kg.

Using a standard equipment for measurement of vibrations [2] (Fig. 3) accelerations on the handle were measured. The following equipment was used for measurements: B&K 4384 and 4374 accelerometers, a B&K 2513 vibration meter, RFT measuring apparatus consisting of a signal amplifier, a low-pass filter, a high-pass filter, an

oscilloscope and a power unit. Signals were recorded using a digital oscilloscope RIGOL DS 1102CD.
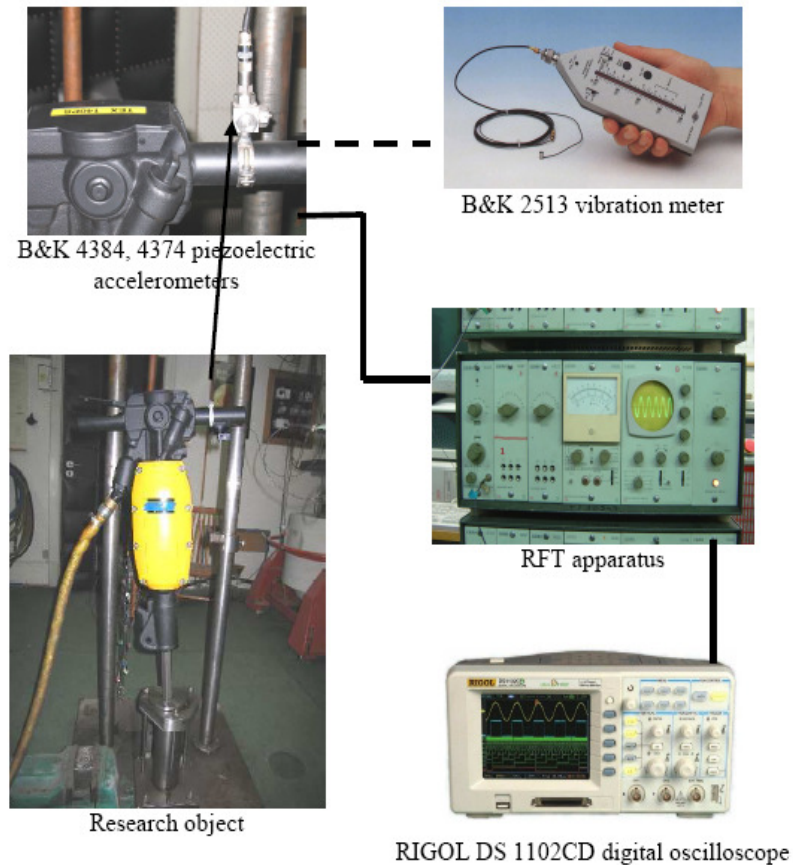

B&K 2513 vibration meter

B&K 4384, 4374 piezoelectric accelerometers

RFT apparatus

Research object

RIGOL DS 1102CD digital oscilloscope

Figure 3. Diagram of measuring equipment used for research

4. Measurement results

The instantaneous runs of vibration acceleration of the handle are shown in Fig. 4.Initial tests showed that the actual frequency of work (of stroking) equals 20 (+/- 2) Hz, which differs from the data given by the manufacturer, who declares it at a level of 25.5 Hz.

During the identification research the running demolition hammer generated impulse forces. This was particularly the case for direction 'z' along the axis of symmetry of the tool, which is simultaneously the main direction of motion of the ram and tool body.
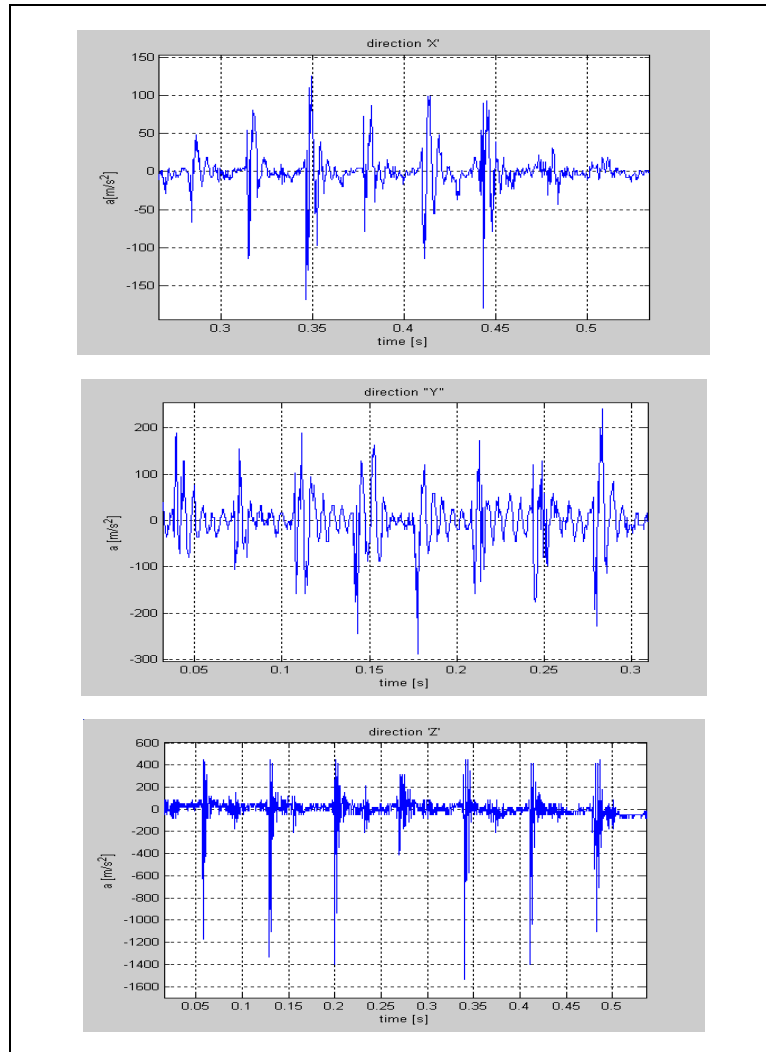
Figure 4. Signals of vibration acceleration recorded for three directions X, Y and Z
during work of the tool held down by a human operator

For directions x and y was observed a significant influence of changing working conditions on the recorded values of acceleration.

Weighted values, RMS values (Lin) and peak values of vibration acceleration were obtained by means of a B&K 2513 integrating vibration meter (Tab.)..

Table. Weighted values, RMS values (Lin) and peak values of vibration acceleration for each direction

Measured value	direction 'x'	direction 'y'	direction 'z'
$a_{weighted}$ [m/s^2]	26	24	30
a_{RMS} [m/s^2]	48	81	152
a_{peak} [m/s^2]	50	94	177
Peak factor CR	1.04	1.16	1.16

The values shown in the table are mean values from five tests conducted for one operator. The values of the peak factor confirm occurrence of impact forces.

5. Conclusion

Work with a demolition hammer having a percussive character of running is very hard, requires a lot of effort, and strains a human operator strongly by vibrations. Practically, it is impossible to hold down the tool with a constant force in the given direction. For further research it is planned to fix the hammer in a special fixture developed specially for this purpose.

References

1. M. W. Dobry, *Nowa generacja zmechanizowanych narzędzi ręcznych dostosowanych do człowieka*, Zeszyty Naukowe Politechniki Poznańskiej, Poznań 2007 r. 47-58
2. T. Kucharski, *System pomiaru drgań mechanicznych*, Wydawnictwo Naukowo-Techniczne, Warszawa 2002, ISBN 83-204-2739-4
3. M. Wojsznis, M. W. Dobry; *Spatial model of a Human-being – Demolition Hammer System*, Vibrations in Physical systems, vol. XXIII, Poznan University of Technology, Poznan 2008, pp. 429-434
4. ISO/FDIS 8662 (EN28662). *Hand- held portable power tools- Measurement of vibrations at handle*. Part 5:Pavement breakers and hammers for construction work.

Badania identyfikacyjne Młota Wyburzeniowego

W pracy przedstawiono wyniki wstępnych badań eksperymentalnych zakupionego młota wyburzeniowego. Młot posiada symetryczny, dwuręczny uchwyt w kształcie litery T, co wymusza u operatora pozycję symetryczną i wyprostowaną. Pomiary wykonano przy wykorzystaniu standardowej aparatury w Zakładzie Wibroakustyki i Bio–Dynamiki Systemów Politechniki Poznańskiej w Laboratorium Dynamiki i Ergonomii Metasystemu: Człowiek – Obiekt Techniczny – Środowisko. Wykonano pomiary przyspieszeń drgań na rękojeści młota w trzech kierunkach x, y, i z. Badania wykazały, że narzędzie generuje w czasie pracy siły o charakterze impulsowym. Szczególnie dotyczy to kierunku „z" wzdłuż osi symetrii narzędzia, który jest jednocześnie głównym kierunkiem ruchu bijaka i korpusu narzędzia. Badania identyfikacyjne narzędzia przeprowadzono w celu weryfikacji modelu dynamicznego systemu Człowiek – Młot Wyburzeniowy.

Abstract only

Abnormal Dispersion of Acoustic Eigenwaves in Anisotropic Plates

V.I. ALSHITS
Institute of Crystallography RAS, 119333 Moscow, Russia
Polish-Japanese Institute of Information Technology, 02-008 Warsaw, Poland

V.N. LYUBIMOV
Institute of Crystallography RAS, 119333 Moscow, Russia

A. RADOWICZ
Kielce University of Technology, 25-314 Kielce, Poland

Lamb waves in elastic anisotropic plates are characterized by an infinite set of dispersion curves. Generally, their intersections are forbidden. However degeneracies in Lamb wave spectra become possible when the plate medium has a symmetry plane parallel to the sagittal plane or to the surfaces. The first symmetry provides splitting of the eigenwaves into the sets of SH waves (polarized orthogonally to the sagittal plane) and in-plane waves (polarized in the sagittal plane). The second leads to their decomposition into the wave systems symmetric and anti-symmetric with respect to the middle plane of the plate. In both cases the wave sub-systems are independent and their dispersion curves may cross each other. It is clear that even infinitesimal perturbations eliminating a symmetry of the problem must exclude infinite number of intersections of the dispersion branches of initially independent systems. Such branch repulsion will mix wave fields with qualitatively different characteristics. A transformed spectrum is formed by new dispersion branches which consist of multiple fragments of initial curves belonging to different sets.

The paper presents three examples of perturbation of a symmetry of initially transversely isotropic elastic plate with the surfaces parallel to the fundamental symmetry axis and the sagittal plane coinciding with the basal symmetry plane: 1) a thin coating of one of the surfaces; 2) a small trigonal perturbation of elastic moduli; and 3) an addition of a weak piezoelectric coupling. These perturbations eliminate a horizontal, or a vertical symmetry plane, or both of them. We shall find for all considered cases the relations between perturbations and branch splittings.

Abstract only

Interfacial Elastic Waves at Twist Boundaries in Transversely Isotropic Media

V.I. ALSHITS

Institute of Crystallography RAS, 119333 Moscow, Russia
Polish-Japanese Institute of Information Technology, 02-008 Warsaw, Poland

V.N. LYUBIMOV

Institute of Crystallography RAS, 119333 Moscow, Russia

A. RADOWICZ

Kielce University of Technology, 25-314 Kielce, Poland

The conditions for existence of Stoneley-type waves localized at the twist interface in the transversely isotropic medium are studied. The considered bi-crystalline structure is formed by the two semi-infinite medium with non-collinear principal axes parallel to the interface. The implicit form of the dispersion equation in terms of the Stroh formalism is found in a general statement. Its approximate analysis is accomplished for the limiting case of small twist angles between principal axes. It is proved the existence theorem for the Stoneley wave solutions in the sector of propagation directions close to the transverse isotropic orientations in the both halves of the structure. The basic parameters of the appropriate localized solutions are found both inside of the sector and on its boundaries.

Wyłączny przedstawiciel
producenta wzbudników drgań
"LDS Test and Measurement Ltd"
w Polsce

Bruel & Kjaer Polska Sp. z o.o.
ul.Goraszewska 12
02-910 Warszawa
Tel.: (22) 858 93 92, Faks: (22) 858 82 21
www.bruel.com.pl
spectris@bruel.com.pl